THESIS REPORT
Ph.D.

S Y S T E M S
R E S E A R C H
C E N T E R
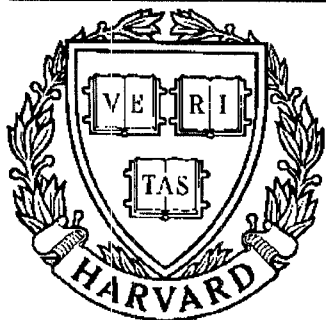
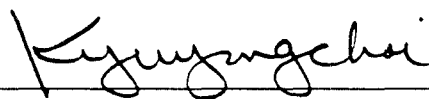# Modeling and Control of Continuous Free Radical Polymerization Reactors

by K.J. Kim
Advisor: K.Y. Choi

Ph.D. 91-12

Approval Sheet

Title of Dissertation: Modeling and Control of Continuous
Free Radical Polymerization Reactors

Name of Candidate: Kee Jeong Kim
Doctor of Philosophy, 1991

Dissertation and Abstract Approved: _____

K. Y. Choi
Associate Professor
Department of Chemical Engineering

Date Approved: _Aug. 26, 1991_

Abstract

Title of Dissertation: Modeling and Control of Continuous
Free Radical Polymerization Reactors

Kee Jeong Kim, Doctor of Philosophy, 1991

Dissertation Directed by: Prof. Kyu Yong Choi
Associate Professor
Department of Chemical Engineering
University of Maryland, College Park, MD.

Nonlinear dynamics of continuous stirred tank reactors for free radical polymerization of styrene have been studied with complex initiator systems such as a binary mixture of monofunctional initiators and bifunctional initiators. The regions of reactor operating conditions which give rise to steady state multiplicity, multiple Hopf bifurcation points, isolas, period doubling bifurcations leading to period-doubling cascades and homoclinics have been identified. The parametric sensitivity of the reactor has also been investigated during the start-up and the steady state operations. Emphasis of the reactor analysis has been placed on the elucidation of the effect of initiator characteristics on the reactor dynamics and resulting polymer molecular weight properties. It has been observed that the presence of more than one monofunctional initiators or dual initiator functionalities makes the reactor dynamics more complex than

a single monofunctional initiator. When the heat transfer coefficient of the reactor wall changes during the polymerization because of viscosity increase, the reactor exhibited simpler dynamic behavior than the case of constant heat heat transfer coefficient. The presence of reactive impurities such as inhibitors in the feed steams also influenced reactor dynamics significantly, depending on their reactivities and concentrations.

A two-time scale extended Kalman filter has been used for on-line estimation and control of polymer molecular weight in continuous and batch polymerization reactors. The effects of model uncertainty and measurement time delay on the filter performance have been investigated through numerical simulations. In the presence of moderate model errors and unknown process disturbances in the continuous polymerization process, the filter showed robust estimation performance in predicting the polymer molecular weight properties when frequent molecular weight measurements are provided. It has been illustrated that the polymer grade change policy can be obtained effectively by using the filter and the steady state process model in the continuous process. The overall filter performance in the batch process was quite similar to that of the continuous process. With relatively large model errors or long measurement time delays, the filter converges slowly. Since the batch processes are operated in finite reaction time, more frequent molecular weight measurements than in continuous processes are required for fast filter convergence.

Modeling and Control of Continuous Free Radical Polymerization Reactors

by
Kee Jeong Kim

Dissertation submitted to the Faculty of the Graduate School
of the University of Maryland in partial fulfillment
of the requirements for the degree of
Doctor of Philosophy
1991

Advisory Committee:

Associate Professor K. Y. Choi, Chairman/Advisor
Professor T. J. McAvoy
Professor T. G. Smith
Assistant Professor N. S. Wang
Professor J. C. Alexander

Dedication

to

My Parents

Acknowledgements

Table of Contents

Appendices   380

References   394

List of Tables

List of Figures

Chapter 1

Introduction

Many polymeric materials are manufactured by batch, semibatch and continuous polymerization processes. Although numerous polymeric materials have been produced for years, diversified enduse requirement and fierce price competition have been forcing the polymerization industry to develop more efficient polymerization methods. In particular, a precise control of polymer properties has become one of the most important objectives in operating modern industrial polymerization processes. Safe operation is another important factor to be considered. Some of these objectives have been accomplished by introducing new catalyst or initiator systems and improved reactor design and reactor control systems [Leaversuch (1986)].

Since many important polymer properties such as molecular weight and molecular weight distribution are complex functions of reactor variables, a

thorough understanding of the polymerization kinetics and reactor behavior is essential for the control of such polymer properties. One of the key problems in controlling the polymer properties is the lack of adequate on-line property sensors. Without rapid and accurate on-line sensors, a direct control of the polymer properties is not possible. Therefore, polymer properties are often controlled indirectly by controlling the primary reactor variables such as temperature, pressure and flow rate of various reactants, solvents and catalysts. When deviations in polymer properties are detected through, for example, laboratory sample analysis, some reactor variables need to be adjusted. Such an indirect control method requires reactor operators extensive plant experience and prescient ability to make necessary adjustments.

One alternative to the direct on-line measurement of polymer properties is to utilize a process model and state estimation technique to predict the polymer properties. In order to use process models for reactor controls, a quantitative understanding of the polymerization kinetics and reactor dynamics is a prerequisite.

The research objectives of this thesis are:

(i) to elucidate steady state and dynamic behavior of continuous polymerization reactors for free radical polymerization of styrene

(ii) to develop a state estimation technique for on-line control of polymer properties and to evaluate its performance in realistic process environ-

ments.

The polymerization systems considered in this study are free radical polymerizations of styrene and methyl methacrylate (MMA) with various initiator systems such as single monofunctional initiators, binary mixture of monofunctional initiators and bifunctional initiators, which are commonly used in the polymer industry. It must be pointed out that the methodology developed in this work for the on-line control of polymer properties in polymerization processes can also be applied to other reaction systems.

This thesis consists of two parts: (i) modeling and analysis of continuous polymerization reactors (Chapters 2, 3, and 4), (ii) on-line estimation and control in continuous and batch polymerization processes (Chapters 5 and 6).

In Chapter 2, a dynamic model is developed for styrene free radical polymerizations with a binary mixture of two monofunctional initiators in a cascade of two continuous stirred tank reactors (CSTR). For each reactor, steady state and dynamic behavior is investigated using a bifurcation analysis package AUTO and numerical model simulations. For bifunctional initiator systems in styrene polymerization, both kinetic models and continuous reactor models are developed in Chapter 3. In particular, the effect of bifunctional initiators on resulting polymer molecular weight is discussed and compared with other initiator systems. Other important factors to be considered in operating and controlling the industrial polymerization processes (e.g., decrease in heat re-

moval efficiency during polymerization and the presence of reactive impurities in the feed) are analyzed in Chapter 4.

The on-line estimation and control of polymer properties in various polymerization processes is discussed in Chapter 5 and 6. In Chapter 5, a two-time scale extended Kalman filter with delayed measurements of polymer molecular weight is applied to a CSTR for styrene polymerization initiated by a binary initiator system. Through numerical simulations, the performance of the filter in the presence of model errors and measurement delays is evaluated at various reactor operating conditions. On-line control of polymer properties is also attempted by incorporating the estimator into a closed loop polymer property control system. In Chapter 6, the performance of the estimation algorithm developed in the previous chapter is tested in a batch reactor for methyl methacrylate polymerization initiated by azobisisobutyronitrile (AIBN). Through numerical simulations for a pilot and an industrial scale batch reactors, the effect of the reactor scale-up on the design of reactor control systems is also discussed.

Chapter 7 is a summary of this work. A few recommendations for future research are also provided in this chapter.

Chapter 2

Dynamics of Continuous Styrene Polymerization Reactors with a Binary Initiator System

2.1. Introduction

Continuous styrene polymerization processes have been in commercial use for years. Continuous stirred tank reactors (CSTR) are widely used in such processes due to uniformity of reactor contents which results in easy control and close reproduction of operating conditions. However, inherent problems of the reactor such as protracted feed blending time, segregation, short circuiting and stagnation become more pronounced at higher monomer conversion and have limited their applications to early stages in the continu-

ous polymerization process. As monomer conversion increases, heat transfer and mixing become less efficient due to increasing viscosity of the reaction mixture. Using specially designed agitators such as anchor or helical agitators, the aforementioned drawbacks can be circumvented and CSTR's can be used for high conversion polymerizations [Uhl and Voznick (1960), Coyle *et al.* (1970), Gawne and Ouwerkerk (1977), Weber (1977)]. In many industrial continuous polymerization processes, more than one reactor is used. For example, in bulk or low solvent styrene polymerization, a CSTR is often used to prepolymerize the monomer to about 30~40 % conversion and the reaction is completed in a specially designed second stage reactor. [Bronstert *et al.* (1972), Carter and Simon (1975), Gawne and Ouwerkerk (1977), Mott and Kozakiewicz (1980)]. High impact polystyrene (HIPS) processes usually employ at least two reactors in series in order to handle the highly viscous polymerizing mass and to produce polymers of desired properties (e.g., molecular weight, rubber morphology, etc.). In such processes, specially designed impellers are used to insure good mixing of viscous mass and thereby achieve high monomer conversion at high temperatures.

Industrial free radical styrene polymerization processes employ a variety of complex initiator systems, such as mixtures of monofunctional initiators or multifunctional initiators, to produce polymers of various grades at intermediate reaction temperature (e.g., 100~160 °C) [Glick (1950), Shusman (1950,1953), D'Alelio (1953), Kamath and Harpell (1978), Kamath (1981)].

When a mixture of monofunctional initiators possessing considerably different thermal stabilities is used, it is quite possible to reduce reaction time and to increase both the monomer conversion and the polymer molecular weight simultaneously through optimal control of the reactor. In a multi-stage CSTR system in which mixed initiators are employed, the temperature can be controlled differently in each stage for better control of the reaction rate and resulting polymer properties. One can also vary the initiator feed composition to improve the reactor performance. Thus, the use of such complex initiator systems enables a polymer reactor engineer to improve the performance of the polymerization reactor without major process equipment changes.

Free radical polymerization of vinyl monomers carried out in CSTR's may exhibit complex steady state and dynamic behavior such as multiple steady states and nonlinear oscillations for certain operating conditions. Such behavior has been observed for both isothermal and nonisothermal operating conditions in various polymerization processes including bulk, solution and emulsion polymerizations. An understanding of such nonlinear reactor behavior is important for the design of reactor control systems for producing the polymers of desired properties with maximum productivity. Many papers have been published on the dynamics of continuous polymerization reactor systems in the literature. However, little has been reported on the behavior of polymerization reactors when initiators other than single monofunctional initiators are used.

In this chapter, the dynamic behavior of a single CSTR and of two CSTR's in series will be investigated for free radical solution polymerization of styrene with a mixture of two initiators having different thermal decomposition rate constants. The emphasis will be placed on the analysis of the effects of various reactor operating conditions on the global reactor behavior and resulting polymer properties.

2.2. Literature Survey

It is well known that continuous chemical reactors can exhibit exotic dynamic behavior (e.g., steady state multiplicity and autonomous oscillations). Such phenomena are caused by inherent nonlinearities, the most common of which is the Arrhenius temperature dependence of the reaction rate. For example, a first order irreversible exothermic reaction in a nonisothermal CSTR may show a strong parametric sensitivity for a small change in its operating or design parameters. There has been a large number of publications on this subject, notably by Schmitz (1975), Bailey (1977), Ray (1977), Varma and Aris (1977), Pismen (1980), Luss (1981), Balakotaiah and Luss (1986), and Ražon and Schmitz (1986). Various multiplicity patterns of steady state profiles reported include **S** shape, inverse **S** shape, isolas, mushrooms and their combinations. Periodic bifurcations observed include Hopf bifurcation, homoclinics (infinite period or saddle-node), limit cycles, period doubling and cas-

cade of period doubling leading to aperiodic oscillations (chaos). The chaotic behavior in chemical reaction systems, which is indicated by the presence of a well defined attractor shaped by folding and stretching intricacy of strips, has been reviewed recently by Hudson and Rössler (1986), Gurel and Gurel (1986) and Doherty and Ottino (1988). The occurrence of such nonlinear dynamics in continuous chemical reactors can have important implications in the design and control of reactors and thus it is important to understand when and how such nonlinear dynamic phenomena would occur for a given reactor system.

Since the early studies of steady state multiplicity and stability of a CSTR by Van Herdeen (1953) and Bilous and Amundson (1955), systematic efforts to understand, analyze and exploit the reactor behavior have made by many workers through a detailed numerical or experimental methods.

2.2.1. Dynamics of a Single CSTR

The simplest lumped parameter system that has been studied most extensively is a single homogeneous exothermic reaction in a nonisothermal CSTR. In the following, we shall provide a brief literature survey on this issue.

2.2.1.1. Steady State Multiplicity and Stability

The first observation of multiple steady states in a continuous chemical reactor was reported by Liljenroth (1918). He found that such multiplicity is caused by the interaction between the external heat transfer resistance and the rate of heat generation by the chemical reaction. However, his report along with a few other pioneering analyses of steady state multiplicity were not recognized until exhumed recently by Schmitz (1975) and Luss (1981).

After Van Herdeen (1953) proposed a simple graphical method to analyze reactor stability using heat generation and removal curves (now known as Van Herdeen diagram), many theoretical and experimental studies have followed. A rigorous analysis of the local stability was first reported by Bilous and Amundson (1955) using Liapunov's first method (perturbation method) and the frequency response method. They utilized the phase plane diagrams to illustrate how the reactor can be reached to its steady state from various initial conditions. They extended their analysis of the open loop system to the closed loop system with feedback controllers [Aris and Amundson (1957, 1959), Nemanic et al. (1959), Schmitz and Amundson (1963)].

Computational methods used for the stability analysis include: Liapunov's direct method [Warden et al. (1964), Berger and Perlmutter (1964a, 1964b, 1965a), Luecke and McGire (1965), Berger and Lapidus (1968), Mauren and Garlid (1968)]; the root locus method [Luyben (1974)]; the reverse

time integral method [Pellegrim (1988)]. A variety of multiplicity analysis technique have also been applied to more complex systems such as two phase reaction systems [Schmitz and Amundson (1963), Luyben (1964)] and systems of imperfect mixing [Yang *et al.* (1974), Puhl and Nicolis (1986)].

There are many experimental evidences of multiple steady states. For example, Furusawa *et al.* (1969) observed up to two stable (upper and lower) steady states in a nonadiabatic CSTR for hydration of propylene oxide. Stabilization of unstable steady state was also studied using feedback controllers by Chang and Schmitz (1975). A review of experimental studies of nonlinear reactor dynamics can be found in Schmitz (1975).

2.2.1.2. Oscillatory Behavior

The occurrence of self-sustained oscillatory behavior in a continuous reactor was pointed out by Bilous and Amundson (1955) using the Van Herdeen diagram and the linear stability analysis. The emergence of oscillatory dynamics was observed when the heat removal curve cross the inflection point of the heat generation curve where the characteristic equation has purely imaginary eigenvalues. Aris and Amundson (1958) observed the emergence of limit cycles in a CSTR with a proportional feedback controller, even though these oscillations were not self-sustained. They also found that the bifurcation of limit cycles may occur at the critical value of a bifurcation parameter in which the steady state loses its stability.

Poincaré bifurcation theory and several other mathematical tools have been used in the study of oscillatory behavior. They include Liapunov's direct method [Warden *et al.* (1964), Leathrum, *et al.* (1964)]; the averaging technique [Luss and Lapidus (1966, 1967)] to predict the existence and stability of limit cycles; perturbation technique [Douglas and Gaitonde (1967), Dorawala and Douglas (1971), Heberling *et al.* (1971), Cohen and Keener (1976)] to predict the form of limit cycles; Fourier expansion [Beek (1972) and Hyun and Aris (1972)] to determine the stability of limit cycles. These theoretical studies have been verified experimentally in various chemical reaction systems by many researchers [Hugo and Wirges (1978), Schmitz *et al.* (1979), Stoukides *et al.* (1982), Gray *et al.* (1984), Vleeschhouwer *et al* (1988)].

An extensive analysis of reactor dynamics and oscillatory behavior reactor has been further carried out by Uppal *et al.* (1974, 1976). They analyzed the local bifurcation phenomena and derived analytical formulae to predict the existence and direction of bifurcation points to periodic solutions and their stabilities using Friedrichs Hopf bifurcation theory [Poor (1973, 1976)]. Such local bifurcation analysis of limit cycles was further extended to the global bifurcation analysis by Keener (1981). He found the occurrence of an infinite period bifurcation (homoclinic orbit) when the branches of periodic solutions are terminated and showed how to find the entire branch of periodic solutions including the points of Hopf bifurcation and infinite period bifurcation using the perturbation method.

When the reaction is highly exothermic, the oscillatory behavior of the reactor can be significantly influenced by solid materials (extraneous thermal capacitance) such as the reactor walls, stirring devices, baffles or packings which interact the reacting fluid via storage and transfer of heat [Chang and Schmitz (1975) and Schmitz *et al.* (1979)]. Using the Lewis number, which is the ratio of intrinsic thermal time constant to intrinsic material time constant, Ray and Hastings (1980) investigated the effect of extraneous thermal capacitance on the dynamic behavior of such reactor systems. The effect of extraneous thermal capacitance on the reactor dynamics has also been studied by Planeaux and Jensen (1986) who included the energy balance equation for the solid phase. Using the normal form theory, they observed other types of bifurcations to invariant tori, isolas of periodic branches. They also found four Hopf points and multiple stable periodic orbits, which are not observed in a two dimensional system without the solid phase energy balance.

When the dynamic process model consists of more than two O.D.E's, bifurcation analysis for complex nonlinear dynamical systems can be carried out using numerical methods. A number of general purpose bifurcation analysis packages are now available. For example, AUTO [Doedel (1981)], DERPAR [Kubíček and Marek (1983)] and BIFOR2 [Hassard *et al.* (1981)] have been used widely in many different fields.

2.2.1.3. Parametric Studies

Following a plethora of reports concerning the existence and stability of multiple steady states and limit cycles, reactor dynamic studies have been focused on the systematic search of the reactor behavior in the operating parameter space. Such parametric study of steady state multiplicity was first reported by Halváček *et al.* (1970). They derived a criterion for the existence of multiplicity using a steady state manifold and observed four different types of steady state solutions (*i.e.*, unique, **S**, unique-isola and mushroom) with several operating parameters as bifurcation parameters.

Uppal *et al.* (1974,1976) classified all possible reactor dynamic behavior including steady state multiplicity, limit cycles and their stabilities in an operating parameter space. They identified nine different regions of dynamic behavior for a simple first order irreversible reaction in a nonisothermal CSTR. Later they found up to seventeen different regions with five different steady state structures (*i.e.*, unique, **S**, unique-isola, **S**-isola and mushroom) with a residence time as a bifurcation parameter. Other workers reported similar analysis [Kauschus *et al.* (1978), Huang and Varma (1980), William and Calo (1981), Kwang and Tsotsis (1983)]. Such parametric analyses have been applied to more complex systems such as higher order single reaction in a CSTR [Vaganov *et al.* (1978), Schmitz *et al.* (1979)] and autocatalytic reactions in an isothermal CSTR [Gray and Scott (1983)]. In particular, the sufficient con-

ditions for the existence of steady state multiplicity and uniqueness criteria for various single reaction systems have been derived [Bosch and Luss (1977a, 197b), Tsotsis and Schmitz (1979), Leib and Luss (1979)]. Calo and Chang (1979, 1980) developed a generalized technique for the exact determination of multidimensional regions of unique and multiple steady states via the catastrophe theory and showed successful applications of this technique to various reaction systems.

A computational procedure for the parametric classification of steady state multiplicity was developed by Balakotaiah and Luss (1981, 1982a) using the singularity theory [Golubitsky and Schaeffer (1979), Golubitsky and Keyfitz (1980, 1985)]. For the simplest reaction system, they identified six different steady state multiplicity patterns (*i.e.*, **S**, inverse **S**, isola, mushroom, **S**-isola and inverse **S**-isola) formed by the hysteresis and isola varieties in a parameter space and also found the winged-cusp point.

2.2.2. Dynamics of Complex Chemical Reaction Systems

When several reactions occur simultaneously in a CSTR, or when more than one reactor is used even for a single reaction, the resulting reactor dynamics become quite complex. In the following, a brief literature review on this issue is presented.

2.2.2.1. Multiple Reactions in a CSTR

For a CSTR in which two consecutive first order exothermic reactions occur, Bilous and Amundson (1953) was the first to point out the presence of up to five steady states. Similar observations have been reported by Westerterp (1962) and Sabo and Dranoff (1970). Hlaváček *et al.* (1972) derived a multiplicity criterion for a two exothermic consecutive reaction system and his techniques for finding the sufficient conditions for multiplicity have been applied to a CSTR in which either two parallel or two consecutive reactions of the first order exothermic or endothermic occur [Luss and Chen (1975), Michelson (1977), Pikos and Luss (1979)]. These studies showed the existence of up to five steady states when both reactions are exothermic or when only one is exothermic. Multiple steady states were also found even for two endothermic reactions in a CSTR.

By utilizing the elementary catastrophy theory and the singularity theory, Balakotaiah and Luss (1982b, 1982c, 1982d, 1983, 1984) conducted a parametric analysis of multiplicity in two different ways: mapping of parameter regions

with different number of steady state solutions and mapping of parameter regions with different bifurcation diagrams (multiplicity patterns). In two consecutive exothermic reactions, they observed the existence of up to five steady states and identified five distinctive regions of multiplicity patterns near the butterfly singularity point which was obtained with the hysteresis and double limit varieties. With the reactor residence time as an independent variable, they identified 36 bifurcation diagrams around the highest order singularity (a higher order pitfork) in the regions of feasible parameters and 12 other bifurcation diagrams in other parts of parameter spaces. They also found that in a CSTR with N parallel reactions there exist $N!$ distinct regions of parameters in each of which $2N + 1$ steady states exist.

The steady state multiplicity for N dimensional system has also been investigated by Retzloff and coworkers [Chicone and Retzloff (1982), Retzloff *et al.* (1987a), Berdonzi *et al.* (1989)]. They found that maximum number of multiple steady states is $2^N - 1$ for $N - 1$ consecutive reactions in a CSTR. This maximum multiplicity criterion has been used to identify steady states in very tiny parameter regions for two consecutive reactions in a CSTR [Jorgensen *et al.* (1984), Farr and Aris (1986), and Starzak and Zarzycki (1989)]. The multiplicity pattern search was also extended to the classification of bifurcation diagrams including periodic solution branches [Byeon and Chung (1889)]. In a CSTR where two consecutive reactions occur, they identified 34 bifurcation diagrams including multiple Hopf bifurcation points that were also found by

Doedel and Heinemann (1983) and Planeaux and Jensen (1986).

Note that all of the multiplicity criteria reviewed above have been derived from a steady state manifold which is a reduced model equation containing the minimum number of intrinsic state variables. When the reaction system is too complicated to be reduced to a steady state manifold, these techniques for multiplicity analysis are not directly applicable. For such complex reaction systems, several different approaches to multiplicity analysis have been reported. Lyberatos *et al.* (1984) derived the multiplicity criteria with the Newton polyhedron method which does not require the reduction of the partial derivatives of the modeling equations or the selection of a bifurcation parameter. Balakotaiah *et al.* (1985) used the Liapunov-Schmidt method to reduce the dimension of the modeling equations before deriving multiplicity criteria with the elementary catastrophe theory. Besides direct derivations of multiplicity criteria, indirect methods of determining the multiplicity of complex reaction networks in an isothermal CSTR have been developed using the deficiency zero theorem and the deficiency one theorem [Feinberg (1987, 1988), Leib *et al.* (1988), Rumschitzki and Feinberg (1988)].

In three or higher order dimensional systems, an increase in the number of potential bifurcation parameters leads to a sequence of period-doubling bifurcations (Feigenbaum sequence), beyond which the attractor changes its character and becomes chaos. Through numerical studies, high order bifurcation and chaotic behavior has been observed in a CSTR where various multiple

reactions occur: two consecutive reactions [Kahlert *et al.* (1981), Jorgensen and Aris (1983)], two parallel reactions [Chan *et al.* (1987)], isothermal auto-catalytic reactions [Gray and Scott (1985)], and three simultaneous reactions [Hudson *et al.* (1986), Retzloff *et al.* (1987b)]. By imposing periodic forcing on the reactor where a single reaction occurs, complex bifurcations have also been found [Mankin and Hudson (1984), Lyberatos *et al.* (1985), McKarnin *et al.* (1988), Shanks and Bailey (1989)]. Through extensive experiments of Belousov-Zhabontinskii reaction in a CSTR, Hudson and coworkers have confirmed the presence of high order bifurcations and chaos [Hudson *et al.* (1979, 1982), Hudson and Mankin (1981, 1982), Lamba and Hudson (1985, 1987)].

2.2.2.2. Cascade of Multiple CSTR's

Since Berger and Perlmutter (1965b) analyzed stability of N-stage cascaded CSTR's using Liapunov's direct method, a few studies of the dynamic behavior of multiple CSTR's have been reported. Even before any theoretical studies of steady state multiplicity for such reactor systems were reported, Horak *et al.* (1971) observed experimentally the existence of up to three stable steady states of the second reactor for autocatalytic reaction of bis-trichloromethy trisulphide in an array of two CSTR's. Varma (1980) showed that a sequence of N CSTR's can have up to $2^{N+1} - 1$ steady states, of which only $N + 1$ are stable.

Kibíček *et al.* (1980) classified parameter regions where different number

of steady states exists in the CSTR with a recycle stream to the first reactor. They found that the second reactor can have up to five steady states and two of them are unstable. With various bifurcation parameters, they observed double isolas and isola-mushroom. For the two cascaded CSTR's without recycle, Svoronos *et al.* (1982) found up to seven steady states in the second reactor. They also identified 22 distinct multiplicity patterns of the second reactor and classified regions of these multiplicity patterns in a parameter space by extending Uppal *et al.*'s works (1974, 1976). The multiplicity patterns in multiple reactor systems were also further studied by Dangelmayr and Stewart (1984) using the singularity theory and the catastrophe theory. The occurrence of high order periodic bifurcations and chaos in this reactor system was reported by Mankin and Hudson (1986).

2.2.3. Dynamics of Continuous Polymerization Reactors

Continuous free radical polymerization reactors can also show complex dynamic behavior due to a huge release of reaction heat and poor heat transfer. In high conversion free radical polymerization, termination reactions involving polymeric radicals becomes diffusion controlled due to increasing viscosity of the reacting fluid and as a result, the reaction rate accelerates even under isothermal conditions. This phenomenon is referred as the gel effect [Trommsdorff et al. (1948)]. Earlier studies on the dynamics of such reactors were reviewed by Imoto (1972) and Ray (1981, 1983).

Continuous polymerization reactor models, in general, can be divided into two subsystems. The first subsystem consists of mass and energy balances and the second subsystem consists of molecular weight moment equations to calculate polymer molecular weight (MW) and molecular weight distribution (MWD). If the polymer properties do not influence the first subsystem variables, the reactor model can be decoupled and the reactor behavior can be analyzed using only the first subsystem of the model.

Earlier studies of continuous polymerization reactors, initiated by Denbigh (1947), have placed emphasis on the development of the second subsystem model for the prediction of polymer properties under isothermal conditions. Denbigh developed various reactor models for homogeneous free radical polymerization where spontaneous initiation, propagation and combination termi-

nation were considered. He calculated MWD by a stepwise algebraic substitution technique. He also found that a CSTR can yield polymers of narrower MWD than a batch reactor. The detailed second subsystem models for homo- and copolymerizations in multiple CSTR's were derived by Amundson and coworkers [Liu and Amundson (1961), Zeman and Amundson (1963, 1965)]. They included all possible chain termination mechanisms such as combination, disproportionation and spontaneous termination into the model. They also developed both exact and approximate (by Taylor expansion) methods for the calculation of MWD from more than 100 nonlinear differential equations of live and dead polymers, which require extensive computation for the explicit MWD. A more efficient calculation method for polymer properties has been developed using moments of live and dead polymers [Ray (1969), Cozewith (1971)].

Continuous polymerization reactor models have been further developed by including chain initiation reactions by initiators [Biesenberger and Tadmor (1965)], the gel effect [Hui and Hamielec (1968, 1969)], chain branching by terminal double bond polymerization [Nagarubramanian and Grassley (1970, 1972), Hyun et al. (1976), Chatterjee et al. (1977), Taylor and Reichert (1985)], imperfect mixing [Tadmor and Biesenberger (1966), Corrigan and Dean (1968), O'Driscoll and Knorr (1969), Mecklenburgh (1970), Nauman (1974), Georgakis and Marini (1981)], volume contraction during polymerization [Schmidt and Ray (1981)], extraneous thermal capacitance [Schmidt

et al. (1984), Teymour and Ray (1989)], and viscosity-dependent heat transfer coefficient [Henderson (1987)]. The effect of periodic reactor operations on the MWD during steady state reactor operation has also been investigated [Laurence and Vasudevan (1968), Ray (1968), Spitz, *et al.* (1976), Meira (1981)]. These mathematical models capable of predicting the polymer molecular weight properties have been validated experimentally for bulk and solution polymerizations of styrene in CSTR's [Duerksen *et al.* (1967), Duerksen and Hamielec (1968)] and methyl methacrylate (MMA) [Terenzi and Cosway (1969)]. Ray (1972) summarized detailed mathematical techniques for the calculations of polymer properties.

The presence of multiple steady states in continuous free radical polymerization reactors was first reported by Hoftyzer and Zwietering (1961). For ethylene polymerization in a nonisothermal CSTR under high pressure, their model prediction shows that as many as five steady states are possible and stable limit cycles may arise at some operating conditions. The presence of five steady states in a continuous polymerization reactor was also found by Amundson and coworkers [Warden and Amundson (1962), Goldstein and Amundson (1965)]. They analyzed steady state multiplicity and stability of the reactor with a generalized free radical polymerization model by extending their earlier studies for classical chemical reactors (§2.2.1.1). For styrene thermal polymerization in a CSTR, Wittimer *et al.* (1965) observed multiple steady states and stable limit cycles with a simple empirical model. These

earlier dynamic studies were not confirmed experimentally and their model did not include the gel effect.

Knorr and O'Driscoll (1970) point out the possibility of multiple steady states caused by the gel effect for styrene polymerization in an isothermal CSTR. The effects of various gel effect correlations on the reactor dynamics for MMA solution polymerization in an isothermal CSTR were discussed by Schmidt and Ray (1981). The presence of multiple steady states in an isothermal CSTR has been observed experimentally for homogeneous polymerization of MMA [Schmidt and Ray (1981), Carratt et al. (1984)] and styrene [Gerrens et al. (1971), Chen et al. (1980a, 1980b, 1982)] and copolymerization of styrene-acrylonitile (SAN) [Balaraman et al. (1982)].

Recently, Henderson (1987) and Herderson and Cornejo (1989) reported and analysis of continuous polymerization reactors where the viscosity of reacting fluid increases by many orders of magnitude and the inside film heat transfer coefficient decreases significantly as monomer conversion increases. For styrene thermal polymerization reactors equipped with various cooling devices, they showed the effect of viscosity dependent heat transfer coefficient on the steady state behavior. They showed that the reactor with a turbine impeller may exceed its design limit at some operating conditions and may exhibit thermal runaway due to poor mixing and heat removal. Shastry and Fan's work (1973) is the unique report on the dynamic behavior in two CSTR's with a recycle. They analyzed the stability of each reactor for homo-

and copolymerization processes using Liapunov's direct method.

The first systematic analysis of the dynamic behavior of continuous polymerization reactors was carried out by Jasinghani and Ray (1977). They observed S-shaped steady state multiplicity and the regions that give rise to unstable limit cycles with Damköhler number as a bifurcation parameter for styrene and MMA bulk polymerizations in a CSTR. They identified the regions of three different types of dynamic behavior in operating parameter space using Uppal *et al.*'s method (§2.2.1.3). For solution homo- and copolymerization of MMA and vinyl acetate (VA) in a CSTR, the dynamic behavior of the reactor was studied by Hamer *et al.* (1984) using Hassard's program (1979). They showed that up to six different dynamic behavior can be observed in the reactor. Schmidt *et al.* (1984) observed the presence of isola with the reactor residence time as a bifurcation parameter through model simulations and experiments for MMA solution polymerization in a nonisothermal CSTR. Their model simulations also showed that up to five steady states are observable at some operating conditions and a small variation in some operating conditions can have an enormous effect on the steady state behavior of the reactor. Such parametric sensitivity has also been observed by many workers [Volter *et al.* (1966), Brooks (1979, 1981), Thiele (1984, 1986)]. For MMA solution polymerization with high solvent volume fraction and excess feed of initiators in a CSTR, Choi (1986) provided analytical criteria to classify multiplicity patterns with a reduced reactor model, using the singularity theory.

25

He identified five distinct parameter regions of steady states with the reactor residence time as a bifurcation parameter. He also shows the effect of reactor dynamics on the polymer properties by calculating the number average chain length (NACL) from the first subsystem variables. Adebekun *et al.* (1988, 1989) further studied the influence of reactor dynamics on NACL and MWD. They also observed the existence of multiple isolas and unusual multiplicity features such as the isola-tuck, which arises from a shift in the isola origin leading to a region of five steady states, through extensive model simulation of MMA solution polymerization in a CSTR.

Teymour and Ray (1989) observed experimentally the presence of limit cycles in a CSTR for VA solution polymerization. Using AUTO, they analyzed various bifurcation behavior of periodic solutions with the first subsystem model which was derived from the volume balance of each component. Validation in fluid density was carried out in their modeling. It should be noted that all other previous reactor models were developed from mass or mole balance of each component. Teymour and Ray (1988) also investigated higher order bifurcation of periodic solutions and chaos in a rescaled parameter space. One of the common features of these dynamic studies is that only single monofunctional initiators such as azobisisobutyronitrile (AIBN) or benzoyl peroxide (BPO) have been considered.

Finally, it should be mentioned that CSTR's for other polymerization systems such as free radical emulsion polymerization and olefin polymerization

with transition metal catalysts may also exhibits similar nonlinear dynamic behavior. For emulsion polymerization in a CSTR, the steady state multiplicity and oscillatory phenomena have been analyzed by Kirillov and Ray (1978), Rawlings and Ray (1987a, 1987b), Schork and Ray (1987), Penlidis *et al.* (1989) and Lu and Brooks (1989). For continuous olefin polymerization reactors, Choi and Ray (1985, 1988) observed the presence of multiple steady states.

2.3. Modeling of Two CSTR's in series

2.3.1. Polymerization Kinetics

The binary mixture of monofunctional initiators considered in this study consists of a slow initiator (initiator A, *tert*-butyl perbenzoate) and a fast initiator (initiator B, benzoyl peroxide). The thermal decomposition rate of the former is much lower than the latter at a given temperature. For example, the half-life of tert-butyl perbenzoate at 100 °C is 12.9 hr and that of benzoyl peroxide is 1 hr. The primary radicals generated by the decomposition of labile groups in both initiators are assumed to be indistinguishable in their activities for styrene polymerization. In the kinetic modeling to follow, the chain transfer to solvent (ethyl benzene), the primary radical termination and induced decomposition reactions of these initiators are assumed negligible. At high reaction temperatures (e.g., above 110 °C), thermal initiation becomes important [Pryor and Coco (1970), Hui and Hamielec (1972)] and thus is included in the kinetic scheme. If the chain termination is assumed to occur exclusively by the combination mechanism in styrene polymerization, the polymerization will proceed as follows:

Initiation by initiators:

$$I_A \xrightarrow{\;k_{d_A}\;} 2R \qquad\qquad (2.1a)$$

28

with transition metal catalysts may also exhibits similar nonlinear dynamic behavior. For emulsion polymerization in a CSTR, the steady state multiplicity and oscillatory phenomena have been analyzed by Kirillov and Ray (1978), Rawlings and Ray (1987a, 1987b), Schork and Ray (1987), Penlidis *et al.* (1989) and Lu and Brooks (1989). For continuous olefin polymerization reactors, Choi and Ray (1985, 1988) observed the presence of multiple steady states.

$$I_B \xrightarrow{k_{d_B}} 2R \qquad\qquad (2.1b)$$

$$R + M \xrightarrow{k_i} P_1 \qquad\qquad (2.1c)$$

Thermal initiation:

$$3M \xrightarrow{k_{d_M}} 2P_1 \qquad\qquad (2.2)$$

Propagation:

$$P_n + M \xrightarrow{k_p} P_{n+1} \qquad (n \geq 1) \qquad\qquad (2.3)$$

Chain transfer to monomer:

$$P_n + M \xrightarrow{k_{fm}} M_n + P_1 \qquad (n \geq 1) \qquad\qquad (2.4)$$
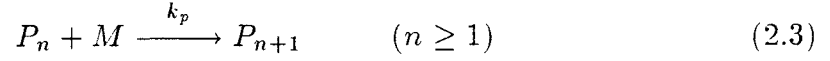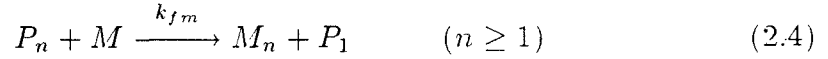
Termination (combination only):

$$P_n + P_m \xrightarrow{k_t} M_{n+m} \qquad (n. m \geq 1) \qquad\qquad (2.5)$$
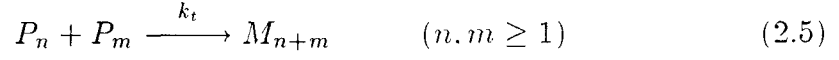
where R is the primary radical, M the monomer, P_n the live polymer with n-repeating units, and M_n the dead polymer with n-repeating units. I_A and I_B are the initiators A and B having different thermal stabilities.

With the kinetic scheme described above, the rate expressions for styrene polymerization with mixed initiators can be expressed as follows:

$$\frac{dI_A}{dt'} = -k_{d_A} I_A \qquad\qquad (2.6)$$

$$\frac{dI_B}{dt'} = -k_{d_B} I_A \qquad\qquad (2.7)$$

$$\frac{dR}{dt'} = 2(f_A k_{d_A} I_A + f_B k_{d_B} I_B) - k_i RM \qquad\qquad (2.8)$$

$$\frac{dP_1}{dt'} = 2k_{d_M} M^3 + k_i RM - k_p MP_1 + k_{fm}M(P - P_1) - k_t PP_1 \qquad (2.9)$$

$$\frac{dP_n}{dt'} = k_p M(P_{n-1} - P_n) - k_{fm} M P_n - k_t P P_n \qquad (n \geq 2) \qquad (2.10)$$

$$\frac{dM}{dt'} = -k_p M P \qquad (2.11)$$

$$\frac{dM_n}{dt'} = k_{fm} M P_n + \frac{1}{2} k_t \sum_{m=1}^{n-1} P_{n-m} P_m \qquad (n \geq 2) \qquad (2.12)$$

where P denotes the total concentration of live polymers.

The key polymer properties of interest are the number average chain length $(\overline{X}_n)$ and the weight average chain length $(\overline{X}_w)$, defined by

$$\overline{X}_n = \frac{\lambda_1^l + \lambda_1^d}{\lambda_0^l + \lambda_0^d} \qquad (2.13)$$

$$\overline{X}_w = \frac{\lambda_2^l + \lambda_2^d}{\lambda_1^l + \lambda_1^d} \qquad (2.14)$$

where λ_k^l and λ_k^d represent the kth moments of live and dead polymer chains, respectively. The moment equations of live and dead polymers can be derived from the above rate expressions.

Live polymers:

$$\lambda_0^l = P \qquad (2.15)$$

$$\lambda_1^l = \frac{P}{1 - \hat{\alpha}} \qquad (2.16)$$

$$\lambda_2^l = \frac{(1 + \hat{\alpha})}{(1 - \hat{\alpha})^2} P \qquad (2.17)$$

Dead polymers:

$$\frac{d\lambda_0^d}{dt'} = P[\hat{\alpha} k_{fm} M + \frac{1}{2} k_t P] \qquad (2.18)$$

$$\frac{d\lambda_1^d}{dt'} = \frac{P}{1-\hat{\alpha}}[\hat{\alpha}(2-\hat{\alpha})k_{fm}M + k_tP] \qquad (2.19)$$

$$\frac{d\lambda_2^d}{dt'} = \frac{P}{(1-\hat{\alpha})^2}[(\hat{\alpha}^3 - 3\hat{\alpha}^2 + 4\hat{\alpha})k_{fm}M + (\hat{\alpha}+2)k_tP] \qquad (2.20)$$

where

$$\hat{\alpha} = \frac{k_pM}{k_{fm}M + k_pM + k_tP}.$$

The three leading moments of live polymers are derived by applying the quasi steady state approximation (QSSA) to active radical species. The polydispersity index $(\overline{PD})$ is a measure of molecular weight distribution broadening and defined by

$$\overline{PD} = \frac{\overline{X}_w}{\overline{X}_n} \qquad (2.21)$$

Although the gel effect in styrene polymerization is not as strong as in other vinyl polymerization such as MMA polymerization, it should be considered in describing the polymerization kinetics at high conversion or low solvent volume fraction. In this study, the empirical gel effect correlation suggested by Hui and Hamielec (1972) for bulk styrene polymerization is used and modified for solution polymerization according to Hamer et $al.$ (1981):

$$g_t(X_1, T) \equiv \frac{k_t}{k_t^*} = \exp[-2(Ax + Bx^2 + Cx^3)] \qquad (2.22a)$$

where

$$A = 2.57 - 5.05 \times 10^{-3}T$$

$$B = 9.56 - 1.76 \times 10^{-2} T \qquad (2.22b)$$

$$C = -3.03 + 7.85 \times 10^{-3} T$$

and

$$x = X_1(1 - f_s). \qquad (2.22c)$$

X_1 is the fractional monomer conversion and x the effective monomer conversion in the presence of solvent with solvent volume fraction of f_s. Here, k_t^* denotes the termination rate constant at zero monomer conversion. Figure 2.1 illustrates the variation in chain termination rate constants predicted by eq. (2.22) for different temperatures and solvent fractions, respectively. The incorporation of the gel effect correlation into the model improves the model accuracy and increases the model complexity as well.

2.3.2. Reactor Model

For free radical polymerization of styrene with mixed initiators in a cascade of two CSTR's of constant volume V_1 and V_2 (Figure 2.2), mass and energy balance equations take the following form:

For the first reactor:

$$V_1 \frac{dM_1}{dt'} = q(M_f - M_1) - V_1 k_p(T_1) M_1 P_1 \qquad (2.23)$$

32
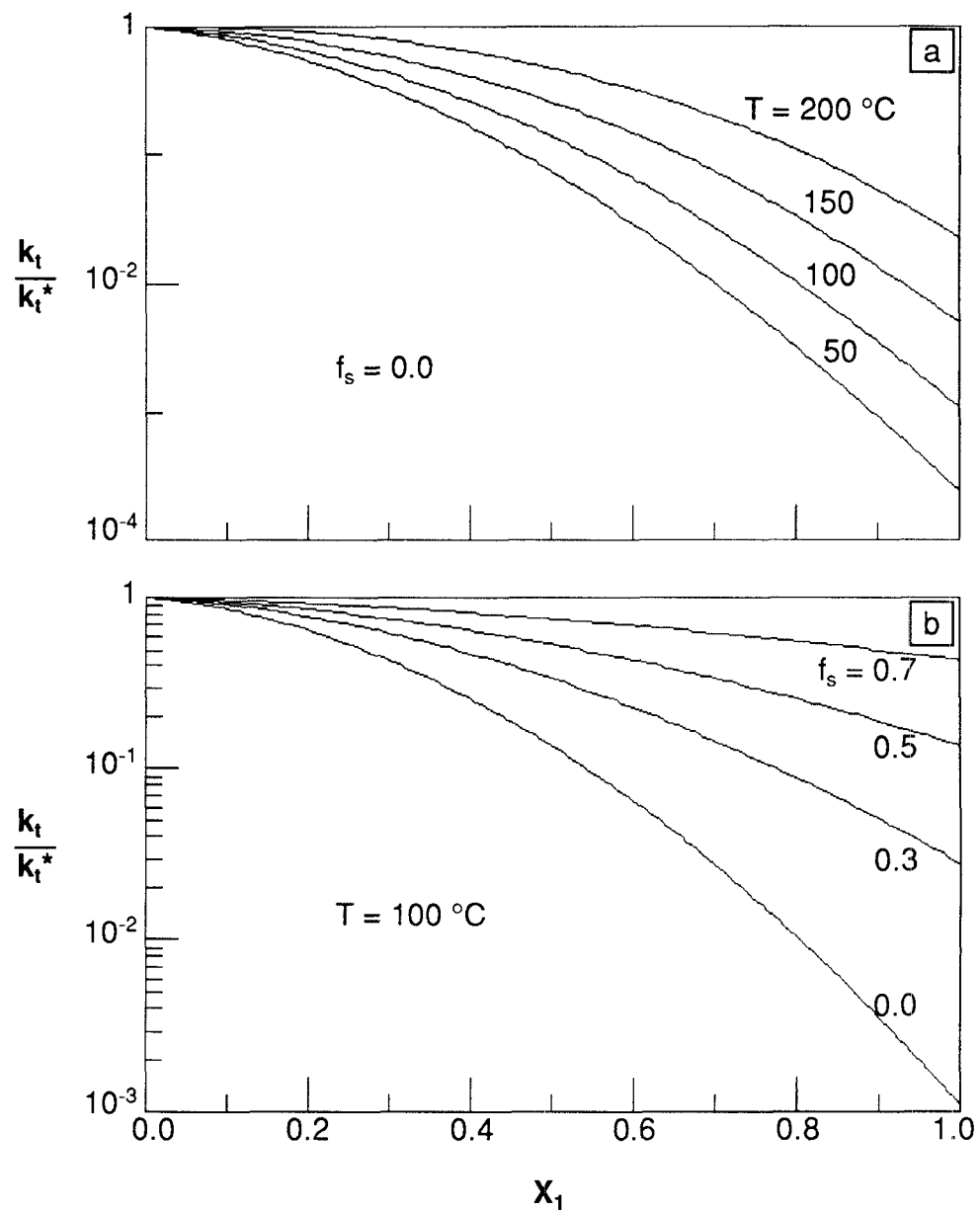
Figure 2.1   Gel effect correlations for styrene polymerization.
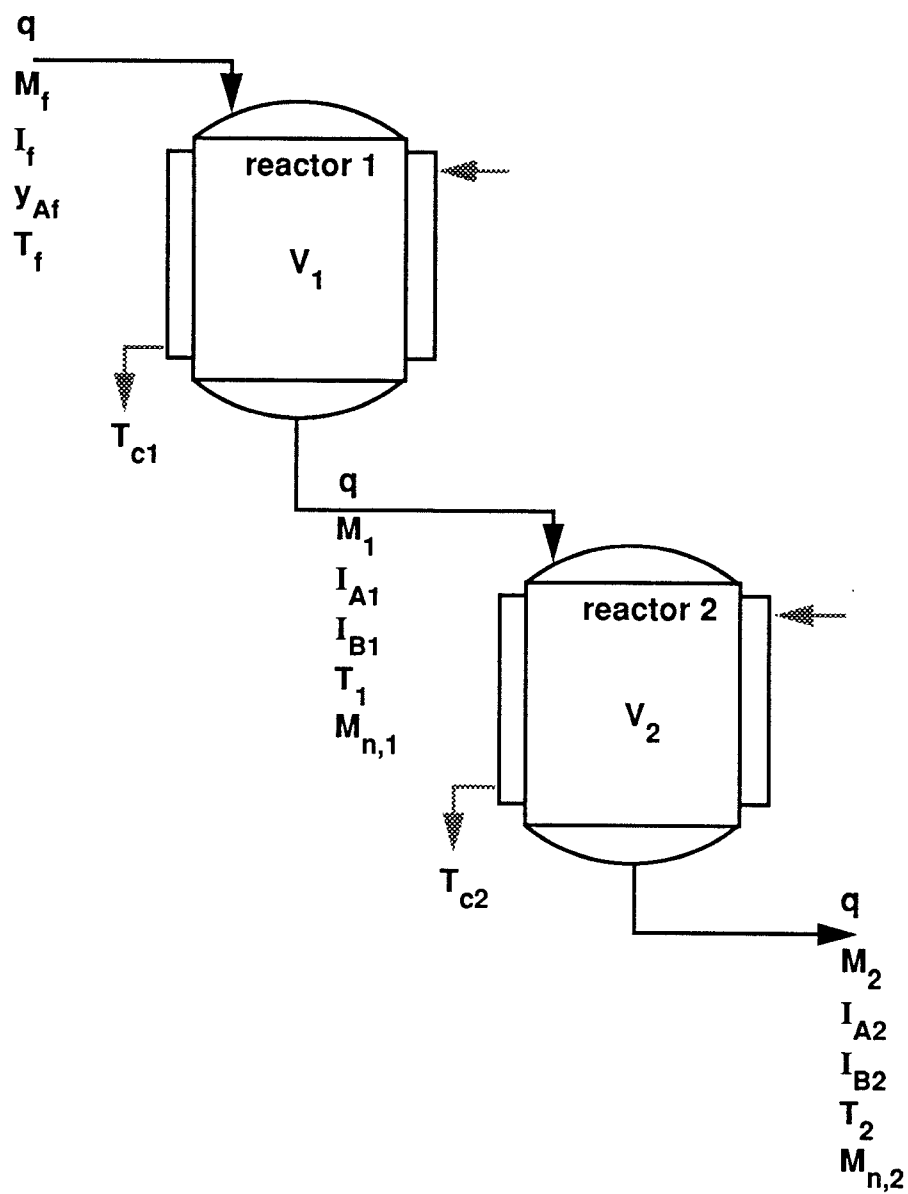
Figure 2.2   Schematic diagram of continuous styrene polymerization reactors with mixed initiators.

$$V_1 \frac{dI_{A1}}{dt'} = q(y_{Af}I_f - I_{A1}) - V_1 k_{d_A}(T_1)I_{A1} \qquad (2.24)$$

$$V_1 \frac{dI_{B1}}{dt'} = q\{(1 - y_{Af})I_f - I_{B1}\} - V_1 k_{d_B}(T_1)I_{B1} \qquad (2.25)$$

$$\rho C_p V_1 \frac{dT_1}{dt'} = \rho C_p q(T_f - T_1) + V_1(-\Delta H)k_p(T_1)M_1 P_1$$

$$- h_{c1} A_{c1}(T_1 - T_{c1}) \qquad (2.26)$$

For the second reactor:

$$V_2 \frac{dM_2}{dt'} = q(M_1 - M_2) - V_2 k_p(T_2)M_2 P_2 \qquad (2.27)$$

$$V_2 \frac{dI_{A2}}{dt'} = q(I_{A1} - I_{A2}) - V_2 k_{d_A}(T_2)I_{A2} \qquad (2.28)$$

$$V_2 \frac{dI_{B2}}{dt'} = q(I_{B1} - I_{B2}) - V_2 k_{d_B}(T_2)I_{B2} \qquad (2.29)$$

$$\rho C_p V_2 \frac{dT_2}{dt'} = \rho C_p q(T_1 - T_2) + V_2(-\Delta H)k_p(T_2)M_2 P_2$$

$$- h_{c2} A_{c2}(T_2 - T_{c2}) \qquad (2.30)$$

where q represents the volumetric flow rate of feed and product streams. The subscript f denotes the feed condition. M_i is the monomer concentration in the ith reactor. I_{Ai} and I_{Bi} the concentrations of initiator A and B, and y_{Af} is the mole fraction of initiator A in the initiator mixture. (*i.e.*, $y_{Af} \equiv I_{Af}/I_f$). T_i is the reactor temperature, h_{ci} the heat transfer coefficient, A_{ci} the effective heat transfer area and T_{ci} the coolant temperature in the ith reactor. Physical properties of the polymerizing mixture (e.g., ρ, C_p, $(-\Delta H)$) are assumed constant.

By applying the quasi-steady state approximation to live polymeric rad-

icals in each reactor, the total concentration of growing polymers in the ith reactor (P_i) can be derived as follows:

$$P_i = \left[\frac{2}{k_t^*(T_i)g_t(X_{1,i}, T_i)} (f_A k_{d_A}(T_i)I_{Ai} + f_B k_{d_B}(T_i)I_{Bi} + k_{d_M}(T_i)M_i^3) \right]^{\frac{1}{2}}$$

(2.31)

where f_A and f_B represent the efficiencies of the initiators A and B, respectively. Note that perfect backmixing has been assumed in our reactor modeling. As mentioned earlier, the use of specially designed impellers such as anchor and helical agitators enables one to achieve a uniform mixing, leading to high monomer conversion (80~85 %) even in a highly viscous polymerizing medium.

The moment equations for live and dead polymers, which comprise the second subsystem, are given in **Appendix A**. By assuming that the chain life time of each live polymer is much shorter than the mean residence time of each reactor, the QSSA is applied in deriving the three leading moments of live polymers. Since the first subsystem is separated from the second subsystem, the reactor dynamics can be determined with the first subsystem model only.

2.3.3. Dimensionless Reactor Model

The reactor modeling equations (2.23)~(2.31) can be reduced to dimensionless form by using the following dimensionless variables and parameters:

$$X_{1,i} = \frac{M_f - M_i}{M_f}, \qquad X_{2,i} = \frac{y_{Af} I_f - I_{Ai}}{y_{Af} I_f},$$

$$X_{3,i} = \frac{(1 - y_{Af}) I_f - I_{Bi}}{(1 - y_{Af}) I_f}, \qquad X_{4,i} = \frac{T_i - T_f}{T_f},$$

$$\alpha_i = \frac{\alpha_{0,i}}{Z}, \qquad \beta = \frac{(-\Delta H) M_f}{\rho C_p T_f}, \qquad \delta_i = \frac{T_{ci} - T_f}{T_f},$$

$$y_{Af} = \frac{I_{Af}}{I_f}, \qquad \eta = \frac{k_{d_{B0}}}{k_{d_{A0}}}, \qquad \epsilon = \frac{E_{d_B}}{E_{d_A}}, \qquad t = \frac{t'}{\theta},$$

$$g_{t,i} = g_t(X_{1,i}, T_i), \qquad Da_1 = \theta Z, \qquad Da_2 = \nu Da_1, \qquad (2.32)$$

$$\zeta = \frac{k_{d_{A0}}}{Z}, \qquad \gamma = \frac{E_p}{RT_f}, \qquad \gamma_d = \frac{E_{d_A}}{RT_f},$$

$$\gamma_a = \frac{E_{d_M} - E_t}{RT_f}, \qquad \gamma_b = \frac{E_{d_A} - E_t}{RT_f}, \qquad \gamma_c = \frac{E_{d_B} - E_t}{RT_f},$$

$$a = \frac{2 k_{d_{M0}} M_f^3}{k_{t0}^*}, \qquad b = \frac{2 f_A k_{d_{A0}} y_{Af} I_f}{k_{t0}^*},$$

$$c = \frac{2 f_B k_{d_{B0}} (1 - y_{Af}) I_f}{k_{t0}^*}$$

where

$$I_f = I_{Af} + I_{Bf}, \qquad \alpha_{0,i} = \frac{h_{ci} A_{ci}}{\rho C_p V_i},$$

$$\theta = \frac{V_1}{q}, \qquad \nu = \frac{V_2}{V_1},$$

$$Z = k_{p0} \exp(-\gamma)[a \exp(-\gamma_a) + b \exp(-\gamma_b) + c \exp(-\gamma_c)]^{\frac{1}{2}}.$$

Note that $X_{2,i}$ and $X_{3,i}$ represent the fractional conversion of initiators A and B in the ith reactor, respectively. I_f is the total feed concentration of the initiator mixture, and y_{Af} the mole fraction of initiator A in the initiator feed mixture. ν denotes the reactor volume ratio. Using the above dimensionless variables and parameters, the following dimensionless modeling equations for the first and the second reactor are obtained:

Reactor 1:

$$\frac{dX_{1,1}}{dt} = -X_{1,1} + Da_1(1 - X_{1,1})Y_1\exp\left[\frac{\gamma X_{4,1}}{1 + X_{4,1}}\right] \qquad (2.33)$$

$$\frac{dX_{2,1}}{dt} = -X_{2,1} + Da_1\zeta(1 - X_{2,1})\exp\left[-\frac{\gamma_d}{1 + X_{4,1}}\right] \qquad (2.34)$$

$$\frac{dX_{3,1}}{dt} = -X_{3,1} + Da_1\zeta\eta(1 - X_{3,1})\exp\left[-\frac{\epsilon\gamma_d}{1 + X_{4,1}}\right] \qquad (2.35)$$

$$\frac{dX_{4,1}}{dt} = -X_{4,1} + \beta\left(X_{1,1} + \frac{dX_{1,1}}{dt}\right) + \alpha_1 Da_1(X_{4,1} - \delta_1) \qquad (2.36)$$

Reactor 2:

$$\frac{dX_{1,2}}{dt} = X_{1,1} - X_{1,2} + Da_2(1 - X_{1,2})Y_2\exp\left[\frac{\gamma X_{4,2}}{1 + X_{4,2}}\right] \qquad (2.37)$$

$$\frac{dX_{2,2}}{dt} = X_{2,1} - X_{2,2} + Da_2\zeta(1 - X_{2,2})\exp\left[-\frac{\gamma_d}{1 + X_{4,2}}\right] \qquad (2.38)$$

$$\frac{dX_{3,2}}{dt} = X_{3,1} - X_{3,2} + Da_2\zeta\eta(1 - X_{3,2})\exp\left[-\frac{\epsilon\gamma_d}{1 + X_{4,2}}\right] \qquad (2.39)$$

$$\frac{dX_{4,2}}{dt} = X_{4,1} - X_{4,2} + \beta\left(X_{1,2} - X_{1,1} + \frac{dX_{1,2}}{dt}\right)$$

$$+ \alpha_2 Da_2(X_{4,2} - \delta_2). \qquad (2.40)$$

Y_i in eqs (2.33)~(2.40) is the dimensionless total concentration of live polymers in the ith reactor:

$$Y_i = \frac{1}{P_f}\left(\frac{P_{x,i}}{g_{t,i}}\right)^{\frac{1}{2}} \qquad (2.41)$$

where P_f and $P_{x,i}$ represent the total concentrations of live polymers in the feed and in the ith reactor, respectively, and they are given by

$$P_f = [a\exp(-\gamma_a) + b\exp(-\gamma_b) + c\exp(-\gamma_c)]^{\frac{1}{2}} \qquad (2.42a)$$

$$P_{x,i} = a(1 - X_{1,i})^3 \exp\left[-\frac{\gamma_a}{1 + X_{4,i}}\right]$$

$$+ b(1 - X_{2,i})\exp\left[-\frac{\gamma_b}{1 + X_{4,i}}\right]$$

$$+ c(1 - X_{3,i})\exp\left[-\frac{\gamma_c}{1 + X_{4,i}}\right]. \qquad (2.42b)$$

where α_i refers to the dimensionless heat transfer coefficient for the ith reactor, β the dimensionless heat of reaction, and Da_i the dimensionless mean residence time of the ith reactor which can be changed experimentally by varying the reactant flow rate.

2.4. Dynamics of the First Reactor

In studying the dynamics of the two CSTR's for styrene polymerization, one may wish to examine the reactor behavior for various reactor operating conditions such as reactant flow rate, coolant temperature, feed temperature, initiator composition, feed initiator concentration, feed monomer concentration, etc. Due to such a multitude of possible reactor operating parameters to vary, a complete parametric analysis of the reactor system would be quite a formidable task. In what follows, however, the analysis will focus mainly on the effect of initiator feed composition (y_{Af}) on the reactor dynamics. Therefore, the variation of other reactor operating parameters may yield some

reactor behavior which are not observed in the present study.

Since there are no recycle streams from the second reactor to the first reactor, the behavior of the first reactor is independent of the behavior of the second. The numerical values of the kinetic and physical constants and the standard reactor operating conditions used in the numerical simulations are listed in Table 2.1.

2.4.1. Steady State and Bifurcation Behavior

At steady state, the LHS of the modeling eqs (2.33)$\sim$(2.36) vanish and the modeling equations are combined into a steady state manifold, F_1, by rearranging the four steady state modeling equations (2.33$\sim$2.36):

$$F_1(X_{1,1}, \boldsymbol{p}_1) = 0 \qquad (2.43)$$

where $\boldsymbol{p}_1$ is the vector of principal operating and design parameters which influence the behavior of the first reactor and defined as

$$\boldsymbol{p}_1 = \{a, b, c, Da_1(\theta), \alpha_1, \beta_1(f_s), \delta_1, y_{Af}\}. \qquad (2.44)$$

For given values of the system parameters, the steady state solutions are obtained. by solving the nonlinear steady state equations (2.33)$\sim$(2.36). Because of the high degree of nonlinearity and interaction in the modeling equations,

Table 2.1   Kinetic and physical constants and the reactor operating conditions for styrene polymerization

---

For Initiator A [slow initiator]: *tert-butyl perbenzoate*,

k_{d_A}=8.439 × 10^{13}exp(-32,000/RT), sec^{-1} *

f_A=0.637 *

For Initiator B [fast initiator]: *benzoyl peroxide*,

k_{d_B}=1.200 × 10^{13}exp(-28,690/RT), sec^{-1} †

f_B=0.6 †

k_{d_M}=2.190 × 10^{5}exp(-27440/RT), (1/mol)^2/sec ‡

k_p=1.051 × 10^{7}exp(-7,060/RT), 1/mol.sec †

k_t^*=1.260 × 10^{9}exp(-1,680/RT), 1/mol.sec †

k_{fm}=2.463 × 10^{5}exp(-10,280/RT), 1/mol.sec †

$(-\Delta H_r)$=16.24 kcal/mol †

ρC_p=0.43 kcal/l°K †

$\alpha_{01} = \alpha_{02} = 2.146 \times 10^{-3}$ sec^{-1},

T_f=343 °K, f_s=0.1, I_f=0.025 mol/l

---

* Product Bulletin Peroxiesters (1983)

† Brandrup and Immergut (1989)

‡ Hui and Hamielec (1972).

some care must be taken in obtaining the steady state solutions to ensure that all feasible solutions are found. In practical situations, one is often interested in knowing whether the steady state multiplicity pattern and stability problems may exist for a given set of system parameters. With parameters δ_1, T_f, I_f and y_{Af} held fixed, the diagrams showing the steady state behavior of the reactor have been constructed by using the computational method suggested in [Balakotaiah and Luss (1984), Golubitsky and Schaeffer (1979)].

The criteria for the hysteresis variety which defines the parameter space at which a continuous change of the parameter causes the appearance or disappearance of hysteresis type multiplicity are:

$$F_1(X_{1,1}, Da_1, \beta_1) = 0 \tag{2.45}$$

$$\frac{\partial F_1}{\partial X_{1,1}}(X_{1,1}, Da_1, \beta_1) = 0 \tag{2.46}$$

$$\frac{\partial^2 F_1}{\partial^2 X_{1,1}}(X_{1,1}, Da_1, \beta_1) = 0 \tag{2.47}$$

where eq (2.45) is obtained from eq (2.43) by fixing α_1 and other system parameters. Here Da_1 (Damköhler number) is chosen as a bifurcation parameter. Across the hysteresis variety, the number of solutions to the steady state equations increases or decreases by two. The isola variety is defined as the parameter space at which the appearance or disappearance of an isolated branch (isola) occurs. The criteria for the isola variety are given by eqs (2.45), (2.46) and:

$$\frac{\partial F_1}{\partial Da_1}(X_{1,1}, Da_1, \beta_1) = 0. \qquad (2.48)$$

For varying α_1 values, eqs (2.45)~(2.47) for the hysteresis variety and eqs (2.45), (2.46) and (2.48) for the isola variety have been solved by using Brown's method which solves nonlinear simultaneous algebraic equations by the modified Newton's method [Brown (1969)]. Figure 2.3 and 2.4 are the diagrams showing the steady state reactor behavior in α_1-f_s plane for different mole fraction values of initiator A (y_{Af}) in the feed initiator mixture. Note that there are four unique regions of steady state behavior separated by the two characteristic curves, Γ_1 and Γ_2 for all cases:

Region I: Unique steady state

Region II: Multiple steady state (**S**-shape curve)

Region III: Isola and unique steady state

Region IV: Isola and multiple steady state (**S**-shape curve).

The region V (mushroom) reported by Choi (1986) for the AIBN initiator system is not observed with the present initiator system. Here, Γ_1 and Γ_2 represent the hysteresis variety and the isola variety, respectively. For all the initiator feed compositions studied (*i.e.*, $y_{Af} = 0.0 \sim 1.0$), isolated branches (isola) [Region III and IV] are observed. Note that the regions III and IV
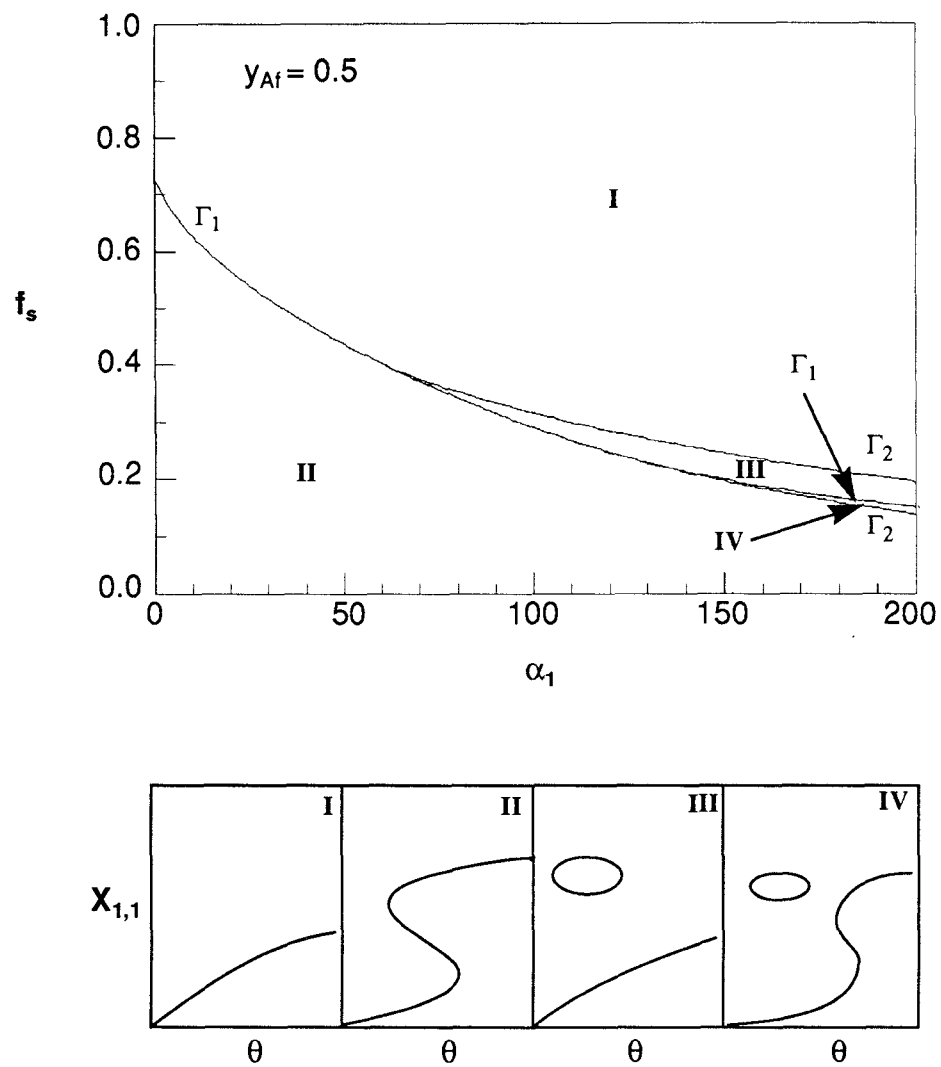
Figure 2.3   Parameter region of each steady state behavior of styrene polymerization in the first CSTR: $I_f = 0.025$ mol/l, $y_{Af} = 0.5$, $T_f = 343$ °K, $T_{c,1} = 363$ °K.
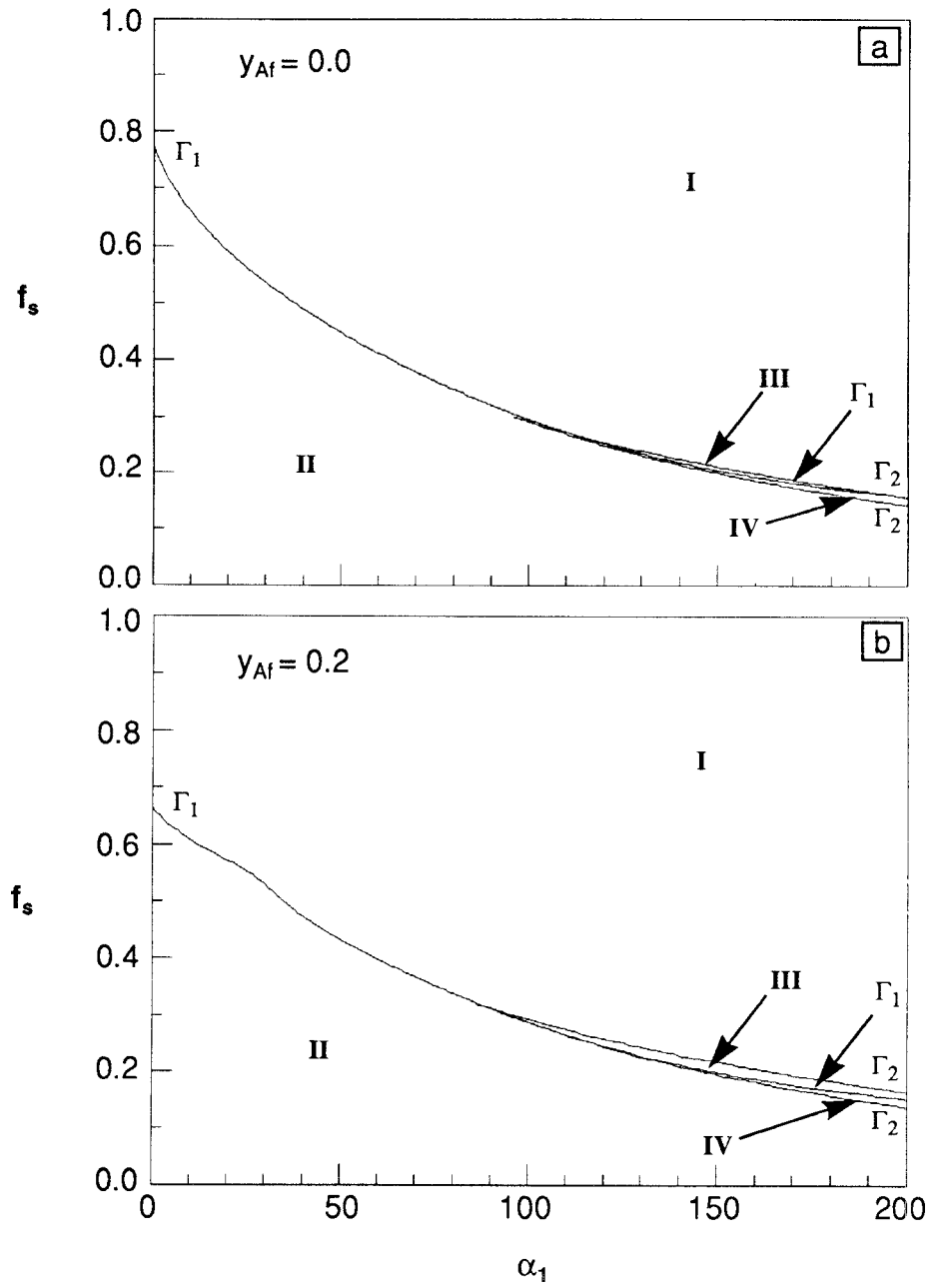
Figure 2.4   Effect of the initiator composition (y_{Af}) on the steady state behavior of styrene polymerization in the first CSTR: I_f= 0.025 mol/l, T_f= 343 °K, $T_{c,1}$= 363 °K.
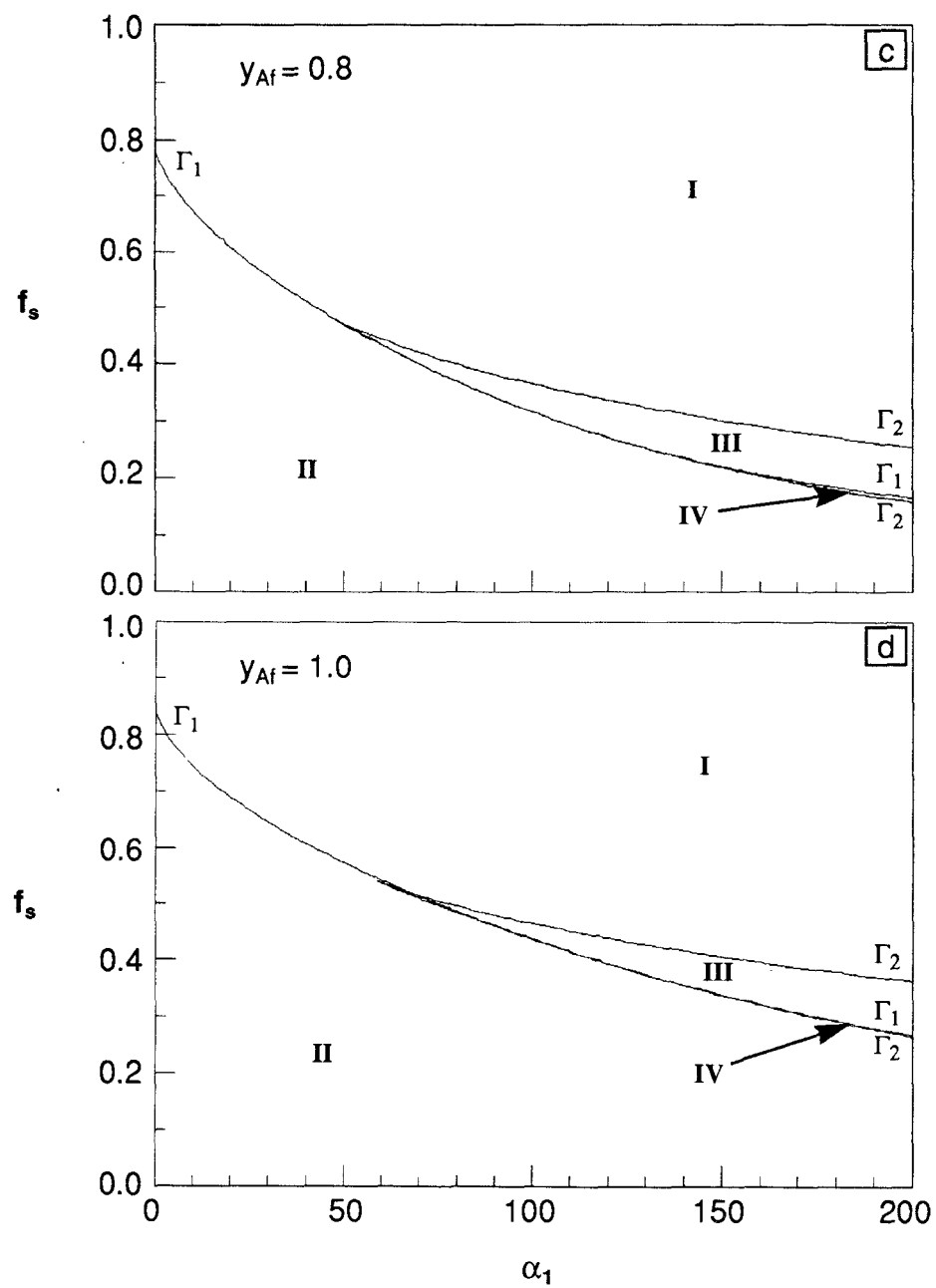
Figure 2.4   (*continued*)

46

become broader as α_1 increases. The existence of isolas has been known for many years in various chemically reacting systems including continuous polymerization reactors [Schmidt *et al.* (1984)]. Since region IV is so small over the whole range of initiator feed composition, it will be practically very difficult or impossible to confirm this tiny region experimentally. For the initiator feed composition below $y_{Af} < 0.2$, region III may also be difficult to observe experimentally (Figure 2.4a and 2.4b). For larger values of y_{Af}, region III becomes little broader (Figure 2.4d). Figure 2.3 and 2.4 also indicate that the multiple steady state behavior is always observable in bulk free radical polymerization (*i.e.*, $f_s = 0.0$). For adiabatic operations (*i.e.*, $\alpha = 0$), only type I and II steady state profiles are observable.

For each initiator feed composition, the steady state profiles of the first reactor state variables (i.e. $X_{1,1}$, $I_{A,1}$, $I_{B,1}$ and T_1), number average degree of polymerization ($\overline{X}_{n,1}$) and the polydispersity ($\overline{PD}_1$) are illustrated in Figures 2.5~2.10. The analysis of steady state and periodic bifurcation branches has been carried out with the numerical package AUTO [Doedel (1981)]. This software package is designed for the semi-interactive determination of such bifurcation branches and their display in graphic form. Starting from a known or calculated steady state value, AUTO can trace the associated steady state branch, determine any steady state or Hopf bifurcation points, and follow the branches emanating from those bifurcation points. On branches of periodic orbits, it can identify period-doubling bifurcation points and follow branches
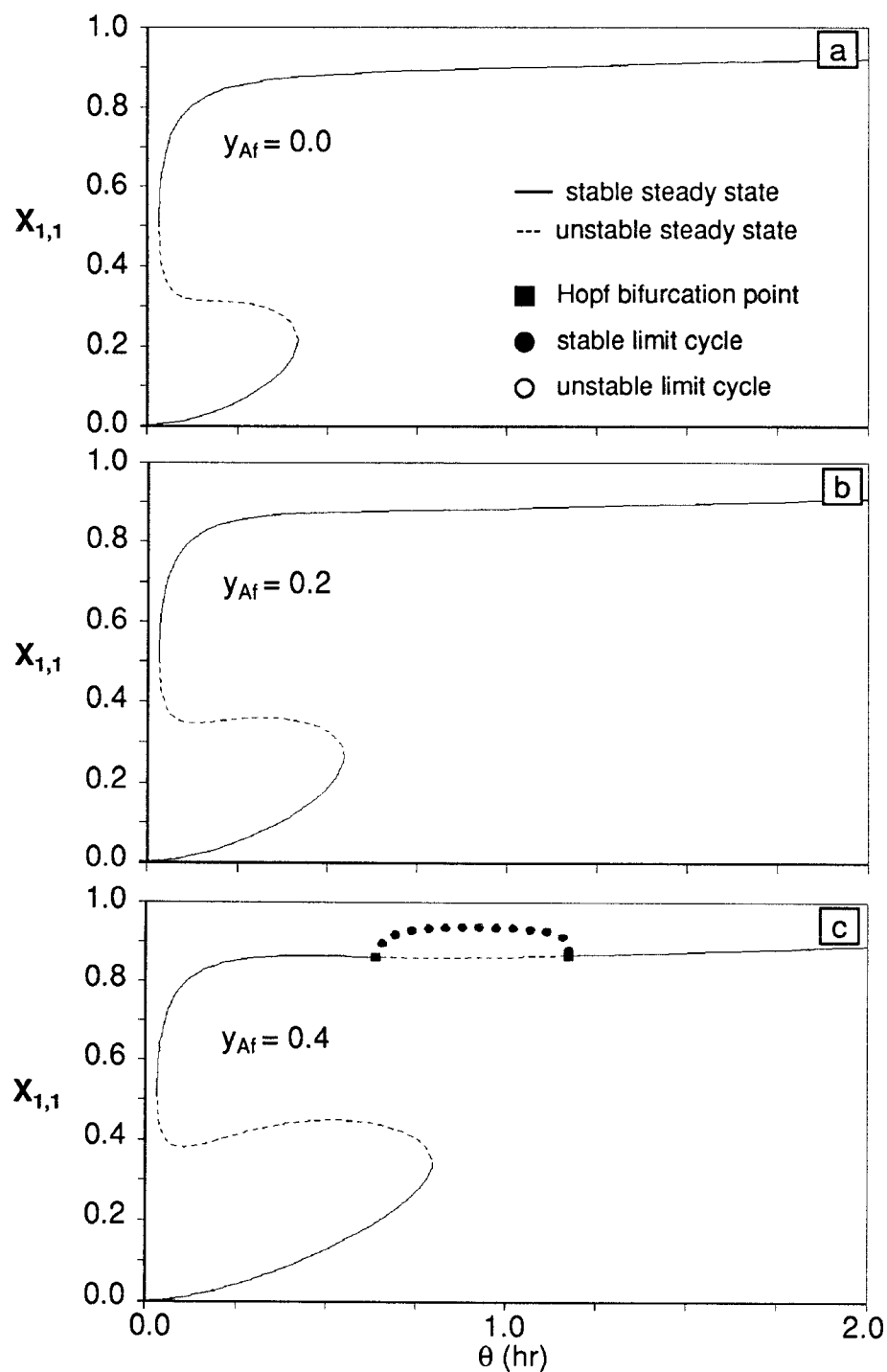
Figure 2.5   Bifurcation diagrams of $X_{1,1}$ with different y_{Af}: $f_s = 0.1$, $I_f =$
0.025 mol/l, $T_f = 343\ ^{\circ}K$, $T_{c,1} = 363\ ^{\circ}K$ (i: period doubling bi-
furcation point, ii: second period doubling bifurcation point,
iii: homoclinic bifurcation point).
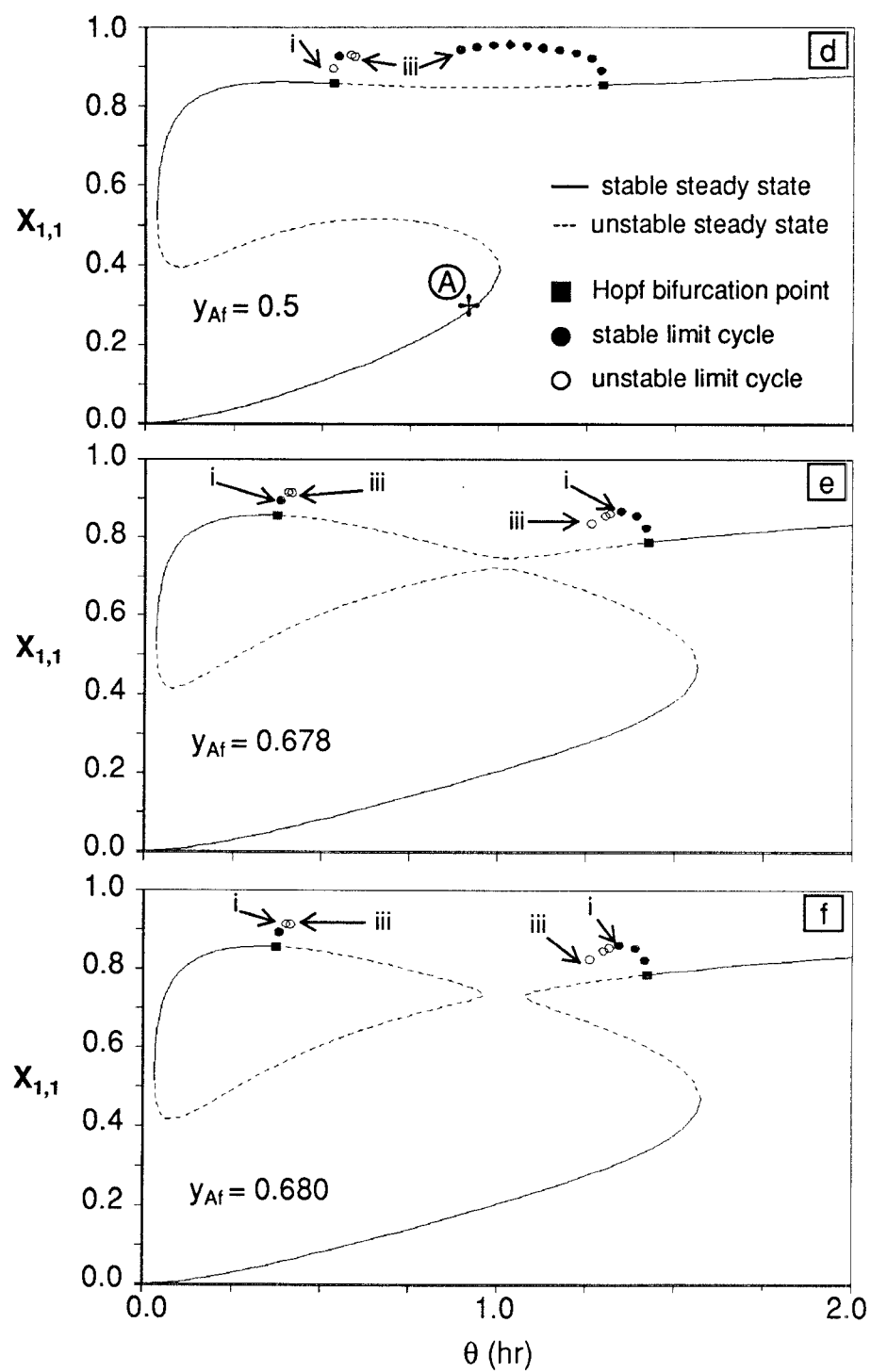
Figure 2.5   (*continued*)
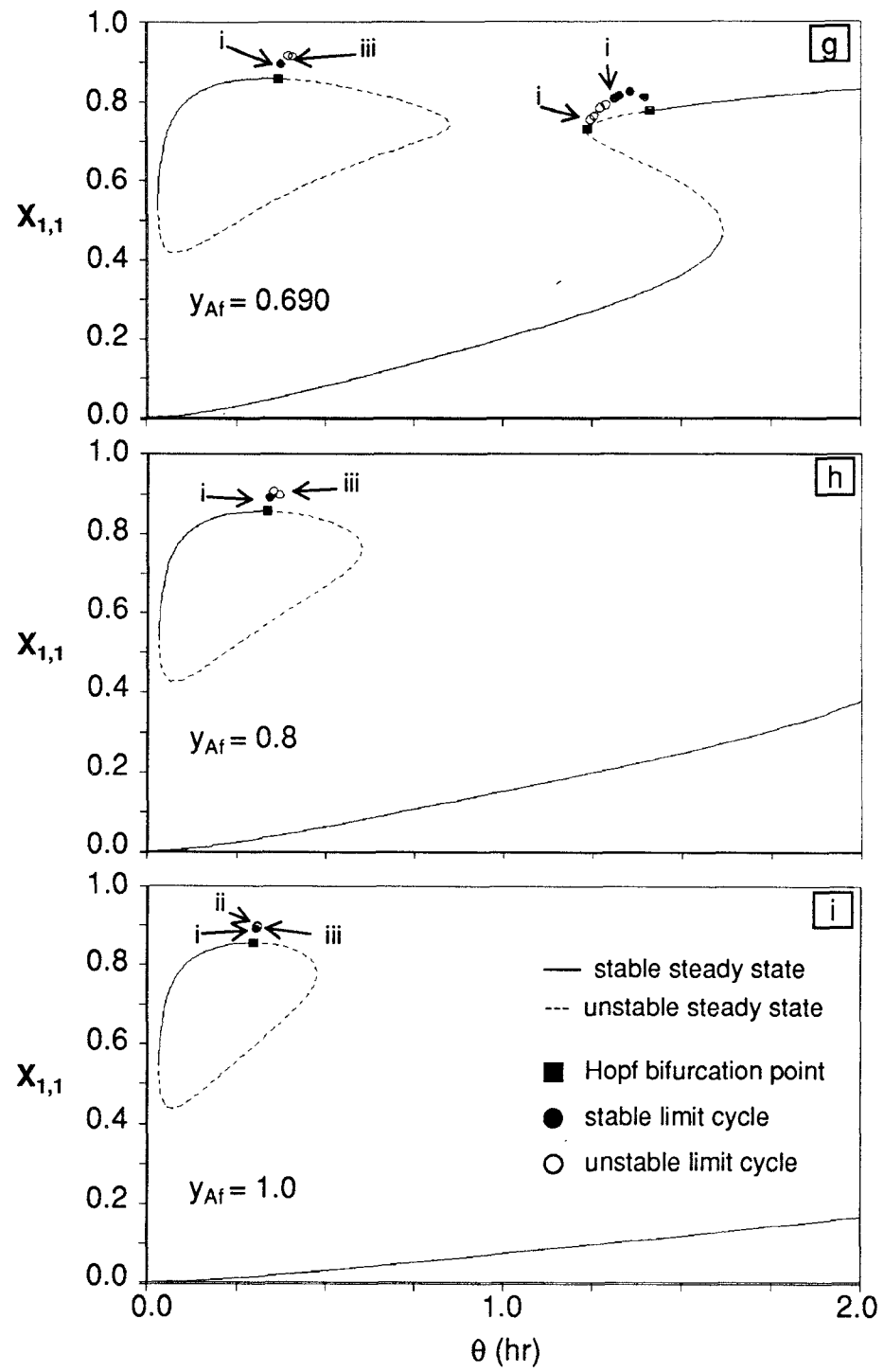
Figure 2.5   (*continued*)
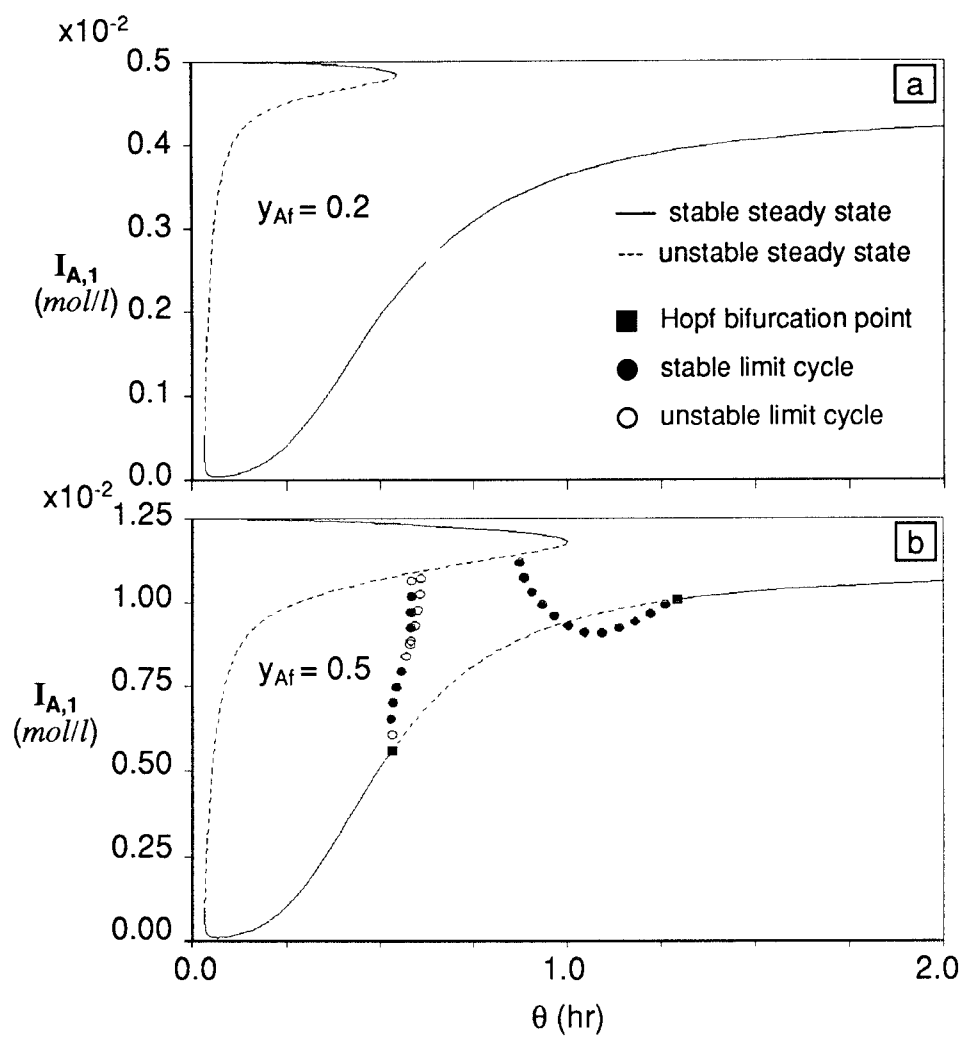
Figure 2.6   Bifurcation diagrams of $I_{A,1}$ with different y_{Af}: $f_s = 0.1$, $I_f = 0.025$ mol/l, $T_f = 343$ °K, $T_{c,1} = 363$ °K.
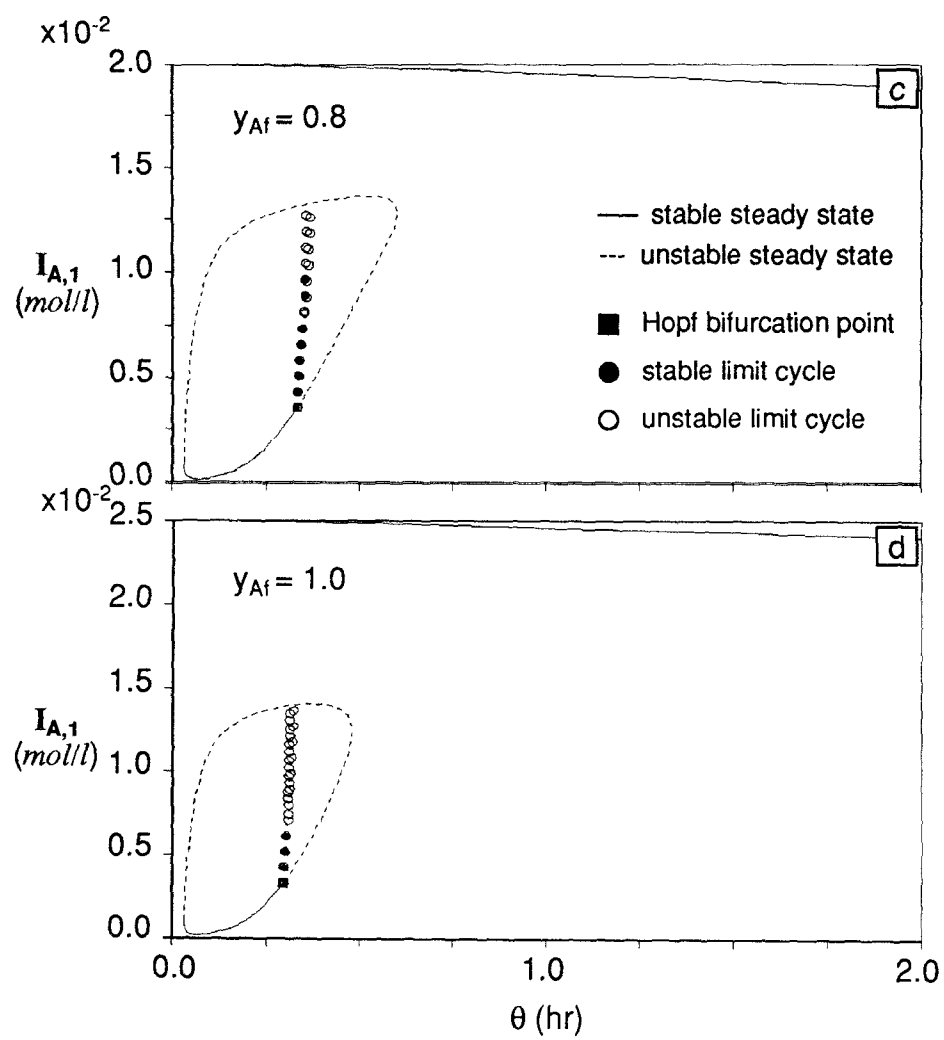
Figure 2.6   (*continued*)
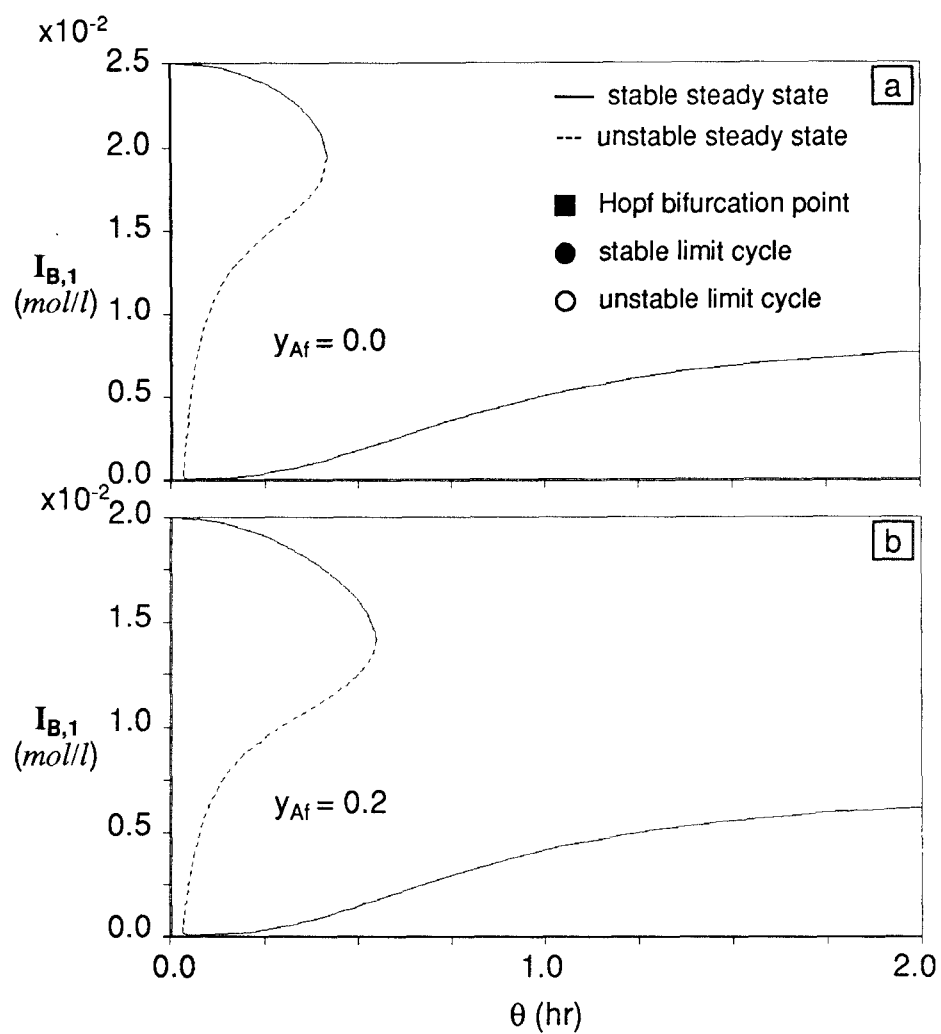
Figure 2.7   Bifurcation diagrams of $I_{B,1}$ with different y_{Af}: $f_s = 0.1$, $I_f = 0.025$ mol/l, $T_f = 343$ °K, $T_{c,1} = 363$ °K.
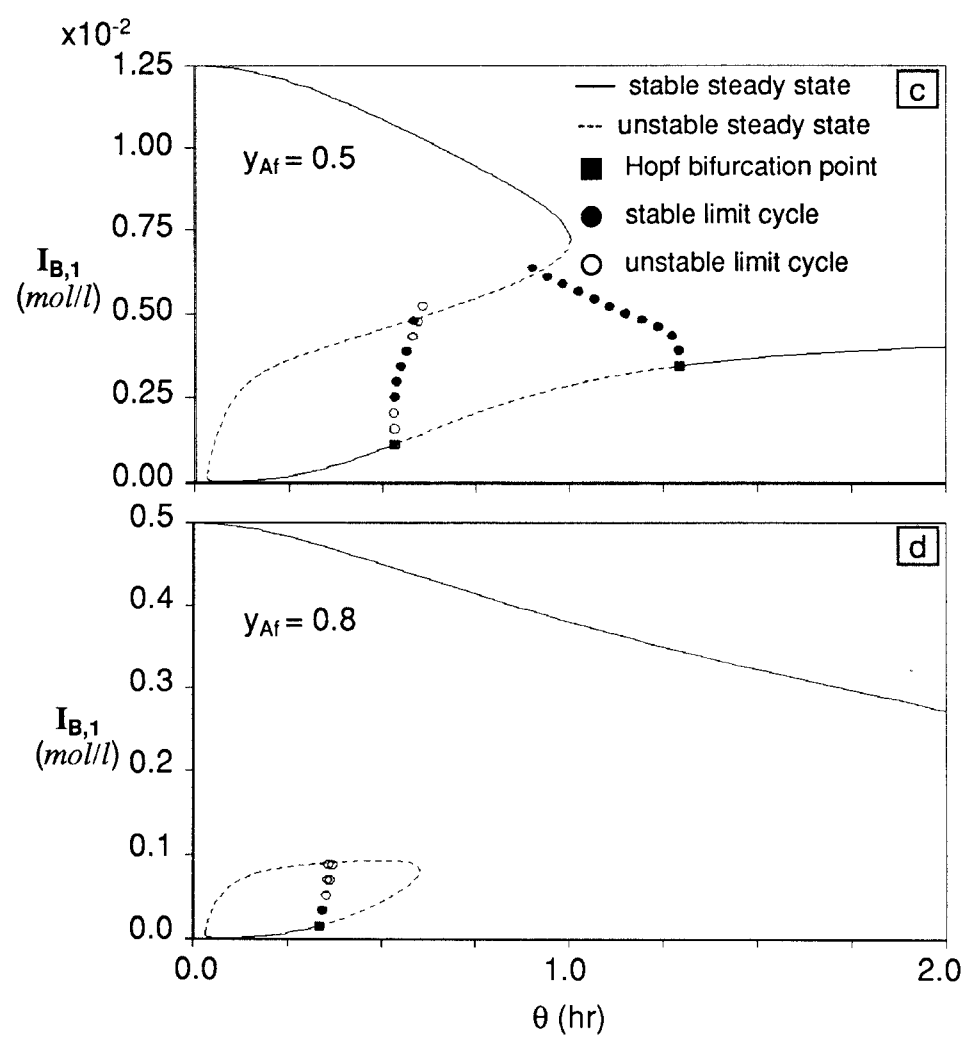
Figure 2.7   (continued)
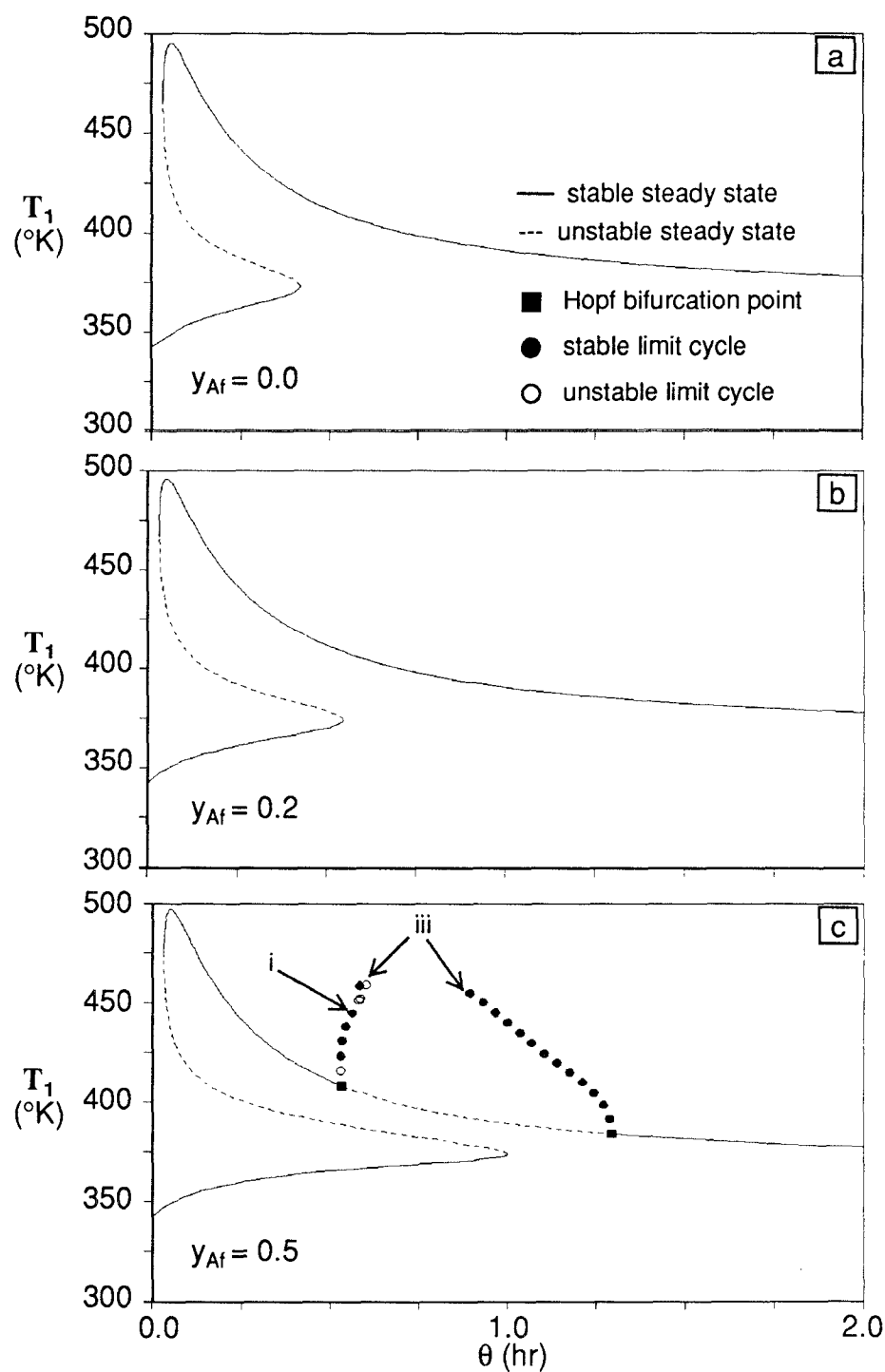
Figure 2.8   Bifurcation diagrams of T_1 with different y_{Af}: $f_s = 0.1$, $I_f =$ 0.025 mol/l, $T_f = 343$ °K, $T_{c,1} = 363$ °K (i: period doubling bifurcation point, ii: second period doubling bifurcation point, iii: homoclinic bifurcation point).
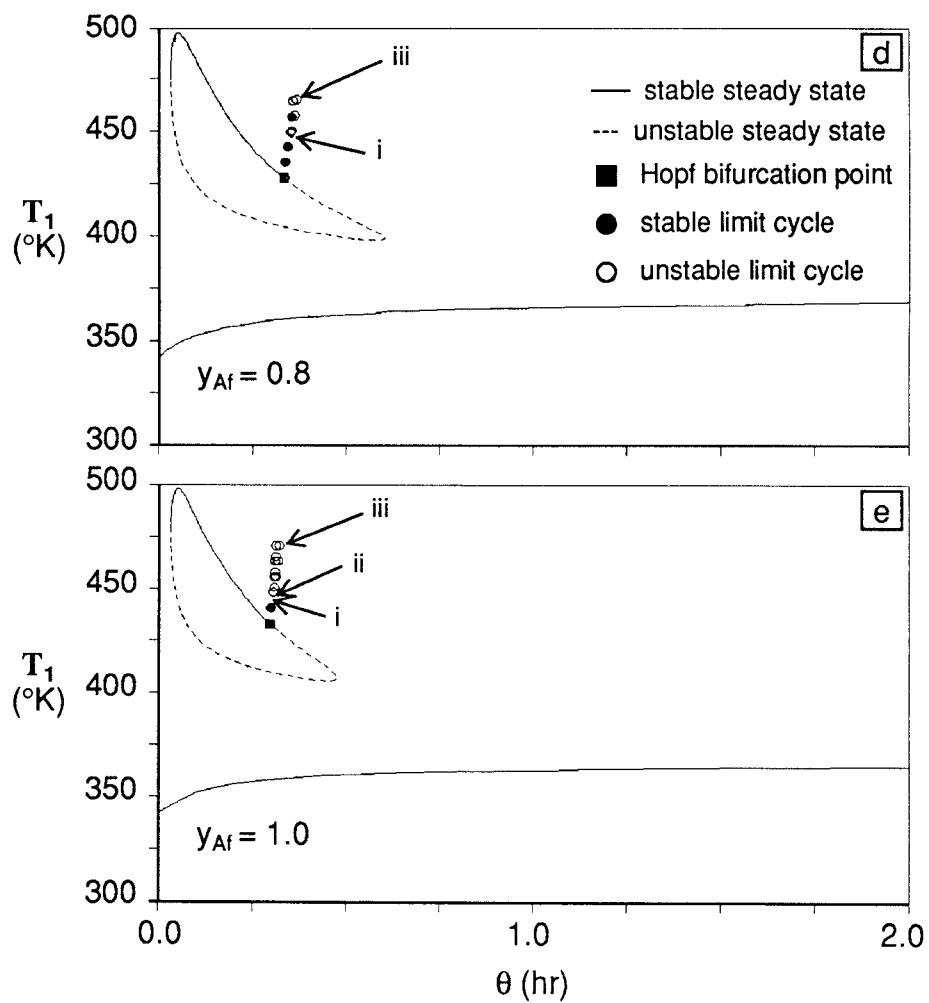
Figure 2.8   (*continued*)
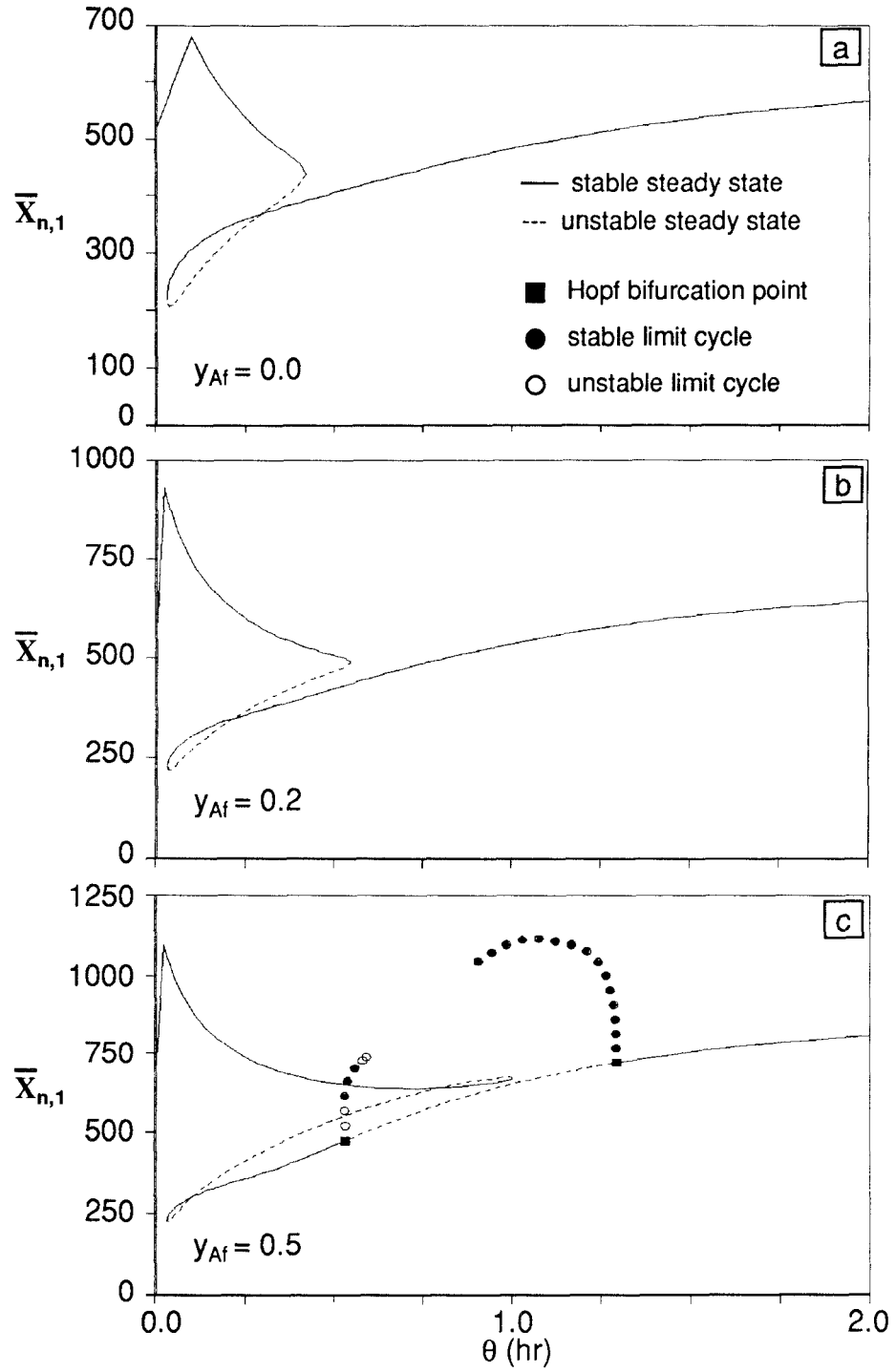
Figure 2.9   Bifurcation diagrams of $\overline{X}_{n,1}$ with different y_{Af}: $f_s=$ 0.1, $I_f=$ 0.025 mol/l, $T_f=$ 343 °K, $T_{c,1}=$ 363 °K.
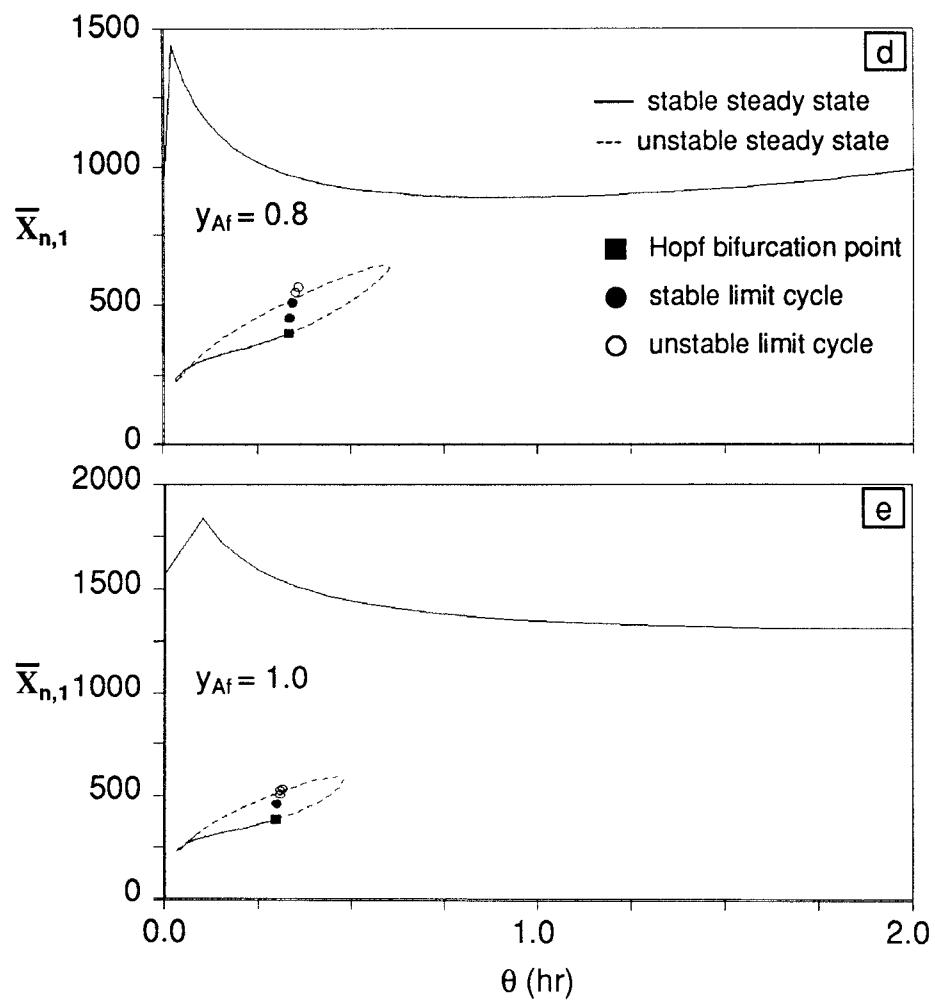
Figure 2.9   (*continued*)
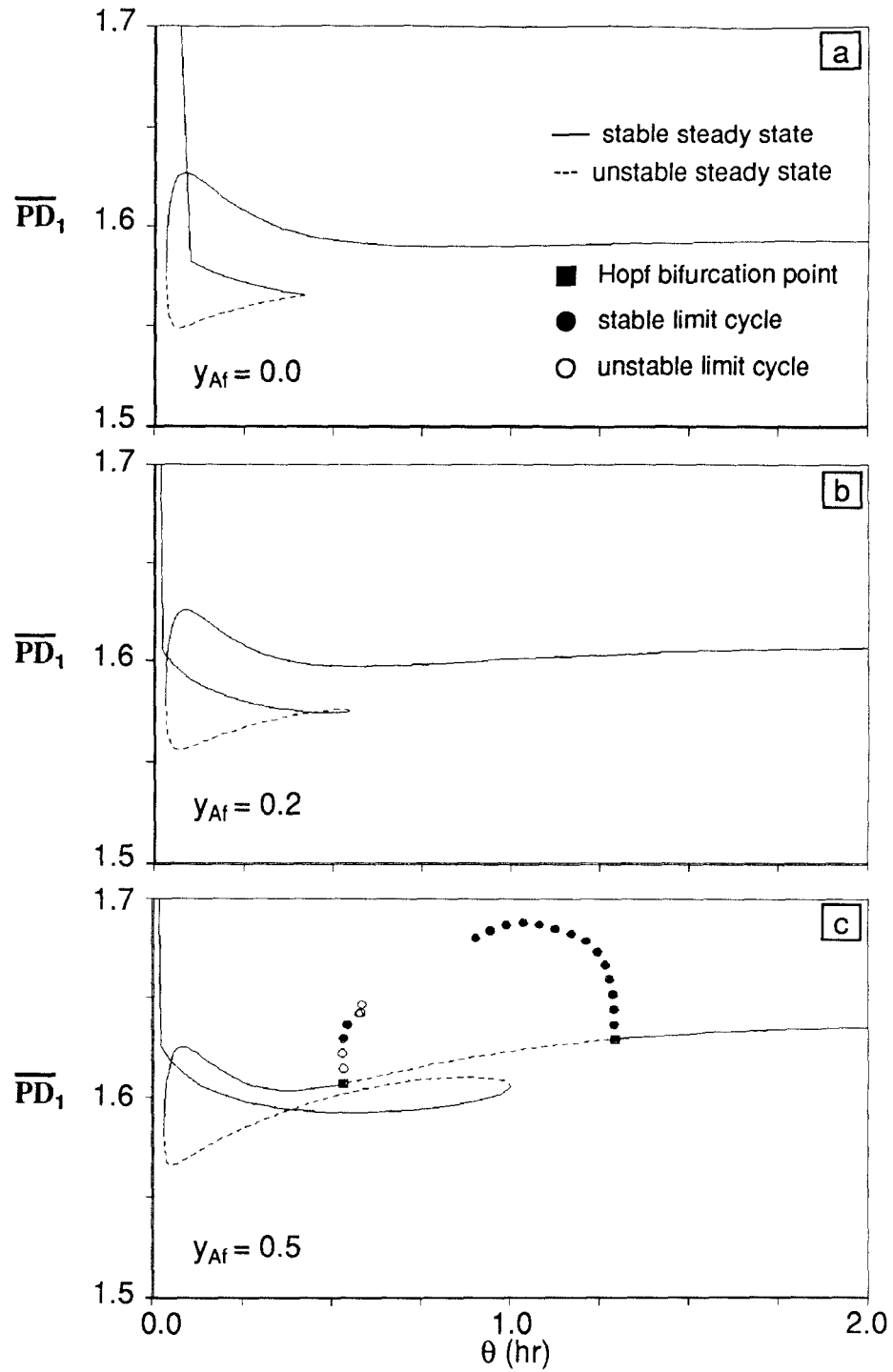
Figure 2.10   Bifurcation diagrams of $\overline{PD}_1$ with different y_{Af}: $f_s = 0.1$, $I_f = 0.025$ mol/l, $T_f = 343$ °K, $T_{c,1} = 363$ °K.
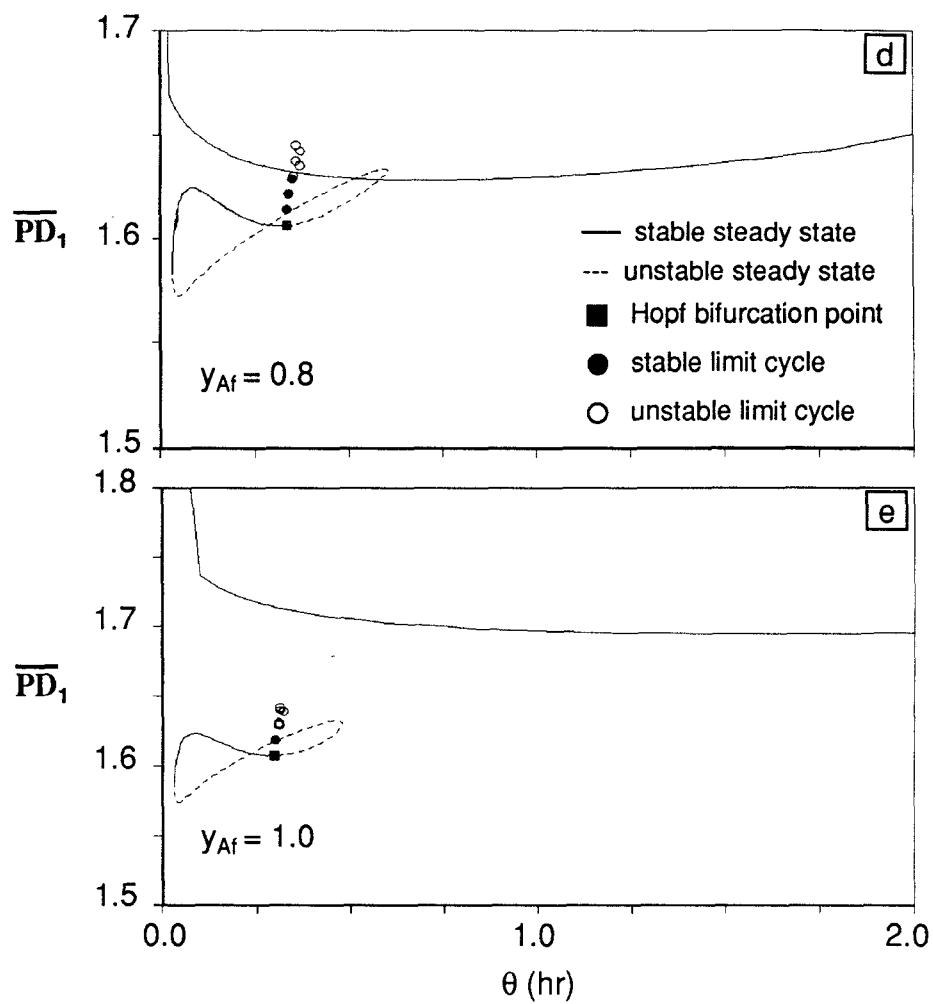
Figure 2.10   (*continued*)

emanating from them. Therefore one can obtain a complete picture of both steady state and periodic bifurcation characteristics of the dynamic systems. Computations are done in a combination of parameter and state space, and thus there are no problems with saddle-node bifurcations (switchbacks).

In Figures 2.5~2.10, steady state branches are exhibited as lines and periodic branches as circles. Solid lines and circles demark asymptotically stable orbits (as determined by a local eigenvalue analysis at steady states and by Floquet exponents at periodic orbits), and dashed lines and open circles demark unstable solutions. For any periodic orbit, the maximum value on that orbit is exhibited. All parameter values in these figures are identical, except y_{Af}.

In Figures 2.5a and 2.5b, there is only one steady state branch, on which there is an exchange of stability at each saddle-node bifurcation. When the feed mixture consists of 20 % A and 80 % B (Figure 2.5b), no noticeable changes from Figure 2.5a in the steady state behavior are observed except some increase in $\overline{X}_{n,1}$ value (Figure 2.9). As the concentration of the *slow initiator* A increases, the reactor behavior changes dramatically. At an intermediate value, a single periodic branch appears. It spans two Hopf bifurcation points (marked by ∎) which spread apart; see Figure 2.5c. At some value of y_{Af}, a homoclinic orbit appears on the branch and the branch separates into two. At $y_{Af} = 0.4$, (Figure 2.5c), there is no indication of period doubling. When period doubling branches first appear, they connect two different points on the

primary periodic branch, and then "go homoclinic" with the primary branch.

At $y_{Af} = 0.5$ (Figure 2.5d), there are also two periodic branches, emanating from Hopf bifurcation points. These branches terminate in homoclinic orbits; that is, the period of the orbits on these branches becomes unbounded. In the limit of the branch, the orbit is asymptotic in both forward and backward time to the unstable stationary point on the middle segment of the steady state branch; see phase plane portraits shown in Figure 2.12, where a "homoclinic limit cycle" is a good approximation to the homoclinic orbit. For this value of y_{Af}, all the orbits on the right periodic branch are stable. The left branch bifurcates almost vertically. It either bifurcates subcritically (to the left) and orbits near the Hopf bifurcation point are unstable, or else bifurcates supercritically, but switches back to the left almost immediately. There is then a switchback to the right, and stability is gained. There is then a period-doubling bifurcation (point (i)). The periodic branch loses its stability, and a second periodic branch bifurcates from it. Orbits on this branch have a period about twice that of those on the first periodic branch (cf., Figures 2.13 and 2.14). This branch also terminates in an unstable homoclinic. There is a second period doubling bifurcation emanating from this secondary branch which is not exhibited, and, depending on the values of y_{Af}, there can be an infinite succession of period doublings — a period doubling cascade — leading to chaos. For values of θ between the two periodic branches, dynamic simulations indicate there are no non-stationary attractors; from any initial

state, the system is attracted to the stable stationary point on the bottom of the steady state branch.

As y_{Af} increases, there are further transitions in the bifurcation branch. An isola is present, with a Hopf bifurcation point, and the right periodic branch has disappeared. The periodic branch emanating from the Hopf branch on the isola terminates in a homoclinic and exhibits period doubling behavior. The transitions are exhibited in Figures 2.5e, 2.5f and 2.5g. The isola appears as a "breaking off" of a portion of the steady state branch. The bifurcation diagrams for values of y_{Af} just below and above the transition point are exhibited in Figures 2.5e and 2.5f, respectively. This breaking off of the isola is similar to that observed by other investigators [Uppal et $al.$ (1976), Choi (1986)], except that the isola breaks off to the left instead of above the main branch, and hence there is no transitional "mushroom". At these values, there is period-doubling behavior also on the right periodic branch. At a slightly larger value of y_{Af} (Figure 2.5g), the right periodic branch "reattaches" to the steady state branch at the saddle-node switchback. As y_{Af} is increased, the two Hopf points come closer together, the period-doubling behavior collapses and disappears, and finally the two Hopf points coalesce and the period branch itself disappears. This occurs for $y_{Af} < 0.7$. Between $y_{Af} = 0.7$ and $y_{Af} = 0.8$ (Figure 2.5h), there is a further transition, in that the steady state branch "straightens out" and loses its saddle-node switchback. Figure 2.5i, with a single slow initiator, is qualitatively the same as Figure 2.5h.

Figures 2.11∼2.14 show phase plane portraits of the bifurcation phenomena such as Hopf bifurcation, homoclinic limit cycle and period doubling limit cycles. These figures represent the reactor transients to the pulse disturbance in y_{Af} (Figure 2.11 and 2.12) or the total initiator feed concentration (Figure 2.13 and 2.14) during the steady state operation of the reactor at each bifurcation point. These diagrams were obtained by solving the reactor modeling equations (2.33)∼(2.36) and the molecular weight moment equations simultaneously. Figure 2.11 exhibits a limit cycle on the left periodic branch of Figure 2.5d. The value of θ is set near the value at the left Hopf point. The orbit is a small amplitude oscillation around the steady state value. In Figure 2.12, an approximation to a homoclinic orbit is exhibited. The value of θ is set at the value of the point on the left periodic branch in Figure 2.5d. The system relaxes to a very long-period orbit. Along the branch of periodic orbits, the period is unbounded, and the limiting orbit is asymptotic in both forward and backward times to an unstable stationary point. The times between the spikes in Figure 2.12a becomes infinite in the limit. The unstable stationary point is approximately at the lower left of the trajectories in Figure 2.12b. The system spends most of its time near that point, making quick excursions through the rest of its orbit.

A period-doubled limit cycle is exhibited in Figure 2.13. The outer and inner segments (Figures 2.13b and 2.13c) are two pieces of the same orbit (the larger and smaller oscillations in Figure 2.13a). In between the inner and
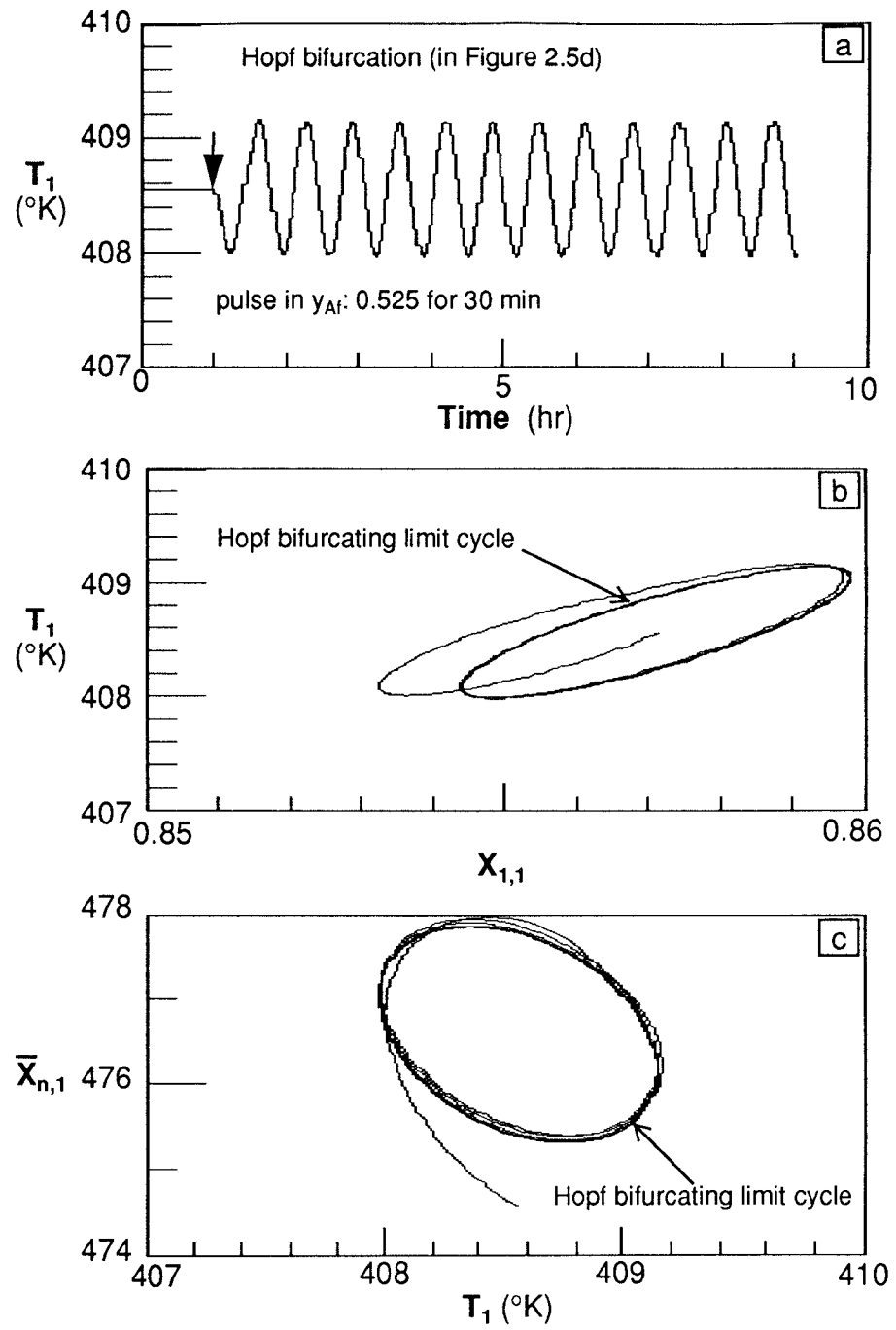
Figure 2.11   Transient response and phase plane portraits of Hopf bifurcation point to pulse change in y_{Af}: $f_s = 0.1$, $I_f = 0.025$ mol/l, $y_{Af} = 0.5$, $T_f = 343$ °K, $T_{c,1} = 363$ °K.
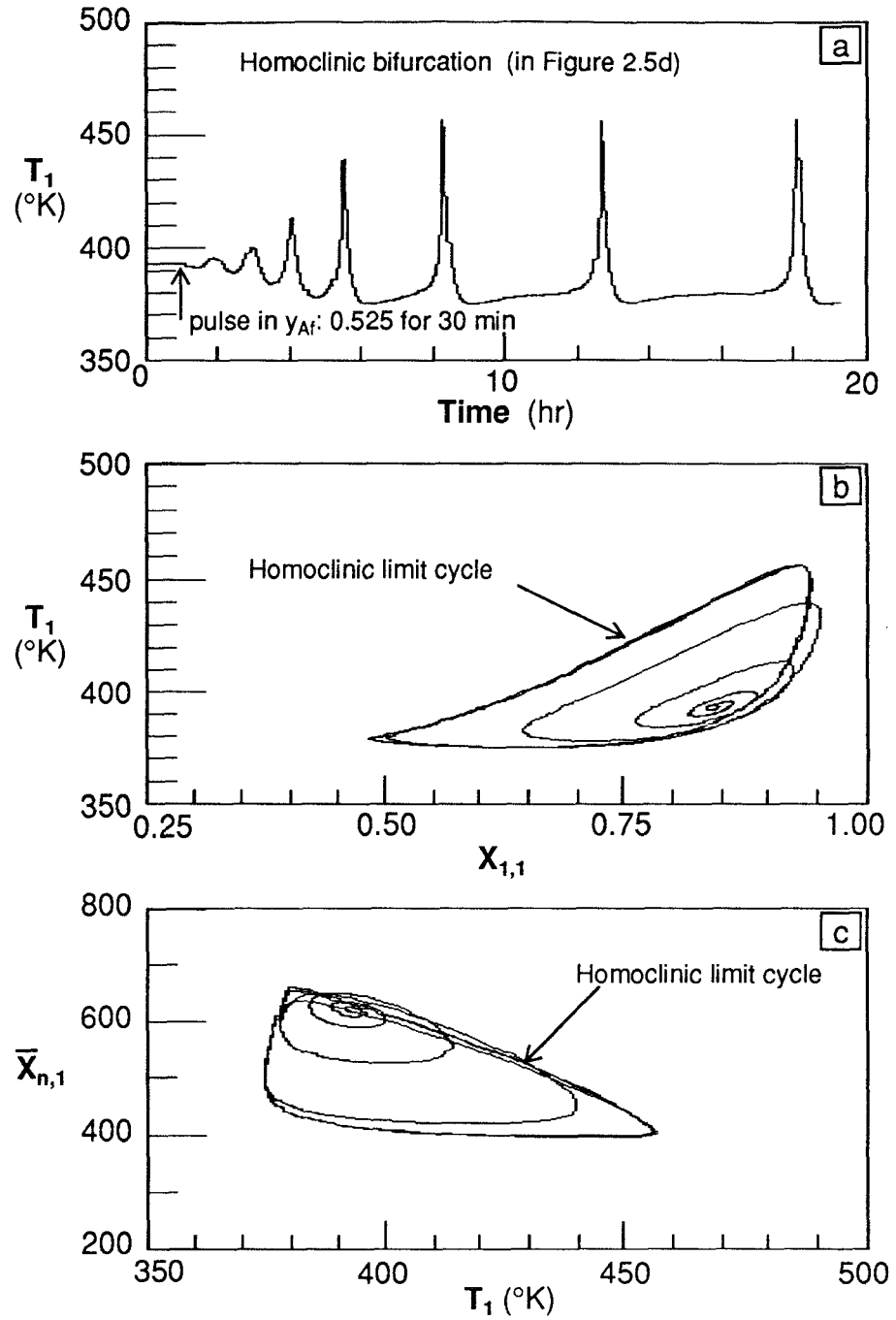
Figure 2.12   Transient response and phase plane portraits of homoclinic bifurcation point to pulse change in y_{Af}: $f_s = 0.1$, $I_f = 0.025$ mol/l, $y_{Af} = 0.5$, $T_f = 343$ °K, $T_{c,1} = 363$ °K.
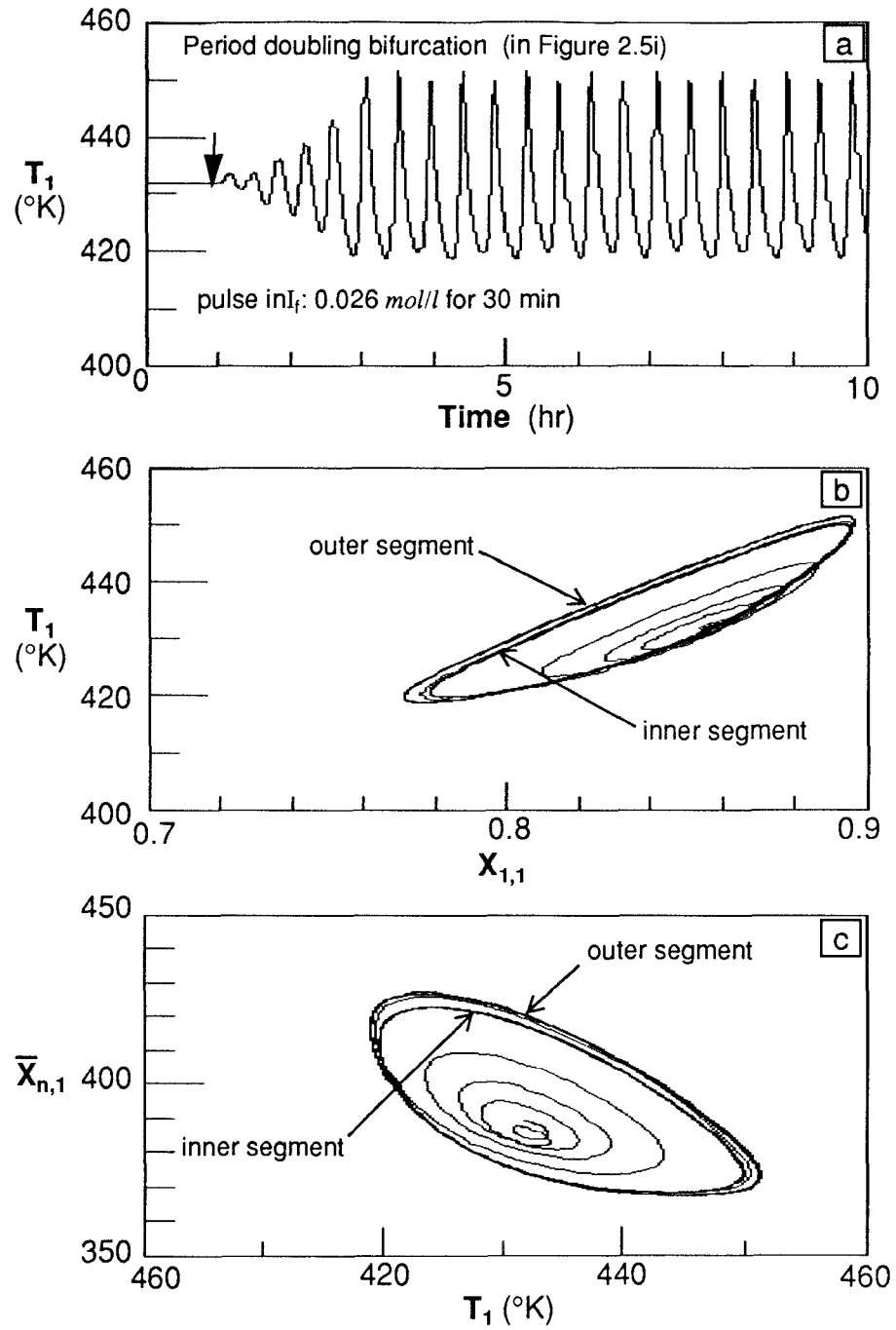
Figure 2.13   Transient response and phase plane portraits of period doubling bifurcation point to pulse change in I_f: $f_s = 0.1$, $I_f = 0.025$ mol/l, $y_{Af} = 1.0$, $T_f = 343$ °K, $T_{c,1} = 363$ °K.
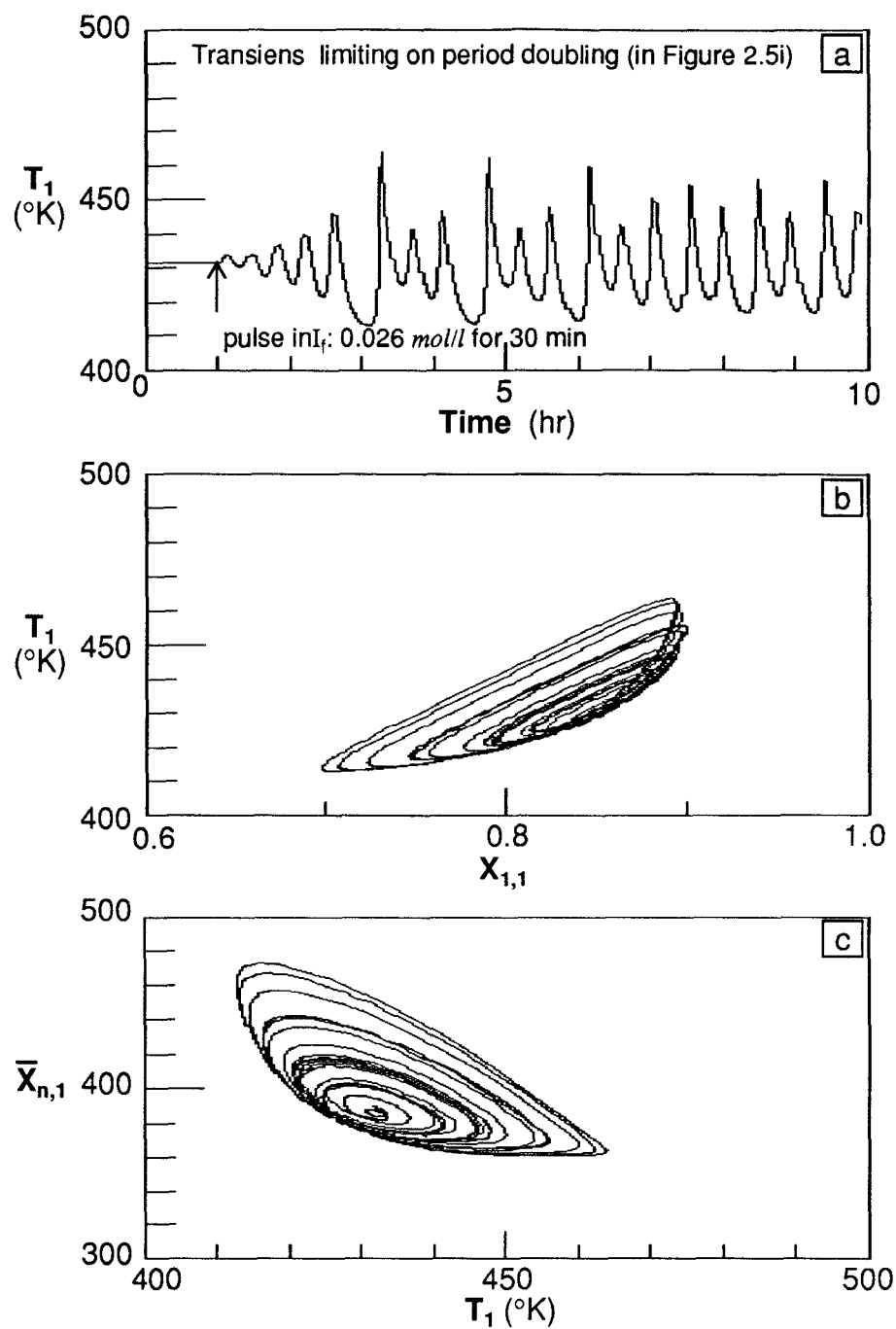
Figure 2.14   Transient behavior limiting on period doubling: $f_s = 0.1$, $I_f = 0.025$ mol/l, $y_{Af}=1.0$, $T_f= 343$ °K, $T_{c,1}= 363$ °K.

outer segments of this orbit , there is an unstable undoubled periodic orbit, which is on the primary periodic branch. The period-doubled orbit and the undoubled orbit form the boundary and center circle of a Möbius band. In Figure 2.14, θ is set a value near that of point (ii) in Figure 2.5i. The orbit exhibits some complicated transitional behavior, and it is not evident if it has settled down to a periodic orbit or not. There is some transient "period 3" behavior and then a transition to something approximating a "period 2" behavior. It may be a chaotic orbit.

The effect of the initiator feed composition (y_{Af}) on the steady state monomer conversion, temperature and the degree of polymerization is illustrated in Figure 2.15 for varying reactor residence time. Note that for a given set of operating parameters, the reactor steady state may change significantly by simply varying the composition of the feed initiator mixture. For those cases illustrated in the figure, the reactor giving intermediate monomer conversion is mostly unstable. As the reactor residence time increases, middle unstable branches become smaller and a wide range of initiator feed composition can be used to regulate both the monomer conversion and the polymer molecular weight. Similar diagrams are also shown in Figure 2.16 for varying feed initiator concentration with fixed initiator feed composition ($y_{Af} = 0.5$). These diagrams such as Figure 2.15 and 2.16 will be useful when one wants to design reactor operating conditions with a binary mixture of slow and fast initiators.
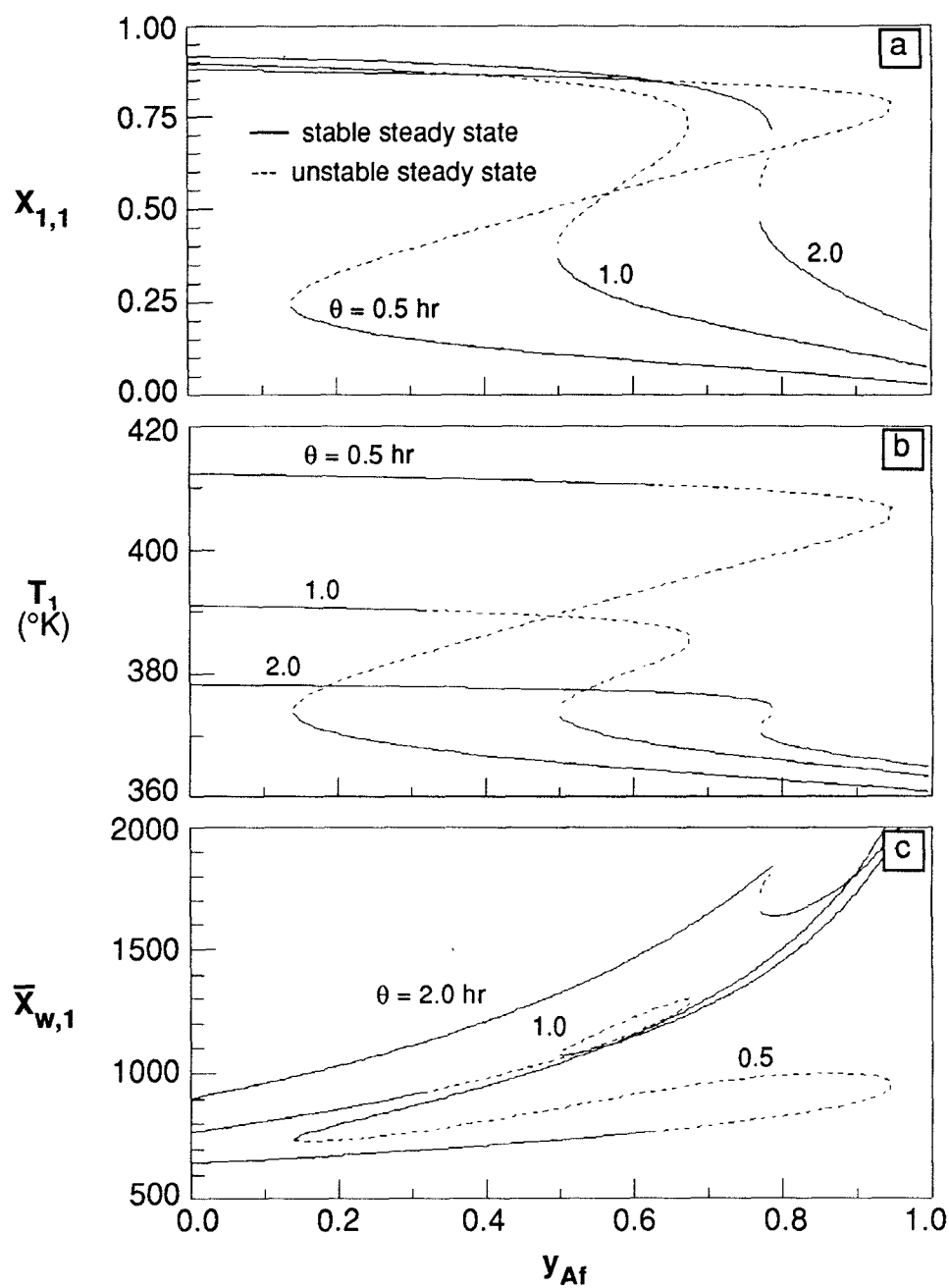
Figure 2.15   Effect of the initiator feed composition on the steady state profiles of $X_{1,1}$, T_1 and $\overline{X}_{w,1}$ with mixed initiators in the first reactor: $f_s=0.1$, $y_{Af}=0.5$, $T_f=343$ °K, $T_{c,1}=363$ °K.

70
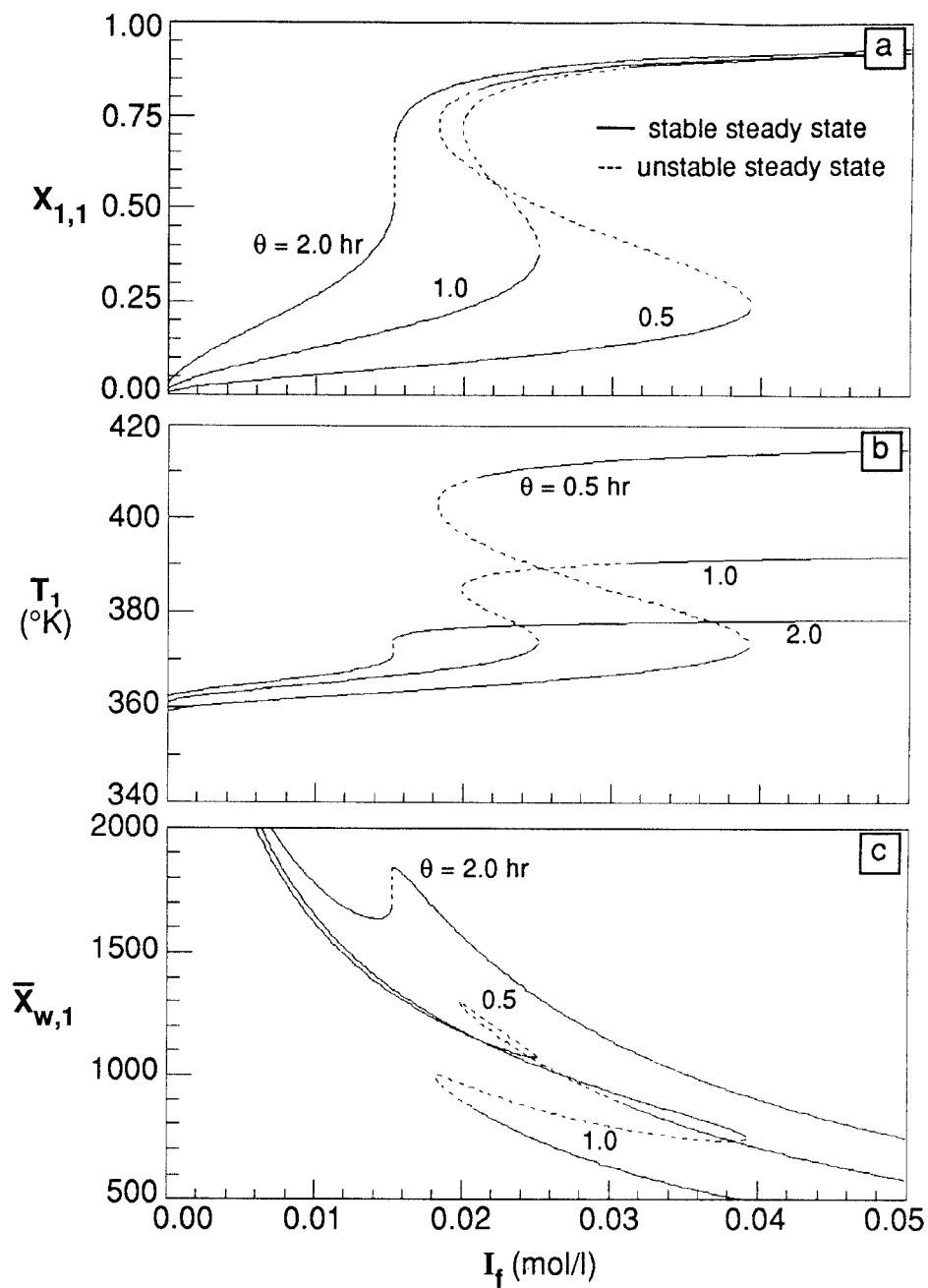
Figure 2.16   Effect of the initiator feed concentration on the steady state profiles of $X_{1,1}$, T_1 and $\overline{X}_{w,1}$ with mixed initiators in the first reactor: f_s=0.1, y_{Af}= 0.5, T_f= 343 °K, $T_{c,1}$= 363 °K.

2.4.2. Transient Behavior

The transient behavior of the first reactor will now be illustrated for various operating conditions: perturbation of steady state and the reactor start-up. Figure 2.17 and 2.18 shows the dynamic response of the polymerization reactor when the feed initiator composition (y_{Af}) is step changed ($\pm$ 60 %). The original steady state is point A in Figure 2.5d which is stable. As the content of more stable or *slow initiator* is increased from $y_{Af} = 0.5$ to 0.8 as shown in Figure 2.18, the reactor state moves smoothly toward a new stable steady state. The steady state temperature decreases only by 5 °C but $\overline{X}_{n,1}$ value increases from 650 to 900, a 38 % increase. The polydispersity also increases slightly. Figure 2.18 also shows that the reactor temperature reaches its new steady state value in one hour whereas it takes about 4 hours for monomer conversion $\overline{X}_{n,1}$, and $\overline{PD}_1$ to reach their new steady state values. However, when the content of the *slow initiator* is decreased from $y_{Af} = 0.5$ to 0.2, a dramatic change in the reactor state occurs as illustrated in Figure 2.17. Note that in less than 30 min after the change in the feed initiator composition is made, both the reactor temperature and monomer conversion increase rapidly and oscillate afterward toward a new upper steady state. The temperature reaches as high as 460 °K in a short time period and this rapid temperature surge may cause a serious heat removal problem or runaway phenomenon. It is also interesting to observe that the polydispersity returns to its original

a

$X_{1,1}$

1.0

0.5

0.0

step change in y_{Af} (0.5→0.2)

b

$I_{i,1}$
(mol/l)

0.02

0.01

0.00

$I_{A,1}$

$I_{B,1}$

c

T_1
(°K)

500

450

400

350

d

$\overline{X}_{n,1}$

800

600

400

200

e

$\overline{PD}_1$

1.9

1.7

1.5

0

5

10

Time (hr)
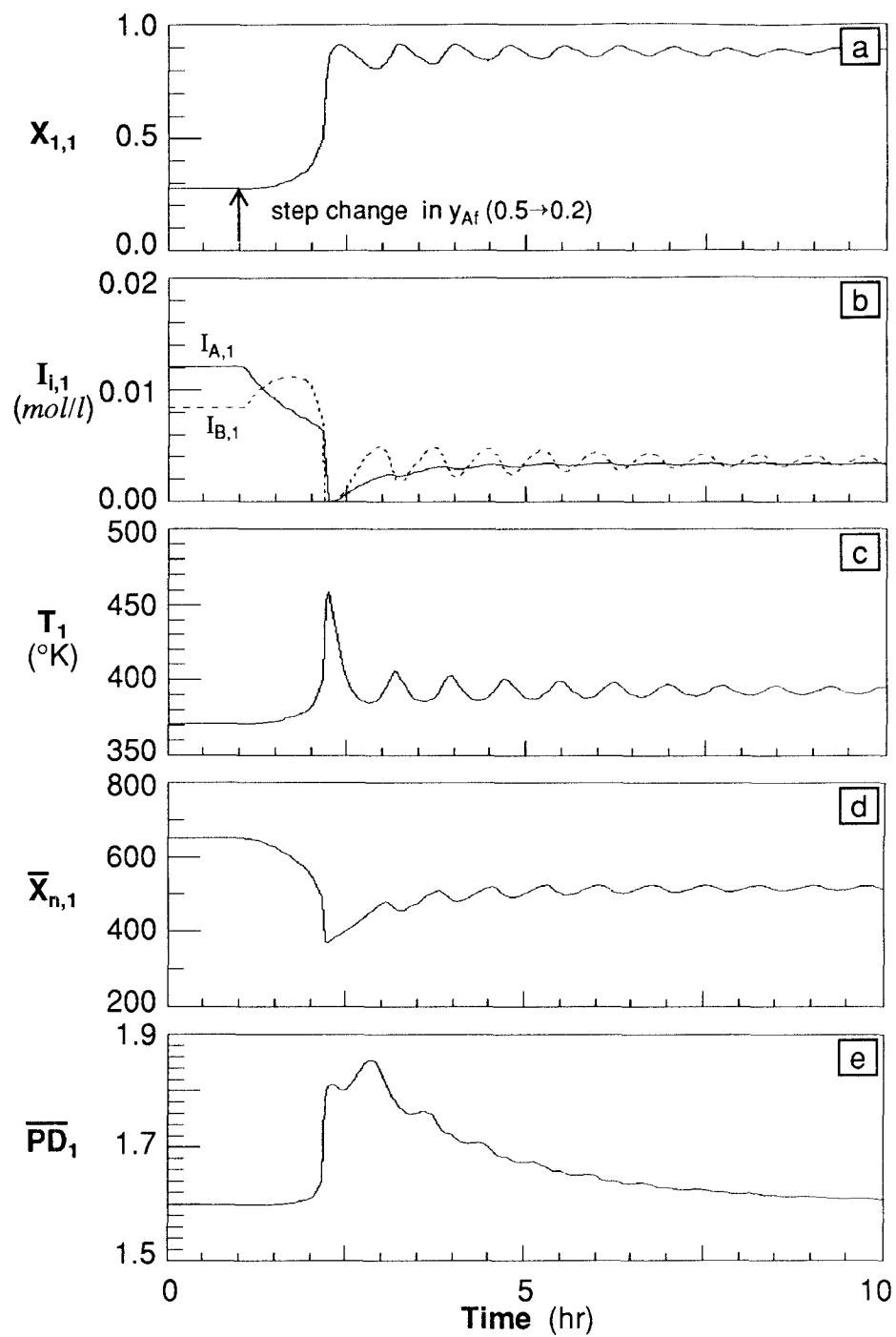
Figure 2.17   Transient response of the first reactor to the step change in the initiator feed composition (-60 %) during the steady state operation: $f_s = 0.1$, $I_f = 0.025$ mol/l, $y_{Af} = 0.5$, $T_f = 343$ °K, $T_c = 363$ °K, $\theta = 0.9$ hr.

73
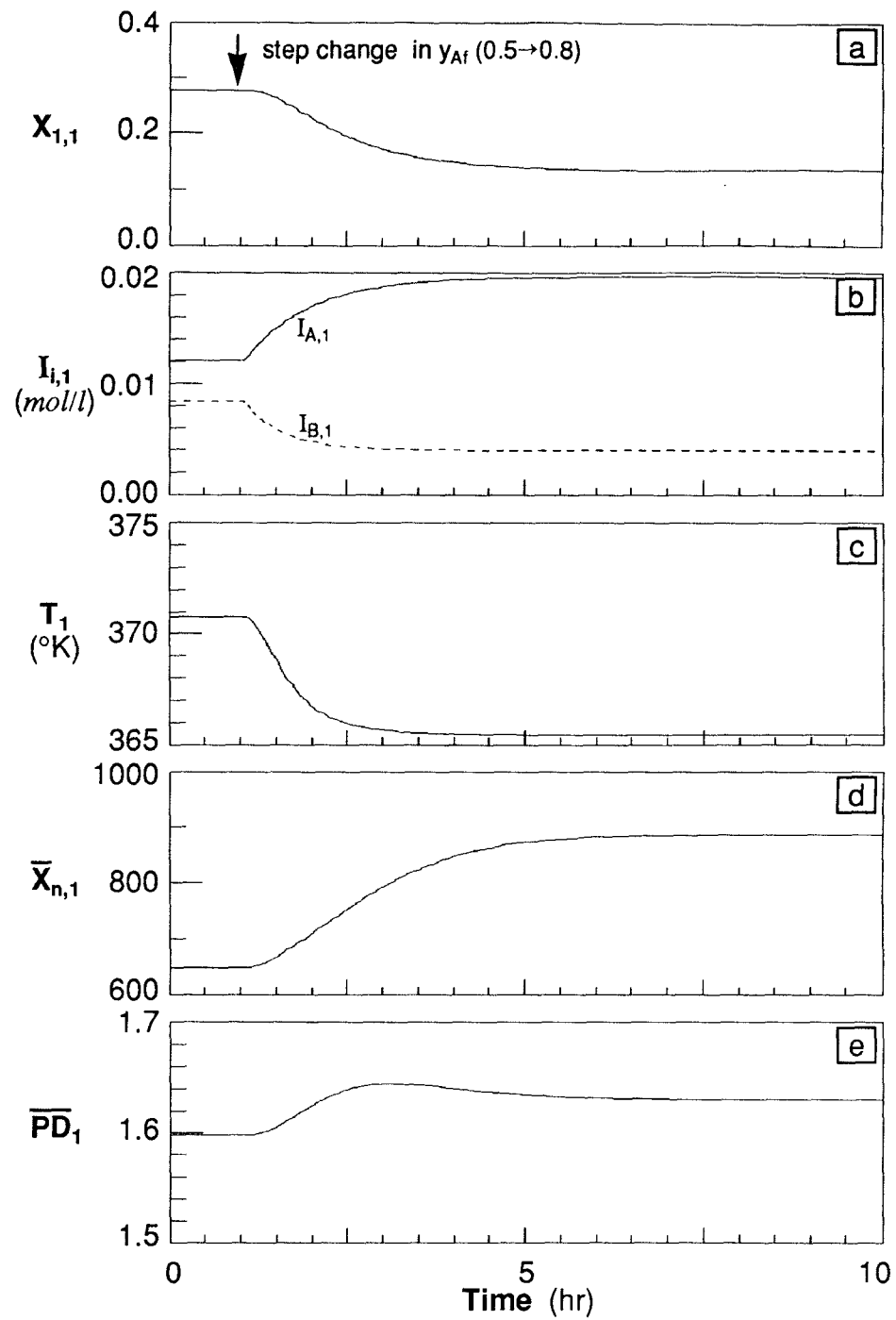
Figure 2.18   Transient response of the first reactor to the step change in
the initiator feed composition (+60 %) during the steady state
operation: $f_s = 0.1$, $I_f = 0.025$ mol/l, $y_{Af} = 0.5$, $T_f = 343$ °K,
$T_c = 363$ °K, $\theta = 0.9$ hr.

value 5 hours after the step change is introduced to the system (Figure 2.17e).

Similar behavior observed in Figure 2.17 and 2.18 is seen in Figure 2.19 and 2.20 where step changes ($\pm$ 20 %) in the total feed initiator concentration (I_f) are made with the initiator composition being held constant at $y_{Af} = 0.5$. Figure 2.19 illustrates again that the time constants for the change in monomer conversion, $\overline{X}_{n,1}$ and $\overline{PD}_1$ are almost the same. Figure 14 shows the transient response of the reactor to the simultaneous changes in both the feed initiator composition (y_{Af}) ($\pm$ 33.4 %) and the feed initiator concentration (I_f) ($\pm$ 50 %). When the content of the *slow initiator* increases (Figure 2.21), the transition of the reactor state to a new steady state occurs with about 3 hours of "induction" before entering a limit cycle. This can be a very dangerous situation because the system appears to move smoothly toward a new steady state before the runaway type transition to the new state occurs. When the content of the *slow initiator* is decreased, reactor runaway to a new steady state occurs almost instantly (Figure 2.22). It is interesting to observe that the polymer molecular weight decreases significantly in both cases whereas the polydispersity value returns to its original value in the case of Figure 2.22.

The start-up transients of the reactor also depend strongly upon the feed initiator concentration and the feed initiator composition. Figure 2.23 and 2.24 illustrate the two cases in which slightly different initiator concentrations are used only to result in significantly different transient behavior.
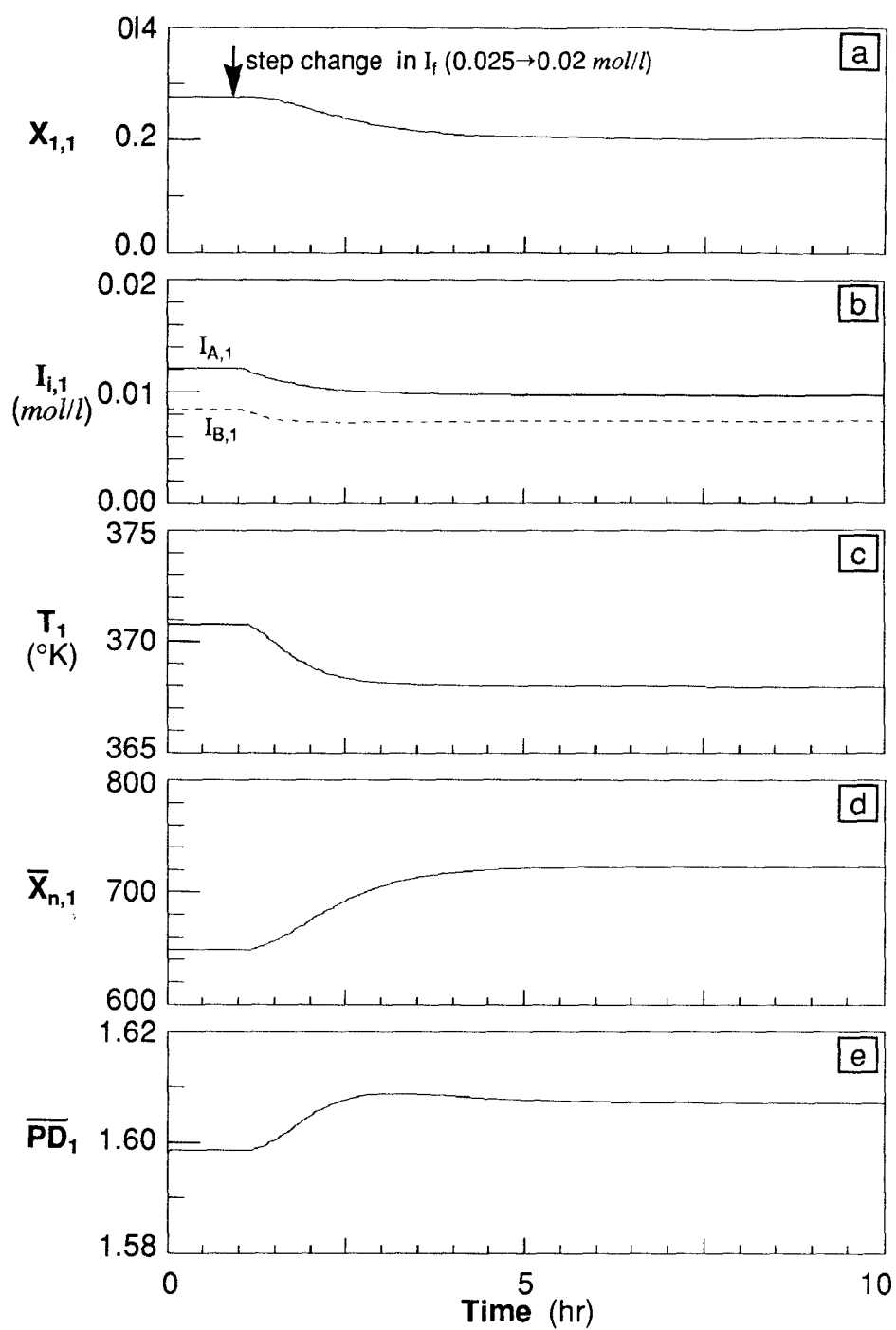
Figure 2.19   Transient response of the first reactor to the step change in the initiator feed concentration (-20 %) during the steady state operation: $f_s = 0.1$, $I_f = 0.025$ mol/l, $y_{Af} = 0.5$, $T_f = 343$ °K, $T_c = 363$ °K, $\theta = 0.9$ hr.

76
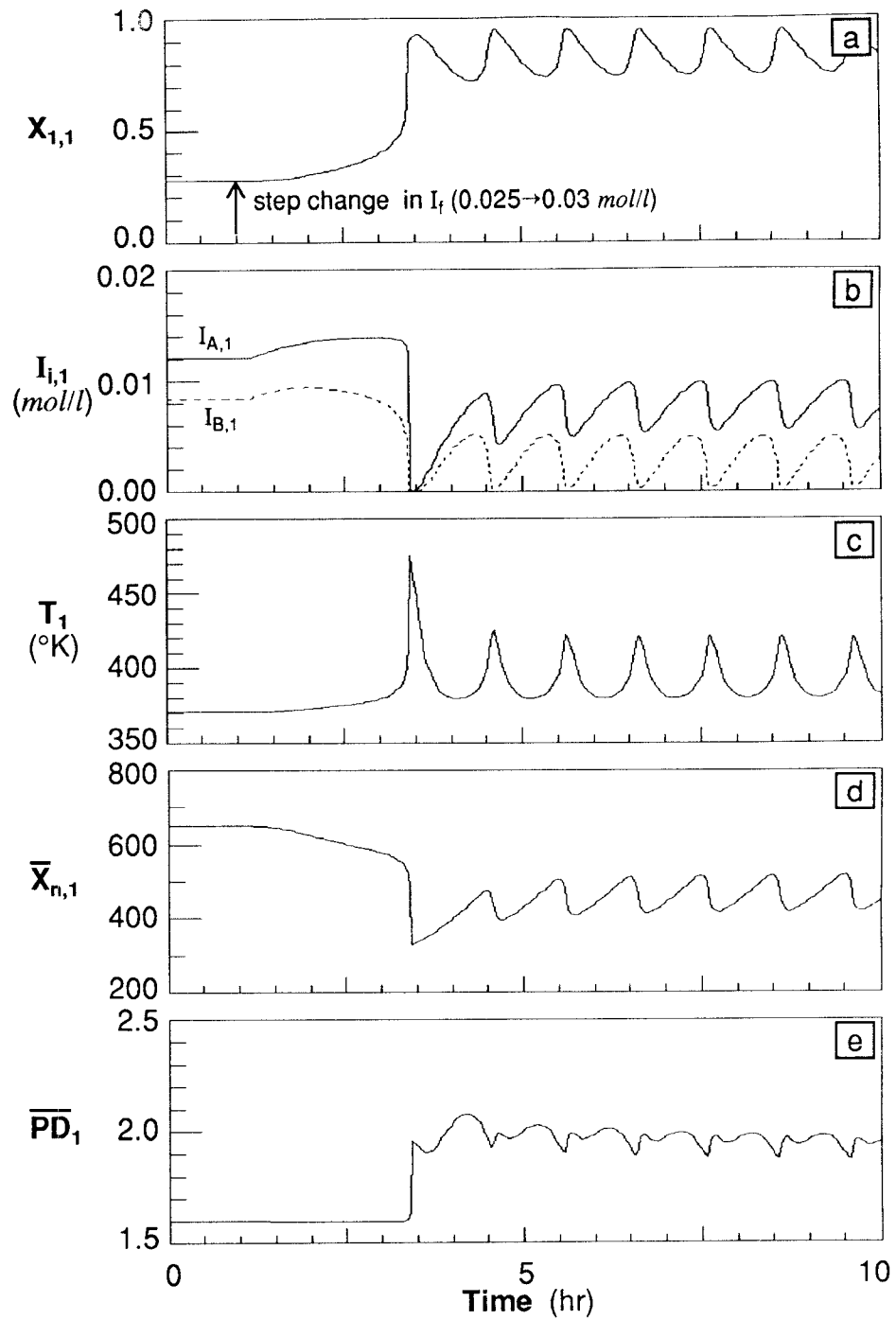
Figure 2.20   Transient response of the first reactor to the step change in the initiator feed concentration (+20 %) during the steady state operation: $f_s = 0.1$, $I_f = 0.025$ mol/l, $y_{Af} = 0.5$, $T_f = 343$ °K, $T_c = 363$ °K, $\theta = 0.9$ hr.
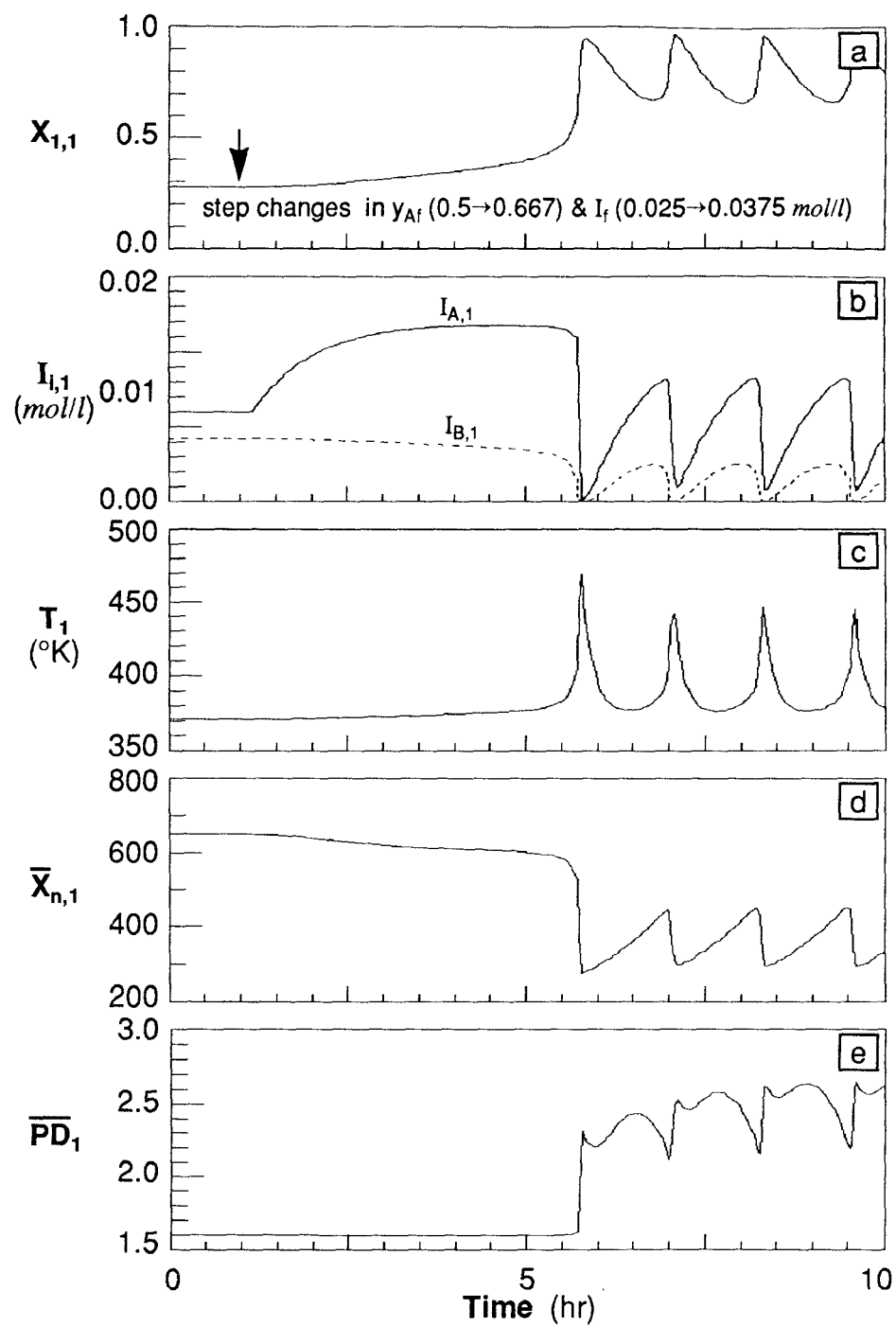
Figure 2.21   Transient response of the first reactor to the step change in composition (+33 %) and concentration (+50 %) of the initiator feed mixture during the steady state operation: $f_s =$ 0.1, $I_f =$ 0.025 mol/l, $y_{Af} =$ 0.5, $T_f =$ 343 °K, $T_c =$ 363 °K, $\theta =$ 0.9 hr.
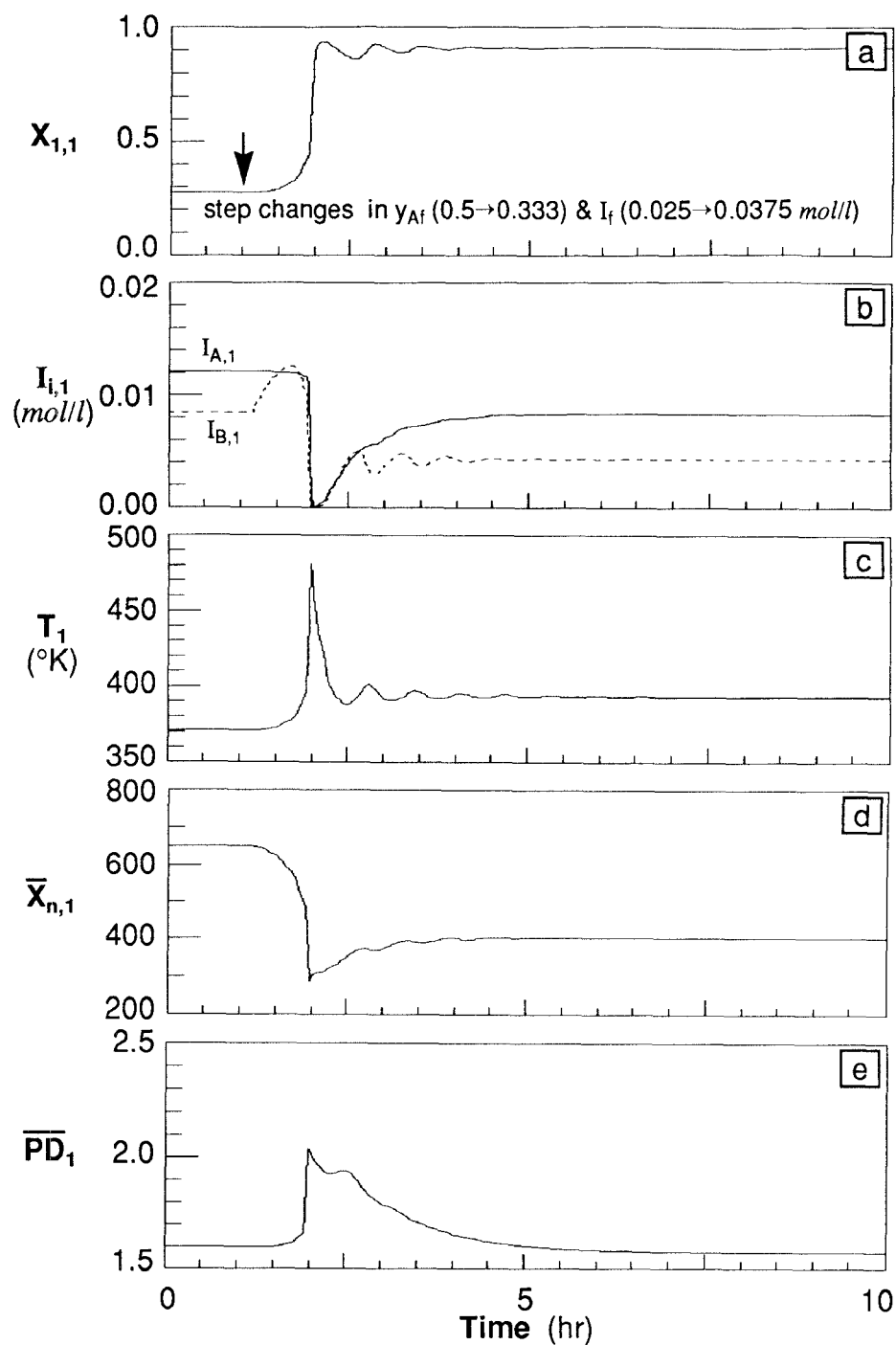
Figure 2.22   Transient response of the first reactor to the step change in composition (-33 %) and concentration (+50 %) of the initiator feed mixture during the steady state operation: $f_s = 0.1$, $I_f = 0.025$ mol/l, $y_{Af} = 0.5$, $T_f = 343\ °K$, $T_c = 363\ °K$, $\theta = 0.9$ hr.
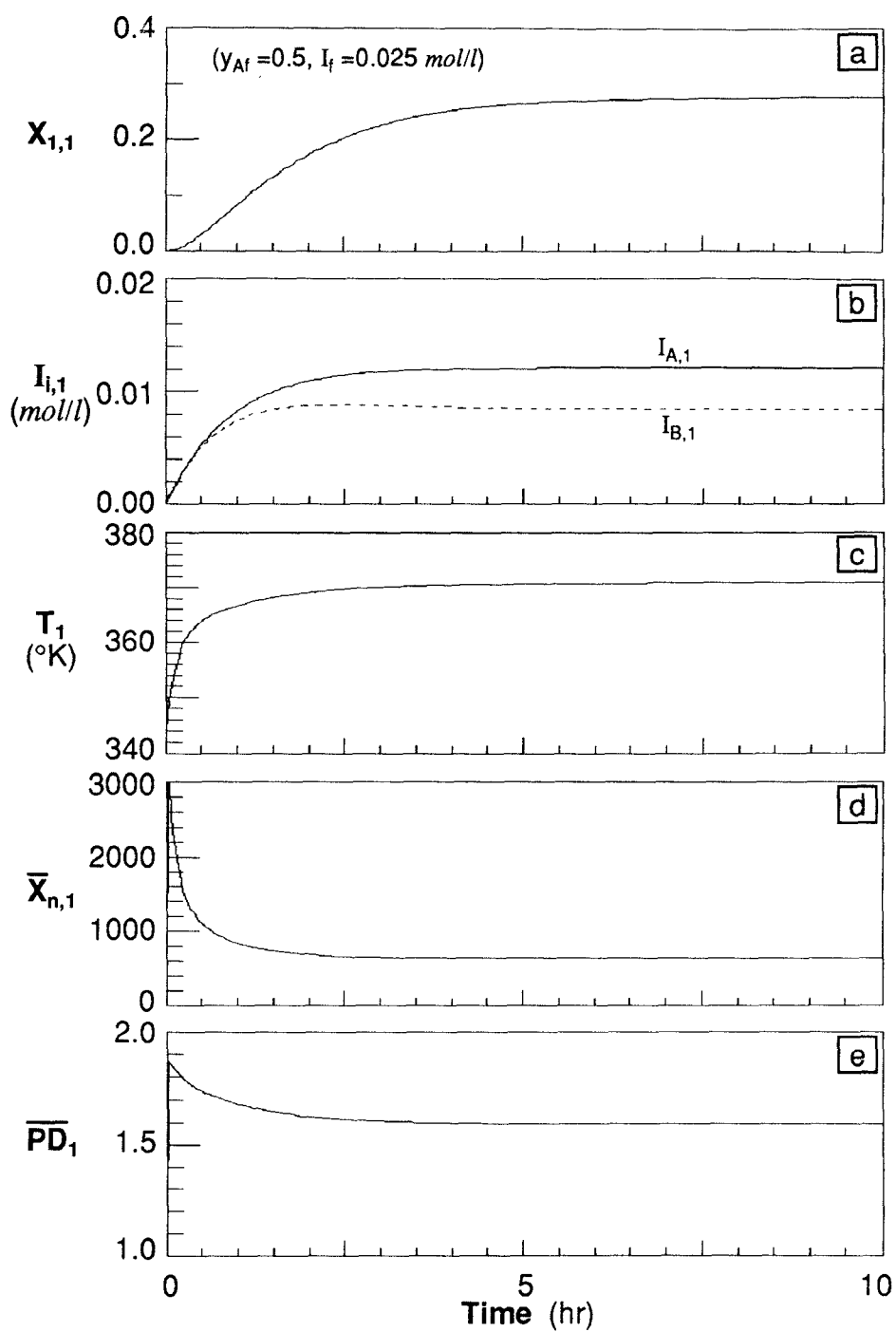
Figure 2.23   Start-up of the first CSTR at the standard operating conditions: $f_s=0.1$, $I_f=0.025$ mol/l, $y_{Af}=0.5$, $T_f=343$ °K, $T_c=363$ °K, $\theta=0.9$ hr.
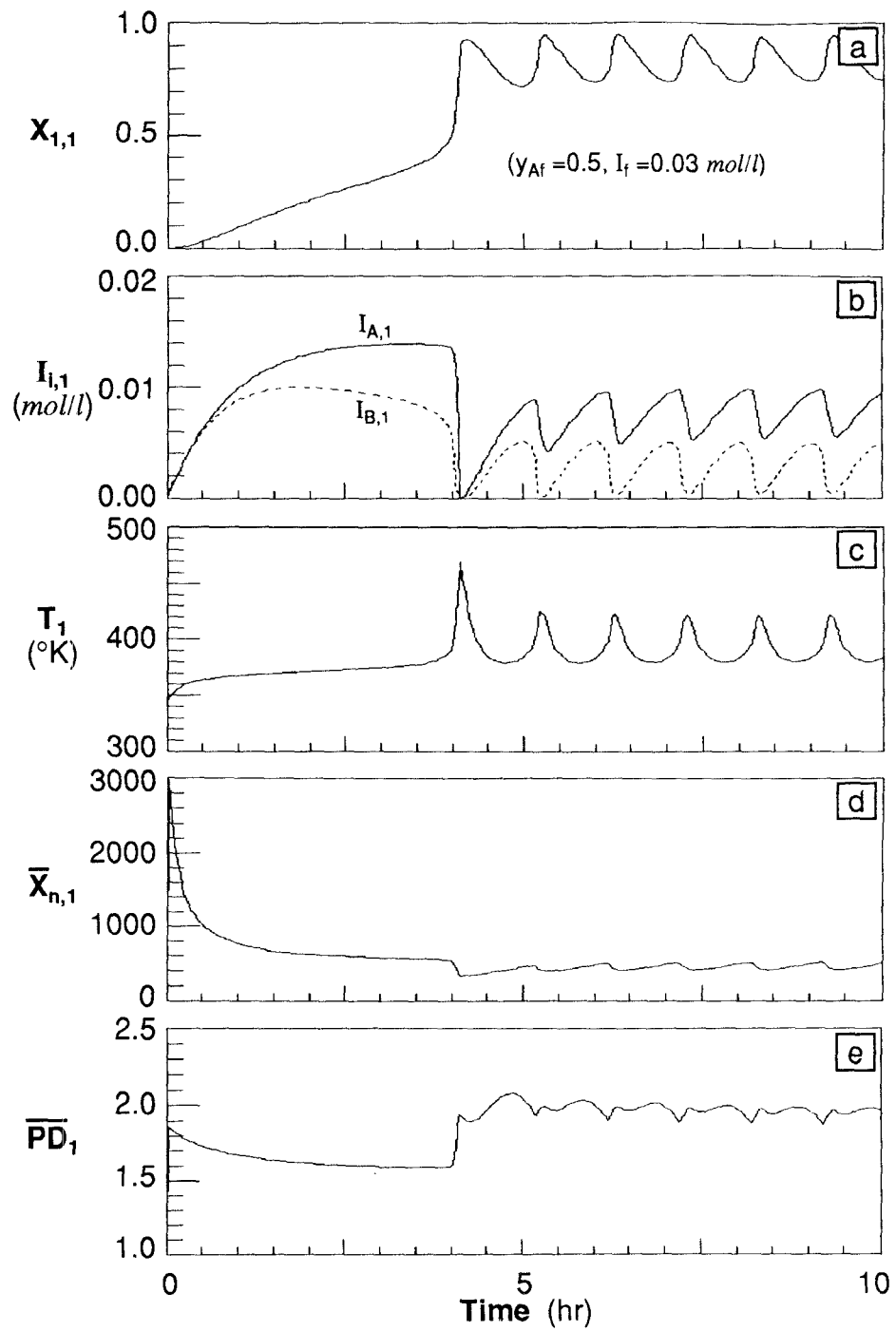
Figure 2.24   Effect of the initiator feed concentration on the start-up of
the first reactor: $f_s = 0.1$, $I_f = 0.030$ mol/l, $y_{Af} = 0.5$, $T_f = 343$ °K, $T_c = 363$ °K, $\theta = 0.9$ hr.

The effect of feed initiator composition is shown in Figure 2.25. The strong nonlinear behavior as observed in both cases suggests that reactor start-up should be done carefully to avoid potentially dangerous situations.

2.5. Dynamics of the Second Reactor

When the second reactor has the same operating conditions (*i.e.* $T_{c,2} = 363\ °K$) and same size (*i.e.*, $\nu = 1$) as the first reactor, it has similar bifurcation behavior to the first reactor, as shown in Figures 2.26~2.31. Here, the fractional conversion of monomer ($X_{1,2}$), the molar concentration of the initiators ($I_{A,2}$, $I_{B,2}$), the reactor temperature (T_2), the number average degree of polymerization ($\overline{X}_{n,2}$), and the polydispersity ($\overline{PD_2}$) of the second reactor are presented for each initiator feed composition. There is a pattern in the manner in which the bifurcation behavior of the second reactor extends that of the first reactor. That is, there are two loops which become isolas as y_{Af} is increased (at different values of y_{Af}). The behavior of the periodic orbits is also repeated. Each of the two loops has a pair of Hopf bifurcations, which lead to branches of periodic orbits, period-doubling cascades, and chaos. One of each pair of Hopf bifurcations lies on the appropriate isola and one disappears as above. Thus for small y_{Af}, the bifurcation diagram with θ as a bifurcation parameter consists of a single branch of stationary points with two loops. For large y_{Af}, the bifurcation diagram consists of one straight branch
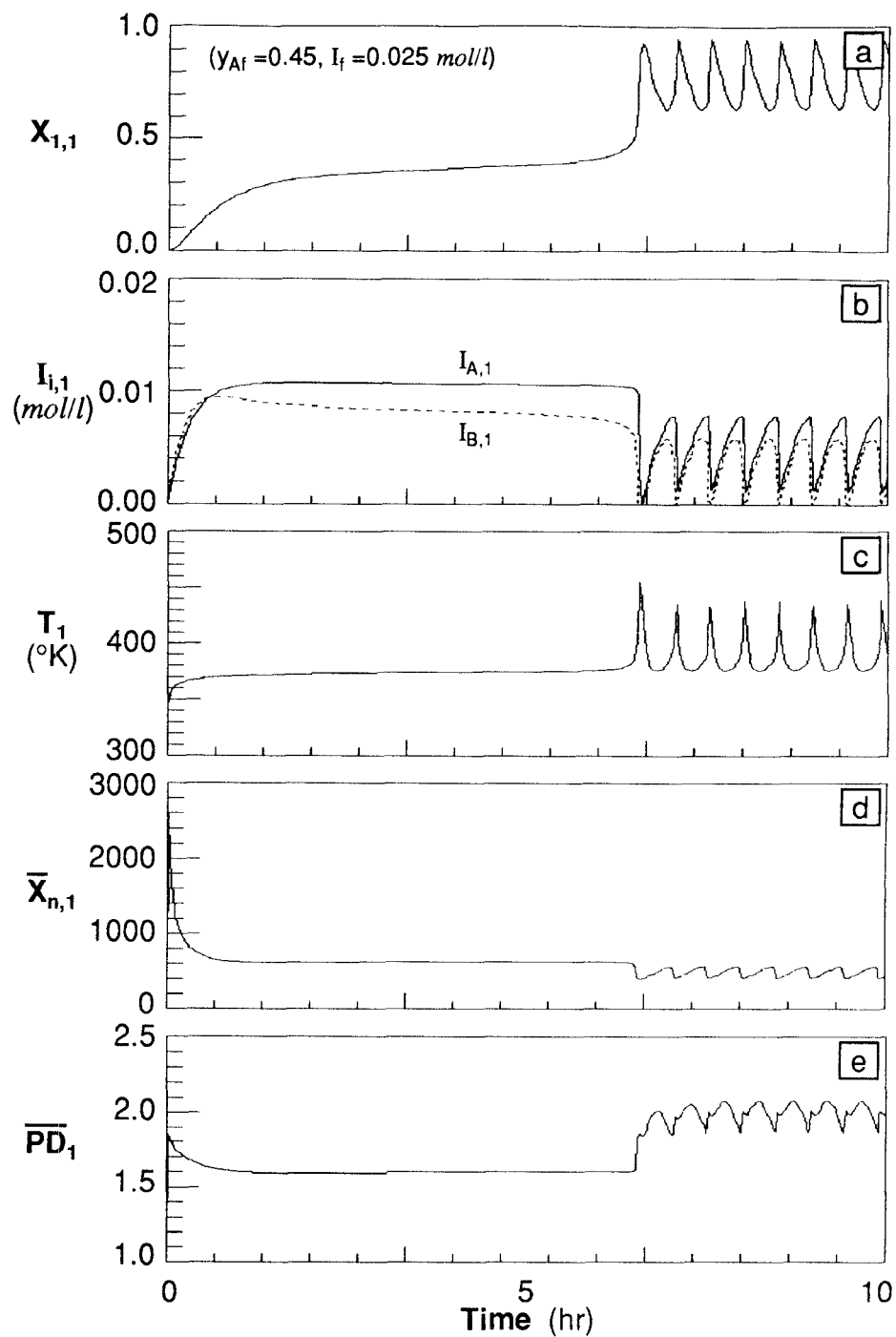
Figure 2.25   Effect of the initiator feed composition on the start-up of the first reactor: $f_s = 0.1$, $I_f = 0.025$ mol/l, $y_{Af} = 0.45$, $T_f = 343$ °K, $T_c = 363$ °K, $\theta = 0.9$ hr.
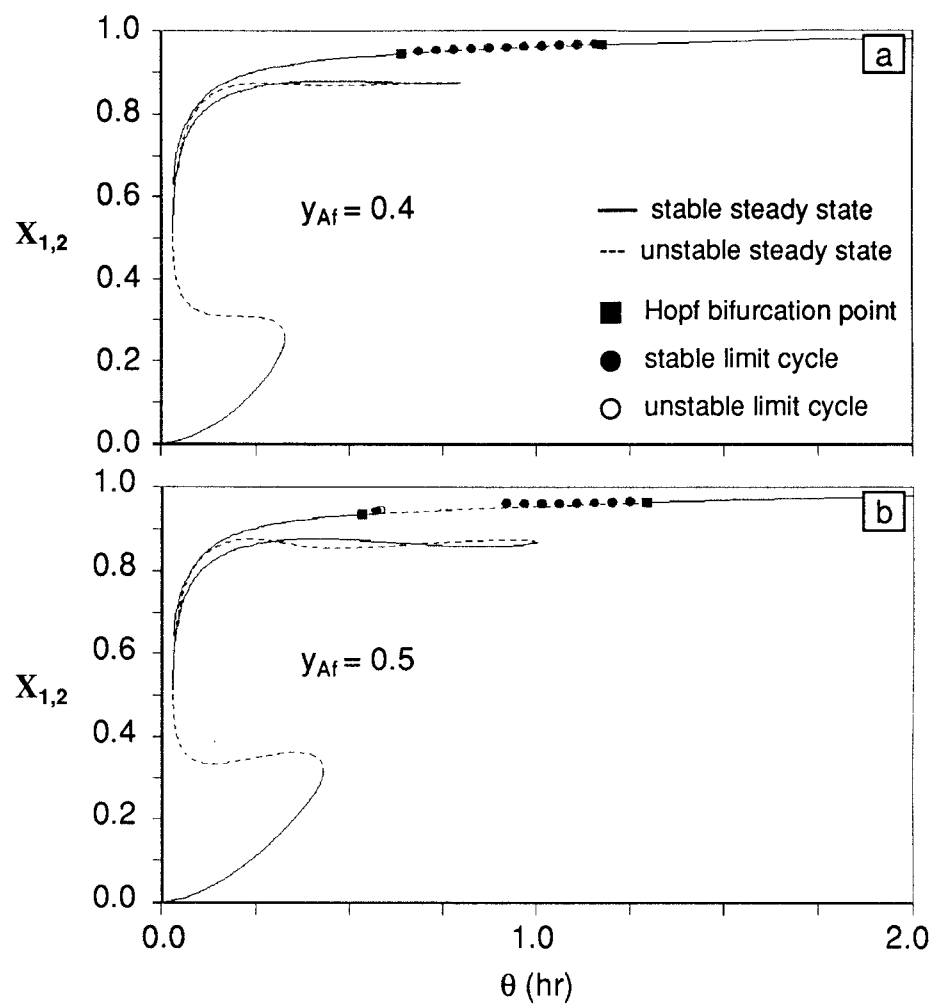
Figure 2.26 Bifurcation diagrams of $X_{1,2}$ with different y_{Af}: $f_s = 0.1$, $I_f = 0.025$ mol/l, $T_f = 343$ °K, $T_{c,1} = T_{c,2} = 363$ °K, $\nu = 1$.
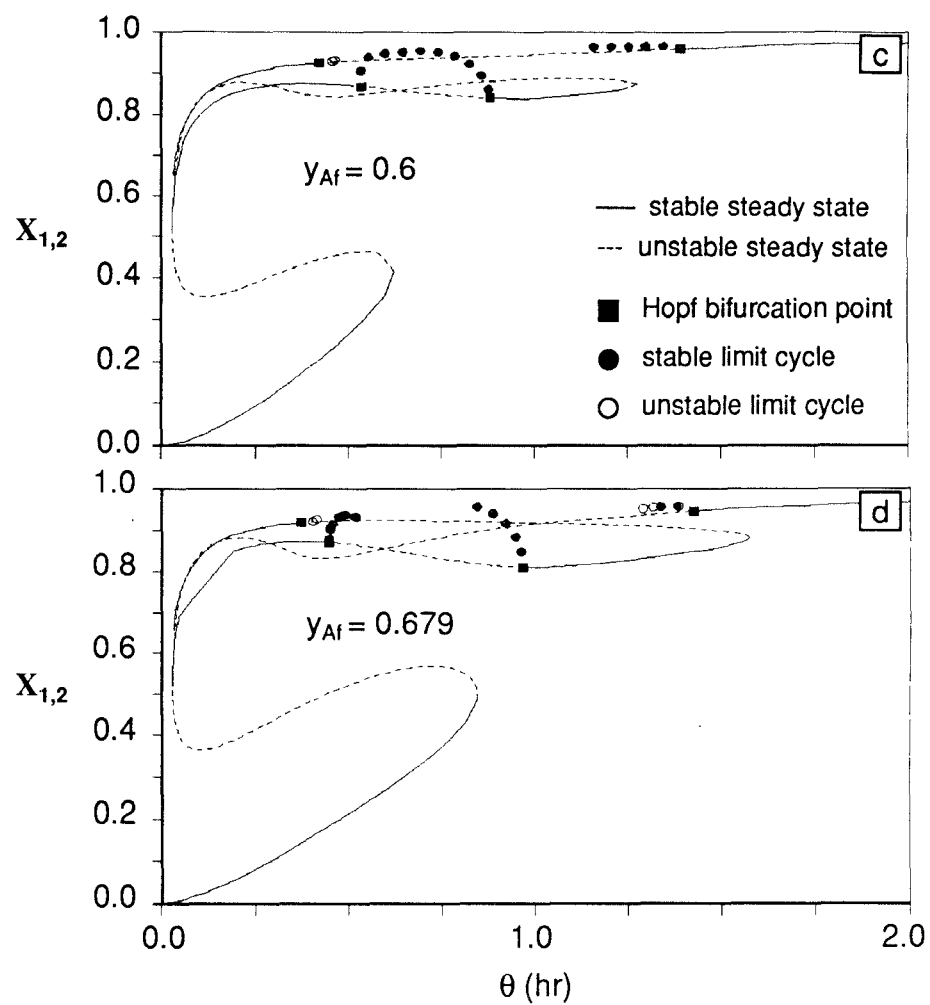
Figure 2.26   (*continued*)
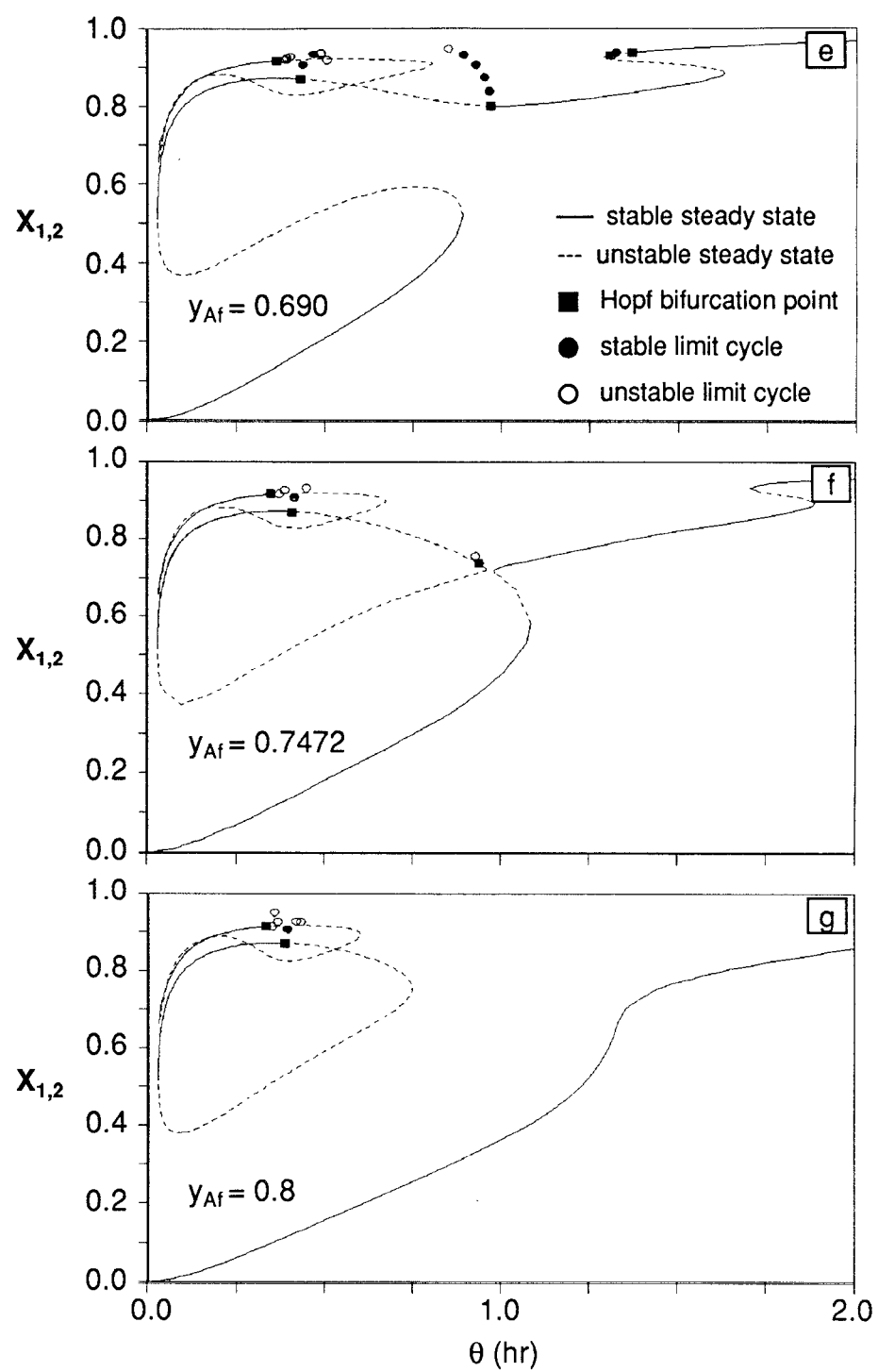
Figure 2.26 (*continued*)
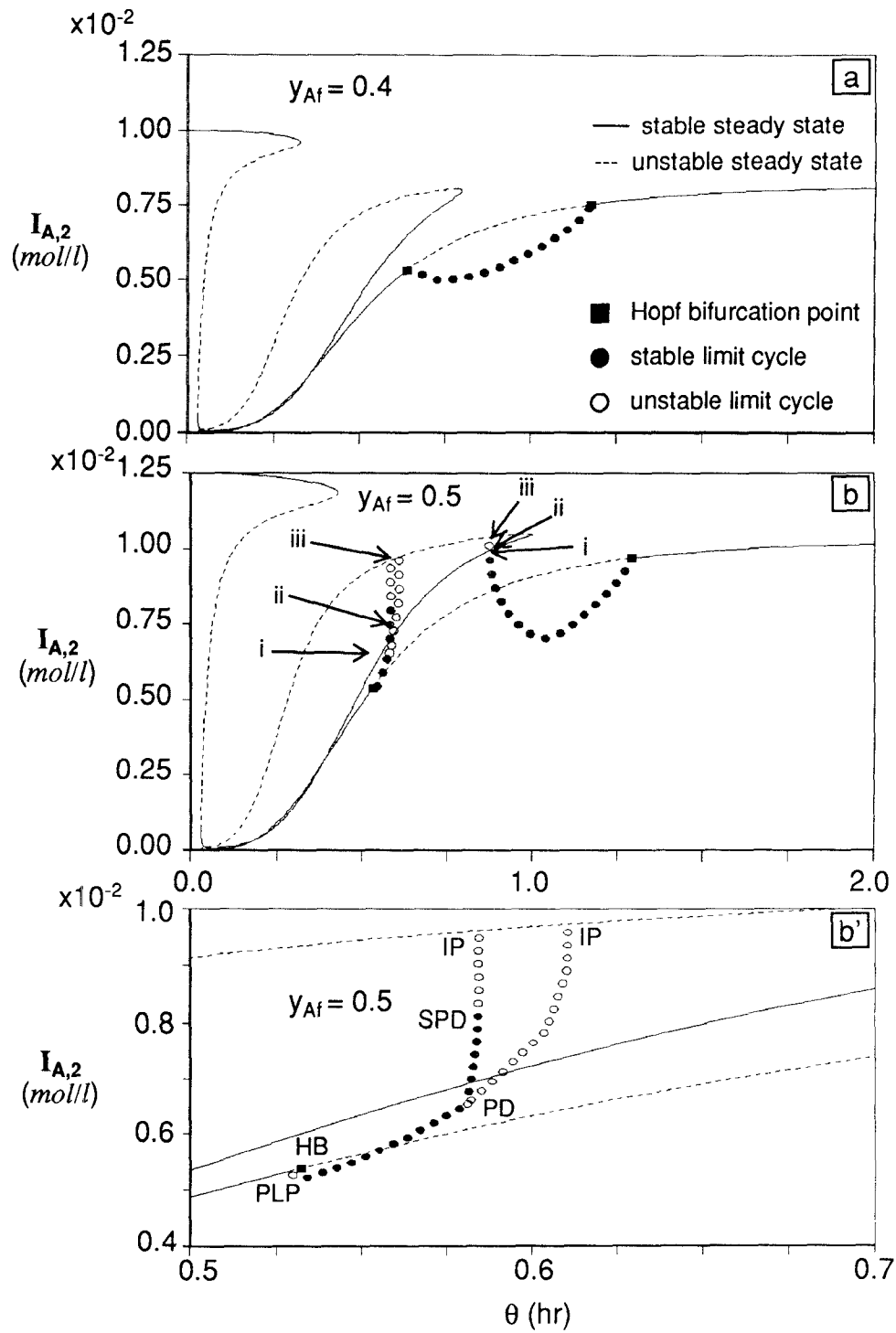
Figure 2.27   Bifurcation diagrams of $I_{A,2}$ with different y_{Af}: $f_s = 0.1$, $I_f = 0.025$ mol/l, $T_f = 343$ °K, $T_{c,1} = T_{c,2} = 363$ °K, $\nu = 1$ (i: period doubling bifurcation point, ii: second period doubling bifurcation point, iii: homoclinic bifurcation point).
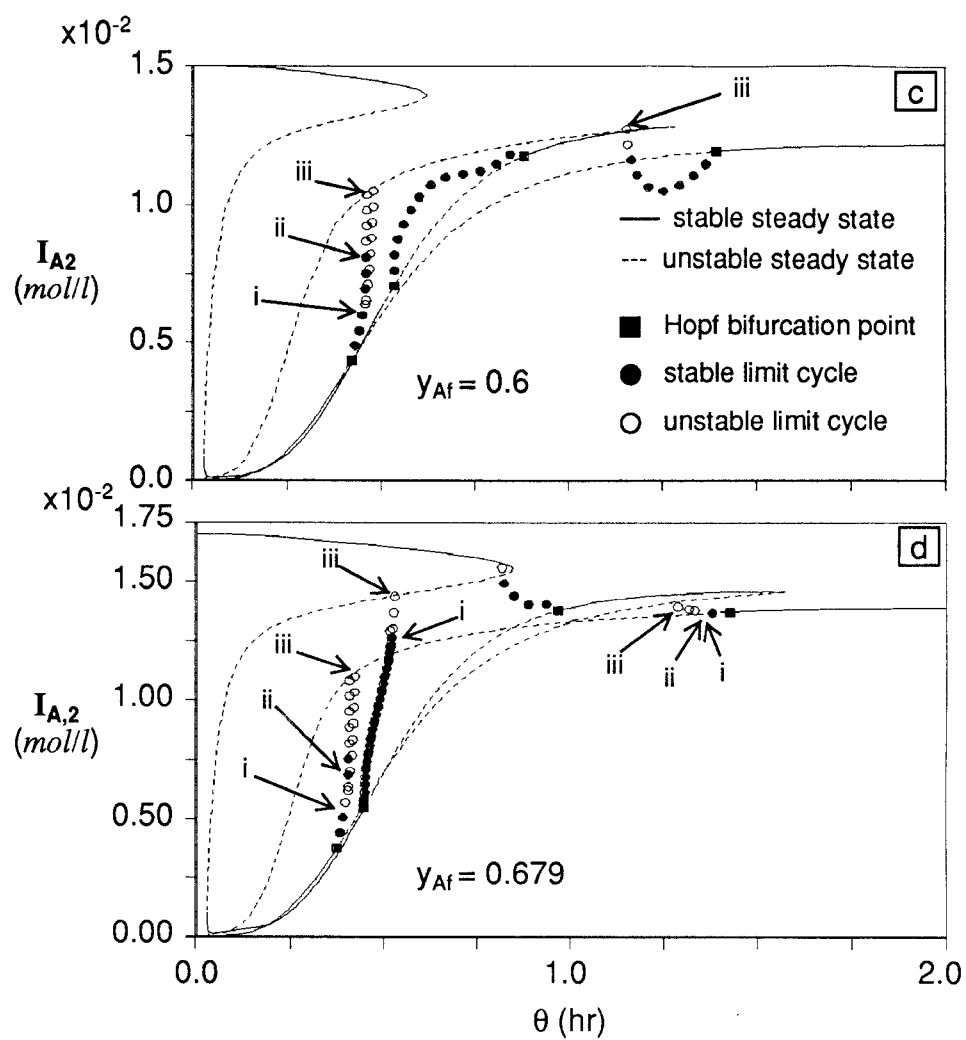
Figure 2.27   (*continued*)
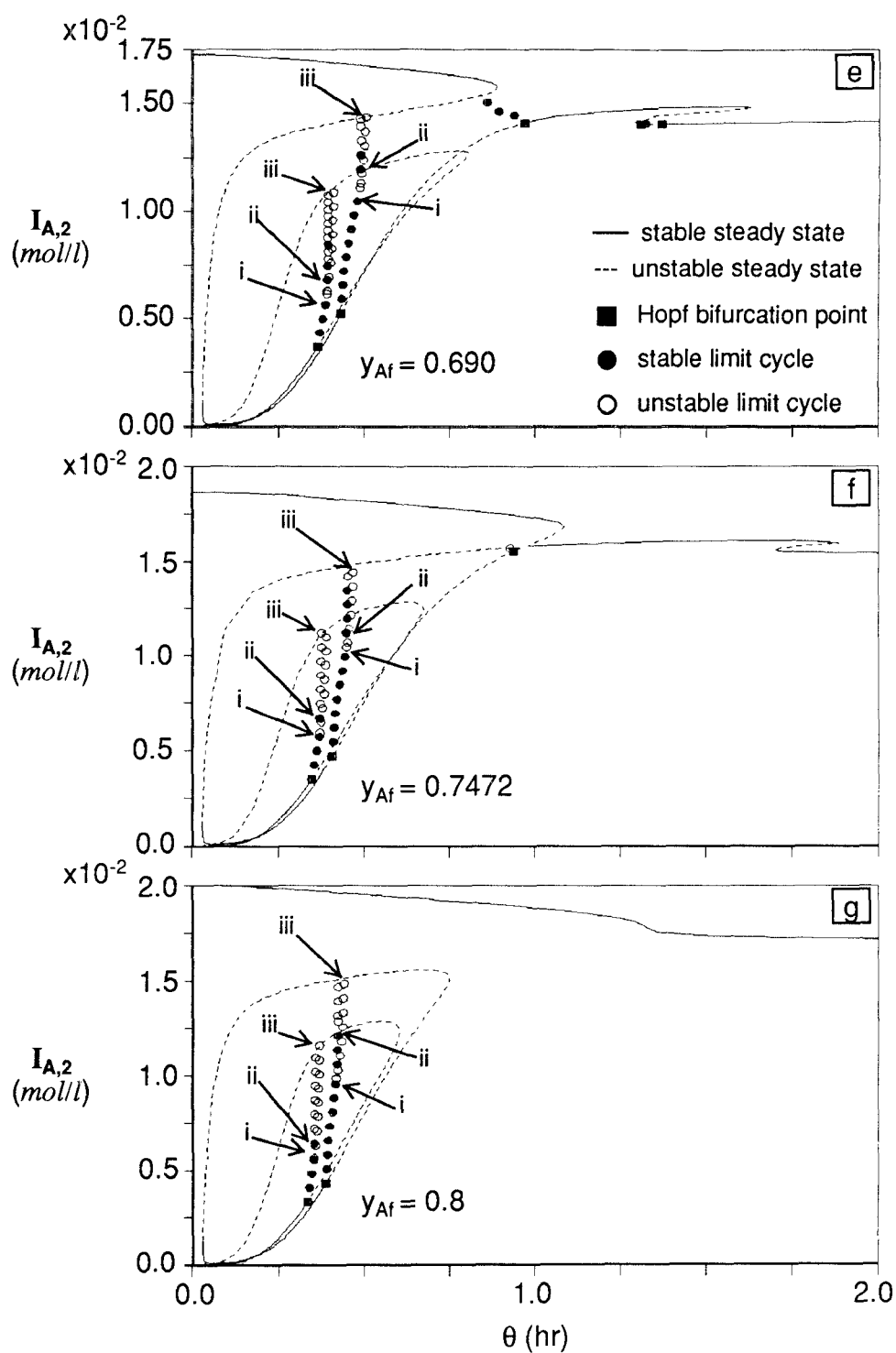
Figure 2.27   (continued)
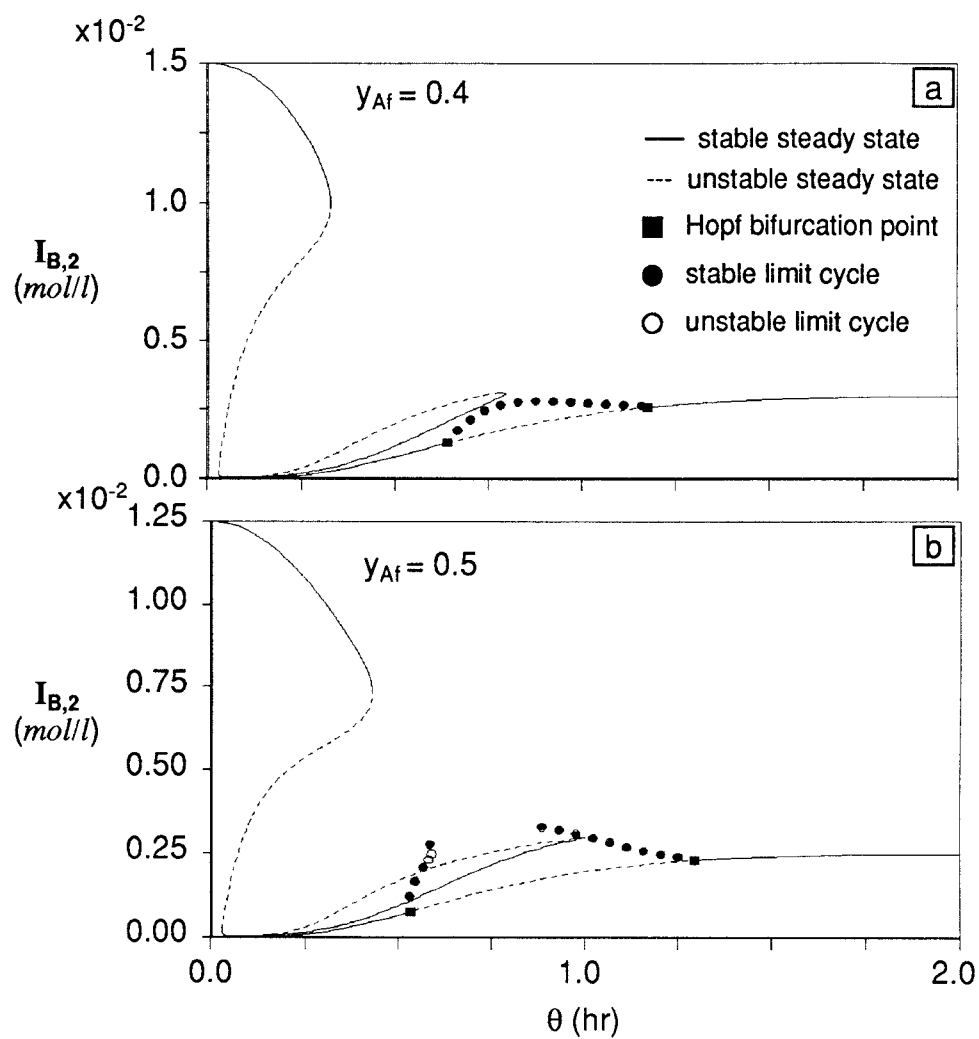
Figure 2.28   Bifurcation diagrams of $I_{B,2}$ with different y_{Af}: $f_s = 0.1$, $I_f = 0.025$ mol/l, $T_f = 343$ °K, $T_{c,1} = T_{c,2} = 363$ °K, $\nu = 1$.
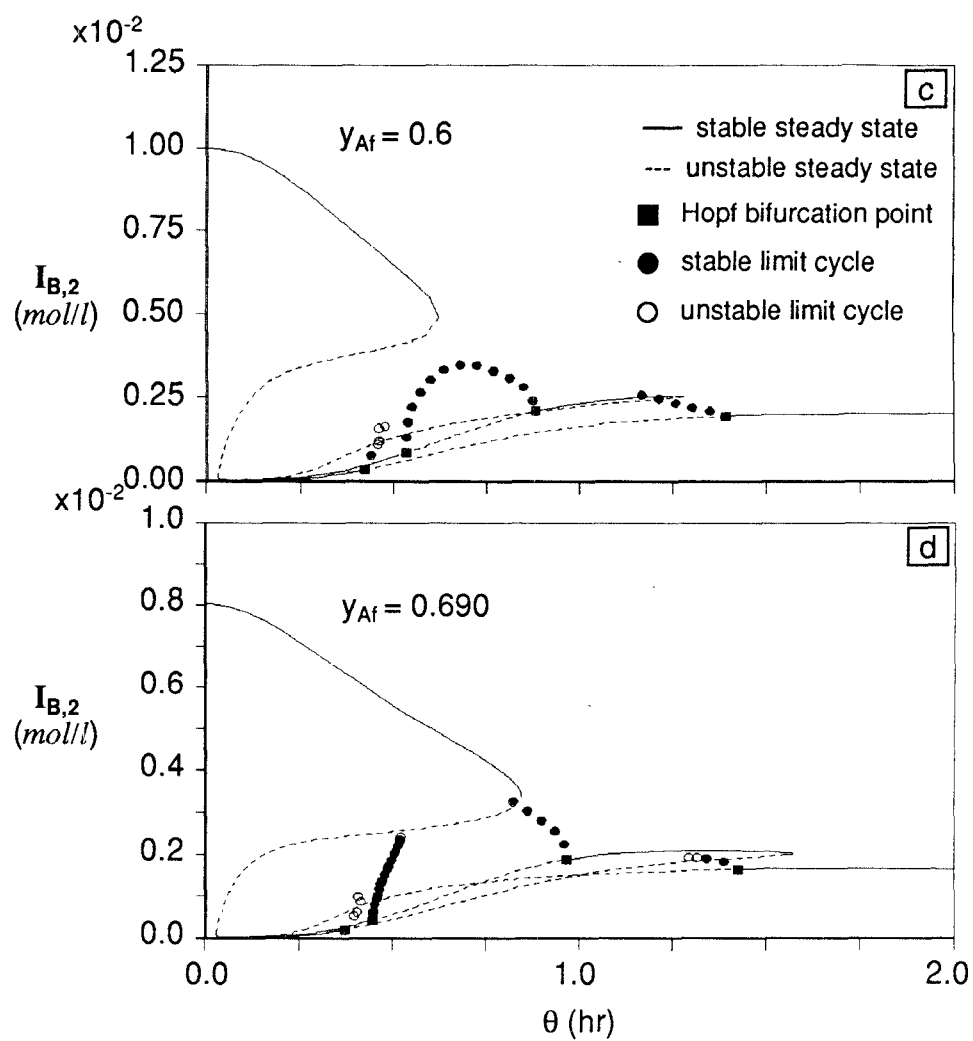
Figure 2.28 (*continued*)
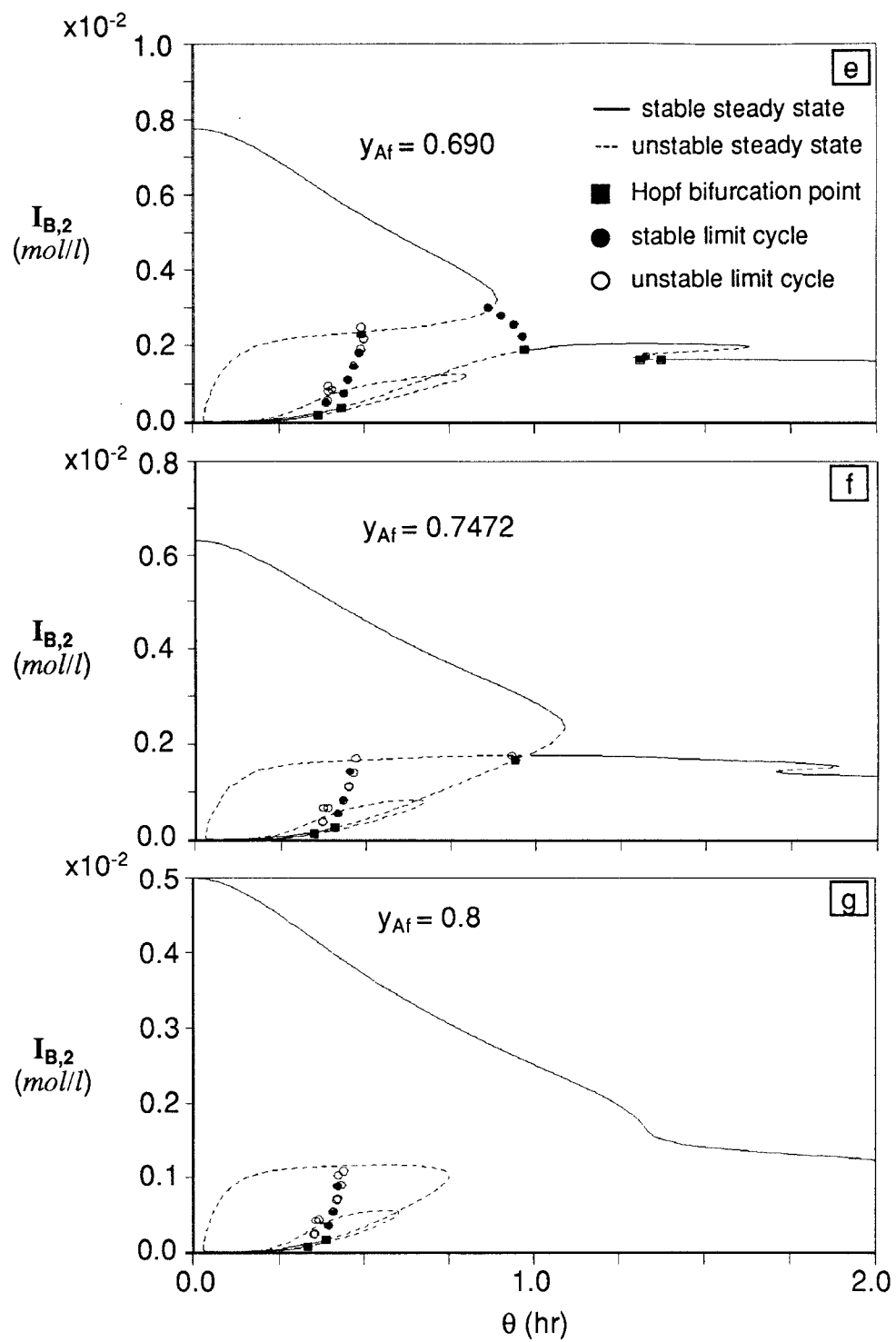
Figure 2.28   (*continued*)
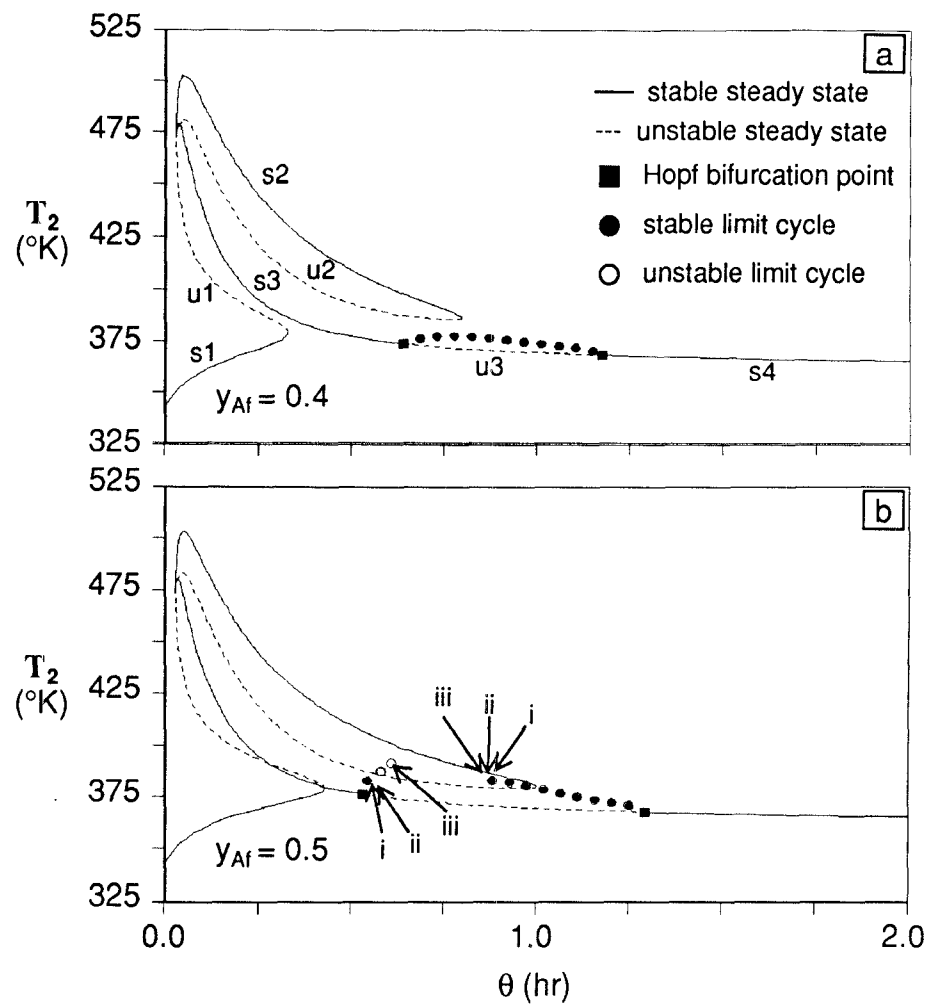
Figure 2.29 — Bifurcation diagrams of T_2 with different y_{Af}: $f_s = 0.1$, $I_f = 0.025$ mol/l, $T_f = 343$ °K, $T_{c,1} = T_{c,2} = 363$ °K, $\nu = 1$ (i: period doubling bifurcation point, ii: second period doubling bifurcation point, iii: homoclinic bifurcation point).

93
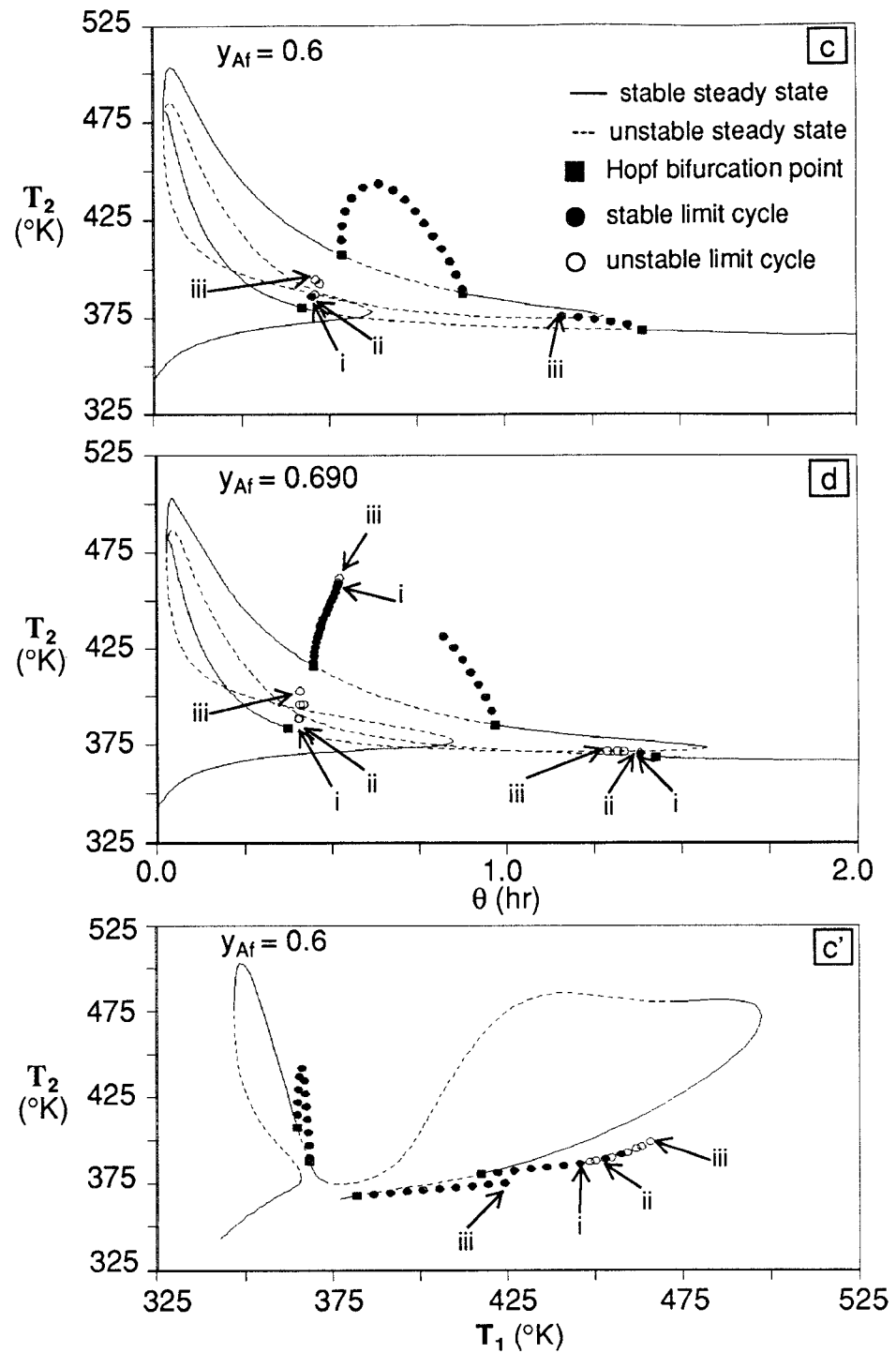
Figure 2.29   (*continued*)
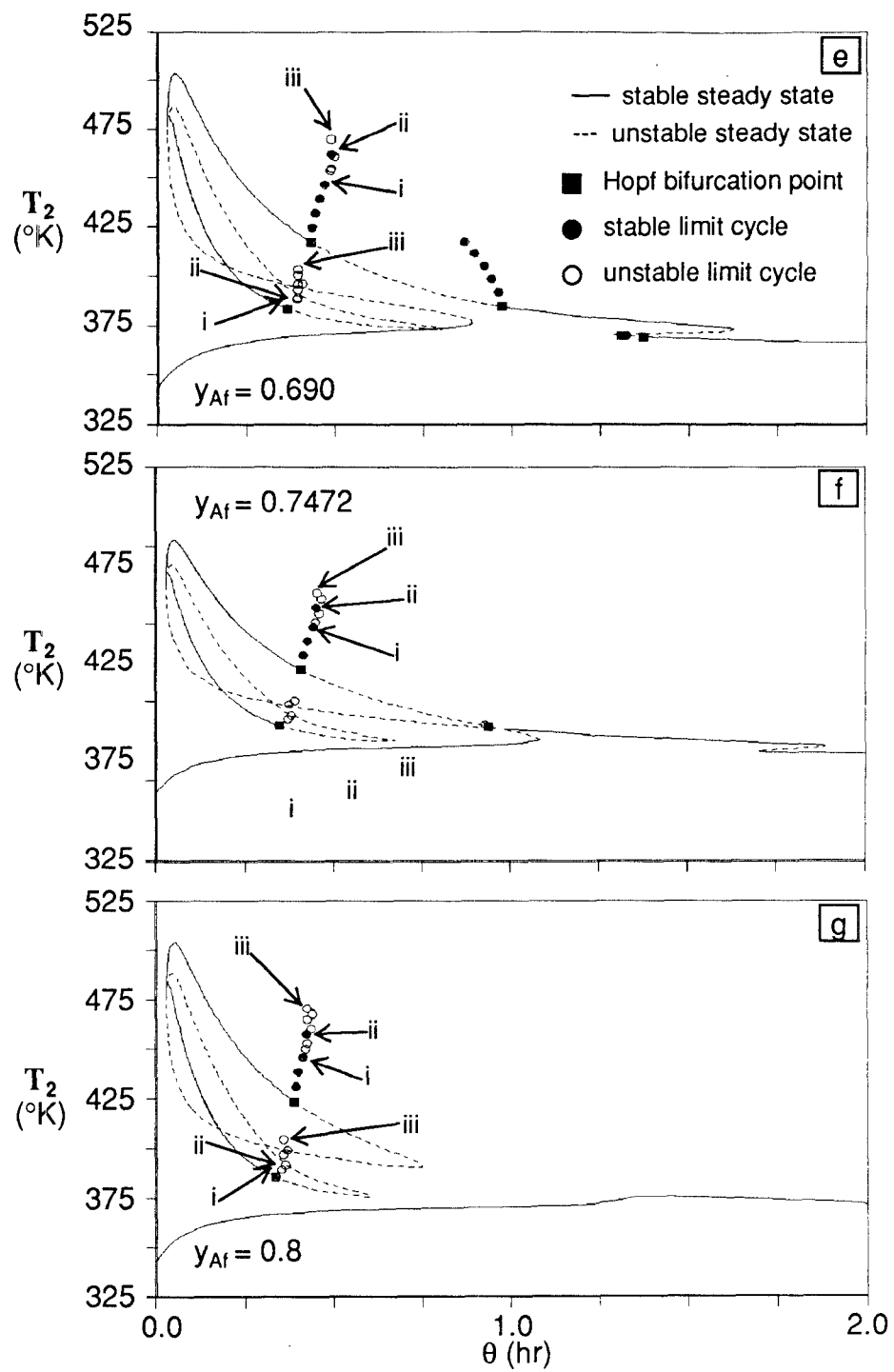
Figure 2.29   (*continued*)
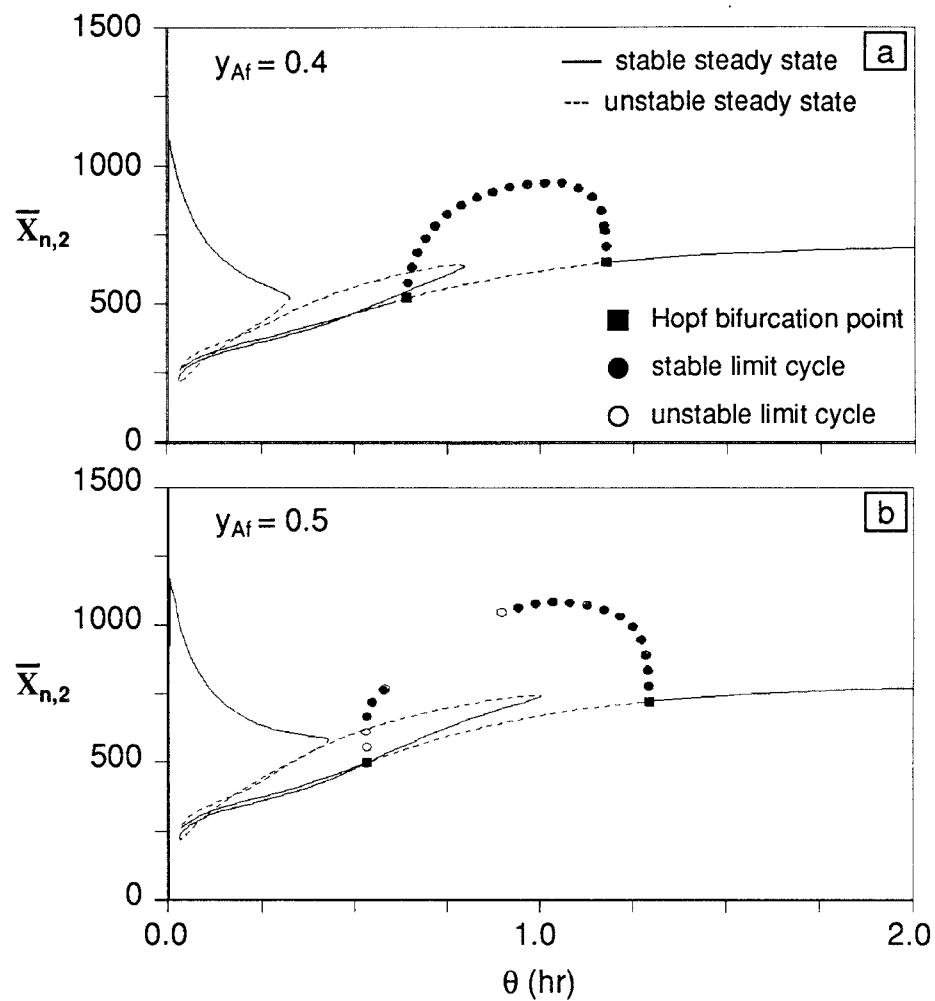
Figure 2.30   Bifurcation diagrams of $\overline{X}_{n,2}$ with different y_{Af}: $f_s = 0.1$, $I_f = 0.025$ mol/l, $T_f = 343$ °K, $T_{c,1} = T_{c,2} = 363$ °K, $\nu = 1$.
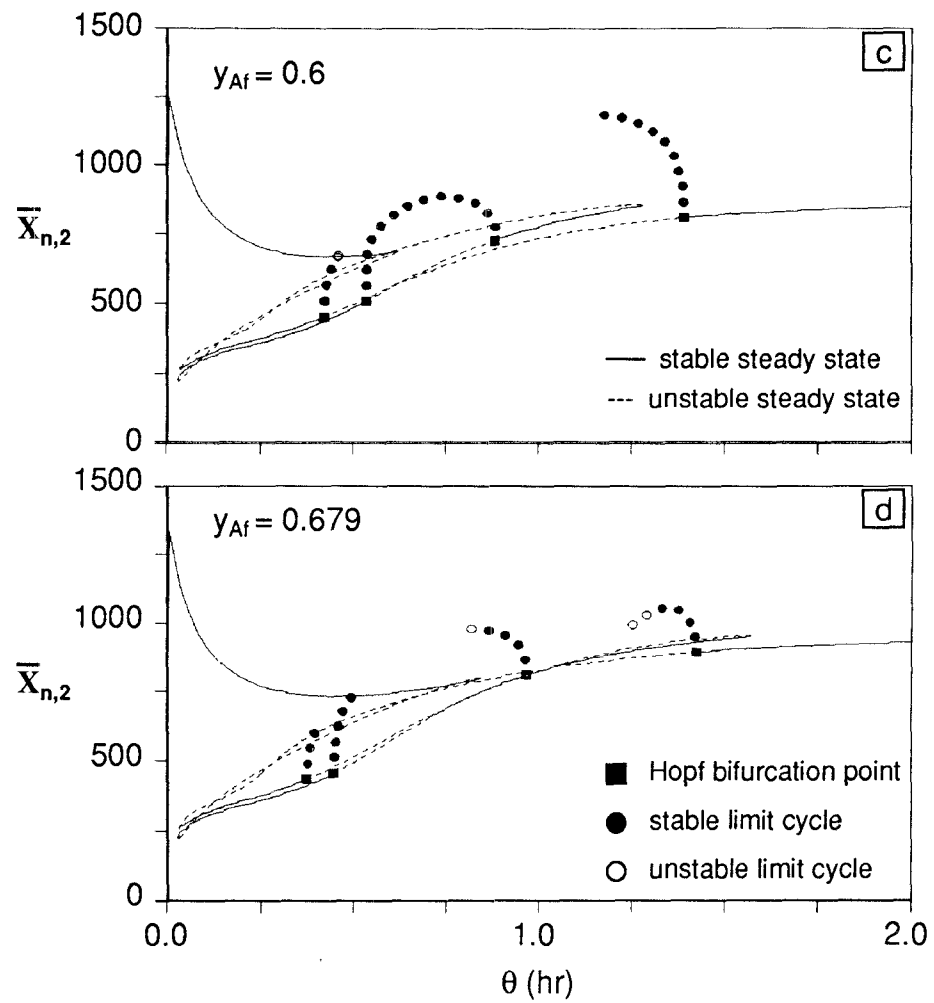
Figure 2.30   (*continued*)
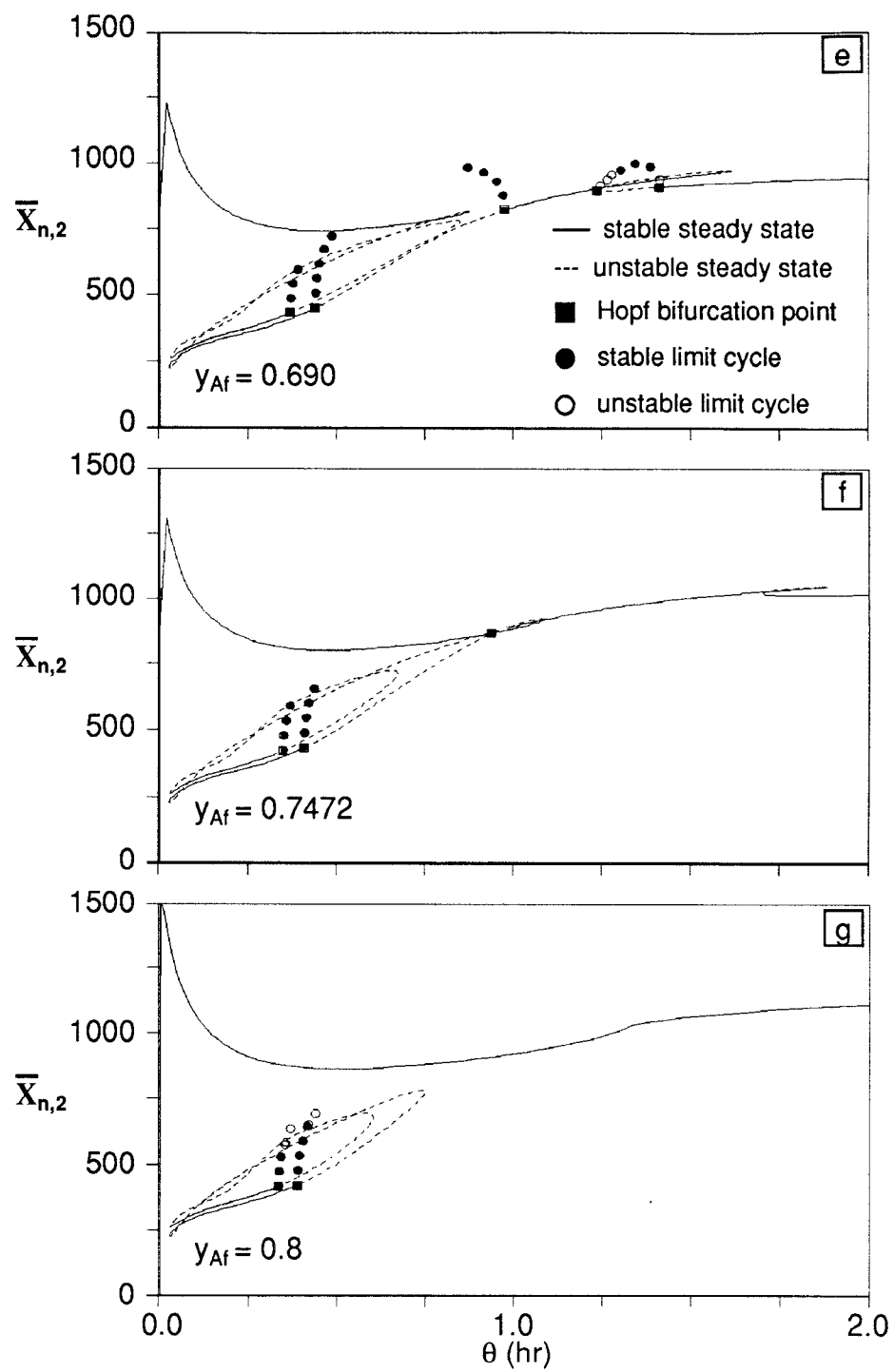
Figure 2.30   (*continued*)
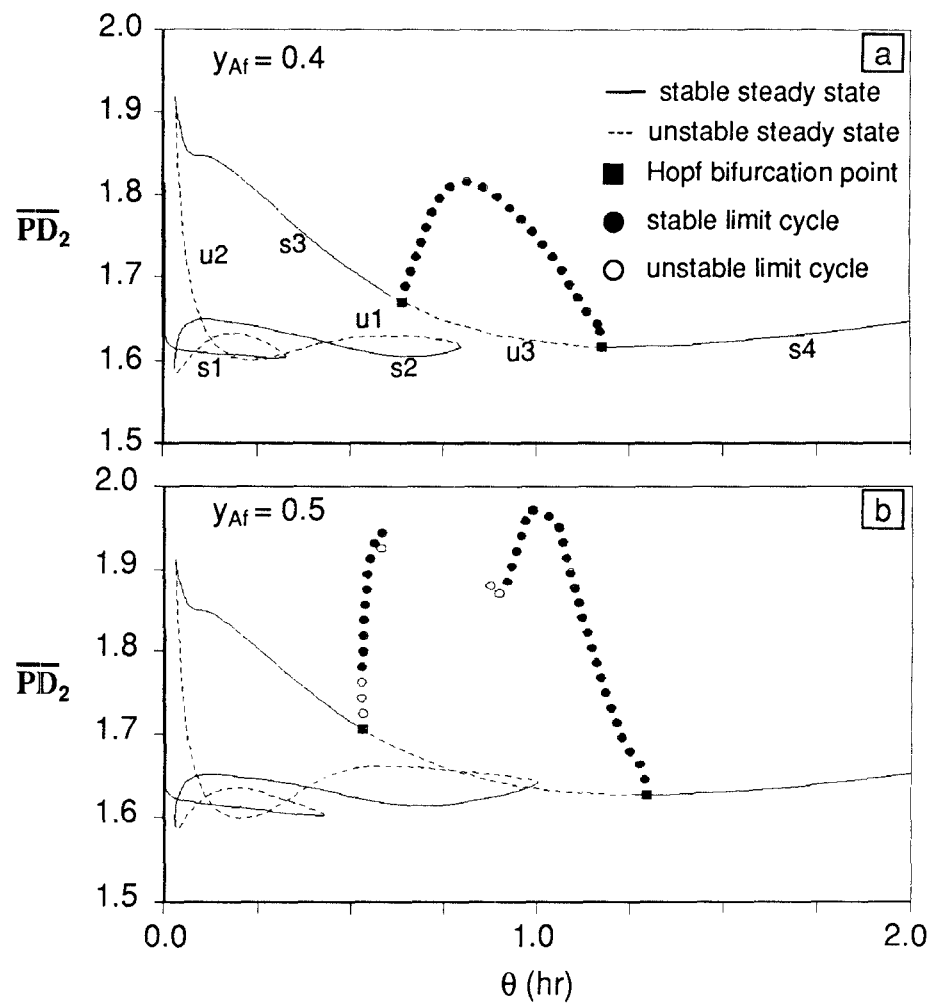
Figure 2.31   Bifurcation diagrams of $\overline{PD_2}$ with different y_{Af}: $f_s = 0.1$,
$I_f = 0.025$ mol/l, $T_f = 343$ °K, $T_{c,1} = T_{c,2} = 363$ °K, $\nu = 1$.
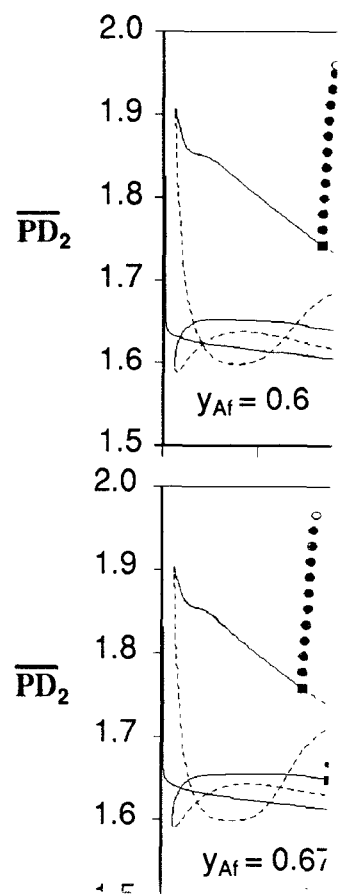
Figure 2.31   (*continued*)
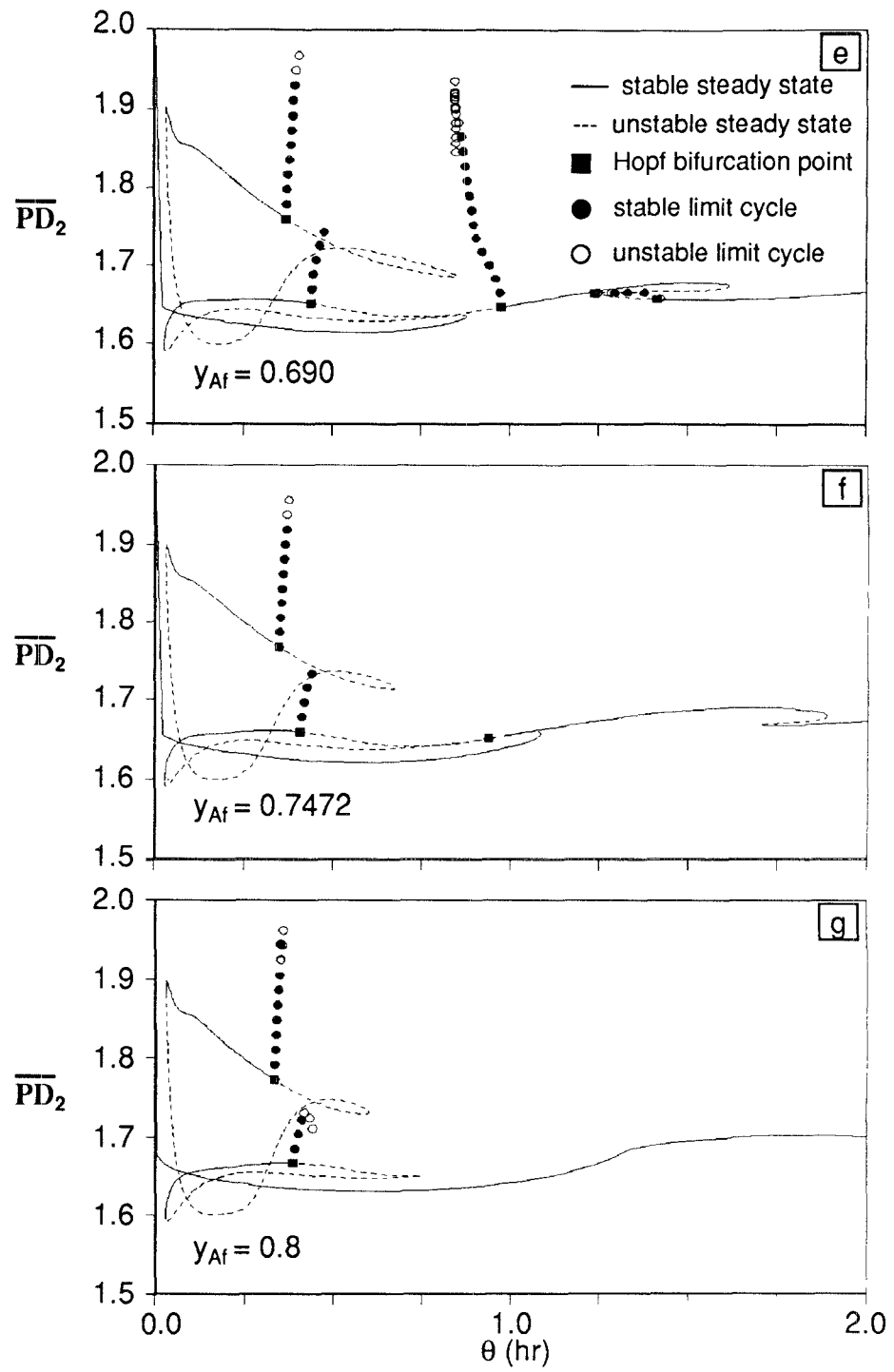
Figure 2.31   (*continued*)

and two isolas; each isola has a Hopf bifurcation off of which a periodic branch bifurcates leading to a period-doubling cascade.

First note that up to five steady states may exist for θ (e.g., $\theta < 0.36$ hr for $y_{Af} = 0.4$) and only three of them are stable. The main solution branch consists of a sequence of steady state [see Figure 2.29a]: (from the left) stable (s1) - unstable (u1) - stable (s2) - unstable (u2) - stable (s3) - unstable (u3) - stable (s4). There are also two Hopf bifurcation points connecting a branch of periodic orbits. All these periodic solutions are asymptotically stable. In the range of intermediate monomer conversion (e.g., $0.3 < X_{1,2} < 0.5$) the steady states are always unstable under the given operating conditions. Although the steady state conversion values are quite different, the steady state temperatures on the lower left branch (s1) and on the upper branch (u3-s4) are very similar.

As y_{Af} is increased to 0.5 (Figure 2.26b), the second reactor exhibits much more complex bifurcation behavior. There is one pair of Hopf bifurcation points as in Figure 2.27a; the branches of periodic orbits are disconnected and they terminate in homoclinics (point iii in Figure 2.27b) where the period of orbits becomes unbounded. Figure 2.27b' shows the details of bifurcation behavior near the left Hopf bifurcation point (HB). Note that there is a periodic limit point (PLP) followed by a branch of stable periodic orbits. The orbits near the Hopf bifurcation points are unstable. There is then a period-doubling (PD) bifurcation from which the two branches of periodic

orbits emanate. The right periodic branch loses its stability and terminates in unstable infinite period (IP) periodic orbits. The left branch bifurcates almost vertically. Note also that there is a second period doubling (SPD) bifurcation off of this branch. This branch eventually terminates in an unstable homoclinic or in infinite period (IP) orbits. As seen in these figures , the amplitudes of oscillations in monomer conversion ($X_{1,2}$) on the periodic branches are quite small; however, the initiator concentrations, the number average degree of polymerization ($\overline{X}_{n,2}$), and the polydispersity ($\overline{PD}_2$) oscillate with much larger amplitudes.

With a further increase in y_{Af} (=0.6) (Figure 2.26c), the branch separates into two branches, and another branch of periodic orbits connects another pair of Hopf bifurcation points. The overall pattern of the emergence of periodic orbits is quite similar to the case of $y_{Af} = 0.5$, as shown in Figure 2.26b. Note that the rightmost periodic orbit terminates in a homoclinic. Figure 2.28c' shows the plot of the steady state temperature of the second reactor vs. the steady state temperature of the first reactor. Here, the loop on the left corresponds to the second loop or isola in the bifurcation diagram, and the loop on the right corresponds to the first loop or isola in the bifurcation diagram. This plot shows, for example, that there is a range of operating conditions for which T_1 is approximately 350 °K, but for which T_2 can range up to 500 °K. For these values of θ, there are several coexisting stable states for the system.

As y_{Af} is increased further to 0.679, the periodic orbits between the Hopf points are disconnected and the second loop becomes larger as illustrated in Figure 2.26d. The lower branch is also extended to the monomer conversion of 0.45. It is interesting to observe in Figure 2.29 that the steady state temperatures near the end of lower branches and in the last segment of upper solution branches are almost identical. In other words, it will be possible to operate the second reactor at high monomer conversion and relatively low temperature. The molecular weights and the polydispersity values are also quite similar. The rightmost branch also has a period doubling bifurcation point (*ii*) and it terminates in a homoclinic (*iii*) as other branches of periodic orbits (Figure 2.27d).

With a further increase in the concentration of t-butyl perbenzoate in the feed (e.g., $y_{Af} = 0.690$), the right-most branch of periodic orbits is connected to the stationary branch by Hopf bifurcation points at both ends (Figure 2.26e). For slightly larger y_{Af}, this branch has disappeared. Figures 2.32 and 2.33 exhibits graphs and phase diagrams for typical periodic orbits. These particular ones exist for $y_{Af} = 0.690$. They are members of the branch of periodic orbits associated with the Hopf bifurcation on the isola, with θ approximately 0.4. From the Hopf point, a branch of periodic orbit bifurcates, terminating in a homoclinic orbit. From this branch a branch of period-doubling orbits bifurcates. A typical member of the branch is exhibited in Figure 2.32a and 2.33a. For much of the time, the orbit is near stationary point.
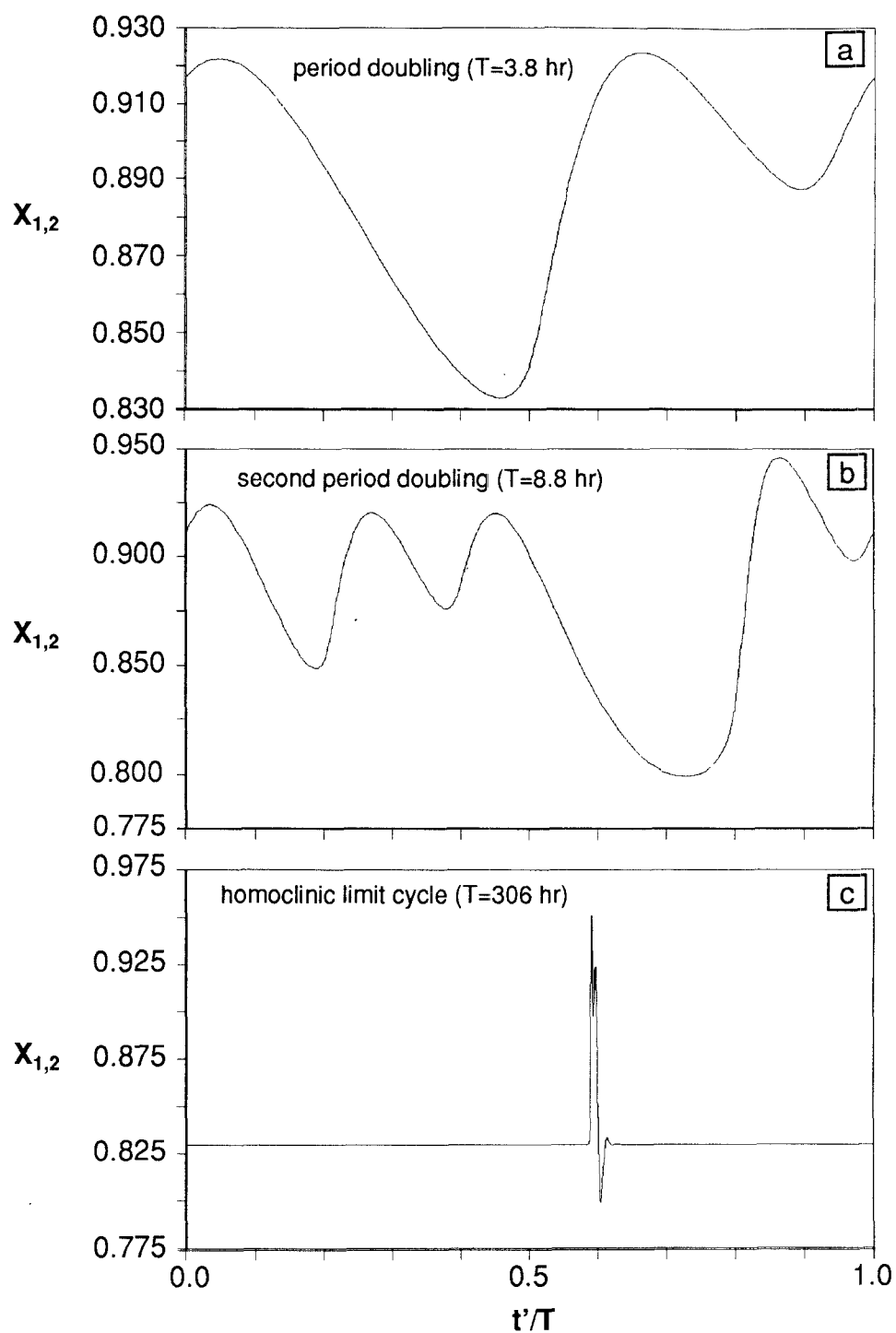
Figure 2.32   Typical periodic behavior of the second reactor: $f_s = 0.1$, $I_f = 0.025$ mol/l, $y_{Af} = 0.690$, $T_f = 343$ °K, $T_{c,1} = T_{c,2} = 363$ °K, $\nu = 1$.
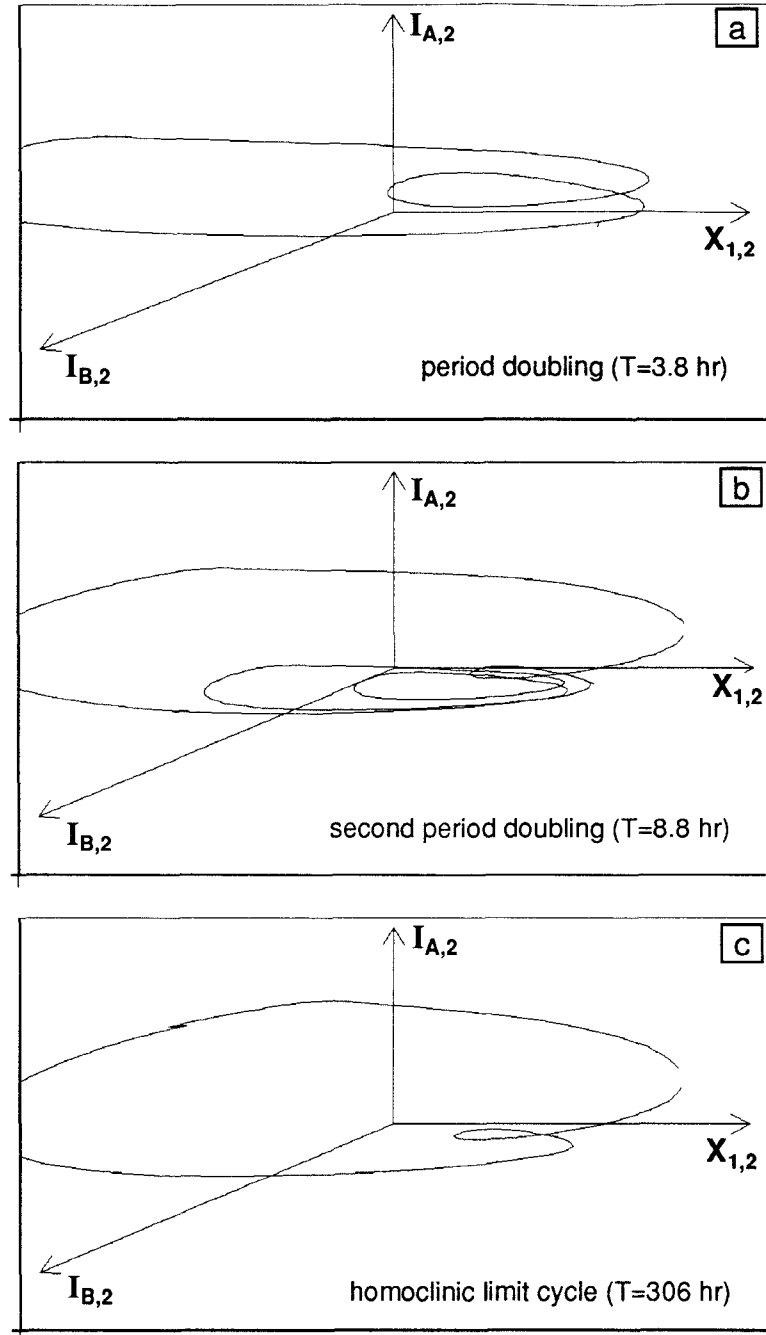
Figure 2.33   Phase plane portraits of typical periodic behavior of the second reactor: $f_s = 0.1$, $I_f = 0.025$ mol/l, $y_{Af} = 0.690k$, $T_f = 343$ °K, $T_{c,1} = T_{c,2} = 363$ °K, $\nu = 1$.

In Figure 2.33c, note that stationary point is near the small jog in the orbit near the left (this jog corresponds to the dip seen in Figure 2.32c). In fact, there is a period doubling cascade of branches bifurcating from the branch; each of these branches terminates in a homoclinic. A typical member of the second period-doubling branch is exhibited in Figure 2.32b and 2.33b

As y_{Af} approaches 0.7472, the right-most branch of periodic orbits disappears and the appearance of an isola is evident and the lower branch is connected to the upper branch as shown in Figure 2.26f. Note that in this case the right-most Hopf bifurcation is not on the main branch of stationary points, but rather on the isola. In Figure 2.26g, the same variables are shown for $y_{Af} = 0.8$. The two isola can be seen, each with a branch of periodic orbits and period doubling. Note that now there is a stable branch where no periodic orbits exist.

So far we have examined the bifurcation behavior of the second reactor which has the same volume as the first reactor. In practical situations, these two reactors may have different reactor volumes. In Figures 34 and 35, the effect of volume ratio ($\nu = V_2/V_1$) is shown for $y_{Af} = 0.5$. The first reactor is fixed at nominal operating conditions [i.e., $\theta = 0.5$, $T_{c,1} = 343$ °K ($\delta_1 = 0.0$)] and the bifurcation parameter is ν, ranging from 0 to 2. Of course, the behavior of the first reactor is independent of ν; only the change of behavior in the second reactor is of interest. The coolant temperature in the second reactor is set at three different values, namely $\delta_2 = 0.029$, $\delta_2 = 0.058$,
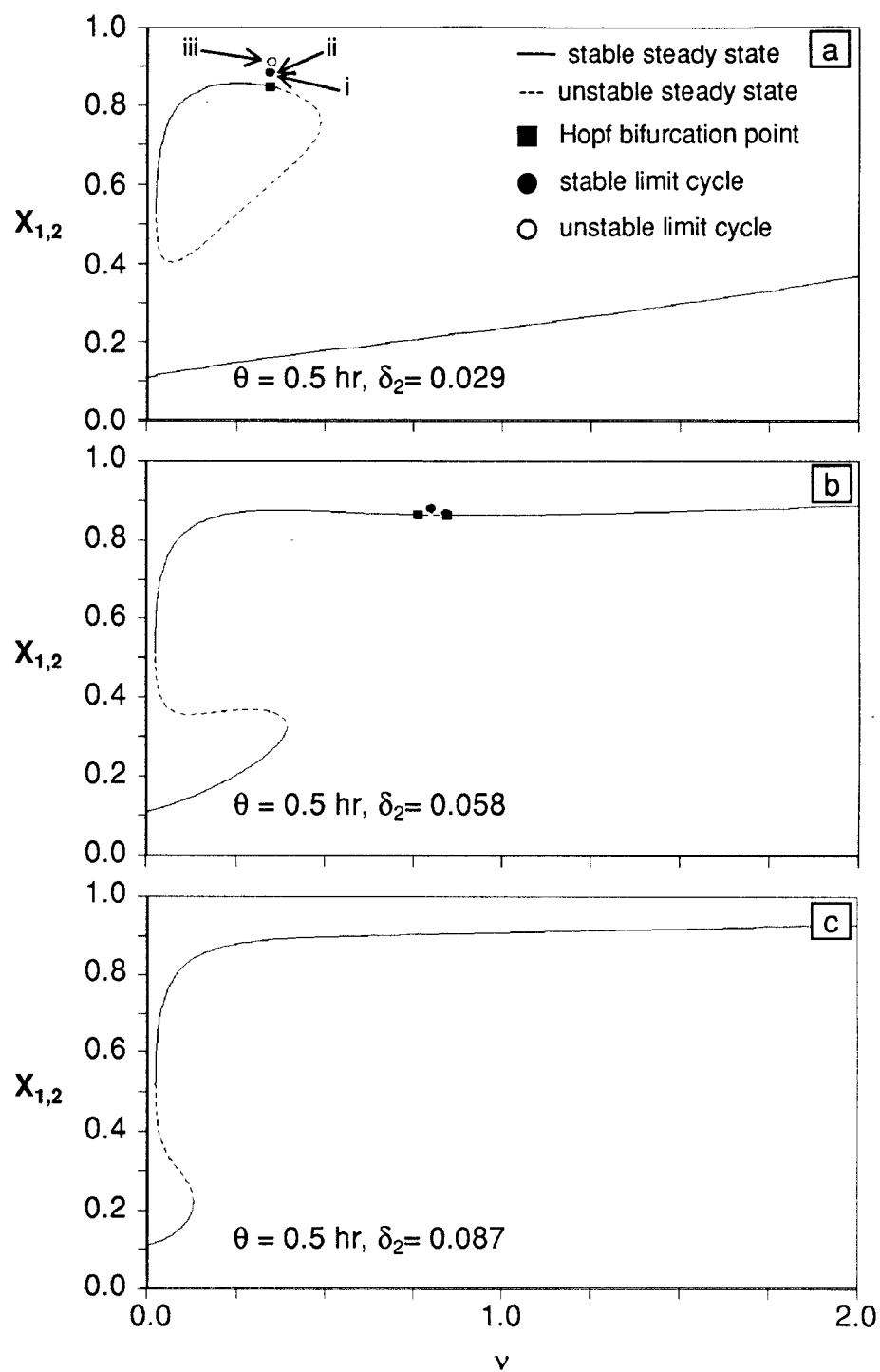
Figure 2.34   Effect of volume ratio (ν) on $X_{1,2}$ for different coolant temperatures in the second reactor: $f_s = 0.1$, $I_f = 0.025$ mol/l, $y_{Af} = 0.5$, $T_f = 343$ °K, $T_{c,1} = 343$ °K, $\theta = 0.5$ hr.
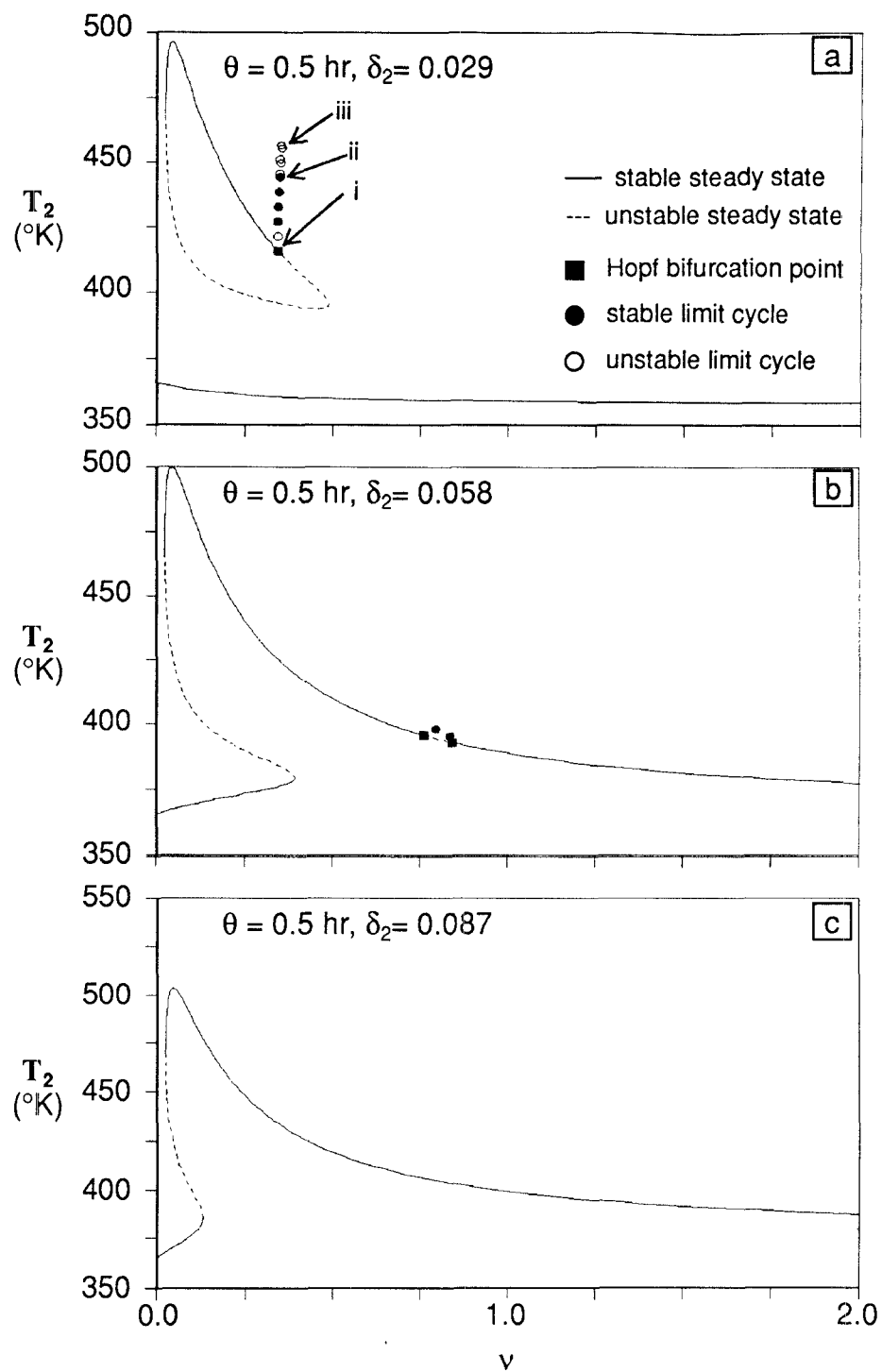
Figure 2.35   Effect of volume ratio (ν) on T_2 for different coolant temperatures in the second reactor: $f_s = 0.1$, $I_f = 0.025$ mol/l, $y_{Af} = 0.5$, $T_f = 343$ °K, $T_{c,1} = 343$ °K, $\theta = 0.5$ hr.

$\delta_2 = 0.087$, corresponding to temperatures 353, 363, 373 °K, respectively. Again, there is a loop in the branch of steady states which breaks off to form an isola, along with the appearance of Hopf bifurcation, periodic branches and chaotic regimes.

In the second reactor, the coolant temperature (δ_2) and the heat transfer coefficient (α_2) are two of the important reactor parameters. Figure 2.36 shows the steady state behavior regions for the first reactor (a) and the second reactor (b). When the first reactor operates in the region III (a point marked by • in Figure 2.36a), the second reactor may exhibit four different steady state behavior as shown in Figure 2.36b with δ_2 and α_2 as free parameters. Here Γ_1 and Γ_2 represent the hysteresis variety and the isola variety, respectively. Note that for large values of α_2, S-shaped steady state curves are always observed for all values of coolant temperature. This indicates that poor heat transfer from the reactor to the cooling jacket is one of the major causes for strong process nonlinearity. Figure 2.36b also illustrates that the steady state behavior of the second reactor can vary with the operating conditions of the first reactor.

In Figures 2.37 and 2.38, the bifurcation parameter is the coolant temperature of the second reactor (δ_2), with the first reactor at a given steady state (marked by • in Figure 2.26a). α_2 value used in these figures is the same as α_1 for the first reactor and only δ_2 is varied. The first reactor is fixed at a steady state value with $y_{Af} = 0.5$, $\theta = 0.5$, and with $\delta_1 = 0.0$. The volume
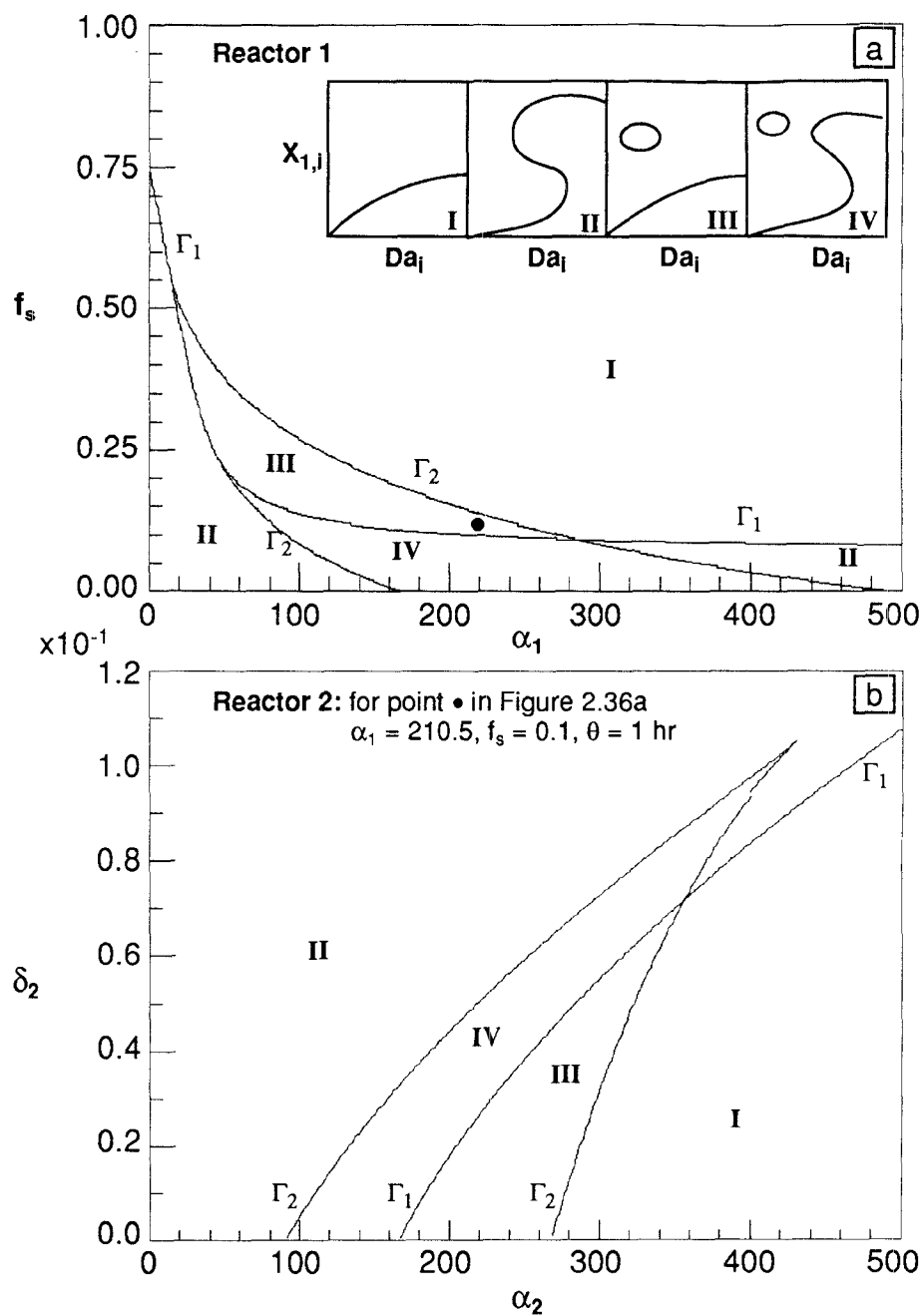
Figure 2.36   Steady state behavior regions in the first and the second reactor: I_f = 0.025 mol/l, y_{Af} = 0.5, T_f = 343 °K, $T_{c,1}$ = 343 °K.

111
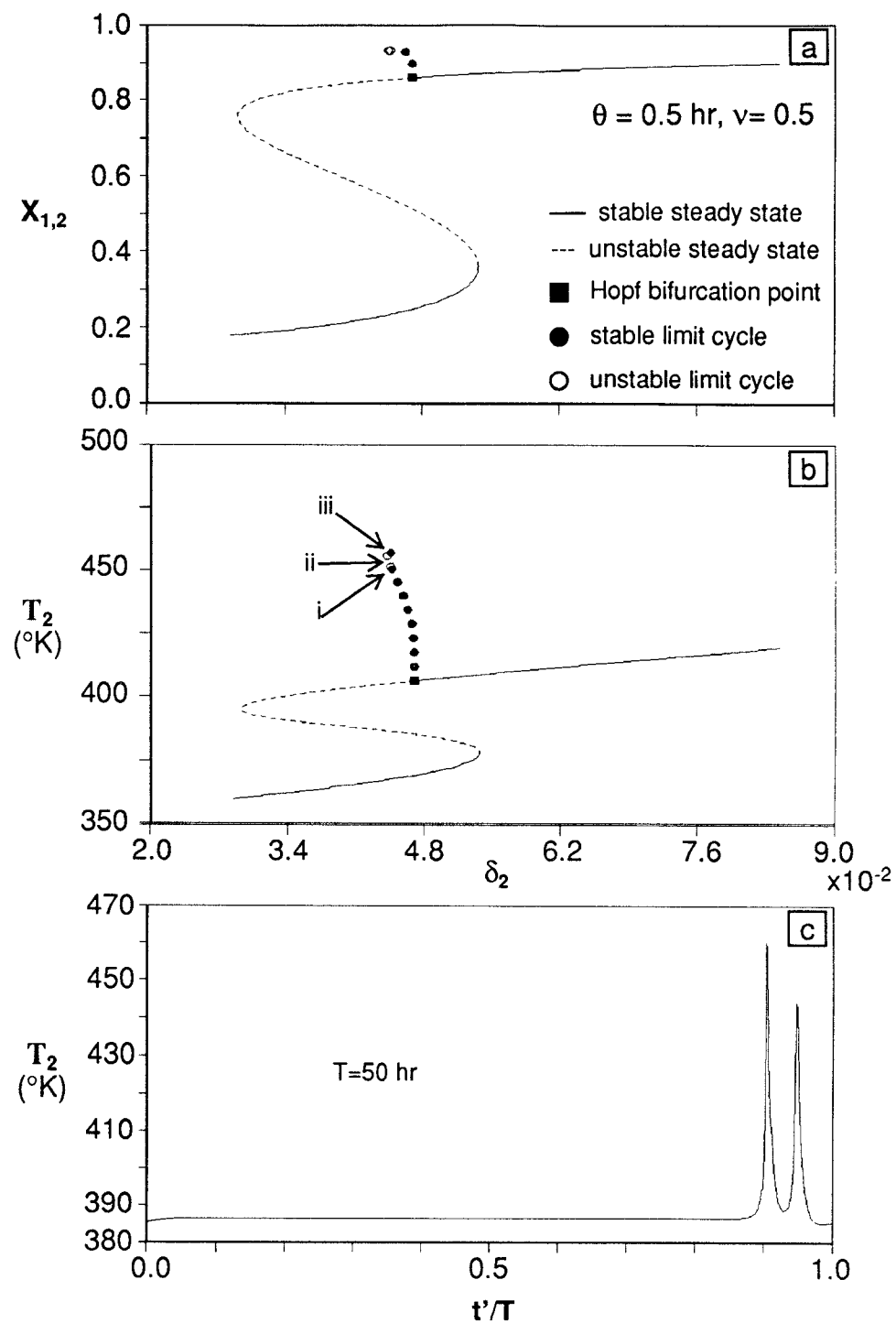
Figure 2.37   Effect of coolant temperature of the second reactor (δ_2) on the reactor behavior: $f_s=$ 0.1, $I_f=$ 0.025 mol/l, $y_{Af}=$ 0.5, $T_f=$ 343 °K, $T_{c,1}=$ 343 °K, $\theta=$ 0.5 hr, $\nu=$ 0.5.
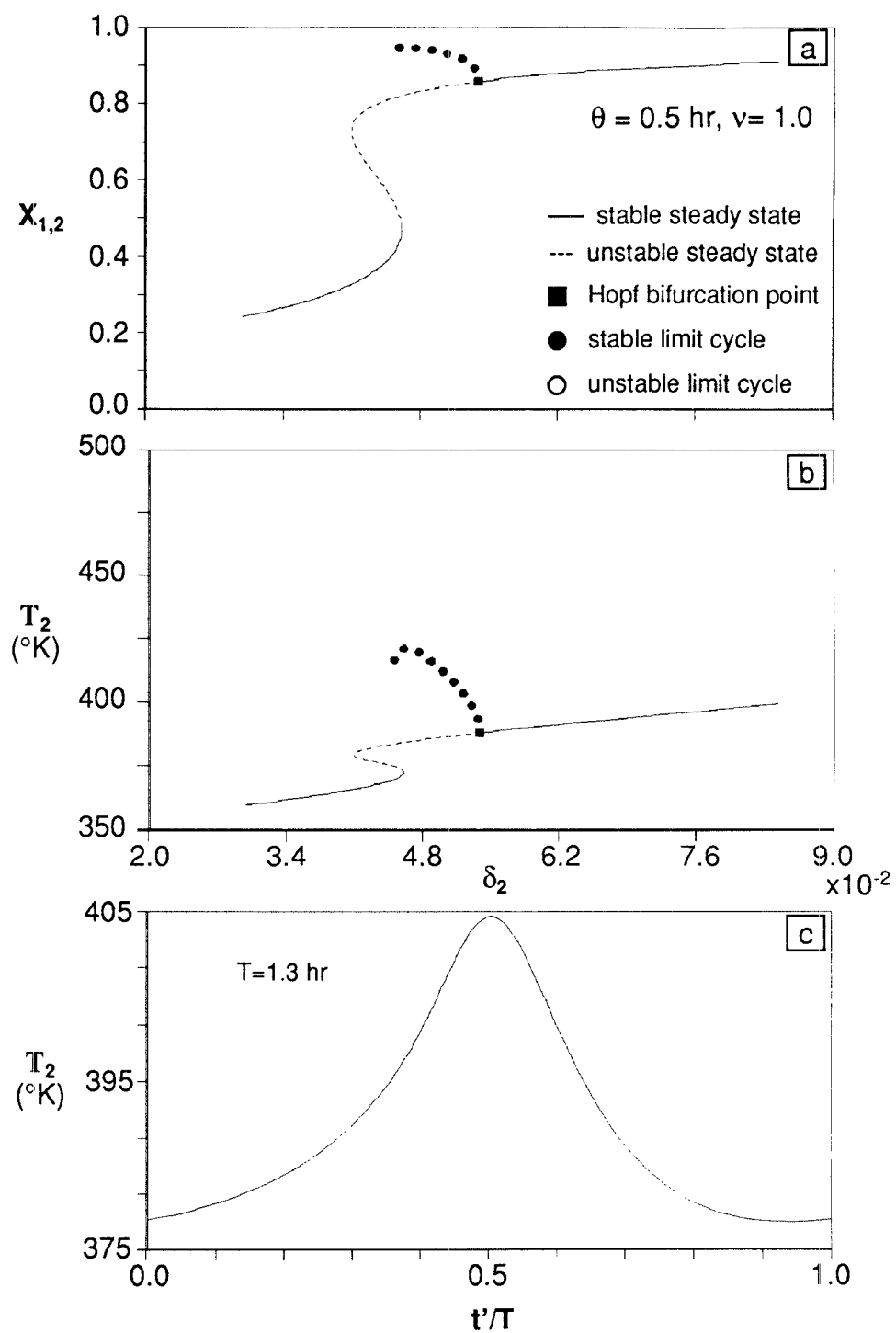
Figure 2.38   Effect of coolant temperature of the second reactor (δ_2) on the reactor behavior:$f_s = 0.1$, $I_f = 0.025$ mol/l, $y_{Af} = 0.5$, $T_f = 343$ °K, $T_{c,1} = 343$ °K, $\theta = 0.5$ hr, $\nu = 1.0$.

ratio ν is set at 0.5 (Figure 2.37) and 1.0 (Figure 2.38). In both case, there is an "S" curve of steady states with a Hopf bifurcation and branches of periodic orbits terminating in homoclinics. For $\nu = 0.5$, there is a period doubling cascade and the resulting chaotic regime, which is evidently not there for $\nu = 1.0$. Graphs of typical periodic orbits are shown in Figures 2.37c and 2.38c. Here, T is the period of oscillation. For $\nu = 0.5$, the orbit is near the homoclinic on the period-doubling branch; for $\nu = 1.0$ is midway on the periodic orbit.

For the cases illustrated in Figures 2.26~2.31, the coolant temperatures in the two reactors were same. In practical operating conditions, the coolant temperature in the second reactor can be different from that in the first reactor. Figures 2.39 and 2.40 show the bifurcation diagrams for the first and the second reactors operating at different coolant temperatures. The coolant temperatures for the first and the second reactor are 343 °K and 360 °K, respectively. These diagrams are similar to those shown in Figure 2.26b. Note that the second reactor exhibits a considerably different dynamic behavior from the first reactor. Figures 2.41 and 2.42 show the transient behavior of the two reactors when the initiator feed composition is changed from 0.5 to 0.35 (30 % less slow initiator in the feed). The initial operating points for both reactors are marked as A in Figures 2.39 and 2.40. Note that the first reactor moves smoothly toward a new stable steady state in less than 3 hours; however, the second reactor, after about 17 hours, runs away to an upper
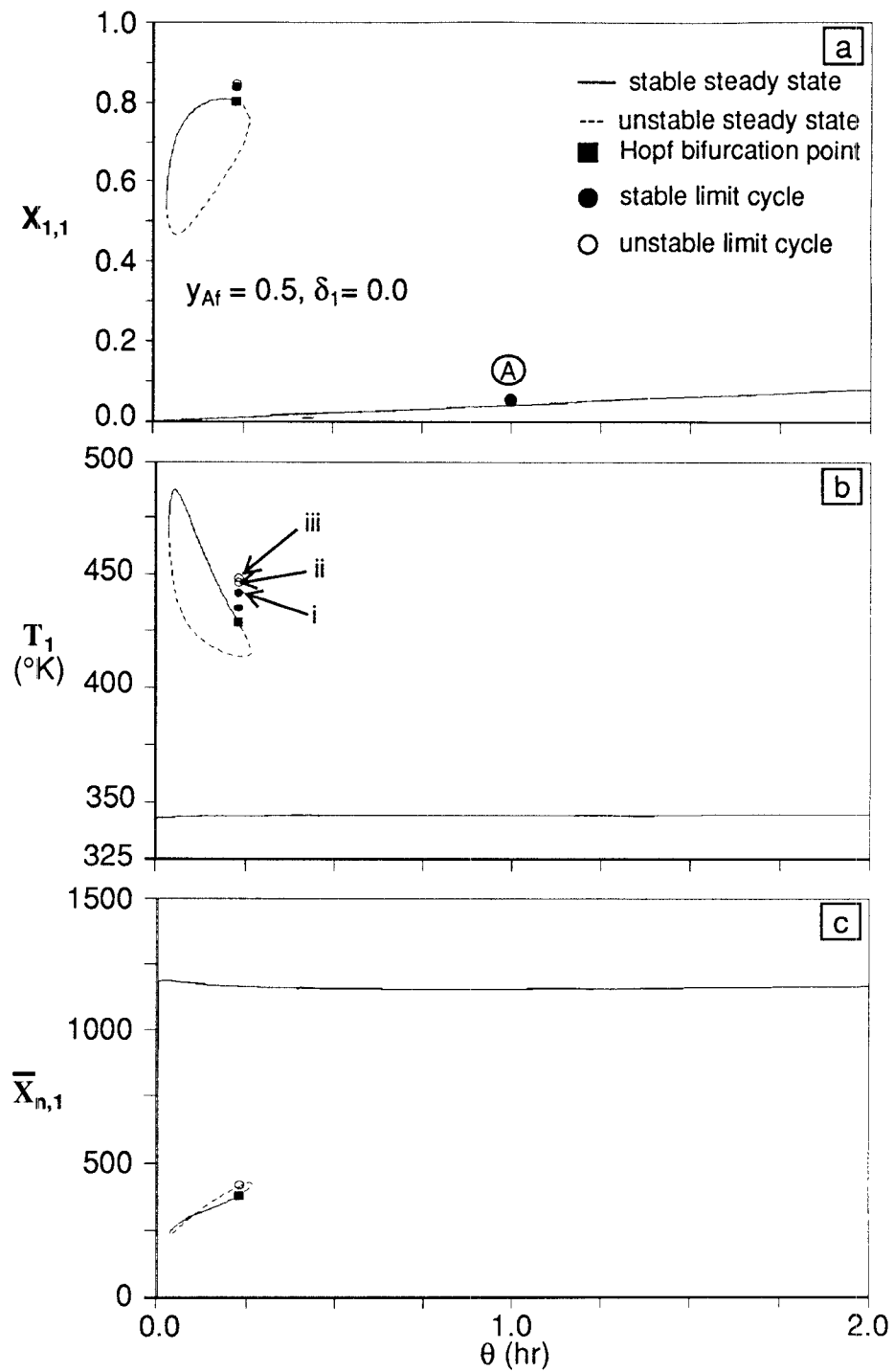
Figure 2.39   Bifurcation diagram of the first reactor with different coolant
temperatures: $f_s= 0.1$, $I_f= 0.025$ mol/l, $y_{Af} = 0.5$, $T_f= 343$
°K, $T_{c,1}= 343$ °K, $T_{c,2}= 363$ °K, $\nu = 1.0$.
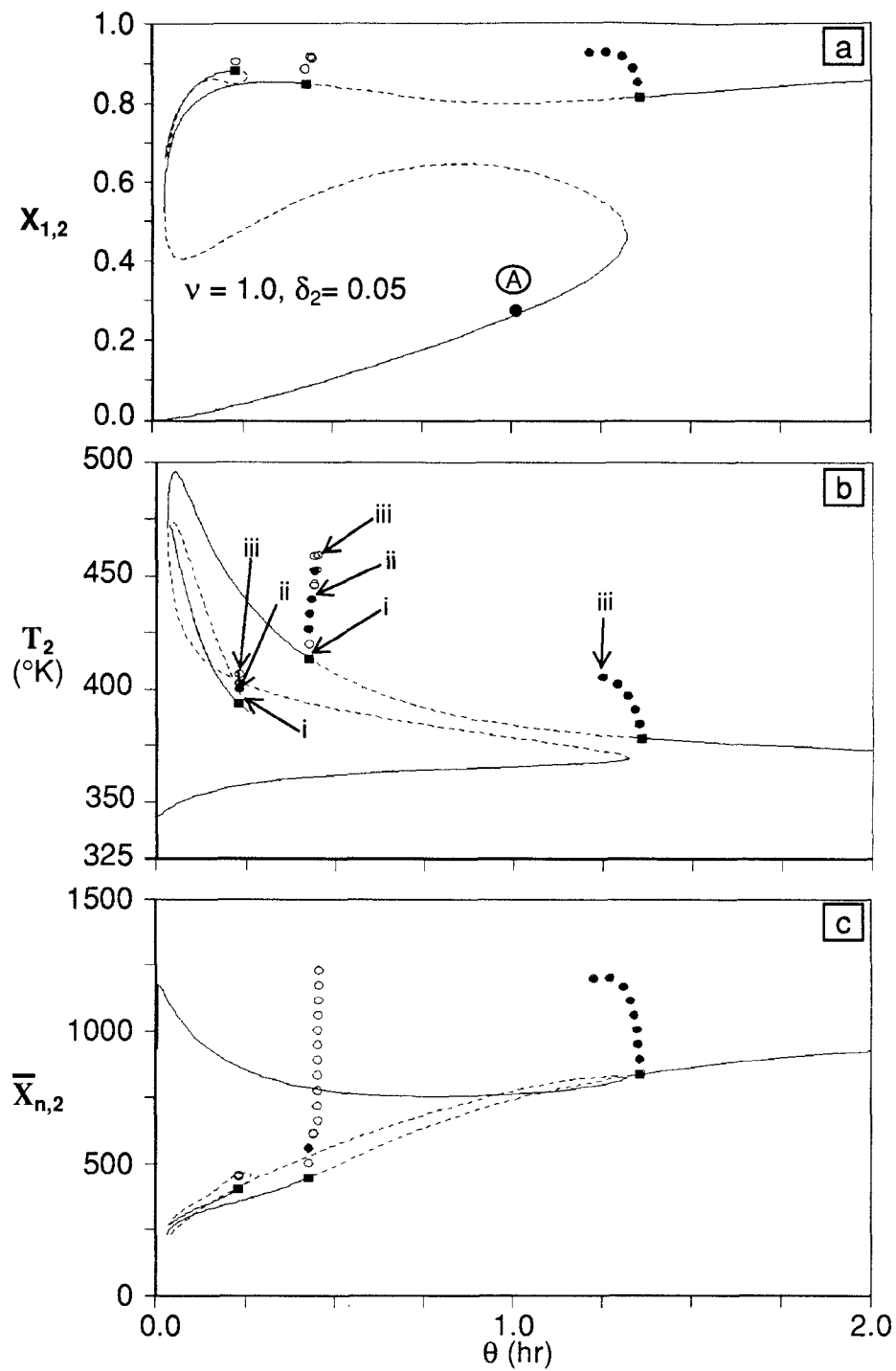
Figure 2.40   Bifurcation diagram of the second reactor with different coolant temperatures: $f_s = 0.1$, $I_f = 0.025$ mol/l, $y_{Af} = 0.5$, $T_f = 343$ °K, $T_{c,1} = 343$ °K, $T_{c,2} = 363$ °K, $\nu = 1.0$.
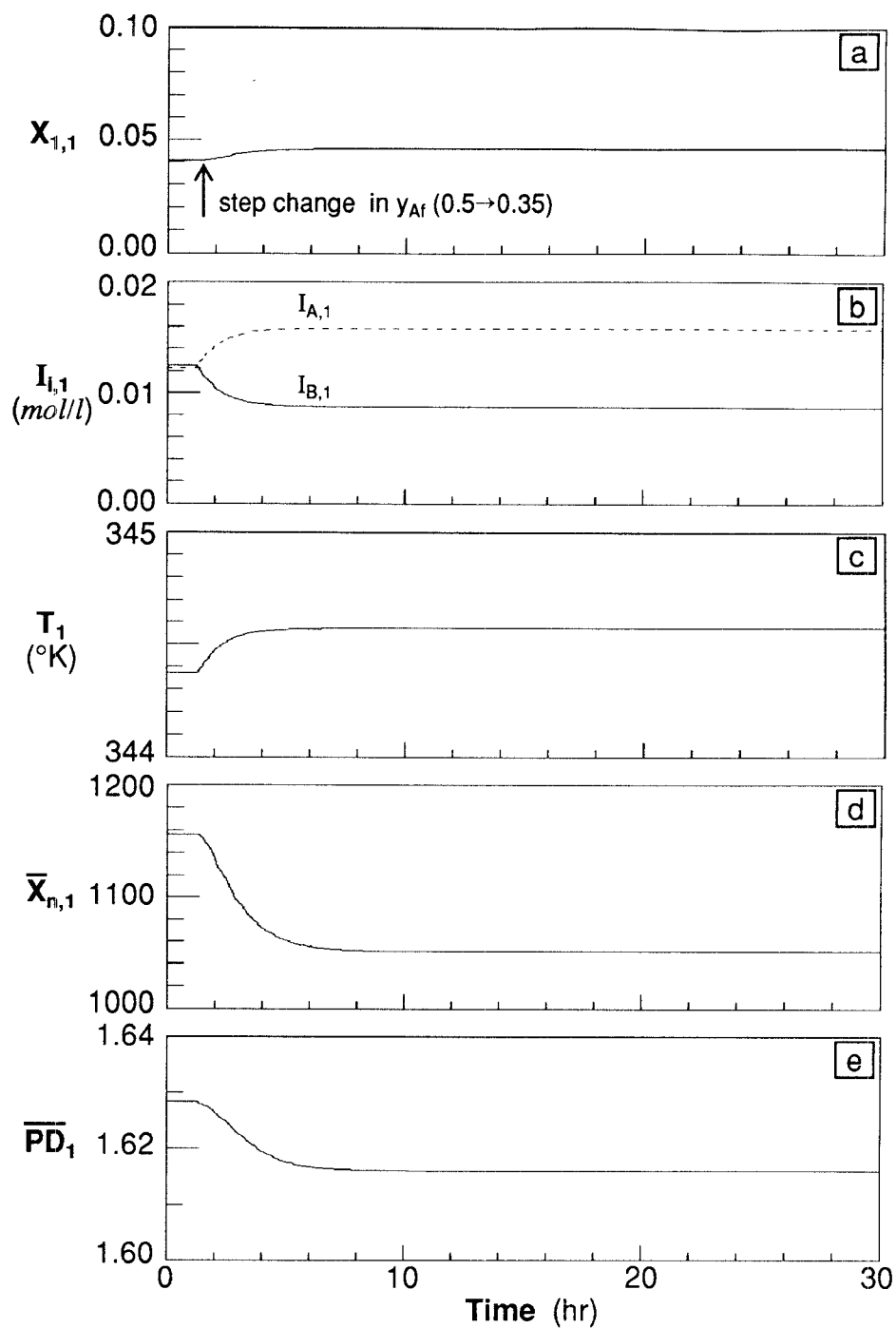
Figure 2.41   Transient response of the first reactor to the step change in y_{Af} during the steady state operation: $f_s = 0.1$, $I_f = 0.025$ mol/l, $y_{Af} = 0.5$, $T_f = 343$ °K, $T_{c,1} = 343$ °K, $T_{c,2} = 363$ °K, $\theta = 1.0$ hr, $\nu = 1.0$.
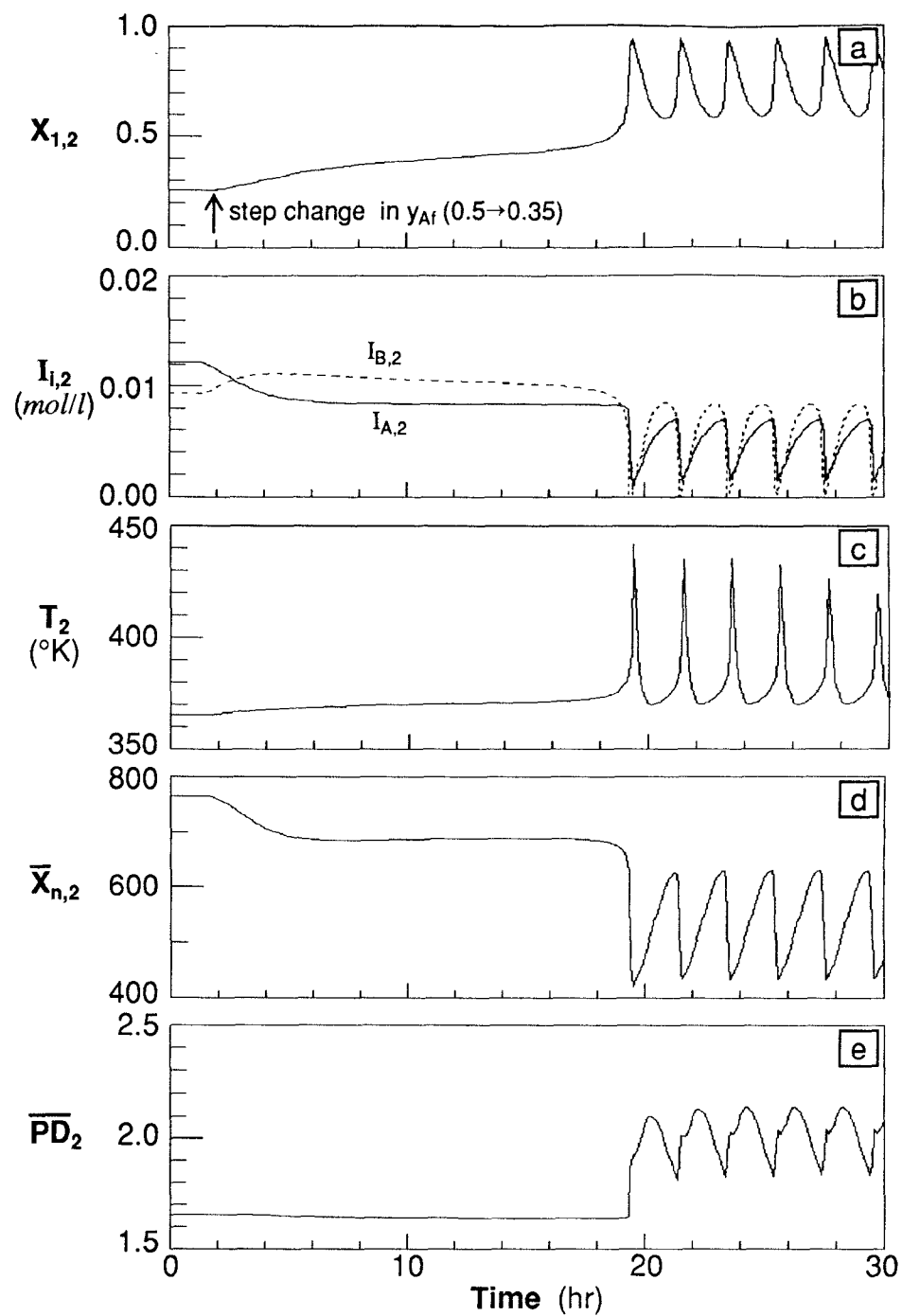
Figure 2.42   Transient response of the second reactor to the step change in y_{Af} during the steady state operation: $f_s = 0.1$, $I_f = 0.025$ mol/l, $y_{Af} = 0.5$, $T_f = 343$ °K, $T_{c,1} = 343$ °K, $T_{c,2} = 363$ °K, $\theta = 1.0$ hr, $\nu = 1.0$.

unstable steady state in an oscillatory manner. The temperature surge is as large as 75 °K. The polymer molecular weight also varies with a large amplitude of oscillation. Such behavior as illustrated in Figure 2.42 can lead to a potentially very dangerous situation. Similar behavior is also observed when the total initiator feed concentration is changed from 0.025 to 0.033 mol/l (Figures 2.43 and 2.44). Figures 2.45 and 2.46 illustrate the reactor transients when the residence time is increased from 1.0 to 1.35 hour. Again, the second reactor exhibits an oscillatory behavior. In this example, the effect of residence time variation on the reactor temperature and the polymer molecular weight is not as large as in the previous examples.
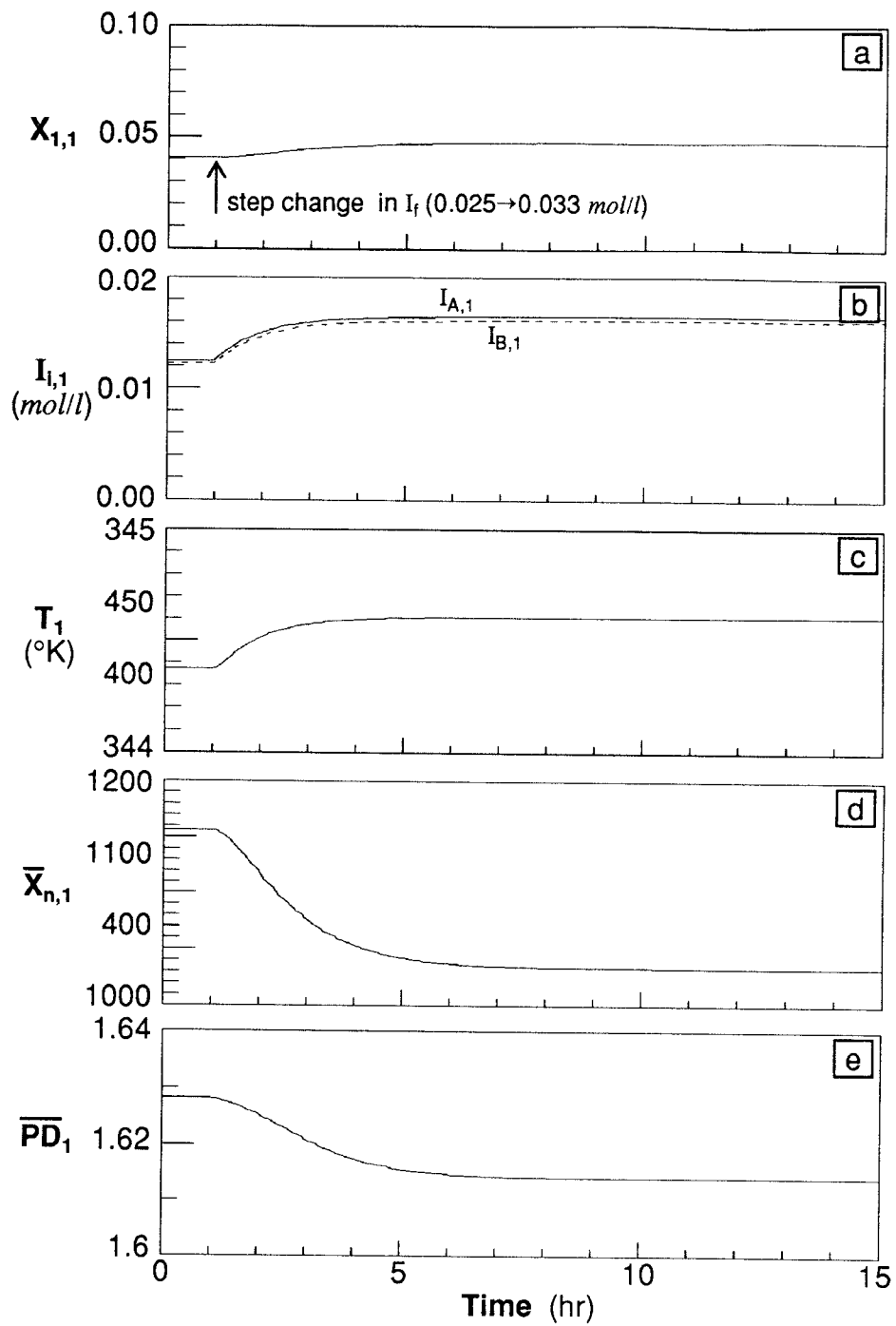
Figure 2.43   Transient response of the first reactor to the step change in I_f during the steady state operation: $f_s = 0.1$, $I_f = 0.025$ mol/l, $y_{Af} = 0.5$, $T_f = 343$ °K, $T_{c,1} = 343$ °K, $T_{c,2} = 363$ °K, $\theta = 1.0$ hr, $\nu = 1.0$.
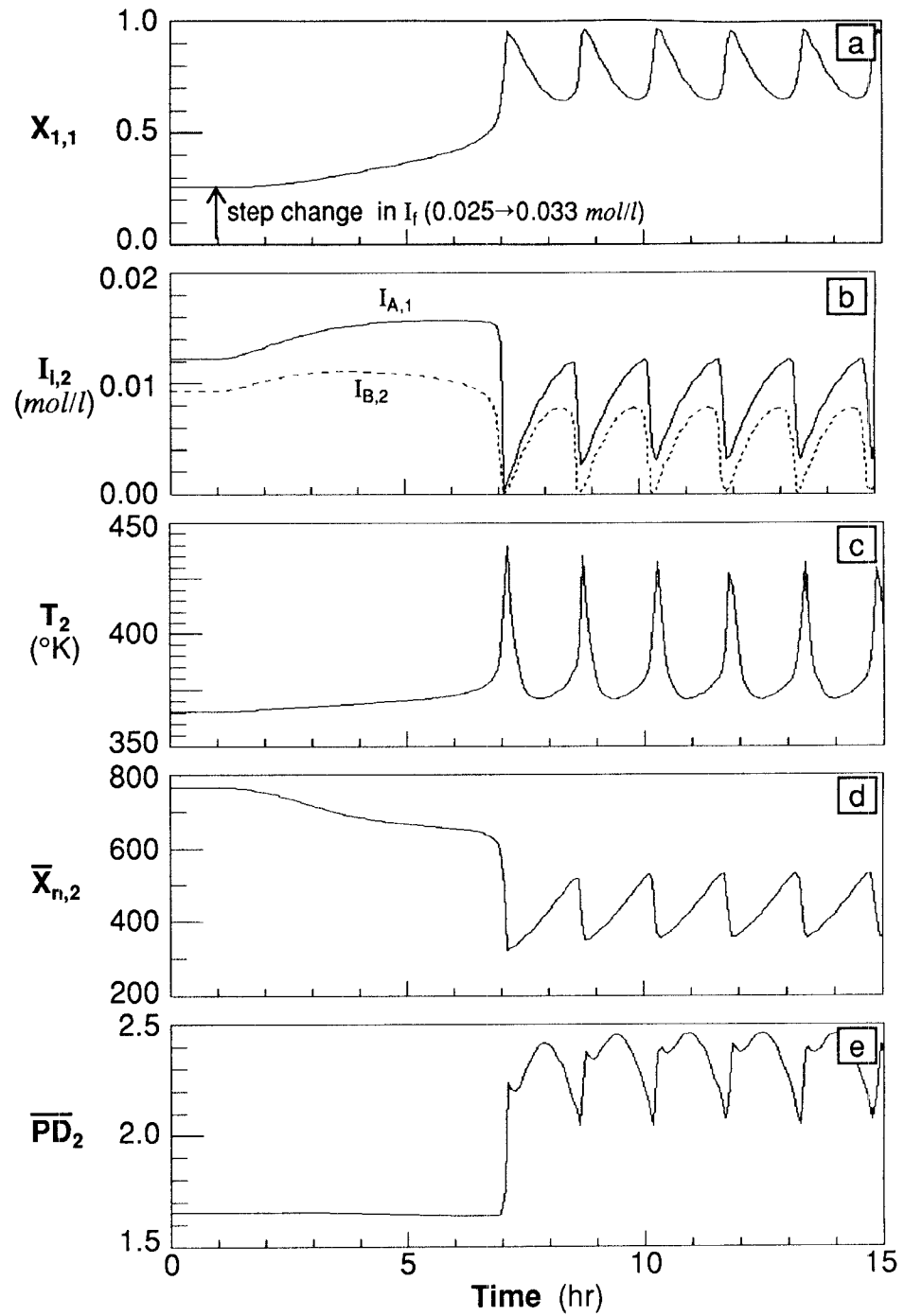
Figure 2.44   Transient response of the second reactor to the step change
in I_f during the steady state operation: f_s= 0.1, I_f= 0.025
mol/l, y_{Af} = 0.5, T_f= 343 °K, $T_{c,1}$= 343 °K, $T_{c,2}$= 363 °K,
θ = 1.0 hr, ν = 1.0.

121
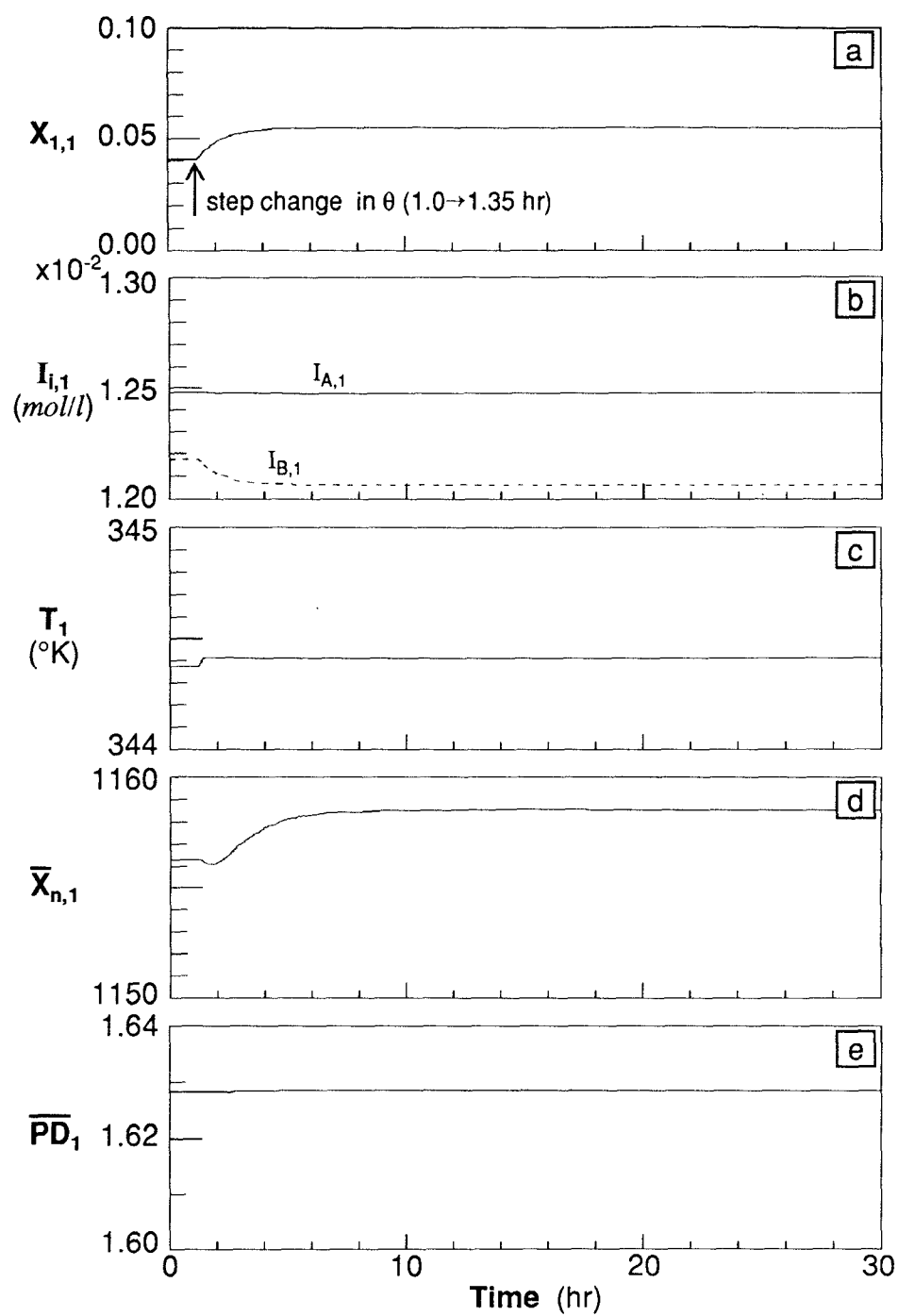
Figure 2.45   Transient response of the first reactor to the step change in θ during the steady state operation: $f_s = 0.1$, $I_f = 0.025$ mol/l, $y_{Af} = 0.5$, $T_f = 343$ °K, $T_{c,1} = 343$ °K, $T_{c,2} = 363$ °K, $\theta = 1.0$ hr, $\nu = 1.0$.
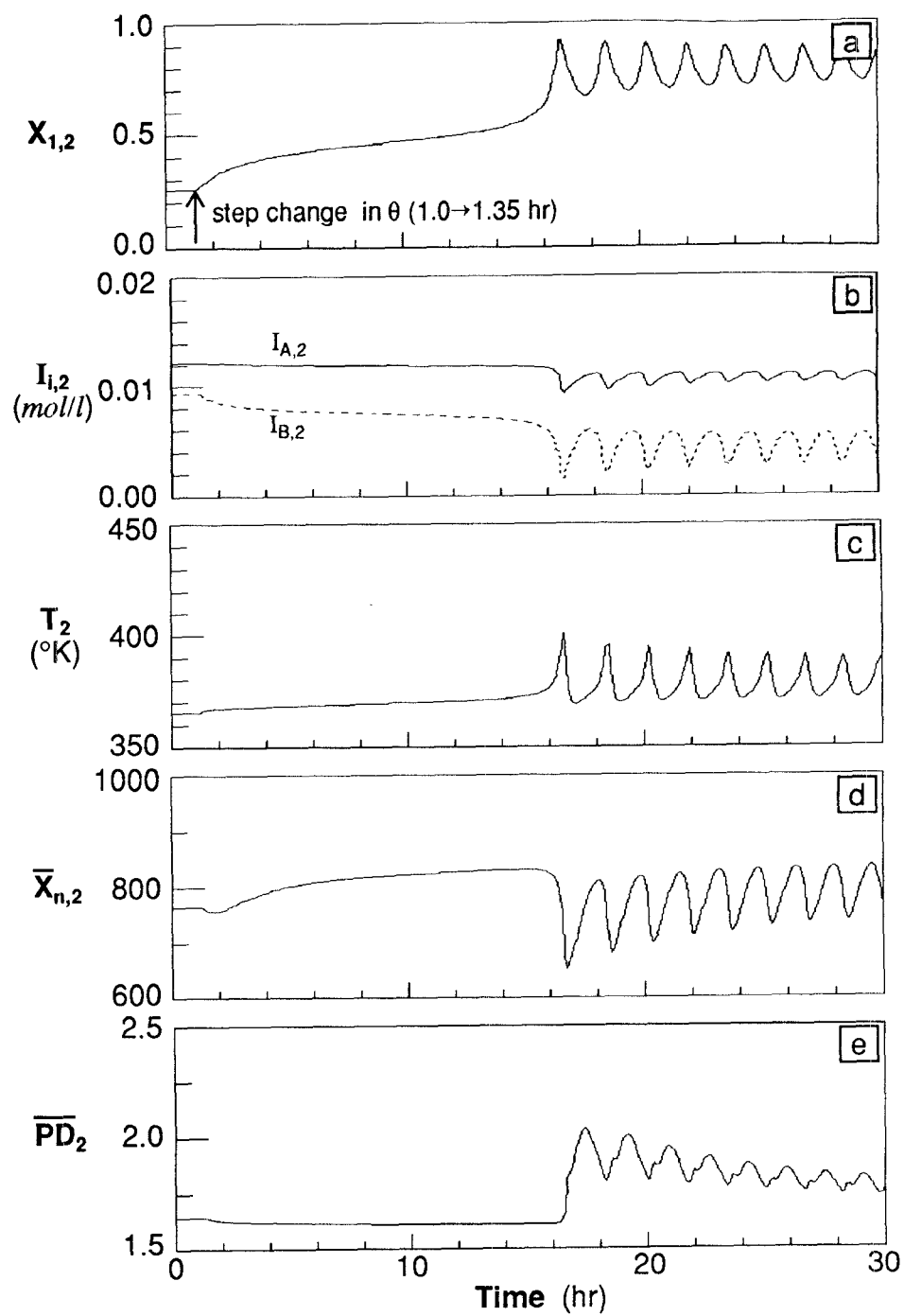
Figure 2.46   Transient response of the second reactor to the step change
in θ during the steady state operation: $f_s = 0.1$, $I_f = 0.025$
mol/l, $y_{Af} = 0.5$, $T_f = 343$ °K, $T_{c,1} = 343$ °K, $T_{c,2} = 363$ °K,
$\theta = 1.0$ hr, $\nu = 1.0$.

2.6. Conclusions

The bifurcation behavior of a cascade of two continuous rectors has been analyzed for styrene solution polymerization with a binary mixture of monofunctional initiators, viz, t-butyl perbenzoate and benzoyl peroxide. The kinetic model used in the model includes the gel-effect and thermal initiation. Compared with single monofunctional initiator systems, the mixed initiator systems exhibit more complex reactor dynamics depending on the feed initiator composition. It has been shown that the polymerization reactor with a binary initiator mixture exhibits quite rich dynamic behavior for some operating conditions. It has been observed that complex bifurcation behavior such as secondary or higher-order bifurcation of a periodic branch and annihilation of multiple periodic branches occur for certain initiator feed compositions. More specifically, multiple Hopf bifurcation points, isolas, period doubling bifurcation leading to a period-doubling cascade and homoclinics have been found. The effects of other reactor design and operating parameters such as the reactor volume ratio, the coolant temperature, and the residence time on the steady state and transient behavior of the two reactors are also reported. It is also illustrated that some process disturbances (e.g., feed initiator composition, initiator concentration, feed flow rate) introduced to the first reactor may change the stability of the second reactor.

2.7. Notation

A_{ci} heat transfer area of the ith reactor (cm^2)

C_p heat capacity of reaction mixture (cal/g°K)

Da_i Damköhler number (dimensionless mean residence time) of

the ith reactor (-)

E_{d_i} decomposition activation energy of initiator i, $i = A, B$ (cal/mol)

E_{d_M} activation energy of thermal initiation (cal/mol)

E_j activation energy of each reaction step j, $j = p, fm, t$ (cal/mol)

f_i efficiency of initiator i, $i = A, B$ (-)

f_s solvent feed volume fraction (-)

g_t gel effect correlation factor, k_t/k_t^* (-)

h_{ci} heat transfer coefficient of the ith reactor (cal/cm^{2}sec°K)

ΔH_r heat of reaction (cal/mol)

I_f concentration of initiator feed mixture (mol/l)

I_{ji} concentration of initiator j in the ith reactor, $j = A, B$ (mol/l)

k_{d_i} decomposition rate constant of initiator i, $i = A, B$ (sec^{-1})

k_{d_M} rate constant of thermal initiation ((1/mol)^2.sec)

k_i initiation rate constant (1/mol.sec)

k_{fm} chain transfer rate constant(1/mol.sec)

k_p propagation rate constant (1/mol.sec)

k_t combination termination rate constant (1/mol.sec)

k_t^* combination termination rate constant at zero monomer conversion (1/mol.sec)

M_i monomer concentration in the ith reactor (mol/l)

M_f monomer feed concentration (mol/l)

$\overline{PD}_i$ polydispersity index of the polymer in the ith reactor (-)

q volumetric feed flow rate (1/sec)

R primary radical concentration (mol/l)

T_i reactor temperature in the ith reactor (°K)

T_{ci} coolant temperature of the ith reactor (°K)

T_f feed temperature (°K)

t dimensionless time in the reactor (-)

t' time (sec)

V_i volume of the ith reactor (cm^3)

x effective monomer conversion in the presence of solvent (-)

$X_{1,i}$ monomer conversion in the ith reactor (-)

$X_{2,i}$ conversion of initiator A in the ith reactor (-)

$X_{3,i}$ conversion of initiator B in the ith reactor (-)

$X_{4,i}$ dimensionless reactor temperature in the ith reactor (-)

$\overline{X}_{n,i}$ number average polymer chain length in the ith reactor (-)

$\overline{X}_{w,i}$ weight average polymer chain length in the ith reactor (-)

y_{Af} mole fraction of initiator A in the initiator feed mixture (-)

Greek Letters

α_i dimensionless heat transfer coefficient of the ith reactor (-)

$\alpha_{0,i}$ effective heat transfer coefficient of the ith reactor (sec^{-1})

$\hat{\alpha}_i$ probability of propagation in the ith reactor (-)

β dimensionless heat of reaction (-)

δ_i dimensionless coolant temperature in the ith reactor (-)

ϵ ratio of decomposition activation energy of initiator B to that of initiator A (-)

γ dimensionless activation energy of propagation reaction (-)

γ_d dimensionless decomposition activation energy of initiator A (-)

η ratio of preexponential factor of decomposition of initiator B to that of initiator A (-)

θ mean residence time of the first reactor (hr)

$\lambda_{k,i}^l$ k-th moment of live polymer chain in the ith reactor (-)

$\lambda_{k,i}^d$ k-th moment of dead polymer chain in the ith reactor (-)

ν volume ratio of the second to the first reactor (-)

ρ density of reaction mixture (g/cm^3)

Chapter 3

Styrene Polymerization with Bifunctional Initiators in a CSTR

3.1. Introduction

With rapidly growing demands for the polymers of precisely controlled properties and of varying grades, there is a growing interest in the polymer industry in applying multifunctional initiators to free radical polymerization of vinyl monomers. The multifunctional initiators are defined as free radical generating initiators containing more than one labile group (e.g., peroxy or azo) having distinctly different thermal stabilities. During the past decades, many works have been reported in the literature on the kinetics of free radical polymerizations and the associated polymerization reactor design and control

problems, as discussed in the previous chapter. Most of these works have been confined to the polymerizations employing a single monofunctional initiator system such as benzoyl peroxide (BPO) and azobisisobutyronitrile (AIBN). In practice, more complex initiator systems such as mixed initiators and bifunctional initiators or multifunctional initiators are widely used in the polymer industry in order to enhance the monomer conversion and to improve polymer properties or to reduce the batch time.

Unlike conventional monofunctional initiators, functional groups in the multifunctional initiators can be decomposed in a controlled manner by varying the polymerization conditions. Therefore, the multifunctional initiators offer an added degree of freedom to polymer reactor engineers in optimizing the polymerization processes more effectively by taking advantage of some unique characteristics of the initiators. For example, it has been illustrated experimentally by some workers [Kamath and Harpell (1978), Sanchez *et al.* (1978)] that the multifunctional initiators can produce polymers of increased molecular weight at high reaction rate when they are used properly. Such an effect is due primarily to the sequential decomposition of the reactive functional groups (peroxy or azo) and repeated reinitiation, propagation, termination and chain transfer reactions. One of the practical advantages of using such multifunctional initiators is that no major modification of reactor equipment is necessary. The multifunctional initiators can also be used for the synthesis of block or graft copolymers by sequential monomer incorporation techniques

[Budtov *et al.* (1976), Ivanchev *et al.* (1976), Walz and Heitz (1978), Piirma and Chou (1979), Gunesin and Piirma (1981), Yamamoto *et al.* (1991)]. Although the concept of using multifunctional initiators in free radical polymerization of vinyl monomers was introduced some years ago [Shah *et al.* (1951), Vuillemenot *et al.* (1965), Prisyazhnyuk and Ivanchev (1970), Ivanchev and Zherebin (1974), Ivanchev (1979)], it is only recently that systematic kinetic modeling and experimental investigation have been reported in the literature [O'Driscoll and Bevington (1985), Choi and Lei (1987), Choi *et al.* (1988), Villalobos *et al.* (1991)].

In this chapter, a kinetic model and experimental model verification will be presented for the free radical styrene polymerization catalyzed by bifunctional initiators. Steady state behavior of a continuous stirred tank reactor for this system will also be studied. In particular, the effect of bifunctional initiators on the polymer molecular weight properties will be elucidated.

3.2. Polymerization Kinetics

The bifunctional initiator systems considered in this study are the diperoxyesters having the following structure:

$$\underset{(A)}{R_1\text{-}OO}\text{-}\overset{\overset{\displaystyle O}{\|}}{C}\text{-}X\text{-}\overset{\overset{\displaystyle O}{\|}}{C}\text{-}\underset{(B)}{OO\text{-}R_2} \qquad (3.1)$$
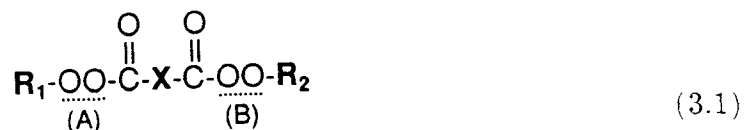
where R_1, R_2 and X represent hydrocarbon ligands. Depending on the structure of R_1 and R_2, the bifunctional initiators are divided into symmetrical and unsymmetrical bifunctional initiators and the peroxides A and B in these initiators exhibit different decomposition characteristics. The difference in the decomposition rates of the peroxide groups depends on the size and the type of the hydrocarbon bridge between the peroxide groups in the main chain of the multifunctional initiator molecule [Ivanchev and Zherebin (1974)].

3.2.1. Symmetrical Bifunctional Initiators

The specific symmetrical initiator system chosen is the diperoxyester studied by Prisyazhnyuk and Ivanchev (1970):

$$CH_3(CH_2)_6\overset{\overset{O}{\|}}{C}\text{-OO-}\overset{\overset{O}{\|}}{C}\text{-}[CH_2CHCl]\text{-}\overset{\overset{O}{\|}}{C}\text{-OO-}\overset{\overset{O}{\|}}{C}(CH_2)_6CH_3 \qquad (3.2)$$
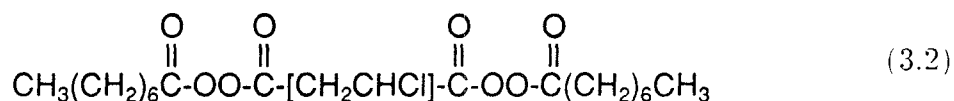
where R_1 and R_2 has same structure $[CH_3(CH_2)_6CO]$. Upon heating, the initiator decomposes into two radical species as follows:

$$I \rightarrow CH_3(CH_2)_6\overset{\overset{O}{\|}}{C}O\bullet + \bullet O\overset{\overset{O}{\|}}{C}\text{-}[CH_2CHCl]\text{-}\overset{\overset{O}{\|}}{C}\text{-OO-}\overset{\overset{O}{\|}}{C}(CH_2)_6CH_3 \qquad (3.3)$$
$$\quad\quad\quad\quad (R)\quad\quad\quad\quad\quad\quad\quad\quad (R')$$
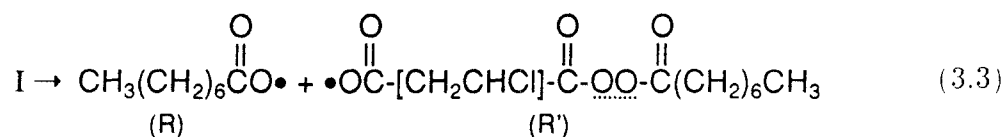
where the primary radical species R' carries an undecomposed peroxide group

131

which may decompose further during the course of polymerization. It is assumed that the peroxide groups of the same structure in the symmetrical initiator as shown in eq (3.2) have the same decomposition rate constants when the ligand between the peroxides is small. If the bridge (*i.e.*, hydrocarbon ligand X) between the peroxide groups is short enough for an inductive effect to be transmitted, the thermal stability of a group will change considerably when the neighboring group decomposes [Ivanchev (1979)]. For the bifunctional initiator shown above, it has been found that the decomposition activation energy of the peroxide group in R' is quite different from that of the peroxides in the original initiator (I). When monomers are polymerized by the radical species R', the polymers will carry labile peroxide groups and such polymers are called reactive polymers or polymeric initiators. Such complex polymerization kinetics caused by the existence of the two radical species (R and R') has been modeled by Choi and Lei (1987), Choi *et al.* (1988) and Villalobos *et al.* (1991). The following kinetic model was proposed by Choi and Lei (1987) and will be applied to a CSTR model in the next section.

A mechanism of polymer formation in free radical polymerization initiated by bifunctional initiators is called poly-recombinational polymerization because reactive macromolecules formed in the early stages of polymerization participate in the reaction through re-initiation, propagation and termination.

Table 3.1   Polymeric species produced from symmetrical bifunctional ini-
tiator

Growing Polymers

$$P_n \; : \; \bullet \text{————OOCR}_1$$

$$Q_n \; : \; \bullet \text{————COO–OOCR}_1$$

$$S_n \; : \; \bullet \text{————} \bullet$$

Inactive Polymers

$$T_n \; : \; \text{R}_1\text{COO–OOC————COO–OOCR}_1$$

$$Z_n \; : \; \text{R}_1\text{COO————COO–OOCR}_1$$

$$M_n \; : \; \text{R}_1\text{COO————OOCR}_1$$

As shown in Table 3.1, six different polymeric species (P_n, Q_n, S_n, T_n, Z_n, and M_n) can be defined in accordance with the nature of the end units of the polymer chains. Note that P_n, Q_n, and S_n are the growing (or live) polymer radicals with n-monomer units and T_n, Z_n, and M_n are the dead polymers of n-monomer units. However, Q_n, T_n, and Z_n species carry undecomposed peroxide groups ($-\text{COO-OOCR}_1$) on the chain ends. Thus, such polymers can be reconverted to active radical species via subsequent thermal decomposition of the peroxides. The decomposition reactions of the primary diperoxyester initiator (I) and the polymeric initiators can be described as follows:

$$I \xrightarrow{2k_{d1}} R + R' \tag{3.4}$$

$$Q_n \xrightarrow{k_{d2}} S_n + R \qquad (n \geq 1) \tag{3.5}$$

$$T_n \xrightarrow{2k_{d2}} Q_n + R \qquad (n \geq 2) \tag{3.6}$$

$$Z_n \xrightarrow{k_{d2}} P_n + R \qquad (n \geq 2) \tag{3.7}$$
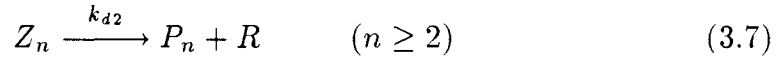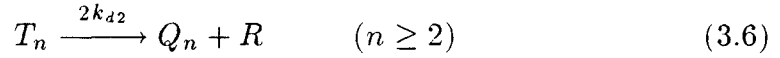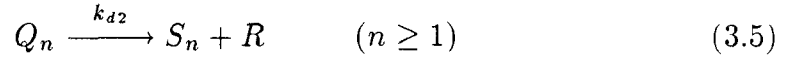
where k_{d1} and k_{d2} denote the decomposition rate constants of the two perox-
ide groups in the primary initiators and in the polymers, respectively. Note
that both the primary initiator (I) and the polymeric species T_n have dual
functionalities because they contain two undecomposed peroxides of equal ac-
tivities. Here, it is assumed that cyclization reaction and thermal initiation do
not occur. The decomposition of primary radical species R' is also assumed
negligible. According to Ivanchev (1979), the decomposition rate constants
of more stable peroxides (*i.e.*, peroxides in Q_n, T_n and Z_n) are independent
of polymer chain length. The initiation of polymer chain propagation by the
primary radicals takes place as follows:

$$R + M \xrightarrow{k_{i1}} P_1 \tag{3.8}$$

$$R' + M \xrightarrow{k_{i2}} Q_1 \tag{3.9}$$

The propagation reactions are:

$$P_n + M \xrightarrow{k_p} P_{n+1} \qquad (n \geq 1) \qquad\qquad (3.10)$$

$$Q_n + M \xrightarrow{k_p} Q_{n+1} \qquad (n \geq 1) \qquad\qquad (3.11)$$

$$S_n + M \xrightarrow{2k_p} S_{n+1} \qquad (n \geq 1) \qquad\qquad (3.12)$$
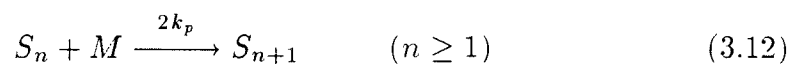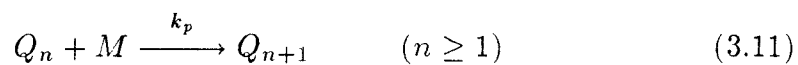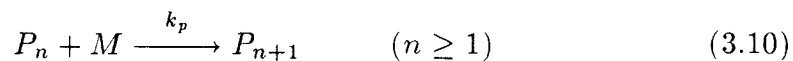
where the propagation rate constants are also assumed to be independent of polymer chain length. Since S_n contains two radicals per molecule, the propagation and the termination reactions involving these polymers occur twice as fast as those involving the other polymeric species. When the termination of growing polymer chains occurs exclusively by combination (e.g., styrene polymerization), the following termination reactions will take place:

$$P_n + P_m \xrightarrow{k_t} M_{n+m} \qquad (n, m \geq 1) \qquad\qquad (3.13)$$

$$P_n + Q_m \xrightarrow{k_t} Z_{n+m} \qquad (n, m \geq 1) \qquad\qquad (3.14)$$

$$P_n + S_m \xrightarrow{2k_t} P_{n+m} \qquad (n, m \geq 1) \qquad\qquad (3.15)$$

$$Q_n + Q_m \xrightarrow{k_t} T_{n+m} \qquad (n, m \geq 1) \qquad\qquad (3.16)$$

$$Q_n + S_m \xrightarrow{2k_t} Q_{n+m} \qquad (n, m \geq 1) \qquad\qquad (3.17)$$

$$S_n + S_m \xrightarrow{4k_t} S_{n+m} \qquad (n, m \geq 1) \qquad\qquad (3.18)$$
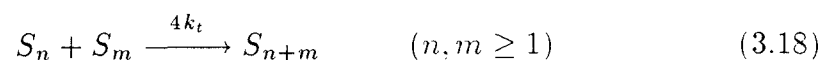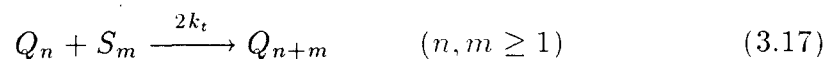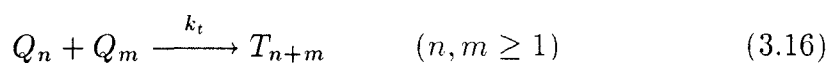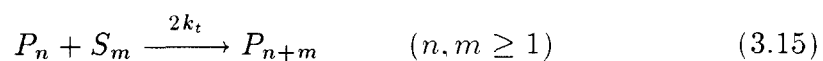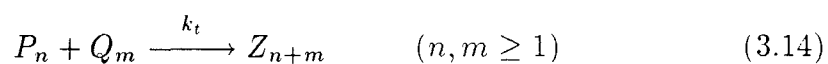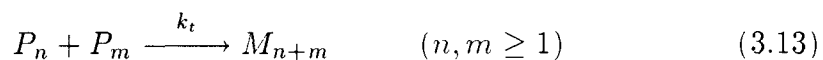
Note that various reactive polymeric species (e.g., Q_n, T_n, Z_n) containing undecomposed peroxide groups are formed by the combination termination

135

reactions and these species, upon subsequent decomposition and polymerization, will lead to the formation of polymers having extended polymer chain lengths. The termination by primary radicals is assumed negligible in the above scheme. In eqs (3.13)~(3.18), the combination termination rate constants for the different polymeric species are assumed to be identical. In this kinetic scheme, chain transfer reactions have not been considered.

With the polymerization mechanism proposed above, a batch polymerization process with the bifunctional initiator can be modeled as follows:

For initiator and primary radicals:

$$\frac{dI}{dt} = -2k_{d1}I \tag{3.19}$$

$$\frac{dR}{dt} = 2f_1 k_{d1}I - k_{i1}RM + k_{d2}(Q + 2T + Z) \tag{3.20}$$

$$\frac{dR'}{dt} = 2f_2 k_{d1}I - k_{i2}R'M \tag{3.21}$$

where f_1 and f_2 are the initiator efficiencies which indicate the fraction of primary radicals (R and R') used for chain initiation.

For growing polymers:

$$\frac{dP_1}{dt} = k_{i1}RM - k_p M P_1 - k_t P_1(P + Q + 2S) \tag{3.22}$$

$$\frac{dP_n}{dt} = k_p M(P_{n-1} - P_n) + k_{d2}Z_n - k_t P_n(P + Q + 2S)$$
$$+ 2k_t \sum_{m=1}^{n-1} P_{n-m}S_m \qquad (n \geq 2) \tag{3.23}$$

$$\frac{dQ_1}{dt} = k_{i2}R'M - k_pMQ_1 - k_{d2}Q_1 - k_tQ_1(P + Q + 2S) \tag{3.24}$$

$$\frac{dQ_n}{dt} = -k_{d2}Q_n + 2k_{d2}T_n + k_pM(Q_{n-1} - Q_n) - k_tQ_n(P + Q + 2S)$$

$$+ 2k_t \sum_{m=1}^{n-1} Q_{n-m}S_m \qquad (n \geq 2) \tag{3.25}$$

$$\frac{dS_1}{dt} = k_{d2}Q_1 - 2k_pMS_1 - 2k_tS_1(P + Q + 2S) \tag{3.26}$$

$$\frac{dS_n}{dt} = k_{d2}Q_n + 2k_pM(S_{n-1} - S_n) - 2k_tS_n(P + Q + 2S)$$

$$+ 2k_t \sum_{m=1}^{n-1} S_{n-m}S_m \qquad (n \geq 2) \tag{3.27}$$

For *temporarily inactive polymers:*

$$\frac{dT_n}{dt} = -2k_{d2}T_n + \frac{k_t}{2} \sum_{m=1}^{n-1} Q_{n-m}Q_m \qquad (n \geq 2) \tag{3.28}$$

$$\frac{dZ_n}{dt} = -k_{d2}Z_n + k_t \sum_{m=1}^{n-1} P_{n-m}Q_m \qquad (n \geq 2) \tag{3.29}$$

For *monomers and dead polymers:*

$$\frac{dM}{dt} = -k_{i1}RM - k_{i2}R'M - k_pM(P + Q + 2S) \tag{3.30}$$

$$\frac{dM_n}{dt} = \frac{k_t}{2} \sum_{m=1}^{n-1} P_{n-m}P_m \qquad (n \geq 2) \tag{3.31}$$

where P, Q, S, T, and Z are the total concentrations of the corresponding polymeric species, *i.e.*,

$$P = \sum_{n=1}^{\infty} P_n \qquad Q = \sum_{n=1}^{\infty} Q_n \qquad S = \sum_{n=1}^{\infty} S_n$$

$$T = \sum_{n=2}^{\infty} T_n \qquad Z = \sum_{n=2}^{\infty} Z_n \tag{3.32}$$

For primary radicals and live polymeric species (P_n, Q_n, and S_n) a quasi-steady state approximation will be employed. In order to compute the molec-

ular weight averages of polymers, the following molecular weight moments are used:

$$\lambda_{\xi,k} \equiv \sum_{n=j}^{\infty} n^k \xi_n \qquad \left[\xi = P, Q, S(j = 1); T, Z(j = 2) \right] \qquad (3.33)$$

$$\lambda_k^d \equiv \sum_{n=2}^{\infty} n^k M_n \qquad (3.34)$$

where $\lambda_{\xi,k}$ and λ_k^d denote the k-th moment of polymeric species ξ and dead polymers, respectively. Detailed moment equations for each polymeric species are derived by Choi and Lei (1987).

3.2.2. Unsymmetrical Bifunctional Initiators

The peroxides A and B in the unsymmetrical bifunctional initiators have significantly different decomposition activation energies due to their structural difference. The specific initiator system chosen is 4-(t-butylperoxycarbonyl-3-hexyl-6-[7-(t-butylperoxycarbonyl)heptyl]cyclohexene:

$$
CH_3(CH_2)_5 \text{---} \bigcirc \text{---} (CH_2)_7 \overset{\overset{\displaystyle O}{\|}}{C}\text{-OO-C(CH}_3)_3 \quad (A) \\
O=C\text{-OO-C(CH}_3)_3 \quad (B) \\
(I)
$$

$$(3.35)$$

in which the primary peroxy ester(A) and the cyclic peroxy ester (B) have

138

decomposition activation energies of 33.5 kcal/mol and 29.8 kcal/mol, respectively [Sanchez *et al.* (1978), Product Bulletin (1986)]. Figure 3.1 illustrates the comparison of the half-life of the two peroxide groups in the bifunctional initiator (M_A and M_B) with those of other popular monofunctional initiators, t-butyl perbenzoate (TBPB), BPO and AIBN. The peroxide (B) is less stable or more reactive than the peroxide (A). Note that the decomposition characteristics of the peroxides (A) and (B) are similar to that of TBPB and BPO, respectively.

The thermal decomposition of the primary initiator (I) occurs via homolytic scission as follows:

$$\text{(3.36a)}$$

$$\text{(3.36b)}$$
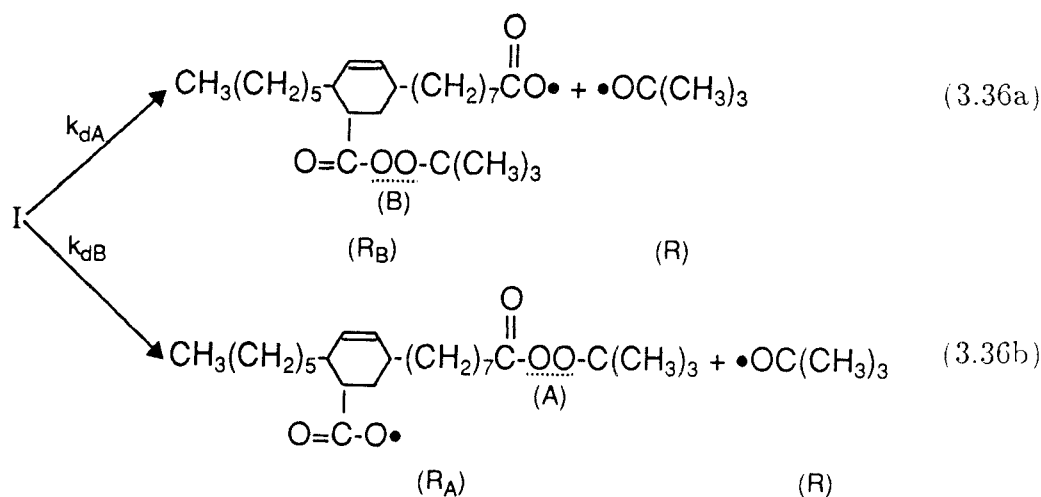
where k_{dA} and k_{dB} denote the decomposition rate constants of peroxide (A)
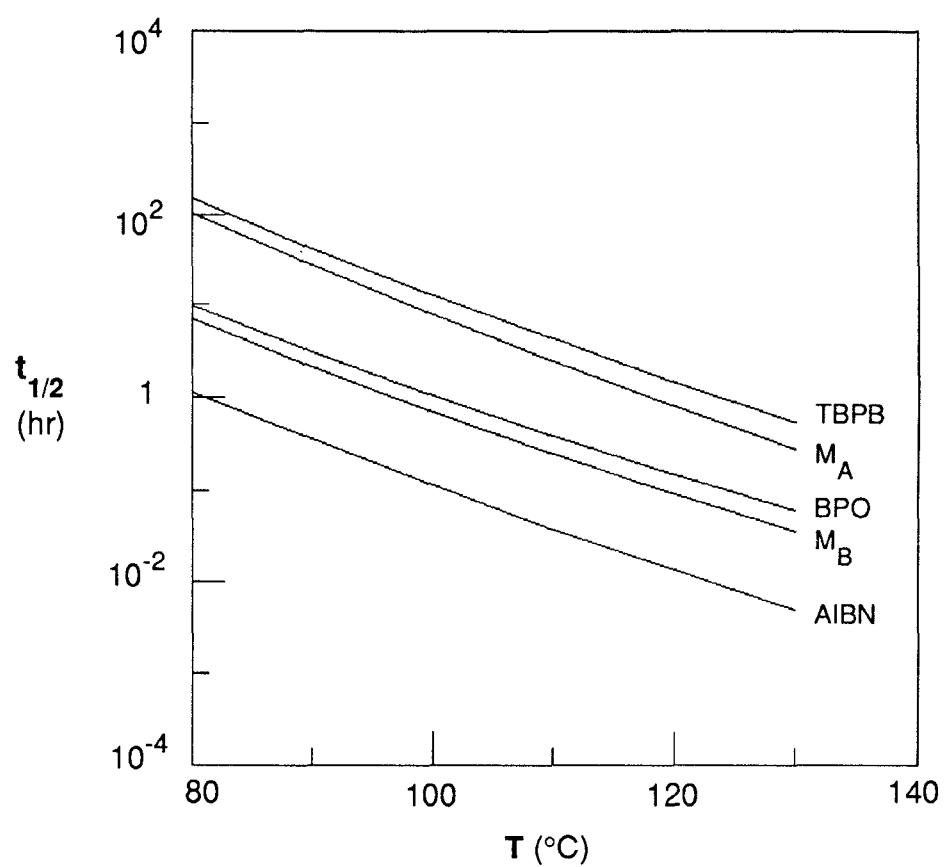
Figure 3.1   Initiator half-life of various initiators.

and (B), respectively. R_A and R_B represent primary radicals with undecomposed peroxide (A) and (B), respectively. During the course of polymerization, those primary radicals (R_A, R_B) can further decompose as follows:

$$R_A \text{ or } R_B \xrightarrow[\text{ or } k_{dB}]{k_{dA}} CH_3(CH_2)_5 \underset{\substack{| \\ O=C\text{-}O\bullet \\ (R')}}{\bigcirc} \text{-}(CH_2)_7 \overset{\overset{\displaystyle O}{\|}}{C}O\bullet + \bullet OC(CH_3)_3 \tag{3.37}$$
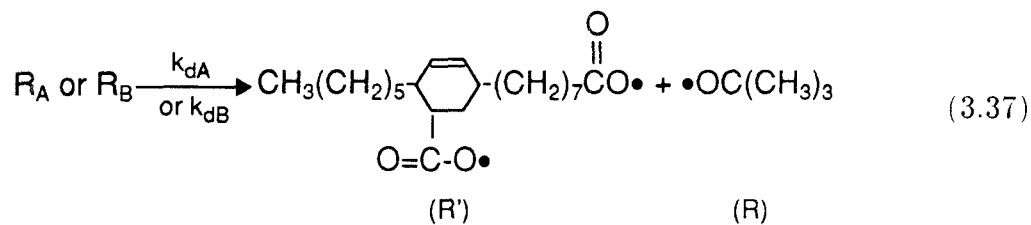
$$\phantom{R_A \text{ or } R_B} (R') (R)$$

Note that diradical species (R') is produced by the decomposition of R_A or R_B. Those primary radicals may undergo decarboxylation reactions; however, there will be no net change in their concentrations by such reactions. It is assumed that induced decomposition (chain transfer to the initiator) and intramolecular rearrangement reactions are negligible.

When these radical species are involved in initiation and propagation reactions, ten unique polymeric species can be defined in accordance with the type of chain end units, as shown in Table 3.2. Note that Q_n and S_n are live monoradicals of n-monomer units carrying undecomposed peroxide group (A) and (B) at the other end of the chain, respectively. Inactive polymeric species U_n, V_n, W_n, U'_n, and V'_n contain undecomposed peroxides which may decompose during the polymerization process.

Table 3.2   Polymeric species produced from unsymmetrical bifunctional initiator

Symbols		Note
P_n	●————|	live polymer without any undecomposed peroxides
Q_n	●————A	live polymer with undecomposed peroxide (A)
S_n	●————B	live polymer with undecomposed peroxide (B)
T_n	●————●	live polymer with diradicals
M_n	|————|	dead polymer without undecomposed peroxides
U_n	|————A	inactive polymer with a single undecomposed peroxide (A)
V_n	|————B	inactive polymer with a single undecomposed peroxide (B)
W_n	A————B	inactive polymer with undecomposed peroxides (A) and (B)
U_n'	A————A	inactive polymer with two undecomposed peroxides (A)
V_n'	B————B	inactive polymer with two undecomposed peroxides (B)

3.2.2.1. Kinetic Model

Similar to the symmetrical bifunctional initiators, a mechanism of free radical polymerization initiated by unsymmetrical bifunctional initiators is poly-recombinational because various types of reactive macromolecules participate in the polymerization repeatedly through re-initiation, propagation and termination. The decomposition reactions of the primary initiator(I) and the radical species R_A and R_B are described by:

$$I \xrightarrow{k_{d_A}} R_B + R \tag{3.38a}$$

$$I \xrightarrow{k_{d_B}} R_A + R \tag{3.38b}$$

$$R_A \xrightarrow{k_{d_A}} R + R' \tag{3.38c}$$

$$R_B \xrightarrow{k_{d_B}} R + R' \tag{3.38d}$$

The initiation reactions are:

$$R + M \xrightarrow{k_i} P_1 \tag{3.39a}$$

$$R_A + M \xrightarrow{k_i} Q_1 \tag{3.39b}$$

$$R_B + M \xrightarrow{k_i} S_1 \tag{3.39c}$$

$$R' + M \xrightarrow{k_i} T_1 \tag{3.39d}$$

Since some polymeric species contain undecomposed peroxides, additional reinitiation reactions will also occur as follows:

$$Q_n \xrightarrow{k_{d_A}} R + T_n \qquad (n \geq 1) \qquad\qquad (3.40a)$$

$$S_n \xrightarrow{k_{d_B}} R + T_n \qquad (n \geq 1) \qquad\qquad (3.40b)$$

$$U_n \xrightarrow{k_{d_A}} R + P_n \qquad (n \geq 2) \qquad\qquad (3.40c)$$

$$V_n \xrightarrow{k_{d_B}} R + P_n \qquad (n \geq 2) \qquad\qquad (3.40d)$$

$$W_n \xrightarrow{k_{d_B}} R + Q_n \qquad (n \geq 2) \qquad\qquad (3.40e)$$

$$W_n \xrightarrow{k_{d_A}} R + S_n \qquad (n \geq 2) \qquad\qquad (3.40f)$$

$$U_n' \xrightarrow{2k_{d_A}} R + Q_n \qquad (n \geq 2) \qquad\qquad (3.40g)$$

$$V_n' \xrightarrow{2k_{d_B}} R + S_n \qquad (n \geq 2) \qquad\qquad (3.40h)$$
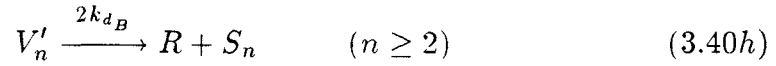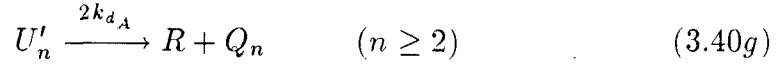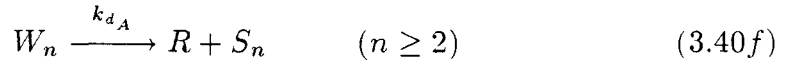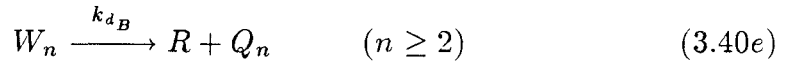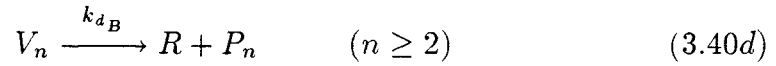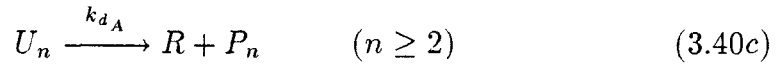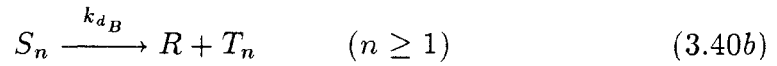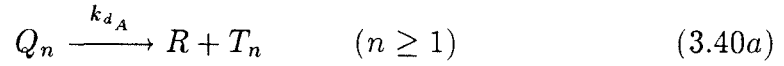
Note that U_n' and V_n' have dual functionalities because they contain two identical undecomposed peroxides.

The thermal initiation by styrene is [Hui and Hamielec (1972)]:

$$3M \xrightarrow{k_{d_M}} 2P_1 \qquad\qquad (3.41)$$

The propagation reactions are:

$$P_n + M \xrightarrow{k_p} P_{n+1} \qquad (n \geq 1) \qquad\qquad (3.42a)$$

$$Q_n + M \xrightarrow{k_p} Q_{n+1} \qquad (n \geq 1) \qquad\qquad (3.42b)$$

$$S_n + M \xrightarrow{k_p} S_{n+1} \qquad (n \geq 1) \qquad\qquad (3.42c)$$

$$T_n + M \xrightarrow{2k_p} T_{n+1} \qquad (n \geq 1) \qquad\qquad (3.42d)$$

144
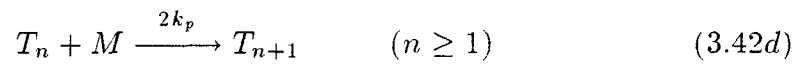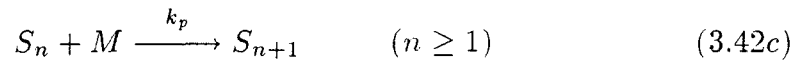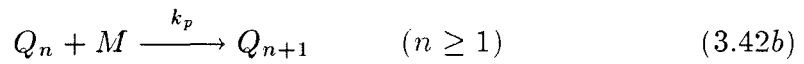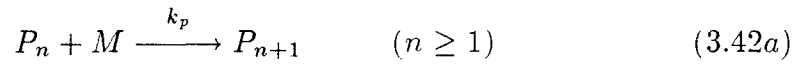
where the propagation rate constants are assumed to be independent of polymer chain length. In the above kinetic scheme, it is also assumed that the reactivity of any free radical species is independent of the polymer chain length [Ivanchev (1979)]. The diradical species (T_n) are assumed not to form any cyclic polymers. Since T_n contains two radicals per molecule, the propagation and termination reactions involving this polymer occur twice as fast as those having only one active radical. When active polymeric species are involved in the chain transfer reactions to monomer, they produce different types of dead or inactive polymeric species according to the endgroups having undecomposed peroxide groups:

$$P_n + M \xrightarrow{k_{fm}} M_n + P_1 \qquad (n \geq 1) \qquad (3.43a)$$

$$Q_n + M \xrightarrow{k_{fm}} U_n + P_1 \qquad (n \geq 1) \qquad (3.43b)$$

$$S_n + M \xrightarrow{k_{fm}} V_n + P_1 \qquad (n \geq 1) \qquad (3.43c)$$

$$T_n + M \xrightarrow{2k_{fm}} P_n + P_1 \qquad (n \geq 1) \qquad (3.43d)$$
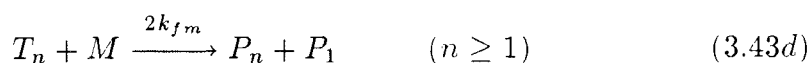
When the termination of growing polymers occurs exclusively by combination (e.g., styrene polymerization), the following termination scheme will be valid:

$$P_n + P_m \xrightarrow{k_t} M_{n+m} \qquad (n, m \geq 1) \qquad (3.44a)$$

$$P_n + Q_m \xrightarrow{k_t} U_{n+m} \qquad (n, m \geq 1) \qquad (3.44b)$$

$$P_n + S_m \xrightarrow{\ k_t\ } V_{n+m} \qquad (n, m \geq 1) \qquad\qquad (3.44c)$$

$$P_n + T_m \xrightarrow{\ 2k_t\ } P_{n+m} \qquad (n, m \geq 1) \qquad\qquad (3.44d)$$

$$Q_n + Q_m \xrightarrow{\ k_t\ } U'_{n+m} \qquad (n, m \geq 1) \qquad\qquad (3.44e)$$

$$Q_n + S_m \xrightarrow{\ k_t\ } W_{n+m} \qquad (n, m \geq 1) \qquad\qquad (3.44f)$$

$$Q_n + T_m \xrightarrow{\ 2k_t\ } Q_{n+m} \qquad (n, m \geq 1) \qquad\qquad (3.44g)$$

$$S_n + S_m \xrightarrow{\ k_t\ } V'_{n+m} \qquad (n, m \geq 1) \qquad\qquad (3.44h)$$

$$S_n + T_m \xrightarrow{\ 2k_t\ } S_{n+m} \qquad (n, m \geq 1) \qquad\qquad (3.44i)$$

$$T_n + T_m \xrightarrow{\ 4k_t\ } T_{n+m} \qquad (n, m \geq 1) \qquad\qquad (3.44j)$$
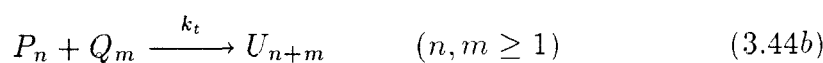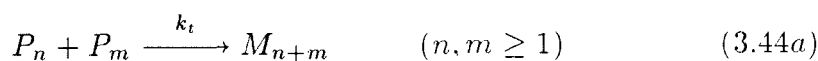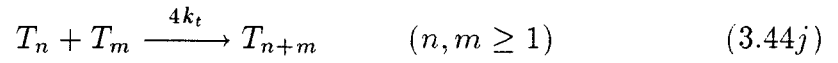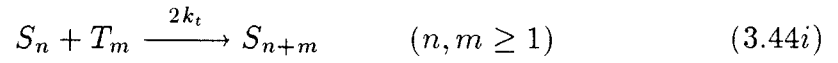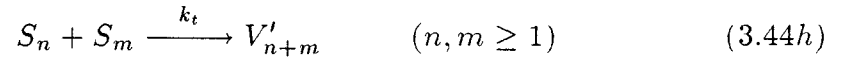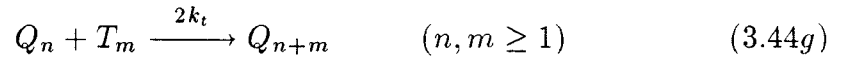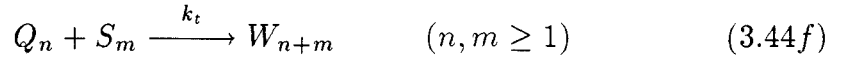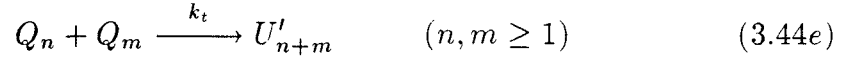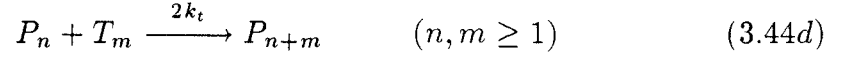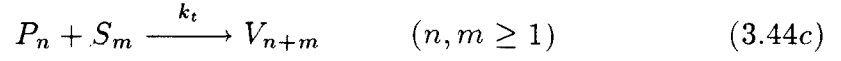
For bulk styrene polymerization, gel effect correlation suggested by Hui and Hamielec (1972) is used:

$$g_t \equiv \frac{k_t}{k_{to}} = \exp[-2(Bx + Cx^2 + Dx^3)] \qquad\qquad (3.45)$$

where x and k_{to} denote the monomer conversion and the termination rate constant at zero monomer conversion, respectively, and:

$$B = 2.57 - 5.05 \times 10^{-3} T(^\circ K)$$

$$C = 9.56 - 1.76 \times 10^{-2} T(^\circ K)$$

$$D = -3.03 + 7.85 \times 10^{-3} T(^\circ K)$$

Due to the density difference between polymer and monomer, the reaction volume of the polymerizing medium changes during the polymerization. Thus, the rate of volume change is described by the following equation:

$$\frac{1}{v}\frac{dv}{dt} = -\left(\frac{\epsilon}{M_o + \epsilon M}\right)\frac{dM}{dt} \tag{3.46}$$

where, M_o is the initial concentration of monomer and ϵ the volume contraction factor defined by:

$$\epsilon = \frac{v_{x=1} - v_{x=0}}{v_{x=0}} \tag{3.47}$$

With the kinetic scheme proposed above, one can derive the rate expressions for various reaction steps as follows:

For initiator and primary radicals:

$$\frac{1}{v}\frac{d}{dt}(Iv) = -(k_{d_A} + k_{d_B})I \tag{3.48}$$

$$\frac{1}{v}\frac{d}{dt}(R_A v) = f_A k_{d_B} I - k_{d_A} R_A - k_i R_A M \tag{3.49}$$

$$\frac{1}{v}\frac{d}{dt}(R_B v) = f_B k_{d_A} I - k_{d_B} R_B - k_i R_B M \tag{3.50}$$

$$\frac{1}{v}\frac{d}{dt}(Rv) = f_R(k_{d_B} + k_{d_A})I + f_R k_{d_A} R_A + f_R k_{d_B} R_B - k_i RM$$

$$+ f_R k_{d_A}(Q + U + V + 2U')$$

$$+ f_R k_{d_B}(S + V + W + 2V') \tag{3.51}$$

$$\frac{1}{dv}\frac{d}{dt}(R'v) = f_{R'} k_{d_A} R_A + f_{R'} k_{d_B} R_B - 2k_i R' M \tag{3.52}$$

where f_A, f_B, f_R and $f_{R'}$ are the initiator efficiencies which indicate the fraction of primary radicals $(R_A, R_B, R$ and R', respectively) involved in chain initiation. It is assumed that the initiator efficiencies are constant during the course of polymerization.

For growing polymers:

$$\frac{1}{v}\frac{d}{dt}(P_1 v) = 2k_{d_M}M^3 + k_i RM + k_{d_A}U_1 + k_{d_B}V_1 - k_p MP_1$$

$$+ k_{fm}(P - P_1 + Q + S + 2T + 2T_1)$$

$$- k_t P_1(P + Q + S + 2T) \qquad (3.53)$$

$$\frac{1}{v}\frac{d}{dt}(P_n v) = k_{d_A}U_n + k_{d_B}V_n + k_p M(P_{n-1} - P_n)$$

$$+ k_{fm}M(2T_n - P_n) - k_t P_n(P + Q + S + 2T)$$

$$+ 2k_t \sum_{m=1}^{n-1} P_{n-m}T_m \qquad (n \geq 2) \qquad (3.54)$$

$$\frac{1}{v}\frac{d}{dt}(Q_1 v) = k_i R_A M - k_{d_A}Q_1 - k_p MQ_1 - k_{fm}MQ_1$$

$$- k_t Q_1(P + Q + S + 2T) \qquad (3.55)$$

$$\frac{1}{v}\frac{d}{dt}(Q_n v) = -k_{d_A}Q_n + k_{d_B}W_n + 2k_{d_A}U'_n + k_p M(Q_{n-1} - Q_n)$$

$$- k_{fm}MQ_n - k_t Q_n(P + Q + S + 2T)$$

$$+ 2k_t \sum_{m=1}^{n-1} Q_{n-m}T_m \qquad (n \geq 2) \qquad (3.56)$$

$$\frac{1}{v}\frac{d}{dt}(S_1 v) = k_i R_B M - k_{d_B}S_1 - k_p MS_1 - k_{fm}MS_1$$

$$- k_t S_1(P + Q + S + 2T) \qquad (3.57)$$

$$\frac{1}{v}\frac{d}{dt}(S_n v) = -k_{d_B}S_n + k_{d_A}W_n + 2k_{d_B}V'_n + k_pM(S_{n-1} - S_n)$$

$$- k_{fm}MS_n - k_tS_n(P + Q + S + 2T)$$

$$+ 2k_t\sum_{m=1}^{n-1}S_{n-m}T_m \qquad (n \geq 2) \qquad (3.58)$$

$$\frac{1}{v}\frac{d}{dt}(T_1 v) = 2k_iR'M + k_{d_A}Q_1 + k_{d_B}S_1 - 2k_pMT_1 - 2k_{fm}MT_1$$

$$- 2k_tT_1(P + Q + S + 2T) \qquad (3.59)$$

$$\frac{1}{v}\frac{d}{dt}(T_n v) = k_{d_A}Q_n + k_{d_B}S_n + 2k_pM(T_{n-1} - T_n)$$

$$- 2k_{fm}MT_n - 2k_tT_n(P + Q + S + 2T)$$

$$+ 2k_t\sum_{m=1}^{n-1}T_{n-m}T_m \qquad (n \geq 2) \qquad (3.60)$$

For monomers and dead polymers:

$$\frac{1}{v}\frac{d}{dt}(Mv) = -k_pM(P + Q + S + 2T) \qquad (3.61)$$

$$\frac{1}{v}\frac{d}{dt}(M_n v) = k_{fm}MP_n + \frac{1}{2}k_t\sum_{m=1}^{n-1}P_{n-m}P_m \qquad (n \geq 2) \ (3.62)$$

For temporarily inactive polymers:

$$\frac{1}{v}\frac{d}{dt}(U_1 v) = -k_{d_A}U_1 + k_{fm}MQ_1 \qquad (3.63)$$

$$\frac{1}{dv}\frac{d}{dt}(U_n v) = -k_{d_A}U_n + k_{fm}MQ_n + k_t\sum_{m=1}^{n-1}P_{n-m}Q_m \qquad (n \geq 2) \ (3.64)$$

$$\frac{1}{v}\frac{d}{dt}(V_1 v) = -k_{d_B}V_1 + k_{fm}MS_1 \qquad (3.65)$$

$$\frac{1}{v}\frac{d}{dt}(V_n v) = -k_{d_B}V_n + k_{fm}MS_n + k_t\sum_{m=1}^{n-1}P_{n-m}S_m \qquad (n \geq 2) \ (3.66)$$

$$\frac{1}{v}\frac{d}{dt}(W_n v) = -(k_{d_A} + k_{d_B})W_n + k_t\sum_{m=1}^{n-1}Q_{n-m}S_m \qquad (n \geq 2) \quad (3.67)$$

$$\frac{1}{v}\frac{d}{dt}(U'_n v) = -2k_{d_A}U'_n + \frac{1}{2}k_t\sum_{m=1}^{n-1}Q_{n-m}Q_m \qquad (n \geq 2) \qquad (3.68)$$

$$\frac{1}{v}\frac{d}{dt}(V_n'v) = -2k_{d_B}V_n' + \frac{1}{2}k_t\sum_{m=1}^{n-1}S_{n-m}S_m \qquad (n \geq 2) \qquad (3.69)$$

where P, Q, S, T, U, V, W, U' and V' are the total concentrations of the corresponding polymeric species, i.e.,

$$P = \sum_{n=1}^{\infty} P_n, \qquad Q = \sum_{n=1}^{\infty} Q_n, \qquad S = \sum_{n=1}^{\infty} S_n,$$

$$T = \sum_{n=1}^{\infty} T_n, \qquad U = \sum_{n=1}^{\infty} U_n, \qquad V = \sum_{n=1}^{\infty} V_n, \qquad (3.70)$$

$$W = \sum_{n=2}^{\infty} W_n, \qquad U' = \sum_{n=2}^{\infty} U_n', \qquad V' = \sum_{n=2}^{\infty} V_n'$$

In order to compute the molecular weight averages of the polymers, molecular weight moments are used:

$$\lambda_{\xi,k} \equiv \sum_{n=j}^{\infty} n^k \xi_n \quad [\xi = P, Q, S, T, U, V(j = 1); W, U', V'(j = 2)] (3.71a)$$

$$\lambda_k^d \equiv \sum_{n=2}^{\infty} n^k M_n \qquad (3.71b)$$

where $\lambda_{\xi,k}$ and λ_k^d denote the k-th moment of polymeric species ξ and dead polymers, respectively. The overall number average chain length (X_N) and weight average chain length (X_W) of the resulting polymers are defined by:

$$X_N = \frac{\sum_{\xi} \lambda_{\xi,1} + \lambda_1^d}{\sum_{\xi} \lambda_{\xi,0} + \lambda_0^d} \quad (\xi = P, Q, S, T, U, V, W, U', V') \qquad (3.72a)$$

$$X_W = \frac{\sum_{\xi} \lambda_{\xi,2} + \lambda_2^d}{\sum_{\xi} \lambda_{\xi,1} + \lambda_1^d} \quad (\xi = P, Q, S, T, U, V, W, U', V') \qquad (3.72b)$$

The number average and weight average chain lengths of each polymeric species are also given by:

$$X_{N,\xi} = \frac{\lambda_{\xi,1}}{\lambda_{\xi,0}}, \qquad X_{W,\xi} = \frac{\lambda_{\xi,2}}{\lambda_{\xi,1}} \qquad (3.73a)$$

$$X_{N,d} = \frac{\lambda_1^d}{\lambda_0^d}, \qquad X_{W,d} = \frac{\lambda_2^d}{\lambda_1^d} \qquad (3.73b)$$

where

$$(\xi = P, Q, S, T, U, V, W, U', V')$$

The polydispersity is a measure of molecular weight distribution broadening and is defined by:

$$PD = \frac{X_W}{X_N} \qquad (3.73c)$$

Using the rate expressions derived above, the molecular weight moment equations can be derived, as given in **Appendix B**. In solving the moment equations, a quasi-steady state approximation is applied to the reaction rates generating the primary radical species and the live polymeric species. The resulting zeroth, first and second moments of live polymers are also shown in **Appendix B**.

3.2.2.2. Model Simulation

The proposed kinetic model for the free radical polymerization cat-alyzed by the unsymmetrical bifunctional initiator system has been used

151

to simulate isothermal batch bulk polymerization of styrene with 4-(t-butylperoxycarbonyl)-3- hexyl-6- [7-(t-butylperoxycarbonyl)heptyl] cyclohexene as an initiator. The numerical values of the kinetic parameters used in our simulations are listed in Table 3.3. Here, the rate constant of chain transfer to monomer was estimated by using the least square method from the data reported in Brandrup and Immergut (1975). Note that the decomposition activation energies of the two peroxides (A) and (B) differ considerably. The monofunctional initiators (M_A and M_B) shown in Table 3.3 are the hypothetical ones used for the purpose of comparison with the bifunctional initiator system.

The two principal parameters which influence the bulk polymerization kinetics and polymer properties for a given free radical initiator system are the reaction temperature and the initiator concentration. Figures 3.2~3.5 show the effects of both reaction temperature and initiator concentration on the monomer conversion and the corresponding number average chain length (NACL) of polystyrene for various initiator systems. Note that the monofunctional initiator M_A is the "slow" initiator or the "high temperature" initiator whereas the initiator M_B is the "fast" initiator or the "low temperature" initiator. In conventional free radical polymerizations with single monofunctional initiators (Figures 3.2 and 3.3), the higher the polymerization temperature is, the lower the resulting polymer molecular weight becomes. Similarly as the higher initiator concentration is used, the lower the polymer molecular

Table 3.3   Numerical values of kinetic parameters for unsymmetrical bifunctional initiators

---

Bifunctional Initiators:

Peroxide (A) : $k_{d_A} = 1.04 \times 10^{15}\exp(\text{-33,500/RT})$, sec^{-1} *

Peroxide (B) : $k_{d_B} = 8.06 \times 10^{13}\exp(\text{-29,800/RT})$, sec^{-1} *

$$f_A = f_B = f_R = f_{R'} = 0.7 \; *$$

Monofunctional Initiators:

M_A : $k_d = 1.04 \times 10^{15}\exp(\text{-33,500/RT})$, sec^{-1}

$\quad f_A = 0.7$

M_B : $k_d = 8.06 \times 10^{13}\exp(\text{-29,800/RT})$, sec^{-1}

$\quad f_B = 0.7$

$k_{d_M} = 2.190 \times 10^5\exp(\text{-27,440/RT})$, (1/mol)^2/sec †

$k_p = 1.051 \times 10^7\exp(\text{-7,060/RT})$, 1/mol.sec ‡

$k_{to} = 1.260 \times 10^9\exp(\text{-1,680/RT})$, 1/mol.sec ‡

$k_{fm} = 7.807 \times 10^6\exp(\text{-12,940/RT})$, 1/mol.sec ‡

$k_i \approx k_p$

$\epsilon = -0.147$ §

$M_o = 8.728$ mol/l

---

*   Product Bulletin Peroxiesters (1983)

‡   Hui and Hamielec (1972).

†   Brandrup and Immergut (1989)

§   Arai *et al.* (1989)
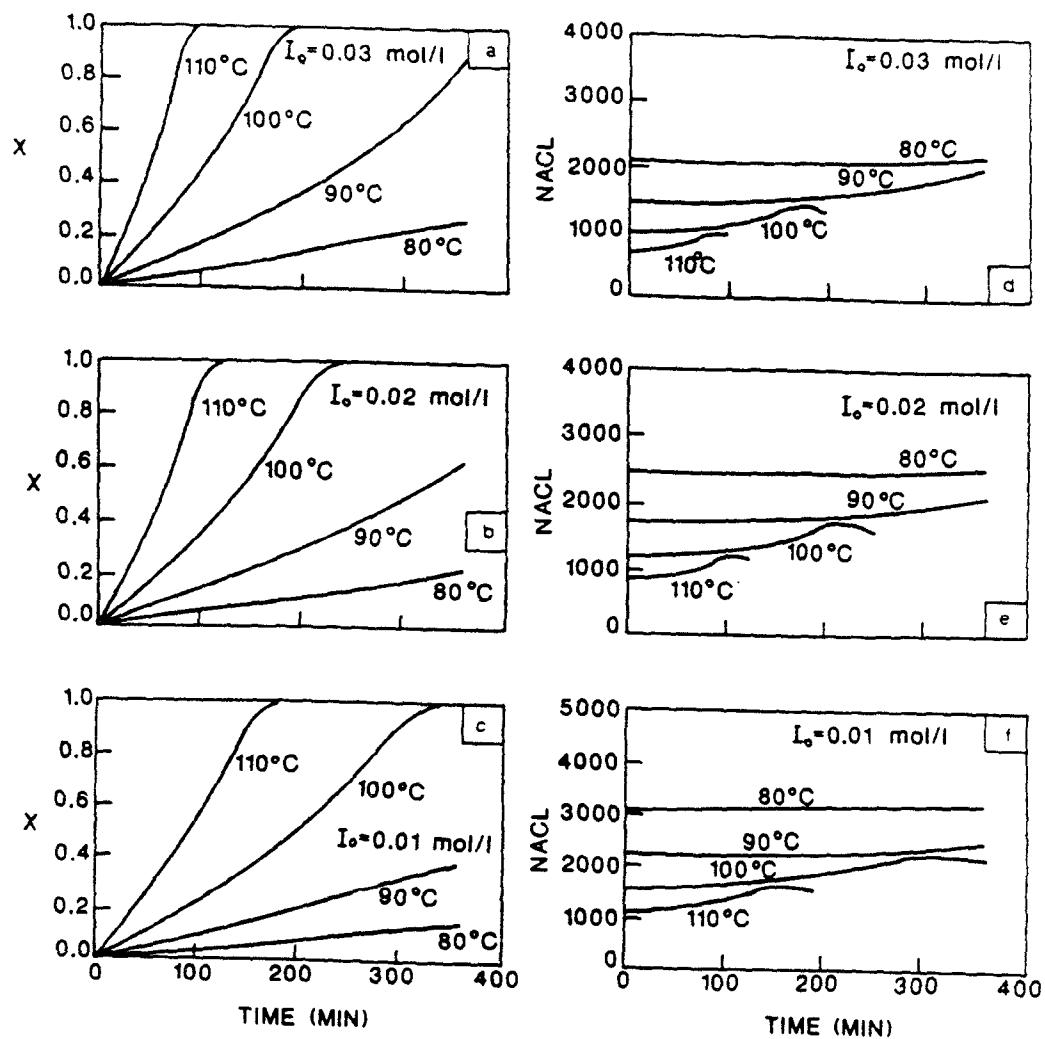
Figure 3.2   Effect of temperature and initiator concentration on monomer conversion and NACL of polystyrene with monofunctional initiator, M_A.
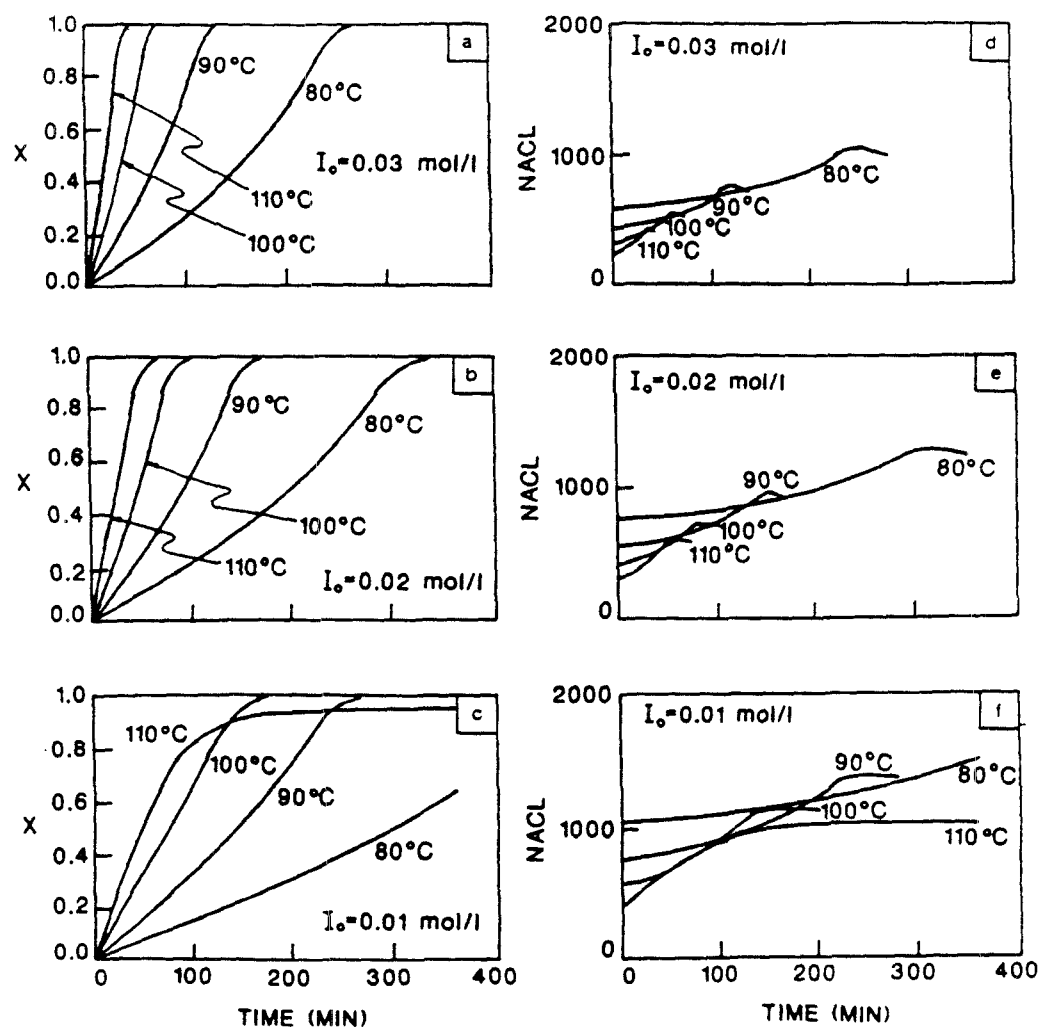
Figure 3.3   Effect of temperature and initiator concentration on monomer conversion and NACL of polystyrene with monofunctional initiator, M_B.
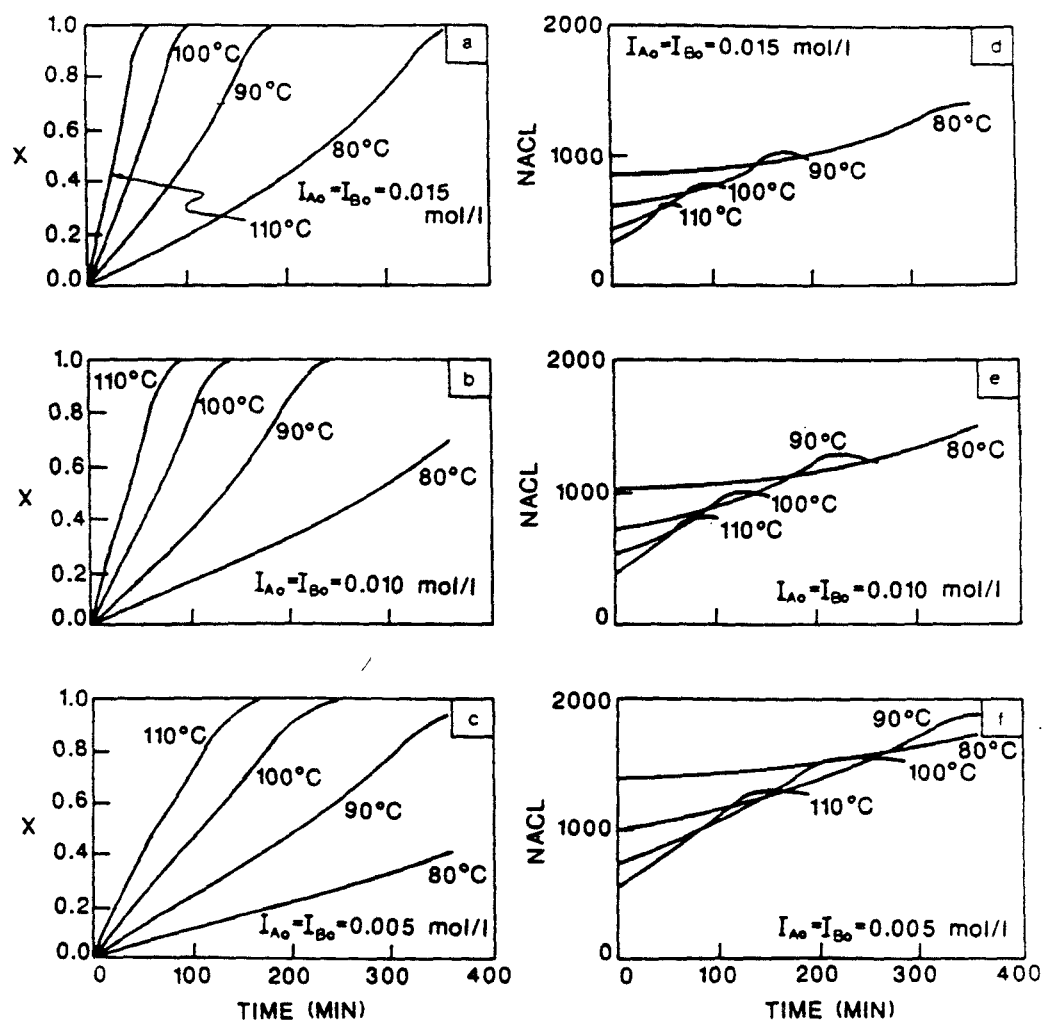
Figure 3.4   Effect of temperature and initiator concentration on monomer conversion and NACL of polystyrene with mixed initiators of M_A and M_B.
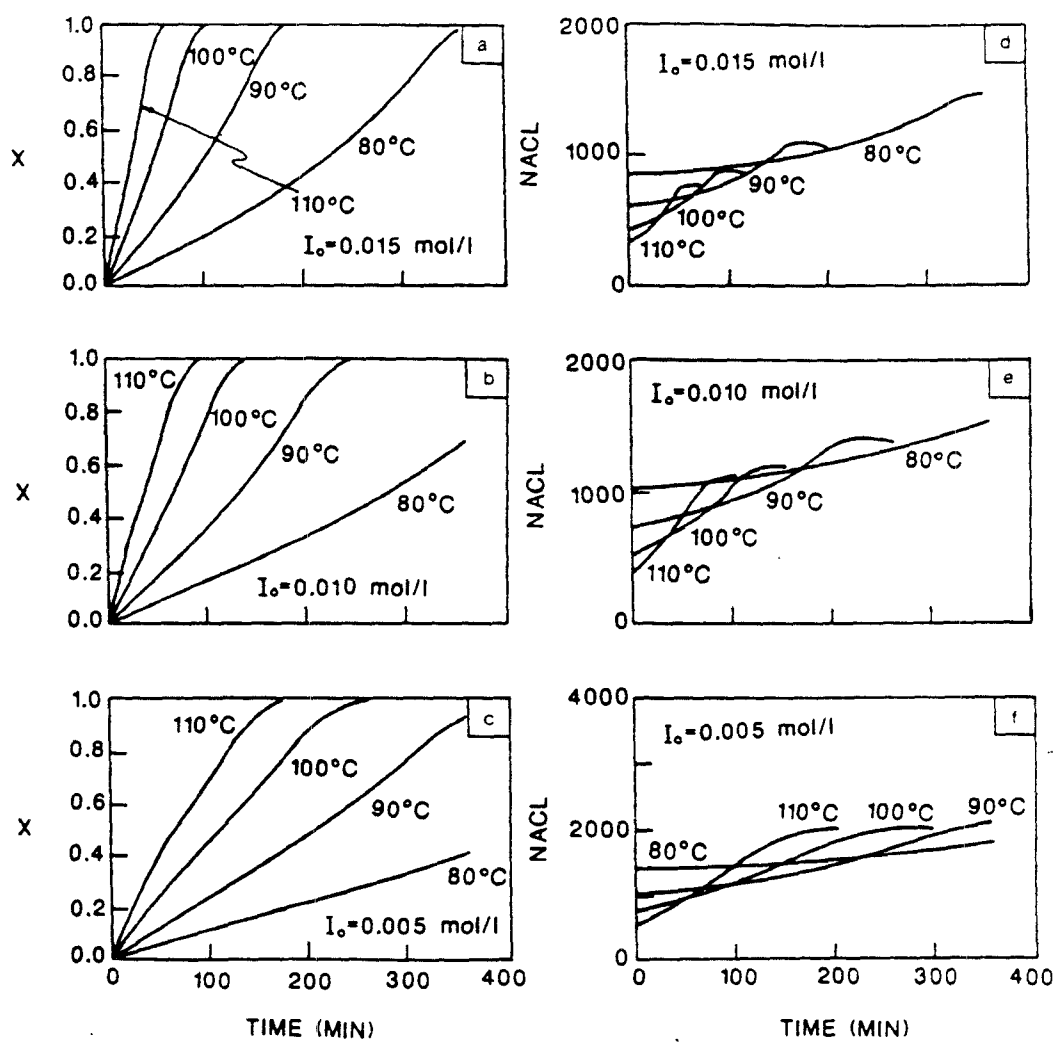
Figure 3.5   Effect of temperature and initiator concentration on monomer conversion and NACL of polystyrene with unsymmetrical bi-functional initiator.

weight becomes. When the monofunctional initiators are used, the monomer conversion and the molecular weight of polymers are influenced by the thermal stability of the peroxides. When the more stable initiator (M_A) is used, higher polymer molecular weight can be obtained than when the less stable initiator (M_B) is used but at lower polymerization rate as shown in Figures 3.2 and 3.3. As shown in Figure 3.4, the mixed initiator system of these two monofunctional initiators bears the advantages of each monofunctional initiator. For instance, the resulting molecular weight is higher than that obtained by the less stable initiator (M_B) alone and the monomer conversion is higher than that by the more stable initiator (M_A) alone. The qualitative effects of temperature and initiator concentration on the monomer conversion and the corresponding molecular weight of polymers for the mixed initiator system are similar to those of the monofunctional initiators.

The effect of unsymmetrical bifunctional initiator is shown in Figure 3.5. At relatively high initiator concentration (e.g., $I_o = 0.015$ mol/l), the profiles of the monomer conversion and the NACL are almost the same as those obtained by the mixed initiator system. However, as the initiator concentration is lower, the dramatic effect of the bifunctional initiator becomes quite clear. Note that high molecular weight and high reaction rate are simultaneously obtained by the use of unsymmetrical bifunctional initiators. Moreover, higher molecular weight is obtained at higher reaction temperature as the monomer conversion increases. Such phenomenon is not observed when single mono-

functional initiator system is employed. Figure 3.6 shows the contours of the reaction temperature and the reaction time on the monomer conversion–NACL plane for the isothermal bulk styrene polymerization with various initiator systems at fixed initial peroxide concentrations. As illustrated in Figure 3.5 and 3.6d, both high NACL and high monomer conversion are obtainable most effectively (e.g., at reduced reaction time) by using the unsymmetrical bifunctional initiators. Figure 3.6 clearly indicates that the use of unsymmetrical bifunctional initiators can broaden the range of reactor operation in producing the polymers of varying grade more effectively than the polymerization systems employing single or mixed monofunctional initiators.

Figure 3.7 illustrates the variations in peroxide concentration for both the bifunctional initiator system and the mixed initiator system at three different temperatures. When the mixed initiator system is used under isothermal reaction conditions, the decomposition of the peroxides depends on the primary initiator concentrations. The presence of the two initiators simply alters the primary radical concentrations in accordance with their thermal decomposition characteristics without any mutual interactions. As a result, the conversion of peroxide groups follows simple first order kinetics. In the bifunctional initiator system, however, the lifetime of the peroxide (A) and (B) which are distributed in the primary initiator and various polymeric species is greatly affected by the reaction conditions and the polymer composition distribution. Since considerable amounts of undecomposed peroxides (A) and
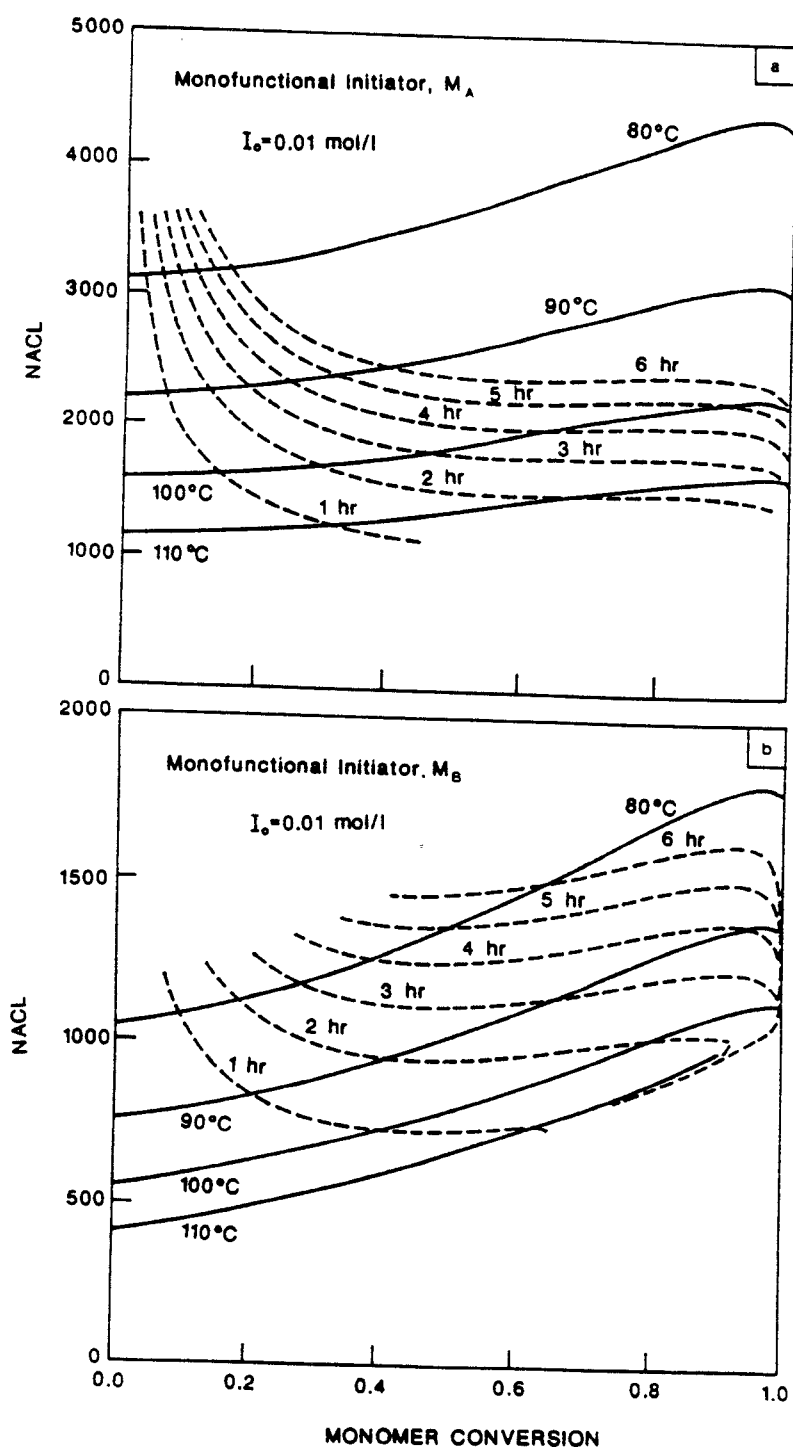
Figure 3.6   Isothermal styrene polymerizations with various initiator systems.
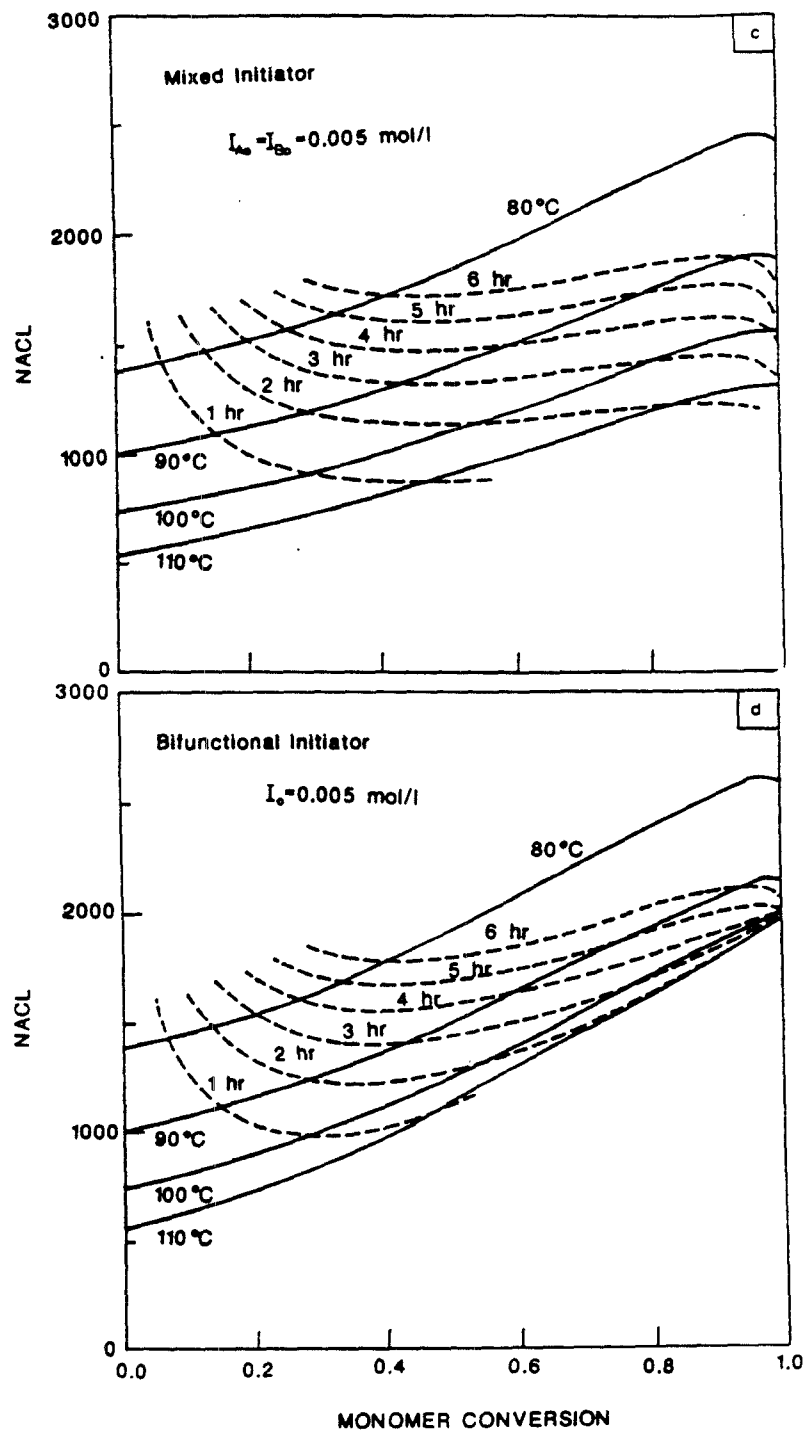
Figure 3.6   (*continued*)

161
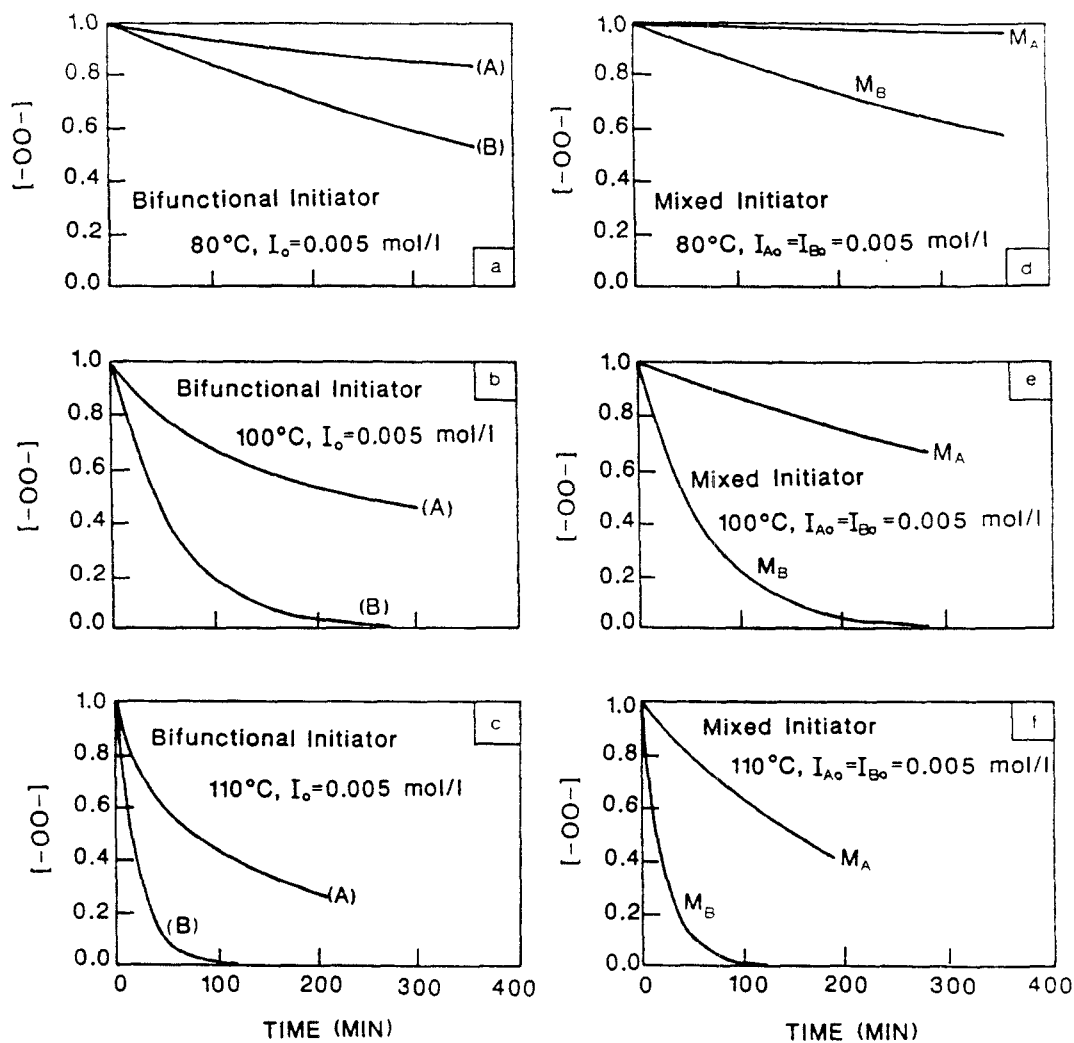
Figure 3.7   Decomposition of peroxides (A) and (B) for bifunctional initiator and mixed initiator systems.

(B) are present in various polymeric species and their decomposition rates are dependent upon the concentrations of those polymeric species (cf. Eqs. (3.52)$\sim$(3.65)), the lifetime of the peroxides (A) and (B) are extended accordingly.

Figures 3.8 and 3.9 show the weight fractions and the corresponding NACLs of various live, dead and inactive polymers for $I_o = 0.005$ mol/l at two different temperatures. Note that in both cases the concentration of diradical species T_n is extremely low. Concentrations of P_n, Q_n and S_n-type live polymers are also considerably lower than those of inactive polymeric species. The NACL of diradical polymeric species T_n is the largest of all active and inactive polymeric species due to its dual functionality. Those live diradical polymeric species are quickly engaged in combination terminations and their contributions to overall polymer molecular weight are negligible due to their extremely low concentrations in the reaction mixture. As the polymerization temperature is increased, the concentrations of inactive polymeric species containing undecomposed peroxides (eg. U_n, V_n, W_n, U'_n and V'_n) decrease with time due to the additional decomposition of both peroxides (A) and (B). Recall that the polymeric species U_n, W_n and U'_n carry more stable undecomposed peroxides (A) and V_n, W_n and V'_n less stable peroxides (B). The NACLs of those inactive polymeric species are very uniform at low temperature but become dispersed with the increase in temperature. Even though the overall NACL of the polymer is dominated by the dead polymer M_n at high temperature
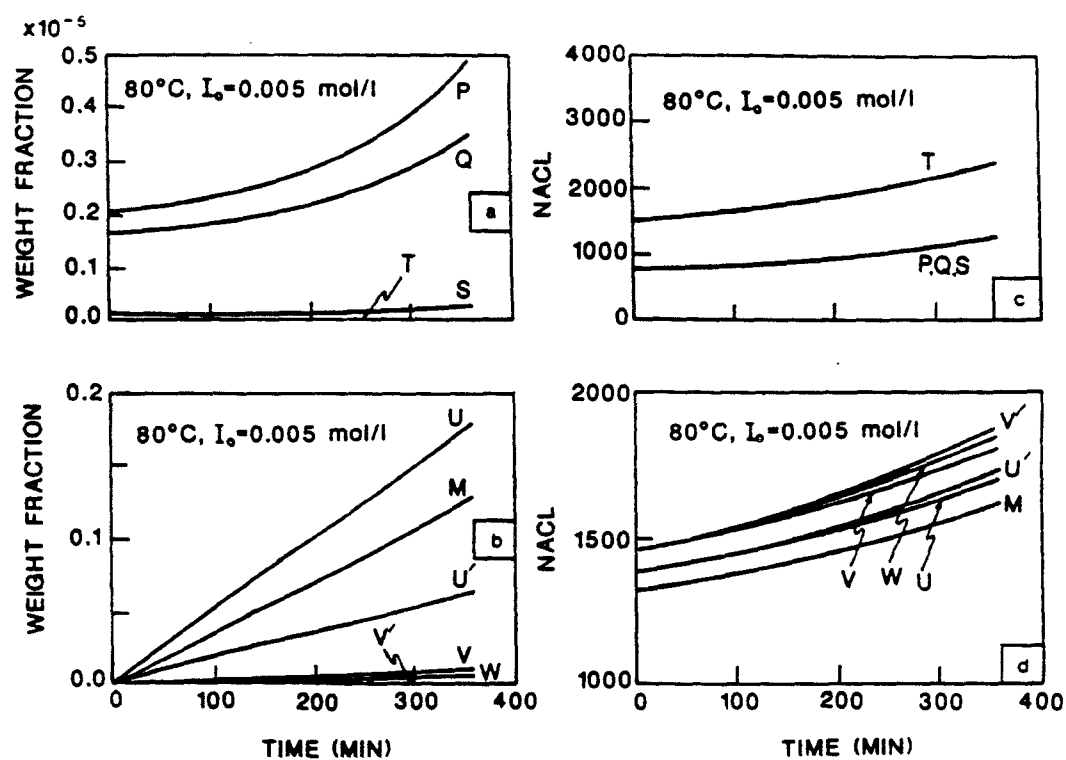
Figure 3.8   Weight fractions and NACLs of various polymeric species with bifunctional initiator at 80 °C, I_o=0.005 mol/l.
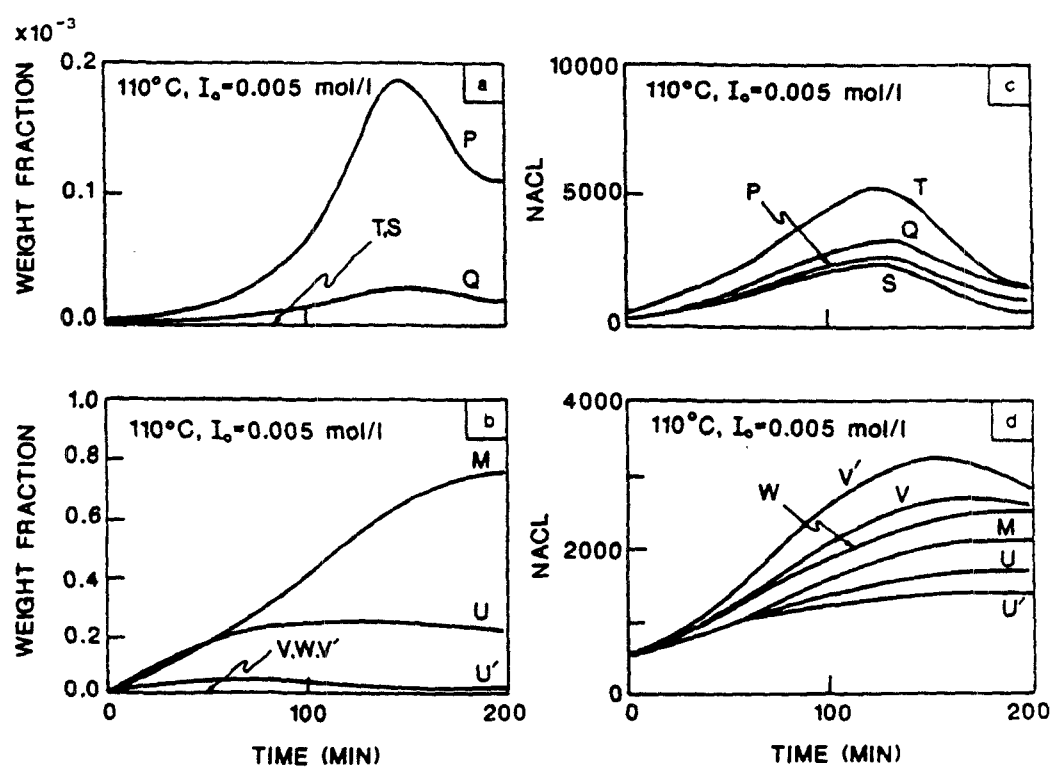
Figure 3.9   Weight fractions and NACLs of various polymeric species
with bifunctional initiator at 110 °C, $I_o = 0.005$ mol/l.

(e.g., 110 °C), the polydispersity of the polymer is affected by the dispersed NACLs of inactive polymeric species as shown in Figure 3.10.

The simulation results of the free radical styrene polymerization with different types of initiators presented in this chapter suggest that the use of the unsymmetrical bifunctional initiators enables one to achieve high monomer conversion and high molecular weight simultaneously by operating the polymerization reactors in an optimal manner. For instance, non-isothermal reactor operations will be advantageous with such bifunctional initiators in reducing the batch time and obtaining polymers of desired high molecular weight and monomer conversion.

3.2.2.3. Experimental Model Validation

The kinetic model for styrene polymerization with the unsymmetrical bifunctional initiators derived in the previous section has been examined experimentally. Polymerization experiments were carried out by Wenru Liang, a visiting professor in our laboratory, using pyrex test tubes under nitrogen atmosphere. Styrene (Aldrich) was purified with Amberlyst resins (Rohm and Hass). The bifunctional initiator 4-(t-butylperoxycarbonyl-3- hexyl-6-[7-(t-butylperoxycarbonyl) heptyl]cyclohexene (Pennwalt-Lucidol Co.) was used as supplied. The polymer samples were dissolved in benzene and precipitated by adding excess methanol. This procedure was repeated several times to ensure that unreacted monomer was completely extracted from the polymer.
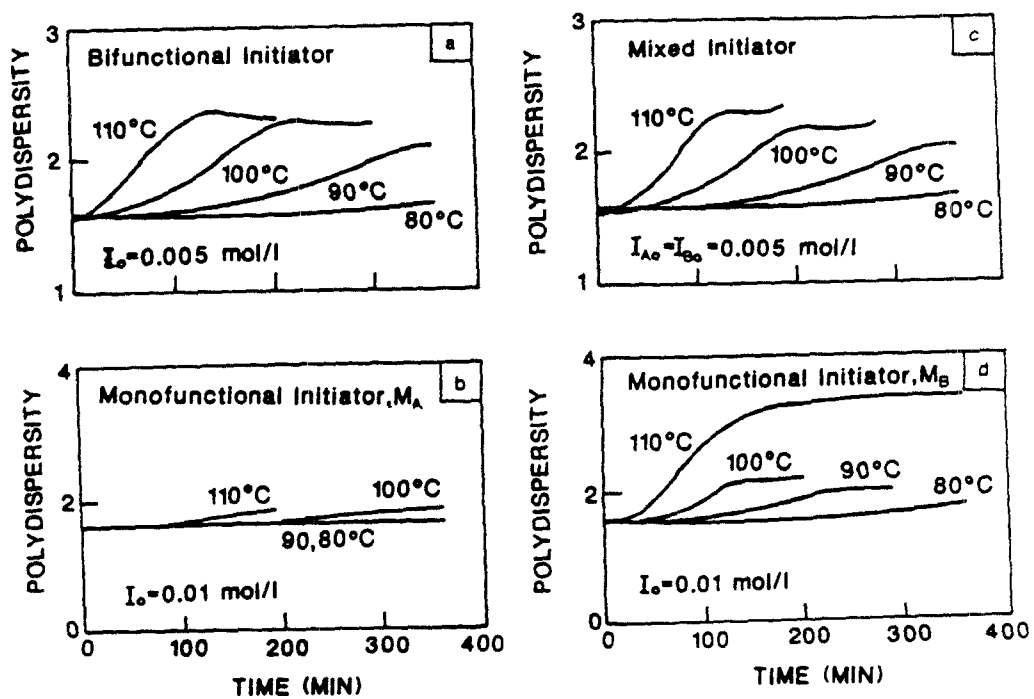
Figure 3.10 Effect of temperature on the polydispersity of polystyrene with various initiator systems.

The samples were dried in vacuo and the monomer conversion was measured by gravimetric method. The experiments were duplicated and the reproducibilities of the experimental data were excellent. The molecular weight and molecular weight distribution of polystyrene were determined by gel permeation chromatography with four Ultrastyragel columns (Waters) and tetrahydrofuran (THF) as a solvent.

Effect of Polymerization Temperature. A first set of experimental runs has been made with an initiator concentration of I_o=0.0042 mol/l at four different temperatures, *i.e.*, 80, 90, 100, 110 °C. Figure 3.11 shows the effect of reaction temperature on monomer conversion. The solid lines represent the model simulations obtained with kinetic parameters given in Table 3.3. In the model, identical initiating efficiencies for the two peroxide groups were assumed. Note that as the reaction temperature increases, an apparent break begins to appear on the monomer conversion curve (e.g., at about 35% conversion at 110 °C). Similar phenomenon has also been observed in the styrene polymerization initiated by polyfunctional initiators [Prisyazhnyuk and Ivanchev (1970), Ivanchev and Zherebin (1974)]. In general, the greater the dissimilarity in the thermal stabilities of the peroxide groups, the more pronounced is the break on the monomer conversion curves. Figure 3.12 shows the model simulations of the variation in the total concentration of undecomposed peroxides (A) and (B) in the reaction mixture at four different temperatures (C_i= [-00-]$_A$/[-00-]$_{A,o}$ or C_i= [-00-]$_B$/[-00-]$_{B,o}$). One can
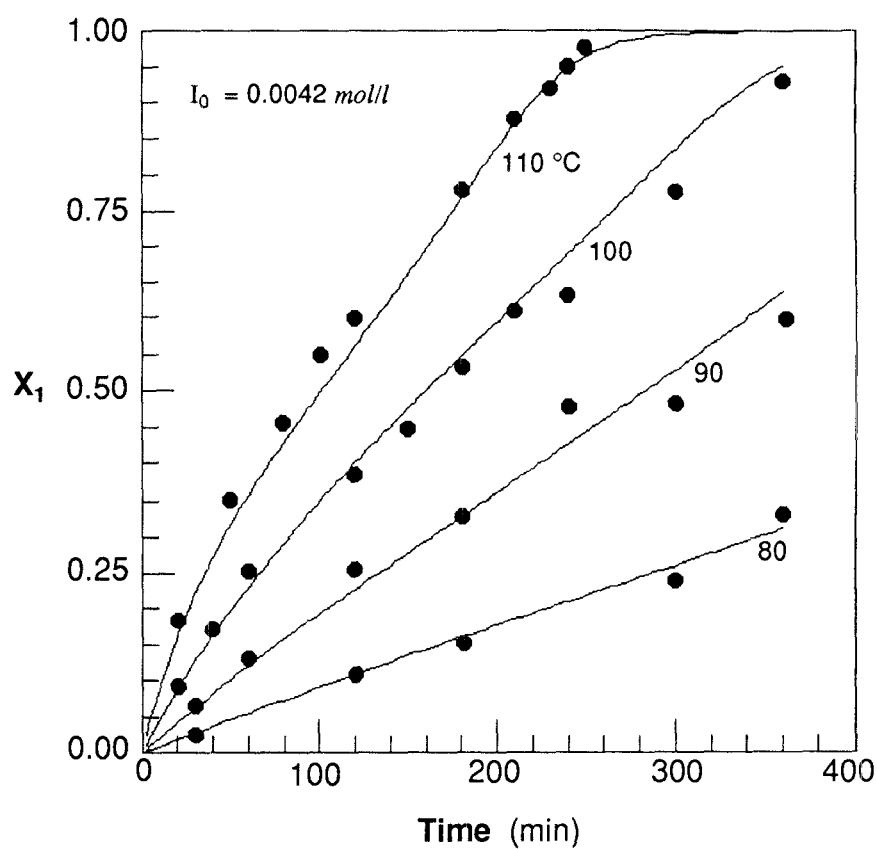
Figure 3.11   Effect of polymerization temperature on monomer conversion, $I_o = 0.0042\text{mol/l}$: •, experimental data; —, model prediction with $f_i = 0.53$ (initiator efficiency).
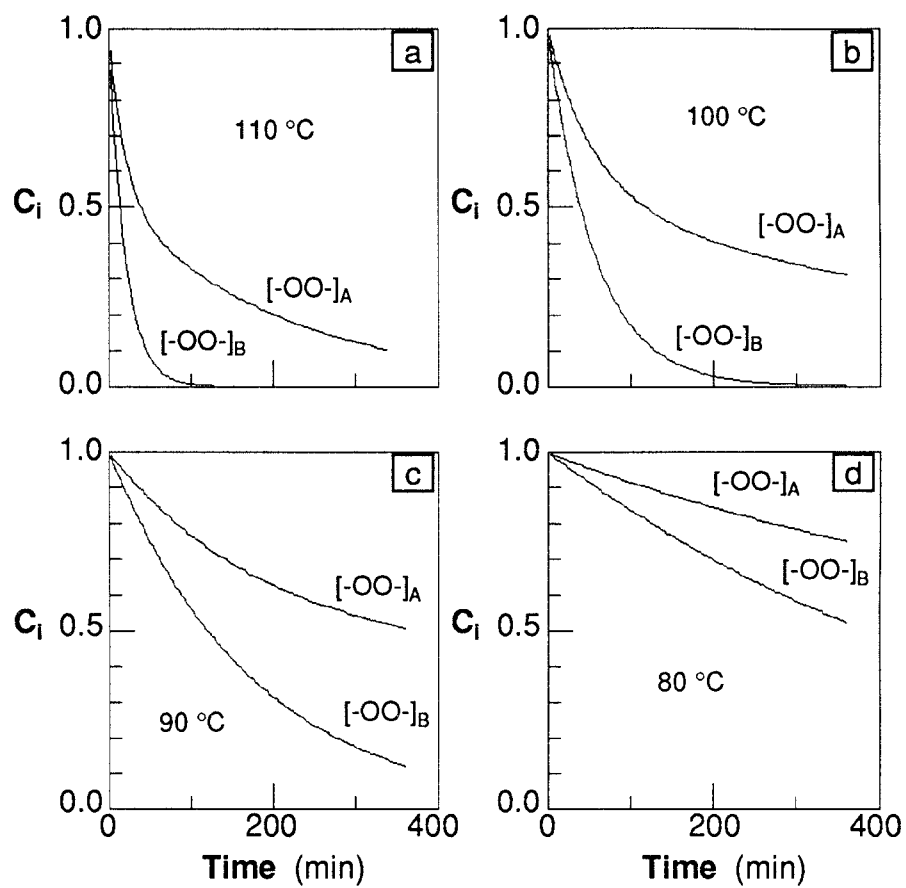
Figure 3.12   Decomposition of peroxides (A) and (B) at different temper-
atures, $I_o = 0.0042$ mol/l (model simulation).

notice that the apparent break on the monomer conversion curve at 110 °C as shown in Figure 3.11 is caused by the disappearance of less stable peroxide (B) and the continuation of the polymerization by the radicals generated from the slowly decomposing peroxide (A). The effect of reaction temperature was also examined at higher initiator concentration (I_o=0.0084 mol/l) and the resulting kinetic curves are shown in Figure 3.13. Again, apparent breaks on the monomer conversion curves appear at high reaction temperatures.

Figure 3.14 shows the number average degree of polymerization (X_n) and the weight average degree of polymerization (X_w) at different polymerization temperatures with I_o=0.0042 mol/l. When styrene polymerization was catalyzed by oligoperoxide initiator having 18 peroxides in a molecule, Ivanchev and Zherebin (1974) observed bimodal molecular weight distribution (MWD) curves. However, in our study of the styrene polymerization catalyzed by the unsymmetrical bifunctional initiator, no bimodality was observed in the MWD. The observed polydispersity values (X_w/X_n) are in the range of 2.0~2.7. Although the predicted molecular weights are slightly higher than the experimental data at 100 and 110 °C, the overall model predictions of the molecular weight are quite satisfactory.

The experimental results shown in Figures 3.11 and 3.14 are rearranged in the number average chain length of the polymer (X_n)–monomer conversion (x_1) plane in Figure 3.15. It is clearly seen that the molecular weight of polystyrene can be increased at high reaction rates by using high
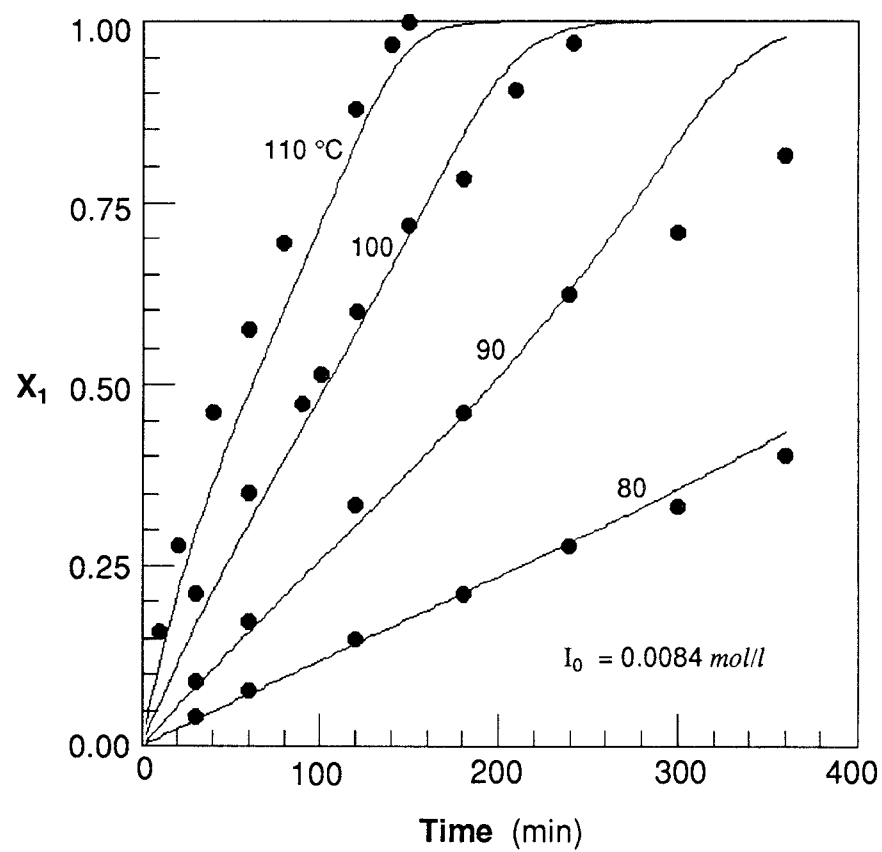
Figure 3.13   Effect of polymerization temperature on monomer conversion, $I_o = 0.0084$ mol/l: •, experimental data; —, model prediction with $f_i = 0.46$.
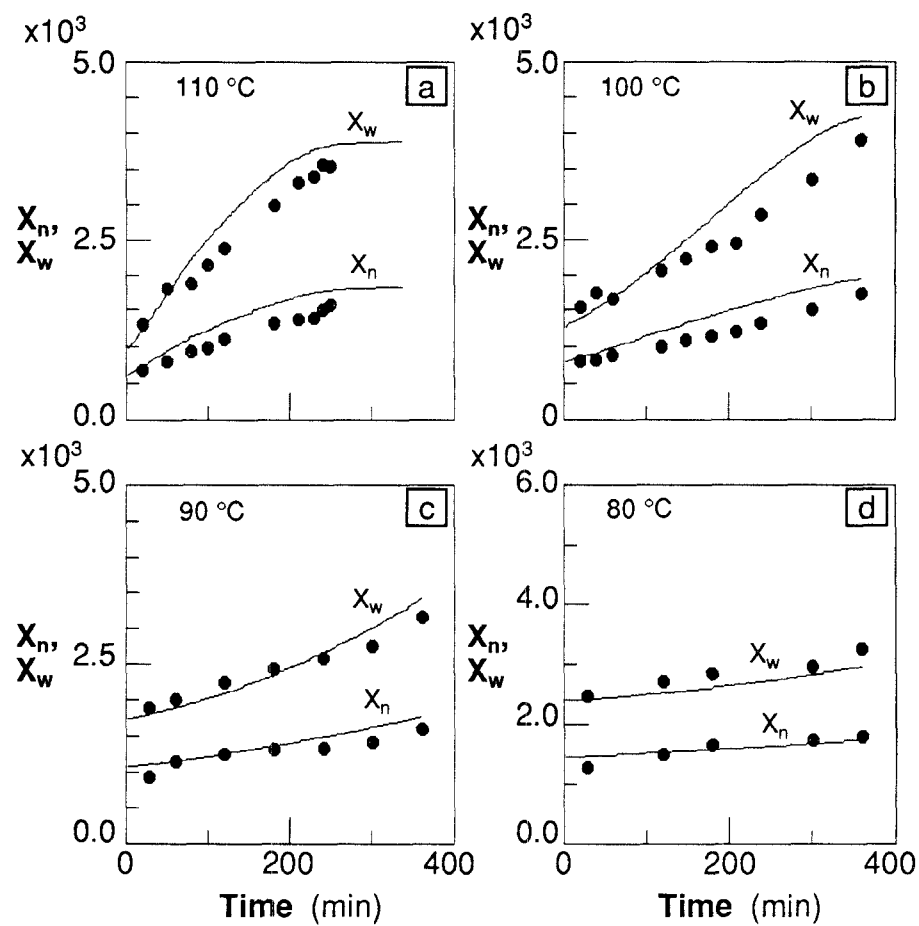
Figure 3.14   Effect of polymerization temperature on X_n and X_w, $I_o =$
0.0042 mol/l: •, experimental data; —, model prediction with
$f_i = 0.53$.
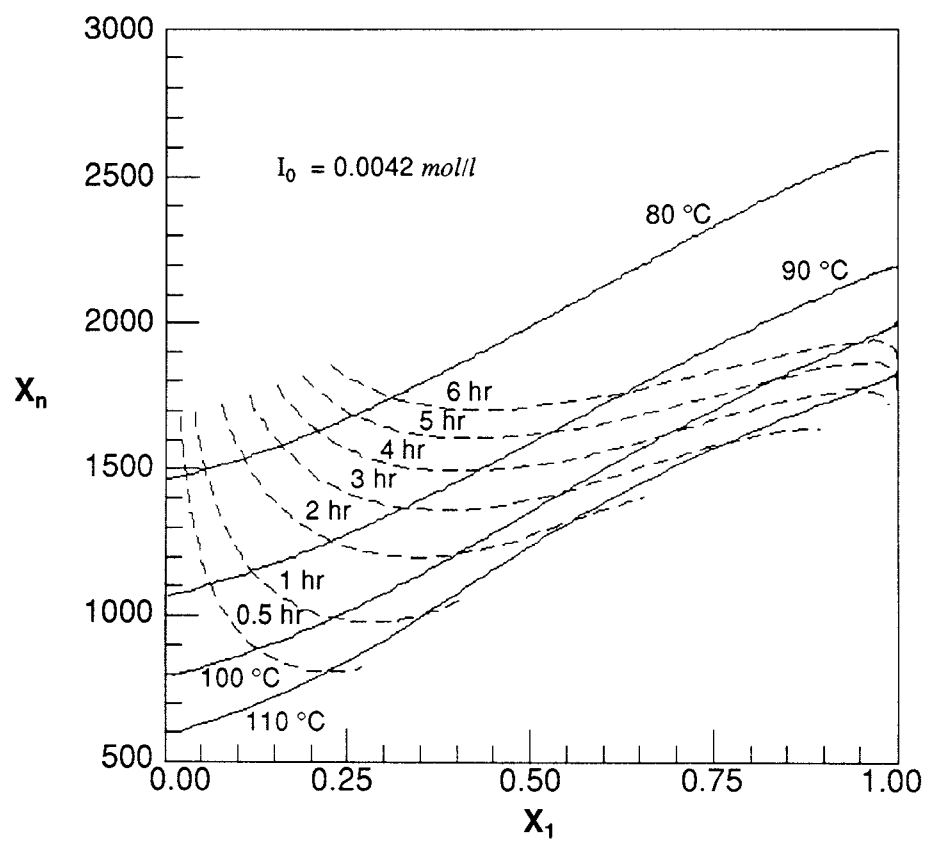
Figure 3.15   Number average chain length (NACL) v.s. monomer conversion (X_1), $I_o = 0.0042$ mol/l (experimental data).

174

polymerization temperature. The high molecular weight obtained at high temperature is due to the initiation of peroxides on the polymer chain ends followed by chain propagation reactions. In free radical polymerization of vinyl monomers with conventional monofunctional initiators, any attempt (e.g., high reaction temperature) to increase the polymerization rate leads to the decreased polymer molecular weight. Thus, the polymerization characteristics observed for the bifunctional initiator system suggests that one can achieve both high polymerization rate and high molecular weight simultaneously by using the bifunctional initiators. Moreover, better polymerization performance may be obtainable by employing nonisothermal polymerization policies. For example, dead-end polymerization which frequently occurs when high temperature is used in order to increase the reaction rate can be avoided by using the bifunctional initiators having both "slowly" decomposing and "rapidly" decomposing labile groups. The decomposition rates of these labile groups can be controlled in an optimal manner by operating the reactor at different temperature levels. As a result, batch styrene polymerization can be improved with the bifunctional initiator. For example, the total batch reaction time can be reduced and the residual peroxide concentration can be minimized by employing the optimal temperature policies.

Composition of Polymerization Mixture   Figure 3.16 shows the model simulations of the concentration profiles of various polymeric species and their number average chain lengths (NACL) during the polymerization.
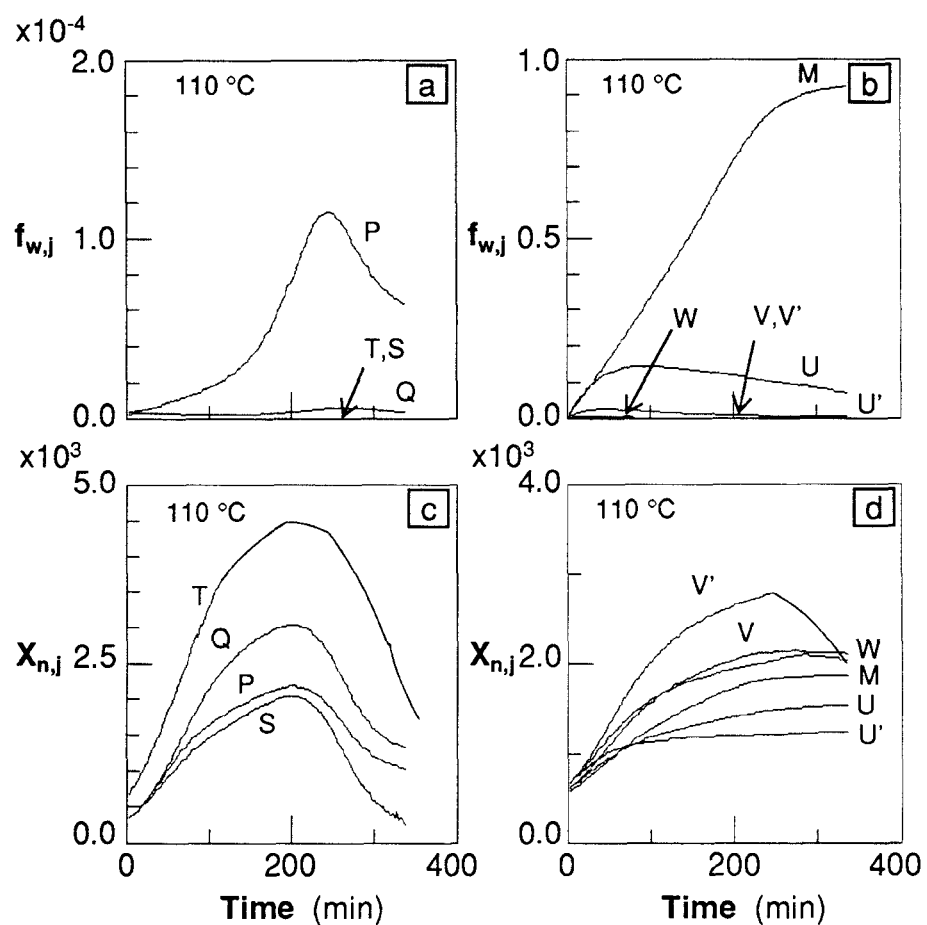
Figure 3.16   Weight fractions and number average chain length (NACL) of various polymeric species, I_o=0.0042 mol/l, 110 °C (model simulation).

Here, $f_{w,i}$ is the weight fraction of the polymer species i. As expected, the diradical polymeric species (T_n) has the longest polymer chain and, in general, live polymeric species (P_n, Q_n, S_n) have higher molecular weights than those of inactive $(U_n, V_n, W_n, U'_n, V'_n)$ and dead polymers (M_n). However, the concentrations of those live polymeric species are very low (see Figure 3.16a) and their contributions to the overall molecular weight are negligible. Figure 3.17 shows the similar diagrams for low temperature (80 °C) polymerization. Polymers such as U_n and U'_n containing undecomposed peroxides will be useful to produce block copolymers by adding other monomers to the reaction mixture and inducing the decomposition of the undecomposed peroxides (A) attached to the polystyrene chain ends. The concentration of undecomposed peroxides (A) and (B) in the polymers at four different reaction temperatures have been computed with the model and are shown in Figure 3.18 as functions of monomer conversion and number average polymer chain length. Here, $C'_{i,A}$ $[C_{i,B}]$ denotes the mole ratio of undecomposed peroxide groups (A) [(B)] to the total peroxide groups present at the beginning. Note that the amount of less stable peroxide (B) is quite small even in the low conversion regime (cf. Figure 2.18b), indicating that the chain propagation is due mainly to the primary radicals generated by the cleavage of O-O linkage in the peroxide (B) of the primary initiator. As the monomer conversion increases, the total amount of undecomposed peroxide (A) in the polymer increases and then gradually decreases with further increase in monomer conversion as those peroxides (A)
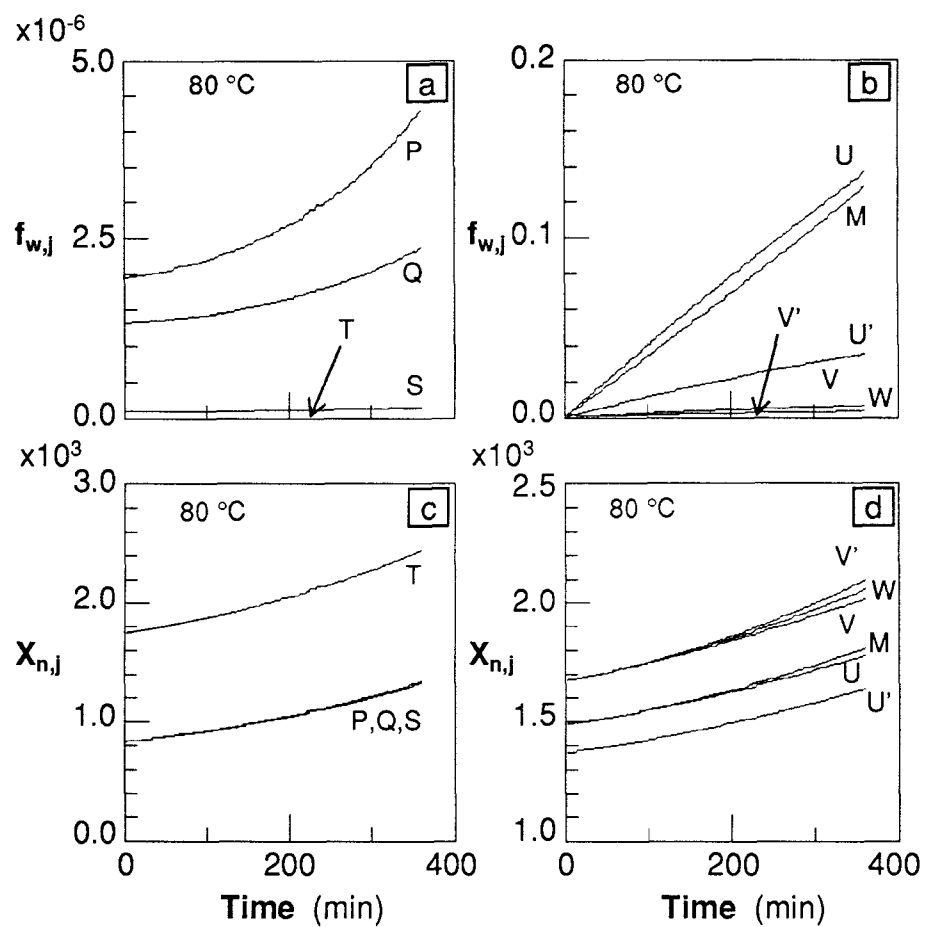
Figure 3.17   Weight fractions and number average chain length (NACL)
of various polymeric species, I_o=0.0042 mol/l, 80 °C (model
simulation).
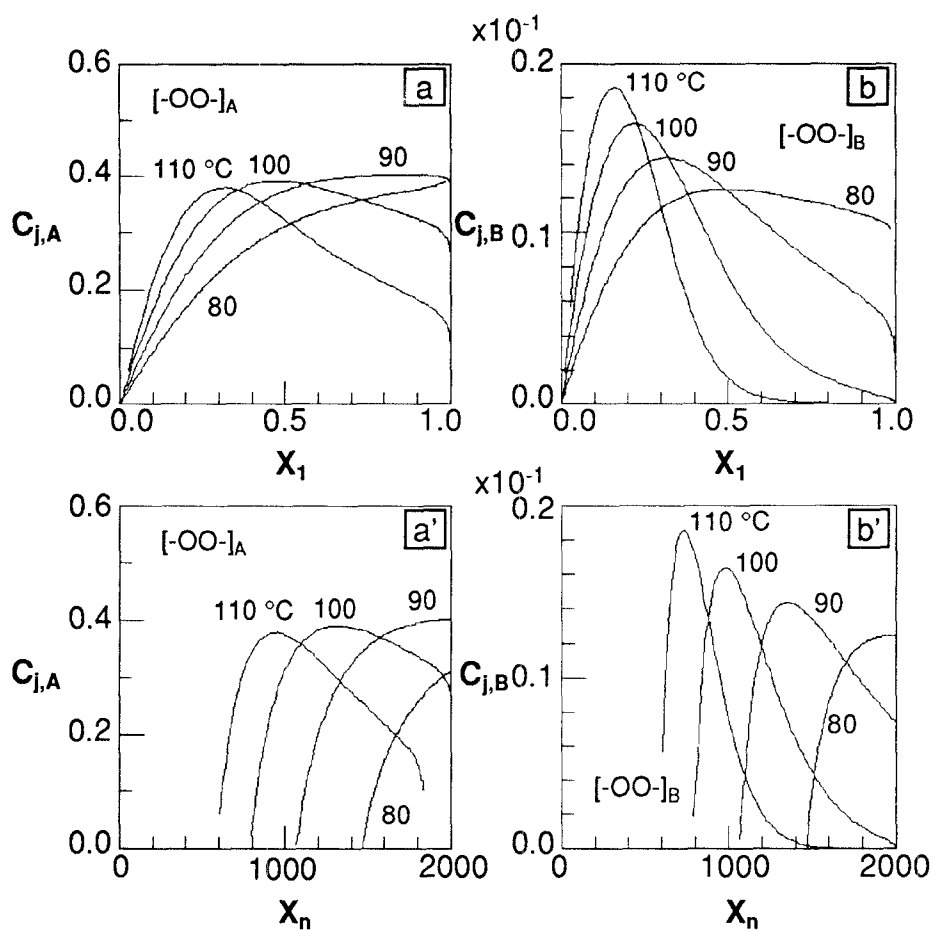
Figure 3.18   Concentration profiles of undecomposed peroxides (A) and (B) in polystyrene as functions of monomer conversion (X_1) and NACL, $I_o = 0.0042$ mol/l; $C_{i,A} = $ [-00-]$_A$/[-00-]$_{A,0}$, $C_{i,B} = $ [-00]$_B$/[-00-]$_{B,0}$ (model simulation).

attached to the polymers decompose. The concentration of the peroxide (A) in the polymer at 110 °C reaches its maximum when the degree of polymerization reaches about 900. The monomer conversion and the average molecular weight which yield the maximum concentrations of undecomposed peroxides (A) and (B) in the polymer decrease as the reaction temperature is increased. Figure 3.18a' and 3.18b' also show that the peroxide group concentration distribution in the polymer becomes narrower as the polymerization temperature is increased.

Figure 3.19 illustrates the average number of O-O groups per polymer chain of average length X_n for given values of monomer conversion ($\beta_A=$ [-OO-]$_A$/[polymer], $\beta_B=$ [-OO-]$_B$/[polymer]). For the slowly decomposing peroxide (A), the number of O-O groups per polymer chain becomes about 0.80~0.85 immediately after the commencement of polymerization and this value decreases gradually with monomer conversion. Note that during the early reaction period, more O-O groups are present in the polymer at higher temperatures; however, as the reaction proceeds, the peroxides in the polymer decompose more rapidly at higher reaction temperatures. The maximum number of less stable peroxide (B) in the polymer chain is only about 0.055~0.080 (Figure 3.19b). This low concentration of peroxide (B) in the polymer chain ends is due to the rapid decomposition of the peroxide (B). The results shown in Figures 3.18 and 3.19 will be very useful when one wants to find proper reaction conditions with the bifunctional initiator for block copolymerization.
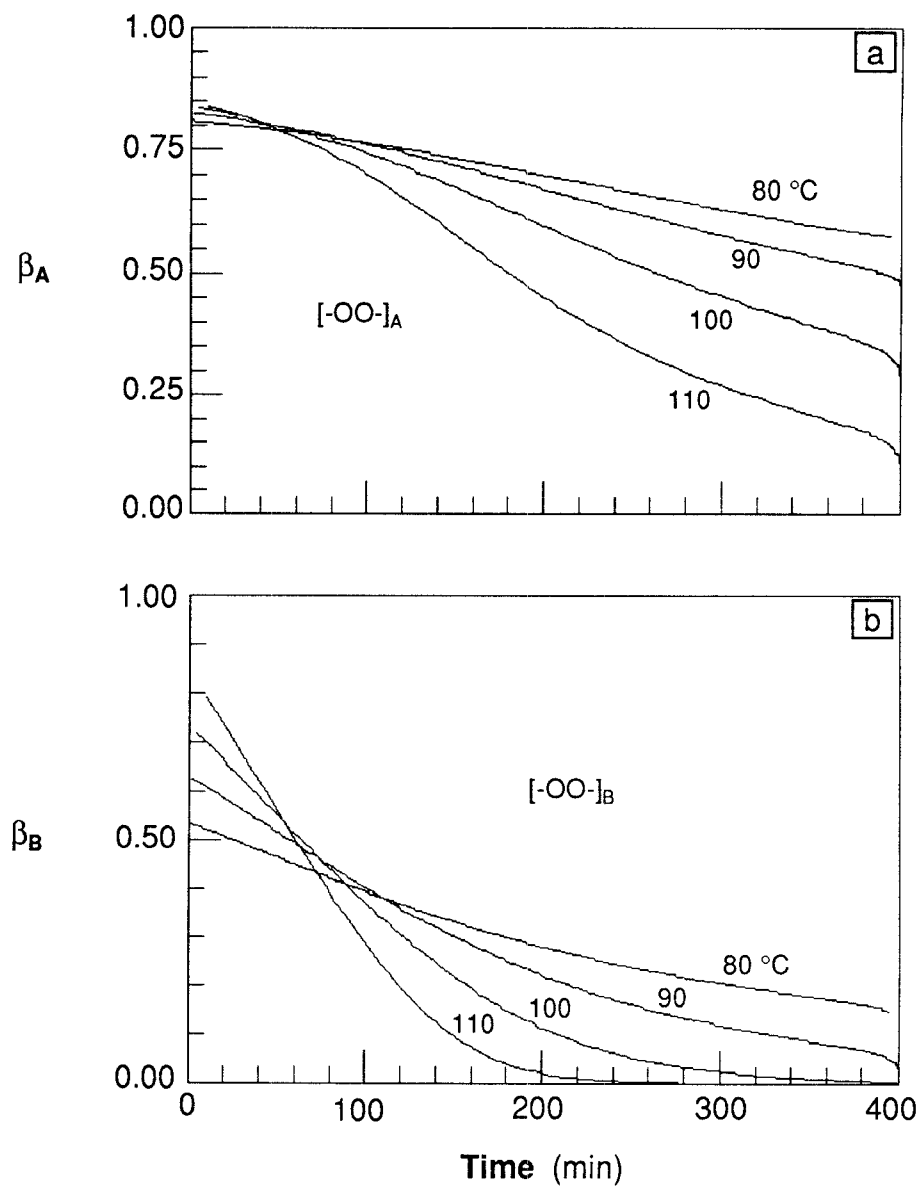
Figure 3.19   Average number of peroxide groups per each polymer chain
for given monomer conversion, $I_o = 0.0042$ mol/l; $\beta_A = $ [-00-
]$_A$/[polymer], $\beta_B = $ [-00-]$_B$/[polymer] (model simulation).

For example, such information as shown in Figures 3.18 and 3.19 will allow one to determine the reaction conditions required to obtain the polymers having desired amounts of undecomposed peroxides and the desired size of polystyrene blocks.

Initiator Efficiency   In predicting the polymerization behavior with the kinetic model, many factors influence the quality of quantitative model predictions. Among these factors, the kinetic parameters (rate constants) are the most important. For the simulation of the kinetic model, accurate rate parameters and initiator efficiency factor (f_i) must be used. Although styrene polymerization has been studied extensively by numerous researchers in the past, there still exists some inconsistency in the numerical values of the kinetic parameters reported in the literature. The rate constants (e.g., propagation, termination, chain transfer reactions) used in our model simulations were obtained mostly from the Polymer Handbook [Brandrup and Immergut (1979)] and the initiator decomposition rate constants were provided by the initiator supplier (Pennwalt-Lucidol Co.). The selected rate parameters have been tested on the bulk styrene polymerization initiated by a monofunctional initiator, t-butyl perbenzoate. The experimental conditions (e.g., initiator concentration and reaction temperature) used were similar to those of bifunctional initiator catalyzed polymerization. It was found that the experimental data (monomer conversion and polymer molecular weight) for this *tert*-butyl perbenzoate system agree very well with the predictions by the kinetic model

developed for monofunctional initiator systems. This test result indicates that the rate constants we used for the simulation of bifunctional initiator catalyzed styrene polymerization are quite accurate.

Unfortunately, however, the exact value of the initiator efficiency factor, which is defined as the fraction of primary radical species which successfully initiate the chain propagation, was unknown for the bifunctional initiator used in our study. Due to the complexity of the polymerization kinetics, it is not feasible to derive from the kinetic model a closed form of test equation required for the estimation of the initiator efficiency factor with experimental data. Therefore, we used the optimal parameter estimation technique in order to determine the initiator efficiency factor for the bifunctional initiator. Theoretically, the two peroxide groups in the initiator [(A) and (B)] may have different initiating efficiencies; however, we assumed that the efficiencies of these peroxides were identical. The induced decomposition reaction was not included in our kinetic scheme described earlier in this paper. Therefore, the initiator efficiency estimated by the optimal search will be an apparent (or overall) initiator efficiency. Using the experimental conversion data obtained at 80~110 °C with an initiator concentration of 0.0042 mol/l, we obtained the efficiency factor of 0.53 . The method used was the Rosenbrock's direct search method [Rosenbrock (1960)]. With this initiator efficiency factor, very satisfactory model predictions were obtained as shown in Figure 3.11. The optimally estimated initiator efficiency factor was further assessed as follows.

As shown in Figure 3.12, the peroxide (B) decomposes much faster than the peroxide (A). Thus, we may assume that during the initial short reaction period, the monomer conversion is due mainly to the radicals generated by the decomposition of the peroxide (B). In other words, we can estimate the initiator efficiency factor by using the initial polymerization rate which can be estimated by extrapolating the polymerization rate to time zero. For this purpose, we used the kinetic model for monofunctional initiators in this short time period. The following equation was used to estimate the initiator efficiency factor f_i:

$$R_{p,o}\left[=-\left(\frac{dM}{dt}\right)_{t=0}\right] = k_p M_o \left(\frac{2 f_i k_{d_B} I_{B,o}}{k_t}\right)^{\frac{1}{2}} \tag{3.74}$$

where $R_{p,o}$ is the initial polymerization rate, M_o the initial monomer concentration, and $I_{B,o}$ the initial concentration of peroxide (B). Figure 3.20 shows the test of this equation. Note that a straight line passing through the origin is obtained. From the slope of this line, the initiator efficiency factor has been found to be 0.562 which is very similar to the value estimated by the optimal search technique (0.53). It is also interesting to observe that the initiator efficiency obtained for the unsymmetrical bifunctional initiator is somewhat lower than that for many monofunctional initiators (e.g., 0.6~0.8). Low overall initiator efficiency factor has also been observed for many other multifunctional initiator systems reported in the literature [Ivanchev and Zherebin (1974), Vuillemenot et al. (1965)]. In general, the initiator efficiency decreases with
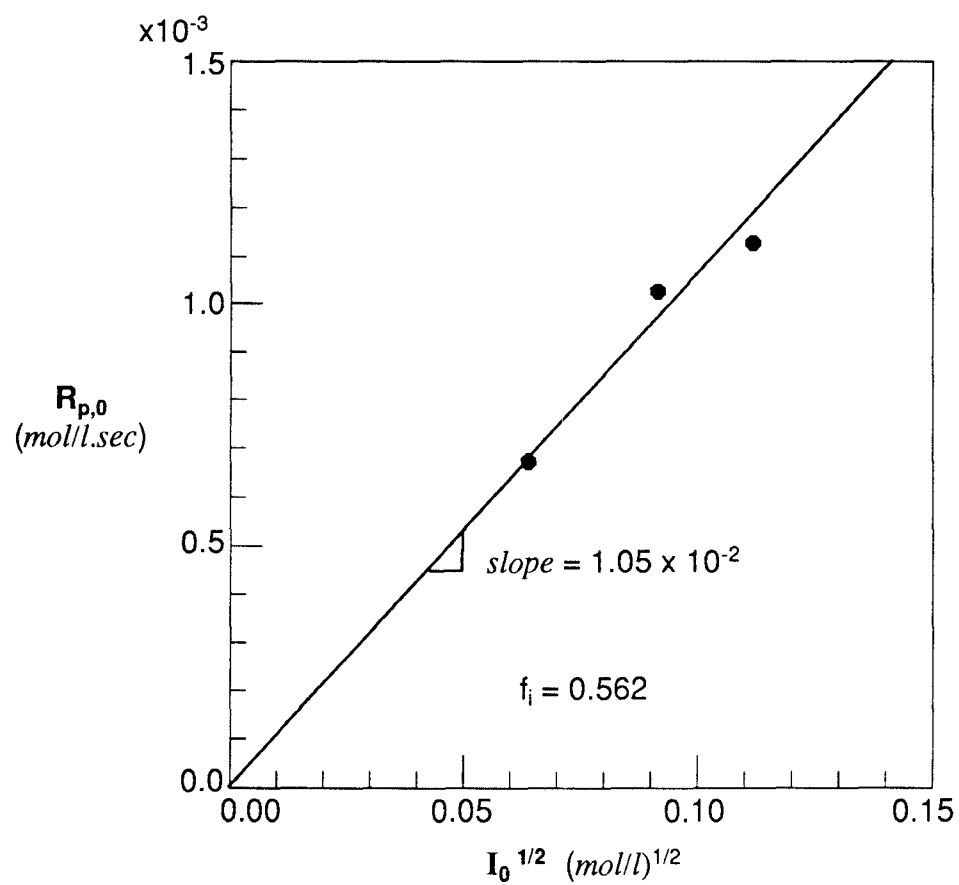
Figure 3.20   Test of equation (4.74) for the estimation of initiator efficiency
factor, 100 °C.

an increase in the number of labile functional groups in the initiator molecule.

Interestingly, it has also been observed that when this optimally estimated initiator efficiency factor (0.53) was used for the polymerization simulations at higher initiator concentrations (e.g., 0.0084 and 0.0126 mol/l), significant deviation from the experimental conversion data has occurred. Figure 3.21 illustrates this point. In particular, the deviation becomes larger at high initiator concentrations as the monomer conversion increases. Therefore, it was decided to estimate the initiator efficiency factors using the experimental data for different initiator concentrations. It has been found that the optimally estimated initiator efficiency factors for I_o=0.0084 mol/l and 0.0126 mol/l were 0.46 and 0.37, respectively. These values are substantially lower than the efficiency factor (0.53) obtained at lower initiator concentration (i.e., I_o=0.0042 mol/l). When these new initiator efficiency factors are used in the model simulations for higher initiator concentration cases, very accurate predictions of monomer conversion are obtained (e.g., Figure 3.13). It is also observed that the initiator efficiency factor decreases linearly with the initiator concentration as illustrated in Figure 3.22. This anomalous behavior suggests that the initiating efficiency of the two peroxide groups may not be identical. It is also probable that some reactions not considered in our model, e.g., primary radical termination and induced decomposition, may become important as the monomer conversion increases at high initiator concentrations.
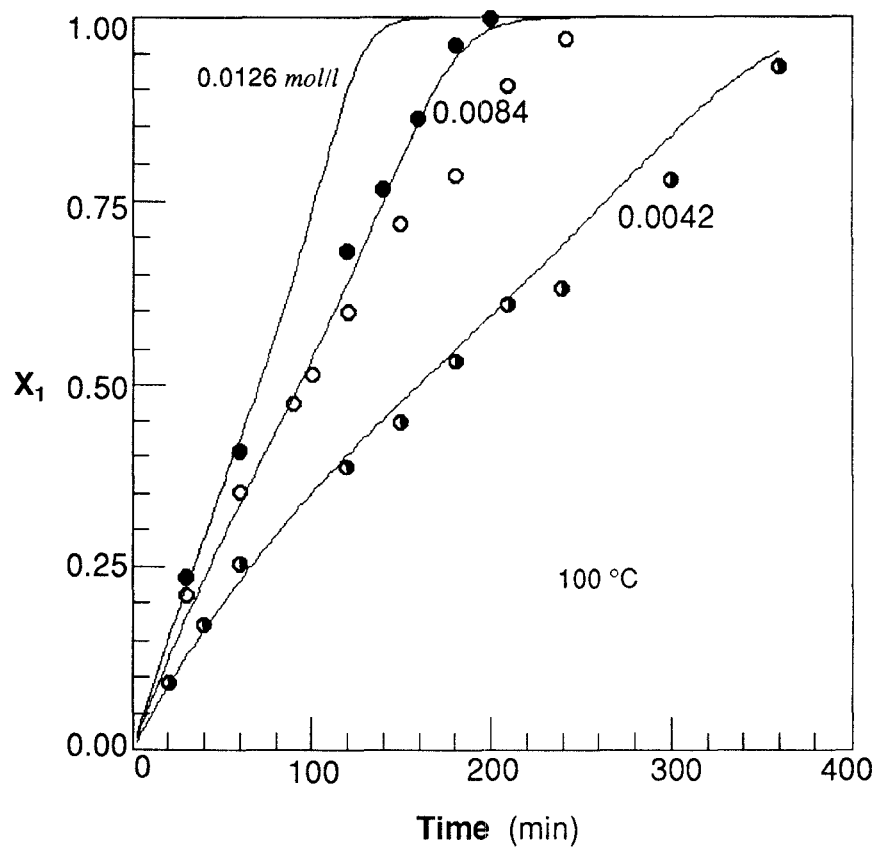
Figure 3.21   Monomer conversion profiles at different initiator concentrations: •, I_o = 0.0126 mol/l; o, I_o = 0.0084 mol/l; o, I_o = 0.0042 mol/l; —, model prediction with f_i = 0.53.

$$f_i = 0.6807 - 18.2\, I_0$$
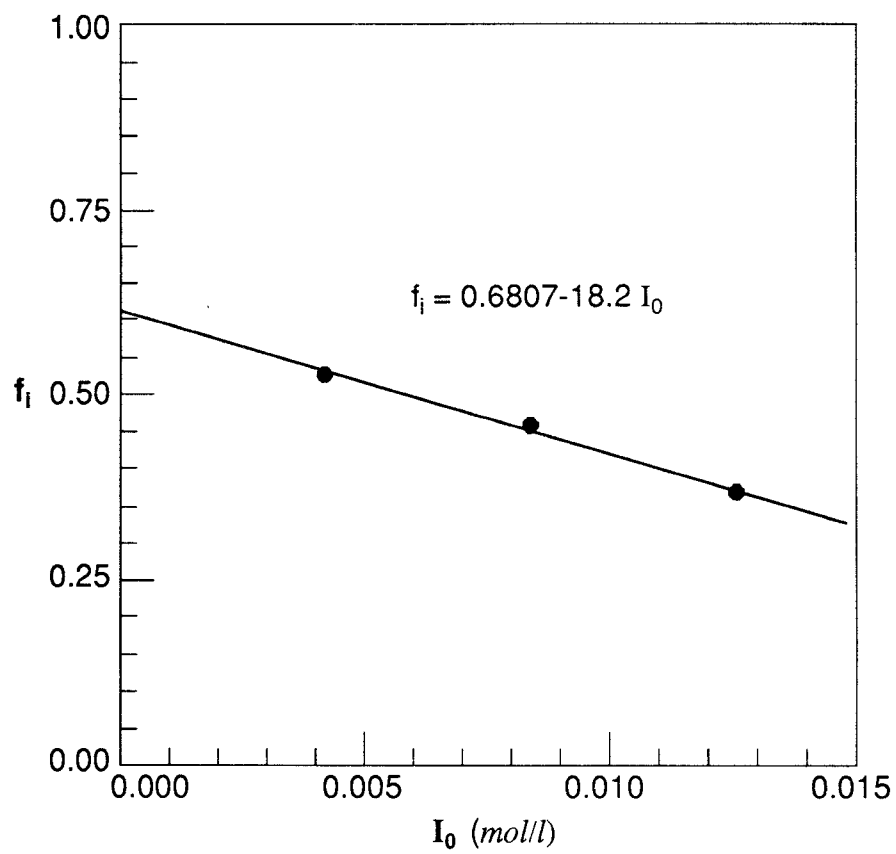
Figure 3.22   Effect of initiator concentration on the initiator efficiency factor, 100 °C.

3.3. Steady State Behavior of a CSTR

3.3.1. Reactor Model

For free radical homopolymerization of styrene with symmetrical bifunctional initiator (§3.2.1), mass and energy balances of a continuous stirred tank reactor of volume V are represented by the following equations:

$$V \frac{dM}{dt'} = q(M_f - M) - V k_p M(P + Q + 2S) \tag{3.75}$$

$$V \frac{dI}{dt'} = q(I_f - I) - 2V k_{d1} I \tag{3.76}$$

$$\rho C_p V \frac{dT}{dt'} = \rho C_p q(T_f - T) + V(-\Delta H_r) k_p M(P + Q + 2S)$$
$$- h_c A_c(T - T_c) \tag{3.77}$$

Here, M is the monomer concentration, I the initiator concentration, and T the reactor temperature. q denotes the volumetric flow rate of feed and product streams, h_c the effective heat transfer coefficient and T_c the coolant temperature. Physical properties of the polymer mixture (e.g. ρ, C_p) are assumed constant. In this model, the effects of thermal initiation and depolymerization which may occur at very high temperatures are ignored. Due to the presence of active polymeric species (P_n, Q_n, S_n) and inactive polymeric species (T_n, Z_n, M_n), the above nonlinear modeling equations become quite complicated.

The moment equations for inactive polymers (species M_n, T_n and Z_n) take the following form:

$$\frac{d\lambda_0^d}{dt'} = -\frac{1}{\theta}\lambda_0^d + \frac{1}{2}k_t\lambda_{P,0}^2 \tag{3.78a}$$

$$\frac{d\lambda_1^d}{dt'} = -\frac{1}{\theta}\lambda_1^d + k_t\lambda_{P,0}\lambda_{P,1} \tag{3.78b}$$

$$\frac{d\lambda_2^d}{dt'} = -\frac{1}{\theta}\lambda_2^d + k_t(\lambda_{P,0}\lambda_{P,2} + \lambda_{P,1}^2) \tag{3.78c}$$

$$\frac{d\lambda_{T,0}}{dt'} = -\frac{1}{\theta}\lambda_{T,0} + \frac{1}{2}k_t\lambda_{Q,0}^2 - 2k_{d2}\lambda_{T,0} \tag{3.79a}$$

$$\frac{d\lambda_{T,1}}{dt'} = -\frac{1}{\theta}\lambda_{T,1} + k_t\lambda_{Q,0}\lambda_{Q,1} - 2k_{d2}\lambda_{T,1} \tag{3.79b}$$

$$\frac{d\lambda_{T,2}}{dt'} = -\frac{1}{\theta}\lambda_{T,2} + k_t(\lambda_{Q,0}\lambda_{Q,2} + \lambda_{Q,1}^2) - 2k_{d2}\lambda_{T,2} \tag{3.79c}$$

$$\frac{d\lambda_{Z,0}}{dt'} = -\frac{1}{\theta}\lambda_{Z,0} + k_t\lambda_{P,0}\lambda_{Q,0} - k_{d2}\lambda_{Z,0} \tag{3.80a}$$

$$\frac{d\lambda_{Z,1}}{dt'} = -\frac{1}{\theta}\lambda_{Z,1} + k_t(\lambda_{P,0}\lambda_{Q,1} + \lambda_{P,1}\lambda_{Q,0}) - k_{d2}\lambda_{Z,1} \tag{3.80b}$$

$$\frac{d\lambda_{Z,2}}{dt'} = -\frac{1}{\theta}\lambda_{Z,2} + k_t(\lambda_{P,0}\lambda_{Q,2} + 2\lambda_{P,1}\lambda_{Q,1} + \lambda_{P,2}\lambda_{Q,0}) - k_{d2}\lambda_{Z,2} \tag{3.80c}$$

The number average polymer chain length (X_N) and the weight average chain length (X_W) are defined by

$$X_N = \frac{\lambda_{P,1} + \lambda_{Q,1} + \lambda_{S,1} + \lambda_{T,1} + \lambda_{Z,1} + \lambda_1^d}{\lambda_{P,0} + \lambda_{Q,0} + \lambda_{S,0} + \lambda_{T,0} + \lambda_{Z,0} + \lambda_0^d} \tag{3.81a}$$

$$X_W = \frac{\lambda_{P,2} + \lambda_{Q,2} + \lambda_{S,2} + \lambda_{T,2} + \lambda_{Z,2} + \lambda_2^d}{\lambda_{P,1} + \lambda_{Q,1} + \lambda_{S,1} + \lambda_{T,1} + \lambda_{Z,1} + \lambda_1^d} \tag{3.81b}$$

where $\lambda_{j,k}$ represents the k-th moment of polymeric species j. The polydispersity index (PD) is a measure of molecular weight distribution broadening and

is defined by the ratio of X_W to X_N. The moment equations (3.78)$\sim$(3.81) are solved simultaneously with reactor modeling equations.

The modeling equations are reduced to dimensionless form by using the following dimensionless variables and parameters:

$$X_1 = \frac{M_f - M}{M_f}, \qquad X_2 = \frac{I_f - I}{I_f}, \qquad X_3 = \frac{T - T_f}{T_f},$$

$$X_p = \frac{P + Q + 2S}{(P + Q + 2S)_f}, \qquad \alpha = \frac{h_c A_c}{\rho C_p V \kappa(T_f)}, \qquad \beta = \frac{(-\Delta H_r)M_f}{\rho C_p T_f},$$

$$\gamma = \frac{E_p}{RT_f}, \qquad \gamma_1 = \frac{E_{d1}}{RT_f}, \qquad \delta = \frac{T_c - T}{T_f}, \qquad (3.82)$$

$$Da = \theta\kappa(T_f), \qquad t = \frac{t'}{\theta}, \qquad K = \frac{2k_{d10}}{\kappa(T_f)}$$

where

$$\kappa(T_f) = k_{p0}(P + Q + 2S)_f \exp(\frac{E_p}{RT_f})$$

The subscript f denotes the feed condition and $(P + Q + 2S)_f$ is the total concentration of live polymers in the reactor at the feed temperature and concentration conditions. Then, the following dimensionless modeling equations are obtained:

$$\frac{dX_1}{dt} = -X_1 + Da(1 - X_1)X_p \exp\left[\frac{\gamma X_3}{1 + X_3}\right] \qquad (3.83)$$

$$\frac{dX_2}{dt} = -X_2 + K Da(1 - X_2)\exp\left[-\frac{\gamma_1}{1 + X_3}\right] \qquad (3.84)$$

$$\frac{dX_3}{dt} = -X_3 + \beta(X_1 + \frac{dX_1}{dt}) - \alpha Da(X_3 - \delta) \qquad (3.85)$$

Note that α refers to the dimensionless heat transfer coefficient, β the dimensionless heat of reaction, and Da the dimensionless mean residence time which can be changed experimentally by varying the reactant flow rate. Because of the high degree of nonlinearity and interaction in the modeling equations, some care must be taken in obtaining the steady state solutions. At steady state, the LHS of the modeling equations (3.83)~(3.85) vanish and the steady state solutions are computed by the following procedure.

(i) For fixed value of Da and β, use eqs (3.84) and (3.85) to obtain:

$$X_{2s} = \frac{KDa\exp[-\frac{\gamma_1}{1+X_{3s}}]}{1 + KDa\exp[-\frac{\gamma_1}{1+X_{3s}}]} \tag{3.86}$$

$$X_{3s} = \frac{\beta X_{1s} + \alpha Da\delta}{1 + \alpha Da} \tag{3.87}$$

where subscript s denotes the steady state condition.

(ii) The dimensionless total live polymer concentration (X_p) is computed by solving the following equations which are from the steady state zeroth moment equations of P, Q and S:

$$a_{11} - a_2(P+Q)P + (a_3 + a_4Q + a_5P)Q = 0 \tag{3.88}$$

$$Q = \frac{1}{2(a_2 - a_4)}[-a_2P - a_3 + \{(a_2P + a_3)^2 + 4a_{12}(a_2 - a_4)\}^{\frac{1}{2}}] \tag{3.89}$$

$$S = -\frac{1}{2}(P+Q) + \frac{1}{2}[(P+Q)^2 + 2(\frac{a_3}{a_2})Q]^{\frac{1}{2}} \tag{3.90}$$

where

192

$$a_{1i} = f_i k_{d10} I_f (1 - X_2) \exp[-\frac{\gamma_1}{1 + X_3}],$$

$$a_2 = k_{t0} g_t \exp[-\frac{\gamma_t}{1 + X_3}], \qquad a_3 = k_{d20} \exp[-\frac{\gamma_d}{1 + X_3}],$$

$$a_4 = \frac{a_2 a_3 \theta}{1 + 2 a_3 \theta}, \qquad a_5 = \frac{2 a_2 a_3 \theta}{1 + a_3 \theta},$$

$$\gamma_t = \frac{E_t}{RT_f}, \qquad \gamma_d = \frac{E_{d2}}{RT_f}.$$

(iii) Substitute the results of steps (i) and (ii) into Eq. (3.83) and solve the resulting nonlinear equation for the monomer conversion for $0 \leq X_1 \leq 1$:

$$F(X_1, Da, \beta) = -X_1 + Da(1 - X_1) X_p \exp(\frac{\gamma X_3}{1 + X_3}) = 0 \qquad (3.91)$$

(iv) Vary Da and repeat steps (i), (ii) and (iii).

This procedure guarantees that all solutions are found for all admissible values of Da. The mathematical expressions of steady state polymer moments are given in **Appendix C**. The numerical values of physical constants, kinetic parameters and standard reactor operating conditions are listed in Table 3.4. Note that the monofunctional initiators (A1 and A2) are hypothetical ones used for the purpose of comparison with the bifunctional initiator system. The behavior of the monofunctional initiator A2 is similar to that of popular azobisisobutyronitrile (AIBN).

3.3.2. Steady State Behavior

The principal parameters which influence the behavior of the continuous

193

Table 3.4   Numerical values of kinetic parameters for symmetrical bifunctional initiators and standard operating conditions

---

Bifunctional initiator:

k_{d1}=8.90 × 10^{10}exp(-23,473/RT), sec^{-1} *

k_{d2}=5.59 × 10^{14}exp(-30,387/RT), sec^{-1} *

f_i=0.23   (i = 1, 2) *

Monofunctional initiators:

(A1) k_d=8.90 × 10^{10}exp(-23,473/RT), sec^{-1}

f=0.23

(A2) k_d=5.59 × 10^{14}exp(-30,387/RT), sec$-$1

f=0.23

k_p=1.051 × 10^7exp(-7,060/RT), 1/mol.sec †

k_t=1.255 × 10^9exp(-1,680/RT), 1/mol.sec †

$(-\Delta H_r)$=16.2 Kcal/mol †

ρC_p=0.4 Kcal/l°K †

T_f=300 °K, T_c=303 °K, I_f=0.05 mol/l

f_s=0.0~1.0, α=0~100

---

* Prisyazhnyuk and Ivanchev (1979)

† Brandrup and Immergut (1989)

194

styrene solution polymerization reactors are Da (or θ), α, β (or f_s), γ, γ_1 and δ. For given values of the system parameters the steady states may be calculated by solving the steady state nonlinear equations (3.83)~(3.85). In practical situations, one is often interested in knowing the steady state multiplicity pattern existing for a given set of system parameters. With parameters δ, T_f and I_f held fixed, the diagram showing the steady state behavior of the reactor has been constructed by using the singularity theory (§2.4.1). Figure 3.23 is a such diagram in α-β plane for the bifunctional initiator system. Note that five unique regions of steady state behavior are identified:

Region I   :   Unique steady state

Region II :   Multiple steady state (S-shape curve)

Region III: Isola and unique steady state

Region IV: Isola and multiple steady state (S-shape curve)

Region V :   Mushroom

Here, Γ_1 (Γ_2) represents the hysteresis (isola) variety which defines the parameter space at which a continuous change of the parameter causes the appearance or disappearance of hysteresis (isola) type multiplicity. The criteria for both varieties are given in eqs (2.45)~(2.48). In regions III and IV, isolated branches (isola) are observed. The isola cannot be obtained by simply varying the reactor residence time and a special control scheme is required
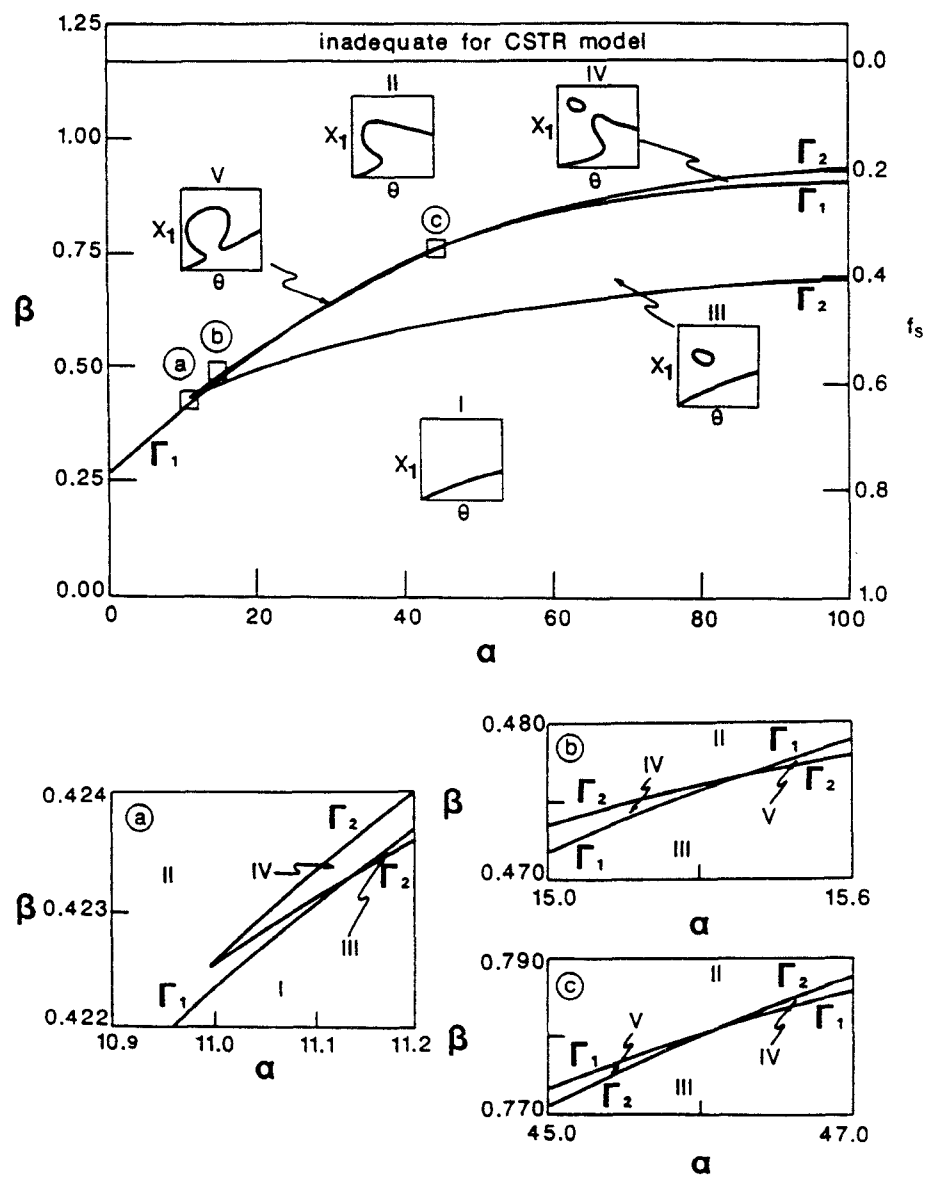
Figure 3.23   Steady state behavior regions for styrene polymerization in a
CSTR with bifunctional initiator. $\delta=0.01$, $I_{fB}=0.025$ mol/l.

to operate the reactor at such steady state conditions. Since regions IV and V are so small, it will be practically very difficult to confirm these tiny regions experimentally. This means that most of the reactor behavior will be represented by region I, II and III for practical operating conditions. It is also interesting to observe that unique steady state behavior is never expected in bulk free radical polymerization reactors (*i.e.*, $f_s = 0.0$). For adiabatic polymerization (*i.e.*, $\alpha = 0.0$), only type I and II steady state profiles will appear. Figures 3.24 and 3.25 show the similar steady state behavior for the monofunctional initiator systems A1 and A2, respectively. The overall structures of the steady state behavior regions for the bifunctional initiator system and for the monofunctional initiator systems are quite similar. The concentration of peroxide groups in the initiator feed stream is held fixed at the same value for all cases, *i.e.*, $I_{fB} = \frac{1}{2}I_{fA1} = \frac{1}{2}I_{fA2}$.

The steady state profiles of the reactor state variables (*i.e.*, X_1: monomer conversion, X_2: initiator conversion, T: reactor temperature) are illustrated in Figure 3.26 for these three different initiator systems:

Monofunctional initiator (A1):

$$k_d = 8.90 \times 10^{10} \exp(-23{,}473/RT), \ \ \sec^{-1}$$

$$I_{fA1} = 0.05 \ \text{mol/l}$$

Monofunctional initiator (A2):

$$k_d = 5.59 \times 10^{14} \exp(-30{,}387/RT), \ \ \sec^{-1}$$
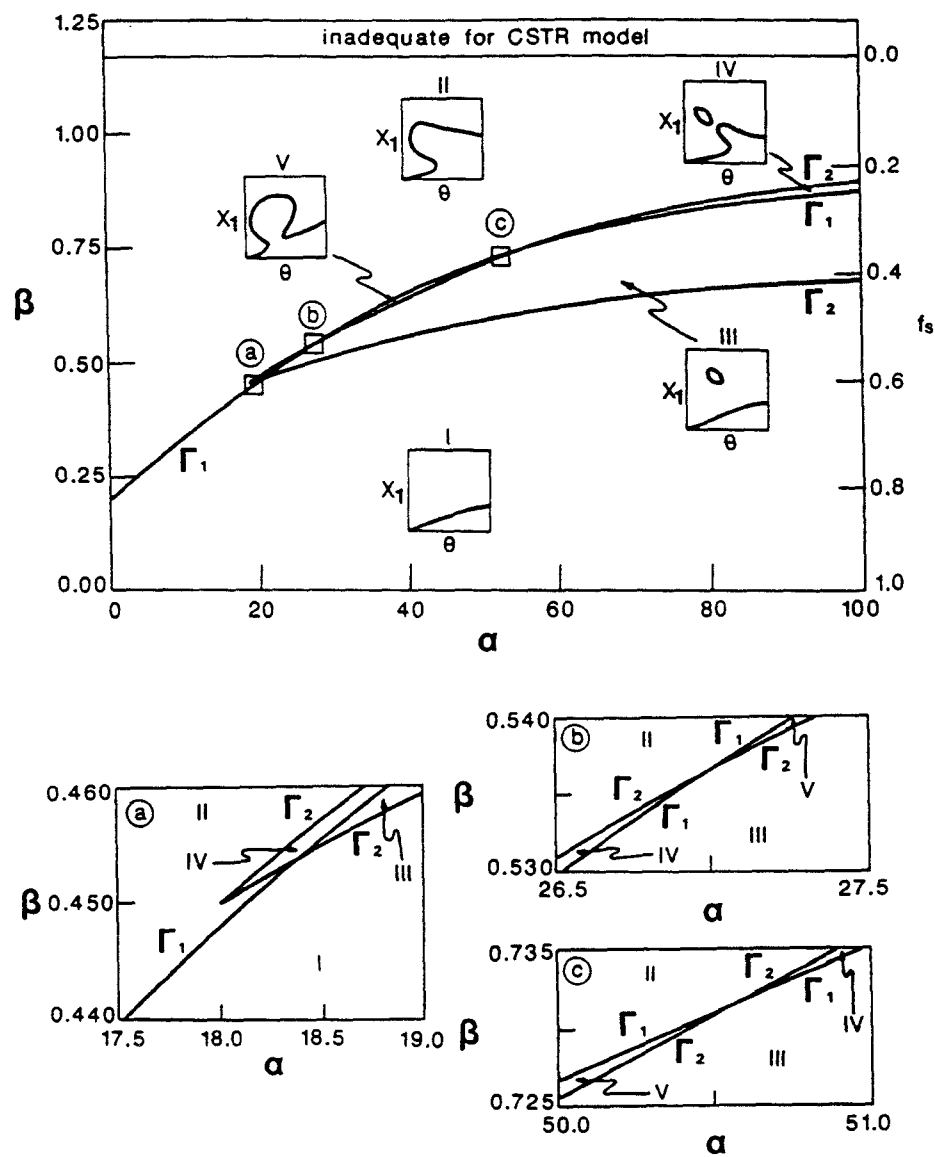
Figure 3.24   Steady state behavior regions for styrene polymerization in a
CSTR with monofunctional initiator A1. $\delta=0.01$, $I_{fA1}=0.05$
mol/l.
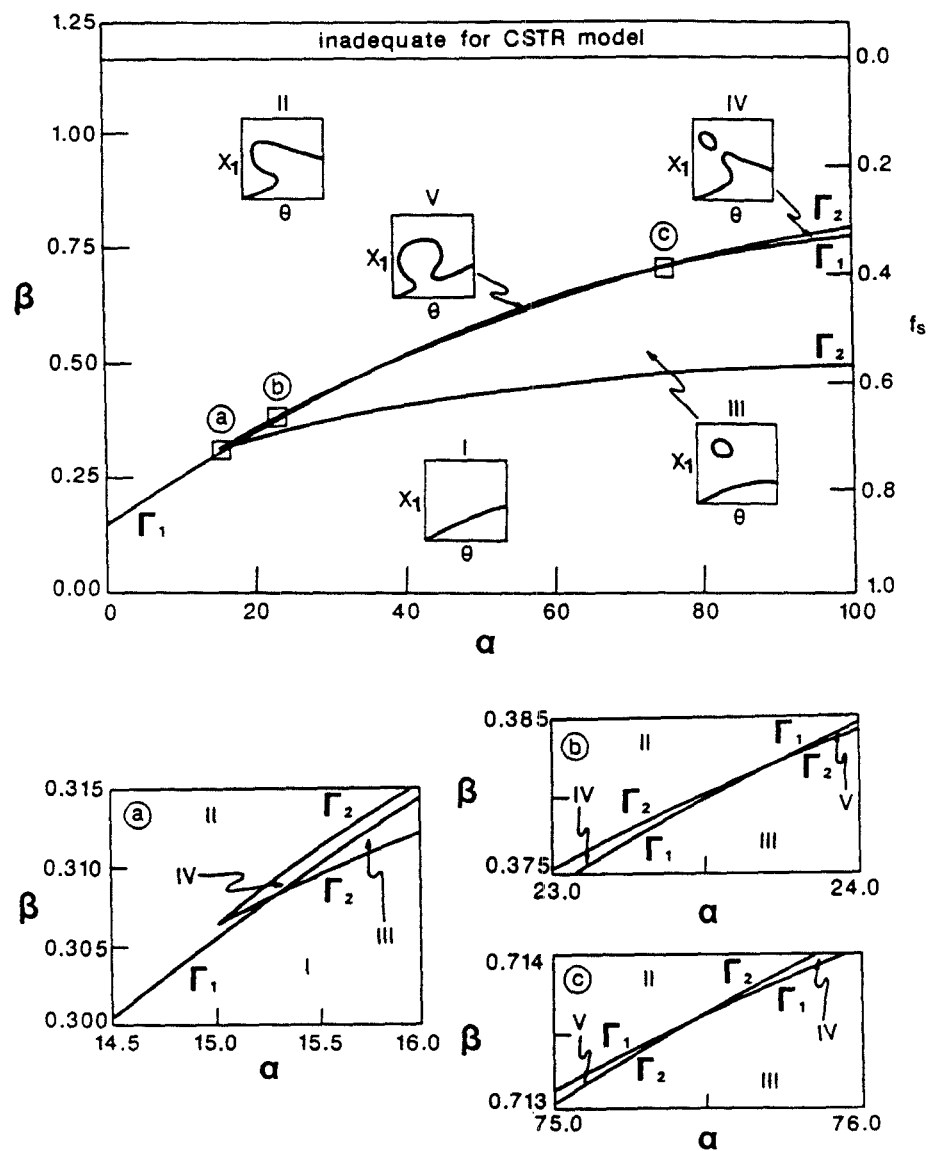
Figure 3.25   Steady state behavior regions for styrene polymerization in a CSTR with monofunctional initiator A2, $\delta=0.01$, $I_{fA2}=0.05$ mol/l.
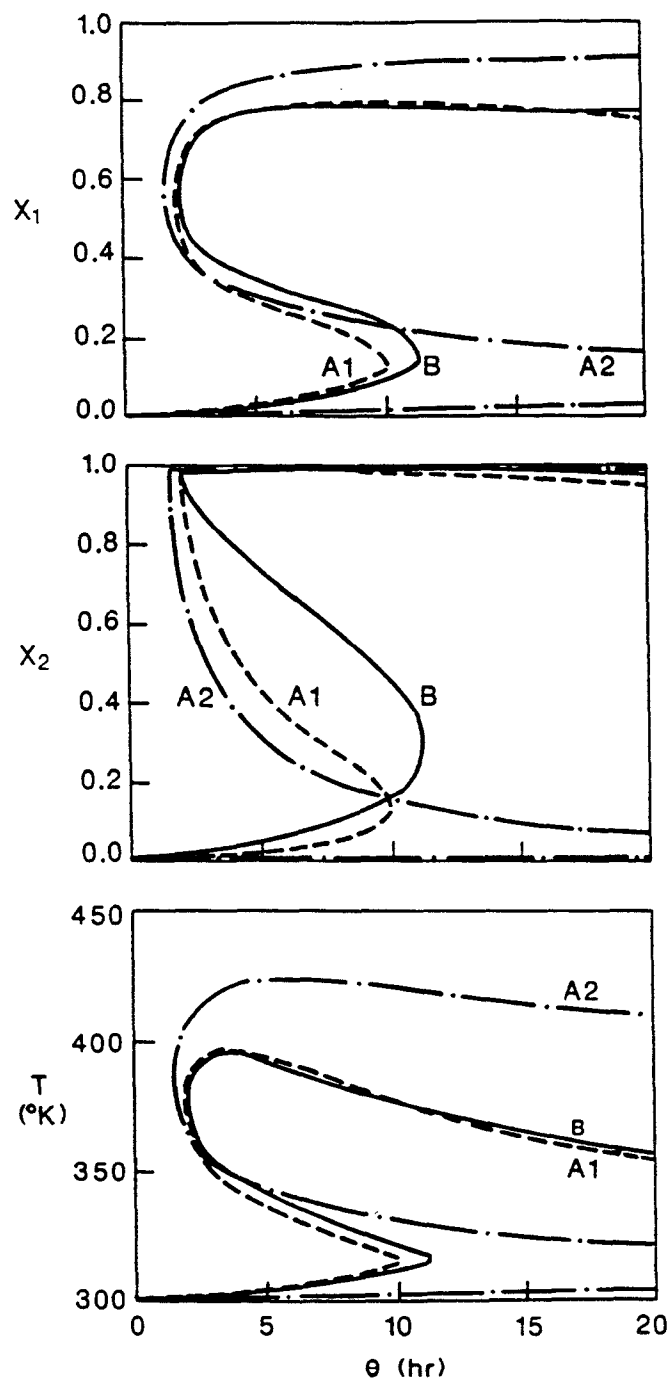
Figure 3.26   Steady state profiles of state variables for three initia-
tor systems: α=15, β=0.5126, δ=0.01, I_{fB}=0.025 mol/l,
I_{fA1}=I_{fA2}=0.05 mol/l.

$$I_{fA2} = 0.05 \text{ mol/l}$$

Bifunctional initiator (B):

$$k_{d1} = 8.90 \times 10^{10} \exp(-23{,}473/RT), \quad \sec^{-1}$$

$$k_{d2} = 5.59 \times 10^{14} \exp(-30{,}387/RT), \quad \sec^{-1}$$

$$I_{fB} = 0.025 \text{ mol/l}$$

Note that the steady state profiles of X_1, X_2 and T for the bifunctional initiator (B) are approximately in the middle of those for the two monofunctional initiator systems. However, the molecular weight properties such as number average chain length (X_N) and polydispersity (X_W/X_N) for the bifunctional initiator system are quite different from those for the monofunctional initiator systems as shown in Figure 3.27. At high monomer conversions, the bifunctional initiator system produces polymers of significantly higher molecular weight than those obtained by the monofunctional initiators. The polydispersity is slightly higher for the bifunctional initiator system than for the monofunctional initiator systems due to the presence of various polymeric species of different chain lengths. The variations of X_N with steady state temperature and monomer conversion are more clearly illustrated in Figure 3.28. The highest conversion is obtainable by using the "slow" initiator (initiator A2) at high temperatures and long residence time; however, both high monomer conversion and high molecular weight of polymers are obtained by using the bifunctional initiator (B) at shorter residence time. The high molecular weight
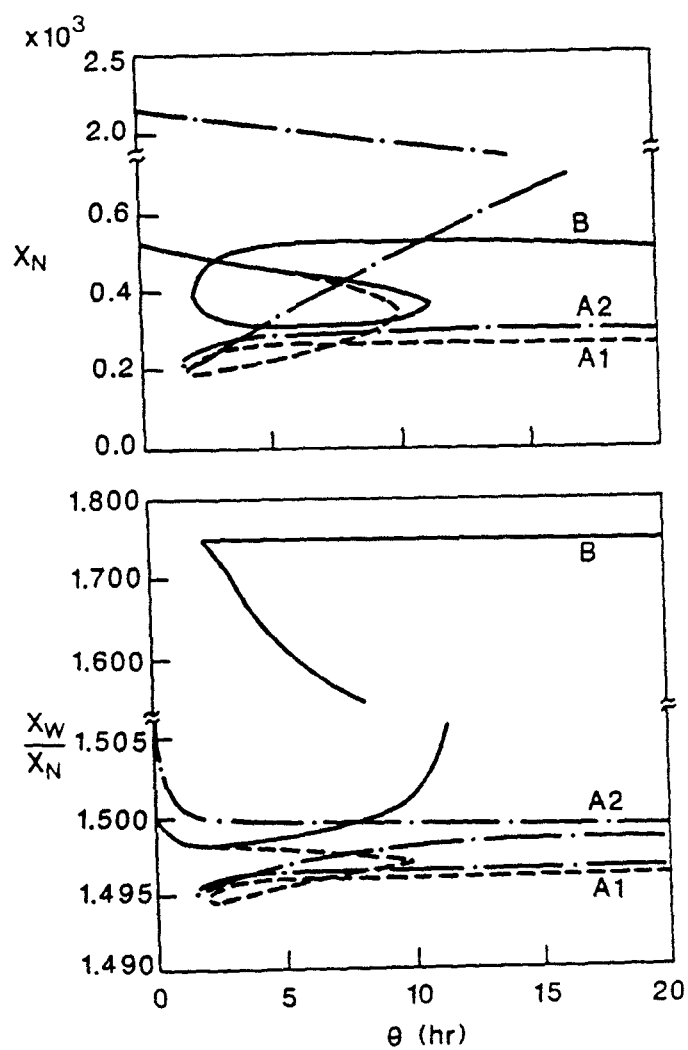
Figure 3.27   Steady state profiles of number average chain length and polydispersity: $\alpha=15$, $\beta=0.5126$, $\delta=0.01$, $I_{fB}=0.025$ mol/l, $I_{fA1}=I_{fA2}=0.05$ mol/l.
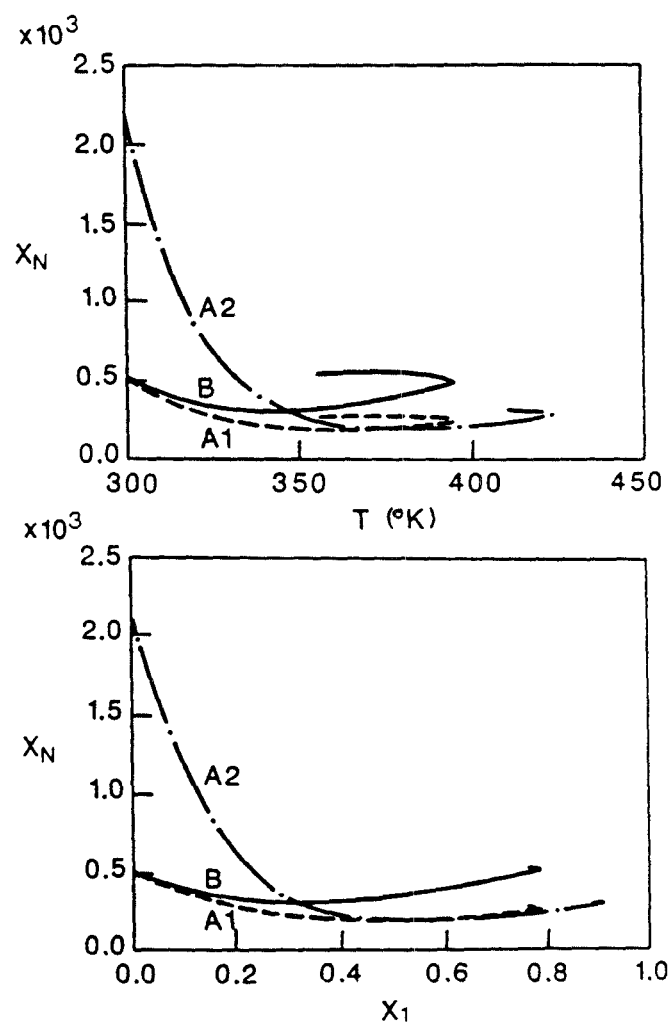
Figure 3.28   Steady state profiles of number average chain lengths vs. temperature and monomer conversion (X_1): $\alpha=15$, $\beta=0.5126$, $\delta=0.01$, $I_{fB}=0.025$ mol/l, $I_{fA1}=I_{fA2}=0.05$ mol/l.

obtained by use of the bifunctional initiator is due to the extended lifetime of peroxide groups which reside in various polymeric species such as Q_n, T_n and Z_n.

Figure 3.29 illustrates the X_N of various inactive polymers and their weight fractions in the polymer. Note that as steady state reaction temperature increases (e.g. upper solution branch, Figure 3.26), the decomposition of the peroxide groups in T_n and Z_n-type polymers is increased and more P_n or Q_n-type polymers are produced. When the growth of these live polymeric radicals is terminated, polymers of much higher molecular weight are obtained. It is also interesting to note in Figures 3.27 and 3.29 that when the concentrations of T_n and Z_n-type polymers are low, polydispersity is lowered due to the reduced heterogeneity of the polymer chain length distribution. The numerical calculation indicates that the concentrations of live polymers (P_n, Q_n and S_n) are an order of magnitude lower than those of inactive polymers as shown in Figure 3.30. This means that the overall polymer molecular weight is determined predominantly by the dead or inactive polymers. Figure 3.29 also shows that Z_n-type polymer is a predominant species when the reactor is operated with residence time shorter than 12 hours. But the highest monomer conversion obtainable is below 20% (Figure 3.26).

The molar concentration (C_j) and the mole fraction (f_{mj}) of undecomposed peroxide groups in the primary initiator and various polymeric species are shown in Figure 3.31. In the middle steady state branch (*i.e.*, $\theta =$
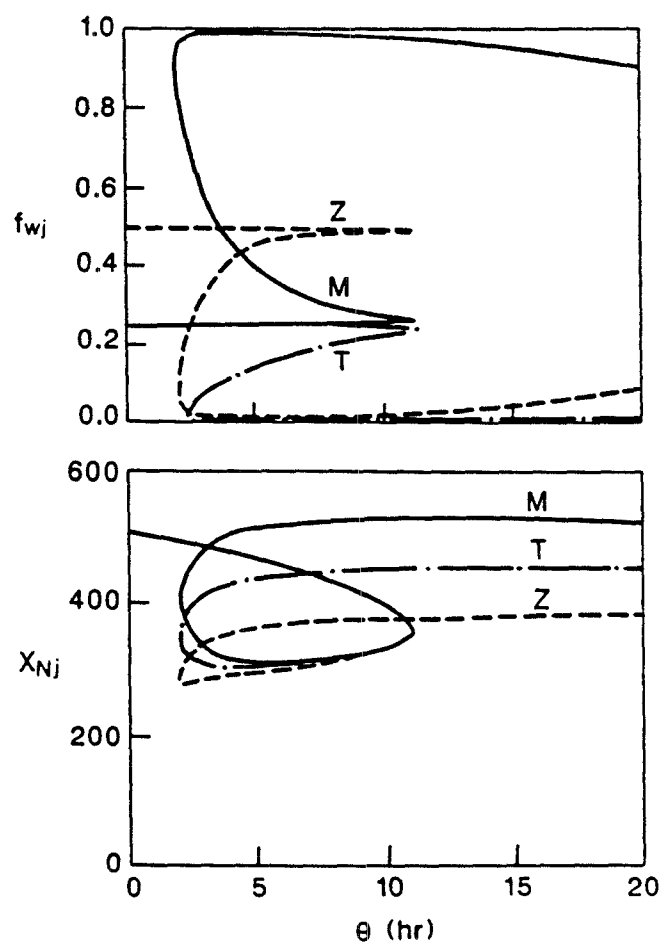
Figure 3.29   Weight fraction and number average chain length profiles
of various inactive polymers: $\alpha=15$, $\beta=0.5126$, $\delta=0.01$,
$I_{fB}=0.025$ mol/l.
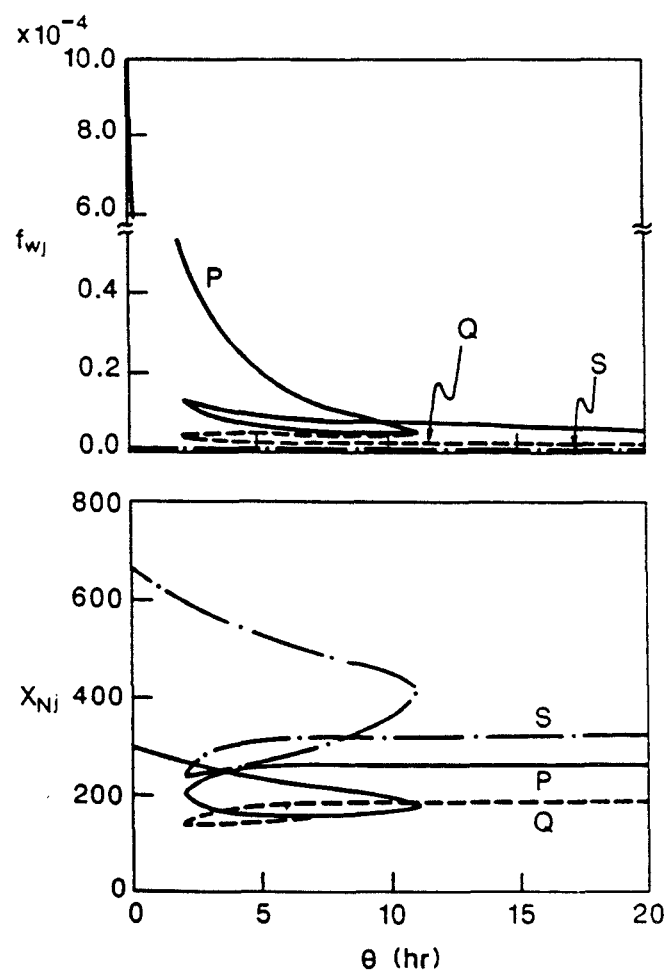
Figure 3.30   Weight fraction and number average chain length profiles of various live polymers: $\alpha=15$, $\beta=0.5126$, $\delta=0.01$, $I_{fB}=0.025$ mol/l.
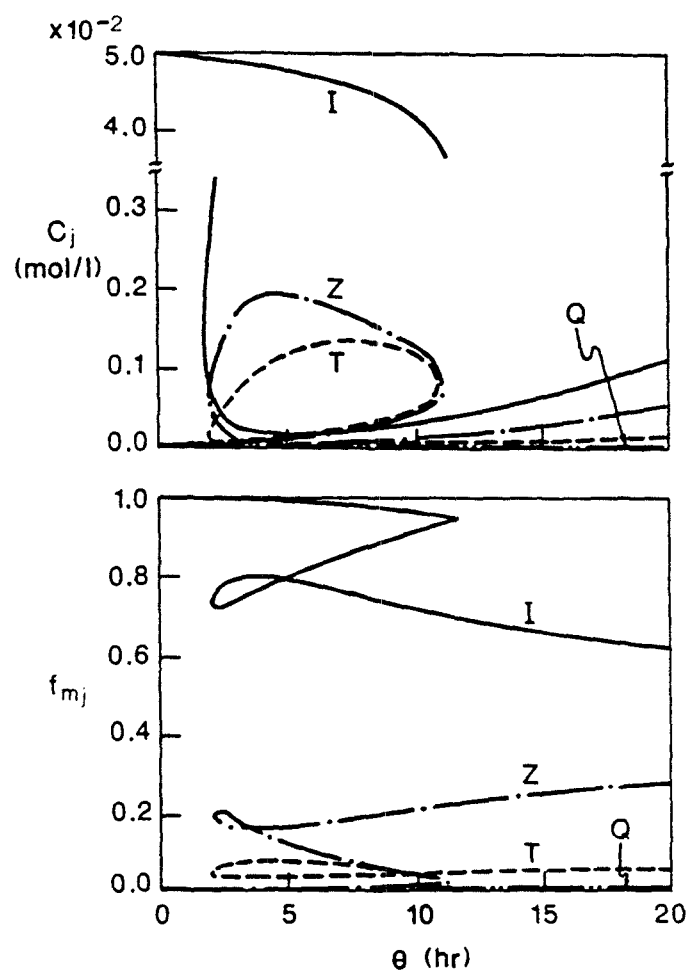
Figure 3.31   Distribution of undecomposed peroxides in various species:
$C_j =$ molar concentration of diperoxide in species j. $f_{mj} =$
mole fraction of peroxides in species j. $\alpha = 15$. $\beta = 0.5126$.
$\delta = 0.01$. $I_{fB} = 0.025$ mol/l.

2~12 hours) where the monomer conversion is about 20~70%, the undecomposed peroxides reside mostly in T_n and Z_n-type polymers. However, as monomer conversion and reactor temperature increase (*i.e.*, upper solution branch), the concentrations of peroxides in those inactive polymers decrease sharply by thermal decomposition and, as a result, the polymer molecular weight increases. If the production of polymers containing high concentration of peroxide is desired, the reactor should be operated at the middle steady state. Such reactor conditions may be practically important, if free radical block copolymerization is performed in a series of CSTRs operating at different polymerization conditions in order to minimize the formation of homopolymers. A special stabilizing control is of course required to operate the reactor at such steady states.

The steady state reactor behavior for three different values of α (dimensionless heat transfer coefficient) with the bifunctional initiator is shown in Figures 3.32 and 3.33. As predicted in Figure 3.23, the S-shaped steady state curves become more exaggerated as α increases for a fixed value of β and an isola begins to appear with further increase in α. Figure 3.33 illustrates that polymer composition also changes significantly with variation in α. Note that the weight fractions of inactive polymers (T_n, Z_n-type) which contain undecomposed peroxide groups increase with α at long reactor residence time (e.g. $\theta > 10$ hrs.).
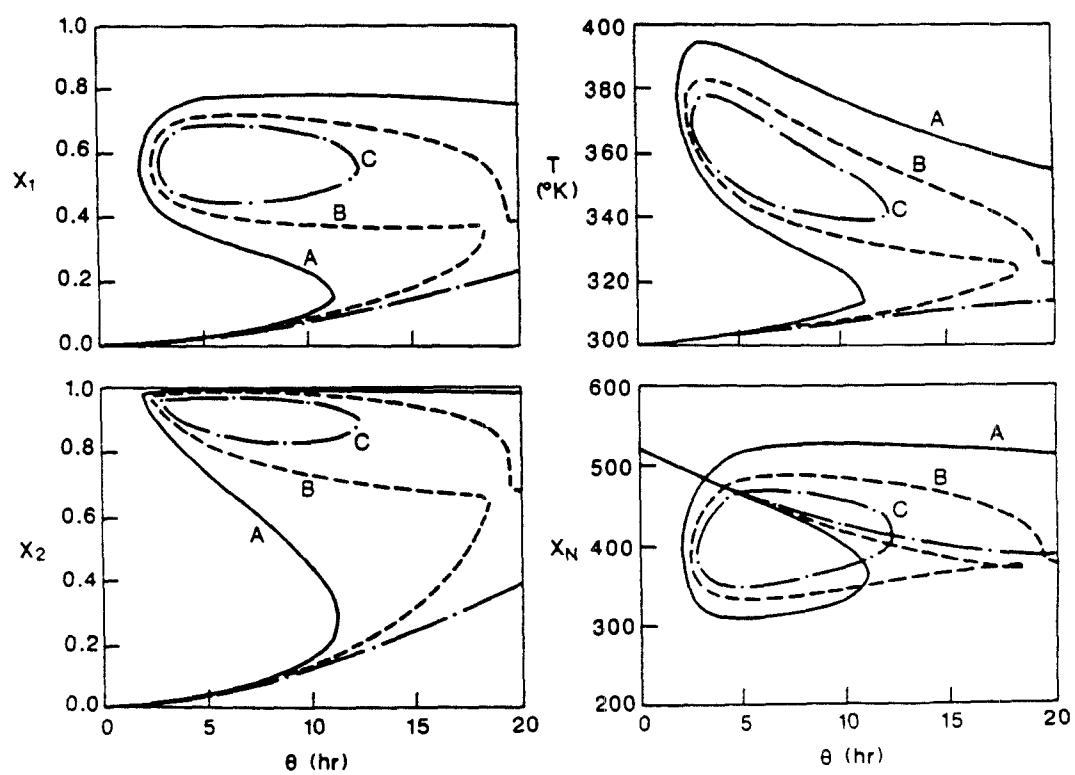
Figure 3.32   Steady state profiles of state variables for varying α values: β=0.5126, δ=0.01. I_{fB}=0.025 mol/l. α: A=15.0, B=19.9. C=22.0.
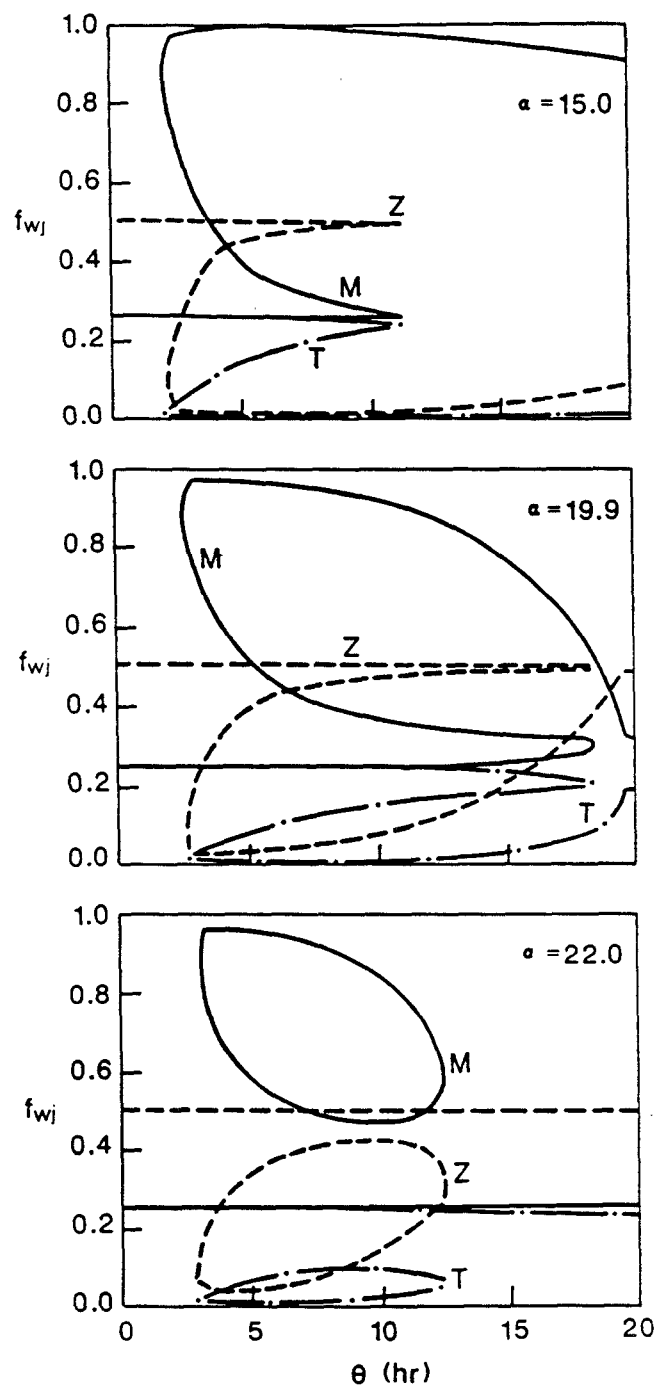
Figure 3.33   Weight fraction profiles of inactive polymers for varying α values: β=0.5126, δ=0.01, I_{fB}=0.025 mol/l.

3.4. Concluding Remarks

Detailed kinetic and reactor models for styrene polymerization initiated by bifunctional initiators have been presented in this chapter. For the polymerization with unsymmetrical bifunctional initiators where the chain termination occurs via combination termination exclusively, ten distinct polymeric species (six with symmetrical bifunctional initiators) are identified in accordance with the nature of the polymer end units. The polymeric species carrying undecomposed peroxides on chain ends can reinitiate the propagation and, as a result, overall lifetime of radicals is extended and the molecular weight of polymer can be significantly increased. Compared with monofunctional initiator systems or mixture of them, the bifunctional initiators provide higher monomer conversion and polymers of higher molecular weight simultaneously due to unequal thermal stabilities of peroxide groups. The effect of the bifunctional initiator is more pronounced at high reaction temperature and low initiator concentration. The proposed model for the unsymmetrical bifunctional initiators has been validated experimentally using 4-(t-butylperoxycarbonyl-3- hexyl-6-[7- (t-butylperoxycarbonyl) heptyl]cyclohexene. These model simulations suggest that the use of bifunctional initiators will provide a new opportunity to polymerization reaction engineers for improving the polymer productivity and controlling the polymer molecular weight properties more efficiently than the use of conventional monofunctional initiators. It is also shown that CSTRs

can be used to produce reactive polymers containing undecomposed peroxide groups.

3.5. Notation

A_c heat transfer area (cm^2)

C_p heat capacity of reaction mixture (cal/mol°K)

Da Damkohler number (-)

E_d decomposition activation energy (cal/mol)

E_p activation energy of propagation (cal/mol)

f_i initiator efficiency (i=A,B,R,R',1,2)

f_s solvent volume fraction (-)

g_t gel effect correlation factor

I_i initiator concentration, mol/l (i=A,B)

k_{d_i} decomposition rate constant of peroxide group i, sec^{-1} (i=A,B,1,2)

k_i initiation rate constant (1/mol.sec)

k_{d_M} thermal initiation rate constant, l^2/mol^2.sec

k_p propagation rate constant, 1/mol.sec

k_{fm} chain transfer rate constant, 1/mol.sec

k_t termination rate constant, 1/mol.sec

k_{to} termination rate constant at zero monomer conversion, 1/mol.sec

M monomer concentration, mol/l

M_f feed monomer concentration (mol/l)

M_o initial concentration of monomer, mol/l

PD polydispersity of polymer

q volumetric feed flow rate (l/sec)

t dimensionless time (-)

t' time (sec)

V reactor volumer (cm^3)

v volume of reaction medium, l

X_1 monomer conversion (-)

X_2 initiator conversion (-)

X_3 dimensionless temperature (-)

X_p dimensionless total live polymer concentration (-)

x monomer conversion

X_N number average chain length of polymer

X_W weight average chain length of polymer

Greek Letters

α dimensionless heat transfer coefficient (-)

β dimensionless heat of reaction (-)

γ dimensionless propagation activatin energy(-)

γ_1 dimensionless decomposition activatin energy (-)

δ dimensionless coolant temperature (-)

ρ density of reaction mixture (mol/l)

ϵ volume contraction factor

$\lambda_{\xi,k}$ k-th moment of polymeric spcies ξ

λ_k^d k-th moment of dead polymer

λ_k^l k-th moment of live polymer

Chapter 4

Heat Transfer and Impurity Effects in Continuous Polymerization Processes

4.1. Introduction

In modeling styrene solution polymerization reactors for the analysis of reactor dynamics in the previous chapters, perfect backmixing and constant wall heat transfer were assumed. However, in reality, as monomer conversion increases the wall heat removal efficiency may decrease because the viscosity of the reacting fluid increases leading to reactor fouling and poor mixing. Recently, it was reported by Henderson (1987) for a continuous styrene thermal polymerization reactor with a turbine agitator that the rate of heat removal

216

decreases significantly as the monomer conversion exceeds 30 % and that an increase of the viscosity can bring the agitator system to a design limit. As a result, the reactor may exhibit potentially dangerous phenomena such as local hot spot formation, fouling at the reactor walls and even thermal runaway. Such problems can be partially solved by using additional heat removal devices such as internal cooling coils, condensers and external heat exchangers with specially designed agitators [Henderson and Cornejo (1989)].

Another factor that can affect the polymerization performance is the presence of reactive impurities (e.g., inhibitors or retarders) in the monomer and/or solvent. Inhibitors or retarders are often added to vinyl monomers prior to shipping and storage to prevent a premature auto-polymerization. Although they are present only in small amount, there is a possibility that they can influence the reactor dynamics and resulting polymer properties.

In this chapter, these forementioned problems encountered in operating and controlling industrial polymerization processes will be discussed through model simulations.

4.2. Effect of Viscosity Dependent Heat Transfer Coefficient

The reactor system considered in this study is a turbine agitated CSTR for styrene solution polymerization with a mixture of tert-butyl perbenzoate (TBPB) and benzoyl peroxide (BPO) as an initiator system. For this polymerization system, the dynamic behavior of ideal CSTR's has been discussed in Chapter 2. In the following, non-ideal heat transfer effects are included in the model and the reactor dynamics are analyzed.

4.2.1. Reactor Model

In modeling the polymerization reactor with a cooling jacket, the same assumptions used in the previous chapter (§2.2.3) are employed except that the heat transfer coefficient is now viscosity dependent. Heat released from the mechanical work of the agitator is assumed negligible. Thus, the structure of the dynamic reactor modeling equations is unchanged from eqs (2.23)~(2.26); however, the heat transfer coefficient is expressed as a function of fluid viscosity to account for the time-varying heat transfer efficiency.

If the thermal resistance in the reactor walls is negligible, the overall heat transfer coefficient of the reactor, h_c, is given by

$$\frac{1}{h_c} = \frac{1}{h_i} + \frac{1}{h_o} \tag{4.1}$$

where h_i and h_o are the inside and the outside film heat transfer coefficients of the reactor, respectively. The outside heat transfer coefficient (h_o) is assumed constant and the inside film heat transfer coefficient (h_i) is estimated from the following empirical correlations suggested for a jacketed reactor [Rase (1977), Henderson (1987)]:

$$\frac{h_i D_r}{k} = 0.51 N_{Re}^{2/3} N_{Pr}^{1/3} \left(\frac{\eta_r}{\eta_w} \right)^{0.14} \quad \text{for} \quad N_{Re} > 100 \qquad (4.2a)$$

$$\frac{h_i D_r}{k} = 0.51 (N_{Re} N_{Pr})^{1/3} \left(\frac{\eta_r}{\eta_w} \right)^{0.2} \quad \text{for} \quad N_{Re} < 100 \qquad (4.2b)$$

where D_r is the reactor diameter and k the thermal conductivity of the reacting fluid. η_r is the viscosity of the bulk liquid phase and η_w the fluid viscosity at the reactor wall surface. N_{Re} is the Reynolds number and N_{Pr} the Prandtl number defined by [Hicks *et al.* (1976), Dickey (1984)]:

$$N_{Re} = \frac{1.66 D_i^2 N \rho_r}{\eta_r} \qquad (4.3a)$$

$$N_{Pr} = \frac{0.01 C_p \eta_r}{k} \qquad (4.3b)$$

where N is the rotational speed (rpm) of the turbine impeller, D_i diameter of the impeller, ρ_r the fluid density and C_p the heat capacity of the reacting fluid.

The viscosity of the reactor fluid is affected by polymer concentration (monomer conversion), temperature, polymer molecular weight and shear rate.

The effect of shear thinning can be significant at high polymer concentration; however, shear thinning effects are negligible at high temperatures [Henderson (1987)]. Mendelson (1979, 1980) proposed the following equation for the temperature dependence of the zero shear viscosity for polymer weight fraction above 0.4:

$$\eta_r = \eta_{200}\exp\left[\frac{E_v}{R}\left(\frac{1}{T} - \frac{1}{473}\right)\right] \quad (cp,\ T\ \text{in}\ °K) \tag{4.4}$$

The viscosity of the polymer solution at 200 °C (η_{200}) is

$$\eta_{200}(cp) = 3.31 \times 10^{-12} X_p^{10.7} M_w^{3.4} \quad (\text{for}\ 0.4 \le X_p \le 1.0) \tag{4.5a}$$

where, X_p is the weight fraction of polymer and M_w the weight average polymer molecular weight. E_v in eq (4.4) is the activation energy for viscous flow and is a function of X_p:

$$E_v = 2300\exp(2.4X_p) \tag{4.5b}$$

The above correlation gives unreasonably small viscosity of the polymer solution when X_p is lower than 0.4. Thus, Eq. (4.4) is modified as follows to cover the whole range of X_p ($0 \le X_p \le 1.0$):

$$\eta_r = \eta_s + \eta_{200}\exp\left[\frac{E_v}{R}\left(\frac{1}{T} - \frac{1}{473}\right)\right] \quad (cp) \tag{4.6}$$

220

where η_s is the viscosity of styrene-ethyl benzene mixture at temperature T and η_s can be estimated by using the following equation [Nishimura (1965)]:

$$\eta_s = 0.667 \exp\left[\frac{2300}{R}\left(\frac{1}{T} - \frac{1}{303}\right)\right] \quad (cp) \tag{4.7}$$

Since the heat transfer resistance through the reactor walls is assumed negligibly small in the jacket, the reactor wall temperature is the same as the coolant temperature in the jacket. The density of the polymer solution (ρ_r) is estimated using the following equation [Hui and Hamielec (1972)]:

$$\rho_r = (1 - X_p)\rho_m + X_p\rho_p \tag{4.8}$$

where ρ_m is the density of monomer and ρ_p the density of polymer. The temperature dependence of ρ_m and ρ_p is given by

$$\rho_m = 0.924 - 9.18 \times 10^{-4}(T - 273.1) \tag{4.9a}$$

$$\rho_p = 1.0848 - 6.05 \times 10^{-4}(T - 273.1) \tag{4.9b}$$

Since the viscosity of the reacting fluid is dependent on the polymer molecular weight, polymer weight fraction and temperature, the polymer molecular weight moment equations are now coupled with mass and energy balance equations in the reactor model. In general, the contribution of live polymers to the overall molecular weight is negligibly small because of their low concentrations. The number average and the weight polymer chain lengths are:

$\overline{X}_n = \lambda_1/\lambda_0$, $\overline{X}_w = \lambda_2/\lambda_1$. The moment equations for dead polymer are given by (A.1)~(A.3) in **Appendix A**.

With the dimensionless variables and parameters defined in Table 4.1, the reactor modeling equations and moment equations for dead polymers are reduced to the following dimensionless form:

$$\frac{dX_1}{dt} = -X_1 + Da(1 - X_1)Y_1 \exp\left\{\frac{\gamma X_4}{1 + X_4}\right\} \tag{4.10}$$

$$\frac{dX_2}{dt} = -X_2 + Da\zeta(1 - X_2)\exp\left\{-\frac{\gamma_d}{1 + X_4}\right\} \tag{4.11}$$

$$\frac{dX_3}{dt} = -X_3 + Da\zeta\eta(1 - X_3)\exp\left\{-\frac{\epsilon\gamma_d}{1 + X_4}\right\} \tag{4.12}$$

$$\frac{dX_4}{dt} = -X_4 + \beta\left(X_1 + \frac{dX_1}{dt}\right) + Da\alpha\phi(X_4 - \delta) \tag{4.13}$$

$$\frac{dX_5}{dt} = -X_5 + DaY_1\left[w_{10}\hat{\alpha}(1 - X_1)\exp\left\{-\frac{\gamma_f}{1 + X_4}\right\}\right.$$
$$\left. + \frac{1}{2}w_{20}Y_2\exp\left\{-\frac{\gamma_t}{1 + X_4}\right\}\right] \tag{4.14}$$

$$\frac{dX_6}{dt} = -X_6 + \frac{DaY_1}{(1 - \hat{\alpha})}\left[w_{11}(1 - X_1)(2\hat{\alpha} - \hat{\alpha}^2)\exp\left\{-\frac{\gamma_f}{1 + X_4}\right\}\right.$$
$$\left. + w_{21}Y_2\exp\left\{-\frac{\gamma_t}{1 + X_4}\right\}\right] \tag{4.15}$$

$$\frac{dX_7}{dt} = -X_7 + \frac{DaY_1}{(1 - \hat{\alpha})^2}\left[w_{12}(1 - X_1)(\hat{\alpha}^3 - 3\hat{\alpha}^2 + 4\hat{\alpha})\exp\left\{-\frac{\gamma_f}{1 + X_4}\right\}\right.$$
$$\left. + w_{22}Y_2(\hat{\alpha} + 2)\exp\left\{-\frac{\gamma_t}{1 + X_4}\right\}\right] \tag{4.16}$$

where Y_1 and Y_2 are given by

$$Y_1 = \frac{1}{P_f}\left(\frac{P_x}{g_t}\right)^{\frac{1}{2}} \tag{4.17a}$$

222

Table 4.1   Dimensionless variables and parameters

$$X_1 = \frac{M_f - M}{M_f}, \qquad X_2 = \frac{y_{Af}I_f - I_A}{y_{Af}I_f}, \qquad X_3 = \frac{(1 - y_{Af})I_f - I_B}{(1 - y_{Af})I_f},$$

$$X_4 = \frac{T - T_f}{T_f}, \qquad X_5 = \frac{\lambda_0}{\lambda_{0,r}}, \qquad X_6 = \frac{\lambda_1}{\lambda_{1,r}}, \qquad X_7 = \frac{\lambda_2}{\lambda_{2,r}},$$

$$y_{Af} = \frac{I_{Af}}{I_f}, \qquad t = \frac{t'}{\theta}, \qquad Da = \theta Z, \qquad \alpha = \frac{\alpha_o}{Z}, \qquad \beta = \frac{(-\Delta H)M_f}{\rho C_p T_f},$$

$$\delta = \frac{T_c - T_f}{T_f}, \qquad \phi = \frac{h_i}{h_i + h_o}, \qquad \eta = \frac{k_{d_B0}}{k_{d_A0}}, \qquad \epsilon = \frac{E_{d_B}}{E_{d_A}},$$

$$\zeta = \frac{k_{d_A0}}{Z}, \qquad \gamma = \frac{E_p}{RT_f}, \qquad \gamma_d = \frac{E_{d_A}}{RT_f}, \qquad \gamma_f = \frac{E_{fm}}{RT_f}, \qquad \gamma_t = \frac{E_t}{RT_f},$$

$$\gamma_a = \frac{E_{dm} - E_t}{RT_f}, \qquad \gamma_b = \frac{E_{d_A} - E_t}{RT_f}, \qquad \gamma_c = \frac{E_{d_B} - E_t}{RT_f},$$

$$P_a = \frac{2k_{dm0}M_f^3}{k_{t0}^*}, \qquad P_b = \frac{2f_A k_{d_A0} y_{Af} I_f}{k_{t0}^*}, \qquad P_c = \frac{2f_B k_{d_B0}(1 - y_{Af})I_f}{k_{t0}^*},$$

$$\alpha_m = \frac{k_{fm0}}{k_{p0}}, \qquad \alpha_t = \frac{k_{t0}^* P_f}{k_{p0}M_f},$$

$$w_{1j} = \frac{k_{fm0}M_f}{\lambda_{j,r}k_{p0}\exp(-\gamma)}, \qquad w_{2j} = \frac{k_{t0}^* P_f}{\lambda_{j,r}k_{p0}\exp(-\gamma)}, \qquad (\text{for} \quad j = 0, 1, 2)$$

where

$$I_f = I_{Af} + I_{Bf}, \quad \alpha_0 = \frac{h_o A_c}{\rho C_p V}, \quad \theta = \frac{V}{q},$$

$$P_f = [P_a\exp(-\gamma_a) + P_b\exp(-\gamma_b) + P_c\exp(-\gamma_c)]^{1/2},$$

$$Z = k_{p0}\exp(-\gamma)P_f$$

$$Y_2 = \frac{(P_x g_t)^{\frac{1}{2}}}{P_f} \qquad (4.17b)$$

where, P_x is the dimensionless concentration of live polymers in the reactor:

$$P_x = P_a(1 - X_1)^3 \exp\left\{-\frac{\gamma_a}{1 + X_4}\right\} + P_b(1 - X_2)\exp\left\{-\frac{\gamma_b}{1 + X_4}\right\}$$
$$+ P_c(1 - X_3)\exp\left\{-\frac{\gamma_c}{1 + X_4}\right\}. \qquad (4.18)$$

The probability of propagation, $\hat{\alpha}$ is represented by the following dimensionless form:

$$\hat{\alpha} = \left[1 + \alpha_m \exp\left(\frac{\gamma - \gamma_f}{1 + X_4}\right) + \left(\frac{\alpha_t Y_2}{1 - X_1}\right)\exp\left(\frac{\gamma - \gamma_t}{1 + X_4}\right)\right]^{-1} \qquad (4.19)$$

where α refers to the dimensionless outside heat transfer coefficient, ϕ the ratio of the inside heat transfer coefficient to the sum of the inside and the outside heat transfer coefficient, β the dimensionless heat of reaction, and Da the dimensionless mean residence time.

4.2.2. Reactor Dynamics

If the reactor wall heat transfer coefficient (h_c) is constant, the reactor model can be divided into two subsystems where the first subsystem (eqs 4.10~4.13) is independent of the second subsystem (eqs 4.14~4.16). In such a

case, the reactor dynamics can be examined using only the first subsystem, as was done in Chapter 2. In the above reactor model, the heat transfer coefficient is a function of polymer concentration, reactor temperature and the polymer molecular weight. Therefore, a complete set of modeling equations including the moment equations must be solved simultaneously. When h_c is constant, the steady state modeling equations (4.10~4.13) can also be reduced to a single nonlinear equation in X_1 (steady state manifold) [eq (2.43)]. However, with the above model, such a reduction of the model equations is not possible and therefore a numerical search is required to identify the regions of steady state multiplicity and bifurcation. For the purpose of comparison with the case of constant heat transfer coefficient, the same numerical values of kinetic parameters, physical constants and standard reactor operating conditions used in Chapter 2 (Table 2.1) are used. The reactor design specifications shown in Table 4.2 are based on the pilot plant scale reactor used by Henderson (1987). The standard solvent (ethyl benzene) volume fraction in the feed (f_s) is 0.1 and the feed is preheated to 70 °C. Note that $y_{Af} = 0.5$ is chosen as a standard feed initiator composition and $I_0 = 0.025$ mol/l as a standard feed concentration of initiator mixture.

The heat transfer coefficient correlations [eqs (4.2a) and (4.2b)] are discontinuous at $N_{Re} = 100$ and the program AUTO used for our bifurcation analysis cannot handle this discontinuity. And of course, h_i is not actually discontinuous. For purposes of computational convenience, h_i is smoothened

Table 4.2   Reactor design specification [Henderson (1987)]

Thermal conductivity of polymer:

k=4.059 × 10^{-4} cal/sec cm °K

Reactor Design Specification:

V=27 l, D_r=25.4 cm, D_i=15.9cm,

N=600 rpm, A_c=3,716 cm^2, $h_o = 3.393 \times 10^{-2}$ cal/sec cm^2 °K,

Reference value of dead polymer moment:

$\lambda_{0,r} = 1.3558 \times 10^{-3}$, $\lambda_{1,r} = 2.1789$, $\lambda_{2,r} = 2.261 \times 10^3$

---

near $N_{Re} = 100$ into a continuous function:

$$h_i = \frac{1}{2}\left[(h_{i1} - h_{i2})\tanh\left\{10(\ln(N_{Re}) - 5)\right\} + h_{i1} + h_{i2}\right] \tag{4.20}$$

Here, h_{i1} is h_i for $N_{Re} > 100$ and h_{i2} is h_i for $N_{Re} < 100$. This smoothing effectively interpolates the heat transfer coefficient in the range $100 < N_{Re} < 200$.

The reactor operating parameters that affect the reactor dynamics are reactor residence time (θ), feed initiator composition (y_{Af}), feed initiator concentration (I_f), feed solvent volume fraction (f_s), and coolant temperature (T_c). Figures 4.1 and 4.2 show the steady state profiles of monomer
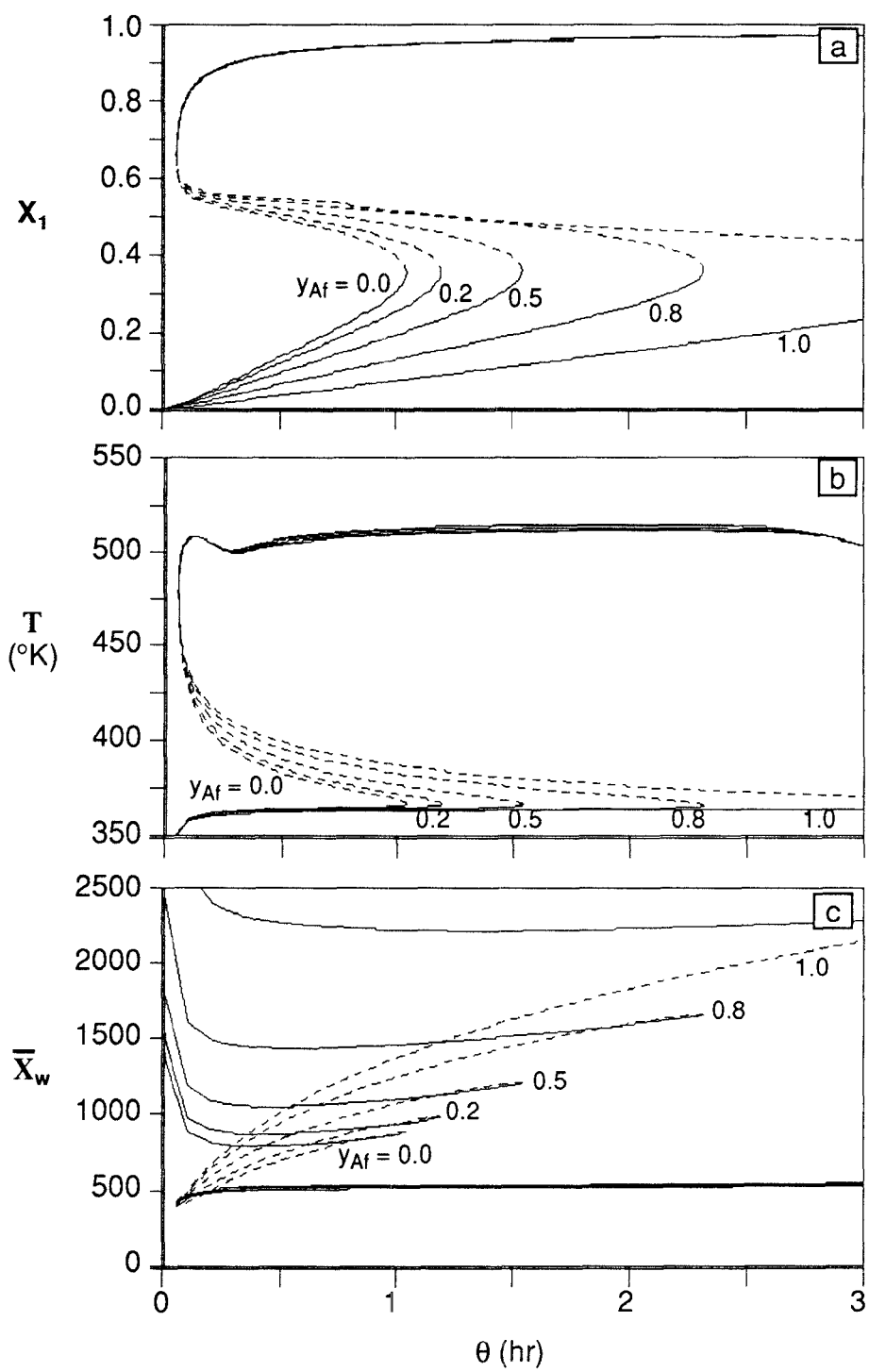
Figure 4.1   Steady state profiles of X_1, T and $\overline{X}_w$ with various y_{Af}: $f_s =$ 0.1, $I_f = 0.025$ mol/l, $T_f = 343$ °K, $T_c = 363$ °K.
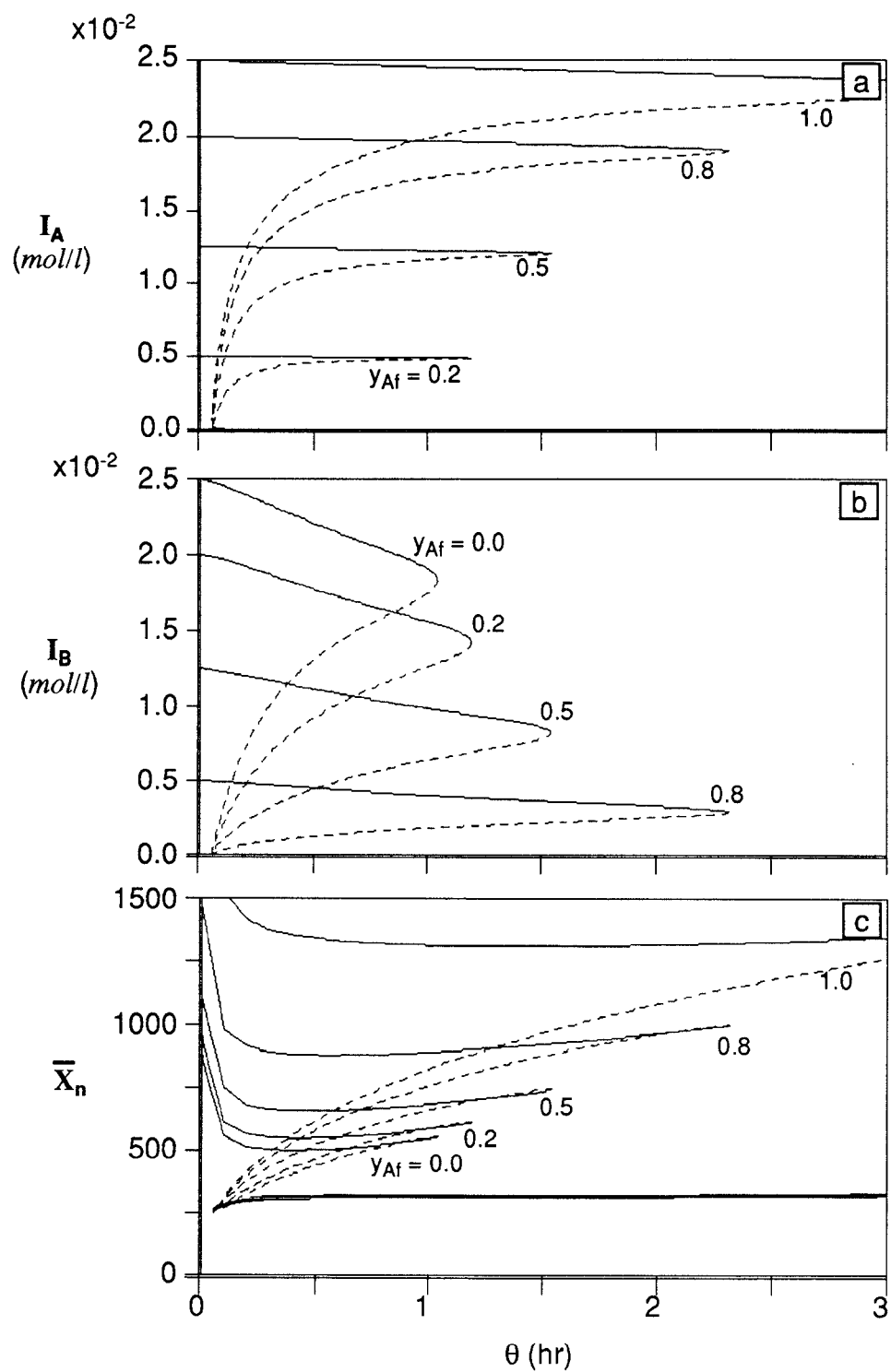
Figure 4.2   Steady state profiles of I_A, I_B and $\overline{X}_n$ with various y_{Af}:
$f_s = 0.1$, $I_f = 0.025$ mol/l, $T_f = 343$ °K, $T_c = 363$ °K.

conversion (X_1), reactor temperature (T), initiator concentrations (I_A, I_B), $\overline{X}_n$ and $\overline{X}_w$ for various feed initiator composition (y_{Af}) with residence time (θ) as a bifurcation parameter. Solid lines and dashed lines represent stable and unstable steady states, respectively. These bifurcation diagrams were obtained by solving the steady state model equations using a numerical package AUTO [Doedel (1981)].

In the analysis of reactor behavior with constant heat transfer coefficient (§2.4), it was shown that the same reactor operating conditions give rise to multiple steady states, isolas, Hopf bifurcations, period doublings, period doubling cascades, homoclinics, etc. Surprisingly, however, as shown in Figures 4.1 and 4.2, rather simple steady state behavior is observed when the viscosity dependent heat transfer coefficient is used in the new model. In §2.4, it was shown that as the feed initiator feed composition varies, there was a dramatic change in the bifurcation behavior (For example, see Figure 2.5). In contrary, no bifurcation to periodic orbits was observed for the entire range of y_{Af} in the present case. It is also seen that the reactor temperature at lower steady states is almost constant for $\theta > 0.2$ hr and is independent of feed initiator feed composition. A similar observation is also made in the upper steady state branch. However, $\overline{X}_n$ and $\overline{X}_w$ values vary significantly with y_{Af} in the lower steady state [upper curves in Figures 4.1c and 4.2c]. The highest polymer molecular weight is obtained when only tert-butyl perbenzoate (slow initiator) is present in the initiator feed stream. The polymer molecular weight at

upper steady states [lower curves in Figures 4.1c and 4.2c] is little affected by the feed initiator composition because, as seen in Figure 4.2a and 4.2b, no undecomposed initiators are present at high reactor temperature. The heat transfer coefficient (h_c) changes markedly in the lower steady state branches as illustrated in Figure 4.3a. Since both the reactor temperature and polymer molecular weight are nearly constant for $\theta > 0.2$ hr, one can easily see that the decrease in h_c is due to the increasing polymer concentration in the reactor. In the upper steady state, essentially no additional polymer production occurs and therefore, the heat transfer coefficient remains almost constant. Figure 4.3b shows the N_{Re} profiles which are qualitatively similar to that of h_c. Notice that the Reynolds numbers in the lower steady state branches [upper curves] are very high, suggesting that the polymer solution is very well mixed. Even in the upper steady state [lower curves], N_{Re} is still above 100.

The viscosities of the polymer solution in the bulk phase (η_r) and at the reactor walls (η_w) are shown in Figures 4.4a and 4.4b. First notice that the maximum bulk phase viscosity is about 3,000 which is lower than the viscosity limit (5,000 cp) a turbine agitator can handle [Henderson (1987)]. At lower steady state branches, there is little difference in the viscosity between the bulk reacting phase and the reactor wall surface [Figures 4.4a and 4.4b]. However, at upper steady states, η_w is about three orders of magnitude larger than η_r, evidently due to a huge temperature difference between the reactor and the coolant. One can easily see that the high viscosity of the fluid at the reactor
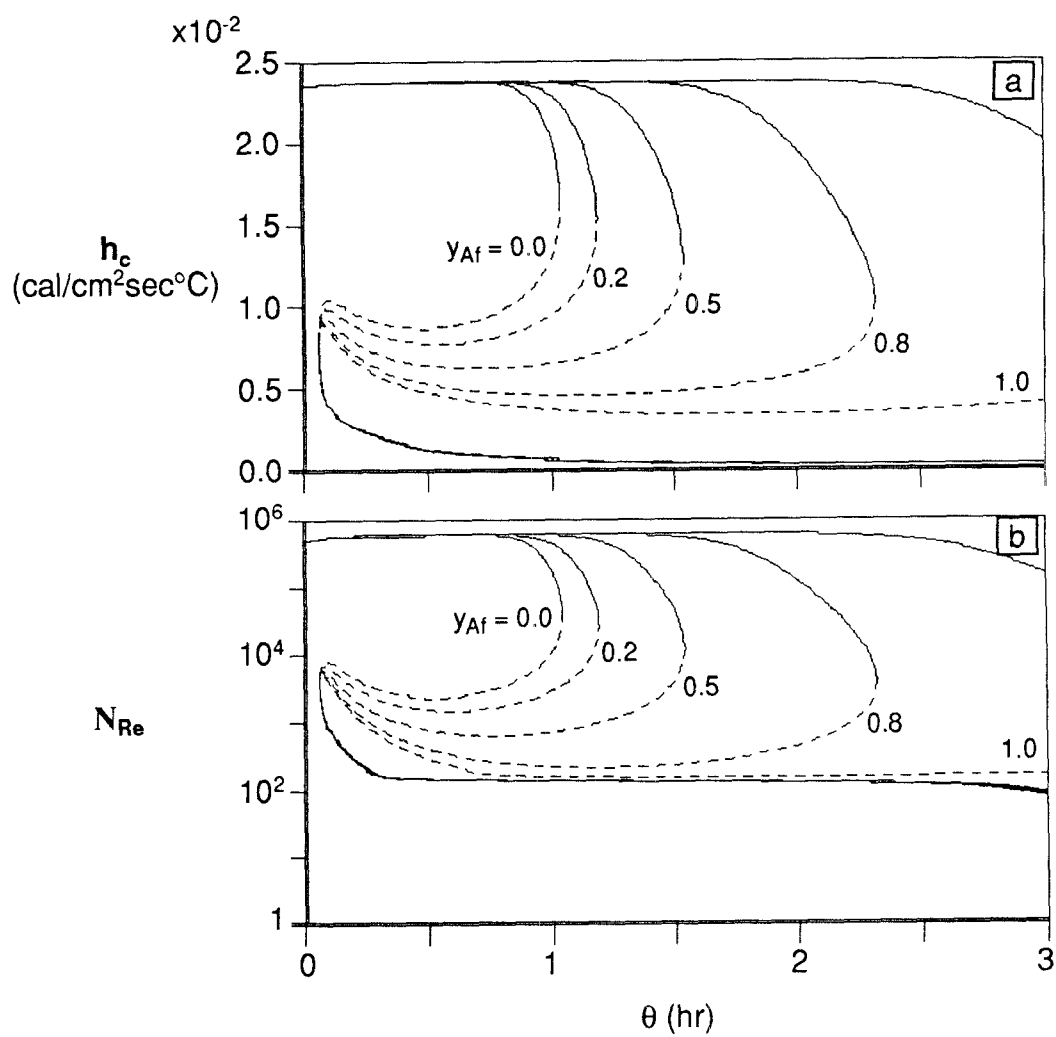
Figure 4.3   Steady state profiles of h_c and N_{Re} with various y_{Af}: $f_s = 0.1$, $I_f = 0.025$ mol/l, $T_f = 343$ °K, $T_c = 363$ °K.
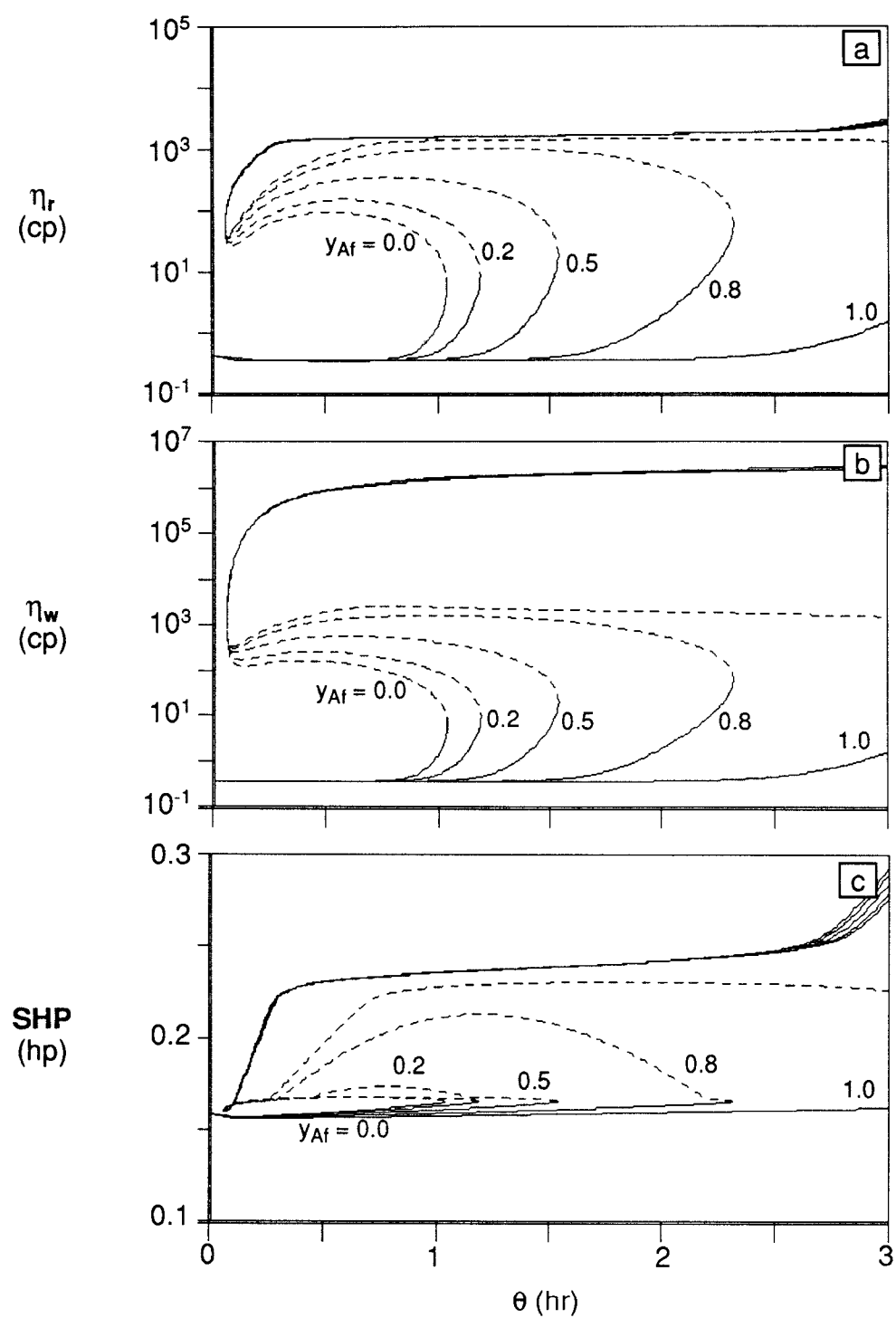
Figure 4.4   Steady state profiles of η_r, η_w, ρ_r and SHP with various y_{Af}:
$f_s = 0.1$, $I_f = 0.025$ mol/l, $T_f = 343$ °K, $T_c = 363$ °K.

Table 4.3   Correlation for required shaft horsepower [Dickey (1984)]

$$SHP = 8.99 \times 10^{-14} f_\eta \rho N^3 D_i^5 \quad \text{(hp)}$$

for $N_{Re} > 900$

$$f_\eta = 1.0$$

for $900 > N_{Re} > 8$

$$f_\eta = \exp\left[3.154 - 0.848 ln N_{Re} + 0.0565 (ln N_{Re})^2\right]$$

for $8 > N_{Re} > 1$

$$f_\eta = \exp\left[3.649 - 0.942 ln N_{Re} - 0.106 (ln N_{Re})^2 + 0.0448 (ln N_{Re})^3\right]$$

for $N_{Re} < 1$

$$f_\eta = 38.4/N_{Re}$$

---

wall also accounts for the decreased heat transfer coefficient, as shown in Figure 4.3a. Figure 4.4c shows the steady state shaft horsepower (SHP) requirements calculated using the correlation suggested by Dickey (1984), as given in Table 4.3. In the range of the reactor operating conditions employed, the driver load is not too high to cause any operational problems.

The feed initiator composition (y_{Af}) and the feed initiator concentration (I_f) are the variables that can also be manipulated by a reactor operator.

Figures 4.5 and 4.6 show the steady state profiles of X_1, I_A, I_B, T, $\overline{X}_n$ and $\overline{X}_w$ for three different residence times with y_{Af} and I_f as bifurcation parameters. In Figure 4.5, the feed initiator concentration is fixed at 0.025 mol/l. It is interesting to observe in Figure 4.5 that no steady state (either stable or unstable) exists to give monomer conversion in the range of 0.5~0.95 unless very small residence time is employed. When the initiator feed concentration is used as a bifurcation parameter, the steady state profiles shown in Figure 4.6 are qualitatively similar to that shown in Figure 4.1. However, for very low initiator concentration, the reactor temperatures at upper steady states are higher and the Reynolds numbers can be much lower than 100 [Figure 4.6e]. Clearly this is due to the increased polymer molecular weight [Figure 4.6c] at low initiator concentrations. Very poor mixing could be possible under such reaction conditions. It is also observed that at $\theta = 1.0$ and 1.5 hr, no steady states exist to give a monomer conversion in the range of 0.6~0.88. Figure 4.7 shows a diagram in which the loci of the limit points of steady state branches are traced as the residence time and the initiator composition or its concentration are varied. For example, with y_{Af} fixed at 0.5, a stable lower steady state is only seen in region I for a very small value of θ. As θ is increased up to 1.6 hr, three steady states exist and with a further increase in θ, the system will have only a single stable upper steady state.

When the solvent volume fraction in the feed stream is used as a bifurcation parameter, steady state profiles as shown in Figure 4.8 are obtained.
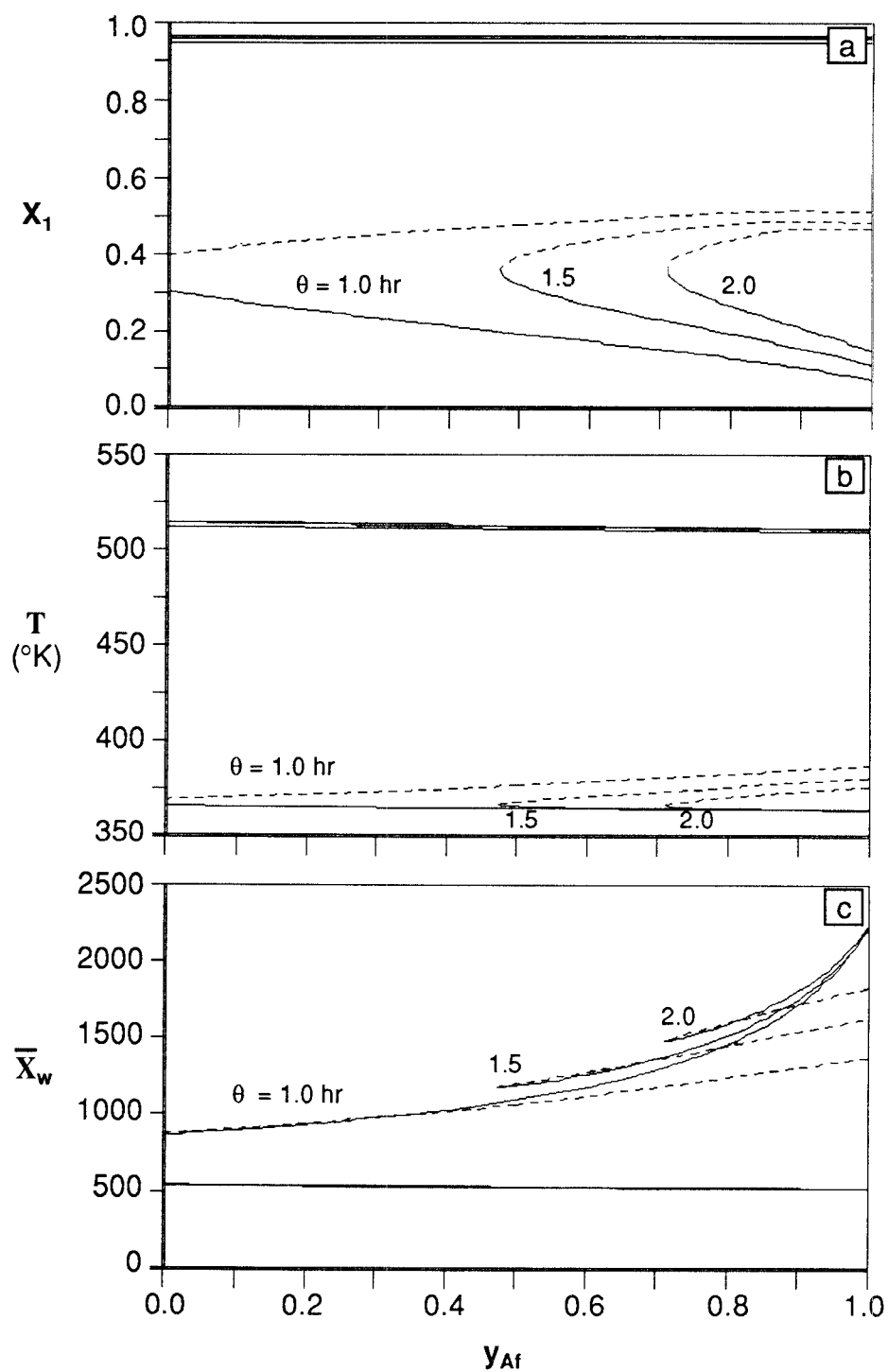
Figure 4.5   Effect of y_{Af} on steady state profiles of the reactor for different θ: $f_s = 0.1$, $I_f = 0.025$ mol/l, $T_f = 343$ °K, $T_c = 363$ °K.
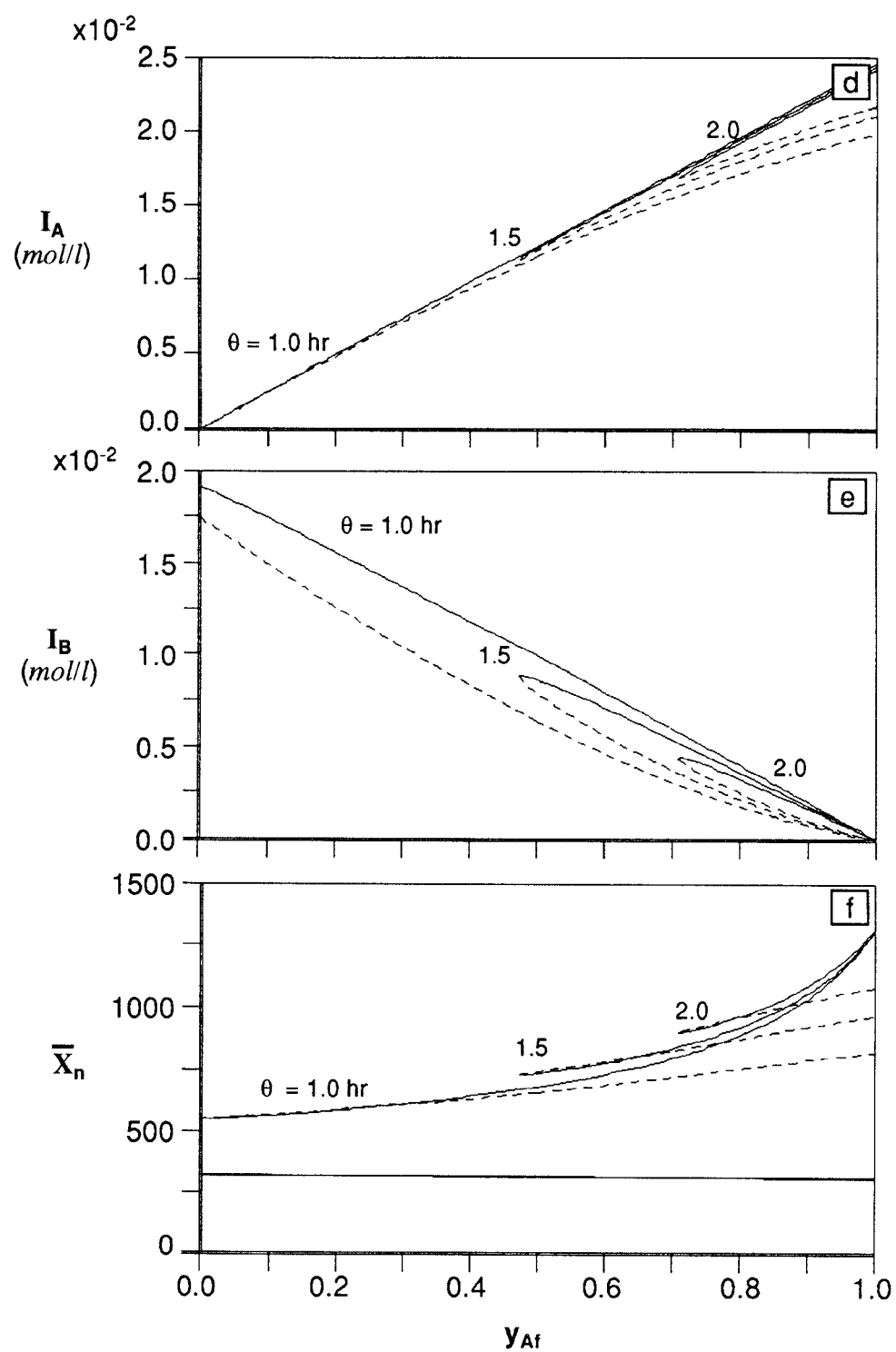
Figure 4.5   (continued)
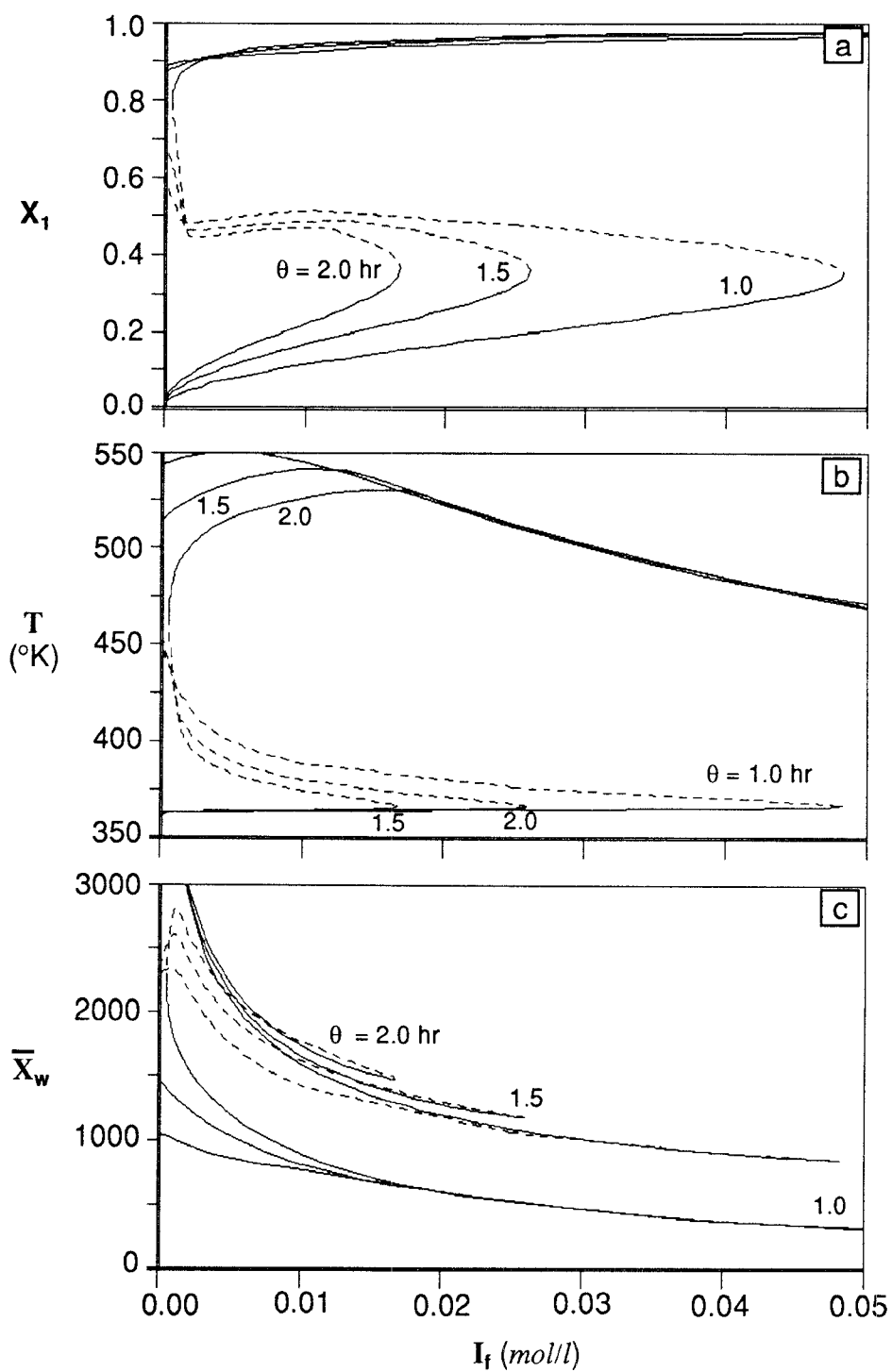
Figure 4.6   Effect of I_f on steady state profiles of the reactor for different *theta*: $f_s = 0.1$, $y_{Af} = 0.5$, $T_f = 343$ °K, $T_c = 363$ °K.
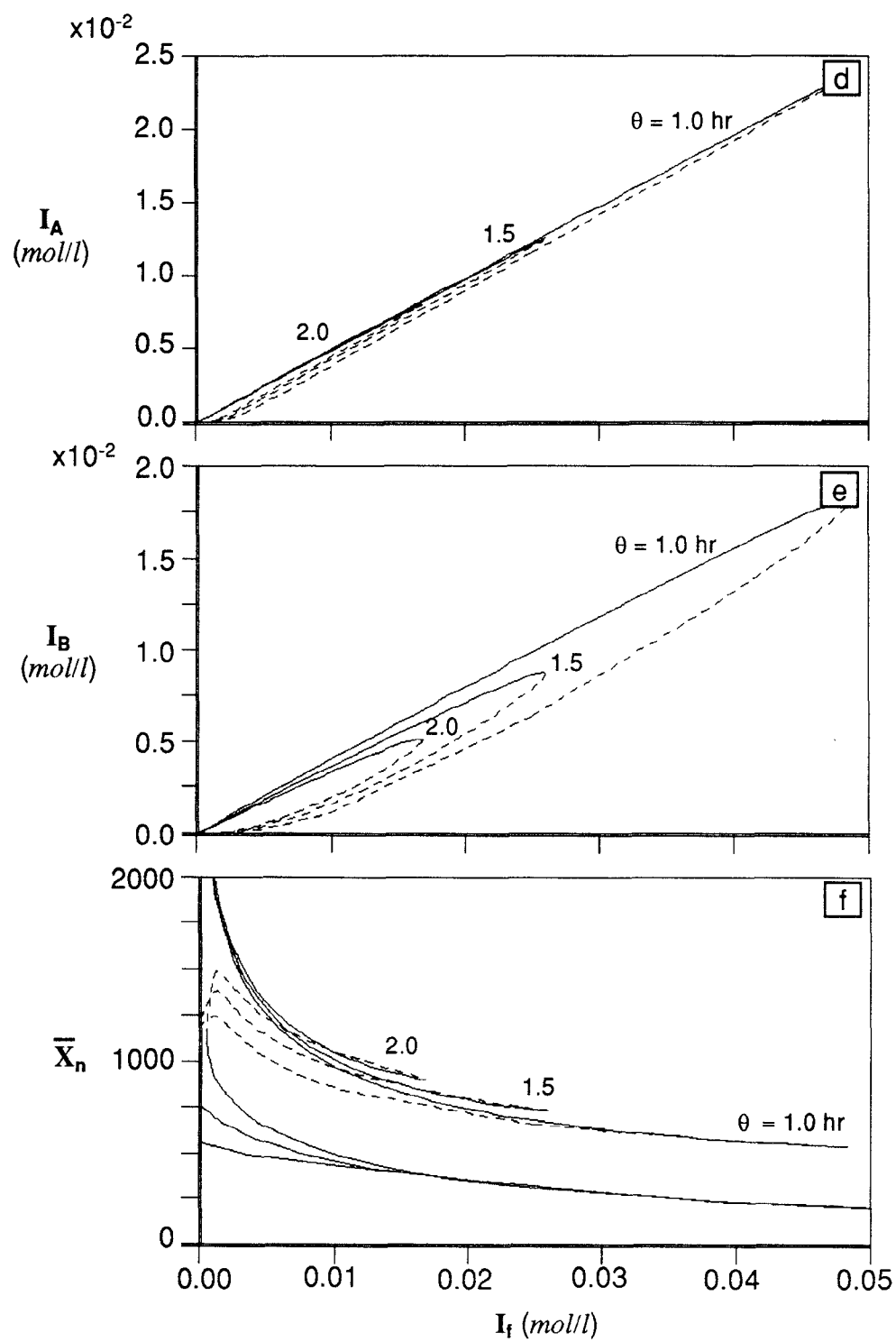
Figure 4.6 *(continued)*
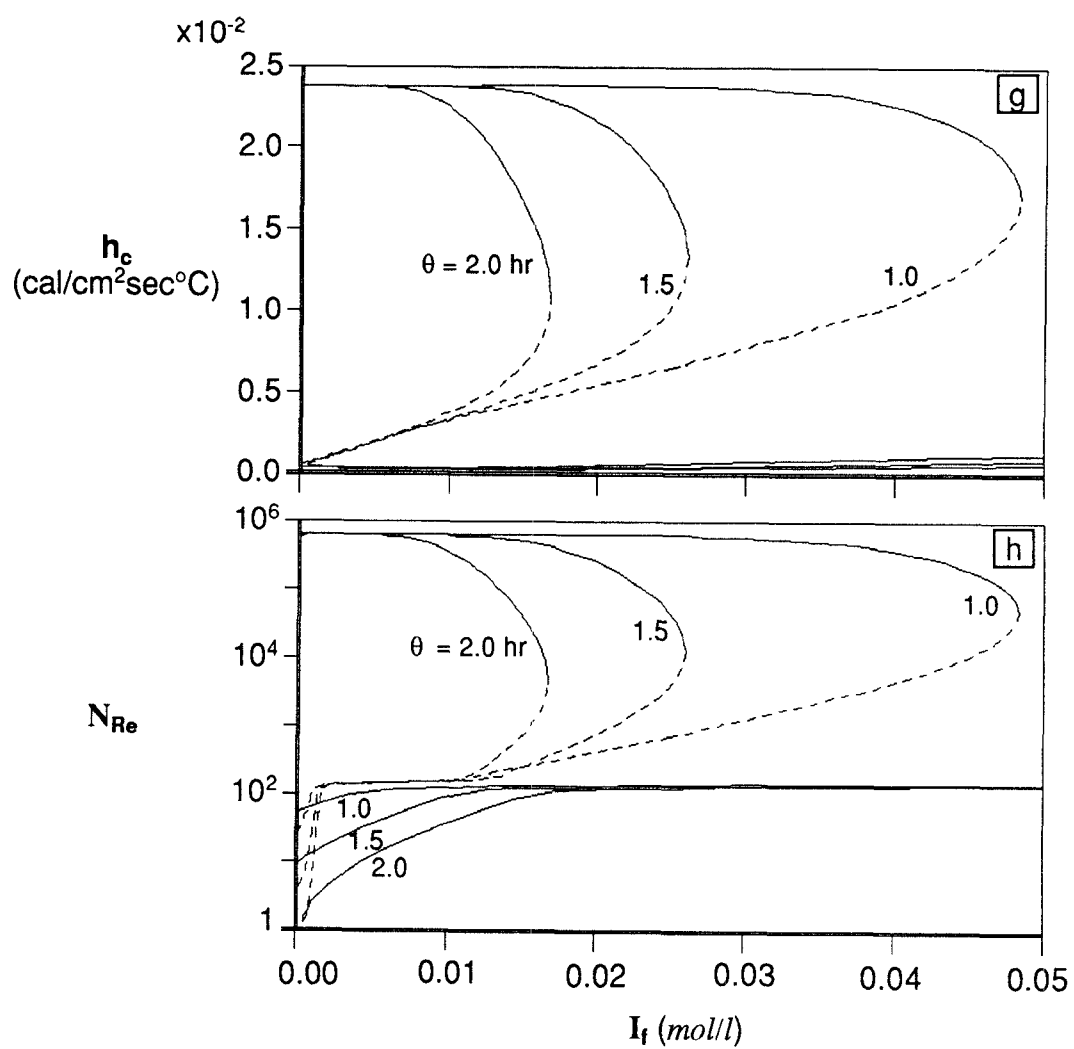
Figure 4.6   (continued)
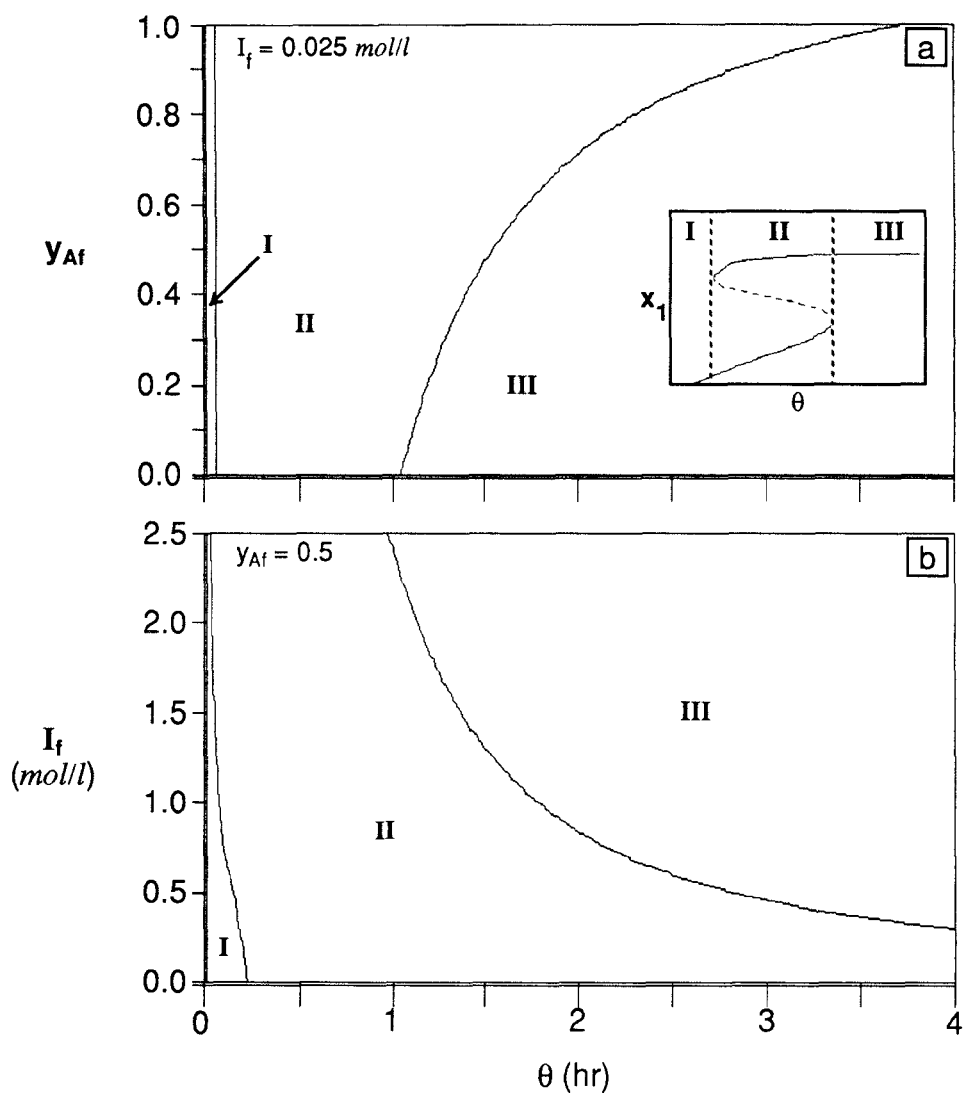
Figure 4.7   Steady state bifurcation structure diagram: $f_s = 0.1$, $T_f = 343\ °K$, $T_c = 363\ °K$.
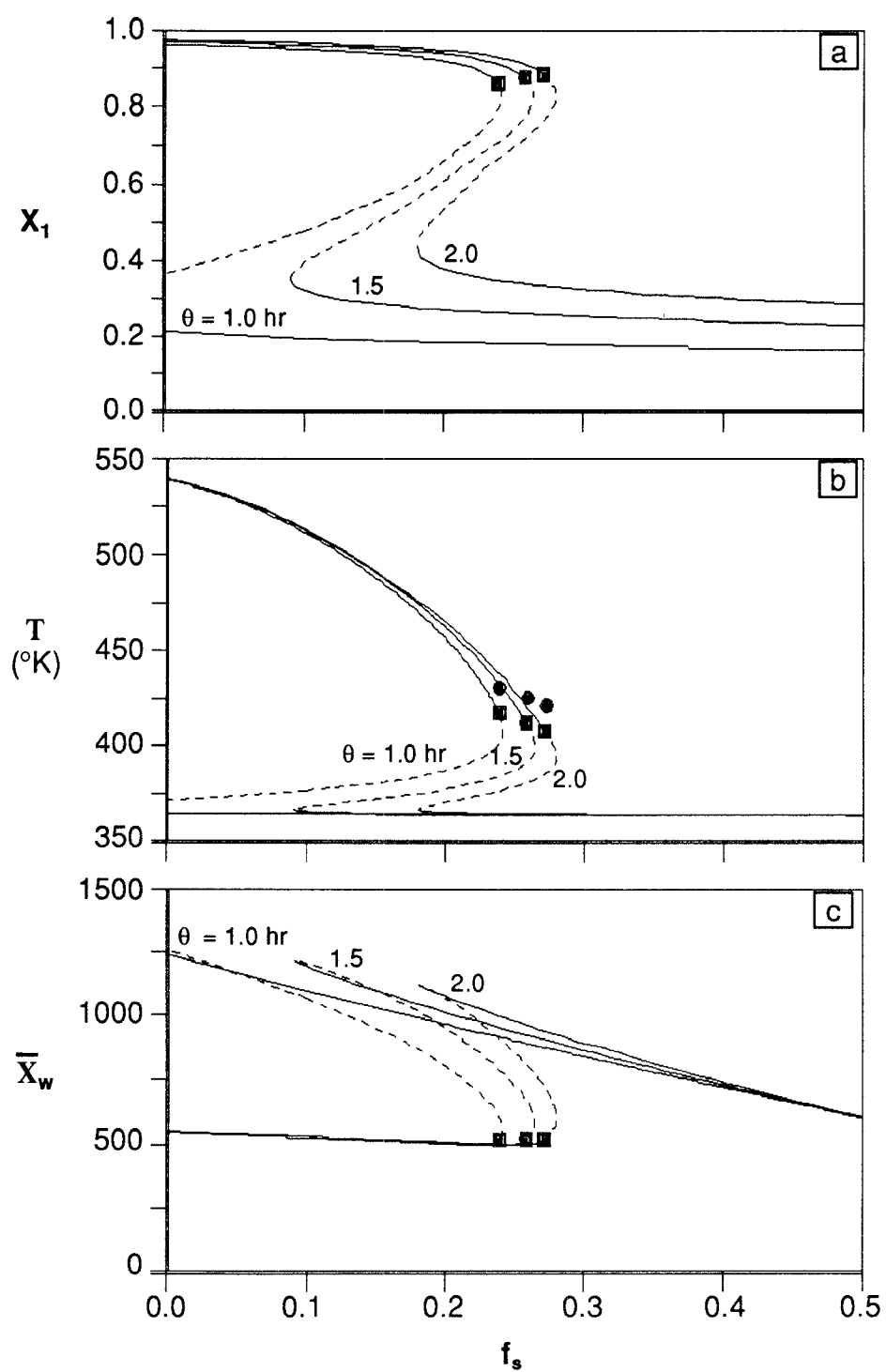
Figure 4.8   Effect of f_s on steady state profiles of the reactor for different
θ: $I_f = 0.025$ mol/l, $y_{Af} = 0.5$, $T_f = 343$ °K, $T_c = 363$ °K.
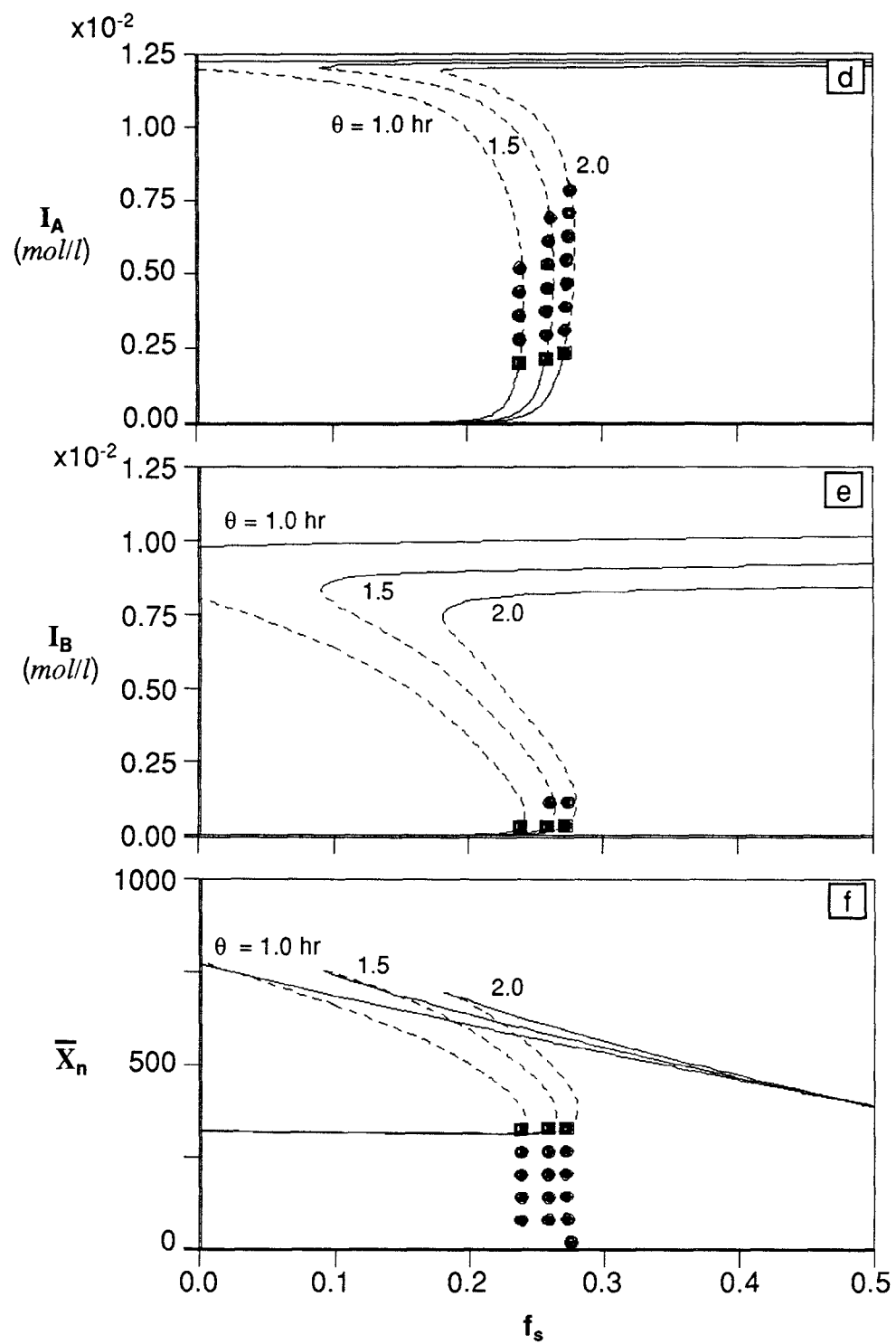
Figure 4.8   (*continued*)

Recall that no bifurcation to periodic solutions was observed so far as f_s was fixed at 0.1. Now as the solvent fraction is increased to about 0.25~0.30, a Hopf bifurcation point (marked by ■) appears and a branch of periodic solution emanates from the Hopf point. The periodic orbit eventually terminates in a homoclinic. Figure 4.9a illustrates the bifurcation behavior in X_1–θ plane. The inset of Figure 4.9a for $f_s = 0.25$ shows that the branch of the periodic solutions (PS) emanating from the Hopf bifurcation point further bifurcates to a stable period doubling (PD) orbit, losing its own stability. It is also interesting to notice that for $f_s = 0.25$ and 0.3, a portion of the upper branch is unstable. Figure 4.9b shows the range of f_s and θ values which yield different bifurcation behavior. Figure 4.10 and 4.11 illustrate the results of dynamic simulations at and near the Hopf point. Note that as the residence time is reduced from 3.86 hr to 3.65 hr, the reactor state is attracted to a stable lower steady state.

The steady state profiles are shown in Figure 4.12 with coolant temperature (T_c) as a bifurcation parameter. The overall qualitative behavior is quite similar to Figure 4.5 in that no steady state exist to give X_1 in the range of 0.55~0.95 for $\theta > 1.0$ hr.

For the control of reactor temperature, a cooling jacket temperature (T_c) is used as a control variable. With a proportional-integral (PI) controller in the temperature control loop, dynamic simulations were carried out with a viscosity dependent heat transfer coefficient and a constant heat transfer
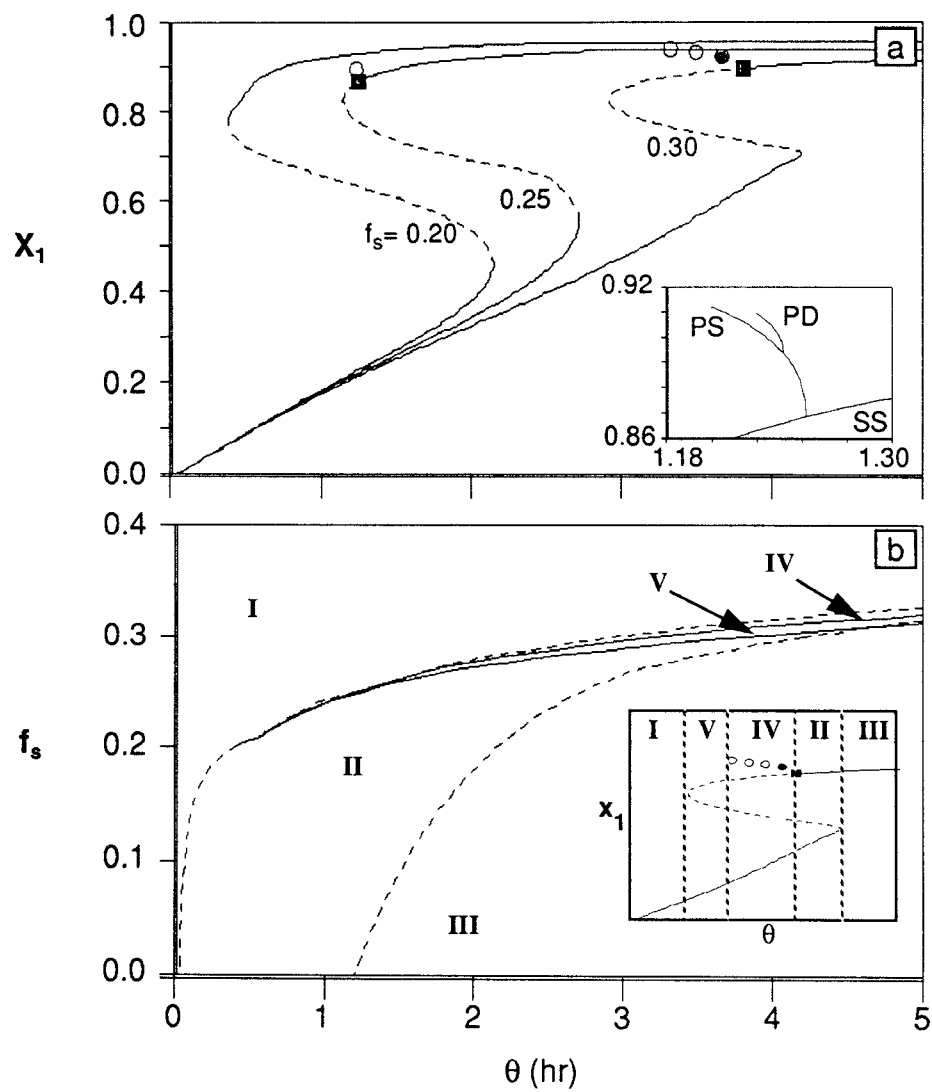
Figure 4.9 Effect of f_s on steady state behavior: $I_f = 0.025$ mol/l, $y_{Af} = 0.5$, $T_f = 343$ °K, $T_c = 363$ °K.
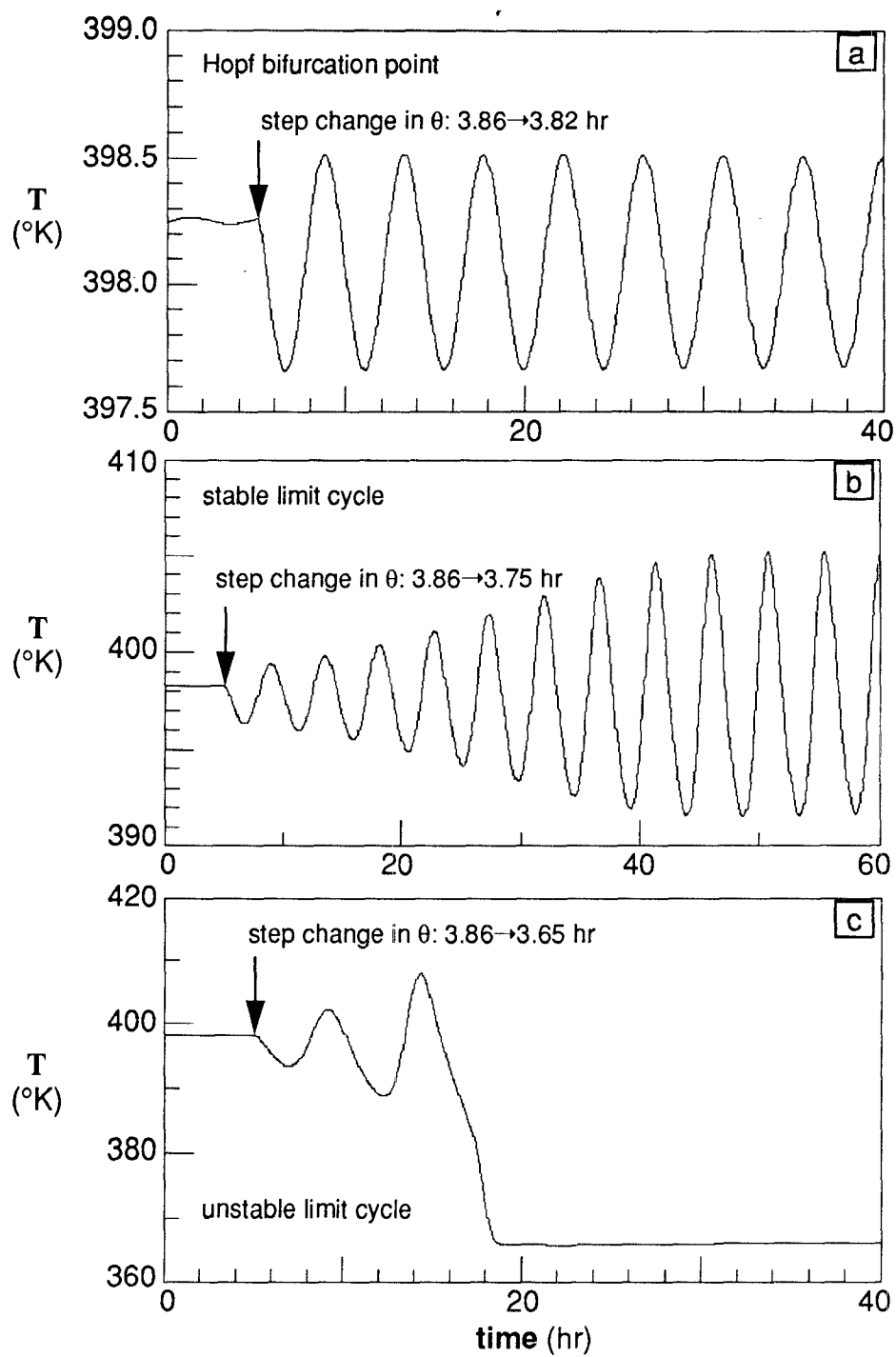
Figure 4.10   Transient reactor response to a step change in θ: $f_s = 0.3$, $I_f = 0.025$ mol/l, $y_{Af} = 0.5$, $T_f = 343\ °K$, $T_c = 363\ °K$.
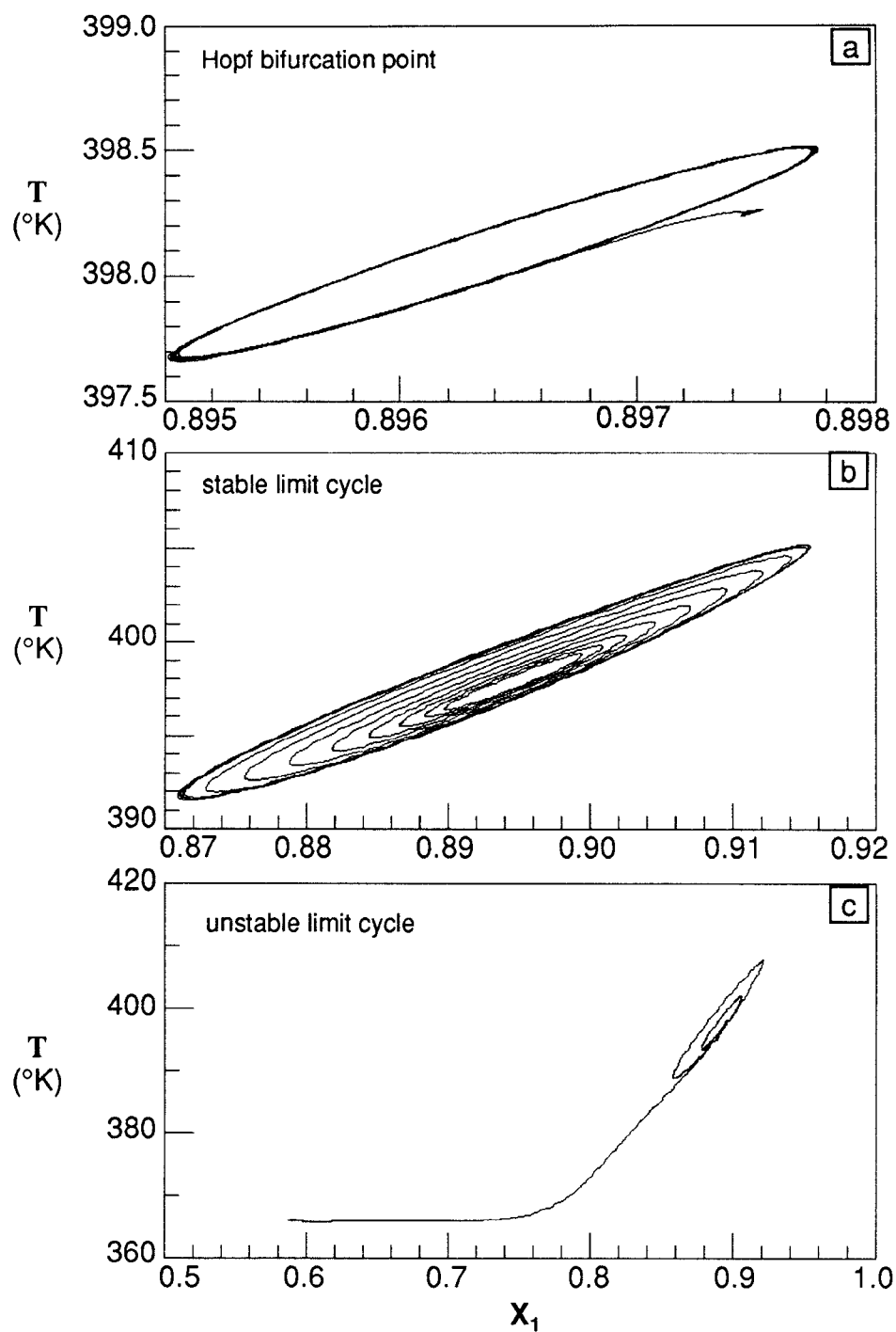
Figure 4.11   Phase plane portraits of transient response to a step change in θ and phase plane portraits: $f_s = 0.3$, $I_f = 0.025$ mol/l, $y_{Af} = 0.5$, $T_f = 343$ °K, $T_c = 363$ °K.
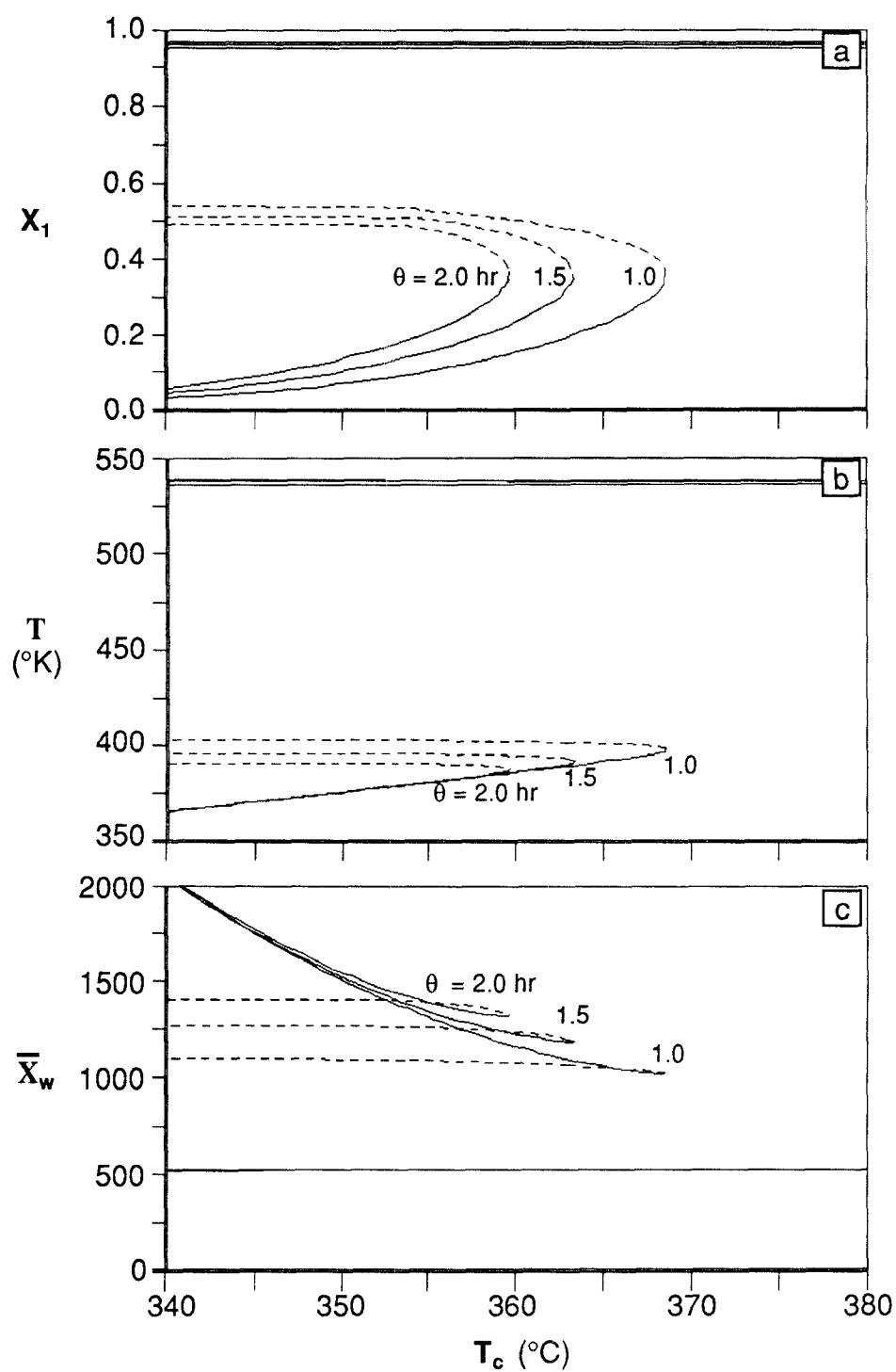
Figure 4.12   Effect of T_c on steady state profiles of the reactor for different θ: $f_s = 0.1$, $I_f = 0.025$ mol/l, $y_{Af} = 0.5$, $T_f = 343$ °K.
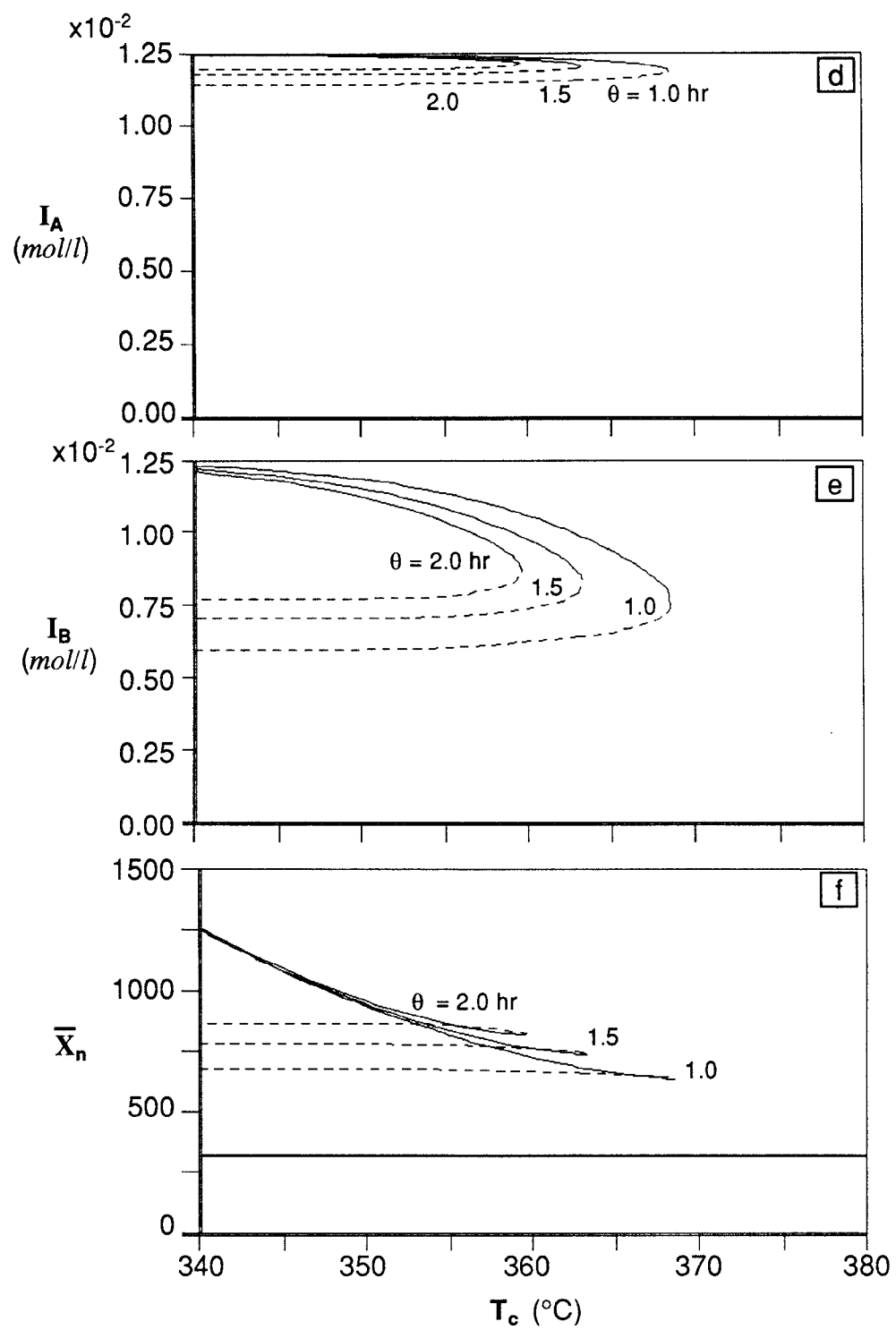
Figure 4.12   (*continued*)

coefficient, respectively. Figure 4.13a and 4.13b show the response of the reactor to a step change in the feed initiator concentration from 0.025 to 0.035 mol/l for both cases. First notice in Figure 4.13b that when the heat transfer coefficient remains unchanged, the reactor temperature is controlled nicely at its set point. However, when the heat transfer coefficient changes, the feedback controller fails to maintain the set point temperature about 3 hours after the step change is made. Such a failure of the temperature control is clearly explained in Figure 4.14. As more initiator is added to the reactor, the monomer conversion increases and the viscosity begins to increase rapidly. As a result, the heat transfer coefficient continues to decrease. As the heat transfer coefficient drops to a very low value after about 3 hours, the reaction heat is not removed adequately through the reactor walls and as a result the reactor runs away to an upper steady state. Figure 4.14e also indicates that the viscosity at the reactor wall increases by a few orders of magnitude. The Reynolds number (N_{Re}) continuously falls to below 100 until the runaway occurs. The reactor simulations shown in Figure 4.14 clearly illustrate that the reactor temperature control can be a serious problem if the heat transfer coefficient changes with reaction conditions.
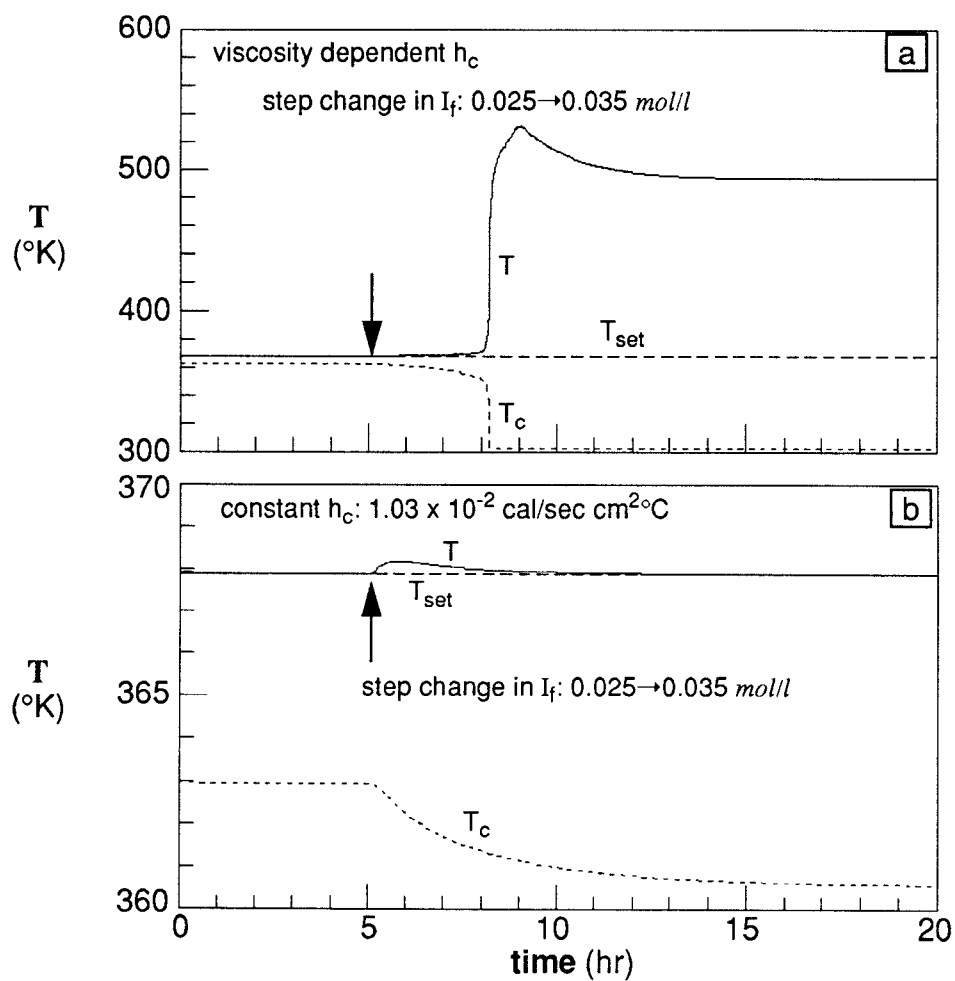
Figure 4.13   Closed loop transients of T to step disturbance in I_f (+40 %) with viscosity dependent h_c (a) and constant h_c: $\theta = 1.5$ hr, $f_s = 0.1$, $I_f = 0.025$ mol/l, $y_{Af} = 0.5$, $T_f = 343$ °K ($K_c = 0.5$ °K, $\tau_I = 0.2$ hr, $303 \leq T_c(°K) \leq 423$).

250
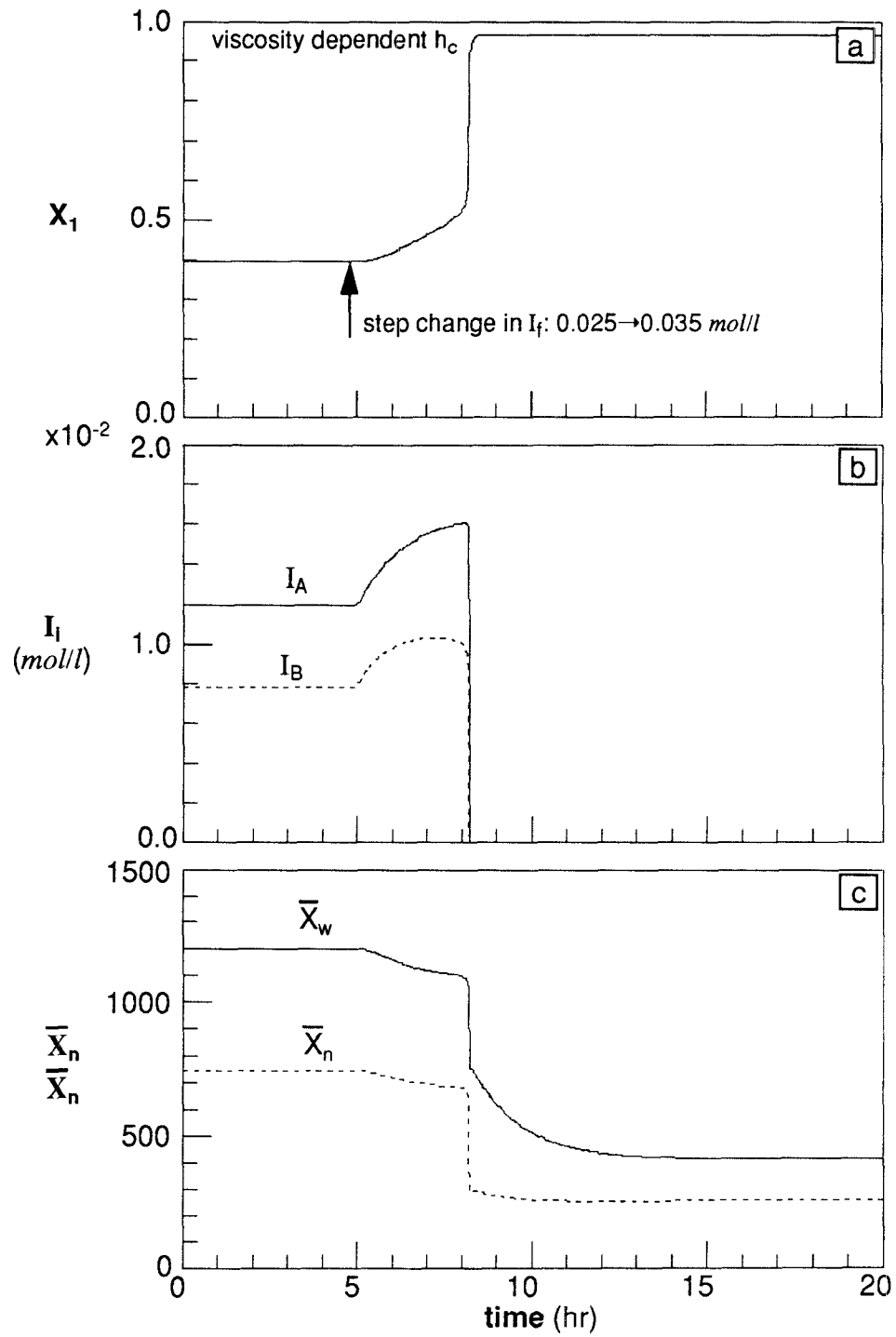
Figure 4.14   Closed loop transients of the reactor to step disturbance in I_f
(+40 %): $\theta = 1.5$ hr, $f_s = 0.1$, $I_f = 0.025$ mol/l, $y_{Af} = 0.5$,
$T_f = 343$ °K ($K_c = 0.5$ °K, $\tau_I = 0.2$ hr, $303 \leq T_c(°K) \leq 423$).

251
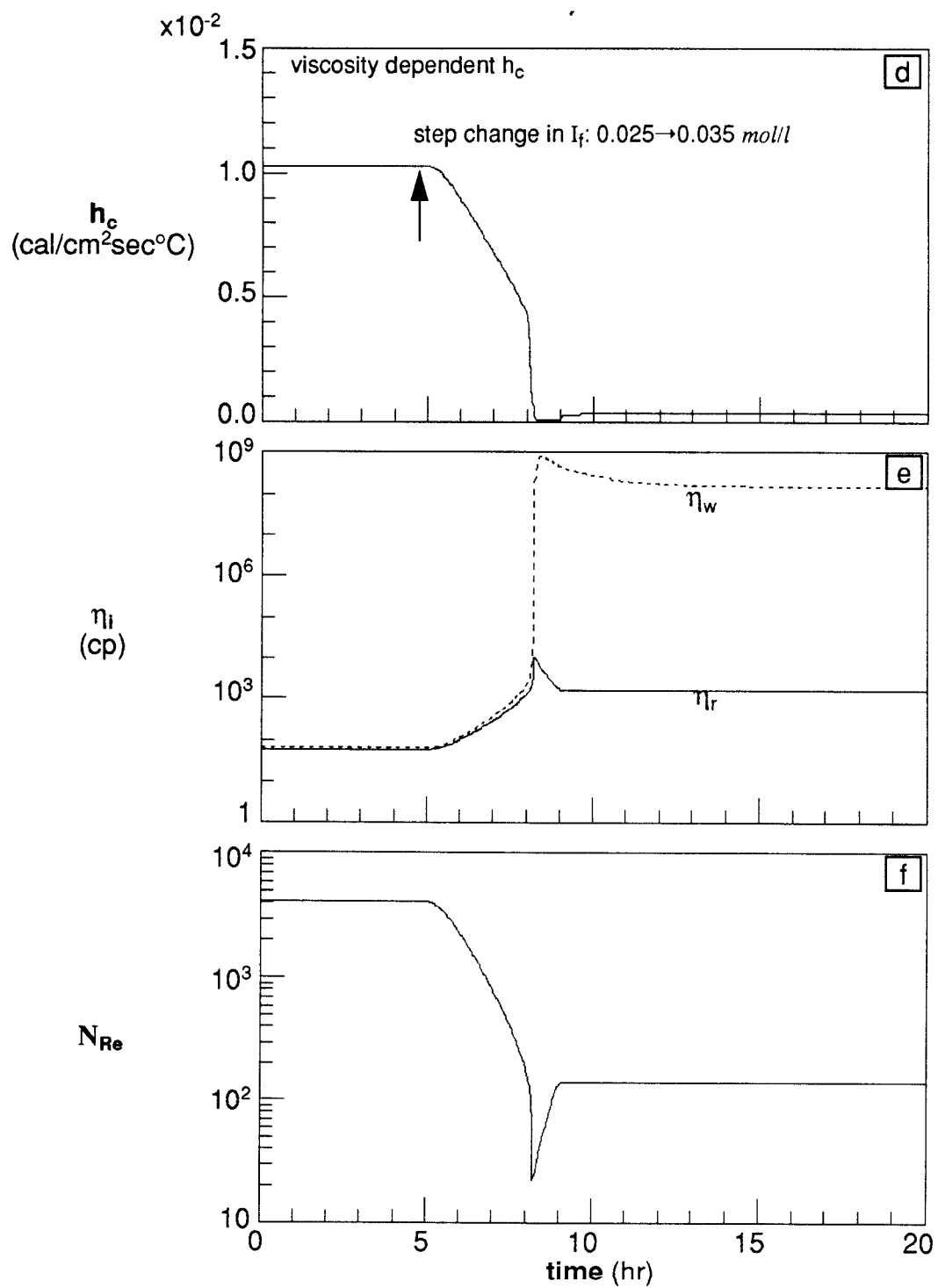
Figure 4.14   (*continued*)

4.2.3. Concluding Remarks

In this section, the steady state and dynamic behavior of a CSTR is investigated for styrene polymerization with mixed initiators. In particular, the effect of various operating parameters such as initiator feed composition, initiator feed concentration, solvent feed volume fraction and coolant temperature have been analyzed. An emphasis has been placed on the elucidation of the effect of viscosity dependent heat transfer coefficient on the reactor behavior. It is observed that the reactor system with viscosity dependent heat transfer coefficient shows a simpler steady state and dynamic behavior than the case with constant heat transfer coefficient. For the solvent volume fraction below 0.2, no bifurcation to periodic solutions occurs; however, as the solvent volume fraction is increased, Hopf bifurcations, period doubling and homoclinic limit cycles are observed. Dynamic simulations of the reactor with varying heat transfer coefficient indicate that some process disturbances can lead to a disastrous reactor runaway even with a feedback temperature controller.

4.3. Effect of Impurities

In this section, the same polymerization system in a CSTR discussed in Chapter 2 is considered except that inhibitors are present in the feed stream.

4.3.1. Reactor Model

Inhibitors or retarders suppress the polymerization by scavenging the primary radicals and terminating the active polymeric chains. Although clear difference between inhibitors and retarders has not been defined, it is determined by the reactivity of each material. Inhibitors, which are highly reactive, mainly attack the primary radicals so that the polymerization cannot occur. Less reactive retarders reduce the radical chains leading to slower polymerization [Bamford and Tipper (1976)]. The inhibition (retardation) mechanism varies from one inhibitor (retarder) to another. For quinone type inhibitors, the inhibition has been known to occur through a two step mechanism [Rintelen *et al.* (1983), Douglas *et al.* (1982), Tüdös *et al.* (1961), Bevington and Ghanem (1959), Cohen (1947)]. In the first step which is the rate determining step, a polymer radical reacts with the inhibitor molecule to form an inhibitor radical of unknown structure. Upon reaction with additional polymer radicals, inactive radical products are formed from this inhibitor radical. The kinetic scheme for inhibition can be represented as follows [Rintelen *et al.* (1983)]:

$$R + I_h \xrightarrow{k_q} Q_0 \qquad\qquad (4.21a)$$

$$P_n + I_h \xrightarrow{k_q} Q_n \qquad (n \geq 1) \qquad\qquad (4.21b)$$

$$Q_0 + R \xrightarrow{k_{tq}} \text{inactive radical} \qquad\qquad (4.21c)$$

$$Q_0 + P_n \xrightarrow{k_{tq}} M_n \qquad (n \geq 1) \qquad\qquad (4.21d)$$

$$Q_n + R \xrightarrow{k_{tq}} M_n \qquad (n \geq 1) \qquad\qquad (4.21e)$$

$$Q_n + P_m \xrightarrow{k_{tq}} M_{n+m} \qquad (n, m \geq 1) \qquad\qquad (4.21f)$$
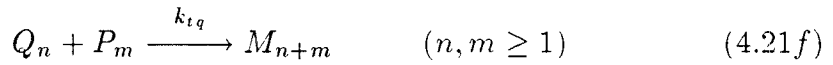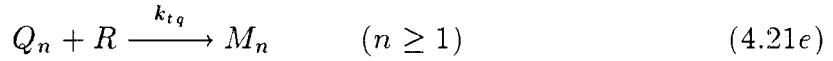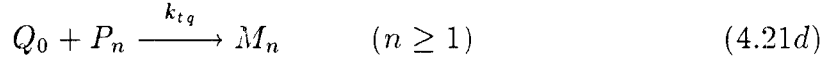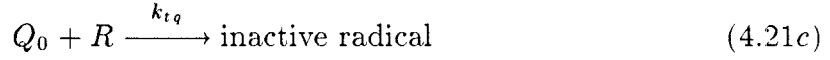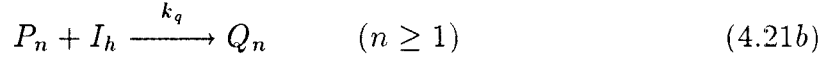
where I_h is the inhibitor, Q_0 the inhibitor radicals formed with the primary radicals and Q_n the inhibitor radicals with n-repeating monomer units.

With the above kinetic scheme, the rate expressions for polymer chains and the inhibitor can be expressed as follows:

$$\frac{dR}{dt'} = 2(f_A k_{d_A} I_A + f_B k_{d_B} I_B) - k_i RM - k_q I_h R$$

$$- k_{tq}(Q_0 + Q)R \qquad\qquad (4.22)$$

$$\frac{dP_1}{dt'} = 2k_{d_M} M^3 + k_i RM - k_p M P_1 + k_{fm} M(P - P_1) - k_t P P_1$$

$$- k_q I_h P_1 - k_{tq}(Q_0 + Q)P_1 \qquad\qquad (4.23)$$

$$\frac{dP_n}{dt'} = k_p M(P_{n-1} - P_n) - k_{fm} M P_n - k_t P P_n - k_q I_h P_n$$

$$- k_{tq}(Q_0 + Q)P_n \qquad (n \geq 2) \qquad\qquad (4.24)$$

$$\frac{dQ_0}{dt'} = k_q R I_h - t_{tq}(R + P)Q_0 \qquad\qquad (4.25)$$

$$\frac{dQ_n}{dt'} = k_q P_n I_h - t_{tq}(R + P)Q_n \qquad (n \geq 1) \qquad\qquad (4.26)$$

$$\frac{dM_n}{dt'} = k_{fm}MP_n + \frac{1}{2}k_t \sum_{m=1}^{n-1} P_{n-m}P_m + k_{tq}Q_0P_n + k_{tq}Q_nR$$

$$+ k_{tq} \sum_{m=1}^{n-1} P_{n-m}Q_m \qquad (n \geq 2) \qquad (4.27)$$

$$\frac{dI_h}{dt'} = -k_qI_h(R+P) \qquad (4.28)$$

where P is the total concentration of active polymer chains and Q the total concentration of inhibitor radical chains.

The three leading moments of each polymeric species are required for the calculation of molecular weight averages of the polymer and they can be derived by defining the moments of the inhibitor radical chain as follows:

$$\lambda_k^q = \sum_{n=1}^{\infty} k^k Q_n + Q_0 \qquad (4.29)$$

All the moment equations for each polymeric species are given in **Appendix D**. Since the concentrations of live polymers and inhibitor radical chains are much lower than that of dead polymers, the molecular weight averages are computed using the dead polymer moments only.

The mass and energy balance equations for a CSTR are expressed as follows:

$$V\frac{dM}{dt'} = q(M_f - M) - Vk_pMP \qquad (4.30)$$

$$V\frac{dI_A}{dt'} = q(I_fy_{Af} - I_A) - Vk_{d_A}I_A \qquad (4.31)$$

$$V\frac{dI_B}{dt'} = q\{I_f(1 - y_{Af}) - I_B\} - Vk_{d_B}I_B \qquad (4.32)$$

$$V\frac{dI_h}{dt'} = q(I_{hf} - I_h) - Vk_qI_h(R + P) \qquad (4.33)$$

$$\rho C_p V\frac{dT}{dt'} = \rho Cpq(T_f - T) + V(-\Delta H)k_p MP - h_c A_c(T - T_c) \quad (4.34)$$

By applying the quasi-steady state approximation to live polymers and inhibitor radical chains in the reactor, the total concentrations of growing polymers (P) and primary radicals (R) can be derived as follows:

$$P = \left[\left(\frac{k_q I_h}{k_t}\right)^2 + 2k_{d_M}M^3 + k_i RM\right]^{1/2} - \left(\frac{k_q I_h}{k_t}\right) \qquad (4.35)$$

$$R = \frac{2f_A k_{d_A} I_A + 2f_B k_{d_B} I_B}{k_i M + 2k_q I_h} \qquad (4.36)$$

Here, it is assumed that $k_i \approx k_p$. The moment equations for dead polymers are:

$$V\frac{d\lambda_0^d}{dt'} = -q\lambda_0^d + VP\left[\hat{\alpha}k_{fm}M + \frac{1}{2}k_t P + \frac{k_q I_h}{(R + P)}(2\hat{\alpha}R + P)\right] \quad (4.37)$$

$$V\frac{d\lambda_1^d}{dt'} = -q\lambda_1^d + \frac{VP}{(1 - \hat{\alpha})}\left[\hat{\alpha}(2 - \hat{\alpha})k_{fm}M + k_t P \right.$$
$$\left. + \frac{2k_q I_h}{(R + P)}(\hat{\alpha}(2 - \hat{\alpha})R + P)\right] \qquad (4.38)$$

$$V\frac{d\lambda_2^d}{dt'} = -q\lambda_2^d + \frac{VP}{(1 - \hat{\alpha})^2}\left[\hat{\alpha}(\hat{\alpha}^2 - 3\hat{\alpha} + 4)k_{fm}M + (\hat{\alpha} + 2)k_t P \right.$$
$$\left. + \frac{2k_q I_h}{(R + P)}\{2\hat{\alpha}(\hat{\alpha}^2 - 3\hat{\alpha} + 4)R + (\hat{\alpha} + 2)P\}\right] \qquad (4.39)$$

With the dimensionless variables and parameters defined in Table 4.4, the reactor modeling equations are reduced to the following dimensionless form:

Table 4.4   Dimensionless variables and parameters

$$X_1 = \frac{M_f - M}{M_f}, \qquad X_2 = \frac{y_{Af} I_f - I_A}{y_{Af} I_f}, \qquad X_3 = \frac{(1 - y_{Af}) I_f - I_B}{(1 - y_{Af}) I_f},$$

$$X_4 = \frac{T - T_f}{T_f}, \qquad X_5 = \frac{\lambda_0^d}{\lambda_{0,r}^d}, \qquad X_6 = \frac{\lambda_1^d}{\lambda_{1,r}^d}, \qquad X_7 = \frac{\lambda_2^d}{\lambda_{2,r}^d},$$

$$X_8 = \frac{I_{hf} - I_h}{I_{hf}} \qquad y_{Af} = \frac{I_{Af}}{I_f}, \qquad t = \frac{t'}{\theta}, \qquad Da = \theta Z, \qquad \alpha = \frac{\alpha_o}{Z},$$

$$\beta = \frac{(-\Delta H) M_f}{\rho C_p T_f}, \qquad \delta = \frac{T_c - T_f}{T_f}, \qquad \psi = \frac{2 k_q}{k_p}, \qquad \eta = \frac{k_{d_{B0}}}{k_{d_{A0}}},$$

$$\epsilon = \frac{E_{d_B}}{E_{d_A}}, \qquad \zeta = \frac{k_{d_{A0}}}{Z}, \qquad \gamma = \frac{E_p}{R T_f}, \qquad \gamma_d = \frac{E_{d_A}}{R T_f}, \qquad \gamma_{d_M} = \frac{E_{d_M}}{R T_f},$$

$$\gamma_f = \frac{E_{fm}}{R T_f}, \qquad \gamma_q = \frac{E_q}{R T_f}, \qquad \gamma_t = \frac{E_t}{R T_f},$$

$$P_a = \frac{\psi k_{p0} I_{hf}}{2 k_{t0}^*}, \qquad P_b = \frac{2 k_{dM0} M_f^3}{k_{t0}^*}, \qquad P_c = \frac{k_{p0} M_f R_f}{k_{t0}^*},$$

$$R_a = 2 f_A k_{d_{A0}} y_{Af} I_f, \qquad R_b = 2 f_B k_{d_{B0}} (1 - y_{Af}) I_f, \qquad R_c = k_{p0} M_f,$$

$$R_d = \psi k_{p0} I_{hf}, \qquad \alpha_m = \frac{k_{fm0}}{k_{p0}}, \qquad \alpha_q = \frac{\psi I_{hf}}{M_f}, \qquad \alpha_t = \frac{k_{t0}^* P_f}{k_{p0} M_f},$$

for $\quad j = 0, 1, 2:$

$$w_{1j} = \frac{k_{fm0} M_f}{\lambda_{j,r}^d k_{p0} \exp(-\gamma)}, \qquad w_{2j} = \frac{k_{t0}^* P_f}{\lambda_{j,r}^d k_{p0} \exp(-\gamma)}, \qquad w_{3j} = \frac{\psi I_{hf}}{\lambda_{j,r}^d},$$

where

$$I_f = I_{Af} + I_{Bf}, \qquad \alpha_0 = \frac{h_o A_c}{\rho C_p V}, \qquad \theta = \frac{V}{q}, \qquad Z = k_{p0} \exp(-\gamma) P_f$$

$$P_f = \left[\{ P_a \exp(\gamma_t - \gamma) \}^2 + P_b \exp(\gamma_t - \gamma_{d_M}) + P_c \exp(\gamma_t - \gamma) \right]^{1/2}$$

$$\qquad - P_a \exp(\gamma_t - \gamma),$$

$$R_f = \frac{R_a \exp(-\gamma_d) + R_b \exp(-\epsilon \gamma_d)}{(R_c + R_d) \exp(-\gamma)},$$

$$\frac{dX_1}{dt} = -X_1 + Da(1-X_1)X_p\exp\left\{\frac{\gamma X_4}{1+X_4}\right\} \tag{4.40}$$

$$\frac{dX_2}{dt} = -X_2 + Da\zeta(1-X_2)\exp\left\{-\frac{\gamma_d}{1+X_4}\right\} \tag{4.41}$$

$$\frac{dX_3}{dt} = -X_3 + Da\zeta\eta(1-X_3)\exp\left\{-\frac{\epsilon\gamma_d}{1+X_4}\right\} \tag{4.42}$$

$$\frac{dX_4}{dt} = -X_4 + \beta\left(X_1 + \frac{dX_1}{dt}\right) + Da\alpha(X_4-\delta) \tag{4.43}$$

$$\frac{dX_5}{dt} = -X_5 + DaX_p\left[w_{10}\hat{\alpha}(1-X_1)\exp\left\{-\frac{\gamma_f}{1+X_4}\right\}\right.$$
$$+ \frac{1}{2}w_{20}X_t\exp\left\{-\frac{\gamma_t}{1+X_4}\right\}$$
$$\left. + \frac{w_{30}(1-X_8)}{X_r+X_p}(\hat{\alpha}X_r + \frac{1}{2}X_p)\exp\left\{-\frac{\gamma_t}{1+X_4}\right\}\right] \tag{4.44}$$

$$\frac{dX_6}{dt} = -X_6 + \frac{DaX_p}{(1-\hat{\alpha})}\left[w_{11}(1-X_1)(2\hat{\alpha}-\hat{\alpha}^2)\exp\left\{-\frac{\gamma_f}{1+X_4}\right\}\right.$$
$$+ w_{21}X_t\exp\left\{-\frac{\gamma_t}{1+X_4}\right\}$$
$$\left. + \frac{w_{31}(1-X_8)}{X_r+X_p}(\hat{\alpha}(2-\hat{\alpha})X_r + X_p)\exp\left\{-\frac{\gamma_t}{1+X_4}\right\}\right] \tag{4.45}$$

$$\frac{dX_7}{dt} = -X_7 + \frac{DaX_p}{(1-\hat{\alpha})^2}\left[w_{12}(1-X_1)(\hat{\alpha}^3 - 3\hat{\alpha}^2 + 4\hat{\alpha})\right.$$
$$\exp\left\{-\frac{\gamma_f}{1+X_4}\right\} + w_{22}X_t(\hat{\alpha}+2)\exp\left\{-\frac{\gamma_t}{1+X_4}\right\}$$
$$+ \frac{w_{32}(1-X_8)}{X_r+X_p}\{(\hat{\alpha}^3 - 3\hat{\alpha}^2 + 4\hat{\alpha})X_r$$
$$\left. + (\hat{\alpha}+2)X_p\}\exp\left\{-\frac{\gamma_t}{1+X_4}\right\}\right] \tag{4.46}$$

$$\frac{dX_8}{dt} = -X_8 + \frac{1}{2}Da\psi(1-X_8)(X_r+X_p)\exp\left\{\frac{\gamma X_4}{1+X_4}\right\} \tag{4.47}$$

where, X_p, X_t and X_r are given by

$$X_p = \left[\left\{ \frac{P_a(1-X_8)}{g_t P_f} \exp\left(\frac{\gamma_t - \gamma}{1+X_4}\right) \right\}^2 + \frac{P_b(1-X_1)^3}{g_t P_f^2} \exp\left(\frac{\gamma_t - \gamma_{d_M}}{1+X_4}\right) \right.$$

$$\left. \frac{P_c(1-X_1)Y_p}{g_t P_f^2} \exp\left(\frac{\gamma_t - \gamma}{1+X_4}\right) \right]^{1/2}$$

$$- \frac{P_a(1-X_8)}{g_t P_f} \exp\left(\frac{\gamma_t - \gamma}{1+X_4}\right) \tag{4.48}$$

$$X_t = X_p g_t \tag{4.49}$$

$$X_r = \frac{R_a(1-X_2)\exp(-\frac{\gamma_d}{1+X_4}) + R_b(1-X_3)\exp(-\frac{\epsilon\gamma_d}{1+X_4})}{P_f\{R_c(1-X_1) + R_d(1-X_8)\}\exp(-\frac{\gamma}{1+X_4})} \tag{4.50}$$

$$Y_p = \frac{P_f}{R_f} X_r \tag{4.51}$$

The probability of propagation, $\hat{\alpha}$ is represented by the following dimensionless form:

$$\hat{\alpha} = \left[1 + \alpha_m \exp\left(\frac{\gamma - \gamma_f}{1+X_4}\right) + \frac{\alpha_t X_t}{1-X_1} \exp\left(\frac{\gamma - \gamma_t}{1+X_4}\right) + \alpha_q \frac{1-X_8}{1-X_1} \right]^{-1} \tag{4.52}$$

Note that the same gel effect correlation (eq 2.22) used in Chap 2 is employed in the above reactor model.

4.3.2. Reactor Dynamics

In the absence of inhibitor, the first subsystem of the reactor model (eqs 4.40~4.43) can be reduced to a steady state manifold (eq 2.43). In such a case, a systematic analysis of the steady state reactor behavior is straightforward (e.g., Chapter 2). However, it is not possible to condense the steady state

Table 4.5   Kinetic constants of inhibitors in styrene polymerization [Rintelen, *et al.* (1983)]

Inhibitor	ψ $(2k_q/k_p)$
4-*tert*-butylcatechol	0.87
4-*tert*-butyl-o-quinone	88.0
1,4-benzoquinone	1,002.0

model equations into a single manifold in the presence of inhibitors. This is because the first subsystem of the reactor model (eqs 4.40~4.43 and 4.47) is too complex and nonlinear. Thus, a numerical search is required for the analysis of steady state bifurcation phenomena.

For the purpose of comparison with the previous cases where no inhibitors are present, the same kinetic and physical parameters as given in Table 2.1 are used. The standard reactor operating conditions are also the same (*i.e.*, I_f = 0.025 mol/l, y_{Af} = 0.5, f_s = 0.1, T_f = 70 °C, T_c = 90 °C, θ = 0.9 hr). Retarders considered in this study are 4-*tert*-butylcatechol and 4-*tert*-butyl-o-quinone and an inhibitor is 1,4-benzoquinone. The kinetic constants for inhibitors are given in Table 4.5.

Figures 4.15~4.17 show the reactor startup transients to different steady states in the presence of 4-*tert*-butylcatechol which is used to stabilize styrene
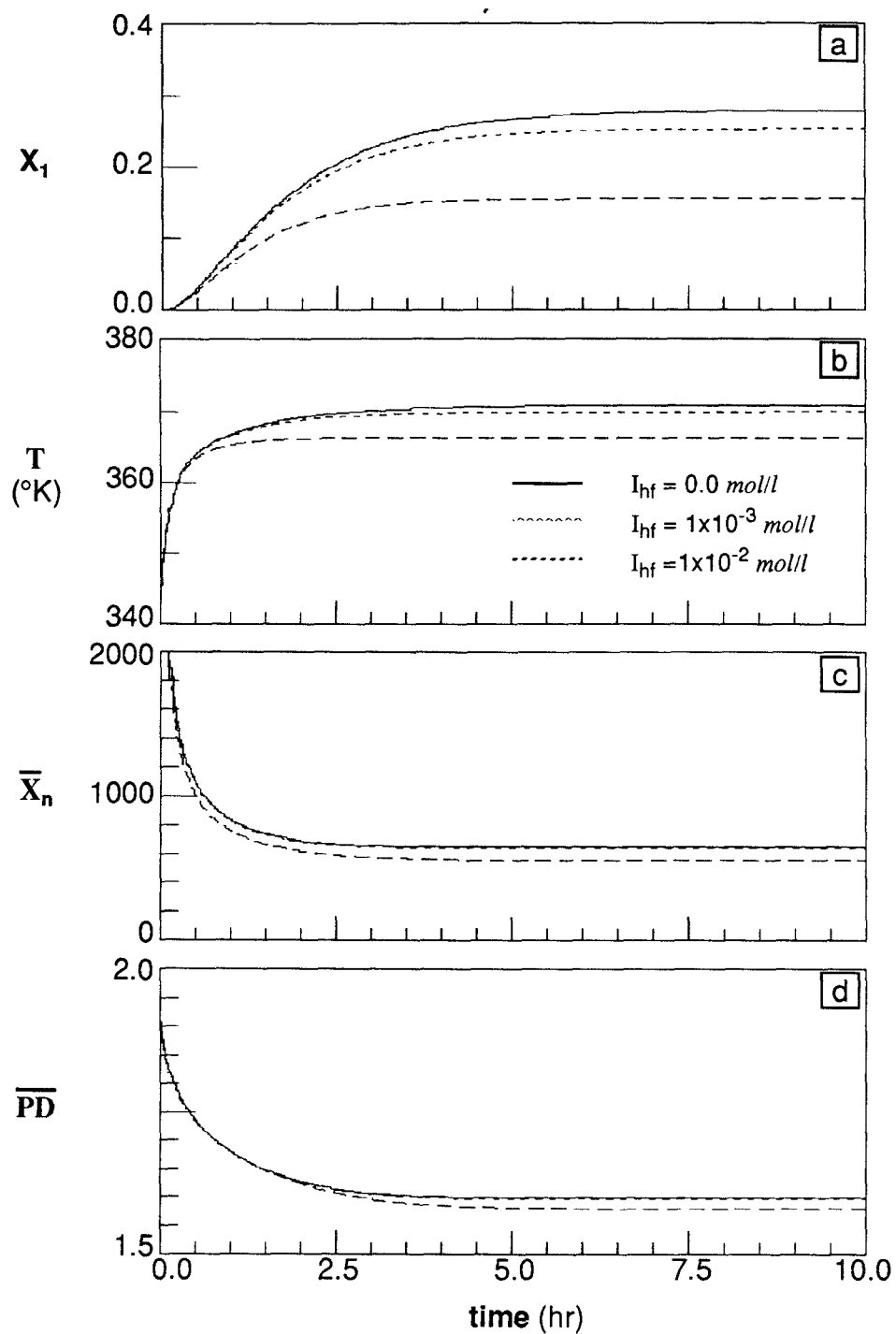
Figure 4.15   Effect of 4-*tert*-butylcatechol on the start-up transients to the lower stable steady state: $\theta = 0.9$ hr, $f_s = 0.1$, $I_f = 0.025$ mol/l, $y_{Af} = 0.5$, $T_f = 343$ °K.
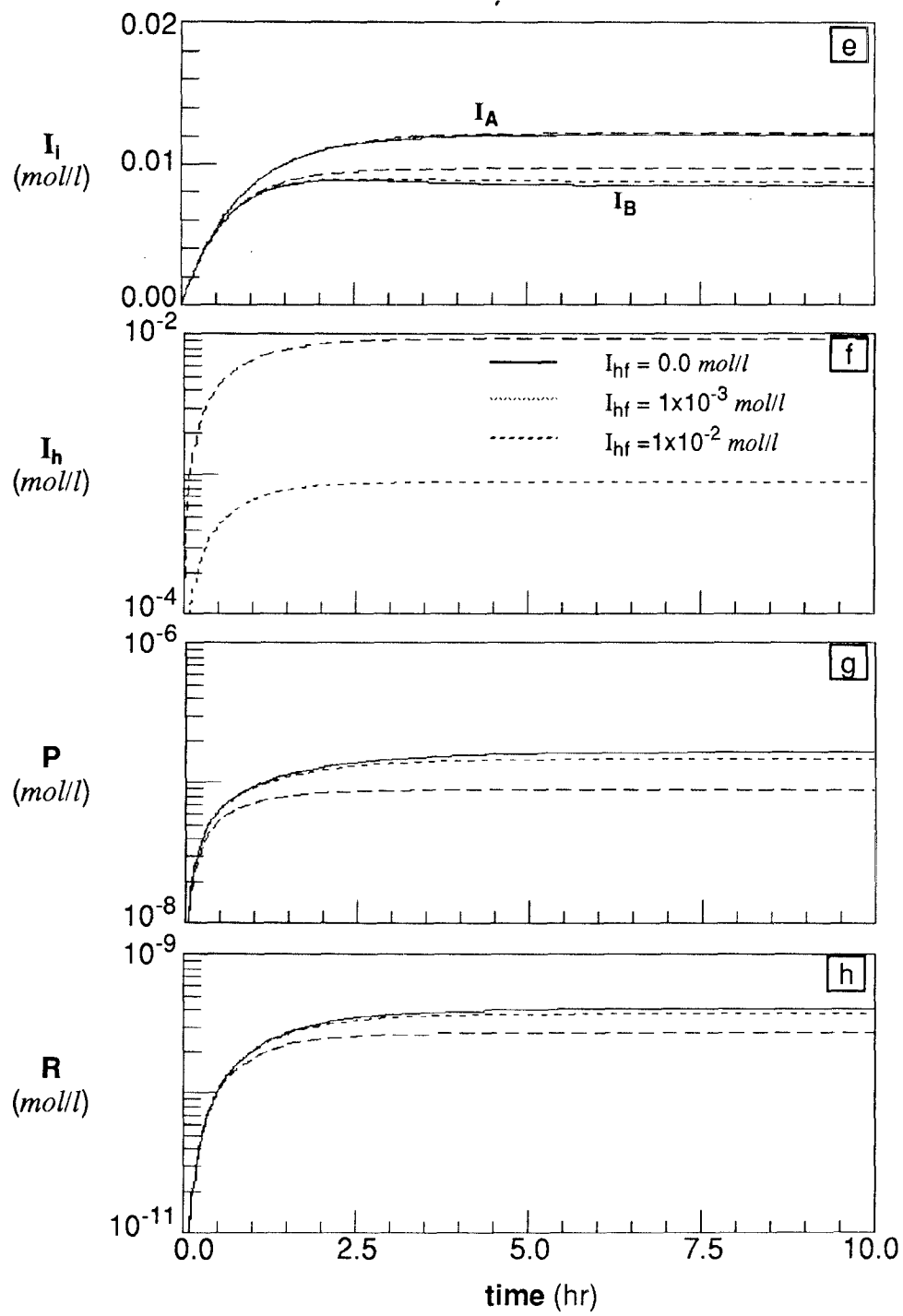
Figure 4.15   (*continued*)
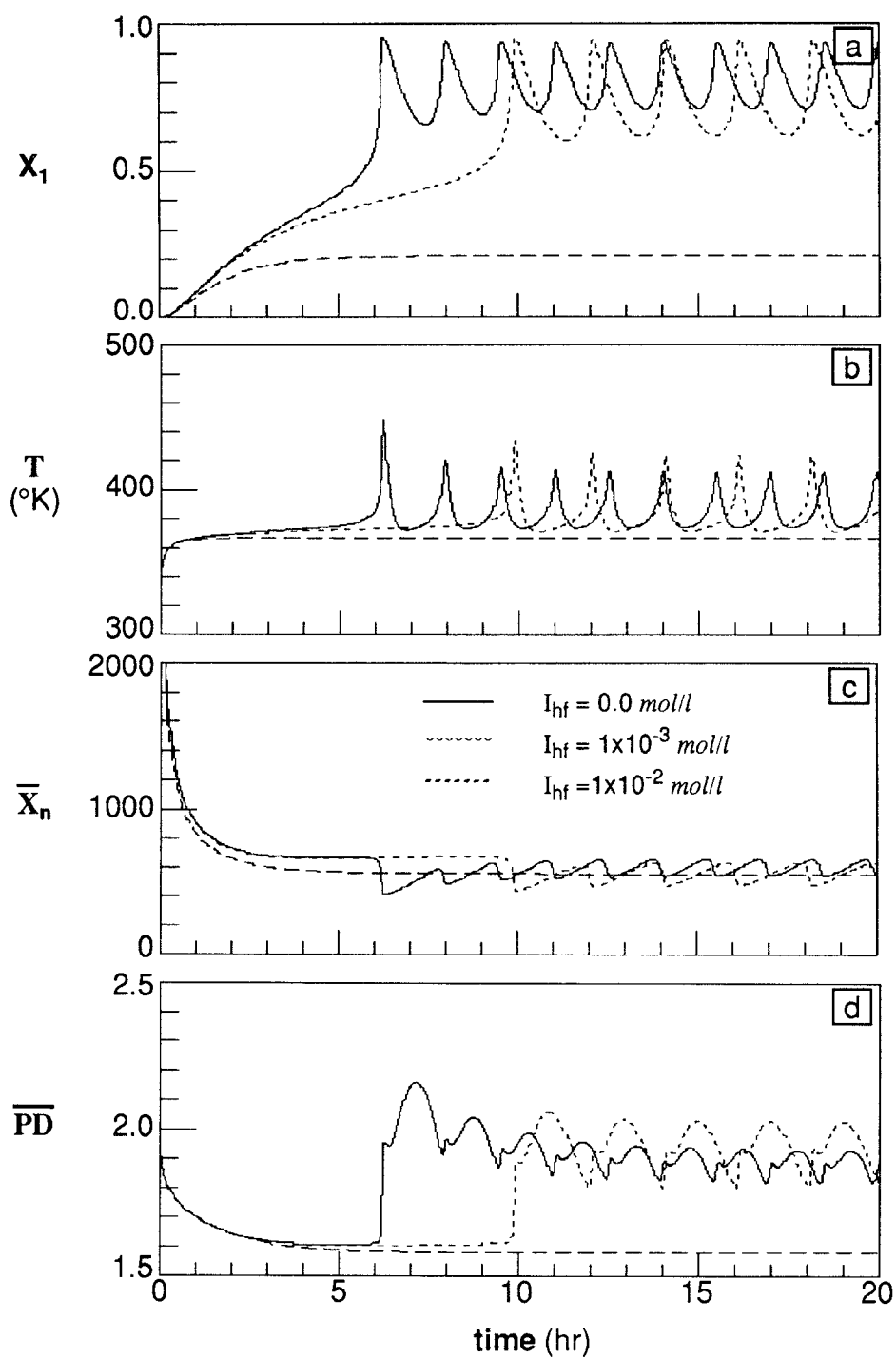
Figure 4.16   Effect of 4-*tert*-butylcatechol on the start-up transients to the
upper unstable steady state: $\theta = 1.2$ hr, $f_s = 0.1$, $I_f = 0.025$
mol/l, $y_{Af} = 0.5$, $T_f = 343$ °K, $T_c = 363$ °K.

a

X_1

1.0

0.5

0.0

b

T (°K)

450

400

350

300

c

$\overline{X}_n$

2000

1000

0

$I_{hf} = 0.0$ *mol/l*

$I_{hf} = 1 \times 10^{-3}$ *mol/l*

$I_{hf} = 1 \times 10^{-2}$ *mol/l*

d

$\overline{PD}$

2.0

1.5

0.0   2.5   5.0   7.5   10.0

time (hr)
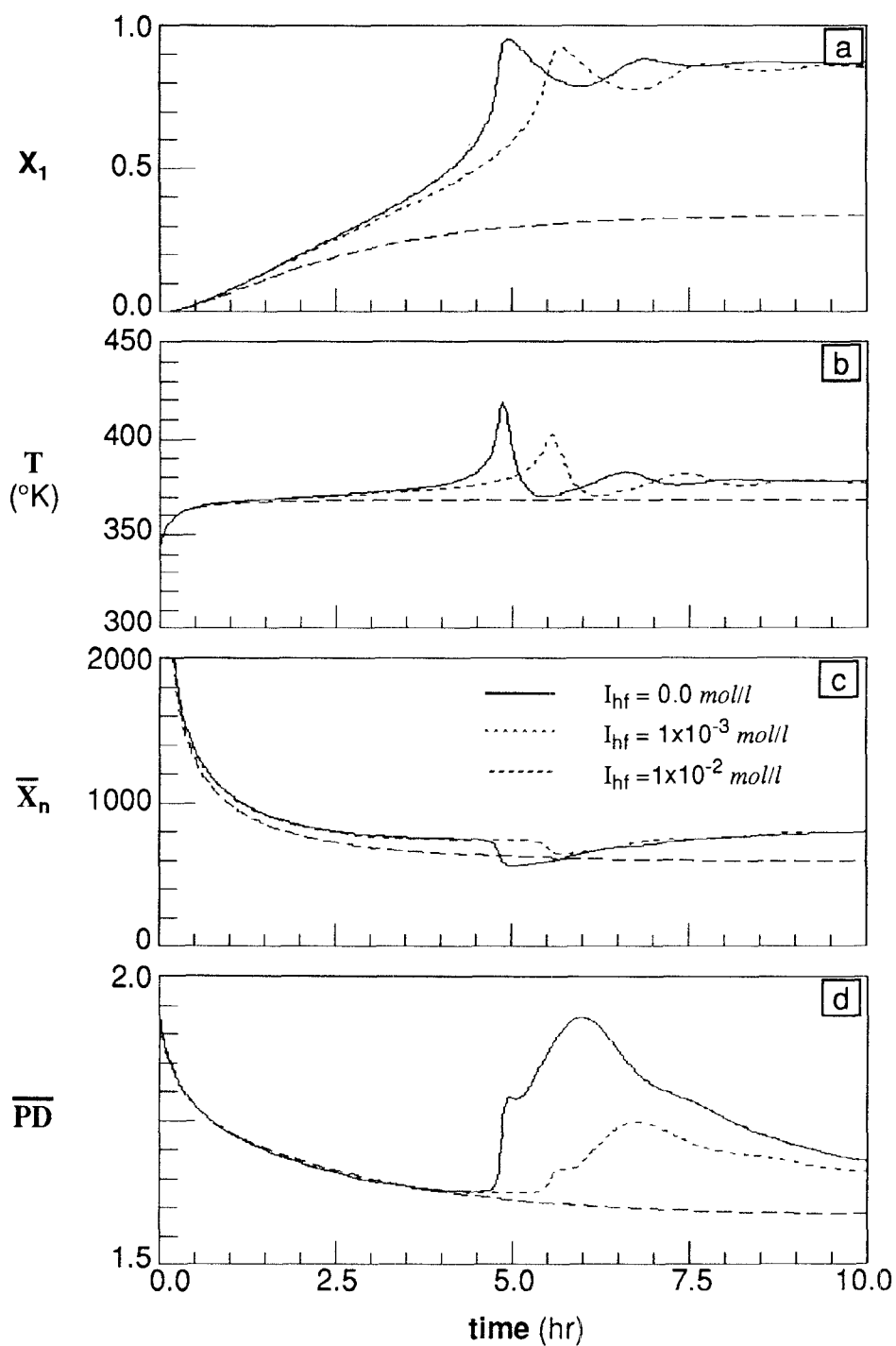
Figure 4.17   Effect of 4-*tert*-butylcatechol on the start-up transients to the upper stable steady state: $\theta = 2.0$ hr, $f_s = 0.1$, $I_f = 0.025$ mol/l, $y_{Af} = 0.5$, $T_f = 343$ °K, $T_c = 363$ °K.

monomer during shipping and storage [Aldrich (1990)]. When the reactor moves to a lower stable steady state (cf. Figure 2.5d), the presence of this retarder has little effect on the steady state stability, as shown in Figure 4.15. As the retarder concentration increases (*i.e.*, 1×10^{-3} mol/l), the concentrations of primary radicals (R) and chain radicals (P) are reduced, resulting in lower monomer conversion (X_1) and lower reactor temperature (Figures 4.15h and 4.15g). The retarder causes the number average chain length ($\overline{X}_n$) and polydispersity ($\overline{PD}$) of the polymer to decrease. When the retarder concentration is 1×10^{-3} mol/l, the steady state multiplicity of the reactor disappears and the reactor state moves to a lower stable steady state, as shown Figures 4.16 and 4.17.

The reactor startup transients are also affected by the reactivity of the inhibitor, ψ, as shown in Figures 4.18 and 4.19. As ψ is increased, suppression of polymerization becomes more pronounced. For the first 2.5 hours during the startup period, 1,4-benzoquinone, which is the strongest inhibitor, suppresses the polymerization completely (Figure 4.18). It also causes the reactor to move to a unique steady state. These figures show clear difference between retarders and inhibitors.

Figure 4.20 and 4.21 illustrate the reactor transients when the step change in the amount of 4-*tert*-butylcatechol is made during the steady state operation. When the reactor is operated at a lower stable steady state, a small amount of the retarder (*i.e.*, 1×10^{-5} mole/l) has little effect. However, the

266
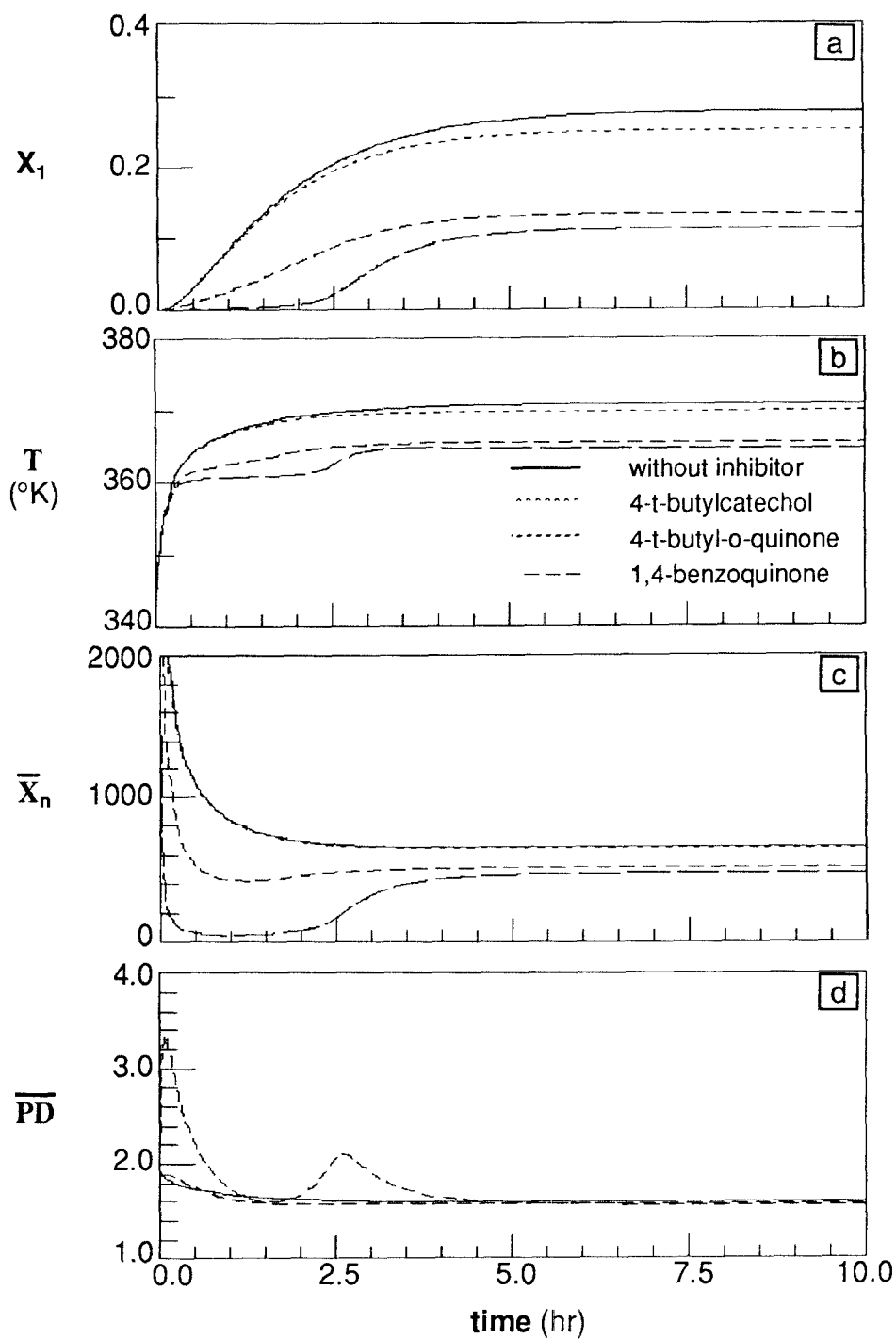
Figure 4.18   Effect of various inhibitors on the start-up transients to the lower stable steady state: $\theta = 0.9$ hr, $f_s = 0.1$, $I_f = 0.025$ mol/l, $y_{Af} = 0.5$, $T_f = 343\,°\mathrm{K}$, $T_c = 363\,°\mathrm{K}$, $I_{hf} = 1.0 \times 10^{-3}$ mol/l.

267
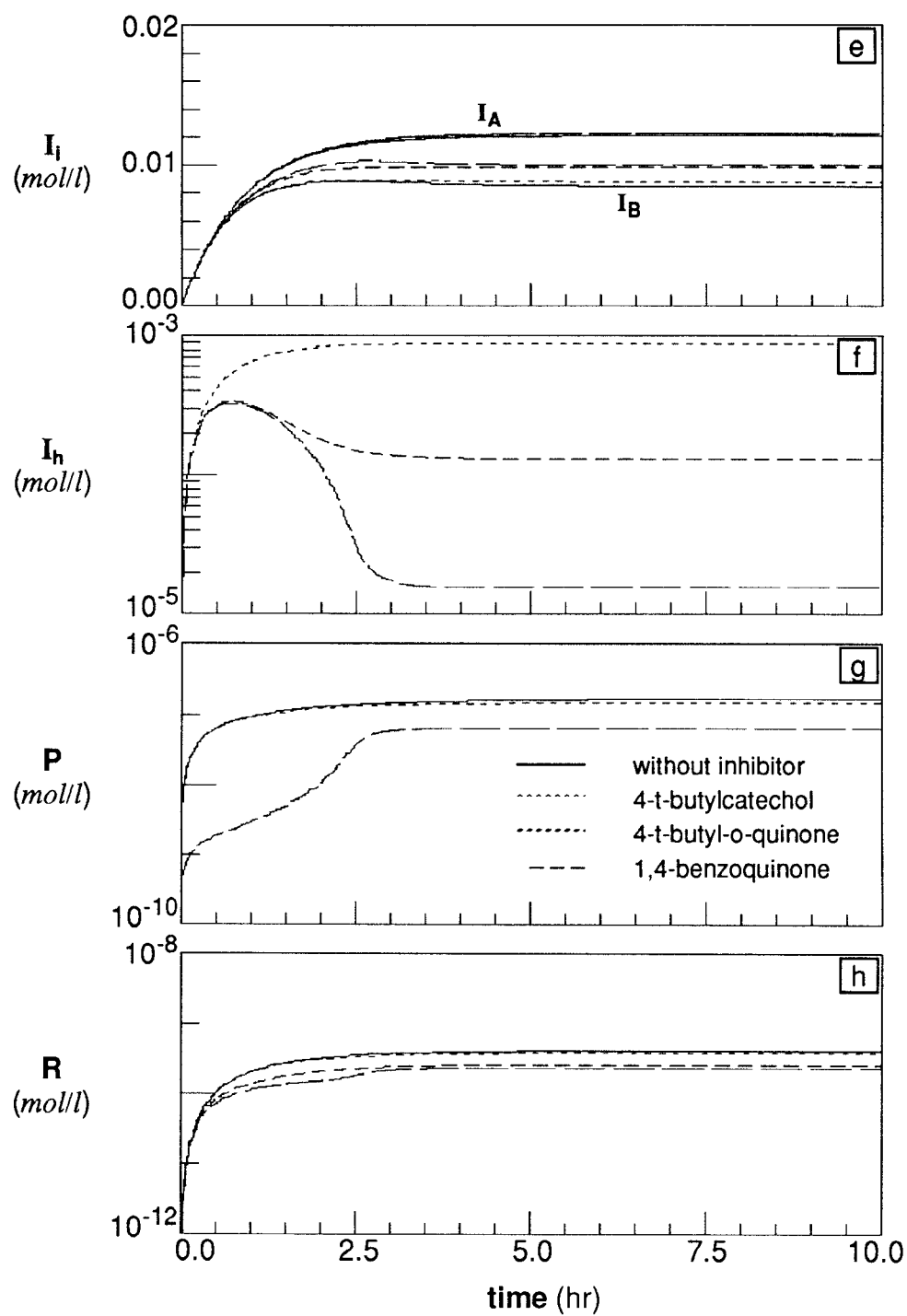
Figure 4.18   *(continued)*
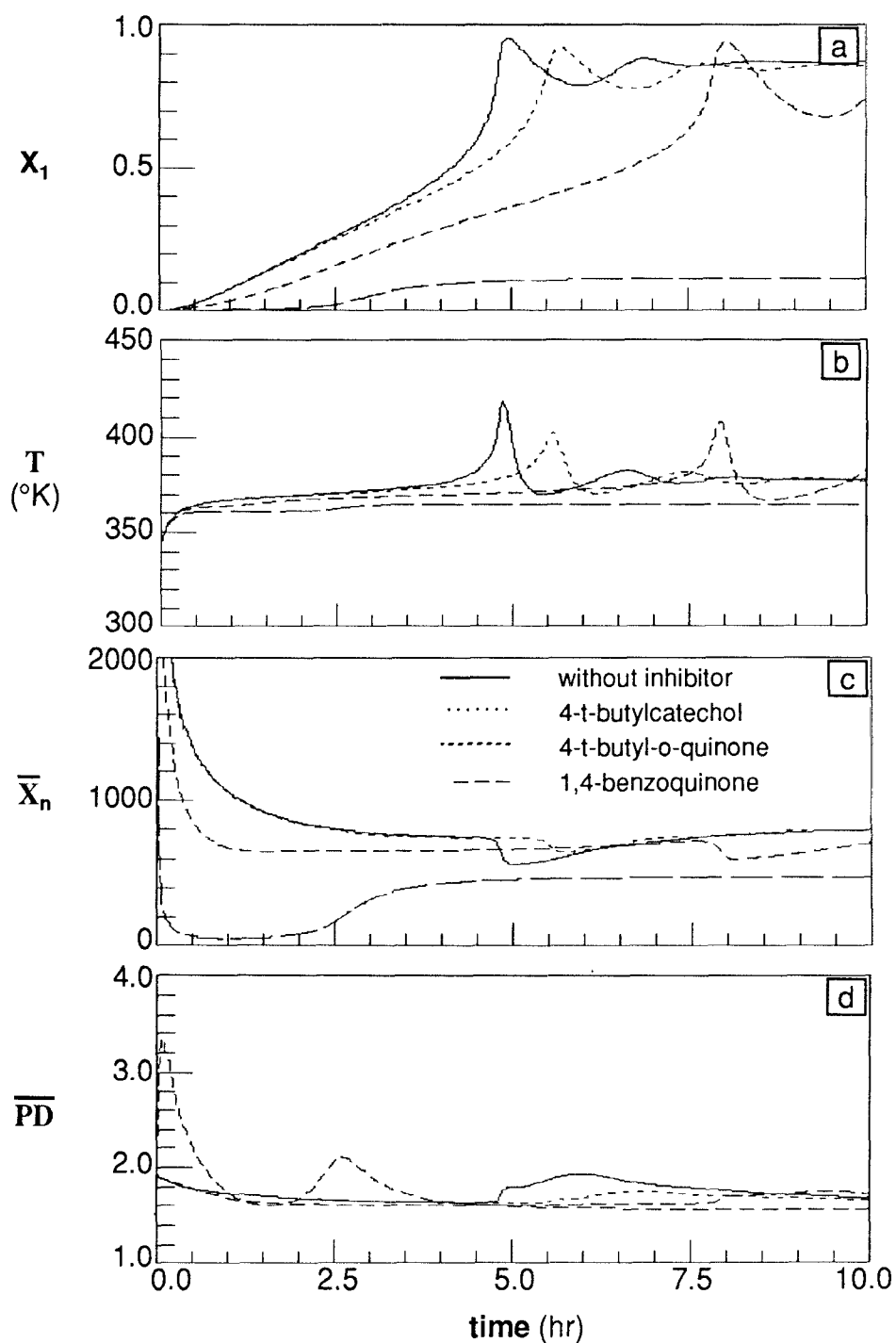
Figure 4.19   Effect of various inhibitors on the start-up transients to the upper stable steady state: $\theta = 2.0$ hr, $f_s = 0.1$, $I_f = 0.025$ mol/l, $y_{Af} = 0.5$, $T_f = 343\,°\mathrm{K}$, $T_c = 363\,°\mathrm{K}$, $I_{hf} = 1.0 \times 10^{-3}$ mol/l.
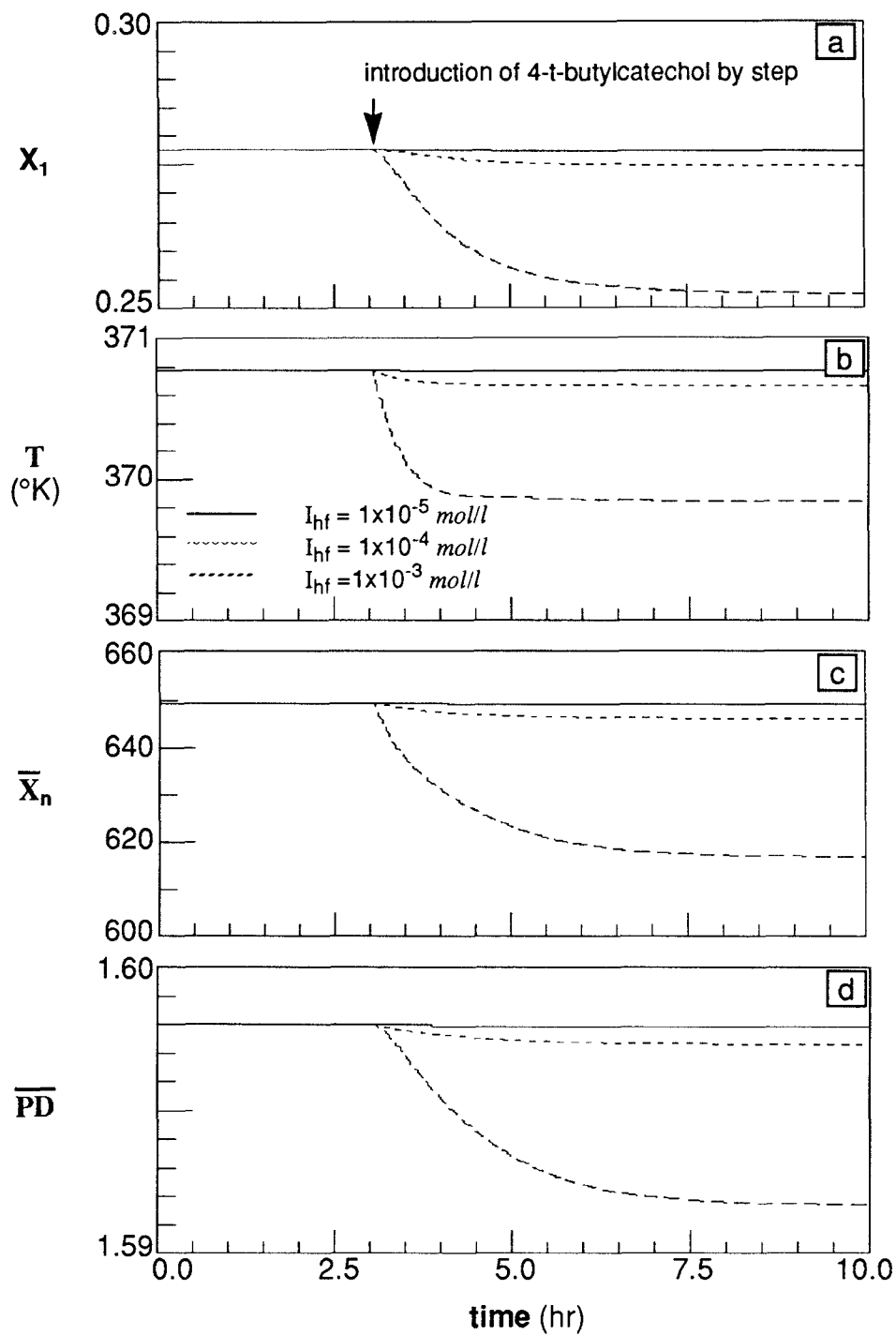
Figure 4.20   Open loop transients to introduction of 4-*tert*-butylcatechol
during steady state operation at the lower stable steady state:
$\theta = 0.9$ hr, $f_s = 0.1$, $I_f = 0.025$ mol/l, $y_{Af} = 0.5$, $T_f = 343$
°K, $T_c = 363$ °K.
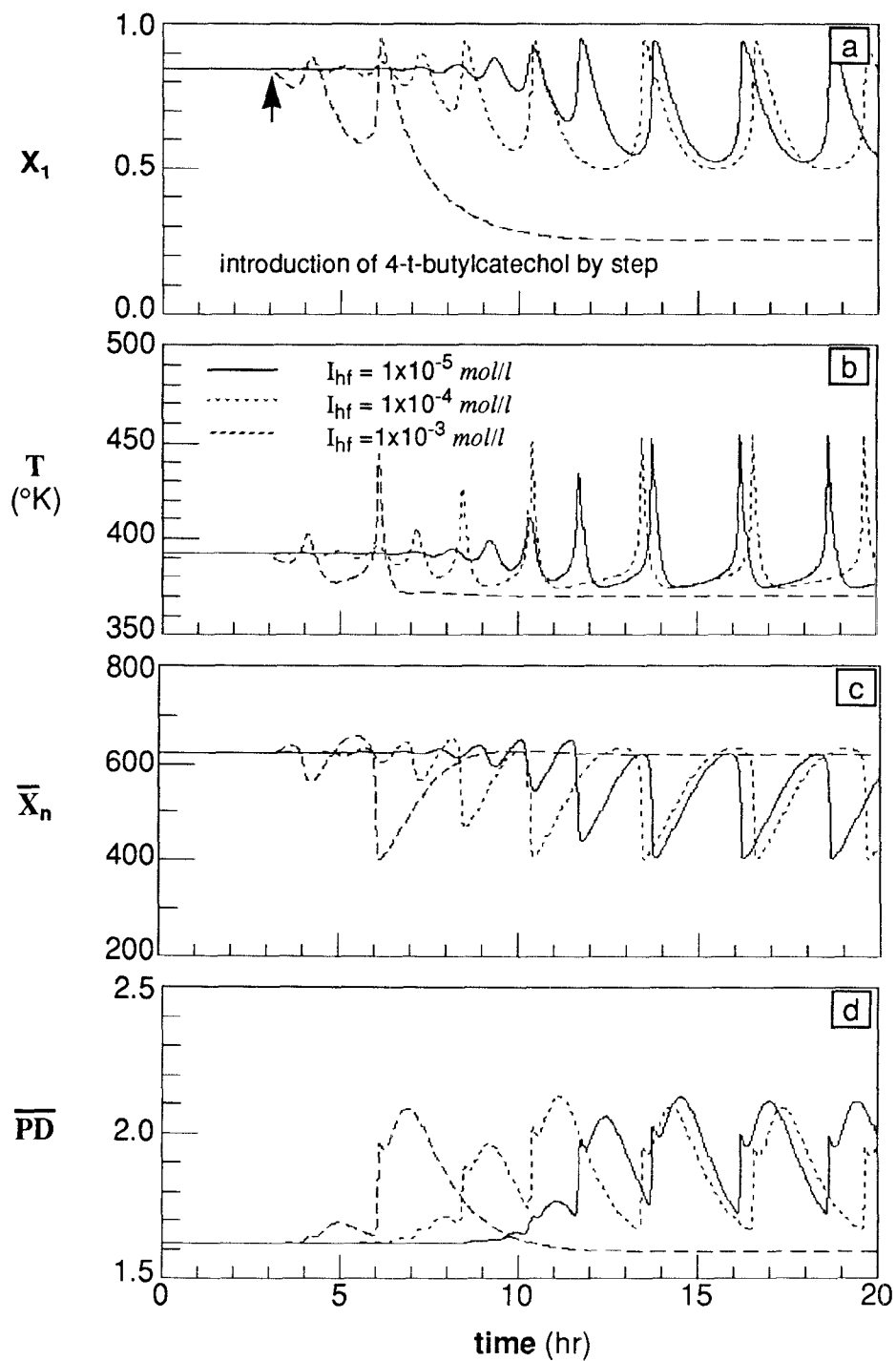
Figure 4.21   Open loop transients to introduction of 4-*tert*-butylcatechol during steady state operation at the upper unstable steady state: $\theta = 0.9$ hr, $f_s = 0.1$, $I_f = 0.025$ mol/l, $y_{Af} = 0.5$, $T_f = 343$ °K, $T_c = 363$ °K.

reactor exhibits oscillatory dynamics when operated at a upper steady state. As the retarder concentration is increased to 1×10^{-3} mole/l, the reactor ceases to exhibit oscillatory dynamics and moves to a new lower stable steady state (Figure 4.21). Similar behavior is observed as the inhibitor reactivity is increased (Figure 4.22).

If the reactor temperature is controlled by manipulating coolant temperature with a PI controller, unstable reactor steady states can be stablized as shown in Figures 4.23 and 4.24. In the presence of small amount of 4-*tert*-butylcatechol (*i.e.*, 1×10^{-5} mole/l), all the reactor variables are perfectly controlled. However, as the retarder concentration increases, monomer conversion and the polymer molecular weight deviate from their original steady state values despite good temperature control. When the inhibitor reactivity is increased, the reactor exhibits similar behavior (Figure 4.25 and 4.25).
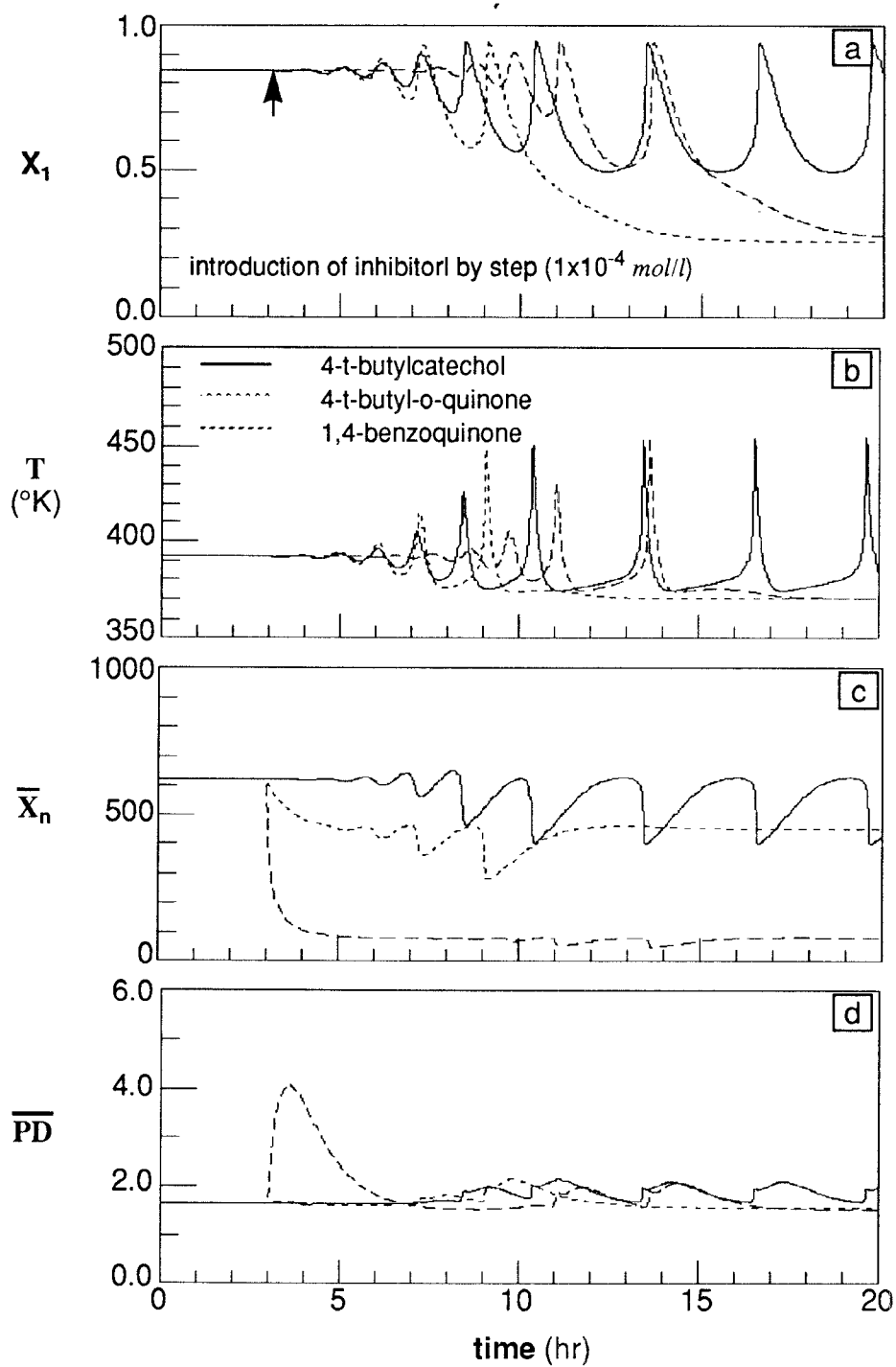
Figure 4.22   Open loop transients to introduction of various inhibitors during steady state operation at the upper unstable steady state: $\theta = 0.9$ hr, $f_s = 0.1$, $I_f = 0.025$ mol/l, $y_{Af} = 0.5$, $T_f = 343$ °K, $T_c = 363$ °K, $I_{hf} = 1.0 \times 10^{-4}$ mol/l.

introduction of 4-t-butylcatechol by step a

X_1

0.50
0.48
0.46
0.44

b

T
(°K)

379
378
377

$I_{hf} = 1 \times 10^{-5}$ *mol/l*
$I_{hf} = 1 \times 10^{-4}$ *mol/l*
$I_{hf} = 1 \times 10^{-3}$ *mol/l*

c

$\overline{X}_n$

675
650
625
600

d

$\overline{PD}$

1.615
1.600

0.0   2.5   5.0   7.5   10.0

time (hr)
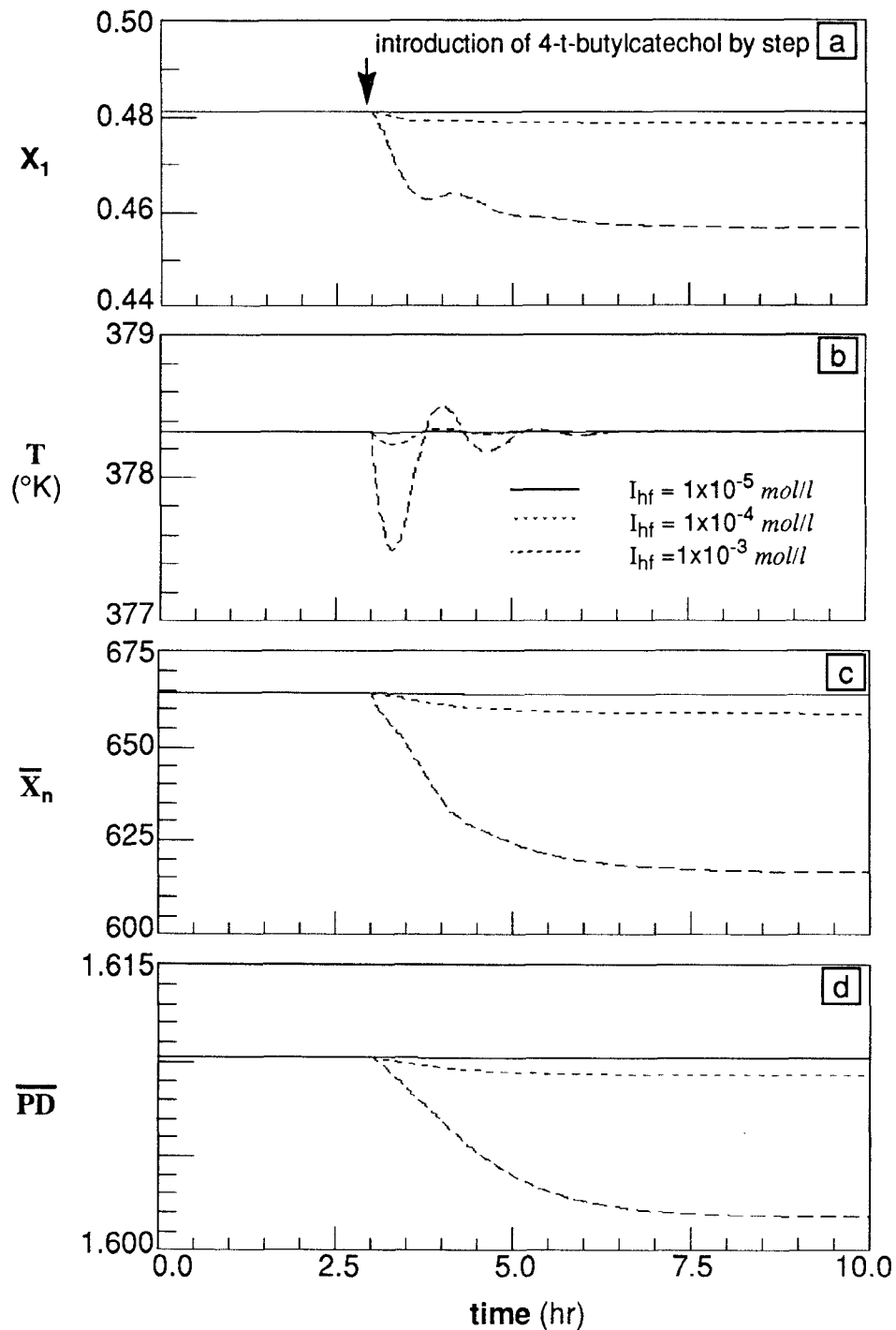
Figure 4.23   Closed loop transients to introduction of 4-*tert*-butylcatechol during steady state operation at the middle unstable steady state: $\theta = 0.9$ hr, $f_s = 0.1$, $I_f = 0.025$ mol/l, $y_{Af} = 0.5$, $T_f = 343$ °K, $T_c = 363$ °K ($K_c = 0.5$ °K, $\tau_I = 0.2$ hr, $303 \leq T_c(°K) \leq 423$).
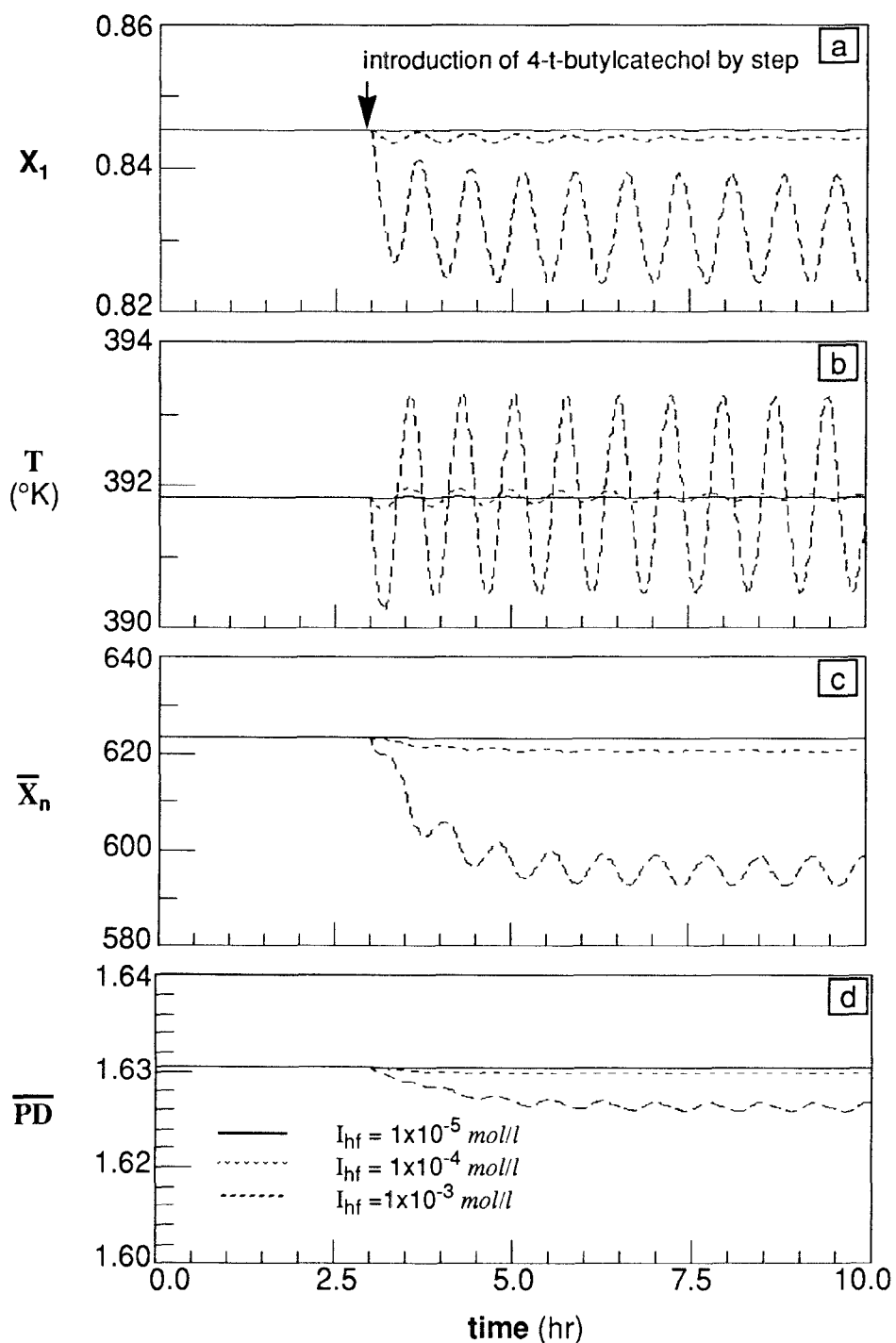
Figure 4.24   Closed loop transients to introduction of 4-*tert*-butylcatechol
during steady state operation at the upper unstable steady
state: $\theta = 0.9$ hr, $f_s = 0.1$, $I_f = 0.025$ mol/l, $y_{Af} = 0.5$,
$T_f = 343$ °K, $T_c = 363$ °K ($K_c = 0.5$ °K, $\tau_I = 0.2$ hr,
$303 \le T_c(°K) \le 423$).
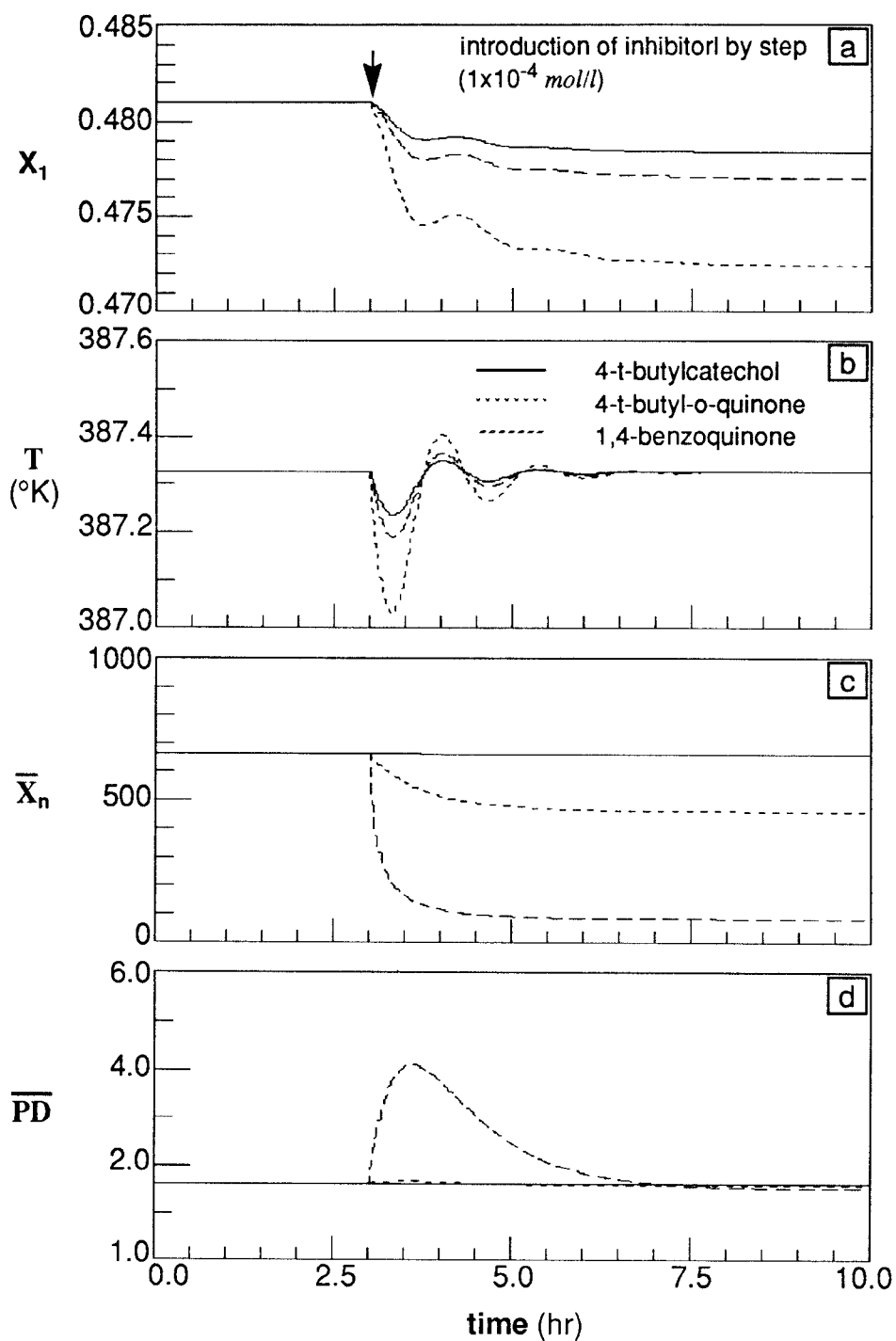
Figure 4.25   Closed loop transients to introduction of various inhibitors during steady state operation at the middle unstable steady state: $\theta = 0.9$ hr, $f_s = 0.1$, $I_f = 0.025$ mol/l, $y_{Af} = 0.5$, $T_f = 343$ °K, $T_c = 363$ °K, $I_{hf} = 1.0 \times 10^{-4}$ mol/l ($K_c = 0.5$ °K, $\tau_I = 0.2$ hr, $303 \le T_c(°K) \le 423$).

276
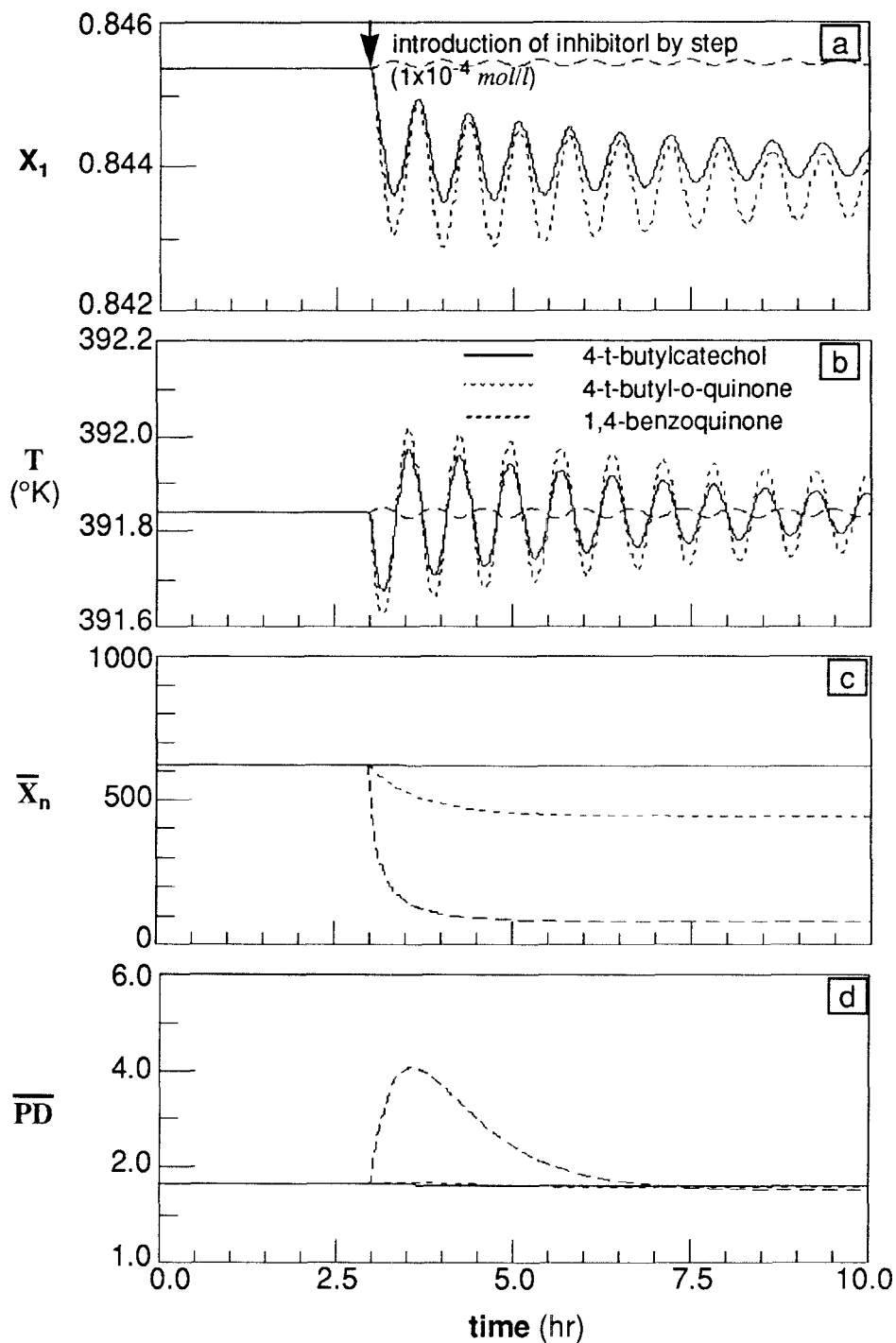
Figure 4.26   Closed loop transients to introduction of various inhibitors
during steady state operation at the upper unstable steady
state: $\theta = 0.9$ hr, $f_s = 0.1$, $I_f = 0.025$ mol/l, $y_{Af} = 0.5$,
$T_f = 343$ °K, $T_c = 363$ °K, $I_{hf} = 1.0 \times 10^{-4}$ mol/l ($K_c = 0.5$
°K, $\tau_I = 0.2$ hr, $303 \leq T_c(°K) \leq 423$).

4.3.3. Concluding Remarks

In this section, the effect of radical scavenging materials such as retarders or inhibitors on the reactor behavior is analyzed for styrene polymerization initiated by mixed initiators in a CSTR. It has been observed that the reactor transients during the startup or steady state operation are affected by the reactivity and the amount of introduced inhibitors. In particular, if the reactor is operated in an unstable or periodic region, a small amount of inhibitor may cause significant change in reactor dynamics. If the reactor temperature is controlled by a feedback PI controller, the reactor shows good control performance in the presence of small amounts of inhibiting materials.

4.4. Notation

A_c heat transfer area of the reactor (cm^2)

C_p heat capacity of reaction mixture ($cal/g°K$)

Da Damköhler number (dimensionless mean residence time) of the reactor (-)

D_i diameter of turbine impeller (cm)

D_r inside diameter of reactor (cm)

E_{di} decomposition activation energy of initiator i, $i = A, B$ (cal/mol)

E_{dm} activation energy of thermal initiation (cal/mol)

E_j activation energy of each reaction step j, $j = p, fm, t$ (cal/mol)

E_v activation energy of viscous flow (cal/mol)

f_i efficiency of initiator i, $i = A, B$ (-)

f_s solvent feed volume fraction (-)

g_t gel effect correlation factor, k_t/k_t^* (-)

h_c overall heat transfer coefficient of the reactor ($cal/cm^2 sec°K$)

h_i inside film heat transfer coefficient of the reactor ($cal/cm^2 sec°K$)

h_o outside film heat transfer coefficient of the reactor ($cal/cm^2 sec°K$)

ΔH_r heat of reaction (cal/mol)

I_f concentration of initiator feed mixture (mol/l)

I_h concentration of inhibitor (mol/l)

I_i concentration of initiator i in the reactor, $j = A, B$ (mol/l)

k thermal conductivity of reaction mixture (cal/cm.sec.°K)

k_{di} decomposition rate constant of initiator i, $i = A, B$ (sec^{-1})

k_{d_M} rate constant of thermal initiation ((l/mol)^2.sec)

k_i initiation rate constant (1/mol.sec)

k_{fm} chain transfer rate constant(1/mol.sec)

k_p propagation rate constant (1/mol.sec)

k_q inhibition rate constant (1/mol.sec)

k_t combination termination rate constant (1/mol.sec)

k_t^* combination termination rate constant at zero monomer

       conversion (1/mol.sec)

k_{tq} termination rate constant of inhibitor radicals (1/mol.sec)

M monomer concentration in the reactor (mol/l)

M_f monomer feed concentration (mol/l)

M_w weight average molecular weight of polymer (g/mol)

N rotating speed of the turbine impeller (rpm)

N_{Re} Reynolds number of the impeller (-)

N_{Pr} Prandtl number in the reactor (-)

Q concentration of inhibitor radicals (mol/l)

q volumetric feed flow rate (1/sec)

R primary radical concentration (mol/l)

T reactor temperature (°K)

T_c coolant temperature of the reactor (°K)

T_f feed temperature (°K)

t dimensionless time in the reactor (-)

t' time (sec)

V volume of the reactor (cm^3)

x effective monomer conversion in the presence of solvent (-)

X_p weight fraction of polymer in the reaction mixture (-)

X_1 monomer conversion in the reactor (-)

X_2 conversion of initiator A in the reactor (-)

X_3 conversion of initiator B in the reactor (-)

X_4 dimensionless reactor temperature in the reactor (-)

X_5 dimensionless zeroth moment of dead polymer (-)

X_6 dimensionless first moment of dead polymer (-)

X_7 dimensionless second moment of dead polymer (-)

$\overline{X}_n$ number average polymer chain length in the reactor (-)

$\overline{X}_w$ weight average polymer chain length in the reactor (-)

y_{Af} mole fraction of initiator A in the initiator feed mixture (-)

Greek Letters

α dimensionless heat transfer coefficient of the reactor (-)

α_0 effective heat transfer coefficient of the reactor (sec^{-1})

$\hat{\alpha}$ probability of propagation in the reactor (-)

β dimensionless heat of reaction (-)

δ dimensionless coolant temperature in the reactor (-)

ϵ ratio of decomposition activation energy of initiator B

to that of initiator A (-)

ϕ ratio of inside heat transfer coefficient to outside heat

transfer coefficient (-)

ψ inhibition constant (-)

γ dimensionless activation energy of propagation reaction (-)

γ_d dimensionless decomposition activation energy of initiator A (-)

γ_{d_M} dimensionless activation energy of thermal initiation (-)

γ_f dimensionless activation energy of chain tranfer to monomer (-)

γ_t dimensionless activation energy of chain termination (-)

η ratio of preexponential factor of decomposition of initiator B

to that of initiator A (-)

η_{200} zero shear viscosity of reacting fluid at 200 °C (cp)

η_r zero shear viscosity of reacting fluid in the bulk phase (cp)

η_s zero shear viscosity of styrene-ethyl benzene mixture (cp)

η_w zero shear viscosity of reacting fluid at the surface of

reactor wall (cp)

θ mean residence time of the reactor (hr)

λ_k k-th moment of dead polymer chain in the reactor (-)

ρ_r density of reaction mixture (g/cm^3)

ρ_m density of styrene monomer (g/cm^3)

ρ_p density of polymer (g/cm^3)

Chapter 5

On-line Estimation and Control of Polymer Properties in a Continuous Polymerization Reactor

5.1. Introduction

One of the most important objectives in operating industrial polymerization processes is a precise control of polymer properties. Since many important polymer properties (e.g., molecular weight (MW), molecular weight distribution (MWD)) are complex functions of reactor variables, good quantitative understanding of the polymerization kinetics and reactor behavior is essential for the control of such polymer properties. In general, on-line control of these polymer properties is difficult mainly because of the lack of adequate on-line

sensors. Without rapid and accurate on-line sensors to measure the polymer properties, a direct control of the polymer properties is not feasible.

In recent years, some on-line sensors for polymerization processes have been developed and they are still an active area of research [Schork and Ray (1983), Technical Bulletin (1987)]. For example, on-line gel permeation chromatography (GPC) is now commercially available for the molecular weight characterization. However, on-line sensors for many other important polymer properties such as copolymer composition, degree of branching, etc. are not readily available at the present time. Even with on-line GPC, some measurement time delay is inevitable due to the requirement of sample preparation prior to chromatographic analysis.

One alternative to the direct on-line measurement of polymer properties is to utilize the process model and state estimation techniques to predict the polymer properties. Since the estimation algorithm is used in conjunction with a dynamic process model, the performance of the filter depends on the quality of the process model being used. In most of the previous works, the model used for state estimation was assumed to be the same as the plant model. In reality, however, it is not always possible to develop a perfect process model, particularly for complex nonlinear systems such as polymerization processes. Therefore, it will be of practical importance to assess the effect of model errors on the performance of the filter.

In this chapter, the two-time scale extended Kalman filter is applied to

a continuous stirred tank styrene polymerization process with a binary initiator mixture for the estimation and control of polymer molecular weight and other reactor state variables. The performance of the filter for various reactor operating conditions and the effect of model errors will be examined through numerical simulations.

5.2. Literature Survey

The Kalman filter is an optimal state estimation method which extracts information concerning states and parameters of the system from noise corrupted observations. Since publication of the classical papers by Kalman (1960) and Kalman and Bucy (1961), the Kalman filter has been applied to many areas including orbit determination, tracking and navigation of satellites, missiles, planes and ships, geographical extrapolation, power systems, and cattle demographics. The historical background and theoretical development of the Kalman filter and its applications have been reviewed by Sorenson (1966, 1970, 1985), Wells and Wismer (1971), Kailath (1974).

From the early 1970s, the Kalman filter and the related nonlinear filter have been applied to chemical processes for state and parameter estimation. Many of the applications reported in the literature are computer simulation studies to evaluate the filter performance: CSTR's [Wells (1971), Kantor (1989)], tubular and packed bed reactors [Gavalas and Seinfeld (1969),

Rutzler (1987)], batch reactors [Bonvin *et al.* (1989)], biochemical reactors [Chattaway and Stephanopoulos (1989), Pomerleau and Perrier (1990)], heat exchangers [Coggan and Noton (1970)], and reaction kinetics [Yuan (1989)]. A few experimental studies have also been reported [Hamilton *et al.* (1973), Stephanopoulos and San (1981, 1984), and Windes *et al.* (1989)]. Filters have also been used in closed loop control systems [Corlis and Luss (1969), Seinfeld *et al.* (1969), West and McGuire (1969), Seinfeld (1970),Wells and Larson (1970), Lynch and Ramirez (1975), Wallman (1979), Wallman *et al.* (1979), Tye (1980), Preisig (1988)]. Extended Kalman filters can be used to detect reactor runaways [King and Gilles (1984, 1990)].

The first application of Kalman filtering to polymerization reactors was the works of Bankoff and coworkers [Jo and Bankoff (1976), Hyun and Bankoff (1976)]. They applied the extended Kalman filter (EKF) to vinyl acetate solution polymerization in an isothermal CSTR. Using two on-line measurements of refractive index and impeller torque, monomer conversion and the weight average molecular weight of the polymer were estimated. Kiparissides *et al.* (1981) developed a suboptimal feedback control algorithm with an EKF for a linearized model of a continuous vinyl acetate emulsion polymerization reactor. For the real time estimation of monomer conversion and the chain length distribution (CLD), Schuler and coworkers developed a decoupled nonlinear estimator with on-line measurements of temperature and refractive index in a batch polystyrene reactor [Schuler and Suzhen (1985),

Schuler and Papadopoulou (1986)]. In semibatch emulsion copolymerization of vinyl acetate and n-butyl acrylate, Dimitratos *et al.* (1988, 1989) applied the adaptive EKF to estimate the copolymer composition from overall monomer concentrations measured by gas chromatography. The filter estimates were used for feedforward/feedback controls to maintain constant copolymer composition. Some efforts have also been made in incorporating delayed off-line measurements of polymer molecular weight into the state estimation algorithm [Ray (1986), Papadopoulou and Gilles (1986), Taylor *et al.* (1986), Ellis *et al.* (1988a, 1988b), Huang (1987), Choi and Khan (1988), Adebekun and Schork (1989)]. An application of such a concept to an industrial process for fluoropolymers has also been known [Richard (1990)]. In Ray's work (1986), polymer property observability and detectability have been analyzed for various combinations of measurement parameters such as temperature, refractive index, density viscosity, low angle light scattering and GPC. It was also shown that delayed off-line measurements can be incorporated into the filter to obtain rapid estimates of polymer molecular weight properties. All these previous works clearly illustrate the feasibility of using the filtering techniques in polymerization processes to improve the polymer molecular weight control.

However, in many of these forementioned literature the effect of model accuracy on the filter performance has not been thoroughly investigated. In view of the fact that perfect process models are very difficult to develop, the assessment of filter performance with imperfect process models becomes an

important issue. In this work, an attempt will be made to control polymer molecular weight with with the extended Kalman filter in the presence of model errors and unknown disturbances.

5.3. Process Model

The reactor system considered is a continuous stirred tank reactor for styrene solution polymerization with a mixture of tert-butyl perbenzoate and benzoyl peroxide, as shown in Figure 5.1. Here, chain transfer by the chain transfer agent (di-n-butyl persulfide) is included into the polymerization mechanism (eqs (2.1)~(2.5)):

$$P_n + A \xrightarrow{k_{f_a}} M_n + P_1 \qquad (n \geq 1) \tag{5.1}$$
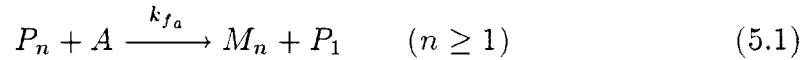
Then, the dynamic modeling equations for a CSTR of volume V take the following form:

$$V\frac{dM}{dt} = q(M_f - M) - Vk_pMP \tag{5.2}$$

$$V\frac{dI_A}{dt} = q(I_f y_{Af} - I_A) - Vk_{d_A}I_A \tag{5.3}$$

$$V\frac{dI_B}{dt} = q\{I_f(1 - y_{Af}) - I_B\} - Vk_{d_B}I_B \tag{5.4}$$

$$\rho C_p V\frac{dT}{dt} = \rho C_p q(T_f - T) + V(-\Delta H)k_pMP$$
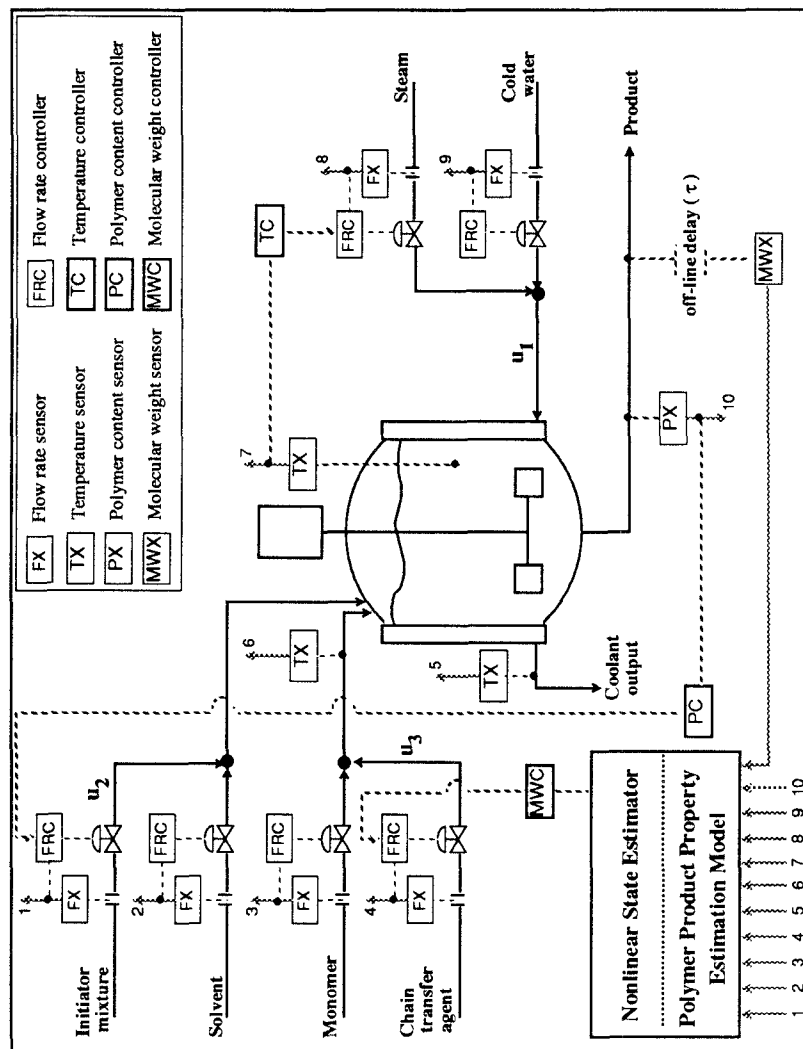
$$- h_c A_c(T - T_c) \tag{5.5}$$

Figure 5.1   Schematic diagram of a continuous styrene polymerization
reactor system with mixed initiator.

$$\rho_c C_{pc} V_c \frac{dT_c}{dt} = \rho_c C_{pc} q_c (T_{cf} - T_c) + h_c A_c (T - T_c) \qquad (5.6)$$

where

$$P = \left[\frac{2}{k_t^* g_t} (k_{d_M} M^3 + f_A k_{d_A} I_A + f_B k_{d_B} I_B) \right]^{\frac{1}{2}} \qquad (5.7)$$

q represents the volumetric feed flow rate and q_c the coolant flow rate. The subscript f denotes the feed condition. M is the monomer concentration in the reactor, I_A and I_B the concentrations of initiator A and B, respectively, and y_{Af} the mole fraction of initiator A in the initiator feed mixture (i.e., $y_{Af} \equiv I_{Af}/I_f$). T is the reactor temperature, h_c the heat transfer coefficient, A_c the effective heat transfer area and T_c the coolant temperature in the reactor jacket. All the assumptions used in §2.3 are applied to deriving the above reactor model. The same gel effect correlation as eq (2.22) is also included into the model.

The molecular weight moment equations required for the molecular weight calculations are:

$$V \frac{d\lambda_0}{dt} = -q\lambda_0 + VP[(k_{f_m} M + k_{f_a} A)\alpha + \frac{1}{2} k_t P] \qquad (5.8)$$

$$V \frac{d\lambda_1}{dt} = -q\lambda_1 + \frac{VP}{(1 - \alpha)} \left[(k_{f_m} M + k_{f_a} A) \right.$$

$$\left. (2\alpha - \alpha^2) + k_t P \right] \qquad (5.9)$$

$$V \frac{d\lambda_2}{dt} = -q\lambda_2 + \frac{VP}{(1 - \alpha)^2} \left[(k_{f_m} M + k_{f_a} A) \right. \qquad .$$

$$(\alpha^3 - 3\alpha^2 + 4\alpha) + k_t P(2 - \alpha)\Big] \qquad (5.10)$$

where, A denotes the concentration of the chain transfer agent. λ_k is the k-th moment of dead polymer, i.e., $\lambda_k \equiv \sum_{n=2}^{\infty} n^k M_n$ where M_n is the concentration of the dead polymer with n repeating monomer units. α is the probability of propagation defined by

$$\alpha = \frac{k_p M}{k_p M + k_{f_m} M + k_{f_a} A + k_t P}. \qquad (5.11)$$

Since the concentration of live polymers is very low, their contribution to the overall molecular weight is assumed to be negligible. The number average and the weight average degree of polymerization are: $\overline{X}_n = \lambda_1/\lambda_0$, $\overline{X}_w = \lambda_2/\lambda_1$.

As discussed in Chapter 2, the continuous styrene polymerization process represented by the modeling equations (5.2)~(5.6) may exhibit strongly nonlinear steady state and dynamic behavior under certain reaction conditions. However, in this work, the reactor operating conditions have been chosen such that the system is always stable. The modeling equations (5.2)~(5.11) are used to simulate the plant. Since it is very difficult, if not impossible, to develop a perfect process model, it is of practical importance to examine the effect of model errors in on-line filtering and control. To do so, numerical values of some parameters of the plant model are changed as follows and the resulting models are designated as model A and model B: in model A(B), all the gel effect parameters are reduced by 5% (10%) from the correct values and

the chain transfer rate constants (k_{fm} and k_{fa}) by 10% (10%). These new models are then used as a basis for filtering.

Figure 5.2 shows the comparison of the steady state and the transient behavior of the process predicted by the plant model and the two inaccurate models (A and B). The reactor was initially at steady state and at $t = 4$ hr, a step change in the reactor residence time (θ) has been made. Here, x_p is the weight fraction of the polymer which is calculated from the monomer conversion. The numerical values of the kinetic parameters, physical constants and standard reactor operating conditions used in the simulations are listed in Tables 2.1 and 5.1. Note that the predictions of x_p, $\overline{X}_n$ and $\overline{X}_w$ by the plant model and the two inaccurate models (A and B) show quite noticeable differences. For example, $\overline{X}_w$ values predicted by model B are nearly 30% larger than the actual plant values. Model A, which has smaller errors than the model B in the gel effect parameters, shows more than 10% error in $\overline{X}_w$. Now we will assume that either model A or model B is the only process model available. Then, using one of these inaccurate models, we will attempt to estimate the process outputs generated by solving the plant model.
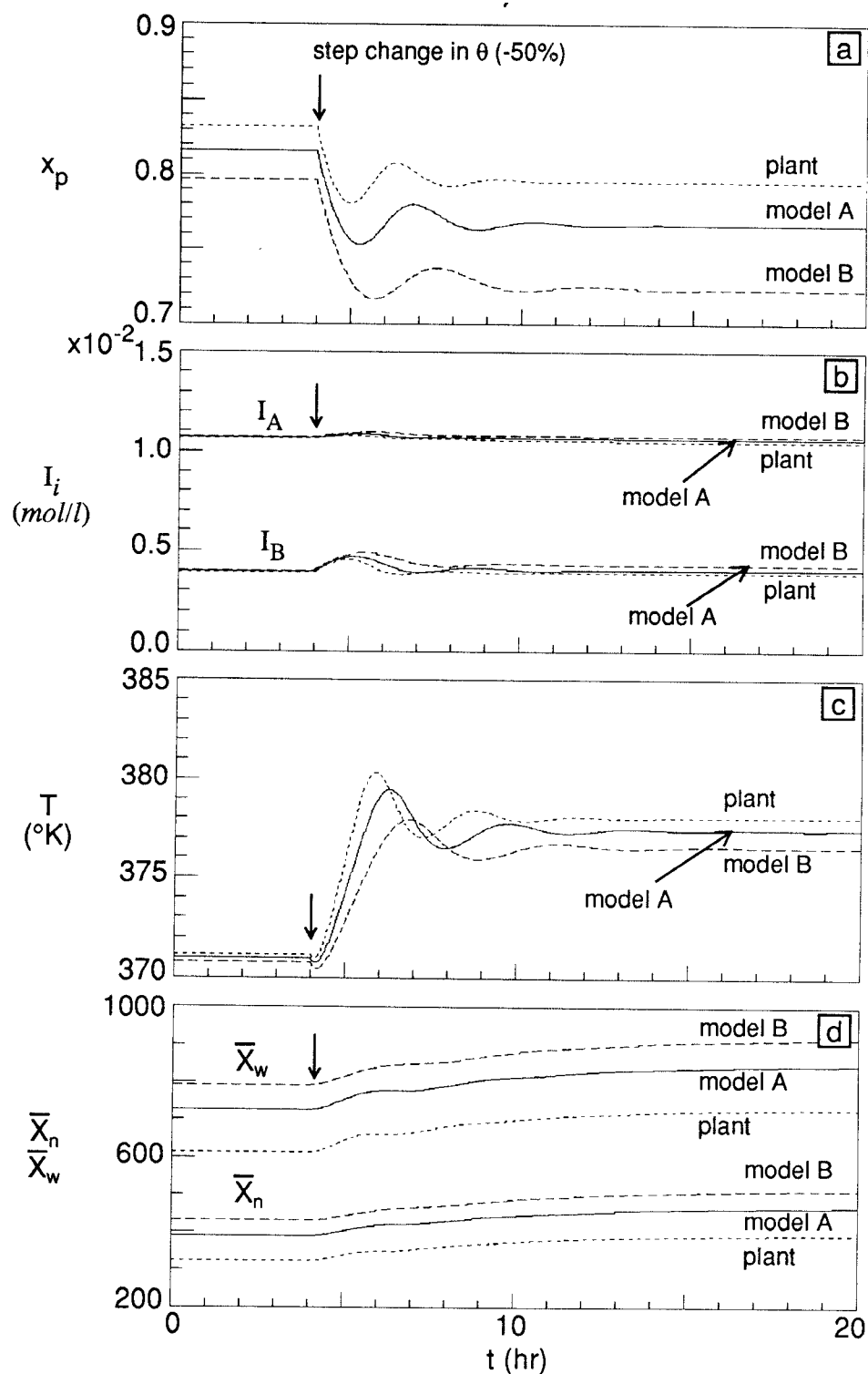
Figure 5.2   Prediction of open loop reactor transients to step change in θ (-50 %) with inaccurate model A ($e_g = -5\%$, $e_t = -10\%$) and model B ($e_g = -10\%$, $e_t = -10\%$).

Table 5.1 Kinetic and physical parameters and standard operating conditions

---

chain transfer agent: *di-n-butyl persulfide*

$$k_{f_a} = 2.523 \times 10^4 \ \exp(-7{,}060/\mathrm{RT}), 1/\mathrm{mol.sec}$$

styrene:

$$M_w = 104.15 \ \mathrm{g/mol}, \quad \rho = 0.906 \ \mathrm{g/cm}^3$$

solvent (*ethyl benzene*):

$$M_w = 106.17 \ \mathrm{g/mol}, \quad \rho = 0.867 \ \mathrm{g/cm}^3$$

standard operating conditions:

$$\frac{h_c A_c}{\rho C_p V} = 2.146 \times 10^{-3} \ \mathrm{sec}^{-1} \quad \nu = 0.516, \quad \theta_c = 30 \ \mathrm{sec},$$

$$f_s = 0.1, \ y_{Af} = 0.5, \ T_f = 343 \ {}^\circ\mathrm{K}, \quad \theta = 4 \ \mathrm{hr}.$$

5.4. Two-Time Scale State Estimation

For non-linear systems, the algorithm of the standard extended Kalman filter (EKF) is described in several texts [Jazwinski (1971), Gleb (1974), Ray (1981b)]. In the continuous styrene polymerization process considered in this study, the reactor temperature and the monomer conversion (or polymer concentration) in the product stream are measured on-line (e.g., by in-line densitometer). The polymer molecular weight and MWD are measured by either on-line or off-line gel permeation chromatography (GPC). When an on-line GPC is available, minimum hold-up time for sample preparation and separa-

tion is about 15 min with a single GPC column [Technical Bulletin (1987)]. If more than one column is used for improved separation efficiency, the measurement delay will be longer than 15 min. If on-line GPC is not available, MW and MWD are measured by off-line GPC. In such a case, there will be much longer time delays (e.g., 60 min or more). In both cases, the time-delayed molecular weight measurement data must be incorporated into the state estimation algorithm so that timely update of MW estimates can be attained.

In order to incorporate the delayed measurement data into the filter, a two time scale filter algorithm is used. The original modeling equations (5.2)∼(5.11) have been converted to dimensionless form using the following dimensionless variables:

$$
\begin{aligned}
x_1 &= \frac{M_f - M}{M_f} & x_2 &= \frac{I_f y_{Af} - I_A}{I_f y_{Af}} & x_3 &= \frac{I_f(1 - y_{Af}) - I_B}{I_f(1 - y_{Af})} \\
x_4 &= \frac{T - T_f}{T_f} & x_5 &= \frac{\lambda_0}{\lambda_{or}} & x_6 &= \frac{\lambda_2}{\lambda_{2r}} & x_7 &= \frac{\lambda_1}{\lambda_{1r}} & x_8 &= \frac{T_c - T_f}{T_f}
\end{aligned}
\tag{5.12}
$$

where, λ_{kr} is the reference value of the kth moment. The modeling equations in dimensionless form and the dimensionless parameters are shown in **Appendix E**.

Table 5.2 summarizes the state estimation algorithm used in our simulations. The process model is corrupted by a noise process $w(t)$. Output data $(y(t))$ are measured with some errors $v(t)$. Q is the covariance of the process model errors and R the covariance of the measurement errors. It is assumed that the noise processes are Gaussian and uncorrelated in time (i.e., white

Table 5.2   Algorithm of standard extended Kalman filter

Process model:

$$\dot{\boldsymbol{x}} = \boldsymbol{f}[\boldsymbol{x}(t), \boldsymbol{u}(t)] + \boldsymbol{w}(t), \quad \boldsymbol{w}(t) \sim N[\boldsymbol{0}, \boldsymbol{Q}(t)]$$

$$\boldsymbol{x}(0) \sim N[\hat{\boldsymbol{x}}_0, \boldsymbol{P}_0]$$

With on-line measurement only:

$$\boldsymbol{y}_{o,k} = \boldsymbol{h}_o(\boldsymbol{x}_k) + \boldsymbol{v}_{o,k}, \quad \boldsymbol{v}_{o,k} \sim N[\boldsymbol{0}, \boldsymbol{R}_{o,k}]$$

With delayed measurement:

$$\boldsymbol{y}_{d_{k-\tau}} = \boldsymbol{h}_d(\boldsymbol{x}_{k-\tau}) + \boldsymbol{v}_{d,k-\tau}, \quad \boldsymbol{v}_{d,k-\tau} \sim N[\boldsymbol{0}, \boldsymbol{R}_{d,k-\tau}]$$

State estimate propagation:

$$\hat{\boldsymbol{x}}(t) = \boldsymbol{f}[\hat{\boldsymbol{x}}(t), \boldsymbol{u}(t)]$$

Error covariance propagation:

$$\dot{\boldsymbol{P}}(t) = \boldsymbol{F}(t)\boldsymbol{P}(t) + \boldsymbol{P}(t)\boldsymbol{F}^T(t) + \boldsymbol{Q}(t)$$

State estimate update at t_k with on-line measurements:

$$\hat{\boldsymbol{x}}_k(+) = \hat{\boldsymbol{x}}_k(-) + \boldsymbol{K}_k[\boldsymbol{y}_{o,k} - \boldsymbol{h}_o\{\hat{\boldsymbol{x}}_k(-)\}]$$

Error covariance update at t_k with on-line measurements:

$$\boldsymbol{P}_k(+) = [\boldsymbol{I} - \boldsymbol{K}_k \boldsymbol{H}_{o,k}]\boldsymbol{P}_k(-)$$

Gain matrix at t_k with on-line measurements:

$$\boldsymbol{K}_k = \boldsymbol{P}_k \boldsymbol{H}_{o,k}^T [\boldsymbol{H}_{o,k} \boldsymbol{P}_k(-)\boldsymbol{H}_{o,k}^T + \boldsymbol{R}_{o,k}]^{-1}$$

where,

$$\boldsymbol{F}(t) = \left.\frac{\partial \boldsymbol{f}[\boldsymbol{x}(t), \boldsymbol{u}(t)]}{\partial \boldsymbol{x}(t)}\right|_{x(t)=\hat{\boldsymbol{x}}(t)}$$

$$\boldsymbol{H}_{o,k} = \left.\frac{\partial \boldsymbol{h}_o(\boldsymbol{x}_k)}{\partial \boldsymbol{x}_k}\right|_{\boldsymbol{x}_k=\hat{\boldsymbol{x}}_k(-)}$$

noise) and also uncorrelated with the initial state. Since the concentration of live polymers is extremely low, the molecular weight averages are determined using the three leading moments for dead polymers only (eqs (5.8)~(5.10)). Then, the first molecular weight moment (λ_1) which is the total weight of the polymer is directly estimated from the monomer conversion measurement. From the measured molecular weights ($\overline{X}_n$ and $\overline{X}_w$) and polymer concentration, the zeroth and the second moments of the polymer can be calculated. Thus, we have total 6 state variables to estimate and they are: monomer conversion (x_1 or polymer concentration, x_p), initiator concentrations (x_2, x_3), temperature (x_4), the zeroth moment (x_5) and the second moment (x_6). The covariance of the model error, $\boldsymbol{Q}(t)$, is a constant diagonal matrix of dimension 6. The covariance of initial estimation error, $\boldsymbol{P}_0$, is also a diagonal matrix. In Table 5.2, $\boldsymbol{x}$ denotes the vector of states and $\hat{\boldsymbol{x}}$ the vector of estimated states. Table 5.2 also shows the two measurements equations, $\boldsymbol{y}_{o,k}$ and $\boldsymbol{y}_{d,k-\tau}$, without and with delayed MW measurements. τ is the MW measurement delay. Each matrix of the measurement error covariances is diagonal: $i.e.$,

$$\boldsymbol{R}_{o,k} = diag\{r_{x_1}^2, r_{x_4}^2\} \tag{5.13}$$

$$\boldsymbol{R}_{d,k-\tau} = diag\{r_{x_1}^2, r_{x_4}^2, r_{x_5}^2, r_{x_6}^2\} \tag{5.14}$$

where r_{x_i} denotes the standard deviation of the measurement error of x_i.

The delayed measurements of polymer molecular weight are incorporated

to the two time scale filter as follows. When the results of delayed MW measurements taken at $t_k - \tau$ are available at time t_k, the old estimates of $\hat{x}_{k-\tau}(-)$ and $P_{k-\tau}(-)$ are corrected using this new information to obtain the updated values:

$$\hat{x}_{k-\tau}^{new}(+) = \hat{x}_{k-\tau}(-) + K_{k-\tau}^{new}[y_{d,k-\tau} - h_d(\hat{x}_{k-\tau}(-))] \qquad (5.15)$$

$$P_{k-\tau}^{new}(+) = [I - K_{k-\tau}^{new} H_{d,k-\tau}]P_{k-\tau}(-) \qquad (5.16)$$

$$K_{k-\tau}^{new} = P_{k-\tau}(-)H_{d,k-\tau}^T \left[H_{d,k-\tau} P_{k-\tau}(-)H_{d,k-\tau}^T \right.$$

$$\left. + R_{d,k-\tau} \right]^{-1} \qquad (5.17)$$

where,

$$H_{d,k-\tau} = \left. \frac{\partial h_d(x_{k-\tau})}{\partial x_{k-\tau}} \right|_{x_{k-\tau} = \hat{x}_{k-\tau}(-)} \qquad (5.18)$$

The superscript *new* is used here to emphasize the fact that updates are made with delayed MW data. After the above reinitialization is done, the propagation equations are solved again forward up to $t_k + \tau$ and at $t_k + \tau$, the same updating procedure is repeated with the delayed data taken at t_k.

Since accurate information concerning noise statistics is rarely available in practice, the model error covariance Q, the measurement error covariance R, the initial estimation error covariance P_0 and the initial state estimate $\hat{x}_0$ are treated as tuning parameters for the estimator. The effects of such tuning parameters on the estimation performance have been discussed elsewhere [Wells (1971), Hamilton *et al.* (1973),Kiparissides *et al.* (1981)]. In general,

when reasonably good process models are used, the estimator performance is relatively insensitive to the initial state estimate $\hat{x}_0$ and the initial estimation error covariance P_0, although they affect the speed of the estimator response. When poor estimates of the initial states or large covariances of the initial state estimation errors are used, the estimator tends to converge slowly to the true system state.

For a linear system, the system is completely observable if all the initial states can be determined from the knowledge of the system control $u(t)$ and the system observation $y(t)$ over some finite time interval [Ray (1981b)]. The observability conditions for non-linear systems are more difficult to derive than those of linear systems. According to [Hwang and Seinfeld (1972), Ray (1981b)], the local observability condition for a non-linear system can be determined by linearizing the system model about a nominal trajectory $\bar{x}(t)$ and conducting linear observability test. If $F(t)$ $(n \times n)$ and $H(t)$ $(m \times n)$ are the jacobian matrices of the linearized process model and the measurement model (h), respectively, at the nominal state $\bar{x}(t)$, then, the system is locally observable if and only if the rank of an $n \times nm$ observability matrix L_0 is n where

$$L_0 \equiv \left[H^T \vdots F^T H^T \vdots (F^T)^2 H^T \vdots \cdots \vdots (F^T)^{n-1} H^T \right]. \tag{5.19}$$

However, it should be noted that there is a possibility that more than two different initial states x_0 may yield the identical observation when the devi-

ation from the nominal state is too large. In such a case, the system is not observable even though the system is locally observable at each point [Hwang and Seinfeld (1972)].

For styrene polymerization in a CSTR considered in this work, the observability matrix (L_o) is expressed as follows when monomer conversion and reactor temperature are measured on-line:

$$
L_o = \begin{pmatrix}
1 & 0 & \vdots & f_{11} & f_{41} & \vdots & f'_{11} & f'_{41} & \vdots & f''_{11} & f''_{41} & \vdots & \\
0 & 0 & \vdots & f_{12} & f_{42} & \vdots & f'_{12} & f'_{42} & \vdots & f''_{12} & f''_{42} & \vdots & \\
0 & 0 & \vdots & f_{13} & f_{43} & \vdots & f'_{13} & f'_{43} & \vdots & f''_{13} & f''_{43} & \vdots & \\
0 & 1 & \vdots & f_{14} & f_{44} & \vdots & f'_{14} & f'_{44} & \vdots & f''_{14} & f''_{44} & \vdots & \cdots \\
0 & 0 & \vdots & 0 & 0 & \vdots & 0 & 0 & \vdots & 0 & 0 & \vdots & \\
0 & 0 & \vdots & 0 & 0 & \vdots & 0 & 0 & \vdots & 0 & 0 & \vdots & \\
\end{pmatrix}
\tag{5.20}
$$

where $\{f_{ij}\}$ are the elements of the Jacobian matrix of the process model (F), $\{f'_{ij}\}$ the elements of F^2 and $\{f''_{ij}\}$ the elements of F^3. The rank of the above observability matrix is 4 which is less than the dimension of the system model (6). Therefore, the two state variables (x_5 and x_6) are not observable. When the molecular weight measurements are provided, the observability matrix L_d becomes

$$
\boldsymbol{L}_d = \begin{pmatrix}
1 & 0 & 0 & 0 & \vdots & f_{11} & f_{41} & f_{51} & f_{61} & \vdots & f'_{11} & f'_{41} & f'_{51} & f'_{51} & \vdots \\
0 & 0 & 0 & 0 & \vdots & f_{12} & f_{42} & f_{52} & f_{62} & \vdots & f'_{12} & f'_{42} & f'_{52} & f'_{51} & \vdots \\
0 & 0 & 0 & 0 & \vdots & f_{13} & f_{43} & f_{53} & f_{63} & \vdots & f'_{13} & f'_{43} & f'_{53} & f'_{53} & \vdots \\
0 & 1 & 0 & 0 & \vdots & f_{14} & f_{44} & f_{54} & f_{64} & \vdots & f'_{14} & f'_{44} & f'_{54} & f'_{54} & \vdots \\
0 & 0 & 1 & 0 & \vdots & 0 & 0 & f_{55} & 0 & \vdots & 0 & 0 & f'_{55} & 0 & \vdots \\
0 & 0 & 0 & 1 & \vdots & 0 & 0 & 0 & f_{66} & \vdots & 0 & 0 & 0 & f'_{66} & \vdots
\end{pmatrix} \cdots
$$

$$(5.21)$$

and the rank of this matrix is 6 and thus the system becomes observable. It must be pointed out that the system is observable only when the molecular weight measurements, albeit delayed, are available.

Figures 5.3 and 5.4 show the performance of the filter with the model A when the reactor residence time is reduced by 50% from the steady state value. Here, the measurement errors have been generated by a pseudo-random number generator and added to the x values to produce the sensor signals (y). The perturbation is assumed to fall within the prespecified standard deviation of each measurement error. For example, it has been assumed that the standard deviation for the measurements are: monomer conversion: ± 0.03, temperature: $\pm 0.5°C$, $\overline{X}_n$ and $\overline{X}_w$: ± 5 %. Sampling time for the on-line measurements of monomer conversion and temperature is 1 min. The numerical values of the initial filter parameters used in our simulations are shown in Table 5.3. In the simulation illustrated in these figures, it is assumed that the change in the feed flow rate (or residence time) has been input to the filter
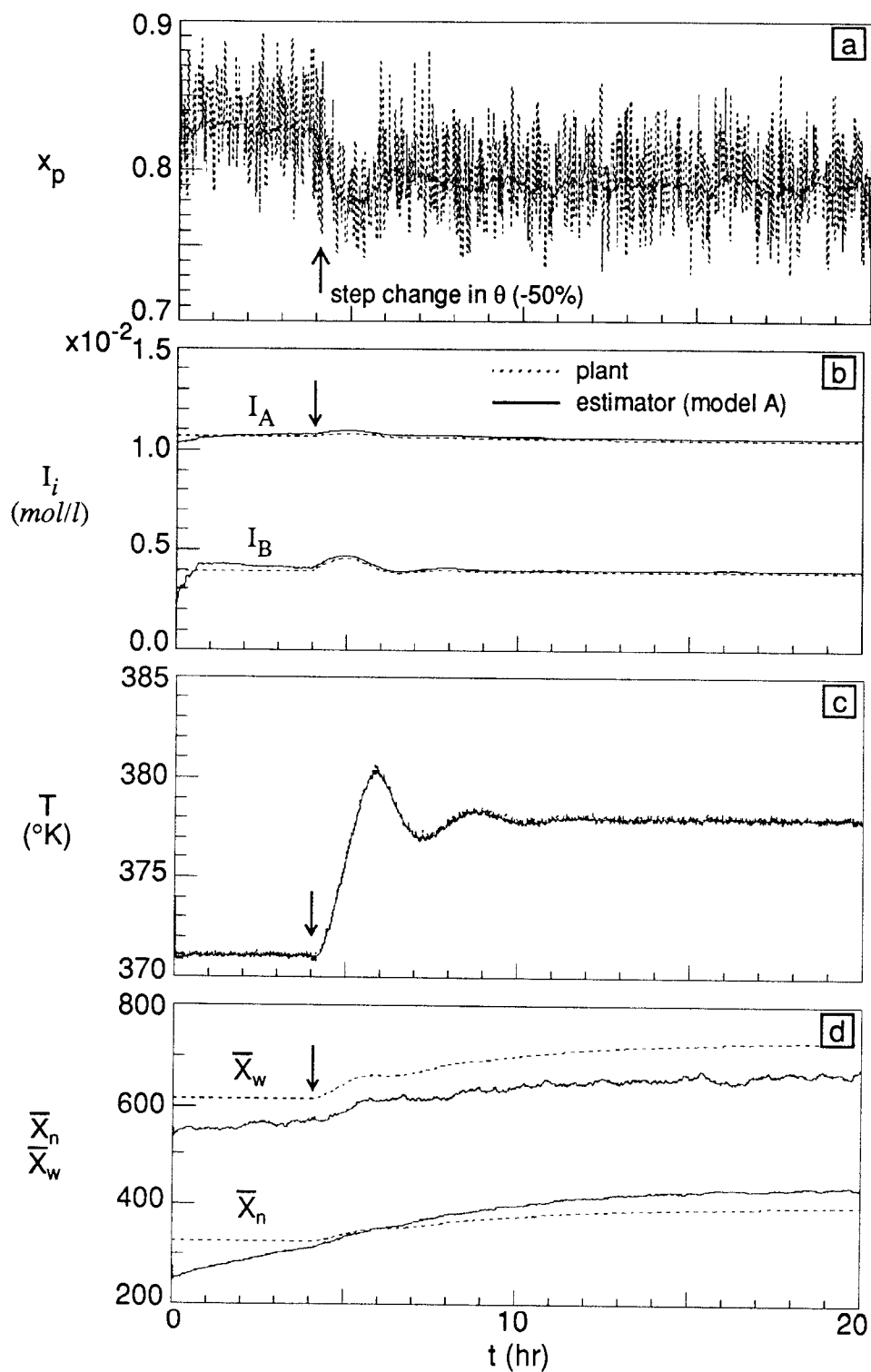
Figure 5.3   Estimation of open loop transients to step change in θ (-50
%) with model A without delayed measurements.
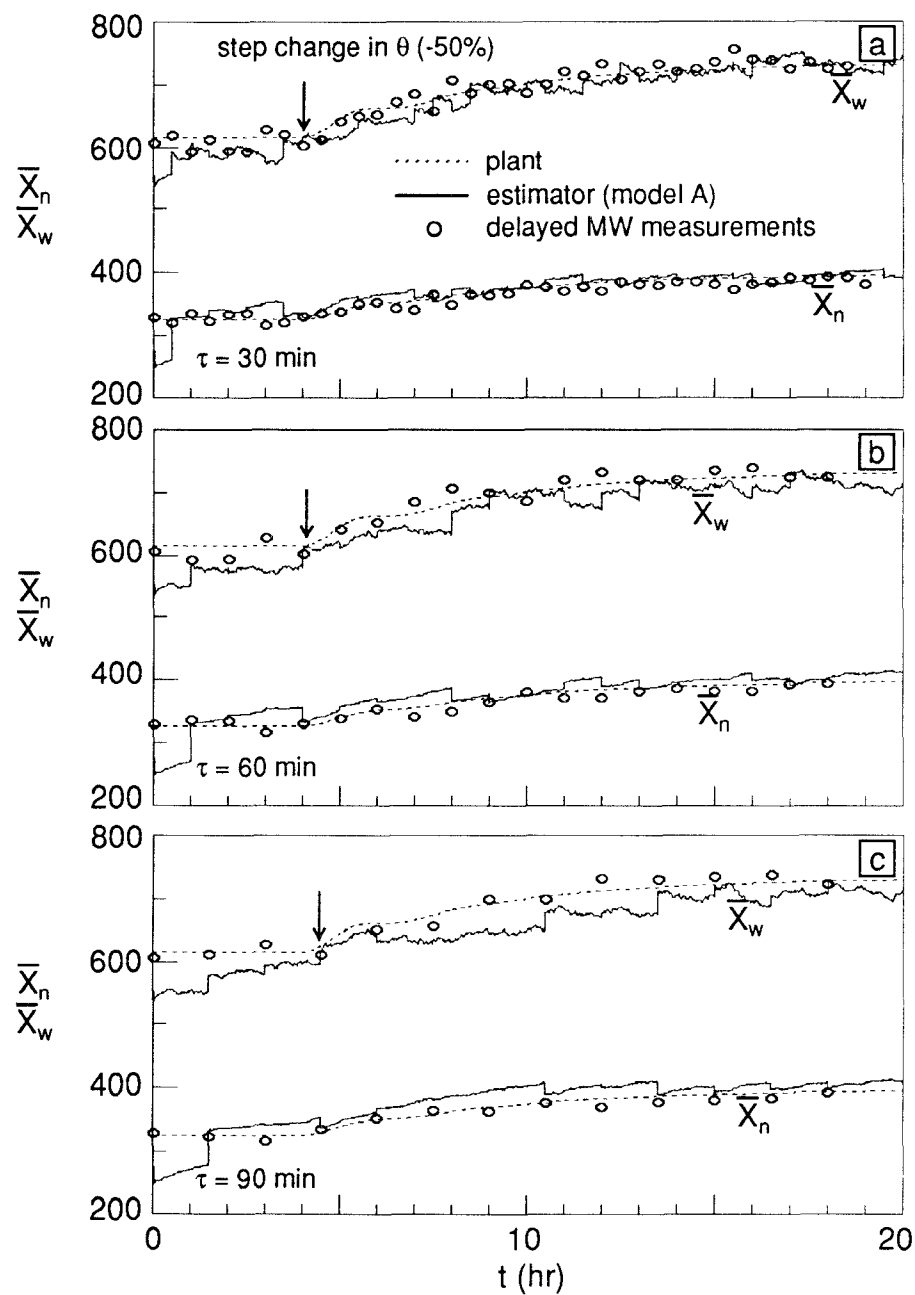
Figure 5.4   Effect of MW measurement delay (τ) on estimation of molecular weight with model A during open loop transients to step change in θ (-50%).
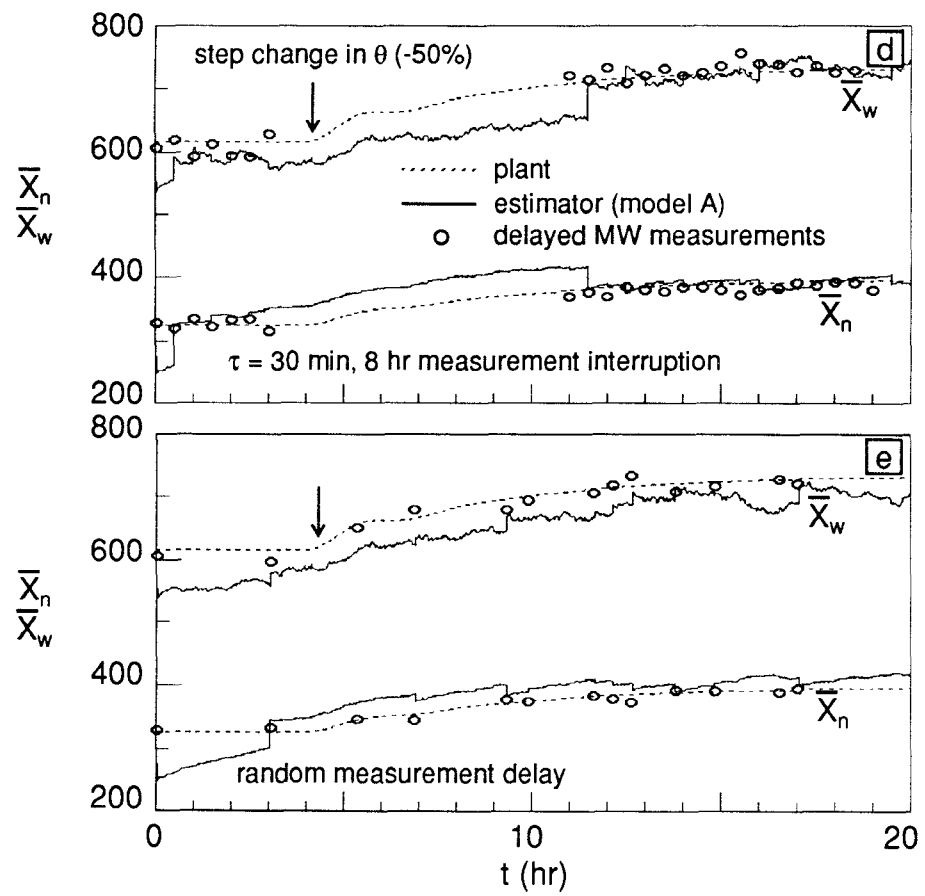
Figure 5.4   *(continued)*

Table 5.3   Numerical values of initial parameters of the state estimator

	model A	model B
$\boldsymbol{Q}(q_{ii} = q_{xi}^2)$	$q_{xi}^2 = 1.0 \times 10^{-3}*$ $q_{xi}^2 = 1.0 \times 10^{-2}\dagger$	$q_{xi}^2 = 1.0 \times 10^{-2}*$ $q_{xi}^2 = 1.0 \times 10^{-1}\dagger$
$\boldsymbol{R}(r_{ii} = r_{xi}^2)$	$r_{x1}^2 = 9.0 \times 10^{-4}$ $r_{x4}^2 = 9.0 \times 10^{-6}$ $r_{x5}^2 = 2.5 \times 10^{-3}$ $r_{x6}^2 = 2.5 \times 10^{-3}$	$r_{x1}^2 = 9.0 \times 10^{-4}$ $r_{x4}^2 = 9.0 \times 10^{-6}$ $r_{x5}^2 = 2.5 \times 10^{-3}$ $r_{x6}^2 = 2.5 \times 10^{-3}$
$\boldsymbol{P}(0)$	$p_{ii}(0) = 0.01\ddagger$	$p_{ii}(0) = 0.01\ddagger$
$\hat{\boldsymbol{x}}_0$	$\hat{x}_{i,0} = 1.2x_i(0)*$ $\hat{x}_{5,0} = 1.3x_5(0)$ $\hat{x}_{6,0} = 1.1x_6(0)$	$\hat{x}_{i,0} = 1.2x_i(0)*$ $\hat{x}_{5,0} = 1.3x_5(0)$ $\hat{x}_{6,0} = 1.1x_6(0)$

* for $i = 1, 2, 3, 4$

† for $i = 5, 6$

‡ for $i = 1, 2, 3, 4, 5, 6$

(Feed flow rates are measured by flow meters and should be available to operators.). As shown in Figure 5.3, the model error has little effect on estimation of monomer conversion and reactor temperature due to their on-line measurements. When model A is used with delayed molecular weight measurements, the quality of estimation of $\overline{X}_w$ and $\overline{X}_n$ improves dramatically, albeit with a slight deterioration in the filter performance with large time delays.

Figure 5.5 shows the time varying profiles of the estimation error covariances for this example with 30 minute delay of MW measurement. Several observations can be made. The uncertainty in the x_1 component, P_{11}, and that in the x_4 component, P_{44}, decrease much more rapidly than do the uncertainties in x_2 and x_3 (initiator concentrations, P_{22} and P_{33}). This stems from the fact that only x_1 and x_4 are measured on-line. The profiles of P_{55} and P_{66} elements of the estimation error covariance matrix shown in Figure 5.4c and 5.4d illustrate how P_{55} and P_{66} change between delayed MW measurements. Note that even with these delayed measurements, the filter estimates converge to the true state rapidly as shown in Figure 5.4. A few elements of the Kalman filter gain matrix are also shown in Figure 5.6. One can observe from this figure that the filter gains remain nearly constant after convergence is attained.

Figure 5.4d illustrates the situation where no measurements are made for 8 hours. As one may expect, the molecular weight prediction during this *blackout period* is very poor because the system is not observable with only two on-line measurements. However, as soon as the MW measurement is resumed the filter converges rapidly to the true state. In practice, the results of product analysis are often available irregularly (*i.e.*, laboratory analysis time may vary). Figure 5.4e shows the filter predictions when unequal sampling periods for off-line MW measurements are used. Here, the sampling periods were determined by a random number generator with a standard deviation
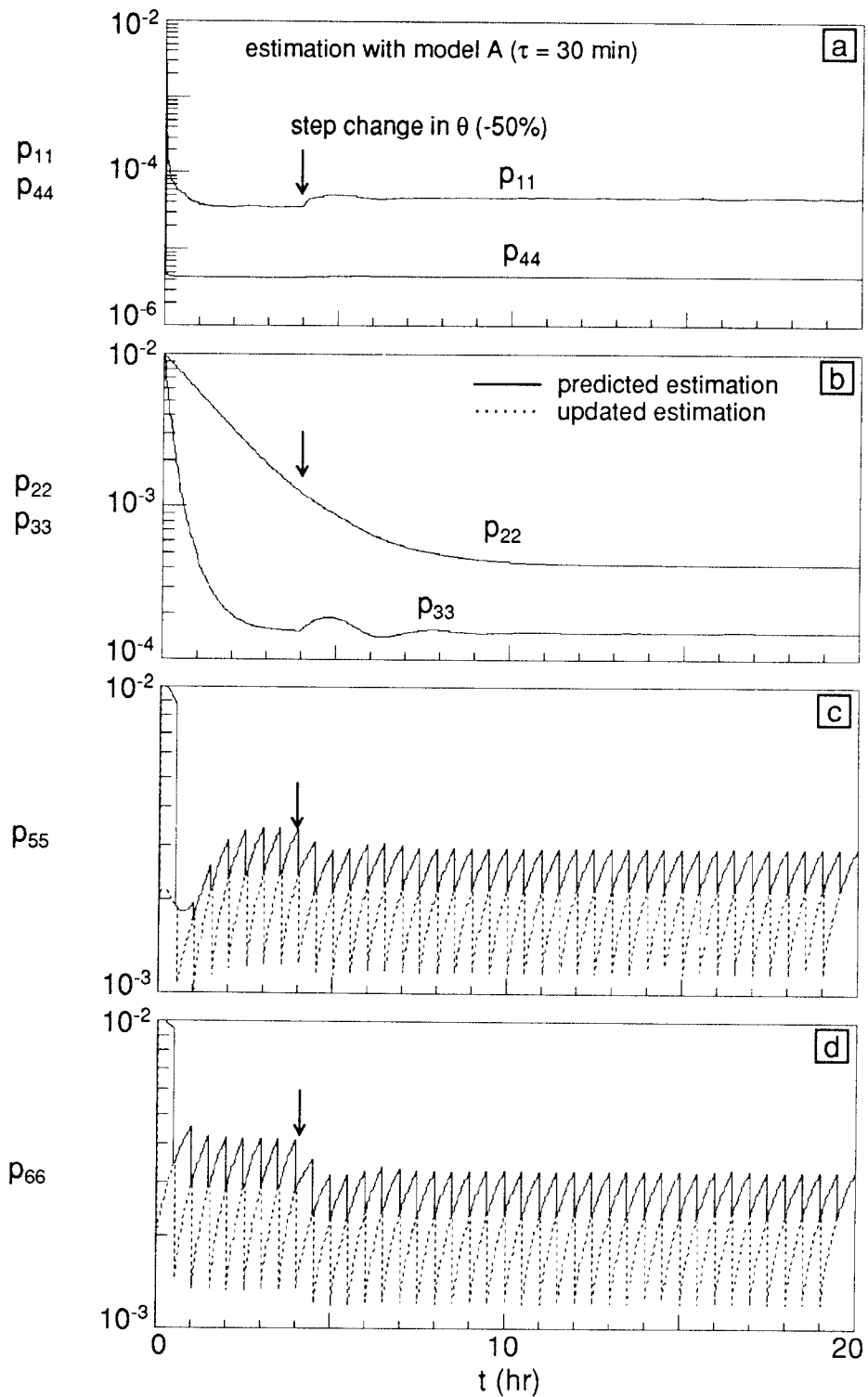
Figure 5.5   Profiles of estimation error covariances during estimation of
open loop transients to step change in θ (-50 %) with model
A and 30 minute MW measurement delay.
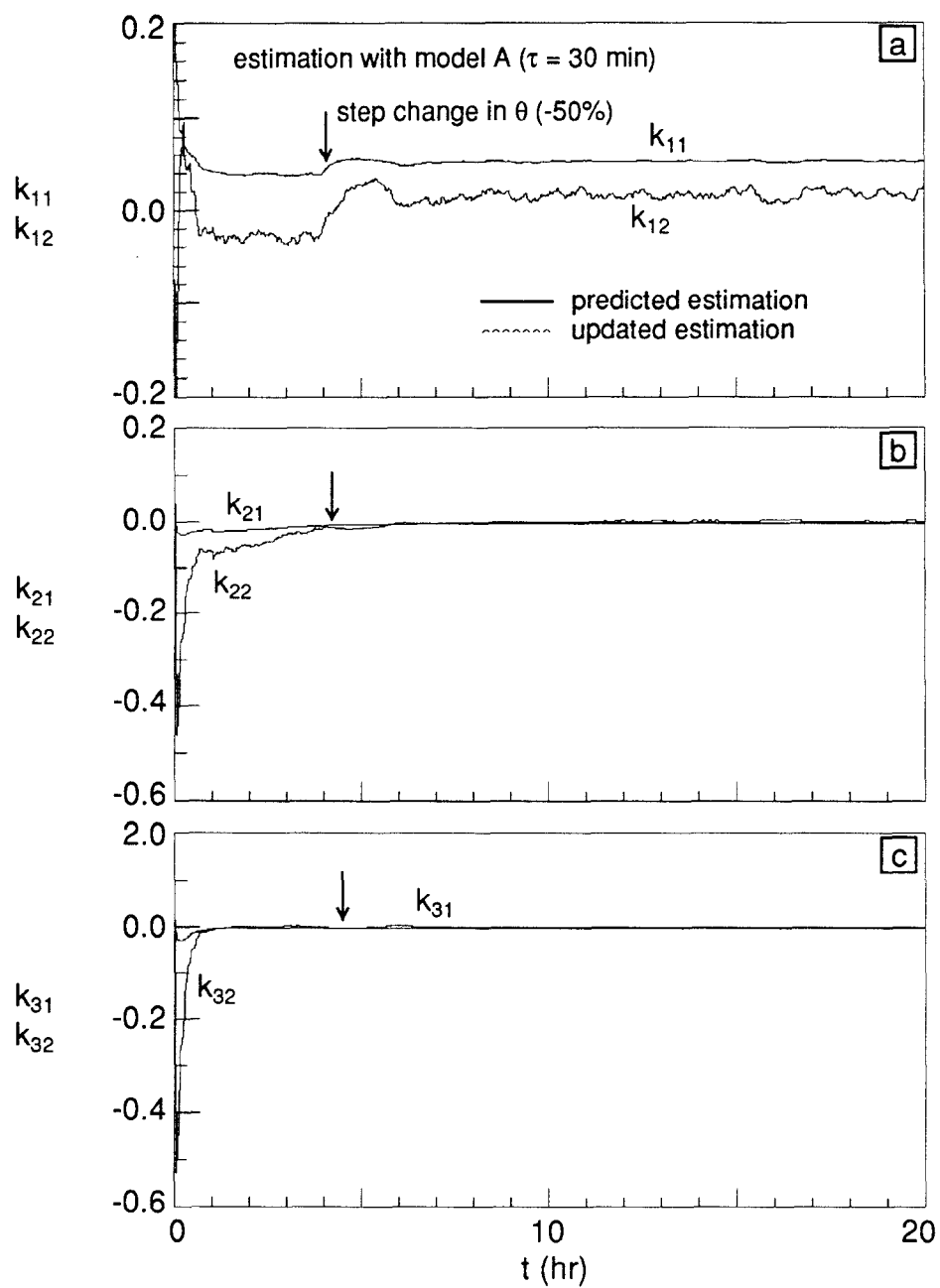
Figure 5.6   Profiles of gains during estimation of open loop transients to step change in θ (-50 %) with model A and 30 minute MW measurement delay.
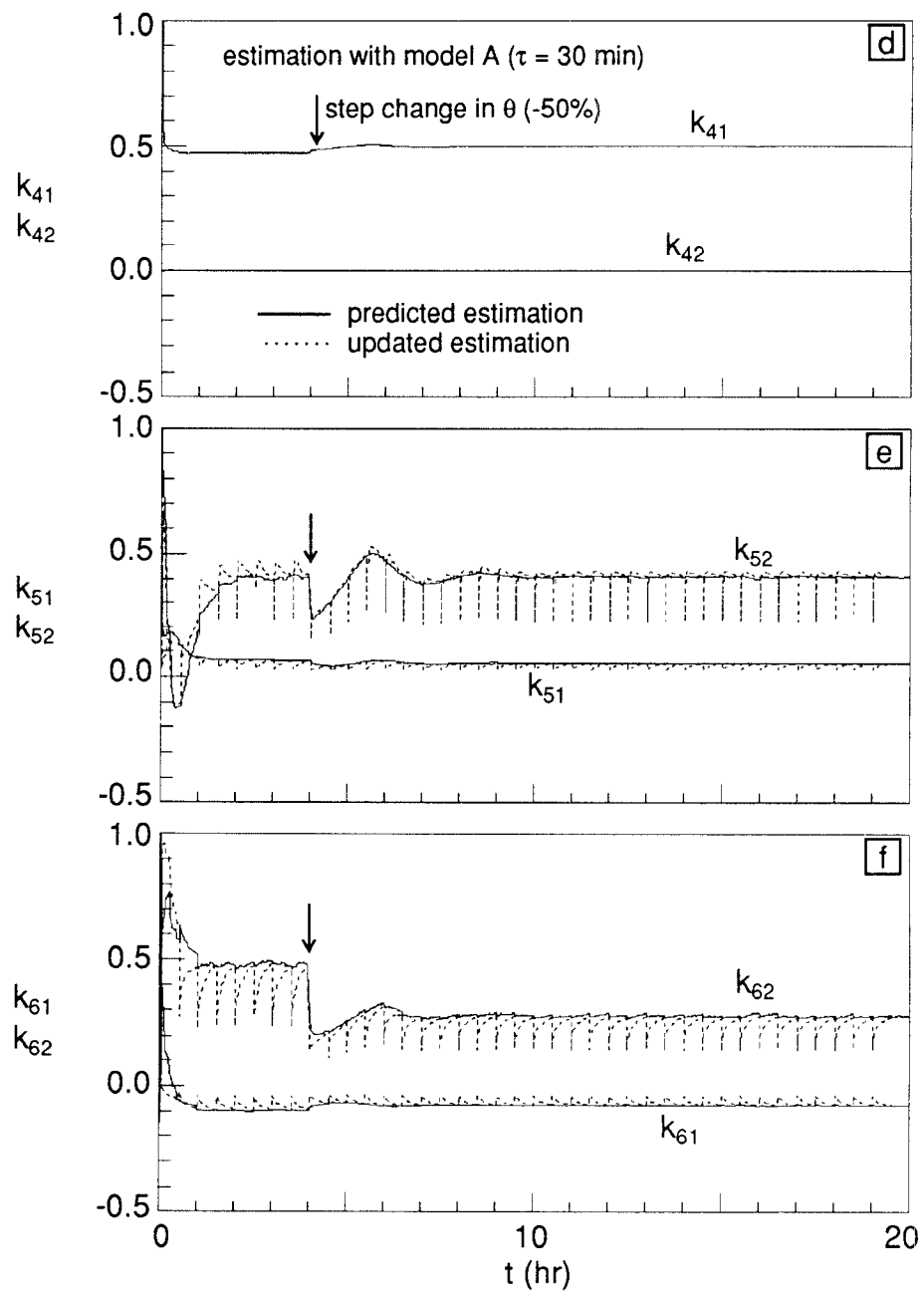
Figure 5.6   (*continued*)

of 45 min from the nominal sampling period of 90 min. Note that the filter performance is better than the case shown in Figure 5.4d but slightly poorer than with equal 90 min intervals between samples (Figure 5.4c). Similar observations can be made in Figures 5.7 and 5.8 for model B. Figure 5.8d and 5.8e indicate that unequal MW sampling gives much better estimates than with an equal but large time delay of 90 min. Considering the model inaccuracy as illustrated in Figure 5.2, one can see that the incorporation of the delayed MW data into the filter even with model B significantly improves the molecular weight predictions. It is also seen that when the modeling error is large, more frequent measurements of the molecular weight are required. Figures 5.9 and 5.10 show the open loop response of the reactor when the reactor residence time is reduced by 75% by increasing the input feed rate. It is seen that the reactor exhibits oscillatory dynamics with a period of oscillation of about 5 hours. With the molecular weight measurements made every 30 min, the filter yields very accurate predictions of molecular weight and initiator concentrations even when the less accurate model B is used for filtering.
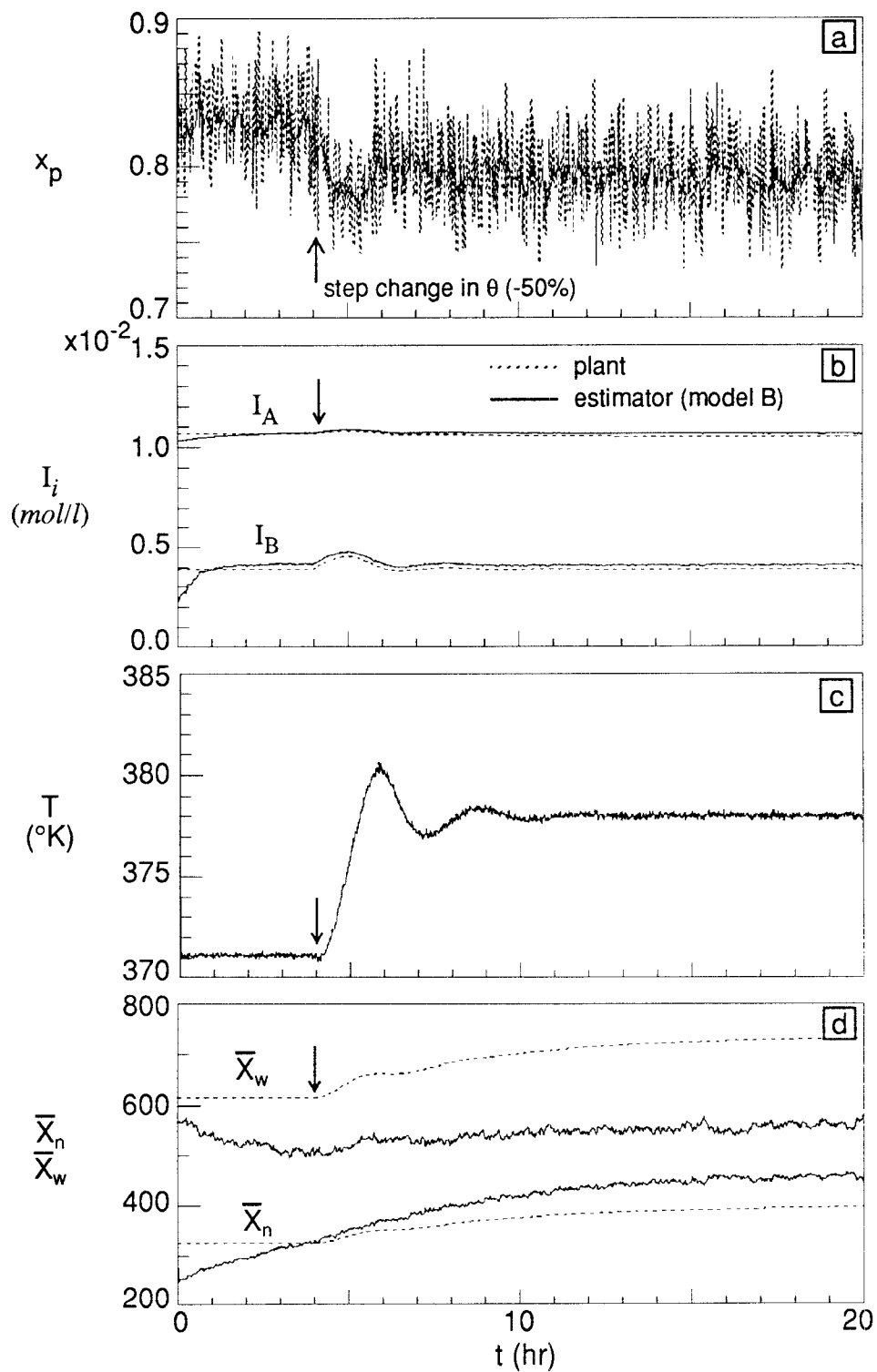
Figure 5.7   Estimation of open loop transients to step change in θ (-50 %) with model B without delayed measurements.
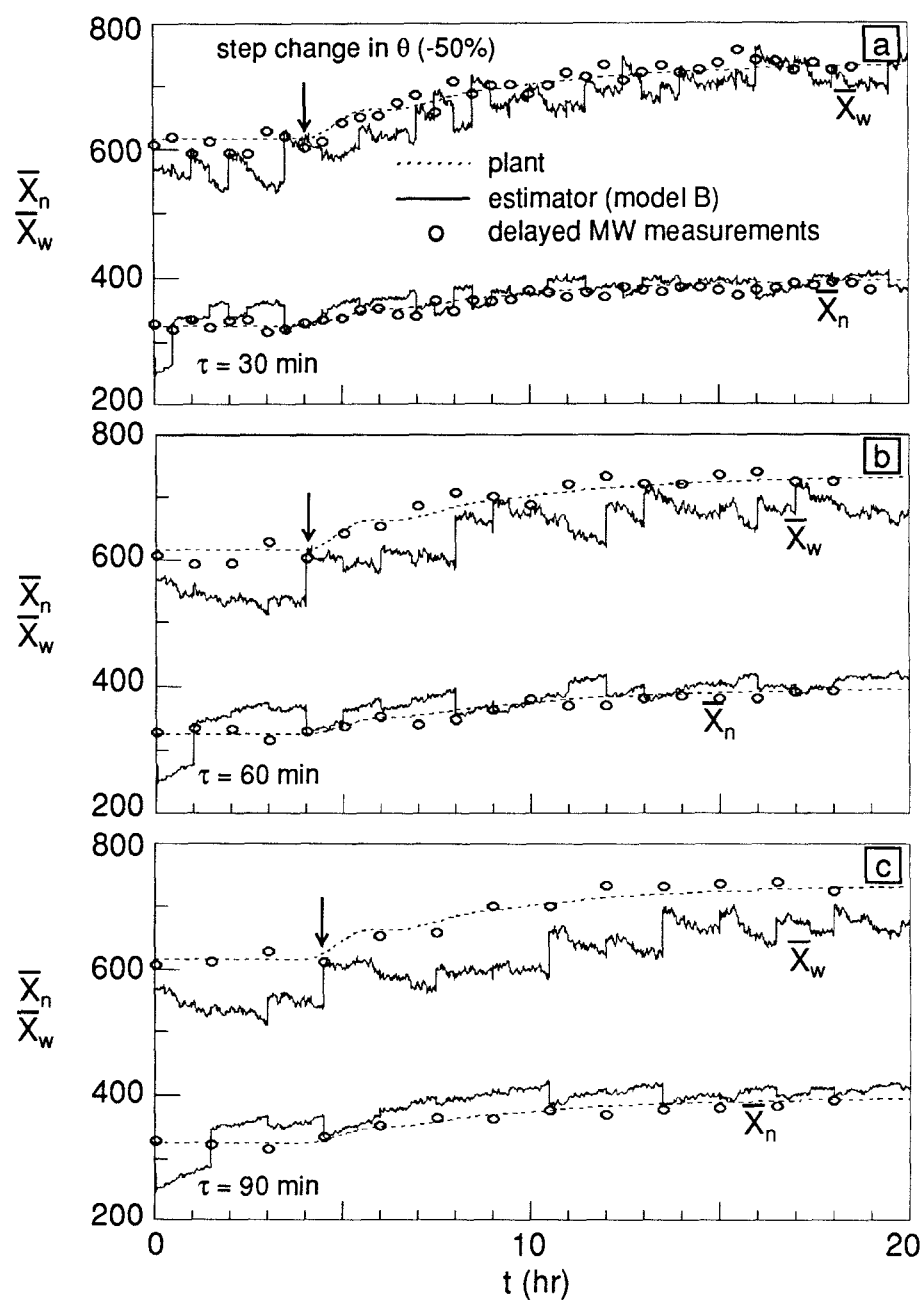
Figure 5.8   Effect of MW measurement delay (τ) on estimation of molecular weight with model B during open loop transients to step change in θ (-50%).
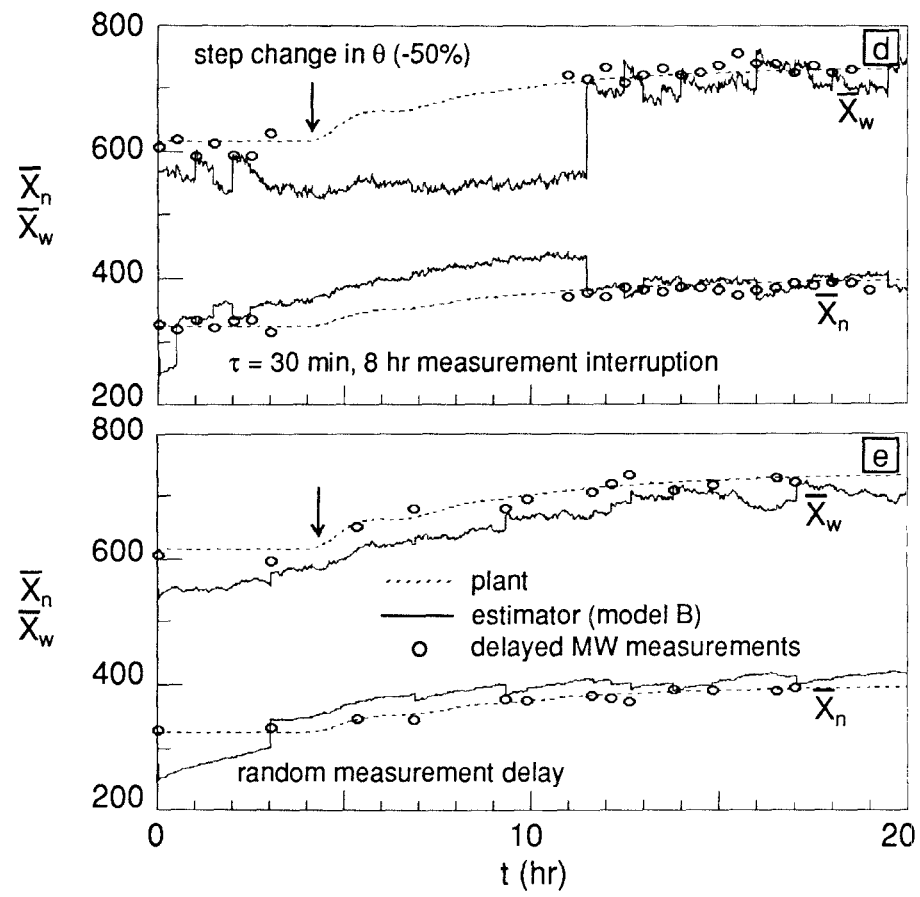
Figure 5.8   (*continued*)
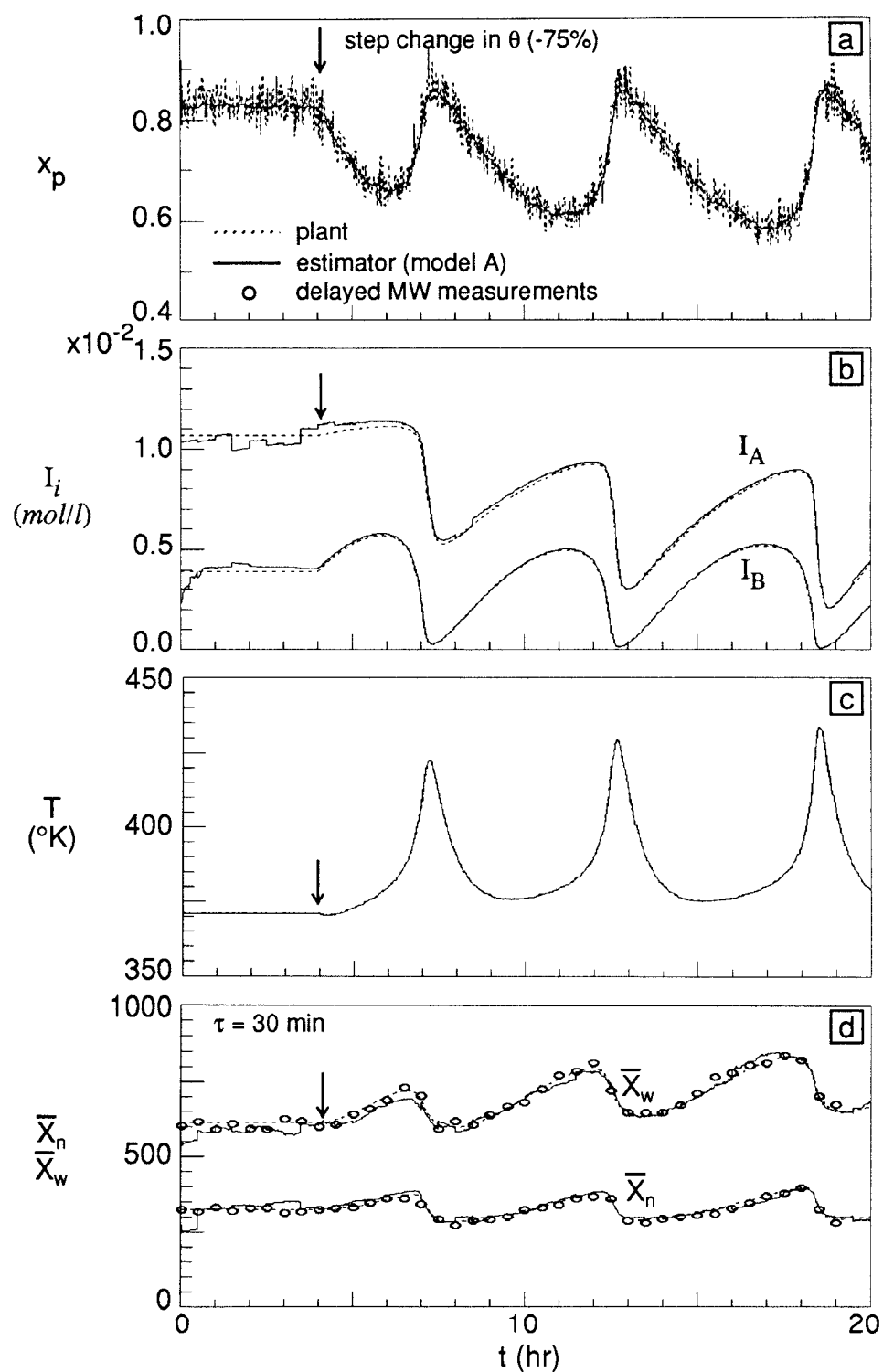
Figure 5.9 Estimator performance with model A and 30 minute delayed MW measurements during oscillatory open loop transients to step change in θ (-75%).
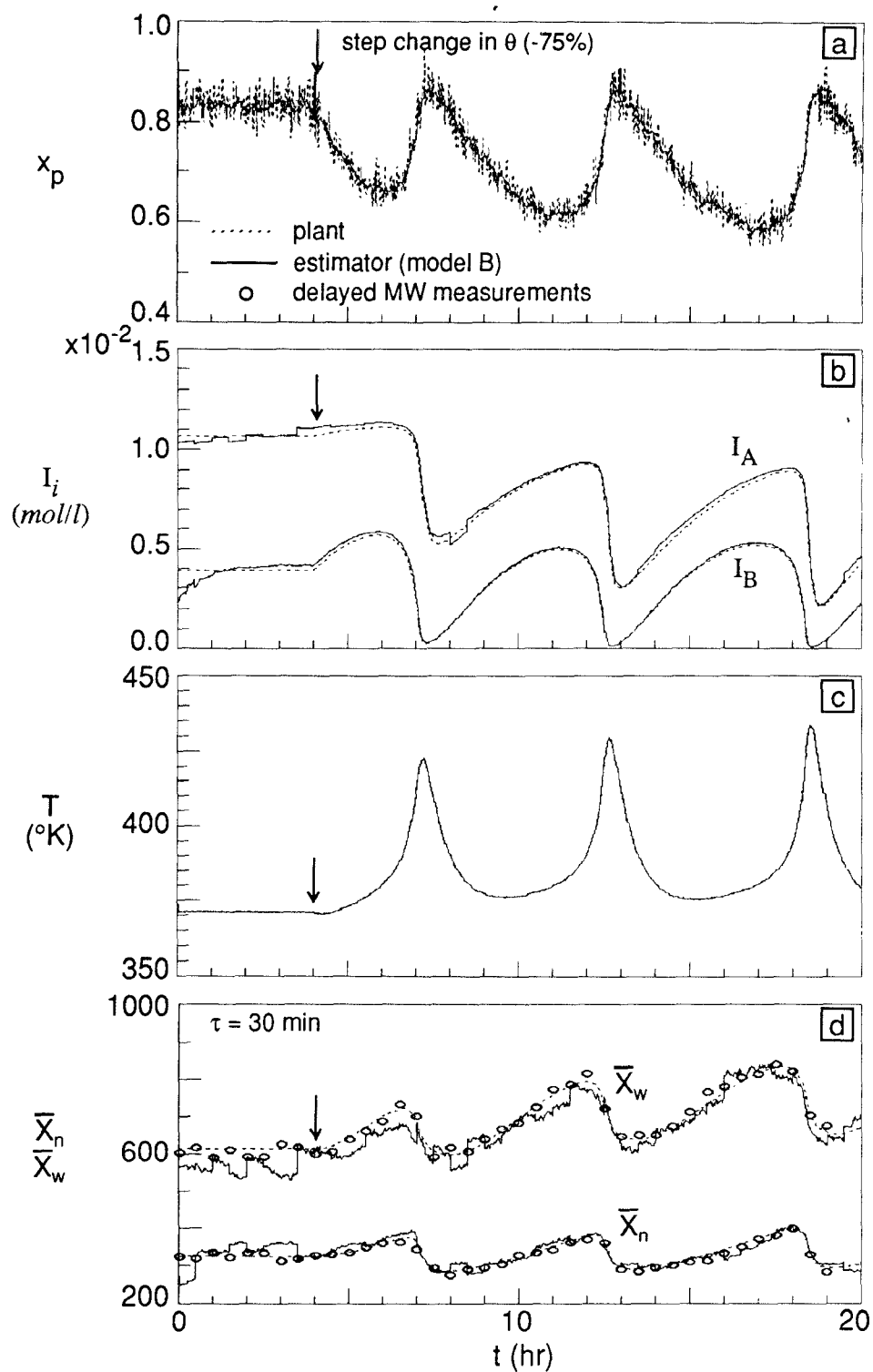
Figure 5.10   Estimator performance with model B and 30 minute delayed MW measurements during oscillatory open loop transients to step change in θ (-75%).

Table 5.4   Parameters of each PI controller

Control variable	T	x_p	$\overline{X}_w$
Manipulated variable	u_1 (T_{cf})	u_2 (I_f)	u_3 (A_f)
Constraints	$303 \le u_1 \le 423$	$0.0 \le u_2 \le 0.1$	$0 \le u_1 \le 10$
Servo control:			
K_c	0.5	0.2 mol/l	-0.002 mol/l
τ_I	1.25 hr	1.25 hr	0.2 hr
Regulatory control:			
K_c	1.2	0.5 mol/l	-0.002 mol/l
τ_I	2.0 hr	5.0 hr	0.2 hr

5.5.   On-line Control of Polymer Molecular Weight

One of the main purposes of using the EKF is to estimate and control the polymer molecular weight on-line with delayed molecular weight measurements. The filter provides molecular weight estimates between the samples and these estimates are used to manipulate the feed rate or concentration of a chain transfer agent.

5.5.1.   Regulatory Control

As shown in Figure 5.1, the reactor temperature is controlled by manipulating the inlet coolant temperature, the monomer conversion by the total

feed initiator concentration (I_f), and $\overline{X}_w$ by the chain transfer agent concentration in the feed stream. It is assumed that flow control valves are perfectly manipulated to regulate the concentrations of various reactants, solvent and initiator. Single loop PI controllers are used and they are tuned manually through numerical model simulations. Optimal control parameter tuning has not been attempted, however. Table 5.4 lists the controller parameters used in the simulations and the range of manipulative variables.

One of the major sources of process disturbance is the feed initiator composition (y_{Af}) which is, in general, very difficult to monitor on-line. Figure 5.11 shows the closed loop responses of the reactor and the filter to a step change in the feed initiator composition (y_{Af}). At $t = 4$ hr, a 50/50 mixture of benzoyl peroxide and tert-butyl perbenzoate initiators has been changed to 0/100. This change in the initiator feed composition is not input to the filter. First note that the control of monomer conversion and temperature is very satisfactory. With 30 min delay of molecular weight measurement (e.g., with on-line GPC), the molecular weight control is also satisfactory. Figure 5.11f shows the performance of the molecular weight controller in the absence of molecular weight measurements for 8 hours (e.g., no MW analysis done by a night shift). During this 8 hr *blackout period*, the estimated molecular weight is lower than the actual value (dotted line); however, as soon as off-line measurements are resumed, the filter starts to provide very accurate estimates of the molecular weight and therefore the MW control becomes very
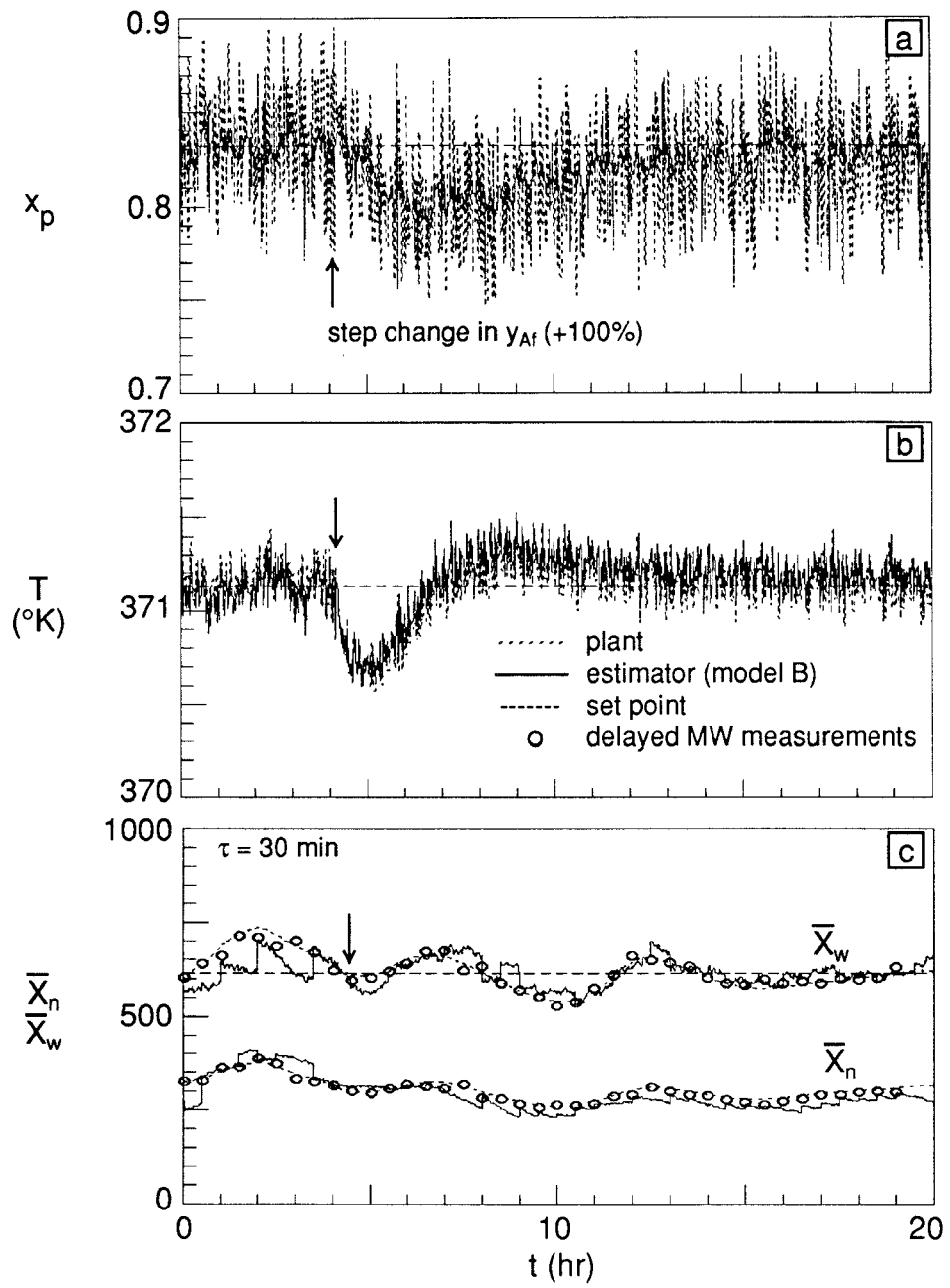
Figure 5.11   Performance of controller and estimator with model B and 30 minute delayed MW measurements during closed loop transients to severe unknown disturbances; step change in y_{Af} (-100 %).

318
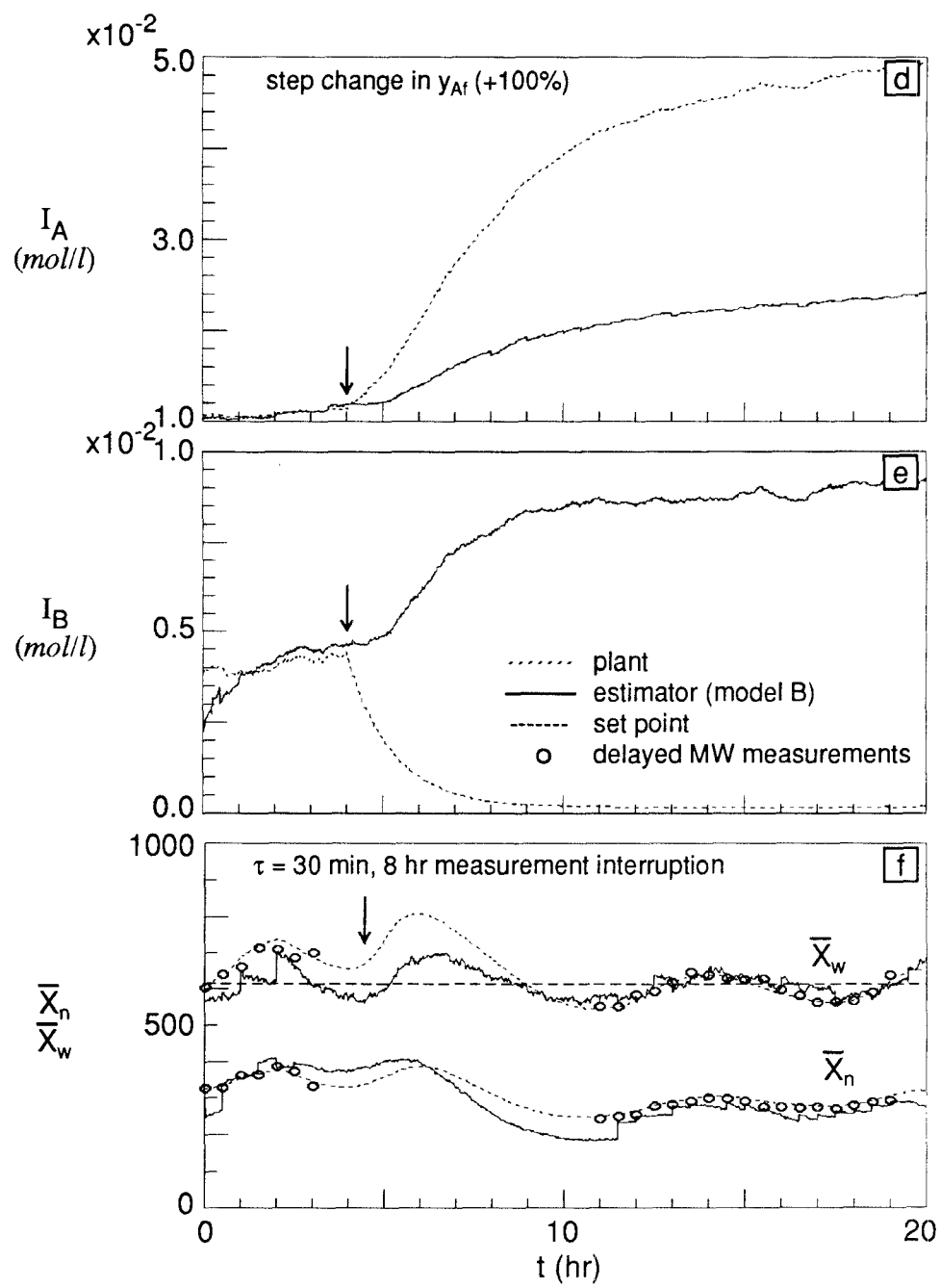
Figure 5.11   (*continued*)
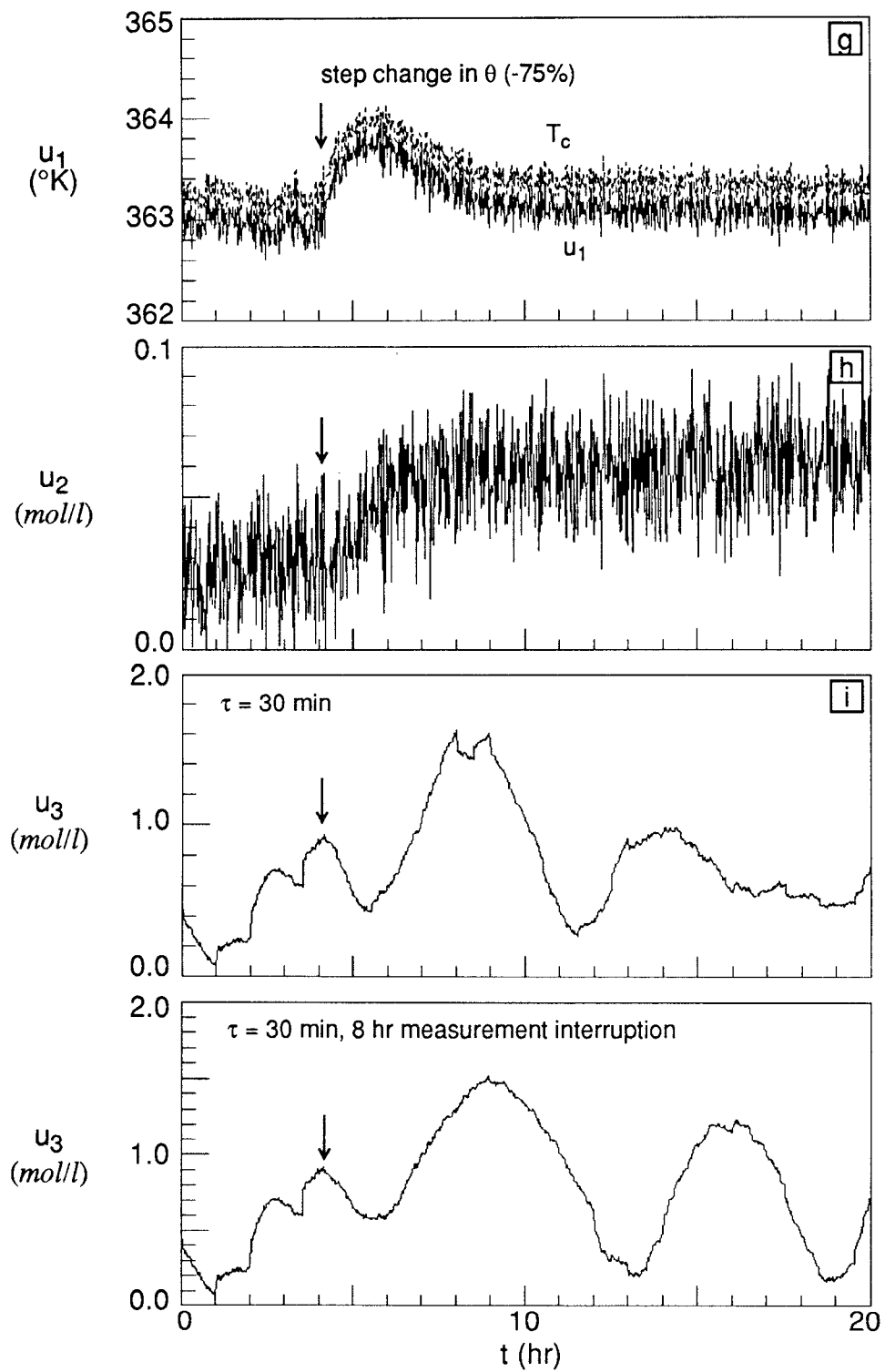
Figure 5.11   (*continued*)

satisfactory again. It should be recalled that the system is not completely observable with only two on-line measurements of monomer conversion and temperature. When model A, which is more accurate than model B, is used, the overall trends are very similar with a slightly better MW control performance.

In general, the initiator concentration in the reactor is very low and much more difficult to measure than other variables. Figure 5.11d and 5.11e show the actual (dashed lines) and estimated (solid lines) initiator concentration profiles. Since the change in the feed initiator composition has not been input to the filter, estimates of the initiator concentrations are very poor. If this change is not detected by the reactor operator, a problem may occur when it is desired to adjust the feed initiator composition in order to change the product grade later on. The effect of unmeasured disturbance was studied by Hamilton *et al.* (1973) for an evaporator. Their simulation results show similar filter behavior to that observed in this work. In order to improve the filter performance, they used large r/q ratio (r = measurement noise covariance, q = process noise covariance). However, in this case, the use of large r/q ratio did not improve the predictions of the initiator concentrations.

In practice, process models and actual plant data can be utilized to detect the source of disturbances in some cases. For example, in the example illustrated in Figure 5.11, the feedback controllers worked almost perfectly to maintain the target values of monomer conversion, temperature and $\overline{X}_w$

in the presence of the disturbance in y_{Af}. However, one can easily observe that the values of the manipulated variables (e.g., I_f, T_{cf}, A (concentration of chain transfer agent)) have been changed after the disturbance has been regulated by the controllers. With such an observation and the process model available, one can reexamine the characteristics of the new steady state. Figure 5.12 illustrates the steady state profiles of reactor variables as a function of y_{Af}. The solid lines and the dotted lines represent the steady states before and after introduction of the disturbance in y_{Af}, respectively. In calculating the new steady state profiles, new values of manipulated variables have been used. First note that the three controlled variables (x_p, T, $\overline{X}_w$) did not change even after y_{Af} has been changed from 0.5 to 1.0. However, one can immediately observe that both I_A and I_B (initiator concentrations) have changed significantly. This indicates that the regulatory control actions were taken to compensate for the change in the initiator concentrations. Then, the reactor operator can have the initiator feedstock checked and make appropriate corrections.
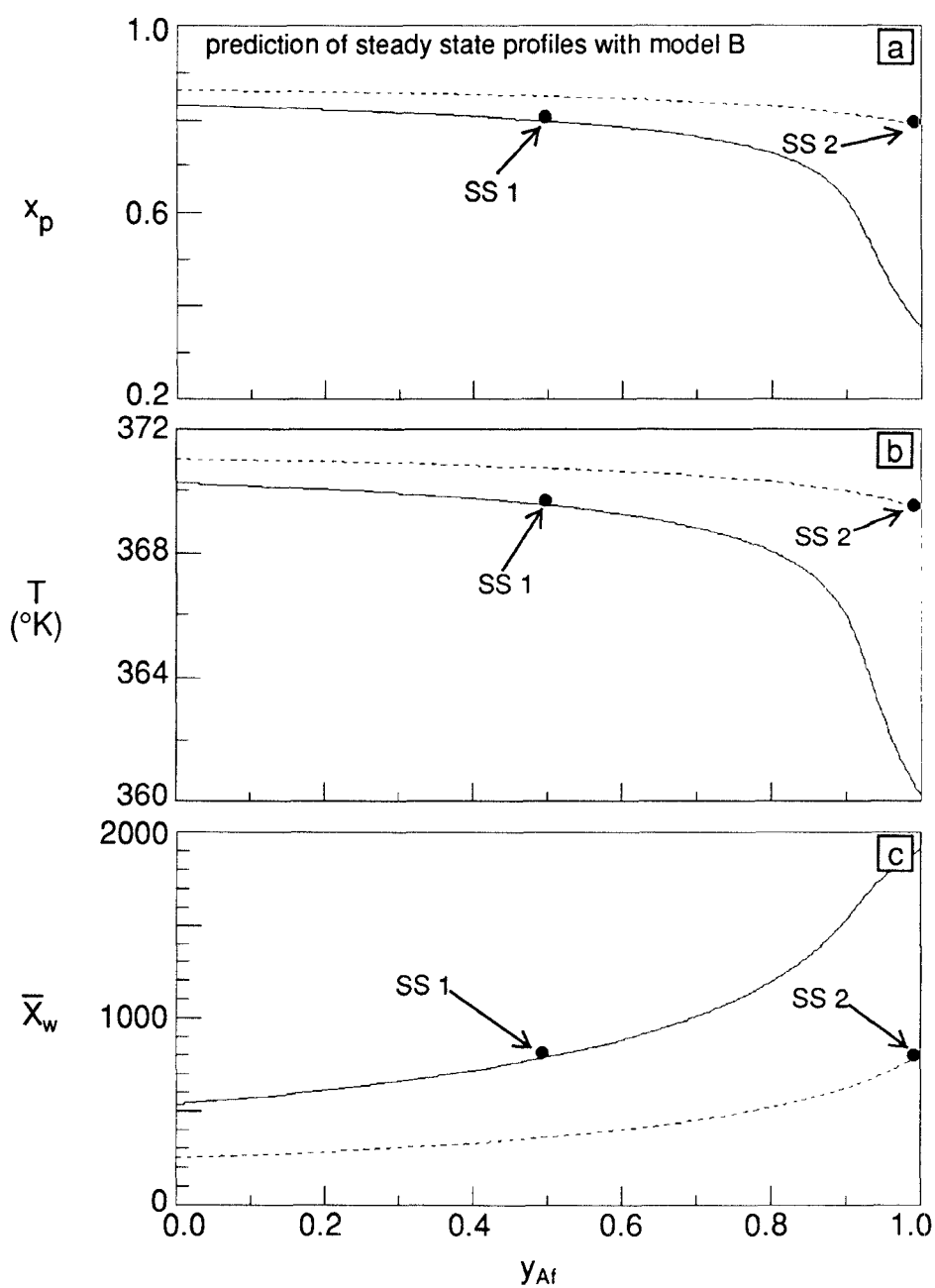
Figure 5.12   Steady state profiles of a function of initiator feed composition with model B before and after control action: SS 1 (before disturbance); $I_f = 0.025$ mol/l, $T_{cf} = 363°$K, $A = 0.5$ mol/l, SS 2 (after disturbance); $I_f = 0.061$ mol/l, $T_{cf} = 363.06°$K, $A = 0.6$ mol/l.
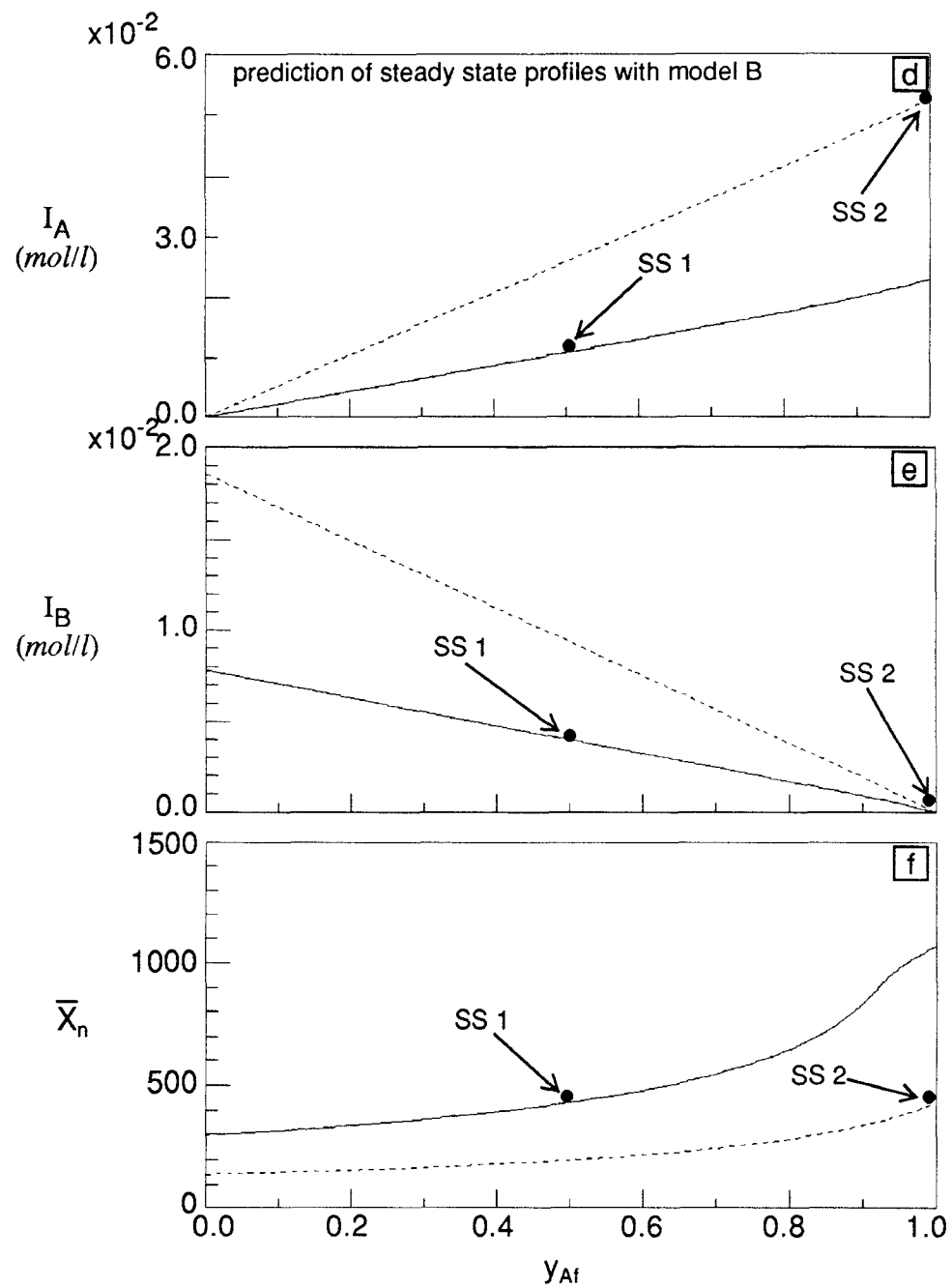
Figure 5.12   (*continued*)

5.5.2. Effect of Measurement delays

Even with on-line GPC, there will be some time delays (15~30 min) in the molecular weight measurement. Thus, in what follows, the effect of time delays on the filter performance will be examined with inaccurate process models. Figure 5.13 shows the results of molecular weight control responding to a step decrease in the reactor residence time by 50% for three different time delays when model A is used. Here, the *estimated* $\overline{X}_w$ values were used for control. Note that as τ increases the deviation of $\overline{X}_w$ from the target value becomes larger and the response is more oscillatory because larger τ causes larger control action in u_3 (chain transfer agent concentration in the feed). With less accurate model B, Figure 5.14 illustrates that the molecular weight control is less satisfactory than with model A even with short delays. The simulation results shown in Figures 5.13 and 5.14 suggest that when the process model is less accurate, more frequent measurements are necessary, which is intuitively obvious. [Note: In the simulations shown in Figures 5.13 and 5.14, the same controller parameters as shown in Table 5.4 have been used.]
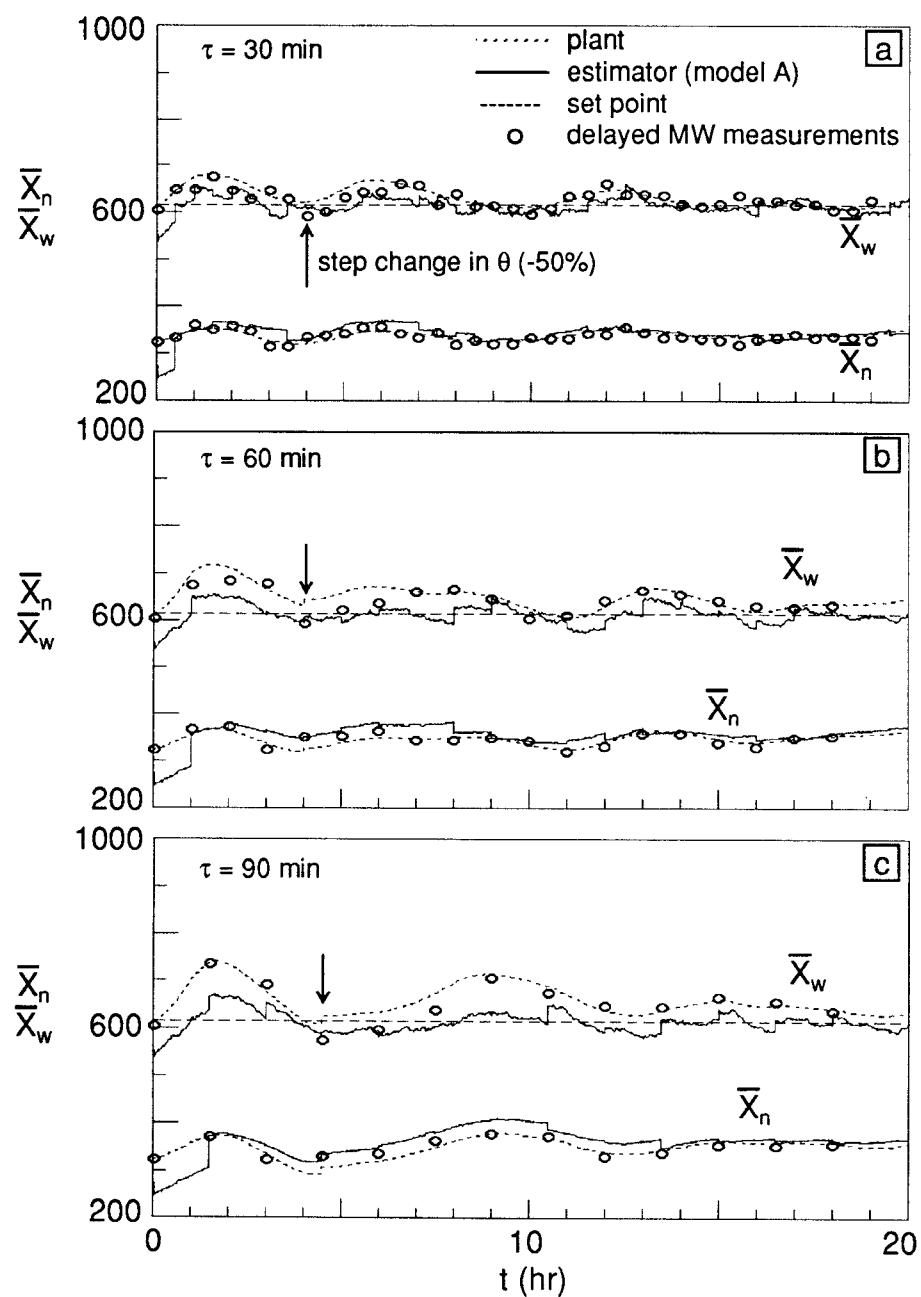
Figure 5.13 Effect of MW measurement delay on control and estimation of molecular weight with model A during closed loop transients to step change in θ (-50%).
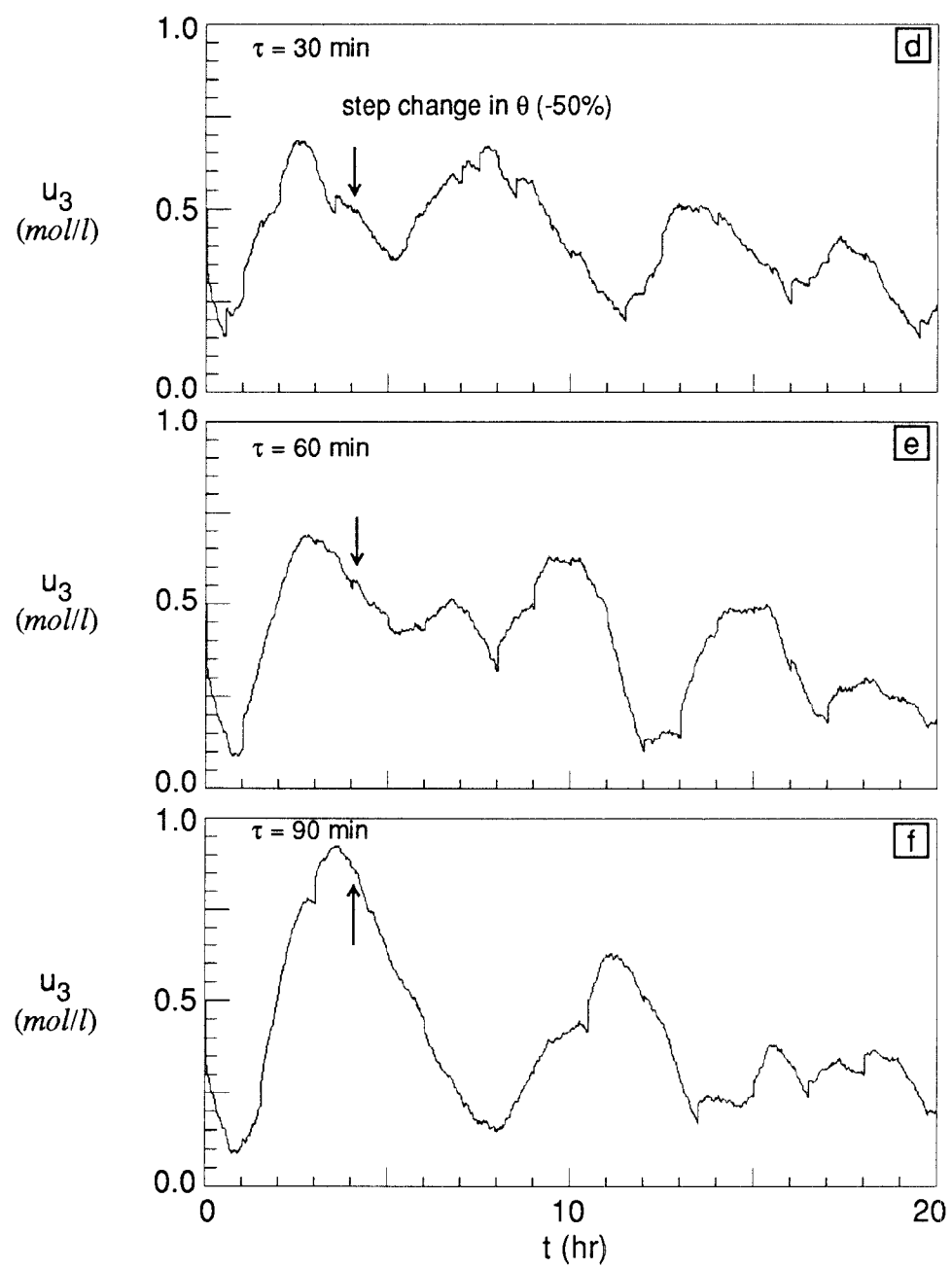
Figure 5.13   (*continued*)
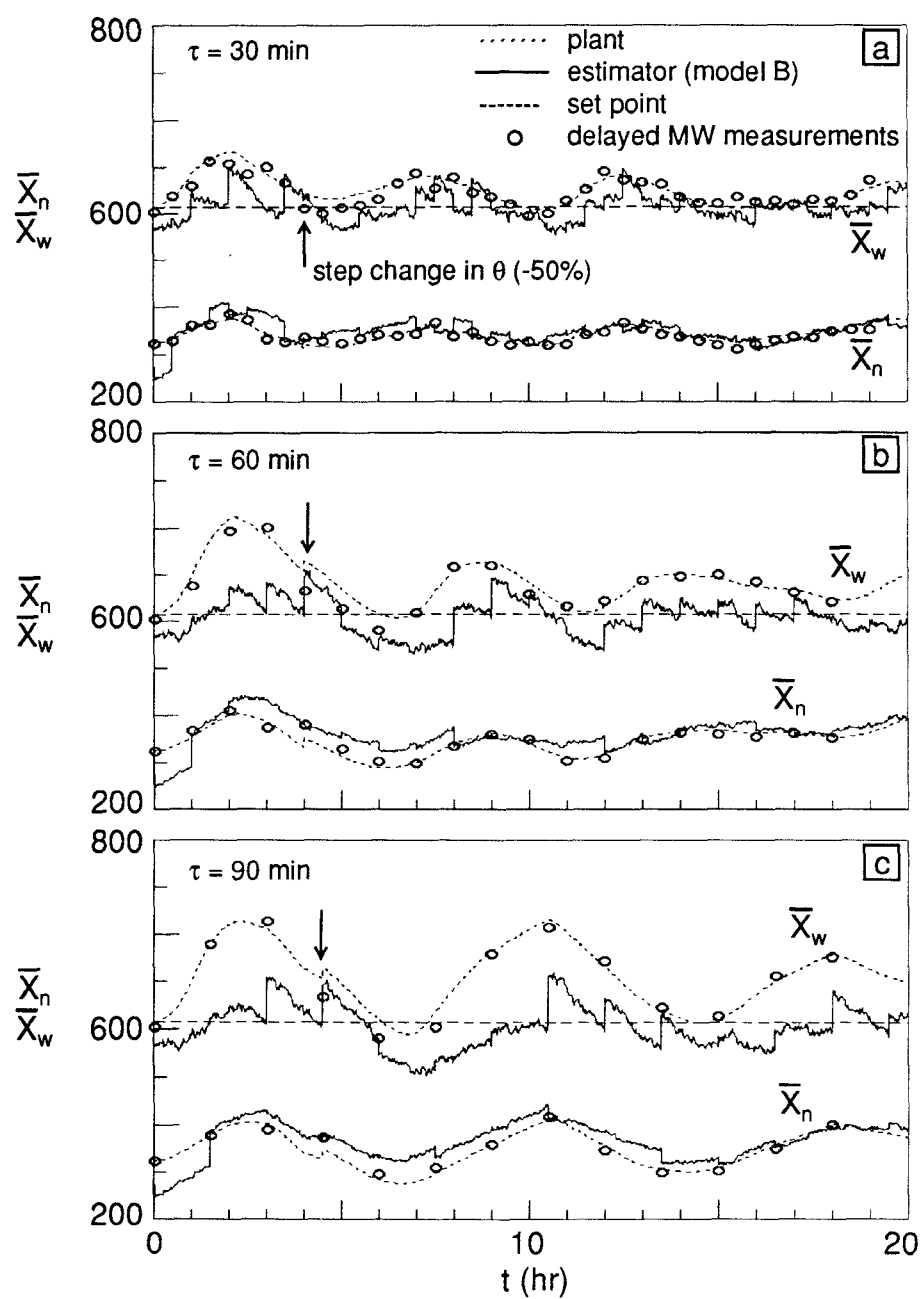
Figure 5.14   Effect of MW measurement delay on control and estimation of molecular weight with model B during closed loop transients to step change in θ (-50%).
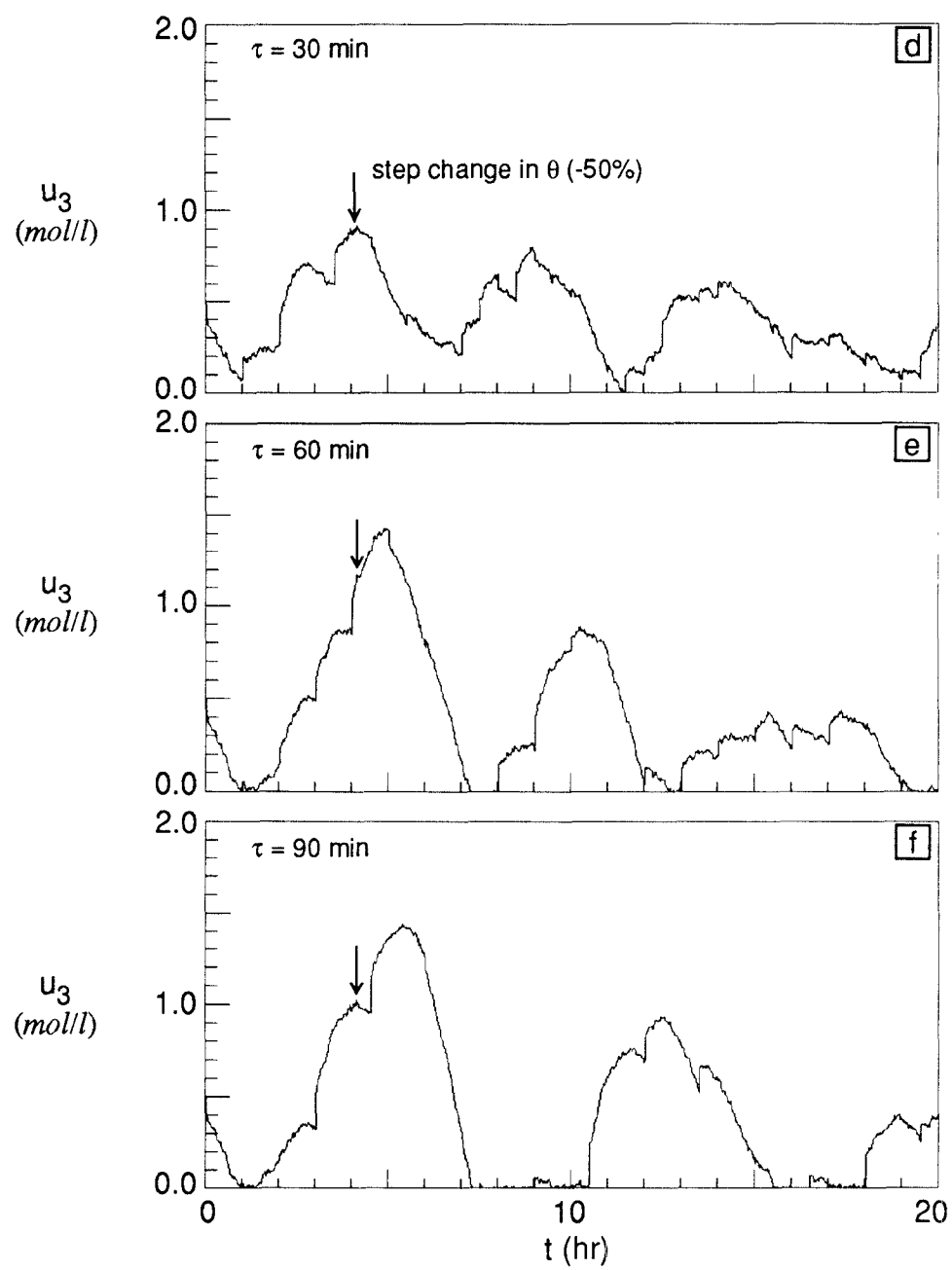
Figure 5.14   (*continued*)

5.5.3. Servo Control

Quite often, it is desired to produce polymers of different grade or properties with an existing reactor system. To do so, some reactor operating conditions may have to be changed in such a way that new target properties can be attained in minimum transition time. One of the key polymer property parameters which affect the end use properties such as melt flow index is the weight average molecular weight or $\overline{X}_w$ (weight average degree of polymerization). Since the $\overline{X}_w$ is controlled by feed chain transfer agent concentration, it is first necessary to see if a new molecular weight is obtainable by changing the chain transfer feed concentration only. Let us suppose that current steady state value of $\overline{X}_w$ is 600 and it is desired to increase the $\overline{X}_w$ value to 1,500. It is also assumed that current monomer conversion and reactor temperature should be maintained. Figure 5.15 shows the $\overline{X}_w$ and $\overline{X}_n$ profiles when the supply of chain transfer agent is completely discontinued. Note that the new steady state $\overline{X}_w$ value is only about 1,300 which is 13% less than the target value. Moreover, the transition time is about 10 hours. Obviously, this is not desirable.

The simulation result shown in Figure 5.15 suggests that in order to increase the $\overline{X}_w$ to 1,500, it will be necessary to change the set points of other reactor variables (e.g., temperature and monomer conversion) simultaneously. This is because the $\overline{X}_w$ is also a function of monomer concentration, initiator
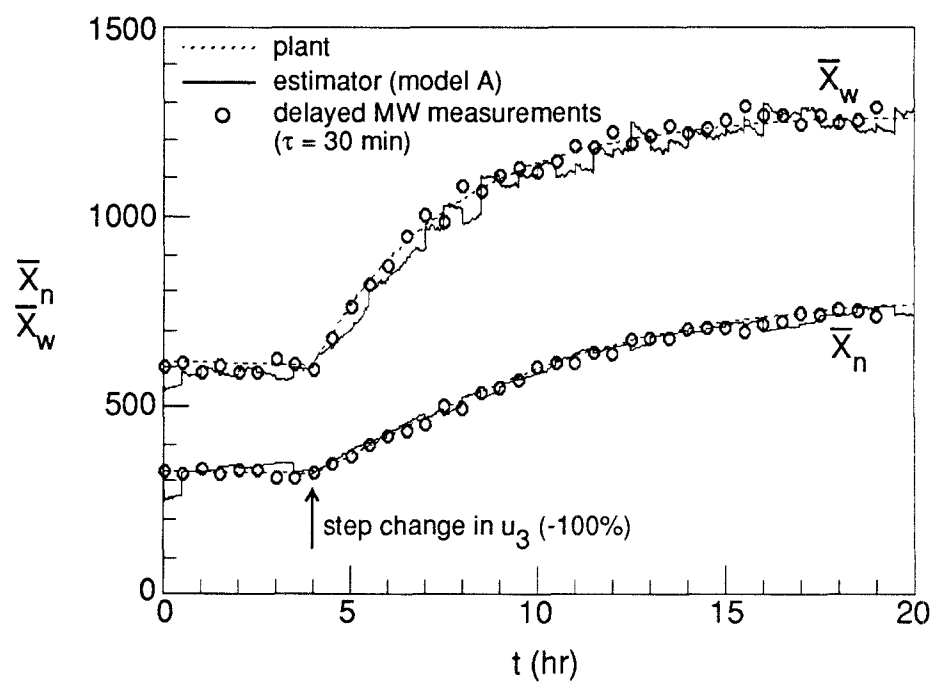
Figure 5.15   Maximum limit of molecular weight control with control variable u_3 only: step change in u_3 (-100%).

concentration and reactor temperature. Since the process models (A and B) are available, one can determine the new set points of reactor temperature and monomer conversion using the steady state diagrams as shown in Figure 5.16 where steady state profiles of monomer conversion, temperature and $\overline{X}_w$ are plotted against the feed initiator concentration for $\theta = 4hr$. In these diagrams, the current operating condition is marked as (A). Note that in order to produce polymers of $\overline{X}_w = 1,500$ (marked as (B)), it is required to change not only the temperature and monomer conversion set points but also the feed initiator concentration. Obviously, there could be a different set of new steady state reaction conditions which may give the same new $\overline{X}_w$ value. For example, one can fix the feed initiator concentration and change the reactor residence time. Figure 5.16 shows that although the new reactor temperature is only slightly lower than the current value, both the new monomer conversion and the feed initiator concentration should be much lower than the current values. Figure 5.17a and 5.17b show the performance of the $\overline{X}_w$ control using delayed measurement data of molecular weight ($\tau = 60$ min) incorporated into the state estimator for model A and B, respectively. In both cases, the target molecular weight is obtained. Moreover, the transition period between the current and new steady states is only about 4 hours which is considerably less than 10 hours as shown in Figure 5.17. Figure 5.17c shows the $\overline{X}_w$ control performance without MW estimator. Here, the delayed measurements of polymer molecular weight are used with a PI controller (The same controller
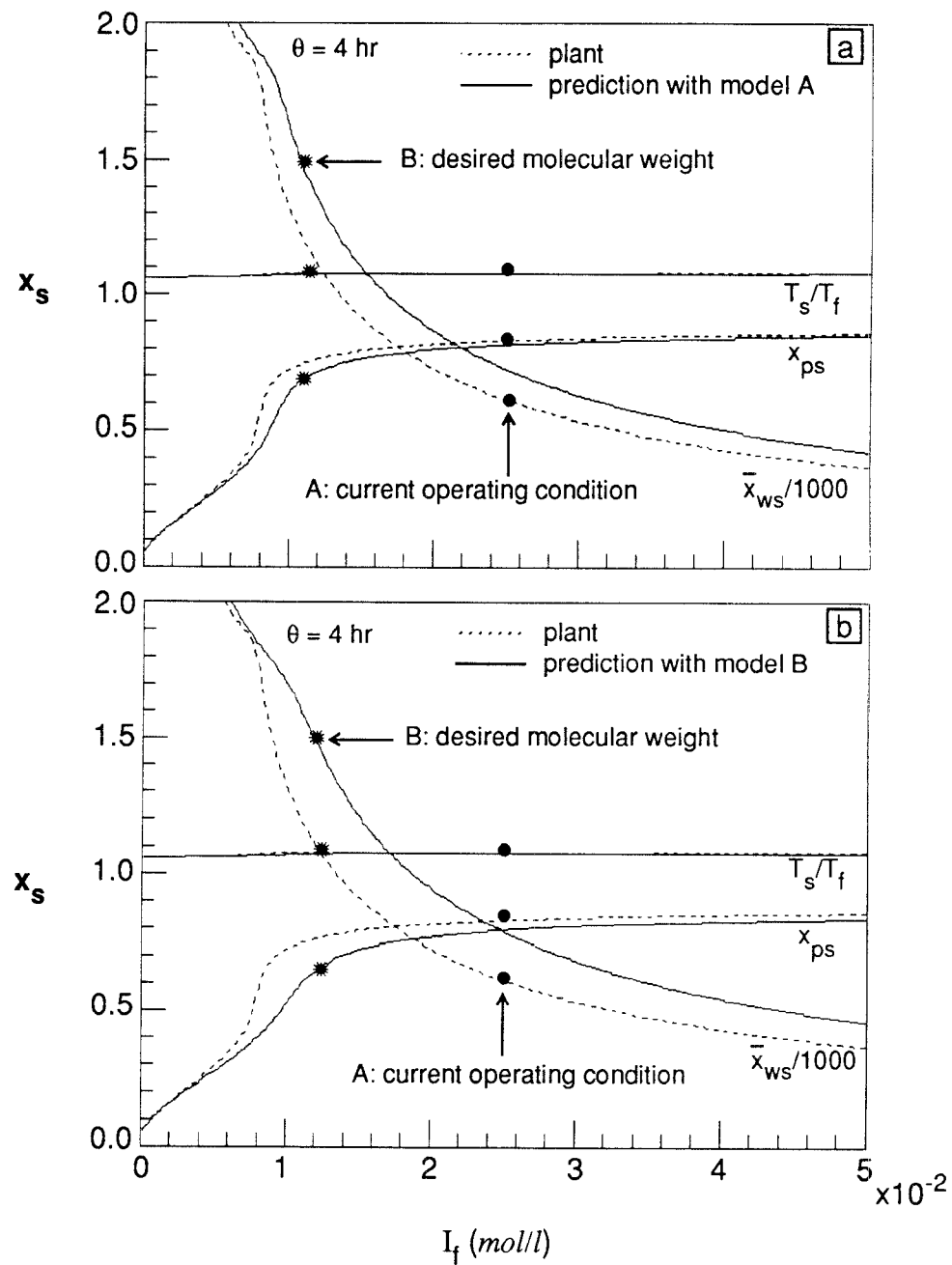
Figure 5.16   Prediction of steady state profiles as function of initiator feed concentration with inaccurate model A and B.
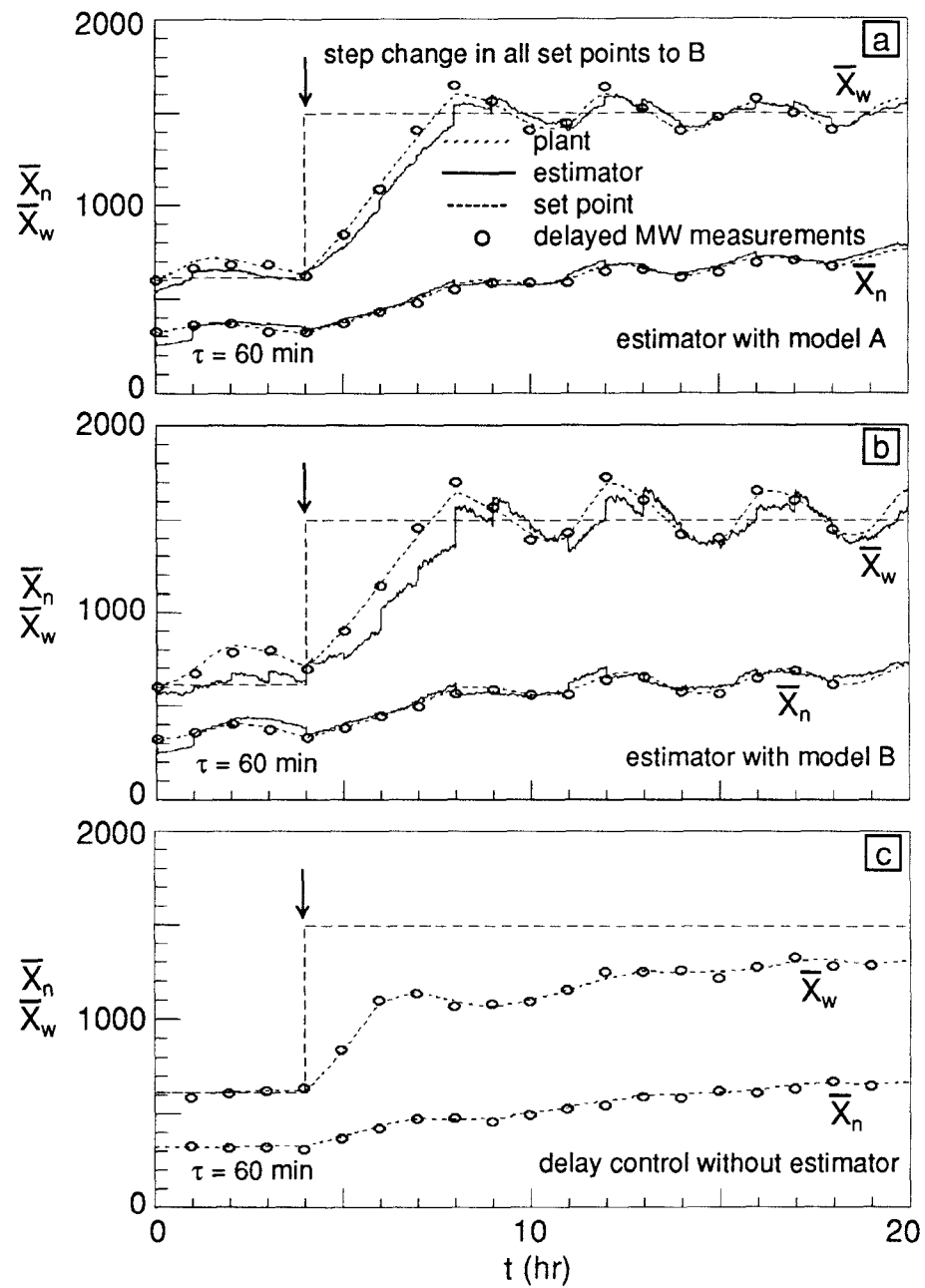
Figure 5.17   Effect of model accuracy on molecular weight control with 60 minute delayed MW measurements based on steady state process model.
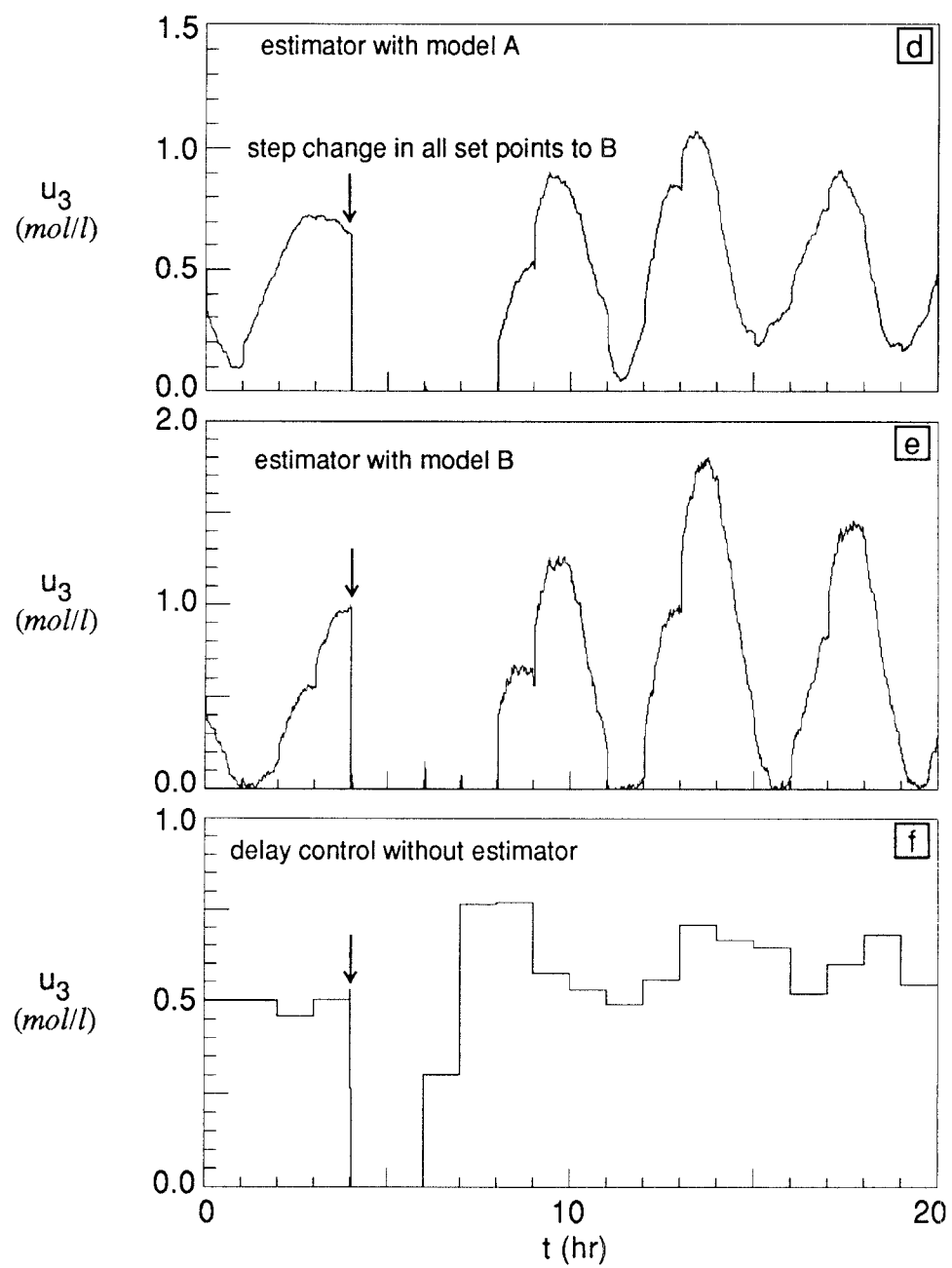
Figure 5.17 (continued)
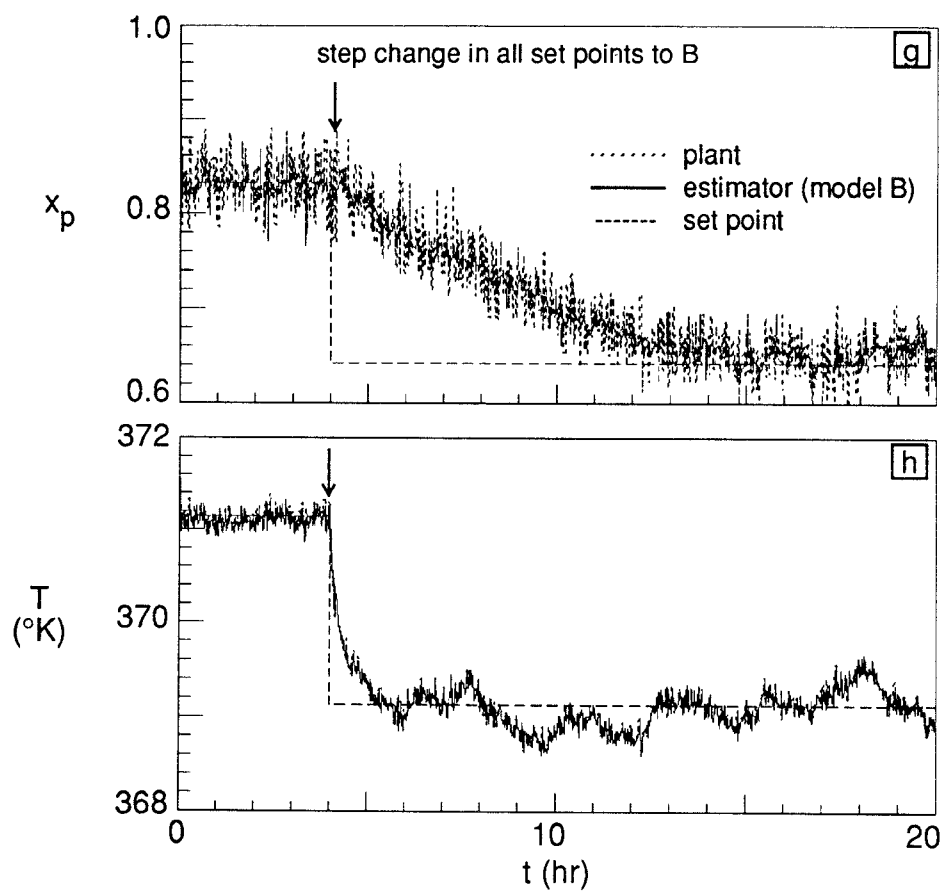
Figure 5.17   *(continued)*

parameters as used in Figure 5.17a and 5.17b were used). Note that the target molecular weight is not attained at all due to integral windup. It should be noted, however, that one can improve the control performance by retuning the controllers on-line. The results shown in Figure 5.17 clearly illustrate the advantage of using an on-line state estimator for servo control in reducing the transition time and obtaining the desired new target values of polymer properties.

5.6. Conclusions

A two time scale extended Kalman filter has been used for the estimation and control of a continuous styrene polymerization reactor. It is shown that even in the presence of some modeling errors, one can obtain quite accurate state estimates when delayed measurement data are incorporated into the filter. This is seen as a main advantage of using the extended Kalman filter with approximate process models. When the model error is large, more frequent MW measurements are required. It has also been illustrated that the polymer grade change can be attained effectively by using the filter in conjunction with the steady state process model.

5.7. Notation

A concentration of chain transfer agent (u_3) (mol/l)

A_c effective heat transfer area (cm^2)

C_p heat capacity of reaction mixture (cal/g$^\circ$K)

C_{p_c} heat capacity of coolant (cal/g$^\circ$K)

f_i efficiency of initiator i, $i = A, B$ (-)

f_s solvent volume fraction (-)

g_t gel effect correlation factor, k_t/k_t^* (-)

h_c overall heat transfer coefficient (cal/cm^{2}sec$^\circ$K)

$(-\Delta H)$ heat of polymerization (cal/mol)

I_f feed concentration of initiator mixture (u_2) (mol/l)

I_i concentration of initiator i in the reactor, $i = A, B$ (mol/l)

k_{d_i} decomposition rate constant of initiator i, $i = A, B$ (sec^{-1})

k_{d_M} rate constant of thermal initiation ((l/mol)^2/sec)

k_i initiation rate constant (1/mol.sec)

k_{fa} rate constant of chain transfer to chain transfer agent (1/mol.sec)

k_{fm} rate constant of chain transfer to monomer (1/mol.sec)

k_p propagation rate constant (1/mol.sec)

k_t termination rate constant (1/mol.sec)

k_t^* termination rate constant at zero monomer conversion (1/mol.sec)

M monomer concentration in the reactor (mol/l)

M_f feed concentration of monomer (mol/l)

P concentration of live polymers (mol/l)

q flow rate of reactant mixture (l/sec)

q_c flow rate of coolant (l/sec)

q_{x_i} standard deviation of model error of x_i, $i = 1, 2, 3, 4, 5, 6$ (-)

r_{x_i} standard deviation of measurement error of x_i, $i = 1, 4, 5, 6$ (-)

T reactor temperature (°K)

T_c coolant temperature in the coolant jacket (°K)

T_{cf} feed temperature of coolant (u_1) (°K)

T_f feed temperature of reactant mixture (°K)

t time (sec)

V reactor volume (cm^3)

V_c volume of coolant jacket (cm^3)

$\overline{X}_n$ number average chain length (-)

$\overline{X}_w$ weight average chain length (-)

x_p polymer weight fraction(-)

y_{Af} initiator feed composition of I_A (-)

Greek Letters

α probability of propagation of a chain radical (-)

θ mean reactor residence time (hr)

θ_c mean residence time of the coolant jacket (hr)

λ_k kth moment of dead polymer (-)

λ_{kr} reference value of kth moment (-)

ν ratio of heat capacity of reaction mixture to that of coolant (-)

ρ density of reaction mixture (g/cm^3)

ρ_c density of coolant (g/cm^3)

τ time delay of off-line measurement (min)

Vectors and Matrices

$\boldsymbol{f}$ system state model

$\boldsymbol{h}$ system measurement model

$\boldsymbol{x}$ system state vector

$\boldsymbol{x}_0$ initial state vector

$\hat{\boldsymbol{x}}$ estimated state vector by the state estimator

$\boldsymbol{u}$ system control vector

$\boldsymbol{v}$ measurement error vector

$\boldsymbol{w}$ model error vector

$\boldsymbol{y}$ measurement vector

$\boldsymbol{F}$ jacobian matrix of $\boldsymbol{f}$

$\boldsymbol{H}$ jacobian matrix of $\boldsymbol{h}$

$\boldsymbol{K}$ Kalman gain matrix

$\boldsymbol{L}_0$ observability matrix

$\boldsymbol{P}$ estimation error covariance matrix

$\boldsymbol{P}_0$ initial estimation error covariance matrix

$\boldsymbol{Q}$ model error covariance matrix

$\boldsymbol{R}$ measurement error covariance matrix

Chapter 6

On-line Estimation and Control of Batch Polymerization Reactors

6.1. Introduction

In the previous chapter, the feasibility of feedback control of polymer molecular weight in a continuous styrene polymerization reactor has been investigated by using a two-time scale extended Kalman filter. During the steady state reactor operations, the feedback control with the filter showed a good regulatory control performance even in the presence of moderate model errors and unknown disturbances. When the desired polymer molecular weight is changed from one value to another, the corresponding new steady state reactor operating condition can be chosen by using the steady state model.

The next step is to determine how the reactor is driven from one steady state to another steady state economically and safely. This control problem is similar to the control problem in batch or semibatch polymerization reactors, *i.e.*, to design optimal controls to achieve desired product specifications in minimum reaction time. Since on-line measurements of polymer properties are also difficult in batch processes, batch polymerization reactors are usually controlled by controlling the reactor temperature profiles which would give desired final polymer properties. Quite often, these temperature profiles are determined empirically or by using process models, if available. When the reactor control policy is determined using the process model, there is always a possibility that the model has some uncertainties and that unknown process disturbances can cause the deviations in the resulting polymer properties from their target values.

Moreover, when a large polymerization reactor is used, the effect of cooling jacket dynamics on the reactor dynamics can be significant [Wu (1985)]. For example, as the holding time of the cooling jacket increases, the reactor temperature response becomes sluggish, which may result in thermal runaway. As discussed in Chapter 4, the heat transfer coefficient of the reactor can also decrease during the course of polymerization. Therefore, on-line state estimation technique can also be useful in batch processes with time varying heat transfer coefficient to improve the MW control.

In this chapter, the performance of the two-time scale extended Kalman

filter is evaluated for the estimation of polymer molecular weight parameters in a batch polymerization reactor. The polymerization system considered here is methyl methacrylate (MMA) solution polymerization initiated by azobisisobutyronitrile (AIBN). The effect of cooling jacket dynamics on the reactor control will also be investigated. In particular, the prediction of the reactor heat transfer coefficient will be attempted using the filter.

6.2. Reactor Model

A kinetic scheme for MMA solution polymerization with AIBN and ethyl acetate as a solvent is shown in Table 6.1. In this kinetic scheme, primary radical termination is assumed negligible. No induced decomposition occurs with AIBN initiator. Chain termination occurs primarily by the disproportionation mechanism. The MMA polymerization is known to exhibit much stronger gel effect than styrene polymerization. In this study, the gel effect correlation proposed by Ross and Laurence (1976) for bulk MMA polymerization is used and modified for solution polymerization:

$$g_t = 0.10575\exp[17.15V_f - 0.01715(T - 273.2)]$$

$$\text{for } V_f > 0.1856 - 2.965 \times 10^{-4}(T - 273.2) \quad (6.1a)$$

$$= 2.3 \times 10^{-6}\exp[75V_f]$$

$$\text{for } V_f \geq 0.1856 - 2.965 \times 10^{-4}(T - 273.2)$$

Table 6.1   Kinetic scheme of MMA polymerization

Initiation by initiators:

$$I \xrightarrow{k_d} 2R$$

$$R + M \xrightarrow{k_i} P_1$$

Propagation:

$$P_n + M \xrightarrow{k_p} P_{n+1} \qquad (n \geq 1)$$
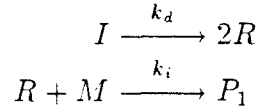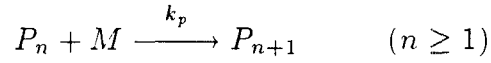
Chain transfer to monomer and solvent:

$$P_n + M \xrightarrow{k_{fm}} M_n + P_1 \qquad (n \geq 1)$$

$$P_n + S \xrightarrow{k_{fs}} M_n + P_1 \qquad (n \geq 1)$$
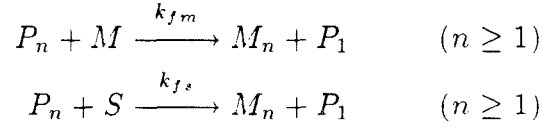
Termination (disproportionation only):

$$P_n + P_m \xrightarrow{k_t} M_n + M_m \qquad (n, m \geq 1)$$
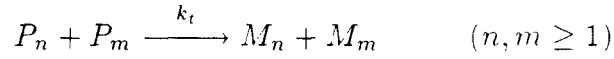
$$g_p = 1.0 \qquad\qquad\qquad \text{for } V_f > 0.05 \qquad (6.1b)$$

$$= 7.1 \times 10^{-5} \exp[171.53 V_f] \qquad \text{for } V_f \geq 0.05$$

where g_t is the gel effect coefficient for chain termination reactions (k_t/k_t^*) and g_p is the gel effect coefficient for chain propagation reactions (k_p/k_p^*). Here the free volume, V_f is defined by

$$V_f = 0.025 + \alpha_m(T - T_{gm})\phi_m + \alpha_p(T - T_{gp})\phi_p + \alpha_s(T - T_{gs})\phi_s \quad (6.1c)$$

$$\alpha_m = 0.001 \qquad \alpha_p = 0.00048 \qquad \alpha_s = 0.0001$$

$$T_{gm} = 167°\text{K} \qquad T_{gp} = 387°\text{K} \qquad T_{gm} = 181°\text{K}$$

The subscripts m, p and s represent monomer, polymer and solvent, respectively. α_j denotes the thermal expansion coefficient and T_{gj} the glass transition temperature of component j. ϕ_j is the volume fraction of each component and expressed by

$$
\begin{aligned}
\phi_m &= \left(\frac{M_o w_m}{1000 \rho_m} \right) \frac{1 - X_1}{1 + \epsilon X_1} \\
\phi_p &= \left(\frac{M_o w_m}{1000 \rho_p} \right) \frac{X_1}{1 + \epsilon X_1} \\
\phi_s &= 1 - (\phi_m + \phi_p)
\end{aligned}
\qquad (6.1d)
$$

where M_o is the initial monomer concentration and X_1 the monomer conversion, respectively. w_m is the molecular weight of monomer and ρ_j the density of component j. Due to a large density difference between the polymer and the monomer, a volume contraction factor, ϵ, is used to account for the density variation of the reaction mixture:

$$
\epsilon = \frac{w_m(1 - f_s)(1/\rho_p - 1/\rho_m)}{w_m(1 - f_s)/\rho_m + w_s f_s/\rho_s}
\qquad (6.2)
$$

where f_s is the mole fraction of solvent.

Then, the mass and energy balance equations for a batch polymerization reactor with a cooling jacket take the following form:

$$\frac{1}{V}\frac{d}{dt'}(MV) = -k_p MP, \qquad\qquad M(0) = M_o \quad (6.3)$$

$$\frac{1}{V}\frac{d}{dt'}(MV) = -k_d I, \qquad\qquad I(0) = I_o \quad (6.4)$$

$$\frac{1}{V}\frac{d}{dt'}(MV) = -k_{fm} SP, \qquad\qquad S(0) = S_o \quad (6.5)$$

$$\rho C_p V \frac{dT}{dt'} = V(-\Delta H)k_p MP - U_c A_c(T - T_c),$$

$$T(0) = T_o \quad (6.6)$$

$$\rho_c C_{pc} V_c \frac{dT_c}{dt'} = \rho_c C_{pc} q_c(T_{cf} - T_c) + U_c A_c(T - T_c),$$

$$T_c(0) = T_{co} \quad (6.7)$$

where M, I, S denote the concentrations of monomer. initiator and solvent. respectively. The subscript c denotes the coolant. Physical properties of the polymerizing mixture and the coolant are assumed constant. The total concentration of live polymers, P, is derived by applying the quasi-steady state approximation to live radical species:

$$P = \left(\frac{2fk_d I}{k_t}\right)^{1/2} \qquad\qquad (6.8)$$

Since the concentration of live polymers is negligibly small. the average molecular weights of the polymer can be calculated from the moments of dead polymers only. The three leading moment equations for dead polymers are

$$\frac{1}{V}\frac{d}{dt'}(\lambda_0 V) = (1 - \alpha)k_p MP \qquad\qquad (6.9)$$

$$\frac{1}{V}\frac{d}{dt'}(\lambda_1 V) = (2-\alpha)k_p M P \tag{6.10}$$

$$\frac{1}{V}\frac{d}{dt'}(\lambda_2 V) = \left(\frac{4-3\alpha+\alpha^2}{1-\alpha}\right)k_p M P \tag{6.11}$$

$$\lambda_j(0) = 0 \quad \text{for } j = 0, 1, 2$$

where the probability of propagation, α, is defined by

$$\alpha \equiv \frac{k_p M}{k_p M + k_{fm} M + k_{fs} S + k_t P} \tag{6.12}$$

The above reactor modeling equations (6.3)~(6.12) can be reduced to a following dimensionless form by using the dimensionless variables and parameters given in Table 6.2:

$$\frac{dx_1}{dt} = -Da(1+\epsilon x_1)x_1 x_2^{1/2}(g_p/g_t^{1/2})\exp\left(-\frac{\gamma}{x_4}\right), \qquad x_1(0) = 1 \tag{6.13}$$

$$\frac{dx_2}{dt} = -Da x_2 \zeta x_2 \exp\left(-\frac{\gamma_d}{x_4}\right) - Da\epsilon x_1 x_2^{3/2}(g_p/g_t^{1/2})\exp\left(-\frac{\gamma}{x_4}\right),$$

$$x_2(0) = 1 \tag{6.14}$$

$$\frac{dx_3}{dt} = -Da\epsilon x_1 x_2^{1/2} x_3 (g_p/g_t^{1/2})\exp\left(-\frac{\gamma}{x_4}\right), \qquad x_3(0) = 1 \tag{6.15}$$

$$\frac{dx_4}{dt} = \beta Da x_1 x_2^{1/2}(g_p/g_t^{1/2})\exp\left(-\frac{\gamma}{x_4}\right) - \Theta(x_4 - \delta), \quad x_4(0) = 1 \tag{6.16}$$

$$\frac{dx_5}{dt} = [\mu_o(1-\alpha) - \epsilon x_5]Da x_1 x_2^{1/2}(g_p/g_t^{1/2})\exp\left(-\frac{\gamma}{x_4}\right),$$

$$x_5(0) = 0 \tag{6.17}$$

$$\frac{dx_6}{dt} = [\mu_1(2-\alpha) - \epsilon x_6]Da x_1 x_2^{1/2}(g_p/g_t^{1/2})\exp\left(-\frac{\gamma}{x_4}\right),$$

$$x_6(0) = 0 \tag{6.18}$$

348

Table 6.2   Dimensionless parameters and variables.

$$x_1 = \frac{M}{M_o}, \qquad x_2 = \frac{I}{I_o}, \qquad x_3 = \frac{S}{S_o}, \qquad x_4 = \frac{T}{T_o},$$

$$x_5 = \frac{\lambda_0}{\lambda_{0,r}}, \qquad x_6 = \frac{\lambda_1}{\lambda_{1,r}}, \qquad x_7 = \frac{\lambda_2}{\lambda_{2,r}},$$

$$\delta = \frac{T_c}{T_o}, \qquad \delta_f = \frac{T_{cf}}{T_o}, \qquad t = t'/t_o \qquad \theta_c = \frac{q_c t_o}{V_c}$$

$$Da = t_o Z, \qquad \zeta = \frac{k_{do}}{Z}, \qquad \beta = \frac{(-\Delta H) M_o}{\rho C_p T_o},$$

$$\epsilon_c = \frac{\rho C_p V}{\rho_c C_{pc} V_c}, \qquad \Theta = \frac{t_o U_c A_c}{\rho C_p V}, \qquad \gamma = \frac{E}{RT_o}, \qquad \gamma_d = \frac{E_d}{RT_o},$$

$$\gamma_m = \frac{E_p - E_{fm}}{RT_o}, \qquad \gamma_s = \frac{E_p - E_{fs}}{RT_o}, \qquad \gamma_t = \frac{E_p - (E_d + E_t)/2}{RT_o},$$

$$\alpha_m = \frac{k_{fmo}}{k_{po}^*}, \qquad \alpha_s = \frac{k_{fmo} S_o}{k_{po}^* M_o}, \qquad \alpha_t = \frac{(2 f k_{do} k_{to}^* I_o)^{1/2}}{k_{po}^* M_o}.$$

$$\text{for} \quad j = 0, 1, 2; \qquad \mu_j = \frac{M_o}{\lambda_{jr}}$$

where

$$Z = k_{po}^* \left(\frac{2 f k_{do} I_o}{k_{to}^*} \right)^{1/2}$$

$$E = E_p + (E_d - E_t)/2$$

$$\frac{dx_7}{dt} = \left[\mu_2 \left(\frac{4 - 3\alpha + a^2}{1 - \alpha} \right) - \epsilon x_7 \right] Dax_1 x_2^{1/2} (g_p / g_t^{1/2}) \exp\left(-\frac{\gamma}{x_4} \right),$$

$$x_7(0) = 0 \quad (6.19)$$

$$\frac{d\delta}{dt} = \theta_c(\delta_f - \delta) + \epsilon_c \Theta(x_4 - \delta), \qquad \delta(0) = \delta_o \quad (6.20)$$

where

$$\alpha = \left[1 + \frac{\alpha_m}{g_p} \exp\left(\frac{\gamma_m}{x_4} \right) + \frac{\alpha_s x_3}{g_p x_1} \exp\left(\frac{\gamma_s}{x_4} \right) + \frac{\alpha_t (g_t x_2)^{1/2}}{g_p x_1} \exp\left(\frac{\gamma_t}{x_4} \right) \right]^{-1} \quad (6.21)$$

The kinetic and physical constants used in the simulations are given in Table 6.3.

The above model has been tested on the experimental data reported by Balke and Hamielec (1973), as shown in Figure 6.1. For the range of reaction temperature and initiator concentration, the model shows a very good agreement with the experimental data. Thus, this model will be used as a plant simulator in the following sections.

Table 4.3   Numerical values of kinetic of physical constants for MMA polymerization

---

$k_d = 1.0 \times 10^{15} \exp(\text{-}30{,}700/RT)$, $\sec^{-1}$ *

   $f_A = 0.44$ *

$k_p^* = 6.6 \times 10^5 \exp(\text{-}4{,}700/RT)$, l/mol.sec *

$k_t^* = 8.0 \times 10^8 \exp(\text{-}2.313/RT)$, 1/mol.sec *

$k_{fs} = 1.2362 \times 10^4 \exp(\text{-}8{,}990/RT)$, 1/mol.sec †

$k_{fm} = 1.9344 \times 10^{11} \exp(\text{-}20{,}262/RT)$, 1/mol.sec †

$\rho_m = 0.9654 - 0.00109 T(C) - 9.7 \times 10^{-7} T^2(C)$, g/cm^3 ‡

$\rho_p = \frac{\rho_m}{0.754 - 9 \times 10^{-4}(T(C) - 70)}$, g/cm^3 ‡

$\rho_s = 0.925 - 1.239 \times 10^{-3} T(C)$, g/cm^3 ‡

$w_m = 100.12$, g/mol, $w_s = 88.1$, g/mol,

$\Delta H_r = \text{-}14.97$ kcal/mol †

$\rho C_p = 0.4$ kcal/l°K †

$\rho_c C_{pc} = 1.0$ kcal/l°K †

$\lambda_{0,r} = 1.86 \times 10^{-3}$ $\lambda_{1,r} = 2.56$ $\lambda_{2,r} = 7{,}420$

---

* Ross and Laurence (1983)

† Brandrup and Immergut (1989)

‡ Schmidt *et al.* (1984).
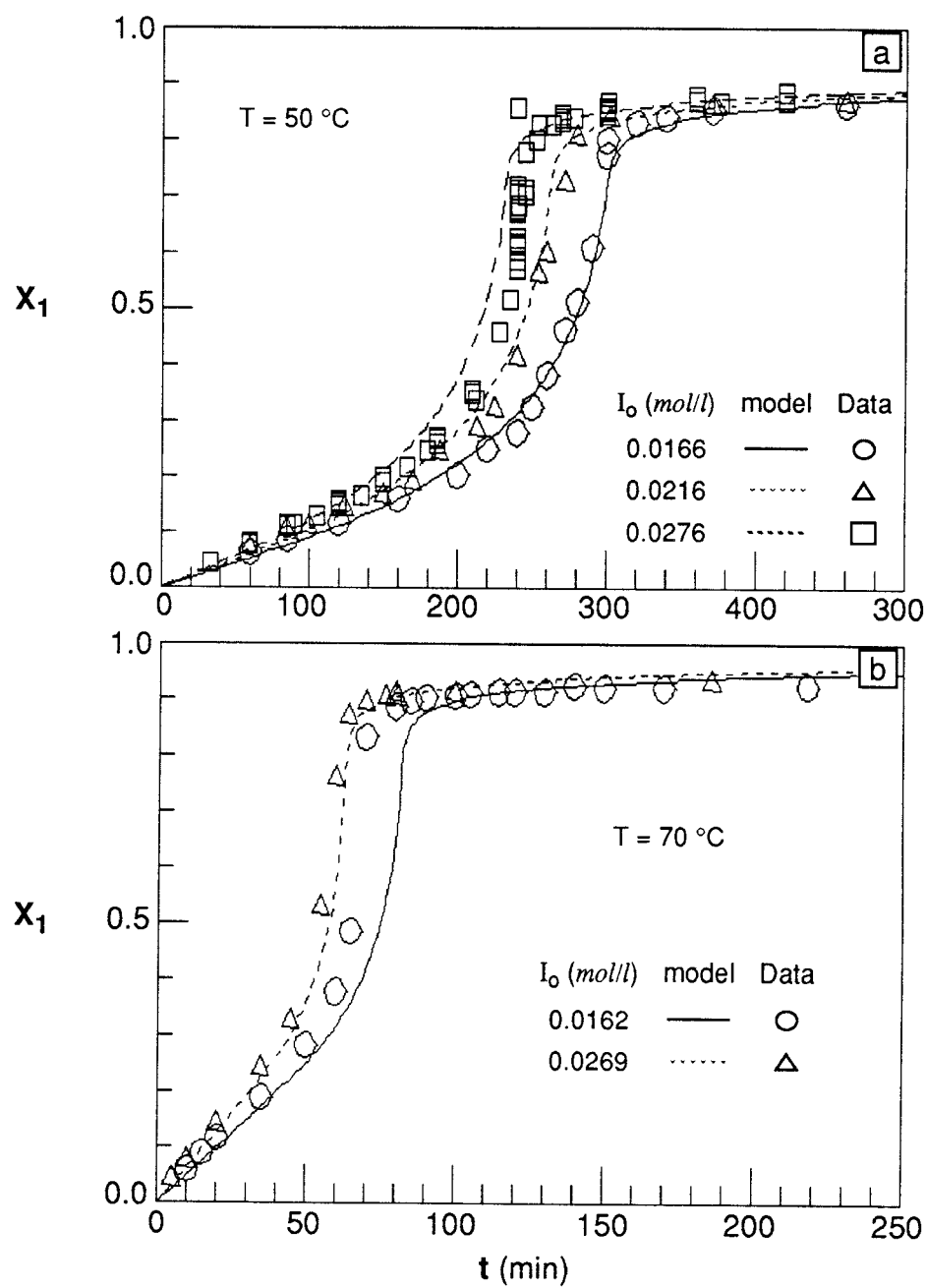
Figure 6.1   Isothermal bulk polymerization of MMA: data from Balke and Hamielec (1973).

6.3. Estimation of Polymer Molecular Weights

The two-time scale state estimation algorithm has been described in §5.4 and will be used here for batch processes. In order to investigate the effect of modeling errors, numerical values of some kinetic parameters in the reactor model are changed from the true values as follows: the rate constant of chain transfer to monomer (k_{fm}) is reduced by 10 %; densities of monomer, solvent and polymer are assumed constant; the gel effect for the propagation rate constant (g_p) is assumed negligible.

The original reactor model is used to simulate the plant and the modified model with inaccurate kinetic parameters is used filtering. It is assumed that the monomer conversion (X_1), the reactor temperature (T), and the coolant inlet and outlet temperatures (T_{cf}, T_c) are monitored on-line. It is desired that the average polymer chain lengths ($\overline{X}_n$, $\overline{X}_w$) are measured by GPC with 30~60 minute time delay. All these measurements are assumed to be corrupted by white noise. From the measured monomer conversion and the initial monomer concentration, the relative concentration of monomer (x_1) and the first moment of dead polymer (x_6), which is the total concentration of the polymer, are directly estimated:

$$x_6 = \frac{\lambda_1}{\lambda_{1,r}} \approx \frac{M_o(1 - X_1)}{\lambda_{1,r}} \qquad (6.22)$$

The zeroth and the second moments of the polymer can be calculated by using

the measured molecular weights and the polymer concentrations:

$$x_5 = \frac{x_6}{\overline{X}_n} \frac{\lambda_{1,r}}{\lambda_{0,r}} \approx \frac{M_o(1-X_1)}{\overline{X}_n \lambda_{0,r}} \tag{6.23a}$$

$$x_7 = \overline{X}_w x_6 \frac{\lambda_{1,r}}{\lambda_{2,r}} \approx \frac{\overline{X}_w M_o(1-X_1)}{\lambda_{2,r}} \tag{6.23b}$$

Thus, there are 5 state variables to estimate and they are: concentrations of monomer (x_1), initiator (x_2), reactor temperature (x_4), the zeroth moment (x_5) and the second moment (x_7). Note that the concentration of solvent is excluded from the estimation algorithm because its consumption by chain transfer reaction is very small and negligible.

The two measurement equations, $\boldsymbol{y}_{o,k}$ and $\boldsymbol{y}_{d,k-\tau}$, without and with delayed MW measurements are expressed as follows:

$$\boldsymbol{y}_{o,k} = \begin{pmatrix} y_{1,k} \\ y_{2,k} \end{pmatrix} = \begin{pmatrix} x_{1,k} \\ x_{4,k} \end{pmatrix} + \boldsymbol{v}_{o,k} \tag{6.24}$$

$$\boldsymbol{y}_{d,k-\tau} = \begin{pmatrix} y_{1,k-\tau} \\ y_{2,k-\tau} \\ y_{3,k-\tau} \\ y_{4,k-\tau} \end{pmatrix} = \begin{pmatrix} x_{1,k-\tau} \\ x_{4,k-\tau} \\ x_{5,k-\tau} \\ x_{7,k-\tau} \end{pmatrix} + \boldsymbol{v}_{d,k-\tau} \tag{6.25}$$

The measurement error covariance for each case is a diagonal matrix:

$$\boldsymbol{R}_{o,k} = diag\{r_{x_1}^2, r_{x_4}^2\} \tag{6.26}$$

$$\boldsymbol{R}_{d,k-\tau} = diag\{r_{x_1}^2, r_{x_4}^2, r_{x_5}^2, r_{x_7}^2\} \tag{6.27}$$

where r_{x_i} is the standard deviation of the measurement error for x_i.

354

Without any MW measurements, the observability matrix L_o is expressed as follows:

$$
L_o = \begin{pmatrix}
1 & 0 & \vdots & f_{11} & f_{31} & \vdots & f'_{11} & f'_{31} & \vdots & f''_{11} & f''_{31} & \vdots & \\
0 & 0 & \vdots & f_{12} & f_{32} & \vdots & f'_{12} & f'_{32} & \vdots & f''_{12} & f''_{32} & \vdots & \\
0 & 1 & \vdots & f_{13} & f_{33} & \vdots & f'_{13} & f'_{33} & \vdots & f''_{13} & f''_{33} & \vdots & \ldots \\
0 & 0 & \vdots & 0 & 0 & \vdots & 0 & 0 & \vdots & 0 & 0 & \vdots & \\
0 & 0 & \vdots & 0 & 0 & \vdots & 0 & 0 & \vdots & 0 & 0 & \vdots &
\end{pmatrix}
\qquad (6.28)
$$

where $\{f_{ij}\}$ are the elements of the Jacobian matrix (F) of the process model, $\{f'_{ij}\}$ the elements of F^2 and $\{f''_{ij}\}$ the elements of F^3. The rank of the observability matrix is 3 and thus the system is not observable. When the MW measurements (delayed) are provided, the observability matrix L_d becomes

$$
L_d = \begin{pmatrix}
1 & 0 & 0 & 0 & \vdots & f_{11} & f_{31} & f_{41} & f_{51} & \vdots & f'_{11} & f'_{31} & f'_{41} & f'_{51} & \vdots & \\
0 & 0 & 0 & 0 & \vdots & f_{12} & f_{32} & f_{42} & f_{52} & \vdots & f'_{12} & f'_{32} & f'_{42} & f'_{52} & \vdots & \\
0 & 1 & 0 & 0 & \vdots & f_{13} & f_{33} & f_{43} & f_{53} & \vdots & f'_{13} & f'_{33} & f'_{43} & f'_{53} & \vdots & \ldots \\
0 & 0 & 1 & 0 & \vdots & 0 & 0 & f_{44} & 0 & \vdots & 0 & 0 & f'_{44} & 0 & \vdots & \\
0 & 0 & 0 & 1 & \vdots & 0 & 0 & 0 & f_{55} & \vdots & 0 & 0 & 0 & f'_{55} & \vdots &
\end{pmatrix}
$$

$$(6.29)$$

where f_{44}, f_{55}, f'_{44} and f'_{55} are non-zero elements. The rank of this matrix is 5 and thus the system is observable.

Figure 6.2 shows the performance of the filter with the inaccurate model during the course of MMA solution polymerization in a pilot scale batch reactor without any controllers. The measurement errors have been generated

Figure 6.2   Estimation of open loop MMA polymerization in a pilot scale batch reactor: $f_s = 0.5$, $I_o = 0.02$ mol/l, $T_o = 30$ °C, $T_{cf} = 60$ °C.

Table 6.4   Design specifications of MMA batch reactors

	Pilot scale	Industrial scale
V (l)	1	19,000
A_c (cm^2)	485	591,000
A_c/V (cm^2/l)	485	31
h_c $(kcal/cm^2 s°K)$	1.086×10^{-5}	0.6788×10^{-5}
θ_c (min)	0.5	2

by a pseudo-random number generator and added to the x values to produce the measured variables (y). The perturbation is assumed to fall within the prespecified standard deviation of each measurement, $i.e.$, ± 0.02 for monomer conversion, ± 0.5 °C for reactor temperature and 5 % for $\overline{X}_n$ and $\overline{X}_w$. Sampling time for the on-line measurements of monomer conversion and temperature is 1 min. The numerical values of the reactor design specification and the initial filter parameters are given in Table 6.4 and 6.5, respectively. Note that the design specification of the pilot plant is for the bench scale pilot reactor in our research laboratory. This reactor is designed to have highly efficient heat removal capacities so that the isothermal operation can be possible even without temperature controllers. As shown in Figures 6.2a and 6.2b, the monomer conversion (X_1), reactor temperature (T) and the initiator conversion (X_2) converges to true value after 150 min. As shown in Figure 6.2b, the reactor temperature is very close to the coolant inlet temperature because the heat

Table 6.5   Numerical values of initial parameters of the filter

Model error covariance, $\boldsymbol{Q}$:

$$q_{11} = 1 \times 10^{-3} \quad q_{22} = 1 \times 10^{-1} \quad q_{33} = 1 \times 10^{-3}$$

$$q_{44} = 1 \times 10^{-1} \quad q_{55} = 1 \times 10^{-1}$$

Measurements error covariance, $\boldsymbol{R}$:

$$r_{11} = 4.0 \times 10^{-4} \quad r_{22} = 2.25 \times 10^{-6}$$

$$r_{33} = 2.5 \times 10^{-3} \quad r_{44} = 2.5 \times 10^{-3}$$

Esstimation error covariance, $\boldsymbol{P}$:

$$p_{11} = 1 \times 10^{-2} \quad p_{22} = 1 \times 10^{-2} \quad p_{33} = 1 \times 10^{-2}$$

$$p_{44} = 1 \times 10^{-2} \quad p_{55} = 1 \times 10^{-2}$$

Initial estimation, $\hat{\boldsymbol{x}}_o$:

$$\hat{x}_{1,o} = 0.95x_1(0) \quad \hat{x}_{2,o} = 0.97x_2(0) \quad \hat{x}_{4,o} = 0.05x_4(0)$$

$$\hat{x}_{5,o} = x_5(0) \quad \hat{x}_{7,o} = 0.95x_7(0)$$

removal capacity of the pilot scale reactor is very large and the jacket holding time is very small. The heat transfer coefficient was also predicted using the energy balance equation of the jacket (6.20) and temperatures of the reactor and the jacket inlet and outlet:

$$\Theta = \frac{1}{\epsilon_c(\hat{x}_4 - \delta)} \left[\frac{d\delta}{dt} - \theta_c(\delta_f - \delta) \right] \qquad (6.30)$$

Θ is the dimensionless heat transfer coefficient, ϵ_c the heat capacity ratio

of reaction mixture to coolant, θ_c the dimensionless jacket holding time, δ the dimensionless jacket temperature and δ_f the dimensionless jacket inlet temperature. All these parameters are defined in Table 6.2. The gradient of coolant temperature in the jacket ($\frac{d\delta}{dt}$) is approximated by using Taylor series expansion. The heat transfer coefficient prediction shown in Figure 6.2c is noisy because jacket wall temperature gradient is quite small and the difference between the inlet and outlet jacket temperature is also small. To improve the prediction of the heat transfer coefficient, the coolant flow rate should be kept low to ensure large temperature differences between the jacket inlet and outlet. Of course, it should not jeopardize the cooling efficiency.

When the delayed MW measurements are not available, the filter predicts the polymer molecular weights ($\overline{X}_n$, $\overline{X}_w$) with large errors because of model errors and no corrective actions (Figure 6.3a). With delayed MW measurements, the MW estimation of the filter improves dramatically (Figures 6.3b and 6.3c). When MW measurements are provided with 30 minute delay, the filter converges after about 150 min. As the measurement time delay increases, the MW estimation converges slowly. Since the polymer properties in a batch reactor are affected by the reaction history, accurate MW estimation and fast convergence of the estimation are required for a feedback control. The simulation results shown in Figures 6.2 and 6.3 indicate that the filter provides an adequate MW prediction; however, if the total batch time is much shorter than 400 min, faster filter convergence will be required. When model errors
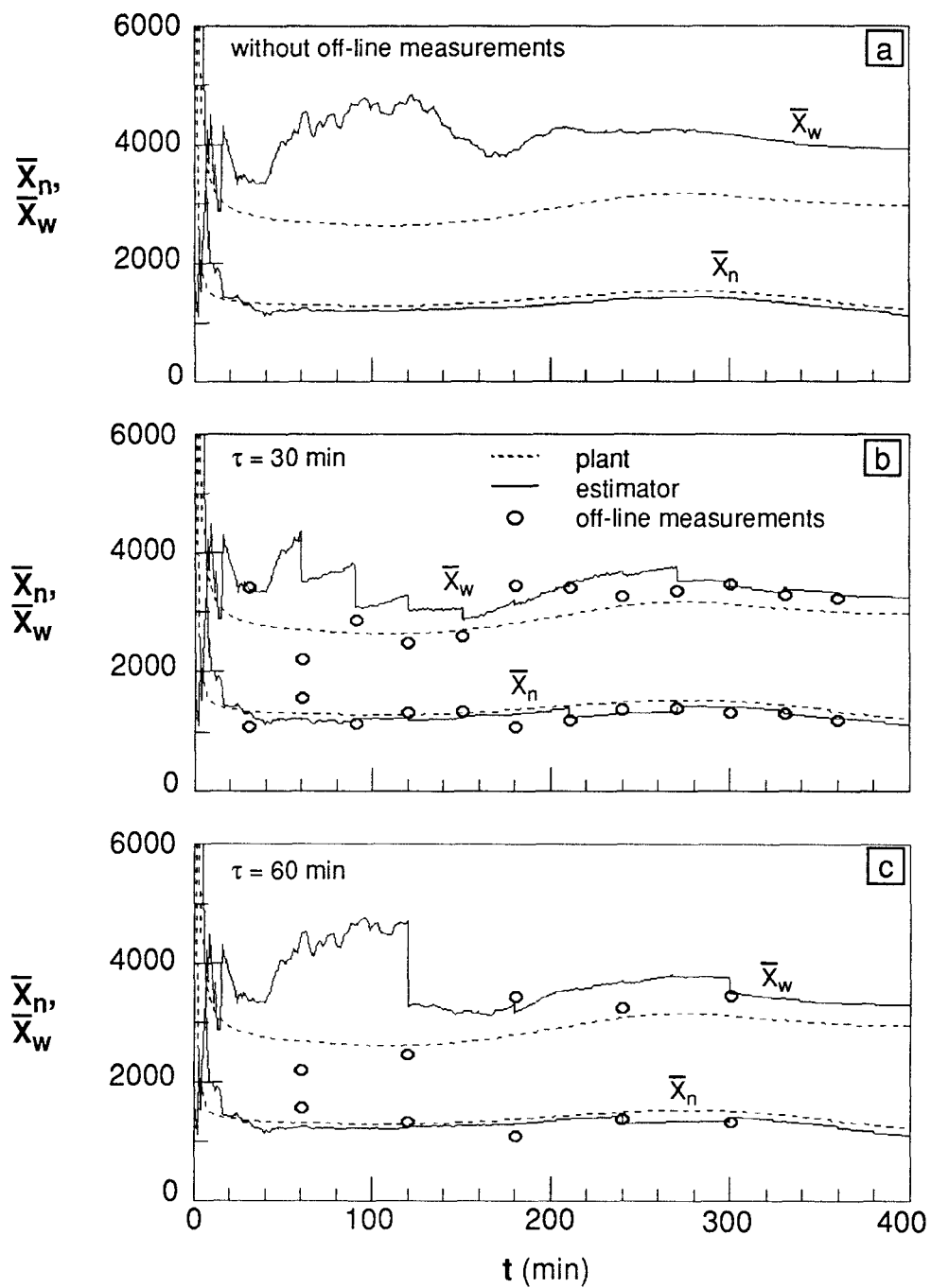
Figure 6.3   Effect of delayed measurements on MW estimation during open loop MMA polymerization in a pilot scale batch reactor: $f_s = 0.5$, $I_o = 0.02$ mol/l, $T_o = 30$ °C, $T_{cf} = 60$ °C.

are significant, the process model used in the estimation algorithm violates its assumption of unbiased white noise. Addition of the following biased disturbance term into the model can improve the estimation algorithm:

$$\dot{\boldsymbol{x}} = \boldsymbol{f}[\boldsymbol{x}(t), \boldsymbol{u}(t)] + \boldsymbol{d}(t) + \boldsymbol{w}(t) \tag{6.31}$$

In Chapter 4, it was shown that the heat transfer coefficient decreases due to the increasing viscosity of the polymerization medium as the monomer conversion and the polymer molecular weight increase. In order to simulate such a case, the heat transfer coefficient is assumed to change as a function of the monomer conversion:

$$h_c = h_{c,o}(1 - 0.7X_1) \tag{6.32}$$

As shown in Figure 6.4, a pilot scale batch reactor is little affected by the decreasing heat transfer coefficient because the heat removal capacity still remains very large (i.e., large heat transfer surface area and short holding time of the jacket). It must be pointed out that the estimation of monomer conversion and reactor temperature is not affected by a small variation in the heat transfer coefficient because they are measured on-line. However, such a variation in h_c slightly deteriorates the quality estimations of initiator conversion and molecular weight with delayed MW measurements (Figure 6.5). When the MW measurements are provided with 30 minute delay, the estimation
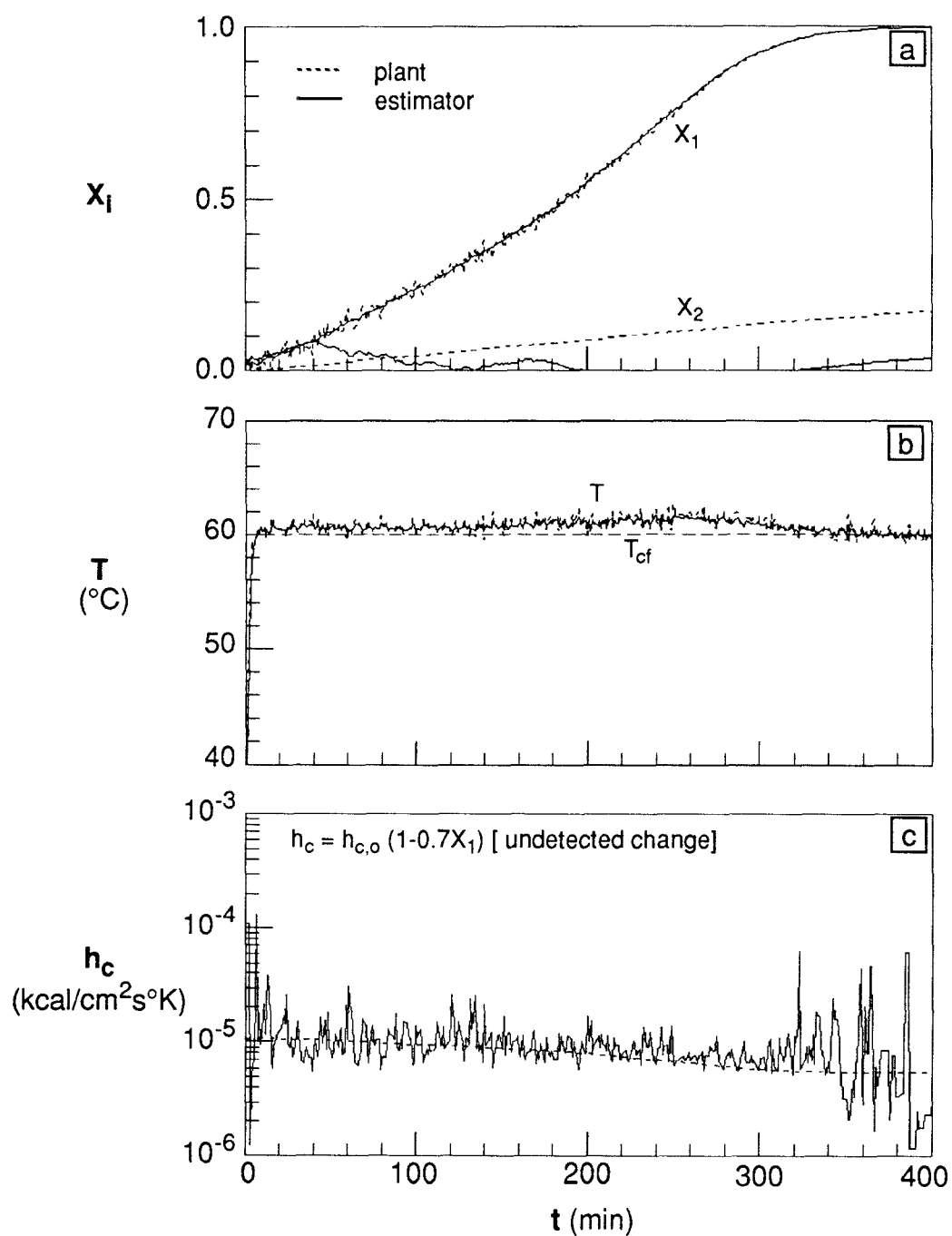
Figure 6.4   Estimation of open loop MMA polymerization in a pilot scale
batch reactor with undetected decrease in heat transfer co-
efficient: $f_s = 0.5$, $I_o = 0.02$ mol/l, $T_o = 30$ °C, $T_{cf} = 60$
°C.
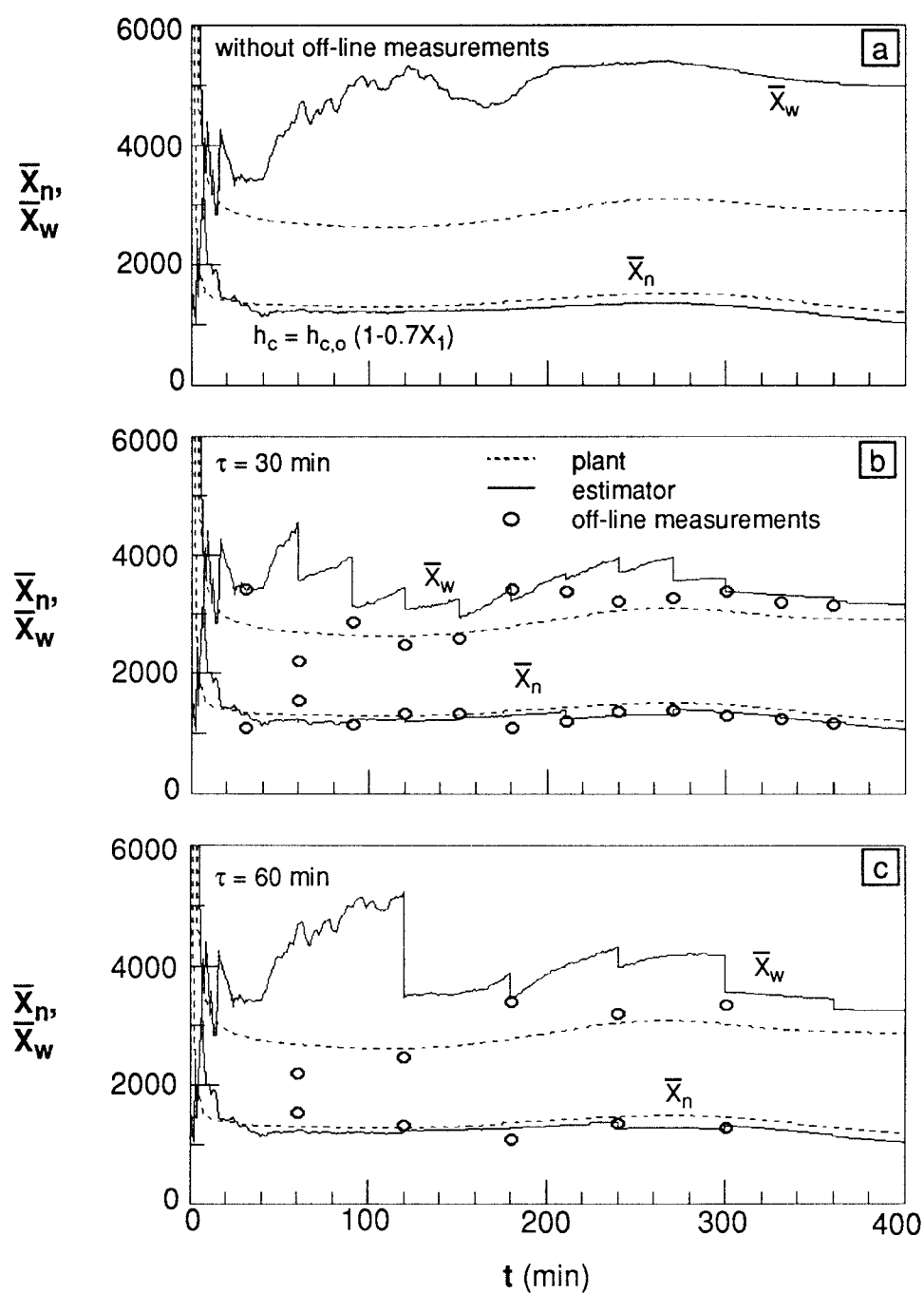
Figure 6.5   Effect of delayed measurements on MW estimation during open loop MMA polymerization in a pilot scale batch reactor with undetected decrease in heat transfer coefficient: $f_s = 0.5$, $I_{cf} = 0.02$ mol/l, $T_o = 30\ ^\circ$C, $T_o = 60\ ^\circ$C.

of $\overline{X}_n$ converges rapidly.

As shown in Table 6.4, when a batch polymerization reactor is scaled up to an industrial scale, the surface area per unit volume of the reactor decreases significantly. Figure 6.6 illustrates MMA solution polymerization in an industrial size batch reactor without temperature control. Since the reaction heat is not removed efficiently, runaway takes place after 90 min. When the coolant temperature is manipulated by a PI controller, the reactor temperature can be maintained at its set point after some oscillations (Figure 6.7b). Here the control parameters were tuned manually through numerical model simulations but extensive controller tuning was not attempted to obtain the best possible control performance. The filter in this case shows a similar performance to that in a pilot scale batch reactor, as shown in Figures 6.7 and 6.8. It is seen that the resulting number average chain length of the polymer ($\overline{X}_n$) is much lower than that in the pilot scale batch reactor because of temperature oscillations. As a result, higher polydispersity ($\overline{X}_w/\overline{X}_n$) is obtained. When the heat transfer coefficient of the industrial size reactor is decreased, the closed loop temperature response becomes sluggish as shown in Figure 6.9. However, the estimation performance of the filter is little affected by h_c variation (Figures 6.9 and 6.10). When the jacket holding time (θ_c) of the reactor is doubled (Figure 6.11), thermal runaway occurs 50 min even with a temperature controller. These figures indicate that the heat removal capacity of a large scale reactor is a very important factor in designing the
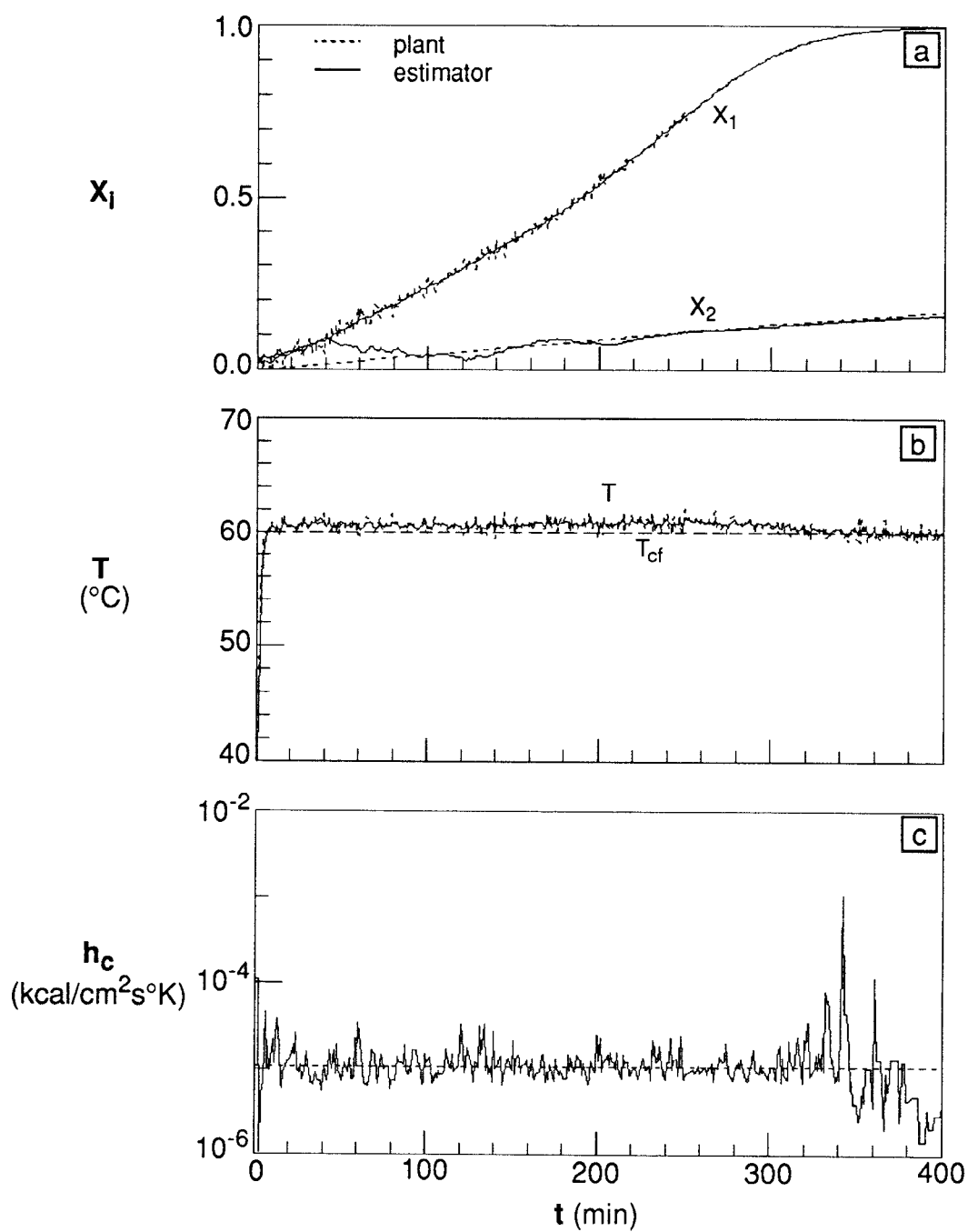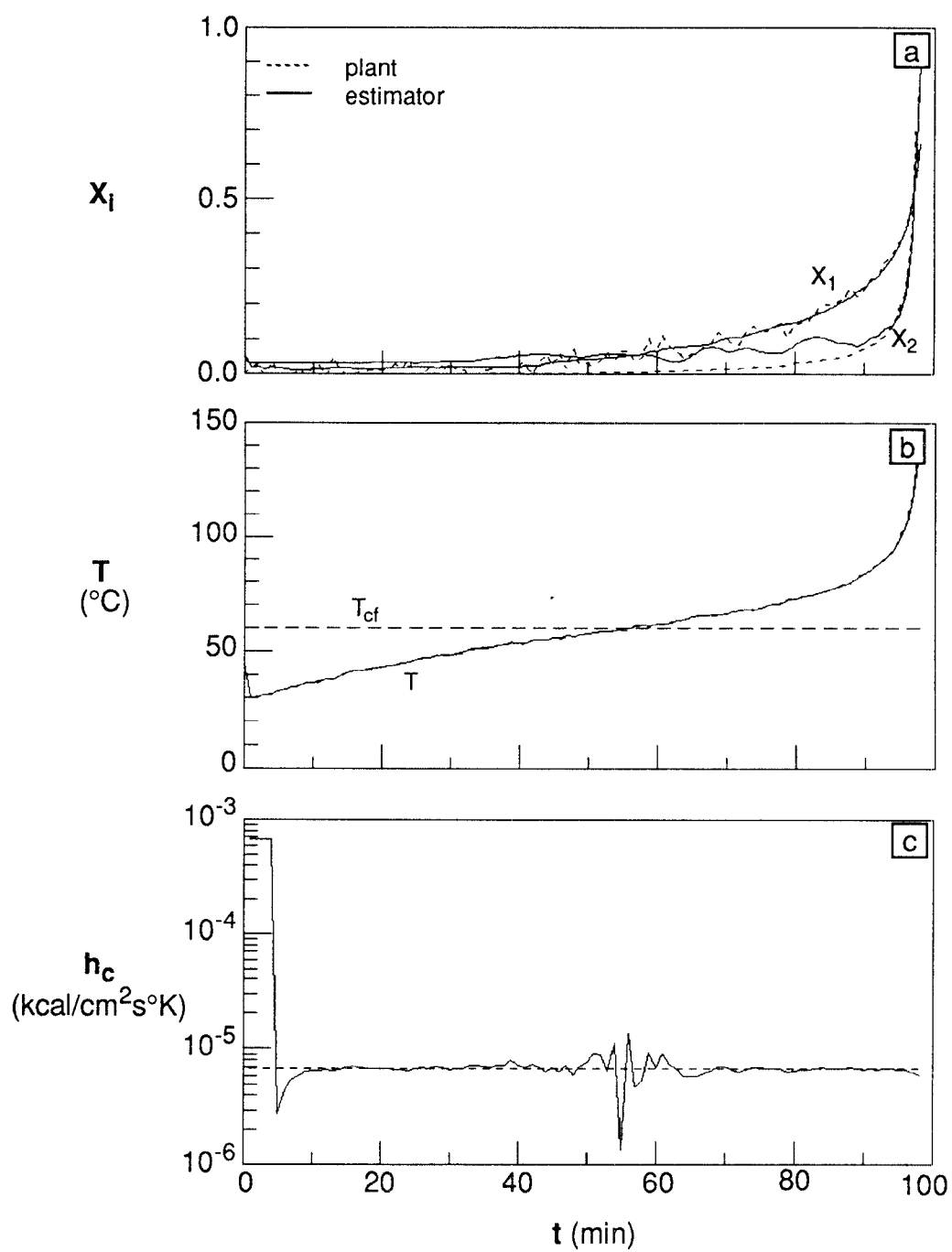
Figure 6.6   Estimation of open loop MMA polymerization in an industrial scale batch reactor: $f_s = 0.5$, $I_o = 0.02$ mol/l, $T_o = 30$ °C, $T_{cf} = 60$ °C.
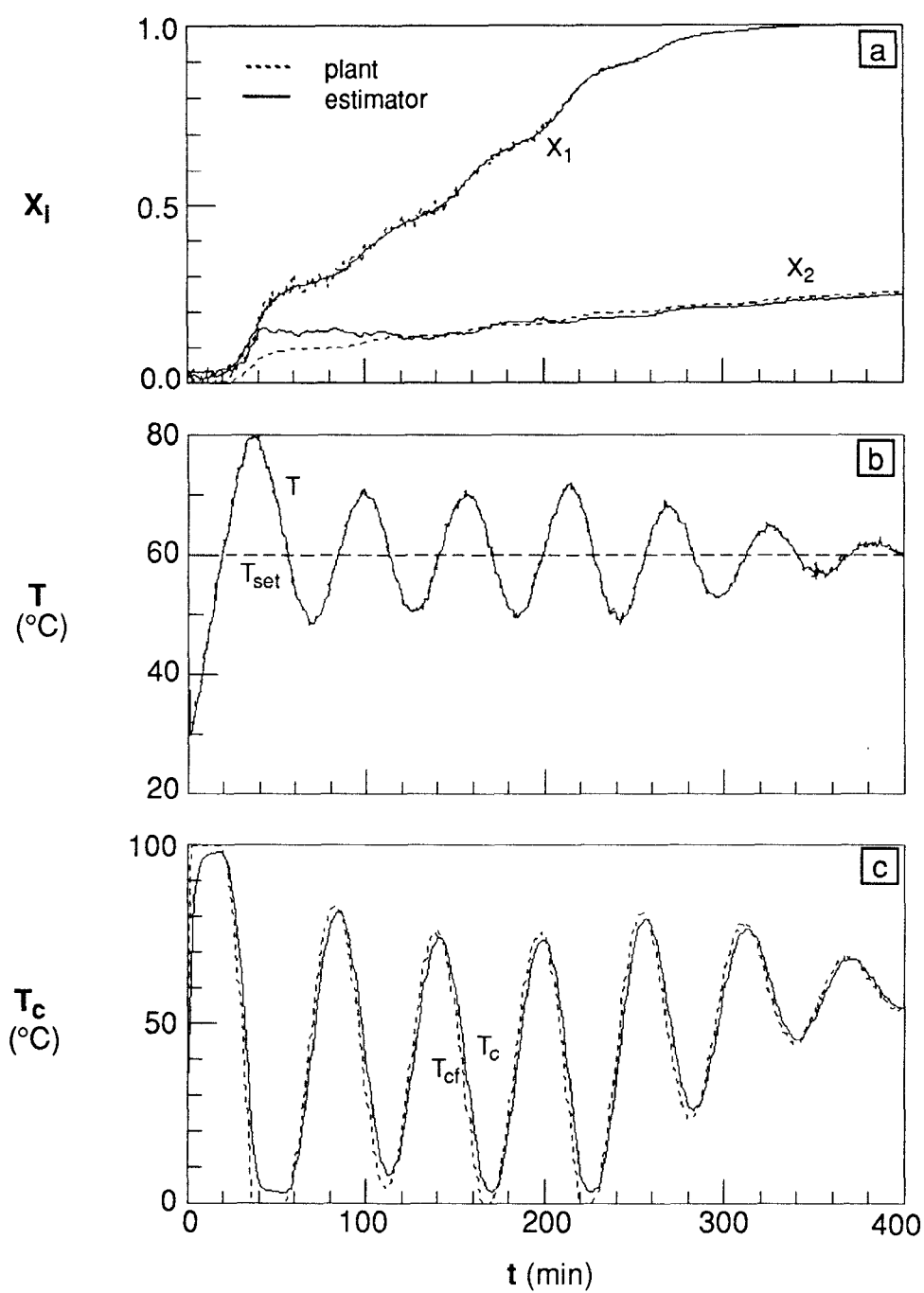
Figure 6.7   Estimation of closed loop MMA polymerization in an industrial scale batch reactor: $f_s = 0.5$, $I_o = 0.02$ mol/l, $T_o = 30$ °C, $T_{set} = 60$ °C, $K_c = 0.8$, $\tau_I = 2$ min, $0 \leq T_{cf}(°C) \leq 100$.

366
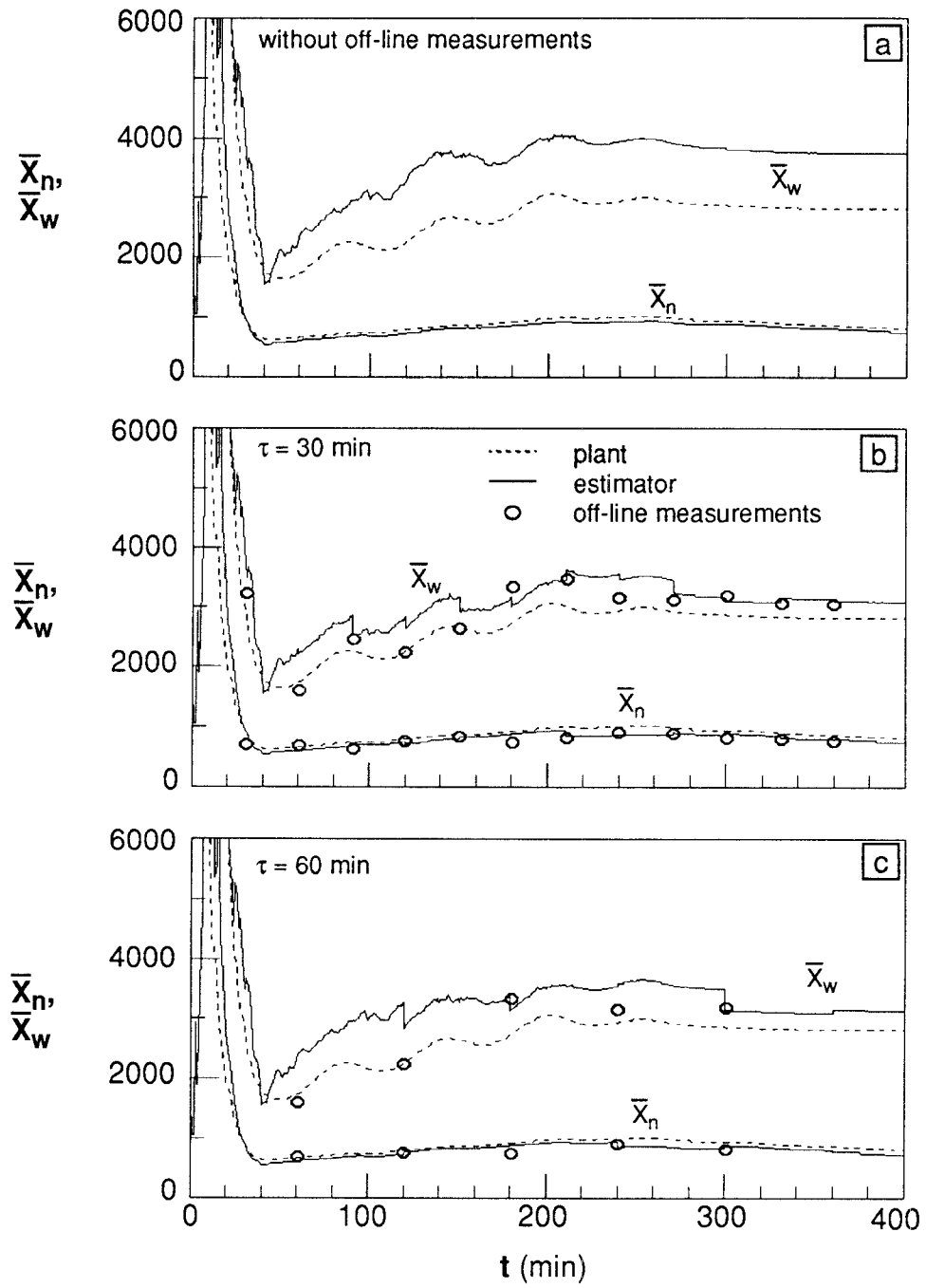
Figure 6.8   Effect of delayed measurements on MW estimation during
closed loop MMA polymerization in an industrial scale batch
reactor: $f_s = 0.5$, $I_o = 0.02$ mol/l, $T_o = 30$ °C, $T_{set} = 60$ °C,
$K_c = 0.8$, $\tau_I = 2$ min, $0 \leq T_{cf}(°C) \leq 100$.
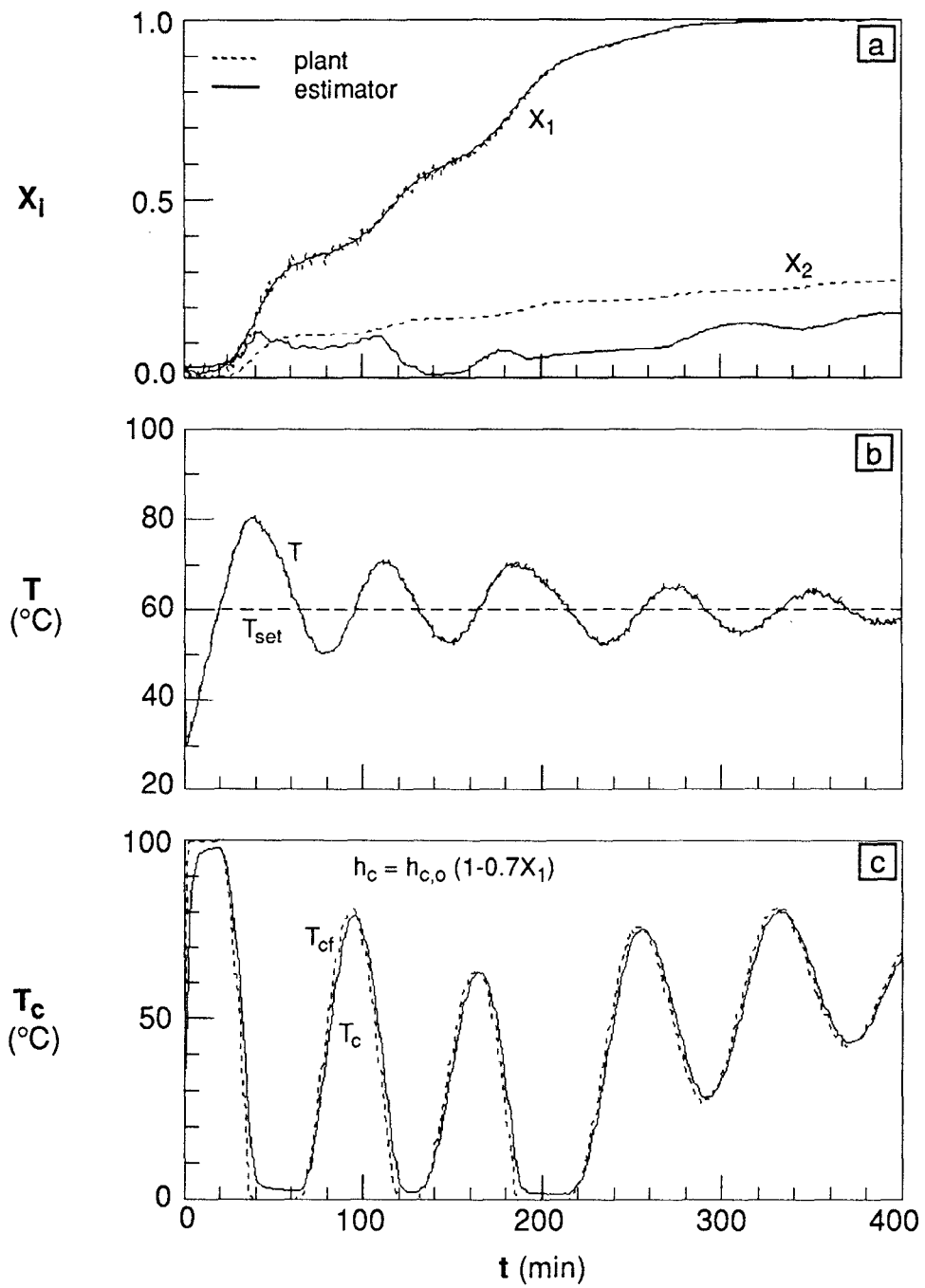
Figure 6.9   Estimation of closed loop MMA polymerization in an indus-
trial scale batch reactor with undetected decrease in heat
transfer coefficient: $f_s = 0.5$, $I_o = 0.02$ mol/l, $T_o = 30$ °C,
$T_{set} = 60$ °C, $K_c = 0.8$, $\tau_I = 2$ min, $0 \le T_{cf}(°C) \le 100$.
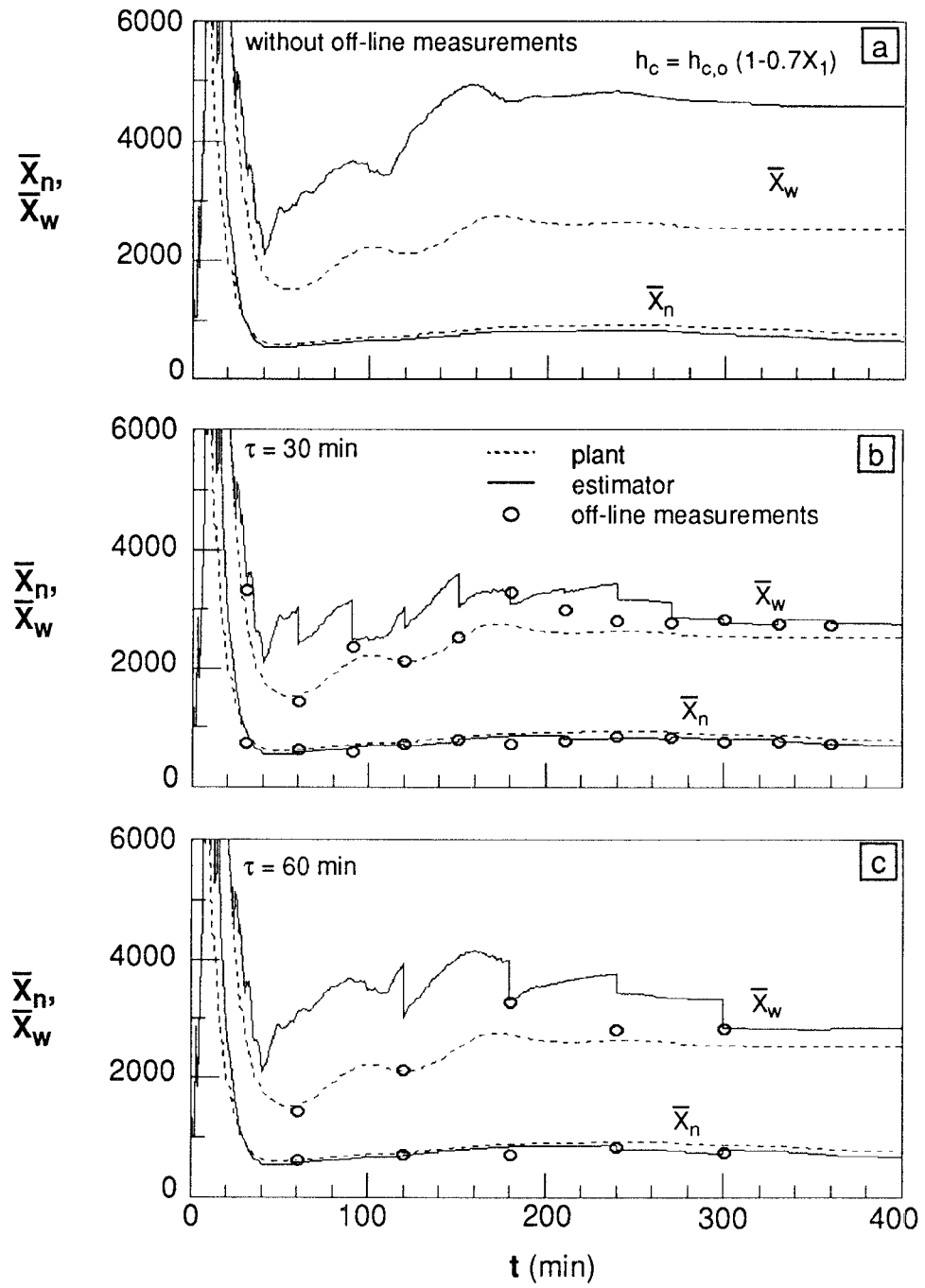
Figure 6.10   Effect of delayed measurements on MW estimation during closed loop MMA polymerization in an industrial scale batch reactor with undetected decrease in heat transfer coefficient: $f_s = 0.5$, $I_o = 0.02$ mol/l, $T_o = 30$ °C, $T_{set} = 60$ °C, $K_c = 0.8$, $\tau_I = 2$ min, $0 \le T_{cf}(°C) \le 100$.
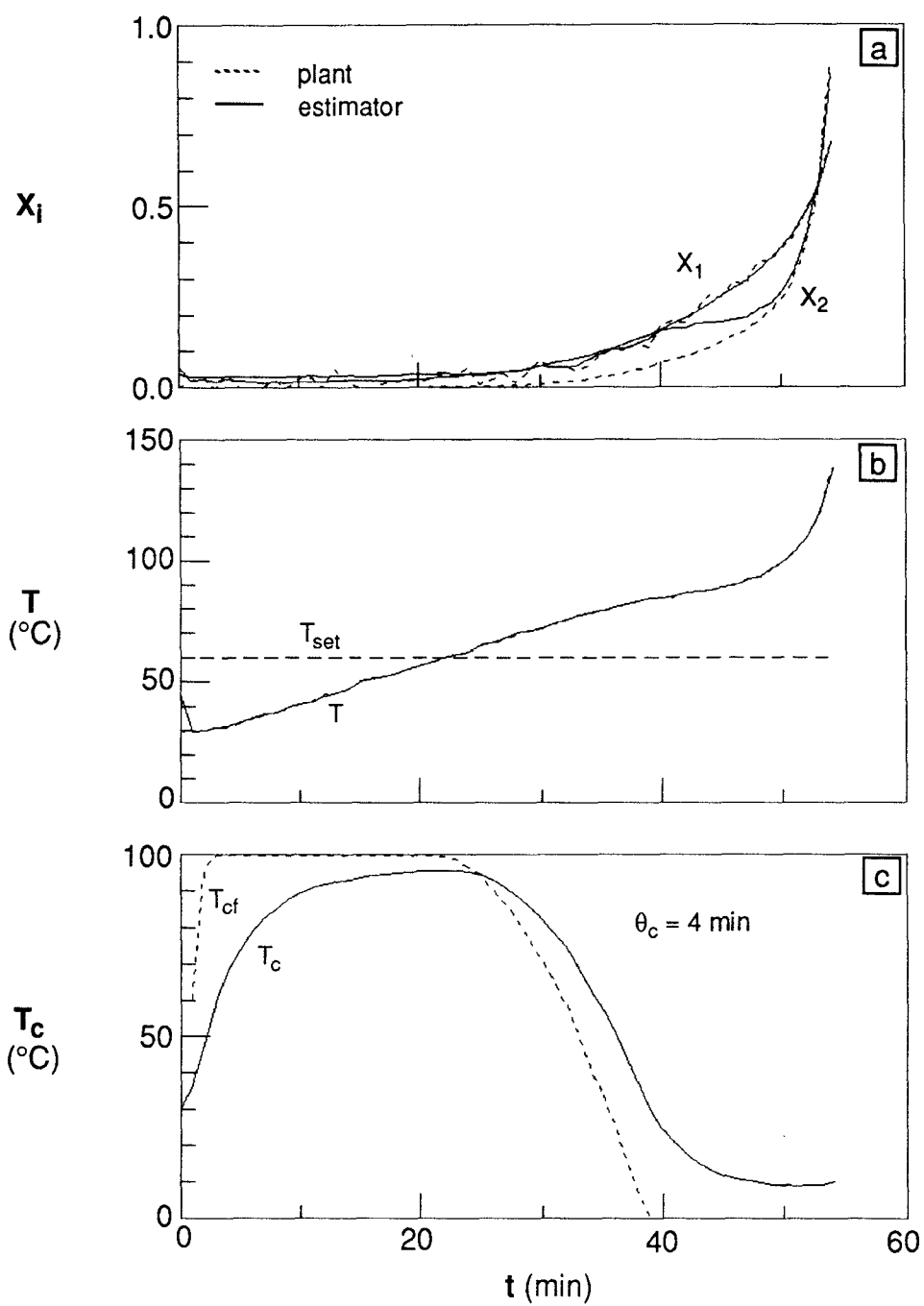
Figure 6.11   Effect of jacket holding time (θ_c) on closed loop MMA poly-
merization in an industrial scale batch reactor: f_s = 0.5,
I_o = 0.02 mol/l, T_o = 30 °C, T_{set} = 60 °C, K_c = 0.8, τ_I = 2
min, $0 \leq T_{cf}(^{\circ}C) \leq 100$.

reactor control policy.

6.4. Conclusions

Performance of the two-time scale extended Kalman filter has been tested through numerical simulations in pilot scale and plant scale batch methyl methacrylate polymerization reactors. It is observed that with the incorporation of delayed measurements of the polymer molecular weight into the filter, satisfactory estimates of reaction variables are obtained even in the presence of unknown disturbances. However, the filter algorithm must be improved for faster convergence if it is incorporated into a feedback control system.

6.5. Notation

A_c effective heat transfer area (cm^2)

C_{p_c} heat capacity of coolant (cal/g$^\circ$K)

Da dimensionless reaction time (-)

f efficiency of initiator (-)

f_s solvent mole fraction (-)

g_p gel effect correlation factor, k_p/k_p^* (-)

g_t gel effect correlation factor, k_t/k_t^* (-)

h_c overall heat transfer coefficient (cal/cm^{2}sec$^\circ$K)

ΔH heat of polymerization (cal/mol)

I_o inital concentration of initiator (mol/l)

k_d decomposition rate constant of initiator (sec^{-1})

k_i initiation rate constant (1/mol.sec)

k_{fm} rate constant of chain transfer to monomer (1/mol.sec)

k_{fs} rate constant of chain transfer to solvent (1/mol.sec)

k_p propagation rate constant (1/mol.sec)

k_p^* propagation rate constant at zero monomer conversion (1/mol.sec)

k_t termination rate constant (1/mol.sec)

k_t^* termination rate constant at zero monomer conversion (1/mol.sec)

M monomer concentration in the reactor (mol/l)

M_o initial concentration of monomer (mol/l)

P concentration of live polymers (mol/l)

q_c flow rate of coolant (l/sec)

q_{ii} standard deviation of model error of x_i, $i = 1, 2, 3, 4, 5$ (-)

r_{x_i} standard deviation of measurement error of x_i, $i = 1, 4, 5, 6$ (-)

T reactor temperature (°K)

T_c coolant temperature in the coolant jacket (°K)

T_{cf} feed temperature of coolant (u_1) (°K)

T_o initial temperature of reactant mixture (°K)

T_s glass transition temperature, for $k = m, p, s$ (°K)

t' time (sec)

t dimensionless time, t'/t_o (-)

t_o reaction time (sec)

V reactor volume (cm^3)

V_c volume of coolant jacket (cm^3)

V_f free volume

$\overline{X}_n$ number average chain length (-)

$\overline{X}_w$ weight average chain length (-)

X_1 monomer conversion(-)

X_2 initiator conversion(-)

x_j dimesionless concentation of j, $j = 1, 2, 3$ (-)

x_4 dimensionless reactor temperature (-)

x_k dimensionless kth moment of dead polymers, $k = 0, 1, 2$ (-)

w_m molecular weight of monomer (g/mol)

Greek Letters

α probability of propagation of a chain radical (-)

α_j coefficients of expansion in the free volume expression for j, $j = m, p, s$

δ dimensionless coolant temperature in the jacket (-)

δ_f dimensionless feed temperature of the coolant (-)

δ_o initial temperature of the coolant, T_{co}/T_o (-)

ϵ volume contraction factor (-)

ϵ_c heat capacity ratio of reaction mixture to coolant (-)

Θ dimensionless heat transfer coefficient of the reactor (-)

θ_c dimensionless holding time of the jacket (-)

λ_k kth moment of dead polymer, $k = 0, 1, 2$ (-)

λ_{kr} reference value of kth moment, $k = 0, 1, 2$ (-)

ρ density of reaction mixture (g/cm^3)

ρ_c density of coolant (g/cm^3)

ρ_j density of component j, $j = m, p, s$ (g/cm^3)

τ time delay of off-line measurement (min)

Vectors and Matrices

$\boldsymbol{f}$ system state model

$\boldsymbol{h}$ system measurement model

$\boldsymbol{x}$ system state vector

x_0 initial state vector

$\hat{x}$ estimated state vector by the state estimator

u system control vector

v measurement error vector

w model error vector

y measurement vector

F jacobian matrix of f

H jacobian matrix of h

K Kalman gain matrix

L_0 observability matrix

P estimation error covariance matrix

P_0 initial estimation error covariance matrix

Q model error covariance matrix

R measurement error covariance matrix

Chapter 7

Summary and Recommendations

Summary of the thesis   A precise control of polymer properties is one of the most important process objectives in operating modern industrial polymerization processes. However, on-line property control is often quite difficult due to the lack of adequate on-line sensors and a poor understanding of process dynamics. This thesis discusses nonlinear steady state and dynamic behavior of continuous polymerization reactors and proposes a computational method for the estimation and control of polymer properties by using a process model and an on-line state estimator.

The first part of this work (Chapter 2, 3 and 4) is devoted to the modeling and analysis of continuous free radical polymerization reactors. Styrene solution polymerization process has been selected as a model system and various initiator systems (e.g., a binary mixture of monofunctional initiators and bi-

functional initiators) have been considered. A new kinetic model is presented for the styrene polymerization with unsymmetrical bifunctional initiators. The continuous polymerization reactors modeled are a single CSTR and a cascade of two CSTR's. With the aid of a bifurcation analysis package AUTO, the regions of reactor operating conditions that give rise to steady state multiplicity, isolas, multiple Hopf bifurcation points, and bifurcations to periodic orbits such as period doubling, period-doubling cascades and homoclinics have been identified and confirmed through numerical model simulations. It was shown that the presence of more than one monofunctional initiator or dual initiator functionalities makes the macroscopic reactor dynamics much more complicated than with a single monofunctional initiator system that was studied by many researchers in the past. The reactor analysis has also been extended from ideal CSTR's to more realistic industrial reactor systems where the wall heat transfer coefficient is no longer constant and reactive impurities are present. Surprisingly, the steady state reactor behavior with viscosity dependent heat transfer coefficient was found to be simpler than that with constant heat transfer coefficient. When the reactive impurities such as inhibitors are present in the feed stream, the reactor dynamics may change significantly, depending on the type of inhibitors and their concentrations.

The second part of this work (Chapter 5 and 6) is concerned with the on-line estimation and control of polymer molecular weight properties in continuous and batch polymerization reactors. A two-time scale filter has been

developed in order to incorporate delayed MW measurement data into the extended Kalman filter. In particular, the effects of model errors and measurement delay time on the filter performance have been investigated through numerical simulations. It was shown that in the presence of some model errors and unknown disturbances, the filter showed a robust performance in predicting the polymer molecular weight properties when frequent MW measurements are provided. It was illustrated that the polymer grade change policy can be obtained effectively by using the steady state process model and filter in continuous polymerization processes.

The filter was also tested in batch polymerization reactors for the solution polymerization of methyl methacrylate. The overall filter performance for the batch process was quite similar to that of continuous polymerization process; however, the model simulations indicate that the filter convergence can be slow if model errors are large or measurement time delays are large. Unlike in continuous processes, batch processes are operated in finite reaction time and therefore more frequent MW measurements than in continuous processes are required to ensure fast filter convergence.

Future work for reactor modeling and analysis   Reactor dynamics were studied to investigate the effect of reactor input conditions on the output variables of the reactor. Due to the nonlinearity of the system, the output variables can have more than one set of steady state operating conditions for

a given set of feed conditions, leading to output multiplicity. It is also possible that more than one set of feed conditions can lead to the same set of output variables, in particular, polymer property parameters (*i.e.*, input multiplicity). The possibility of the input multiplicity in continuous polymerization reactors has been illustrated in this thesis; however, a full investigation of this subject has not been performed. The analysis of input multiplicity would be of interest in designing the reactor operating conditions and controls for efficient product grade changes.

Future work for on-line estimation and control   Although the two-time scale extended Kalman filter developed in this work has shown a good on-line estimation performance, the algorithm needs to be improved in order to be incorporated into feedback control systems. In particular, it will be desirable to improve the estimation algorithm so that the filter converges fast and is less sensitive to model errors. More importantly, experimental testing of the filter on real polymerization reactor systems should be carried out in order to assess the filter performance in realistic environments and to identify some problems that could have been overlooked in the theoretical simulation work as presented in this thesis.

Appendices

Appendix A: Moment Equations of Polymer Chains with Mixed Initiators

A.1. Dead polymers in the first reactor:

$$\frac{d\lambda_{0,1}^d}{dt} = -\lambda_{0,1}^d + \theta P_1 [k_{fm}(T_1)M_1\hat{\alpha}_1 + \frac{1}{2}k_t(T_1,X_{1,1})P_1] \tag{A.1}$$

$$\frac{d\lambda_{1,1}^d}{dt} = -\lambda_{1,1}^d + \frac{\theta P_1}{1-\hat{\alpha}_1}[k_{fm}(T_1)M_1(2\hat{\alpha}_1 - \hat{\alpha}_1^2) + k_t(T_1,X_{1,1})P_1] \tag{A.2}$$

$$\frac{d\lambda_{2,1}^d}{dt} = -\lambda_{2,1}^d + \frac{\theta P_1}{(1-\hat{\alpha}_1)^2}[k_{fm}(T_1)M_1(\hat{\alpha}_1^3 - 3\hat{\alpha}_1^2 + 4\hat{\alpha}_1)$$

$$+ k_t(T_1,X_{1,1})P_1(\hat{\alpha}_1 + 2)] \tag{A.3}$$

A.2. Dead polymers in the second reactor:

$$\frac{d\lambda_{0,2}^d}{dt} = \lambda_{0,1}^d - \lambda_{0,2}^d + \nu\theta P_2[k_{fm}(T_2)M_2\hat{\alpha}_2 + \frac{1}{2}k_t(T_2,X_{1,2})P_2] \tag{A.4}$$

$$\frac{d\lambda_{1,2}^d}{dt} = \lambda_{1,1}^d - \lambda_{1,2}^d + \frac{\nu\theta P_2}{(1-\hat{\alpha}_2)}[k_{fm}(T_2)M_2(2\hat{\alpha}_2 - \hat{\alpha}_2^2)$$

$$+ k_t(T_2,X_{1,2})P_2] \tag{A.5}$$

$$\frac{d\lambda_{2,2}^d}{dt} = \lambda_{2,1}^d - \lambda_{2,2}^d + \frac{\nu\theta P_2}{(1-\hat{\alpha}_2)^2}[k_{fm}(T_2)M_2(\hat{\alpha}_2^3 - 3\hat{\alpha}_2^2 + 4\hat{\alpha}_2)$$

$$+ k_t(T_2,X_{1,2})P_2(\hat{\alpha}_2 + 2)] \tag{A.6}$$

A.3. Live polymers in the ith reactor: ($i = 1,2$)

$$\lambda_{0,i}^l = P_i \tag{A.7}$$

$$\lambda_{1,i}^l = \frac{P_i}{1-\hat{\alpha}_i} \tag{A.8}$$

$$\lambda_{2,i}^l = \frac{(1 + \hat{\alpha}_i)}{(1 - \hat{\alpha}_i)^2} P_i \qquad (.A.9)$$

where,

$$\lambda_{k,i}^d = \sum_{n=2}^{\infty} n^k M_{n,i},$$

$$\lambda_{k,i}^l = \sum_{n=1}^{\infty} n^k P_{n,i},$$

$$\hat{\alpha}_i = \frac{k_p(T_i) M_i}{k_{fm}(T_i) M_i + k_p(T_i) M_i + k_t(T_i, X_{1,i}) P_i}$$

Appendix B: Moments of Live Polymers with Unsymmetrical Bifunctional Initiator

B.1. Primary radical concentrations:

$$R_A = \frac{f_A k_{d_B} I}{k_{d_A} + k_i M} \tag{B.1}$$

$$R_B = \frac{f_B k_{d_A} I}{k_{d_B} + k_i M} \tag{B.2}$$

$$R' = \frac{f_{R'}}{2k_i M}(k_{d_A} R_A + k_{d_B} R_B) \tag{B.3}$$

$$R = \frac{f_R}{k_i M}\{(k_{d_A} + k_{d_B})I + k_{d_A}(Q + U + W + 2U')$$

$$+ k_{d_B}(S + V + W + 2V') + k_{d_A} R_A + k_{d_B} R_B\} \tag{B.4}$$

B.2. Concentrations of primary live polymers:

$$P_1 = \frac{2k_{d_M} M^3 + k_i RM + k_{d_A} U_1 + k_{d_B} V_1}{(k_p + k_{fm})M + k_t(P + Q + S + 2T)}$$

$$+ \frac{k_{fm} M(P + Q + S + 2T + 2T_1)}{(k_p + k_{fm})M + k_t(P + Q + S + 2T)} \tag{B.5}$$

$$Q_1 = \frac{k_i R_A M}{k_{d_A} + (k_p + k_{fm})M + k_t(P + Q + S + 2T)} \tag{B.6}$$

$$S_1 = \frac{k_i R_B M}{k_{d_B} + (k_p + k_{fm})M + k_t(P + Q + S + 2T)} \tag{B.7}$$

$$T_1 = \frac{2k_i R' M + k_{d_A} Q_1 + k_{d_B} S_1}{2[(k_p + k_{fm})M + k_t(P + Q + S + 2T)]} \tag{B.8}$$

B.3. Zeroth moments of live polymers:

$$k_t P^2 + k_t(Q + S)P - [(f_R k_{d_A} + k_{fm}M)Q + (f_R k_{d_B} + k_{fm}M)S$$

$$+ 4k_{fm}MT + A_o] = 0 \tag{B.9}$$

$$k_t Q^2 + [k_{d_A} + k_{fm}M + k_t(P + S)]Q - B_o = 0 \tag{B.10}$$

$$k_t S^2 + [k_{d_B} + k_{fm}M + k_t(P + Q)]S - C_0 = 0 \tag{B.11}$$

$$k_t T^2 + [k_t(P + Q + S) + k_{fm}M]T - \frac{1}{2}(k_{d_A}Q + k_{d_B}S + D_o) = 0 \tag{B.12}$$

where,

$$A_o = 2k_{d_M}M^3 + k_{d_A}U + k_{d_B}V$$

$$+ f_R[(k_{d_B} + k_{d_A})I + k_{d_A}(U + W + 2U')$$

$$+ k_{d_B}(V + W + 2V') + k_{d_A}R_A + k_{d_B}R_B] \tag{B.13}$$

$$B_o = k_i R_A M + 2k_{d_A}U' + k_{d_B}W \tag{B.14}$$

$$C_o = k_i R_B M + k_{d_A}W + 2k_{d_B}V' \tag{B.15}$$

$$D_o = 2k_i R'M \tag{B.16}$$

B.4. First moments of live polymer:

$$\lambda_{P,1} = \frac{2(k_{fm}M + k_t P)\lambda_{T,1} + A_1}{k_{fm}M + k_t(P + Q + S)} \tag{B.17}$$

$$\lambda_{Q,1} = \frac{2k_t Q\lambda_{T,1} + B_1}{k_{d_A} + k_{fm}M + k_t(P + Q + S)} \tag{B.18}$$

$$\lambda_{S,1} = \frac{2k_t S\lambda_{T,1} + C_1}{k_{d_B} + k_{fm}M + k_t(P + Q + S)} \tag{B.19}$$

384

$$\lambda_{T,1} = \frac{D_{1_A}}{2D_{1_B}} \qquad (B.20)$$

where,

$$A_1 = 2k_{d_M}M^3 + k_iRM + k_{d_A}\lambda_{U,1} + k_{d_B}\lambda_{V,1} + k_pMP$$

$$+ k_{fm}M(P + Q + S + 2T) \qquad (B.21)$$

$$B_1 = k_iR_AM + 2k_{d_A}\lambda_{U',1} + k_{d_B}\lambda_{W,1} + k_pMQ \qquad (B.22)$$

$$C_1 = k_iR_BM + k_{d_A}\lambda_{W,1} + 2k_{d_B}\lambda_{V',1} + k_pMS \qquad (B.23)$$

$$D_{1_A} = 2k_iR'M + \frac{k_{d_A}B_1}{k_{d_A} + k_{fm}M + k_t(P + Q + S)}$$

$$+ \frac{k_{d_B}C_1}{k_{d_B} + k_{fm}M + k_t(P + Q + S)} + 2k_pMT \qquad (B.24)$$

$$D_{1_B} = k_{fm}M + k_t(P + Q + S) - \frac{k_{d_A}k_tQ}{k_{d_A} + k_{fm}M + k_t(P + Q + S)}$$

$$- \frac{k_{d_B}k_tS}{k_{d_B} + k_{fm}M + k_t(P + Q + S)} \qquad (B.25)$$

B.5. Second moments of live polymers:

$$\lambda_{P,2} = \frac{2(k_{fm}M + k_tP)\lambda_{T,2} + A_2}{k_{fm}M + k_t(P + Q + S)} \qquad (B.26)$$

$$\lambda_{Q,2} = \frac{2k_tQ\lambda_{T,2} + B_2}{k_{d_A} + k_{fm}M + k_t(P + Q + S)} \qquad (B.27)$$

$$\lambda_{S,2} = \frac{2k_tS\lambda_{T,2} + C_2}{k_{d_B} + k_{fm}M + k_t(P + Q + S)} \qquad (B.28)$$

$$\lambda_{T,2} = \frac{D_{2_A}}{2D_{2_B}} \qquad (B.29)$$

where,

$$A_2 = 2k_{d_M}M^3 + k_iRM + k_{d_A}\lambda_{U,2} + k_{d_B}\lambda_{V,2} + k_pM(2\lambda_{P,1} + P)$$

$$+ k_{fm}M(P + Q + S + 2T) + 4k_t\lambda_{P,1}\lambda_{T,1} \qquad (B.30)$$

$$B_2 = k_i R_A M + 2 k_{d_A} \lambda_{U',2} + k_{d_B} \lambda_{W,2} + k_p M (2 \lambda_{Q,1} + Q)$$

$$+ 4 k_t \lambda_{Q,1} \lambda_{T,1} \qquad (B.31)$$

$$C_2 = k_i R_B M + k_{d_A} \lambda_{W,2} + 2 k_{d_B} \lambda_{V',2} + k_p M (2 \lambda_{S,1} + S)$$

$$+ 4 k_t \lambda_{S,1} \lambda_{T,1} \qquad (B.32)$$

$$D_{2_A} = 2 k_i R' M + \frac{k_{d_A} B_2}{k_{d_A} + k_{fm} M + k_t (P + Q + S)}$$

$$+ \frac{k_{d_B} C_2}{k_{d_B} + k_{fm} M + k_t (P + Q + S)}$$

$$+ 2 k_p M (2 \lambda_{T,1} + T) + 4 k_t \lambda_{T,1}^2 \qquad (B.33)$$

$$D_{2_B} = k_{fm} M + k_t (P + Q + S) - \frac{k_{d_A} k_t Q}{k_{d_A} + k_{fm} M + k_t (P + Q + S)}$$

$$- \frac{k_{d_B} k_t S}{k_{d_B} + k_{fm} M + k_t (P + Q + S)} \qquad (B.34)$$

Appendix C: Steady State Polymer Moments with Symmetrical Bifunctional Initiator

C.1. Inactive Polymers

C.1.1. Zeroth moments:

$$\lambda_0^d = \frac{1}{2}\theta k_t P^2 \tag{C.1}$$

$$\lambda_{Z,0} = \frac{\theta k_t PQ}{1 + \theta k_{d2}} \tag{C.2}$$

$$\lambda_{T,0} = \frac{\theta k_t Q^2}{2(1 + 2\theta k_{d2})} \tag{C.3}$$

C.1.2. First moments:

$$\lambda_1^d = \theta k_t P \lambda_{P,1} \tag{C.4}$$

$$\lambda_{Z,1} = \frac{\theta k_t (P \lambda_{Q,1} + Q \lambda_{P,1})}{1 + \theta k_{d2}} \tag{C.5}$$

$$\lambda_{T,1} = \frac{\theta k_t Q \lambda_{Q,1}}{1 + 2\theta k_{d2}} \tag{C.6}$$

C.1.3. Second moment:

$$\lambda_2^d = \theta k_t (P \lambda_{P,2} + \lambda_{P,1}^2) \tag{C.7}$$

$$\lambda_{Z,2} = \frac{\theta k_t (2\lambda_{P,1}\lambda_{Q,1} + P\lambda_{Q,2} + Q\lambda_{P,2})}{1 + \theta k_{d2}} \tag{C.8}$$

$$\lambda_{T,2} = \frac{\theta k_t (\lambda_{Q,1}^2 + Q\lambda_{Q,2})}{1 + 2\theta k_{d2}} \tag{C.9}$$

C.2. Live Polymers

C.2.1. First moments:

$$\lambda_{P,1} = -\frac{(a_1 + b_1\lambda_{Q,1})}{c_1} \qquad (C.10)$$

$$\lambda_{Q,1} = -\frac{d_1}{e_1} \qquad (C.11)$$

$$\lambda_{S,1} = \frac{k_p M_f (1 - X_1)S + \frac{1}{2}k_{d2}\lambda_{Q,1}}{k_t(P + Q)} \qquad (C.12)$$

C.2.2. Second moments:

$$\lambda_{P,2} = -\frac{(a_2 + b_2\lambda_{Q,2})}{c_2} \qquad (C.13)$$

$$\lambda_{Q,2} = -\frac{d_2}{e_2} \qquad (C.14)$$

$$\lambda_{S,2} = \frac{k_p M_f (1 - X_1)(2\lambda_{S,1} + S) + 2k_t\lambda_{S,1}^2 + \frac{1}{2}k_{d2}\lambda_{Q,2}}{k_t(P + Q)} \qquad (C.15)$$

where

$$a_1 = 2f_1 k_{d1} I_f (1 - X_2) + k_p M_f (1 - X_1)P + k_{d2}(Q + 2T + Z)$$

$$+ \frac{2k_p M_f (1 - X_1)SP}{P + Q} \qquad (C.16)$$

$$b_1 = \frac{k_{d2}P}{P + Q} + \frac{\theta k_t k_{d2} P}{1 + \theta k_{d2}} \qquad (C.17)$$

$$c_1 = \frac{\theta k_t k_{d2} Q}{1 + \theta k_{d2}} - k_t(P + Q) \qquad (C.18)$$

$$d_1 = 2f_2 k_{d1} I_f (1 - X_2) + k_p M_f (1 - X_1)Q$$

$$+ \frac{2k_p M_f (1 - X_1)SQ}{P + Q} \qquad (C.19)$$

$$e_1 = \frac{k_{d2}Q}{P + Q} - k_t(P + Q) + \frac{2\theta k_t k_{d2} Q}{1 + 2\theta k_{d2}} - k_{d2} \qquad (C.20)$$

388

$$a_2 = 2f_1 k_{d1} I_f (1 - X_2) + k_p M_f (1 - X_1)(2\lambda_{P,1} + P)$$

$$+ k_{d2}(Q + 2T + Z) + 4k_t \lambda_{P,1} \lambda_{S,1}$$

$$+ \frac{2\theta k_t k_{d2} \lambda_{P,1} \lambda_{Q,1}}{1 + \theta k_{d2}}$$

$$+ \frac{2k_p M_f (1 - X_1) P (2\lambda_{S,1} + S) + 4k_t P \lambda_{S,1}^2}{P + Q} \qquad (C.21)$$

$$b_2 = \frac{k_{d2} P}{P + Q} + \frac{\theta k_t k_{d2} P}{1 + \theta k_{d2}} \qquad (C.22)$$

$$c_2 = \frac{\theta k_t k_{d2} Q}{1 + \theta k_{d2}} - k_t (P + Q) \qquad (C.23)$$

$$d_2 = 2f_2 k_{d1} I_f (1 - X_2) + k_p M_f (1 - X_1)(2\lambda_{Q,1} + Q)$$

$$+ \frac{2\theta k_t k_{d2} \lambda_{Q,1}^2}{1 + 2\theta k_{d2}} + 4k_t \lambda_{Q,1} \lambda_{S,1}$$

$$+ \frac{2k_p M_f (1 - X_1)(2\lambda_{S,1} + S) Q + 4k_t Q \lambda_{S,1}^2}{P + Q} \qquad (C.24)$$

$$e_2 = \frac{2\theta k_t k_{d2} Q}{1 + 2\theta k_{d2}} - k_{d2} - k_t (P + Q) + \frac{k_{d2} Q}{P + Q} \qquad (C.25)$$

Appendix D: Moment Equations of Polymer Chains with Inhibitor

D.1. Dead polymers:

$$\frac{d\lambda_0^d}{dt'} = P\left[\hat{\alpha}k_{fm}M + \frac{1}{2}k_tP + \frac{k_qI_h}{(R+P)}(2\hat{\alpha}R + P)\right] \tag{D.1}$$

$$\frac{d\lambda_1^d}{dt'} = \frac{P}{(1-\hat{\alpha})}\left[\hat{\alpha}(2-\hat{\alpha})k_{fm}M + k_tP + \frac{2k_qI_h}{(R+P)}(\hat{\alpha}(2-\hat{\alpha})R + P)\right] \tag{D.2}$$

$$\frac{d\lambda_2^d}{dt'} = \frac{P}{(1-\hat{\alpha})^2}\left[\hat{\alpha}(\hat{\alpha}^2 - 3\hat{\alpha} + 4)k_{fm}M + (\hat{\alpha} + 2)k_tP\right.$$
$$\left. + \frac{2k_qI_h}{(R+P)}\{2\hat{\alpha}(\hat{\alpha}^2 - 3\hat{\alpha} + 4)R + (\hat{\alpha} + 2)P\}\right] \tag{D.3}$$

D.2. Live polymers:

$$\lambda_0^l = P \tag{D.4}$$

$$\lambda_1^l = \frac{P}{1-\hat{\alpha}} \tag{D.5}$$

$$\lambda_2^l = \frac{(1+\hat{\alpha})}{(1-\hat{\alpha})^2}P \tag{D.6}$$

D.3. Inhibitor radical chains:

$$\lambda_0^Q = \frac{k_q}{k_{tq}}I_h \tag{D.7}$$

$$\lambda_1^Q = \frac{R + \lambda_1^l}{R + P}I_h \tag{D.8}$$

$$\lambda_2^Q = \frac{R + \lambda_2^l}{R + P}I_h \tag{D.9}$$

where,

$$\lambda_k^d = \sum_{n=2}^{\infty} n^k M_n,$$

$$\lambda_k^l = \sum_{n=1}^{\infty} n^k P_n,$$

$$\lambda_k^Q = \sum_{n=1}^{\infty} n^k Q_n + Q_0,$$

$$\hat{\alpha} = \frac{k_p M}{k_p M + k_{fm} M + 2 k_q I_h + k_t P}$$

Appendix E: Dimensionless Process Model and Parameters

E.1. Dimensionless Model:

$$\frac{dx_1}{dt} = -x_1 + Da_1(1-x_1)Y_1\exp\left[\frac{\gamma_p x_4}{1+x_4}\right] \tag{E.1}$$

$$\frac{dx_2}{dt} = -x_2 + Da_2(1-x_2)\exp\left[-\frac{\gamma_{d_a}}{1+x_4}\right] \tag{E.2}$$

$$\frac{dx_3}{dt} = -x_3 + Da_3(1-x_3)\exp\left[-\frac{\gamma_{d_b}}{1+x_4}\right] \tag{E.3}$$

$$\frac{dx_4}{dt} = -x_4 + \beta Da_1(1-x_1)Y_1\exp\left[\frac{\gamma_p x_4}{1+x_4}\right] - Da_4(x_4-x_8) \tag{E.4}$$

$$\frac{dx_5}{dt} = -x_5 + \alpha Da_{01}Y_1(1-x_1)\exp\left[-\frac{\gamma_{fm}}{1+x_4}\right]$$
$$+ \alpha Da_{02}Y_1\exp\left[-\frac{\gamma_{fa}}{1+x_4}\right]$$
$$+ Da_{03}Y_1Y_2\exp\left[-\frac{\gamma_t}{1+x_4}\right] \tag{E.5}$$

$$\frac{dx_6}{dt} = -x_6 + \frac{(\alpha^3-3\alpha^2+4\alpha)}{(1-\alpha)^2}Da_{21}Y_1(1-x_1)\exp\left[-\frac{\gamma_{fm}}{1+x_4}\right]$$
$$+ \frac{(\alpha^3-3\alpha^2+4\alpha)}{(1-\alpha)^2}Da_{22}Y_1\exp\left[-\frac{\gamma_{fa}}{1+x_4}\right]$$
$$+ \frac{(2+\alpha)}{(1-\alpha)^2}Da_{23}Y_1Y_2\exp\left[-\frac{\gamma_t}{1+x_4}\right] \tag{E.6}$$

$$\frac{dx_7}{dt} = -x_7 + \frac{(2\alpha-\alpha^2)}{(1-\alpha)}Da_{11}Y_1(1-x_1)\exp\left[-\frac{\gamma_{fm}}{1+x_4}\right]$$
$$+ \frac{(2\alpha-\alpha^2)}{(1-\alpha)}Da_{12}Y_1\exp\left[-\frac{\gamma_{fm}}{1+x_4}\right]$$
$$+ \frac{Da_{13}Y_1Y_2}{(1-\alpha)}\exp\left[-\frac{\gamma_t}{1+x_4}\right] \tag{E.7}$$

$$\frac{dx_8}{dt} = \frac{\theta}{\theta_c}(\delta_f-x_8) - \nu Da_4(x_4-x_8) \tag{E.8}$$

where

$$Y_1 = \frac{1}{P_f}\left(\frac{P_x}{g_t}\right)^{\frac{1}{2}} \qquad (E.9)$$

$$Y_2 = \frac{1}{P_f}(P_x g_t)^{\frac{1}{2}} \qquad (E.10)$$

$$P_f = \left[a\exp(-\gamma_1) + b\exp(-\gamma_2) + c\exp(-\gamma_3)\right]^{\frac{1}{2}} \qquad (E.11)$$

$$P_x = a(1 - x_1)^3\exp\left[-\frac{\gamma_1}{1 + x_4}\right] + b(1 - x_2)\exp\left[-\frac{\gamma_2}{1 + x_4}\right]$$
$$+ c(1 - x_3)\exp\left[-\frac{\gamma_3}{1 + x_4}\right] \qquad (E.12)$$

$$\alpha^{-1} = 1 + \alpha_m\exp\left[-\frac{\gamma_4}{1 + x_4}\right] + \frac{\alpha_a}{(1 - x_1)}\exp\left[-\frac{\gamma_5}{1 + x_4}\right]$$
$$+ \frac{\alpha_t Y_2}{(1 - x_1)}\exp\left[-\frac{\gamma_6}{(1 + x_4)}\right] \qquad (E.13)$$

E.2. Dimensionless Parameters:

$$\alpha_0 = \frac{h_c A_c}{\rho C_p V} \qquad \beta = \frac{(-\Delta)M_f}{\rho C_p T_f} \qquad \delta_f = \frac{T_{cf} - T_f}{T_f} \qquad \nu = \frac{\rho C_p V}{\rho_c C_{p_c} V_c} \qquad \theta_c = \frac{V_c}{q_c}$$

$$\gamma_p = \frac{E_p}{RT_f} \qquad \gamma_{d_a} = \frac{E_{d_A}}{RT_f} \qquad \gamma_{d_b} = \frac{E_{d_B}}{TR_f} \qquad \gamma_{fm} = \frac{E_{fm}}{RT_f} \qquad \gamma_{fa} = \frac{E_{fa}}{RT_f} \qquad \gamma_t = \frac{E_t}{RT_f}$$

$$\gamma_1 = \frac{E_{d_M} - E_t}{RT_f} \qquad \gamma_2 = \gamma_{d_a} - \gamma_t \qquad \gamma_3 = \gamma_{d_b} - \gamma_t \qquad \gamma_4 = \gamma_{fm} - \gamma_p$$

$$\gamma_5 = \gamma_{fa} - \gamma_p \qquad \gamma_6 = \gamma_t - \gamma_p \qquad \alpha_m = \frac{k_{fm0}}{k_{p0}} \qquad \alpha_a = \frac{k_{fa0}A}{k_{p0}M_f} \qquad \alpha_t = \frac{k_{t0}^* P_f}{k_{p0}M_f}$$

$$Da_1 = \theta k_{p0}\exp(-\gamma_p)P_f \qquad Da_2 = \theta k_{d_A 0} \qquad Da_3 = \theta k_{d_B 0} \qquad Da_4 = \theta\alpha_0$$

$$Da_{i1} = \frac{\theta k_{fm0}P_f M_f}{\lambda_{ir}} \qquad Da_{i2} = \frac{\theta k_{fa0}P_f A}{\lambda_{ir}} \qquad Da_{i3} = \frac{\theta k_{t0}^* P_f^2}{\lambda_{ir}} \quad \text{(for } i = 0, 1, 2)$$

$$a = \frac{2k_{d_M 0}M_f^3}{k_{t0}^*} \qquad b = \frac{2f_A k_{d_A 0}I_f y_{Af}}{k_{t0}^*} \qquad c = \frac{2f_B k_{d_A 0}I_f(1 - y_{Af})}{k_{t0}^*}$$

$$t = \frac{t'}{\theta} \qquad \theta = \frac{V}{q}$$

References

Adebekun, D. K. and Schork, F. J., "Continuous solution polymerization reactor control. 2. Estimation and nonlinear reference control during methyl methacrylate polymerization", *Ind. Eng. Chem. Res.*, **28**, 1846-1861 (1989).

Adebekun, D. K., Kwalik, K. M. and Schork, F. J., "Steady state multiplicity during solution polymerization of methyl methacrylate in a CSTR", *Chem. Eng. Sci.*, **44**, 2269-2281 (1989).

Adebekun, D. K., Kwalik, K. M. and Schork, F. J., "Steady state and dynamic behavior of a continuous polymerization reactor", *AIChE Annual Meeting*, Washington D.C. (1988).

Aldrich, *Catalog Handbook of Fine Chemicals*, Milwaukee, WI, 1990.

Allen, I., Marshall, W. R. and Wightman, G. E., "Continuous bulk polymerization of styrene", *U.S. Pat.*, **2,496,653** (1950).

Arai, K., Yamaguchi, H., Saito, S., Sarachina, E. and Yamamoto, T., "A kinetic study of bulk thermal polymerization of styrene", *J. Chem. Eng. Japan*, **19**, 413-419 (1986).

Aris, R. and Amundson, N. R., "An analysis of chemical reactor stability and control – I, II", *Chem. Eng. Sci.*, **7**, 121-147 (1959).

Aris, R. and Amundson, N. R., " Stability of some chemical systems under control", *Chem. Eng. Prog.*, **53**, 227-230 (1957).

Bailey, J. E., "Periodic phenomena", in Lapidus, L. and Amundson, N. R. (eds), *Chemical Reactor Theory. A Review*, Prentice Hall, Englewood Cliff, NJ, 1977.

Balakotaiah, V. and Luss, D., "Steady state multiplicity features of lumped parameter chemically reacting systems", in *Dynamics of Nonlinear Systems*, ed by Hlaváček, V., 1-46, Gordeon and Breach Science, New York, 1986.

Balakotaiah, V. and Luss, D., "Input multiplicity in lumped parameter systems", *Chem. Eng. Commun.*, **39**, 309-322 (1985).

Balakotaiah, V. and Luss, D., "Global analysis of the multiplicity features of multi-reaction lumped-parameter systems", *Chem. Eng. Sci.*, **39**, 865-881 (1984).

Balakotaiah, V. and Luss, D., "Multiplicity features of reacting system. Dependence of the steady states of a CSTR on the residence time", *Chem. Eng. Sci.*, **38**, 1709-1721 (1983).

Balakotaiah, V. and Luss, D., "Analysis of the multiplicity patterns of a CSTR", *Chem. Eng. Commun.*, **19**, 185-189 (1982a).

Balakotaiah, V. and Luss, D., "Exact steady state multiplity criteria for two consecutive or parallel reactions in lumped parameter systems", *Chem. Eng. Sci.*, **37**, 433-445 (1982b).

Balakotaiah, V. and Luss, D., "Structure of the steady state solutions of lumped parameter chemically reacting systems", *Chem. Eng. Sci.*, **37**, 1611-1623 (1982c).

Balakotaiah, V. and Luss, D., "A novel method for determining the multiplicity features of multi-reaction systems", *ACS Symp. Ser.*, **196**, 65-75 (1982d).

Balakotaiah, V. and Luss, D., "Analysis of the multiplicity patterns of a CSTR", *Chem. Eng. Commun.*, **13**, 111-132 (1981).

Balakotaiah, V., Luss, D. and Keyfitz, B. L., "Steady state multiplicity analysis of lumped parameter systems described by a set of algebraic equations", *Chem. Eng. Commun.*, **36**, 121-147 (1985).

Balaraman, K. S., Kulkarni, B. D. and Mashelkar, R. A., "Multiplicity of states in continuous stirred copolymerization reactors: its existence and consequences", *Chem. Eng. Commun.*, **16**, 349-360 (1982).

Balke, S. T. and Hamielec, A. E., "Bulk polymerization of methyl methacrylate", *J. Appl. Poly. Sci.*, **17**, 905-949 (1973).

Bamford, C. H. and Tipper, C. F. H., *Chemical Kinetics, Free Radical Polymerization*, vol 14A, Elsevier Scientific Publishing Co., New York, 1976.

Beek, J., "Small oscillations in undisturbanced autonomous systems", *AIChE J.*, **18**, 228-230 (1972).

Berdonzi, B., Chan, P. C. H. and Retzloff, D. G., "Maximal steady state multiplicity of two consecutive first-order reactions in a constant-flow stirred tank reactor", *Chem. Eng. Sci.*, **44**, 436-442 (1989).

Berger, A. J. and Lapidus, L., "On the use of Krasovkii's theorem for stability analysis", *AIChE J.*, **14**, 356 (1968).

Berger, J. S. and Perlmutter, D. D., "An extensive region of asymptotic reactor stability", *Chem. Eng. Sci.*, **20**, 147-156 (1965a)

Berger, J. S. and Perlmutter, D. D., "Stability of cascaded reactors", *Ind. Eng. Sci. Fundam.*, **4** 90-93 (1965b)

Berger, J. S. and Perlmutter, D. D., "Chemical reactor stability by Liapunov's direct method", *AIChE J.*, **10**, 233-238 (1964a)

Berger, J. S. and Perlmutter, D. D., "The effect of feedback control on chemical reactor stability", *AIChE J.*, **10**, 238-245 (1964b)

396

Bevington, J. C. and Ghanem, N. A., "The mechanism of inhibition and retardation in radical polymerizations. V", *J. Chem. Soc.*, 2071-2075 (1959)

Biesenberger, J. A. and Tadmor, Z., "Molecular weight distribution in continuous linear addition polymerization", *J. Appl. Poly. Sci.*, **9**, 3409-3446 (1965).

Bilous, O. and Amundson, N. R., "Chemical reactor stability and sensitivity", *AIChE J.*, **1**, 513-521 (1955).

Bonvin, D., De Valliere, P. and Rippin, D. W. T., "Applications of estimation techniques to batch reactors – I. Modeling thermal effects", *Comp. Chem. Eng.*, **13**, 1-9 (1989).

Bosch, B. V. D. and Luss, D., "Uniqueness and multiplity criteria for an n-th order chemical reaction", *Chem. Eng. Sci.*, **32**, 203-212 (1977a).

Bosch, B. V. D. and Luss, D., "Pitfalls in the prediction of steady state multiplicity by negative order kinetics", *Chem. Eng. Sci.*, **32**, 560-562 (1977b).

Brandrup, J. and Immergut, E. H., *Polymer Handbook*, 3rd ed., Wiley, New York, 1989.

Bronstert, K., Echte, A. Hofmann, J., "Production of rubber-modified vinylaromatic polymers", *U.S. Pat.*, **3,658,946** (1972).

Brooks, B. W., "Dynamic behavior of a continuous-flow polymerization reactor", *Chem. Eng. Sci.*, **36**, 589-593 (1981).

Brooks, B. W., "Start-up and dynamic behavior of a chemical reactor", *Chem. Eng. Sci.*, **34**, 1417-1419 (1979).

Brown, K. M., "A quadratically convergent Newton-like method based upon Gaussian elimination", *SIAM J. Numer. Anal.*, **6**, 560-569 (1969).

Budtov, V. P., Ivanchev, S. S., Belyayev, V. M., Romanova, O. S. and Otradina, G. A., "Branching parameters of comb-like polystyrene obtained using a polyperoxide initiator", *Poly. Sci. U.S.S.R.*, **18**, 2662-2667 (1976).

Butala, D. N., "Modeling and optimal control of polymerization reactor", *Ph. D. Thesis*, University of Maryland, College Park, MD (1990).

Byeon, K. H. and Chung, I. J., "Analysis of the multiple hopf bifurcation phenomena in a CSTR with two consecutive reactions – the singularity theory approach", *Chem. Eng. Sci.*, **44**, 1735-1742 (1989).

Calo, J. M. and Change, H. C., "Catastrophe theory and chemical reactors: exact uniqueness for the CSTR, catalyst particle and packed bed reactor", *Chem. Eng. Sci.*, **35**, 264-272 (1980).

Carratt, G. M., Shervin, C. R. and Soong, D. S., "Experimental study and computer simulation of a two-stage continuous polymerization process for the production of methyl methacrylate", *Poly. Eng. Sci.*, **24**, 442-454 (1984).

Carter, D. E. and Simon, R. H. M., "Continuous mass polymerization process for polyblend", *U.S. Pat.*, **3,903,202** (1975).

Chan, P. C. H., Retzloff, D. G., Mohamed, R., Berdonzi, B., Chicone, C. and Offin, D., "The dynamic behavior and chaos for two parallel reactions in a continuous stirred tank reactor", *Chem. Eng. Commun.*, **57**, 105-138 (1987).

Chang, H. C. and Calo, J. M., "Exact criteria for uniqueness and multiplicity of an nth order chemical reaction via a catastrophe theory approach", *Chem. Eng. Sci.*, **34**, 285-299 (1979).

Chang, M. and Schmitz, R. A., "An experimental study of oscillatory states in a stirred reactor", *Chem. Eng. Sci.*, **30**, 21-34 (1975).

Chatterjee, A, Park, W. S. and Grassley, W. W., "Free radical polymerization with long chain branching: continuous polymerization of vinyl acetate in *t*-butanol", *Chem. Eng. Sci.*, **32**, 167-178 (1977).

Chen, H. T., Kuan, C. N. and Lin, D. J., "Photopolymerization in an isothermal and continuous stirred tank reactor: concentration stability", *AIChE J.*, **28**, 214-219 (1982).

Chen, H. T., Kuan, C. N., Setthachayanon, S. and Chartier, P. A., "Photopolymerization in a continuous stirred tank reactor: experiment", *AIChE J.*, **26**, 672-675 (1980a).

Chen, H. T., Chartier, P. A. and Setthachayanon, S., "Influence of initiation mode on stability and control of a chain reaction", *Poly. Eng. Sci.*, **20**, 1197-1204(1980b).

Chicone, C. and Retzloff, D. G., "Dynamics of the CR equations modeling a constant flow stirred tank reactor", *Nonlinear Anal. Theo. Math. Appl.*, **6**, 983-1000 (1982).

Coggen , G. C. and Noton, A. R. M., "Discrete-time sequential state and parameter estimation in chemical engineering", *Trans. Instn. Chem. Eng.*, **48**, T255-T264 (1970).

Chattaway, T. and Stephanopoulos, G., "Adaptive estimation of bioreactors: monitoring and plasmid instability", *Chem. Eng. Sci.*, **44**, 41-48 (1989).

Choi, K. Y., "Analysis of steady state of free radical solution polymerization in a continuous stirred tank reactor", *Poly. Eng. Sci.*, **26**, 975-981 (1986).

Choi, K. Y. and Khan, A. A., "Optimal state estimation in the transesterification stage of a continuous polymerization terephthalate condensation polymerization process", *Chem. Eng. Sci.*, **43**, 749-762 (1988).

Choi, K. Y. and Lei, G. D., "Modeling of free radical polymerization of styrene catalyzed by bifunctional initiators", *AIChE J.*, **33**, 2067-2076 (1987).

Choi, K. Y. and Ray, W. H., "The dynamic behavior of continuous stirred bed reactors for the solid catalyzed gas phase polymerization of propylene", *Chem. Eng. Sci.*, **43**, 2587-2604 (1988).

Choi, K. Y. and Ray, W. H., "The dynamic behavior of fludized bed reactors for the solid catalyzed gas phase olefin polymerization", *Chem. Eng. Sci.*, **40**, 2261-2279 (1985).

Choi, K. Y., Liang, W. R. and Lei, G. D., "kinetics of bulk styrene polymerization catalyzed by symmetrical bifunctional initiators", *J. Appl. Poly. Sci.*, **35**, 1547-1562 (1988).

Cohen, D. S. and Keener, J. S., "Multiplicity and stability of oscillatory states in a continuous stirred tank reactor with exothermic consecutive reactions A → B → C", *Chem. Eng. Sci.*, **31**, 115-122 (1976).

Cohen, S. G., "Products of initiation, retardation and inhibition of peroxide induced polymerization of styrene", *J. Poly. Sci.*, **2**, 511-521 (1947).

Corlis, R. G. and Luss, R., "Use of residuals in the identification and control of two-input, single-output systems", *Ind. Eng. Chem. Fundam.*, **8**, 246-253 (1969).

Corrigan, T. E. and Dean, M. J., "The effect of backmixing on the molecular weight distribution of polymers", *J. Macromol. Sci. – Chem.*, **A2**, 645-662 (1968).

Coyle, C. K., Hirschland, H. E., Michel, B. J. and Oldshue, J. Y., "Heat transfer to jackets with close clearance impellers in viscous materials", *Can. J. Chem. Eng.*, **48**, 275-278 (1970).

Cozewith, C., "Calculation of molecular weight for polymers produced in continuous flow stirred reactor", *J. Appl. Poly. Sci.*, **15**, 2855-2863 (1971).

D'Alelio, G. F., "Catalytic polymerization process", *U.S. Pat*, **2,656,334** (1953).

Dangelmayr, G. and Stewart, I., "Classification and unfolding of sequential bifurcation", *SIAM J. Math. Anal.*, **15**, 423-445 (1984).

Denbigh, K. G., "Continuous reactions Part II: the kinetics of steady state polymerization", *Trans. Faraday Soc.*, **43**, 648-660 (1947).

Dickey, D. S., "Program chooses agitator", *Chem. Eng.*, **91**, 73-81 (1984)

Dimitratos, J., Georgakis, C., El-Aasser, M.S. and Klein. A., "Dynamic modeling and state estimation for an emulsion copolymerization reactor", *Comp. Chem. Eng.*, **13**, 21 - 33 (1989).

Dimitratos, J., Georgakis, C., El-Aasser, M.S. and Klein, A., "Composition control and Kalman filtering in emulsion copolymerization", *Amer. Cont. Conf.*, Atlanta, GA, 1988.

Doedel, E. J., "AUTO: A Program for the automatic bifurcation and analysis of autonomous systems", *Congr. Numer.*, **30**, 265-284 (1981).

Doedel, E. J. and Heinemann, R. F., "Numerical computation of periodic solution branches and oscillatory dynamics of the stirred tank reactor with $A \rightarrow B \rightarrow C$ reactions", *Chem. Eng. Sci.*, **38**, 1493-1499 (1983).

Doherty, M. F. and Ottino, J. M., "Chaos in deterministic systems: strange attractors, turbulence and applications in chemical engineering", *Chem. Eng. Sci.*, **43**, 139-183 (1988).

Dorawala, T. G. and Douglas, J. M., "Complex reactions in oscillatory reactors", *AIChE J.*, **17**, 1506-1㇒ ㇒ (1971).

Douglas, J. M. and Gaitonde, N. Y., "Analytical estimate of the performance of chemical oscillations", *Ind. Eng. Chem. Fund.*, **6**, 265-267 (1967).

Douglas, T. L., Von Bramer, P. T. and Jenkins. W. L., "Screen and select vinyl monomer inhibitors", *Hydrocarbon Process.*, 109-112 (1982)

Duerksen, J. H., Hamielec, A. E. and Hodgins, J. W., "Polymer reactors and molecular weight distribution: Part I. Free radical polymerization in a continuous stirred tank reactor", *AIChE J.*, **13**, 1081-1087 (1967).

Duerksen, J. H. and Hamielec, A. E., "Polymer reactors and molecular weight distribution. IV. Free radical polymerization in a steady state stirred tank reactor train", *J. Poly. Sci.: Part C*, **25**, 155-156 (1968).

Ellis, M. F., Taylor, T. W., Gonzales, V. and Jensen, K. F., "Estimation of the molecular weight distribution in batch polymerization", *AIChE J.*, **34**, 1341-1353 (1988a).

Ellis, M. F., Taylor, T. W. and Jensen, K. F., "On-line estimation of conversion and the molecular weight distribution in batch methyl methacrylate solution polymerization", *Amer. Cont. Conf.*, Atalanta, GA, 1988b.

Farr, W. W. and Aris, R., "Reflections on the multiplicity of steady states of the stirred tank reactor", *Chem. Eng. Sci.*, **41**, 1385-1402 (1986)

Feinberg, M., "Chemical reaction network structure and the stability of complex isothermal reactors – II", *Chem. Eng. Sci.*, **43**, 1-25 (1988).

Feinberg, M., "Chemical reaction network structure and the stability of complex isothermal reactors – I", *Chem. Eng. Sci.*, **42**, 2229-2268 (1987).

Furusawa, T., Nishimura, H. and Miyauchi, T., "Experimental study of a bistable continuous stirred tank reactor", *J. Chem. Eng. Japan*, **2**, 95-100 (1969).

Gavalas, G. R. and Seinfeld, J. H., "Sequential estimation of states and kinetic parameters in tubular reactors with catalyst decay", *Chem. Eng. Sci.*, **24**, 625-636 (1969).

Gawne, G. and Ouwerkerk, C., "Process for the manufacture of impact-resistant polyvinyl aromatic compound", *U.S. Pat.*, **4,011,284** (1977).

Georgakis, C. and Marini, L., "The effect of mixing on steady state and stability characteristics of low density polyethylene vessel reactors", *ACS Symp. Ser.*, **196**, 591-602 (1981).

Gerrens, H., Kuchner, K. and Ley, G., "Zur Konzentrationsstabilität des isothermen reaktors bei der kontinuierlichen Emulsionspolymerisation von styrol", *Chem. Ing. Tech.*, *43*, 693-698 (1971).

Gleb, A., *Applied Optimal Estimation*, MIT Press, Cambridge, 1974.

Glick, S. E., "Process for polymerizing styrene in contact with benzoyl peroxide and di (tertiary butyl) peroxide", *U.S. Pat.*, **2,534,120** (1950).

Goldstein, R. P. and Amundson, N. R., "An analysis of chemical reactor stability and control – Xb, XI, XII", *Chem. Eng. Sci.*, **20**, 449-527 (1965).

Golubitsky, M. and Keyfitz, B. L., "A qualitative study of the steady state solution for a continuous stirred tank chemical reactor", *SIAM J. Math. Anal.*, **11**, 316-329 (1980).

Golubitsky, M. and Schaeffer, D. G., *Singularities and Groups in Bifurcation Theory* , vol 1, Springer-Verlag, New York, 1985.

Golubitsky, M. and Schaeffer, D. G., "A theory for imperfect bifurcation via singularity theory", *Commun. Pure Appl. Math.*, **32**, 21-98 (1979).

Gray, P., Griffiths, J. F., Hasko, S. M. and Mullins, J. R., "Exotic behavior in the continuous flow, stirred-tank reactor (CSTR): experimental studies of oscillation and of isola and mushroom patterns in stationary states under gaseous condition", *ICE Symp. Ser.*, **87**, 101-109 (1984).

Gray, P. and Scott, S. K., "Sustained oscillations and other exotic, patterns of behavior in isothermal reactions" *J. Phys. Chem.*, **89**, 22-32 (1985).

Gray, P. and Scott, S. K., "Autocatalytic reactions in the isothermal, continuous stirred tank reactor: isolas and other forms of multiplicity", *Chem. Eng. Sci.*, **38**, 29-43 (1983).

Gunesin, B. S. and Piirma, I., "Block copolymer obtained by free radical mechanism – II. Butyl acrylate and methyl methacrylate", *J. Appl. Poly. Sci.*, **26**, 3103-3115 (1981).

Gurel, O. and Gurel, D., "Horantian (Chaotic) dynamics of oscillating chemically reactions", in *Dynamics of Nonlinear Systems*, ed by Hlaváček, V., 155-192, Gordeon and Breach Science, New York, 1986.

Halaváček, V., Kubíček, M. and Jelínek, J., "Modeling of chemical reactors – XVIII. Stability and oscillatory behavior of the CSTR", *Chem. Eng. Sci.*, **25**, 1441-1461 (1970).

Halaváček, V., Kubíček, M. and Višňák, K., "Modeling of chemical reactors – XXVI. Multiplicity and Stability analysis of a continuous stirred tank reactor with exothermic consecutive reaction A → B → C", *Chem. Eng. Sci.*, **27**, 719-742 (1972).

Hamer, J. W., Akarmov, T. A. and Ray, W. H., "The dynamic behavior of continuous polymerization reactors – II. Nonisothermal solution homopolymerization and copolymerization in a CSTR", *Chem. Eng. Sci.*, **36**, 1897-1914 (1981).

Hamilton, J. C., Seborg, D. E., and Fisher, D. G., "An experimental evaluation of Kalman filtering", *AIChE J.*, **19**, 901 - 909 (1973).

Hassard, B. D., Kazarinoff, N.D. and Wan, Y. H., *Theory and Application of Hopf Bifurcation, London Math. Soc. Lect. Note Ser.*, **41**, Cambridge Univ. Press., Cambridge, 1981.

Hassard, B. D. "The numerical evaluation of Hopf bifurcation formula", *Information Linkage between Applied Mathematics and Industry*, Academic Press, New York, 1979.

Heberling, P. V. and Gaitonde, N. Y. and Douglas, J. M., "Multiple limit cycle in a continuous stirred-tank reactor", *AIChE J.*, **17**, 1506-1508 (1971).

Henderson, L. S., "Stability analysis of polymerization in continuous, stirred tank reactors", *Chem. Eng. Prog.*, **83(3)**, 42-50 (1987).

Henderson, L. S. and Cornejo, R. A., "Temperature control of continuous, bulk styrene polymerization reactors and the influence of viscosity: an analytical study", *Ind. Eng. Chem. Res.*, **28**, 1644-1653 (1989).

Hicks, R. W., Morton, J. R. and Fenic, J. G., "How to design agitators for desired process response", *Chem. Eng.*, **83**, 102-110 (1976).

Hoftyzer, P. J. and Zwietering, T. N., "The characteristics of a homogenized reactor for the polymerization ethylene", *Chem. Eng. Sci.*, **14**, 241-251 (1961).

Horak, J., Jiracek, F. and Krausova, L., "Experimental study of the behavior of an isothermal continuous stirred tank reactor in the course of an autocatalytic reaction", *Chem. Eng. Sci.*, **26**, 1-10 (1971)

Huang, D. T. and Varma, A., "On the reference time in the multiplicity analysis for CSTRs", *Chem. Eng. Sci.*, **35**, 1806-1809 (1980)

Huang, K. T., "Control of batch and semibatch free radical solution polymerization using GPC molecular weight monitoring", *Ph. D. Thesis*, University of Maryland, 1987.

Hudson, J. L. and Mankin, J. C., "Chaos in the Belousov-Zhabontinskii reaction", *J. Chem. Phys.*, **74**, 6171-6177 (1981).

Hudson, J. L. and Rössler, O. E., "Chaos and complex Oscillations in stirred chemical reactor", in *Dynamics of Nonlinear Systems*, ed by Hlaváček, V., 193-219, Gordeon and Breach Science, New York, 1986.

Hudson, J. L., Hart, M. and Marinko, D., "An experimental study of multiple peak periodic and nonperiodic oscillation in the Belousov-Zhabontinskii reaction", *J. Chem. Phys.*, **71**, 1601-1606 (1979).

Hudson, J. L., Rössler, O. E. and Killory, H., "A four-variable chaotic chemical reaction", *Chem. Eng. Commun.*, **46**, 159-166 (1986).

Hugo, P. and Wirges, H. P., "Theoretical and experimental study of self-sustained oscillation in a stirred tank reactor", *ACS Symp. Ser.*, **65**, 498-511 (1978).

Hui, A. W. and Hamielec, A. E., "Thermal polymerization of styrene at high conversion and temperature. An Experimental study", *J. Appl. Poly. Sci.*, **16**, 749-769 (1972).

Hui, A. W. and Hamielec, A. E., "Polymer reactors and molecular weight distribution", *Ind. Eng. Chem. Fundam.*, **8**, 105-111 (1969).

Hui, A. W. and Hamielec, A. E., "Polymer reactors and molecular weight distribution. Part V. Free radical polymerization in a transient stirred tank reactor train", *J. Poly. Sci.: Part C*, **25**, 167-189 (1968).

Hwang, M. and Seinfeld, J. H., "Observability of nonlinear system", *J. Opt. Theor. Appl.*, **10**, 67 - 77 (1972).

Hyun, J. C. and Aris, R., "The control of a stirred tank reactor with hysteresis in the control element – I, II", *Chem. Eng. Sci.*, **27**, 1341-1370 (1972).

Hyun, J. C. and Bankoff, S. G., "Continuous polymerization of vinyl acetate – II. On-line estimation of process drift", *Chem. Eng. Sci.*, **31**, 953-958 (1976).

Hyun, J. C., Grassley, W. W. and Bankoff. S. G., "Continuous polymerization of vinyl acetate – I. Kinetic modeling", *Chem. Eng. Sci.*, **31**, 945-952 (1976).

Ide, Y. and White, J. L., "Rheological phenomena in polymerization reactors: rheological properties and flow patterns around agitators in polystyrene-styrene solutions", *J. Appl. Poly. Sci.*, **18**, 2997-3018 (1974).

Imoto, T., "Recent trends in the development of reaction engineering – polymerization reaction engineering", **Int. Chem. Eng.**, **12**, 546-553 (1972).

Ivanchev, S. S., "New views on initiation of radical polymerization in homogeneous and heterogeneous systems. Review", *Poly. Sci. U.S.S.R.*, **20**, 2157-2181 (1978).

Ivanchev, S. S., Budtov, V. P., Romantsova, O. N., Belyayev, V. M., Romanova, O. S., Podosenova, N. G. and Otradina, G. A., "Synthesis of comb-like polystyrene and properties of its dilute solutions", *Poly. Sci. U.S.S.R.*, **18**, 1150-1176 (1976).

Ivanchev, S. S., Zherebin, Y. I., "Radical polymerization of styrene involving participation of the macromolecules in the initiation reaction", *Poly. Sci. U.S.S.R.*, **16**, 956-963 (1974).

Jasinghani, R. and Ray, W. H., "On the dynamic behavior of a class of homogeneous continuous stirred tank polymerization reactors", *Chem. Eng. Sci.*, **32**, 811-825 (1977).

Jazwinski, A. H., *Stochastic Processes and Filtering Theory*, Academic Press, New York, 1970.

Jo, J. H. and Bankoff, S. G., "Digital monitoring and estimation of polymerization reactors", *AIChE J.*, **22**, 361-369 (1976).

Jorgensen, D. V., Farr, W. W. and Aris, R., "More on the dynamics of a stirred tank with consecutive reactions", *Chem. Eng. Sci.*, **39**, 1741-1752 (1984).

Jorgensen, D. V. and Aris, R., "On the dynamics of a stirred tank with consecutive reactions", *Chem. Eng. Sci.*, **38**, 45-53 (1983).

Kahlert, C., Rössler, O. E. and Varma, A., "Chaos in a continuous stirred tank reactor with two consecutive first order reactions, one exo-, one endothermic", in *Modeling of Chemical Reacting System*, ed. by Ebert, K. H., Deuflhard, P. and Jäger, W., 355-365, Springer-Verlag, New York, 1981.

Kaliath, T., "A view of three decades of linear filtering theory", *IEEE Trans. Inform. Theory*, **IT20**, 146-181 (1974).

Kalman, R. E., "A new approach to linear filter and prediction problems", *Trans. ASME J. Bas. Eng.*, **82**, 35-45 (1960).

Kalman, R. E. and Bucy, R. S., "New results in linear filtering and prediction theory", *Trans. ASME J. Bas. Eng.*, **83**, 95-108 (1961).

Kamath, V. R., "New initiators for polystyrene offer big efficiencies", *Modern Plastics*, **58**, 106-110 (1981).

Kamath, V. R. and Harpell, G. A., "Free radical polymerization using mixed initiator systems at two thermally distinct polymerization stages", *U.S. Pat.*, **4,129,703** (1978).

Kantor, J. C., "A finite dimensional nonlinear observer for an exothermic stirred-tank reactor", *Chem. Eng. Sci.*, **44**, 1503-1510 (1989).

Kauschus, W., Demont, J. and Hartman, K., "On the steady state of continuous stirred tank reactor", *Chem. Eng. Sci.*, **33**, 1283-1285 (1978)

Keener, J. P., "Infinite period bifurcation in simple chemical reactors", in *Modeling of Chemical Reacting System*, ed. by Ebert, K. H., Deuflhard, P. and Jäger, W., 126-137, Springer-Verlag, New York, 1981.

Kirillov, V. A. and Ray, W. H., "The mathematical modeling of continuous emulsion polymerization reactors", *Chem. Eng. Sci.*, **33**, 1499-1506 (1978).

King, R. and Gilles, E. D., "Multiple filter methods for detection of hazardous states in an industrial plant", *AIChE. J.*, **36**, 1697-1706 (1990).

King, R. and Gilles, E. D., "Dynamics and runaway of chemical reactors", *AIChE. Ann. Meeting*, San Fransisco, 1984.

Kiparissides, C. and MacGrgor, J. F. and Hamielec, A. E., "Suboptimal stochastic control of a continuous latex reactor", *AIChE J.*, **27**, 13-20 (1981).

Knorr, R. S. and O'Driscoll, "Multiple steady states, viscosity and high conversion in continuous free radical polymerization", *J. Appl. Poly. Sci.*, **14**, 2683-2696 (1970).

Kubíček, M. and Marek, M., *Computational Methods in Bifurcation Theory and Dissipative Structures*, Springer-Verlag, New York, 1983.

Kubíček, M., Hofmann, H., Hlaváček and Sinkule, J., "Multiplicity and stability in a sequence of two nonadiabatic nonisothermal CSTR", *Chem. Eng. Sci.*, **35**, 987-996 (1980).

Kwang, V. K. and Tsotsis, T. T., "Fine structure of the CSTR parameter space", *AIChE J.*, **29**, 343-347 (1983).

Lamba, P. and Hudson, J. L., "Experiments on bifurcations to chaos in a forced chemical reactor", *Chem. Eng. Sci.*, **42**, 1-8 (1987).

Lamba, P. and Hudson, J. L., "Experimental evidence of multiple oscillatory states in a continuous reactor", *Chem. Eng. Commun.*, **32**, 369-375 (1985).

Laurence, R. L. and Vasudevan, G., "Performance of a polymerization reactor in periodic operation", *Ind. Eng. Chem. Des. Dev.*, **7**, 427-433 (1968).

Leathrum, J. F., Johnson, E. F. and Lapidus, L., "A new approach to the stability and control of nonlinear processes", *AIChE J.*, **10**, 16-25 (1964).

Leaversuch, R., "Solid polystyrene gets tougher glossier, and more versatile", *Modern Plastics*, **63(11)**, 54-57 (1986).

Leib, T. M. and Luss, D., "Exact uniqueness and multiplicity criteria for an nth order reaction in a CSTR", *Chem. Eng. Sci.*, **36**, 210-212 (1981).

Leib, T. M., Rumschitzki, D. and Feinberg, M., "Multiple steady states in complex isothermal CFSTRs – I.", *Chem. Eng. Sci.*, **43**, 321-328 (1988).

Liljenroth, F. G., "Starting and stability phenomena of ammonia-oxidation and similar reactions", *Chem. Metall. Eng.*, **19(6)**, 287-193 (1918).

Liu, S. L. and Amundson, N. R., "Analysis of polymerization kinetics and the use of a digital computer", *Rubber Chem. Technol.*, **34**, 995-1133 (1961).

Lu, Y. J. and Brooks, B. W., "Effects of start-up procedure on the emulsion polymerization of vinyl acetate in a continuous flow back-mixed reactor", *Chem. Eng. Sci.*, **44**, 857-871 (1989).

Luecke, R. H. and McGuire, M. L., "Chemical reactor stability by Liapunov's direct method", *AIChE J.*, **11**, 749-750 (1965).

Luss, D., "Steady state multiplicity of chemically reacting systems", *in Modeling of Chemical Reaction Systems*, ed by Ebert, K. H., Deuflhord, P. and Jäger, W., Springer-Verlag, New York, 1981.

Luss, R. and Chen, G. T., "Steady state multiplity of lumped parameter systems in which two parallel chemical reaction occur", *Chem. Eng. Sci.*, **30**, 1483-1495 (1975).

Luss, R. and Lapidus, L., "An averaging technique for stability analysis", *Chem. Eng. Sci.*, **21**, 159-181 (1966).

Luss, R. and Lapidus, L., "Multiple limit cycle in a CSTR", *AIChE J.*, **18**, 1060-1061 (1972).

Luyben, W. L., "Effect of reaction rate on the open loop stability of chemical reactors", *AIChE J.*, **20**, 175-177 (1974).

Luyben, W. L., "Stability of autorefrigerated chemical reactors", *AIChE J.*, **12**, 662-668 (1966).

Lyberatos, G., Kusztz, B. and Bailey, J. E., "Versal matrix families, normal forms and higher order bifurcations in dynamic chemical systems", *Chem. Eng. Sci.*, **40**, 1177-1189 (1985).

Lyberatos, G., Kusztz, B. and Bailey, J. E., "Steady state multiplicity and bifurcation analysis via the Newton polyhedron approach", *Chem. Eng. Sci.*, **36**, 947-960 (1984).

Lynch, E. B. and Ramierz, W. F., "Real-time time-optimal control of a stirred tank reactor using Kalman filtering for state estimation", *AIChE J.*, **21**, 799-804 (1975).

Mankin, J. C. and Hudson, J. L., "The dynamics of coupled nonisothermal continuous stirred tank reactors", *Chem. Eng. Sci.*, **41**, 2651-2661 (1986).

Mankin, J. C. and Hudson, J. L., "Oscillatory and chaotic behavior of a forced exothermic chemical reaction", *Chem. Eng. Sci.*, **39**, 1807-1814 (1984).

Mankin, J. C., Lamba, P. and Hudson, J. L., "Transition between periodic and chaotic states in a continuous stirred tank reactor", *ACS Symp. Ser.*, **196**, 145-154 (1982).

Mauren, C. J. and Garlid, K. L., "Stability of naturally bounded nonlinear systems", *AIChE J.*, **14**, 3-8 (1968).

McKarnin, M. A., Schmidt, L. D. and Aris, R., "Response of nonlinear oscillators to forced oscillations: three chemical reaction case studies", *Chem. Eng. Sci.*, **43**, 2833-2844 (1988).

Mecklenburgh, J. C., "The influence of mixing on the distribution of copolymerization compositions", *Can. J. Chem. Eng.*, **48**, 279-285 (1970).

Meira, G. R., "Forced oscillations in continuous polymerization reactors and molecular weight distribution control. A survey", *J. Macromol. Sci. - Rev. Macromol. Chem.*, **C20**, 207-241 (1981).

Mendelson, R. A., "Concentrated solution viscosity behavior of elevated temperature – Polystyrene in ethyl benzene", *J. Rheology*, **24**, 765-781 (1980).

Mendelson, R. A., "A method for viscosity measurements of concentrated polymer solutions in volatile solvents at elevated temperature", *J. Rheology*, **23**, 545-556 (1979).

Michelson, M. L., "Steady state multiplicity of lumped parameter system with two parallel reactions", *Chem. Eng. Sci.*, **32**, 454-456 (1977).

Mott, C. L. and Kozakiewicz, B. A., "Impact polymer process", *U.S. Pat.*, **4,221,883** (1980).

Nagasubramanian, K. and Grassley, W. W., "Continuous reactors in free radical polymerization with branching", *Adv. Chem. Ser.*, **109**, 81-84 (1972).

Nagasubramanian, K. and Grassley, W. W., "Continuous reactors in free radical polymerization with branching – I, II", *Chem. Eng. Sci.*, **25**, 1459-1569 (1970).

Nauman, E. B., "Mixing in polymer reactors", *J. Macromol. Sci.* – *Revs. Macromol. Chem.*, **C10**, 75-112 (1974).

Nemanic, D. J., Tierney, J. W., Aris, R. and Amundson, N. R., "An analysis of chemical reactor stability and control -IV", *Chem. Eng. Sci.*, **11**, 199-206 (1959).

Nishimura, N., "Viscosities of concentrated polymer solutions", *J. poly. Sci. A*, **3**, 237-253 (1965).

O'Driscoll, K. F. and Bevington, J. C., "The effect of multifunctional initiators on molecular weight in free radical polymerization", *Euro. Poly. J.*, **21**, 1039-1043 (1985).

O'Driscoll, K. F. and Knorr, R., "Multicomponent polymerization. II. The effect of mixing on copolymerization in continuous stirred tank reactors", *Macromolecules*, **5**, 507-515 (1969).

Papadopoulou, S. and Gilles, E. D., "Continuous estimation of the chain length distribution in a polymerization considering time discrete gel-permeation chromatographic measurement", in Reichert, K. H. and Geiseler, W. (eds), in *Polymer Reaction Engineering*, 243-272, Huthig & Wepf, New York, 1986.

Pellegrini, L., Biardi, G. and Grottoli, M. G., "Determination of the region of asymptotic stability for a CSTR", *Comput. Chem. Eng.*, **12**, 237-241 (1988).

Penlidis, A., MacGregor, J. F. and Hamielec, A. E., "Continuous emulsion polymerization: design and control of CSTR trains", *Chem. Eng. Sci.*, **44**, 273-281 (1989).

Piirma, I. and Chou, L. P. H., "Block copolymers obtained by free radical mechanism – I. Methyl methacrylate and styrene", *J. Appl. Poly. Sci.*, **24**, 2051-2070 (1979).

Pikos, C. A. and Luss, D., "Steady state multiplicity of lumped parameter systems in which two consecutive or two parallel irreversible first order reactions occur", *Chem. Eng. Sci.*, **34**, 919-927 (1979).

Pismen, L. M., "Kinetic instabilities in man-made and natural reactors", *Chem. Eng. Sci.*, **35**, 1950-1978 (1980).

Planeaux, J. B. and Jensen, K. F., "Bifurcation phenomena in CSTR dynamics: a system with extraneous thermal capacitance", *Chem. Eng. Sci.*, **41**, 1497-1523 (1986).

Pomerleau, Y. and Perrier, M., "Estimation of multiple specific growth rates in Bioprocesses", *AIChE. J.*, **36**, 207-215 (1990).

Poor, A. B., "On the theory and application of the Hopf-Friedrichs bifurcation theory", *Arch. Rational Mech. Anal.*, **60**, 371-393 (1973).

Poor, A. B., "A model equation arising from chemical reactor theory", *Arch. Rational Mech. Anal.*, **52**, 358-388 (1973).

Preisig, H. A., "The use of differential information for batch reactor control", *Amer. Cont. Conf.*, Atlanta, GA, 1988.

Prisyazhnyuk, A. I. and Ivanchev, S. S., "Deperoxides with differing thermal stabilities of the peroxide groups as initiators of radical polymerization and block copolymerization", *Poly. Sci. USSR*, **12**, 514-524 (1970).

Product Bulletin Peroxiesters, *Pennwalt-Lucidol Co*, New York (1983).

Pryor, W. A. and Coco, J. H., "Computer simulation of the polymerization of styrene. The mechanism of thermal initiation and the importance of primary radical termination", *Macromolecules*, **3**, 500-508 (1970).

Puhl, A., Nicolis, G., "Micromixing and multiple steady state transition in a CSTR", *Chem. Eng. Sci.*, **41**, 3111-3117 (1986).

Rase, H. F., *Chemical Reactor Design for Process Plants*, Vol 1, John Wiley, New York (1977).

Rawlings, J. B. and Ray, W. H., "Emulsion polymerization reactor stability: simplified model analysis", *AIChE J.*, **33** 1663-1677 (1987a).

Rawling, J. B. and Ray, W. H., "Stability of continuous emulsion polymerization reactors: a detailed model analysis", *Chem. Eng. Sci.*, **42**, 2767-2777 (1987b).

Ray, W. H., "Polymerization reactor control", *IEEE Control System Magazine*, **August**, 3-8 (1986).

Ray, W. H., "Current problems in polymerization reaction engineering", *ACS Symp. Ser.*, **226**, 101-133 (1983).

Ray, W. H., "Dynamic behavior of polymerization reactors", in *Modeling of Chemical Reaction Systems*, ed. by Ebert, K. H., Deuflhard, P. and Jäger, W., Springer-Verlag, New York, 1981a.

Ray, W.H., *Advance Process Control*, McGraw-Hill, New York, 1981b.

Ray, W. H., "Bifurcation phenomena in chemically reacting system", in *Application of Bifurcation Theory*, ed by Robinwitz, P. H., 285-315, Academic Press, 1977.

Ray, W. H., "On the modeling of polymerization reactors", *J. Macromol. Sci. – Revs. Macormol. Chem.*, **C8**, 1-56 (1972).

Ray, W. H., "Periodic operation of polymerization reactors", *Ind. Eng. Chem. Des. Dev.*, **7**, 422-426 (1968).

Ray, W. H. and Hastings, S. P., "The influence of the Lewis number on the dynamics of chemically reacting systems", *Chem. Eng. Sci.*, **35**, 589-595 (1980).

Raźon, L. and Schmitz, R., "Multiplicities and instabilities in chemically reacting systems – A review", *Chem. Eng. Sci.*, **42**, 1005-1047 (1987).

Retzloff, D. G., Chan, P. C. H., Mohamed, R., Offin, D. and Chicone, C. "Maximal multiplicity of the critical points of the CR equation modeling

a constant flow stirred tank reactor", *J. Math. Anal. Appl.*, **124**, 327-338 (1987).

Retzloff, D. G., Chan, P. C. H., Chicone, C. Offin, D. and Mohamed, R., "Chaotic behavior in the dynamical system of a continuous stirred tank reactor", *Physica* **25D**, 131-154 (1987b).

Richards, J. R., (*personal communication*), 1990.

Rintelen, T., Riederle, K. and Kirchner, K., "Transfer of kinetic models from batch to continuous reactors with special regard to the formation of oligomers and the effect of retarders during styrene polymerization", in *Polymer Reaction Engineering*, ed by Reichert, K. H. and Geiseler, W., 270-286, Hanser Publishers, New York, 1983

Rosenbrock, H. H., "An automatic method for finding the greatest and least value of a function", *Comput. J.*, **3**, 175-184 (1960).

Ross, R. T. and Laurence, R. L., "Gel effect and free volume in the bulk polymerization of methyl methacrylate", *AIChE Symp. Ser.*, **72**, 74-79 (1976).

Rumschitzki, D. and Feinberg, M., "Multiple steady states in complex isothermal CFSTRs – II.", *Chem. Eng. Sci.*, **43**, 329-337 (1988).

Rutzlwer, W., "Nonlinear and adaptive parameter estimation methods for tubular reactors", *Ind. Eng. Chem. Res.*, **26**, 325-333 (1987).

Sabo, D. S. and Dranoff, J. S., "Stability analysis of a continuous stirred tank reactor with consecutive reactions", *AIChE J.*, **16**. 211-217 (1970).

Sanchez, J., Kamath, V. R. and Halas, J. C., "Unsymmetrical diperoxides and processes of use in polymerizing unsaturated monomers", *U.S. Pat.*, **4,079,074** (1978).

Schmidt, A. D., Clinch, T. A. and Ray, W. H., "The dynamic behavior of continuous polymerization reactors – III. An experimental study of multiple

steady states in solution polymerization", *Chem. Eng. Sci.*, **39**, 419-432 (1984).

Schmidt, A. D. and Ray, W. H., "The dynamic behavior of continuous polymerization reactors – I. Isothermal solution polymerization", *Chem. Eng. Sci.*, **36**, 1401-1410 (1981).

Schmitz, R. A., Boutz, R. R., Ray, W. H. and Uppal, A., "The dynamic behavior of a CSTR: some comparison of theory and experiment", *AIChE J.*, **25**, 289-297 (1979)

Schmitz, R. A., "Multiplicity, stability and sensitivity of states in chemically reacting systems – A review", *Adv. Chem. Ser.*, **148**, 156-211 (1975).

Schmitz, R. A. and Amundson, N. R., "An analysis of chemical reactor stability and control – Va,b", *Chem. Eng. Sci.*, **18**, 265-289, 391-414 (1963).

Schmitz, R. A. and Amundson, N. R., "An analysis of chemical reactor stability and control – VI", *Chem. Eng. Sci.*, **18**, 265-289, 415-445 (1963).

Schork, F. J. and Ray, W. H., "The dynamics of continuous emulsion polymerization of methylmethacrylate", *J. Appl. Poly. Sci.*, **34**, 1259-1276 (1987).

Schork, F. J. and Ray, W. H., "On-line measurement of surface tension and density with application to emulsion polymerization", *J. Appl. Poly. Sci.*, **28**, 407-430 (1983).

Schuler, H. and Papadopoulou, S., "Real-time estimation of the chain length distribution in a polymerization reactor – II. Comparison of the estimated and measured distribution function", *Chem. Eng. Sci.*, **41**, 2681-2683 (1986).

Schuler, H. and Suzhen, Z., "Real-time estimation of the chain length distribution in a polymerization reactor", *Chem. Eng. Sci.*, **40**, 1891-1904 (1985).

Seinfeld, J. H., "Optimal stochastic control of nonlinear systems", *AIChE J.*, **16**, 1016-1022 (1970).

Seinfeld, J. H., Gavalas, G. R. and M. Hwang, "Control of nonlinear stochastic systems", *Ind. Eng. Chem. Fundam.*, **8**, 257-262 (1969).

Shah, H. A., Leonard, F. and Tobolsky, A. V., "Phthalyl peroxide as a polymerization initiator", *J. Poly. Sci.*, **7**, 537-541 (1951).

Shanks, B. H. and Bailey, J. E., "Application of the feedback-induced bifurcation method to a catalytic reaction system", *Chem. Eng. Sci.*, **44**, 901-913 (1989).

Shastry, J. S. and Fan, L. T., "Stability analysis in polymerization reactor systems", *Chem. Eng. J.*, **6**, 129-143 (1973).

Shusman, T., "Polymerization of styrene", *U.S. Pat.*, **2,656,334** (1953).

Shusman, T., "Peroxy polymerization of vinyl aromatic compounds", *U.S. Pat.*, **2,521,754** (1950).

Simon, R. H. M. and Chappelear, D. C., "Technology of styrene polymerization reactors and processes, *ACS Symp. Scr.*, **104**, 71-112 (1979).

Sorenson, H. W., *Kalman Filtering: Theory and Application*, IEEE Press, NewYork, 1985.

Sorenson, H. W., "Least-square estimation: from Gauss to Kalman", *IEEE Spectrum*, **7**, 63-88 (1970).

Sorenson, H. W., "Kalman filtering techniques", in *Advances in Control Systems*, ed by Leondes, C. T., 219-292, Academic Press, New York, 1966.

Spitz, J. J., Laurence, R. L. and Chappelear, D. C., "An experimental study of a polymerization reactor in periodic operation", *AIChE Symp. Ser.*, **72**, 86-101 (1976).

Starzak, M. and Zarzycki, R., "Singular points in the problem of steady state multiplicity for the stirred tank with consecutive reactions", *Chem. Eng. Sci.*, **44**, 1205-1213 (1989).

Stephanopoulos, G. and San, K. Y., "On-line estimation of the state of biochemical reactors", *ACC Symp. Ser.*, **196**, 155-164 (1981).

Stephanopoulos, G. and San, K. Y., "Studies on on-line bioreactor identification. I. Theory", **Biotech. Bioeng.**, **26**, 1176-1188 (1984).

Stoukides, M., Seimanides, S. and Vayenos, C., "Rate Oscillation during propylene oxide oxidation on silver films in a continuous stirred reactor", *ACS Symp. Ser.*, **169**, 165-178 (1982).

Svoronos, S., Aris, R. and Stephanopoulos, G., "On the behavior of two stirred tanks in series", *Chem. Eng. Sci.*, **37**, 357-366 (1982).

Tadmor, Z. and Biesenberger, J. A., "Influence of segregation on molecular weight distribution in continuous linear polymerizations", *Ind. Eng. Chem. Fundam.*, **5**, 336-343 (1966).

Taylor, T. W. and Reichert, K. H., "The influence of reactor type and operating conditions on the molecular weight distribution in vinyl acetate polymerization", *J. Appl. Poly. Sci.*, **30**, 227-250 (1985).

Taylor, T. W., Gonzales, V. and Jenson, K. F., "Modeling and control of the molecular weight distribution in methyl methacrylate polymerization", in Reichert, K. H. and Geiseler, W. (eds), in *Polymer Reaction Engineering*, 261-273, Huthig & Wepf, New York, 1986.

Technical Bulletin B103, *Millipore Corporation*, Milford, MA (1987).

Terenzi, J. F. and Cosway, H. F., "Engineering study of continuous polymerization of acrylic monomers", *Ind. Eng. Chem. Fundam.*, **8**, 199-205 (1969).

Teymour, F. and Ray, W. H., "The dynamic behavior of continuous polymerization reactors – IV. Dynamic stability and bifurcation analysis of an experimental reactor", *Chem. Eng. Sci.*, **44**, 1967-1982 (1989).

Teymour, F. and Ray, W. H., "Complex dynamics of solution polymerization reactors", *AIChE Annual Meeting*, Washington D.C. (1988).

Thiele, R., "Dynamic behavior, stability and optimum startup regime for a bulk copolymerization reactor", *Chem. Eng. Sci.*, **41**, 1123-1130 (1986).

Thiele, R., "Dynamic behavior and stability of continuous reactors for bulk polymerization", *Ins. Chem. Eng. Symp. Ser.*, **87**, 125-134 (1984).

Trommsdorff, V. E., Köhle, H. and Lagally, P., "Zue polymerisation des methacrylsäuremethylesters", *Makro. Chem.*, **1**, 169-198 (1948).

Tsotsis, T. T. and Schmitz, R. A., "Exact uniqueness and multiplicity criteria for a positive-order Arrhenius reaction in a lumped system", *Chem. Eng. Sci.*, **34**, 135-137 (1979).

Tüdös, F., Kende, I. and Azori, M., "Kinetics of the inhibition of styrene polymerization by nitro compounds", *J. Poly. Sci.*, **53**, 17-25 (1961)

Tye, C., "On-line computer control of a nuclear reactor using optimal control and state estimation methods", *Proc. 6th IFAC/IFIP Conf.*, Düsseldorf, Germany, 1980.

Uhl, V. W. and Voznick, H. P., "The anchor agitator", *Chem. Eng. Prog.*, **56**, 72-77 (1960).

Uppal, A., Ray, W. H. and Poor, A. B., "The classification of the dynamic behavior of continuous stirred tank reactor - Influence of reactor residence time", *Chem. Eng. Sci.*, **31**, 205-214 (1976).

Uppal, A. and Ray, W. H. and Poor, A. B., "On the dynamic behavior of continuous stirred tank reactor", *Chem. Eng. Sci.*, **29**, 967-985 (1974).

Vaganov, D. A., Samoilanko, N. G. and Abramov, V. G., "Parametric regimes of continuous stirred tank reactors", *Chem. Eng. Sci.*, **33**, 1133-1140 (1978)

Van Herdeen, C., "Autothermic processes. Properties and reactor design", *Ind. Chem. Eng.*, **45**, 1242-1247 (1953).

Varma, A., "On the number and stability of a sequence of continuous flow stirred tank reactors", *Ind. Eng. Chem. Fundam.*, **19**, 316-319 (1980).

Varma, A. and Aris, R., "Stirred pots and empty tube", in Lapidus, L. and Amundson, N. R. (eds), *Chemical Reactor Theory. A Review*, Prentice-Hall, Englewood Cliff, NJ, 1977.

Villalobos, M. A., Hamielec, A. E. and Wood, P. E., "Kinetic model for short-cycle bulk styrene polymerization through bifunctional initiators", *J. Appl. Poly. Sci.*, **42**, 629-641 (1991).

Vleeschhouwer, P. H. M., Vermeulen, D. P. and Fortuin, J. M. H., "Transient behavior of a chemically reacting system in a CSTR", *AIChE J.*, bf 34, 1736-1739 (1988).

Volter, B. V., Salnikov, I. E., Sofiev, A. E. and Shatkhan, F. A., "Dynamics and optimization of the polymerization processes", *Third Cogr. IFAC*, London (1966).

Vuillemenot, J., Barbier, B., Riess, G. and Banderet, A., "Contribution a l'Etunde de la cinetique de formation de polymeres sequences par voie radicalaire", *J. Poly. Sci., Part A*, **3**, 1969-1984 (1965).

Wallman, P. H., "Reconstruction of unmeasured quantities for nonlinear dynamic processes", *Ind. Eng. Chem. Fundam.*, **18**, 327-333 (1979).

Wallman, P. H., Silva, J. M. and Foss, A. S., "Multivariable integral controls for fixed-bed reactors", *Ind. Eng. Chem. Fundam.*, **18**, 392-399 (1979).

Waltz, R. and Hertz, W., "Preparation of $(AB)_n$ type block copolymers by use of polyazoesters", *J. Poly. Sci. Poly. Chem. Edn.*, **16**, 1808-1814 (1978).

Warden, R. B. and Amundson, N. R., "Stability and control of addition polymerization reactions. A theoretical study", *Chem. Eng. Sci.*, **17**, 725-734 (1962).

Warden, R. B., Aris, R. and Amundson, N. R., "An analysis of chemical reactor stability and control – VIII", *Chem. Eng. Sci.*, **19**, 149-172 (1964).

Weber, A. P., "Continuous-flow reactor for high viscosity materials", *U.S. Pat.*, **4,007,016** (1977).

Wells, C. H., "Application of modern estimation and identification techniques to chemical processes", *AIChE J.*, **17**, 966 - 973 (1971).

Wells, C. H. and Larson, R. E., "Application of combined optimum control and estimation theory to direct digital control", *Proc. IEEE*, **58**, 16-22 (1970).

Wells, C. H. and Wismer, D. A., "Advances in process control applications", in *Advances in Control Systems*, ed by Leondes, C. T., 217-253, Academic Press, New York, 1971

West, H. H. and McGuire, M. L., "Optimal feedforward-feedback control of dead time systems", *Ind. Eng. Chem. Fundam.*, **8**, 253-257 (1969).

Westerterp, K. R., "Maximum allowable temperature in chemical reactors", *Chem. Eng. Sci.*, **17**, 423-433 (1962).

William, D. C. and Calo, J. M., "Fine structure of the CSTR parameter space", *AIChE J.*, **27**, 514-516 (1981).

Windes, L. C., Cinar, A. and Ray, W. H., "Dynamic estimation of temperature and concentration profiles in a packed bed reactor", *Chem. Eng. Sci.*, **44**, 2087-2106 (1989).

Wittmer, P., Anker, T., Gerrens, H. and Romeis, H., "Zum dynamischen verhalten von polymerisationsreaktoren", *Chem. Ing. Tech.*, **4**, 392-399 (1965).

Wu, R. S. H., "Dynamic thermal analyzer for monitoring batch processes", *Chem. Eng. Prog.*, **81**, 57-61 (1985).

Yamamoto, T., Aoshima, K., Ohmura, H., Moriya, Y., Suzuki, N. and Oshibe, Y., "New manufacturing processes for block and graft copolymers by radical reactions", *Polymer*, **32**, 19-28 (1991).

Yang, T. C., Weinstein, H. and Bernstein, B., "Investigation of the multiplicity of steady states with the generalized recycle reactor model", *Adv. Chem. Ser.*, **133**, 532-544 (1974).

Yuan, W., "Estimation of states and parameters by invariant imbedding technique", *Chem. Eng. Sci.*, **44**, 1665-1674 (1989).

Zeman, R. and Amundson, N. R., "Continuous polymerization models – I. Polymerization in continuous stirred tank reactors", *Chem. Eng. Sci.*, **20**, 331-361 (1965).

Zeman, R. and Amundson, N. R., "Continuous models for polymerization", *AIChE J.*, **9**, 297-302 (1963).

Curriculum Vitae

Name: Kee Jeong Kim

Permanent address: 924-14 Siheung-dong, Kuro-gu, Seoul. Korea

Degree and data to be conferred: Ph. D., 1991

Date of birth: February 7, 1959

Place of birth: Seoul, Korea

Secondary education: Seoul Technical High School
Seoul, Korea
February, 1977

College institutions attended	Dates	Degree	Date of Degree
University of Maryland	8/85-8/91	Ph.D.	12/91
Ajou University, Suwon, Korea	3/81-2/83	M.S.	2/83
Ajou University, Suwon, Korea	3/77-2/81	B.S.	2/81

Major: Chemical Engineering

Professional position held:

Mar 1981 - Dec 1982	Teaching Assistant, Ajou University, Suwon, Korea
Sep 1986 - Aug 1991	Research Assistant, Systems Research Center, University of Maryland

Publications

Hur, B. K., Kim, K. J. and Mok, Y. I., "Effect of Drop Size of Toluene on the Relative Viscosity in the Toluene-Glycerin Dispersion", *J. Korean Ins. Chem. Eng.*, **24(6)**, 459-466 (1986).

Butala, D., Kim, K. J. and Choi, K. Y., "Free radical polymerization with multifunctional initiators having peroxides of unequal thermal stabilities", *AIChE Annual Meeting*, New York, 1987.

Kim, K. J. and Choi, K. Y., "Steady State Behavior of A Continuous Stirred Tank Reactor of Styrene Polymerization with Bifunctional Free Radical Initiators", *Chem. Eng. Sci.*, **43(4)**, 965-977 (1988).

Kim, K. J., Alexander, J. C. and Choi, K. Y., "Dynamics Two CSTR's in Series for Styrene Polymerization with a Binary Initiator System", *AIChE Annual Meeting*, San Fransisco, 1989.

Kim, K. J. and Choi, K. Y., "Modeling of Free Radical Polymerization of Styrene Catalyzed by Unsymmetrical Bifunctional Initiators", *Chem. Eng. Sci.*, **44(2)**, 297-312 (1989).

Kim, K. J., Liang, W. R. and Choi, K. Y., "Bulk Free Radical Polymerization of Styrene with Unsymmetrical Bifunctional Initiators", *Ind. Eng. Chem. Res.*, **28**, 131-138 (1989).

Kim, K. J. and Choi, K. Y., "Estimation and Control of Continuous Stirred Tank Polymerization Reactors", *American Control Conference*, San Diego, 1990.

Kim, K. J., Alexander, J. C. and Choi, K. Y., "Dynamics of a CSTR for Styrene Polymerization Initiated by a Binary Initiator System", *Poly. Eng. Sci.*, **30(5)**, 279-290 (1990).

Kim, K. J., Alexander, J. C. and Choi, K. Y., "Dynamics of a Cascade of Two Continuous Stirred Tank Polymerization Reactors with a Binary Initiator Mixture", *Poly. Eng. Sci.*, **31**, 333-352 (1991).

Kim, K. J. and Choi, K. Y., "On-Line Estimation and Control of a Continuous Stirred Tank Polymerization Reactor", *J. Proc. Cont.*, **1**, 96-110 (1991).

Kim, K. J., Alexander, J. C. and Choi, K. Y., "Dynamics of a CSTR for Styrene Polymerization Initiated by a Binary Initiator Mixture – II. Effect of Viscosity Dependent Heat Transfer Coefficient", *Poly. Eng. Sci.*, *in press* (1991).

Kim, K. J. and Choi, K. Y., "Continuous Olefin Copolymerization with Soluble Ziegler-Natta Catalysts", *AIChE J.*, **37**, 1255-1260 (1991).